Nuclear Safety
NEA/CSNI/R(2012)6
February 2012
www.oecd-nea.org

OECD

International Standard Problem No. 50

ATLAS Test, SB-DVI-09: 50% (6-inch) Break of DVI line of the APR1400 Final Integration Report

Volume I
Analysis of Blind/Open Calculations

AEN NEA

NUCLEAR ENERGY AGENCY

Unclassified **NEA/CSNI/R(2012)6/PART1**

Organisation de Coopération et de Développement Économiques
Organisation for Economic Co-operation and Development **23-Feb-2012**

English text only

NUCLEAR ENERGY AGENCY
COMMITTEE ON THE SAFETY OF NUCLEAR INSTALLATIONS

International Standard Problem N° 50
ATLAS Test, SB-DVI-09: 50% (6-inch) Break of DVI line of the APR1400
Final Integration Report

Volume I
Analysis of Blind/Open Calculations

This document is only available in PDF.

JT03316483

Complete document available on OLIS in its original format

NEA/CSNI/R(2012)6/PART1
Unclassified
English text only

ORGANISATION FOR ECONOMIC CO-OPERATION AND DEVELOPMENT

The OECD is a unique forum where the governments of 34 democracies work together to address the economic, social and environmental challenges of globalisation. The OECD is also at the forefront of efforts to understand and to help governments respond to new developments and concerns, such as corporate governance, the information economy and the challenges of an ageing population. The Organisation provides a setting where governments can compare policy experiences, seek answers to common problems, identify good practice and work to co-ordinate domestic and international policies.

The OECD member countries are: Australia, Austria, Belgium, Canada, Chile, the Czech Republic, Denmark, Estonia, Finland, France, Germany, Greece, Hungary, Iceland, Ireland, Israel, Italy, Japan, Luxembourg, Mexico, the Netherlands, New Zealand, Norway, Poland, Portugal, the Republic of Korea, the Slovak Republic, Slovenia, Spain, Sweden, Switzerland, Turkey, the United Kingdom and the United States. The European Commission takes part in the work of the OECD.

OECD Publishing disseminates widely the results of the Organisation's statistics gathering and research on economic, social and environmental issues, as well as the conventions, guidelines and standards agreed by its members.

NUCLEAR ENERGY AGENCY

The OECD Nuclear Energy Agency (NEA) was established on 1 February 1958. Current NEA membership consists of 30 OECD member countries: Australia, Austria, Belgium, Canada, the Czech Republic, Denmark, Finland, France, Germany, Greece, Hungary, Iceland, Ireland, Italy, Japan, Luxembourg, Mexico, the Netherlands, Norway, Poland, Portugal, the Republic of Korea, the Slovak Republic, Slovenia, Spain, Sweden, Switzerland, Turkey, the United Kingdom and the United States. The European Commission also takes part in the work of the Agency.

The mission of the NEA is:

- to assist its member countries in maintaining and further developing, through international co-operation, the scientific, technological and legal bases required for a safe, environmentally friendly and economical use of nuclear energy for peaceful purposes, as well as
- to provide authoritative assessments and to forge common understandings on key issues, as input to government decisions on nuclear energy policy and to broader OECD policy analyses in areas such as energy and sustainable development.

Specific areas of competence of the NEA include the safety and regulation of nuclear activities, radioactive waste management, radiological protection, nuclear science, economic and technical analyses of the nuclear fuel cycle, nuclear law and liability, and public information.

The NEA Data Bank provides nuclear data and computer program services for participating countries. In these and related tasks, the NEA works in close collaboration with the International Atomic Energy Agency in Vienna, with which it has a Co-operation Agreement, as well as with other international organisations in the nuclear field.

THE COMMITTEE ON THE SAFETY OF NUCLEAR INSTALLATIONS

"The Committee on the Safety of Nuclear Installations (CSNI) shall be responsible for the activities of the Agency that support maintaining and advancing the scientific and technical knowledge base of the safety of nuclear installations, with the aim of implementing the NEA Strategic Plan for 2011-2016 and the Joint CSNI/CNRA Strategic Plan and Mandates for 2011-2016 in its field of competence.

The Committee shall constitute a forum for the exchange of technical information and for collaboration between organisations, which can contribute, from their respective backgrounds in research, development and engineering, to its activities. It shall have regard to the exchange of information between member countries and safety R&D programmes of various sizes in order to keep all member countries involved in and abreast of developments in technical safety matters.

The Committee shall review the state of knowledge on important topics of nuclear safety science and techniques and of safety assessments, and ensure that operating experience is appropriately accounted for in its activities. It shall initiate and conduct programmes identified by these reviews and assessments in order to overcome discrepancies, develop improvements and reach consensus on technical issues of common interest. It shall promote the co-ordination of work in different member countries that serve to maintain and enhance competence in nuclear safety matters, including the establishment of joint undertakings, and shall assist in the feedback of the results to participating organisations. The Committee shall ensure that valuable end-products of the technical reviews and analyses are produced and available to members in a timely manner.

The Committee shall focus primarily on the safety aspects of existing power reactors, other nuclear installations and the construction of new power reactors; it shall also consider the safety implications of scientific and technical developments of future reactor designs.

The Committee shall organise its own activities. Furthermore, it shall examine any other matters referred to it by the Steering Committee. It may sponsor specialist meetings and technical working groups to further its objectives. In implementing its programme the Committee shall establish co-operative mechanisms with the Committee on Nuclear Regulatory Activities in order to work with that Committee on matters of common interest, avoiding unnecessary duplications.

The Committee shall also co-operate with the Committee on Radiation Protection and Public Health, the Radioactive Waste Management Committee, the Committee for Technical and Economic Studies on Nuclear Energy Development and the Fuel Cycle and the Nuclear Science Committee on matters of common interest."

NEA/CSNI/R(2012)6

OECD/NEA/CSNI
International Standard Problem No. 50

ATLAS Test, SB-DVI-09: 50% (6-inch) Break of DVI line of the APR1400

Final Integration Report

Volume I

Analysis of Blind/Open Calculations

K.Y. Choi, W.P. Baek, S.Cho, H.S. Park, K.H. Kang, Y.S. Kim, H.T. Kim

Thermal Hydraulics Safety Research Division

Korea Atomic Energy Research Institute

Executive Summary

This report describes final prediction results by system analysis codes during the OECD/NEA ISP-50 exercise, targeting a 50% Direct Vessel Injection (DVI) line break integral effect test performed with the Advanced Thermal-Hydraulic Test Loop for Accident Simulation (ATLAS), which has been operated by Korea Atomic Energy Research Institute (KAERI) for accident simulations of advanced Pressurized Water Reactors (PWRs). This ISP-50 exercise has been performed in two consecutive phases: "blind" and "open" phases. The main objectives of the blind phase were to assess capability of the current-leading safety analysis codes in reproducing the overall thermal-hydraulic phenomena for the DVI line break scenario and to investigate how much "user effects" the safety analysis codes have. The open phase aimed at assessing prediction capability of the multi-dimensional behavior observed in the ISP-50 test, especially in the upper annulus down-comer region and examining how much the "user effects" can be reduced for given integral effect data. In addition, limitation of the current safety analysis codes was investigated and directions where further code improvement is required were suggested.

The submitted calculation results were analyzed and compared with the experimental data qualitatively as well as quantitatively. The 17 and 16 calculation results in "blind" and "open" phases, respectively, were categorized into 4 sub-groups according to the code similarity, and such a grouping enabled us to make more clarified comparison with the experimental data. Information on the actual boundary conditions was attached in Appendix-A. All figures comparing the 86 parameters with the test data in "blind" phase were included in Appendix-B. More expanded figures comparing the 144 parameters with the test data in "open" phase were included in Appendix-D. Additional complementary figures comparing multiple parameters were included in Appendix-E. Reports prepared by the participants in the blind and the open phases are attached in Appendix-C and Appendix-F, respectively without any modification.

In the present ISP-50 test, the observed major sequence of events are an opening of Main Steam Safety Valves (MSSV), a Low Pressurizer Pressure (LPP) trip, a Reactor Coolant Pump (RCP) trip, a Main Feed Water (MFW) isolation, a Safety Injection Pump (SIP) actuation, and a Safety Injection Tank (SIT) actuation and the set point for each event is directly related to the primary or the secondary pressures. Thus, good prediction of the primary pressure behavior leads to good prediction of the calculated sequence of events. Most open calculations showed much better agreement with the data than the blind calculations. Especially, the participants who showed an excellent prediction of the primary pressure also showed an outstanding agreement in prediction of the major sequence of events. The opening of the MSSVs played a role in reducing the secondary pressure and the heat removal rate from the primary system.

Great difficulty was found in the prediction of the secondary pressure. Incorrect prediction of the secondary pressure caused different timing of the opening of the MSSVs. Most predictions over-estimated the secondary pressure behavior. When the secondary heat loss to environment was modeled, the better agreement with the test data was obtained. Modeling of the secondary heat loss is highly recommended for correct reproduction of the secondary pressure behavior.

Reproduction of the asymmetric loop seal clearing behavior seemed to cause great difficulties for most participants. Acceptable reproduction of the loop seal clearing was not made in most calculations, particularly with respect to occurrence order and timing in four intermediate loops. Only three among sixteen calculations succeeded in predicting the same locations of the loop seal clearing to the test data. The location of the loop seal clearing and the number of cleared loop seals do not seem to be important from a viewpoint of safety. However, the timing of the 1st loop seal clearing is considered to be important as the loop seal clearing affects overall transient behavior.

One of the most important code prediction capabilities during small break loss of coolant accidents is an estimation of the break flow discharging from a break location. The break flow is also one of the most dominant factors to determine the primary depressurization. In general, prediction of the initial peak flow rate as well as the later single-phase steam flow rate was acceptable. There was a wide variation among participants in prediction of the discharge of two-phase mixture observed in the earlier phase prior to the loop seal clearing. A few participants adjusted the discharge coefficients and succeeded in calculating the reasonable two-phase break flow rate, but other participants calculated lower two-phase flow rate than the test data. Participants' experience and expertise were used to obtain a better agreement in the primary pressure by adjusting the discharge coefficient, but it was not always effective. In fact, adjustment of the discharge coefficients by code users is not a desirable approach. More investigation on the critical flow model of each code is required to minimize the user effects on the code calculation results.

Multi-dimensional phenomena such as Emergency Core Cooling (ECC) water mixing in the upper down-comer observed in the test were highlighted in terms of code prediction capability in the subsequent open phase. It was found that the code's prediction capability of the 3-D down-comer mixing phenomena was not satisfactory in most calculations even in the open phase. During the ISP-50 test, cold ECC water was introduced by a SIP and three SITs at a different time. The SIP injected ECC water into the down-comer annulus through the DVI nozzle opposite to the broken DVI nozzle and three SITs injected ECC water through the intact three

DVI nozzles. At the time of SIP injection, the down-comer annulus was full of hot water and it was observed that the cold ECC water was well mixed with the hot inventory. However, this vigorous and instant mixing was not predicted appropriately by codes. In most calculations, the fluid temperature of the intact loop side annulus was much lower than that of the broken side annulus. That is, azimuthal temperature stratification was predicted even in lower down-comer region. This incorrect prediction seems to be due to limitation of the one-dimensional code. It is suggested that momentum flux in lateral direction needs to be improved for realistic simulation of the down-comer fluid mixing. Compared with other calculations, the NRC's calculation utilizing 3-dimensional modeling of the reactor pressure vessel showed a better predictability for the ECC mixing in the down-comer.

A noticeable multi-dimensional Peak Cladding Temperature (PCT) distribution was also highlighted in this ISP-50 exercise. Partial core uncovery was observed during the test, resulting in temperature excursion up to 587.7K in the side region of the core, not the center region. It has been estimated from three dimensional code calculations that the mass flux distribution over the core cross section, peaking at the center, seems to be the most plausible reason for the maximum PCT in the side region of the core. A negative mass flux at the side region of the core was obtained in the 3-D code calculation. As the current ISP-50 does not provide the detailed local information on the local mass flux in the core region, it was difficult to reach a solid conclusion, but the three-dimensional aspect in the core region is worthy of further investigation. The temperature excursion was very closely related to the inventory distribution in the reactor pressure vessel. In particular, the down-comer water level was under-estimated in most codes. Recovery of the down-comer water level after the SIT injection was modest compared with the data. Boiling in the down-comer region could be over-estimated in the code simulation.

Great user effects were also found in this ISP-50 exercise especially in the blind phase. The user effects, in general, arise due to many reasons such as the ill-preparation of input caused by simple mistake, misunderstanding of the given boundary and initial condition(s), misunderstanding how to properly use the computer code, misunderstanding of the phenomena that appeared during the test scenario, misunderstanding of the models incorporated in the computer codes, etc. Several computer codes with various nodalization methods were also used. Therefore, it was surely hard to define them quantitatively in the present phase, but great user effects resulting from the combination of the possible reasons were again found, confirming that user effect is still one of the major issues in connection with the system thermal-hydraulic code application. Careful modeling is recommended when the code input is prepared to analyze phenomena without relevant experimental data.

Following the BEMUSE Phase II procedure for evaluating the nodalization quality, the primary and the secondary inventories of the code models were compared with the measured geometric data as the inventories significantly affect the transient behavior. Compared with the primary inventory, the secondary inventory showed much larger errors. About 50% calculations fulfilled the global acceptability Q_A<1.0 with an Acceptable Error (AE) of 5%.

In addition to the qualitative comparison of the selected major parameters and thermal-hydraulic phenomena, quantitative comparisons were performed using the Fast Fourier Transform Based Method (FFTBM) to compare the overall accuracy of the submitted calculations. Open calculations showed better prediction accuracy than the blind calculations in terms of average amplitude (AA) value. Average improvement for each time interval was 19%, 16%, and 12%, respectively. It has also been confirmed that the FFTBM is a useful method to quantify code prediction accuracy, though it has some limitations. Among the selected key parameters, the hot leg flow rate and the SIT flow rate were the most dominant parameters degrading the total prediction accuracy. Besides, as most participants experienced a difficulty in predicting the occurrence order and the timing of the loop seal clearing, the water level in the intermediate legs was not properly predicted. On the contrary, the prediction accuracy of the break flow rate was relatively good. It was due to the efforts of the participants to capture the measured flow rate and the primary pressure. As all the code groups showed the similar prediction capability, no concrete conclusions could be made in this ISP-50 exercise on the relative accuracy of a specific code or a code group.

The ISP-50 is the first-ever international cooperative program focusing on the DVI line break LOCA as well as the direct vessel injection of ECC water whose configuration is different from those of many conventional PWRs. In general the present ISP-50 gives a wide and very valuable outlook of the actual status of code performance in that various codes were tested against the same test data. Different results with the same code depending on users, which was observed apparently in the blind phase, confirms that user effects is still one of the major issues connected with the system thermal-hydraulic code applications. A feedback on the Committee on Safety of Nuclear Installations (CSNI) Integral Test Facility validation matrix issued on July 1996 could be envisaged.

Table of Contents

Volume I

Volume II

Volume III

List of Tables

List of Figures

Abbreviations and Symbols

AA : Average Amplitude
AE : Acceptable Errors
APR1400 : Advanced Power Reactor, 1400 MWe
ATLAS : Advanced Thermal-Hydraulic Test Loop for Accident Simulation
BDFT : Bi-Directional Flow Tube
CAPS : CSNI Activity Proposal Sheet
CEA : Commissariat a l'Energie Atomique
CIAE : China Institute of Atomic Energy (China)
CL : Cold Leg
CLI : Cold Leg Injection
CSNI : Committee on Safety of Nuclear Installations (OECD/NEA)
DC : Down-comer
DAS : Data Acquisition System
DVI : Direct Vessel Injection
ECC : Emergency Core Cooling
ECO : Economizer
FFTBM : Fast Fourier Transform Based Method
FORTUM : Fortum Nuclear Services Ltd. (Finland)
FW : Feed water
Gidropress : OKB Gidropress (Russia)
GRS : Gesellschaft fur Anlagen-und Reaktorsicherheit mbH (Germany)
HL : Hot Leg
HSE : Health and Safety Executive (UK)
IL : Intermediate Leg (or Cross-over Leg)
ISP : International Standard Problem
JAEA : Japan Atomic Energy Agency
JNES : Japan Nuclear Energy Safety Organization
KAERI : Korea Atomic Energy Research Institute
KEPCO : Korea Electric Power Corporation
KEPRI : Korea Electric Power Research Institute (now KEPCO RI)
KFKI/AEKI : Atomic Energy Research Institute (Hungary)
KHNP : Korea Hydro & Nuclear Power Co., Ltd.
KINS : Korea Institute of Nuclear Safety
KNF : Korea Nuclear Fuel Co., Ltd. (now KEPCO NF)
KOPEC : Korea Power Engineering Company, Inc. (now KEPCO E&C)
KTH : Royal Institute of Technology (Sweden)

LOCA : Loss of Coolant Accident
LPP : Low Pressurizer Pressure
MFW : Main Feed Water
MSIV : Main Steam Isolation Valve
MSSV : Main Steam Safety Valve
NEA : Nuclear Energy Agency (OECD)
NPIC : Nuclear Power Institute of China (China)
NRC : Nuclear Regulatory Commission (USA)
NRI : Nuclear Research Institute (Czech Republic)
OPR1000 : Optimized Power Reactor, 1000 MWe
PRG : Program Review Group
PCT : Peak Cladding Temperature
PIRT : Phenomena Identification Ranking Tabulation
PSI : Paul Scherrer Institute (Switzerland)
RCP : Reactor Coolant Pump
RCS : Reactor Coolant System
RHR : Residual Heat Removal
RPV : Reactor Pressure Vessel
RRT : Round Robin Tests
RWT : Refueling Water Storage Tank
SBLOCA : Small Break Loss of Coolant Accident
SIP : Safety Injection Pump
SIT : Safety Injection Tank
SG : Steam Generator
UNIPI : University of Pisa (Italy)
VTT : Technical Research Center (Finland)
WF : Weighted Frequency
WGAMA : Working Group on Analysis and Management of Accident (OECD)

1. Introduction

KAERI has been operating an integral effect test facility, the ATLAS for accident simulations for the OPR1000 and the APR1400 which are in operation and under construction in Korea, respectively. [Baek *et al.*[1], 2005; *Choi et al.*[1], 2006]. The ATLAS program started in 1997 under a nuclear R&D mid- and long-term project funded by the Korean government. Since a complete installation of the ATLAS in 2005, several commissioning tests have been performed successfully [Kim *et al.*, 2008]. Subsequently, the first preliminary integral effect test for a small break LOCA (SBLOCA) with a break size equivalent to a 3-inch cold leg break was performed in 2006 [*Choi et al.*[2], 2008].

In 2007, the ATLAS was extensively used for a broad range of integral effect tests on the reflood phase of a large break LOCA (LBLOCA) in order to resolve two safety issues of the APR1400 raised by a regulatory organization during its licensing process. Afterwards, the ATLAS was modified to have a configuration for simulating the DVI line break accidents of the APR1400 at the beginning of 2008. In the APR1400, DVI nozzles are located 2.1m above elevation of centerline of the cold leg nozzles. The DVI-adopted plants treat a DVI line break as another spectrum among the SBLOCAs in their safety analysis because a DVI nozzle directly attached to a reactor vessel is vulnerable to a postulated break from a safety viewpoint. The thermal hydraulic phenomena in the rector pressure vessel (RPV) down-comer might be different from the cold leg injection (CLI) plants during the postulated design basis accidents. In the event of a DVI line break, the vapor generated in the core is introduced to the RPV down-comer through the hot legs, the steam generators and the cold legs. Then the vapor should pass through the upper part of the RPV down-comer to be discharged through the broken DVI nozzle. Therefore, the behavior of the two-phase flow in the upper annulus down-comer is expected to be complicated and relevant models need to be implemented into safety analysis codes in order to predict these thermal hydraulic phenomena correctly. So far there is not enough integral effect test data for the DVI line breaks which can demonstrate the progression of the DVI line break accident realistically. The test data for the DVI line breaks can be used for an assessment and improvement of safety analysis codes. Hence, sensitivity tests for different DVI line break sizes were performed in 2008 [Choi *et al.*[3], 2008; Choi *et al.*[4], 2011]. Integral effect database for four break sizes were established; 5%, 25%, 50%, and 100%.

After a series of DVI line break tests were completed, the tests for small break LOCA (SBLOCA) commenced at the end of 2008. In order to provide integral effect database for SBLOCA of the APR1400, sensitivity tests for different break sizes of the cold leg were conducted. In addition, parameter survey tests were also taken into account in a test matrix in order to investigate the effects of break location. The same combination of safety injection

systems used in the DVI line break tests was applied. This parameter survey test results with different break locations will be a unique data which can be used for evaluation of the effects of the break location on the safety of the APR1400.

Among the DVI line break scenarios, 50% of the cross section of a DVI nozzle would be of interest because this break size is on the edge of the criterion provided by the EPRI requirement where a core uncovery should be prevented by a best-estimate methodology [EPRI, 1995]. In particular, the thermal-hydraulic phenomena occurring in the upper annulus down-comer region between the DVI nozzle and the cold leg nozzles are expected to be complicated due to the countercurrent flow of the upward break flow and the downward safety injection flow. Therefore, the relevant models need to be incorporated into the safety analysis codes in order to predict these thermal hydraulic phenomena correctly.

In the present ISP-50 exercise, the predictions of a 50% DVI line break accident of the APR1400 with different best-estimate computer codes are compared with each other and above all with the results of a carefully specified experimental study. This exercise would contribute to assessing the code's modeling capabilities and to identifying any deficiencies of the best-estimate system codes of the participants against the obtained integral effect data on the DVI line break accident.

1.1 Background and brief History

The ATLAS has been used to provide the unique test data for the 2(hot legs) x 4(cold legs) reactor coolant system with a direct vessel injection (DVI) of emergency coolant; this will significantly expand the currently available data bases for code validation. International Standard Problem (ISP) exercise using the ATLAS facility would significantly contribute to the enhancement of understanding on the behavior of nuclear reactor systems with the DVI and to the assessment of existing and new thermal-hydraulic analysis codes such as TRACE, CATHARE, RELAP, TRAC, ATHLET, CATHENA and MARS.

Since the first ISP exercise was performed for the problem of the Edwards' Pipe in 1973, the NEA/CSNI has sponsored a considerable number of international activities to promote the exchange of experience between its Member countries in the use of nuclear safety codes and testing materials. A primary goal of these activities is to increase confidence in the validity and accuracy of analytical tools or testing procedures which are needed to warrant the safety of nuclear installations, and to demonstrate the competence of involved institutions. Three main areas of CSNI-sponsored international comparative studies include international standard problems (ISPs), computational benchmark studies (Benchmarks), and round robin tests (RRT).

Up to now, forty nine ISPs were carried out by utilizing test facilities worldwide. A good review on the previous ISPs was summarized in the literature [OECD/NEA, 2000].

An International Standard Problem (ISP) exercise using the ATLAS was proposed and discussed at the 10th plenary meeting of the NEA Committee on the Safety of Nuclear Installations (CSNI) Working Group on Analysis and Management of Accidents (WGAMA) in September 2007. The discussion at the WGAMA plenary meeting with possible participants revealed that a DVI line break scenario would be attractive for the ISP exercise. At the 11th WGAMA meeting in October 2008, KAERI submitted a specified ISP proposal and a relevant CAPS (CSNI Activity Proposal Sheet) as well based on a DVI line break scenario for Program Review Group (PRG) approval, after final endorsement by WGAMA members. Subsequently, the ISP exercise with the ATLAS facility focusing on a DVI line break scenario was finally approved by the CSNI meeting in December 2008 and was numbered by ISP-50. Major milestones of the ISP-50 are summarized in Table 2.3-1.

Considering the very limited integral effect test data on DVI line break, this exercise has provided the participants with the opportunity to understand the relevant thermal hydraulic behavior and to assess existing thermal-hydraulic system codes against the test data. It has also contributed to international familiarization and validation of the ATLAS, which is one of the major nuclear safety research facilities. Among the integral effect test database established by KAERI, 50% break scenario of the DVI nozzle was determined by considering technical importance and by incorporating with comments from the participants. The DVI line break is an important accident scenario for several advanced PWRs but relevant data are very limited. Both regulators and industry require relevant experimental data and reliable prediction tools.

The first "blind" phase started by holding a kick-off meeting in April, 2009. This first workshop (kick-off meeting), where 11 organizations attended, was held at KAERI in April, 21-22, 2009 to finalize the ISP-50 specifications. As agreed at the first workshop, ISP-50 working page (www.oecd-nea.org/download/isp-50) was constructed and opened under NEA web site in May, 2009. The specification was finalized by incorporating answers to the questions and comments on the proposed specifications and it was distributed in June, 2009. The agreed test was successfully performed by the operating agency, KAERI in July, 2009. Information document on actual test conditions and procedure was distributed in August, 2009. The experimental data were not released until the calculation results were made available for a comparison. All participants were requested to submit their calculation results to the operating agency for a comparison by the end of 2009.

In the "blind" phase, a total of 17 calculation results were submitted from 13 organizations.

In particular, KOPEC and EDO Gidropress submitted two and four different calculation results, respectively. CIAE was the latest to join the "blind" calculation of the ISP-50 and contributed to the ISP-50 by submitting their calculation results with the RELAP5/MOD3.3 code. A few participants showed their intentions to join the following the "open" phase due to lack of available resources. Seven leading safety analysis codes were used in the "blind" phase, including RELAP5/MOD3, TRACE, MARS-KS, KORSAR, TECH-M-97, APROS, and ATHLET. As an output specification, 86 parameters considered to be worthy of comparison were selected and requested.

The second workshop was held at OECD headquarter in May 25-26, 2010 to present and to discuss the blind calculation results and future steps. Experimental results and overview of the comparison of the calculation results were presented by the operating agency. Quantitative comparison result of the submitted calculations by FFTBM was also presented and discussed. It was agreed to keep the FFTBM results for the blind phase but with highlighting some precautions regarding the use of this FFTBM method. The participants also discussed the parameters for which a comparison of calculated and experimental results would be interesting as well as the physical phenomena in down-comer and loop seal clearing. In particular 3-D phenomena (e.g., temperature distribution, flow in the down-comer) may be of prime interest. Temperature and condensation rates at injection points, differential pressures, and void fraction distribution (e.g., in the down-comer and in the core) were suggested. JAEA and NRC accepted to help KAERI to point out the 3-D behaviour in the down-comer and in the core. Some participants expressed the need for additional information in order to improve their understanding and interpretation of the test and hence in order to improve their calculation results in the post-test phase. In addition, importance of upper head to down-comer bypass and its role in loop seal clearing as well as 3-dimensional nature of the flow in the upper part of the down-comer was highlighted. It was agreed that the participants would send their requests to KAERI in written form within 2 weeks. KAERI compiled the requests and analyzed the requests and answered by issuing detailed test report for 50% DVI line break simulation.

The "open" phase followed the "blind" phase right after the second workshop. In response to the request for additional experimental data, the operating agency released the detailed experimental information as well as the detailed cladding temperature distribution. A total of 269 parameters for major thermal hydraulic variables were open to the participants. Detailed cladding temperatures for 264 different locations inside the core were also distributed to the participants. In addition, the operating agency delivered revised specifications for output submission, where 144 of 269 parameters were requested to examine the 3-D phenomena in the reactor pressure vessel as well as the asymmetric loop behavior. PSI (Switzerland) and KFKI/AEKI (Hungary) took part in this "open" phase.

Although the program schedule experienced a little delay, calculation results in the open phase were submitted from October, 2010 to March, 2011. A total of 16 calculation results were collected from 11 countries. As the CATHARE code was used by KFKI/AEKI and the calculation by the TECH-M-97 code (GP4) was not submitted in the "open" phase, the number of code used in the ISP-50 was seven: RELAP5/MOD3, TRACE, MARS-KS, KORSAR, APROS, CATHARE, and ATHLET. In order to apply the FFTBM, which can quantify the improvement of the "open" calculation against the "blind" calculation, 12 more cladding temperature data were additionally requested. By the help of wholehearted cooperation of the participants, the requested additional data were successfully collected in due time. A final integration report was prepared with help of participants by the operating agency to incorporate the results in the "blind" phase.

1.2 Objectives of the ATLAS ISP-50

A best-estimate safety analysis methodology for the DVI line break accidents needs to be developed to identify the uncertainties involved in the safety analysis results. Such best-estimate safety analysis methodology will contribute to defining a more precise specification of safety margins and thus lead to a greater operational flexibility. In particular, the co-existing of upward and downward flows in the down-comer above the cold leg are one of the important phenomena specific to the APR1400 because its DVI nozzles are located above the elevation of the cold leg. However, such an effort focusing on the complex thermal hydraulic phenomena occurring in the upper down-comer region has never been reported yet due to a lack of an integral effect database on the DVI line break accidents.

Generally, the current ATLAS ISP-50 aims at:

- Better understanding of thermal-hydraulic phenomena in the upper annulus down-comer region during the DVI period.
- Generation of integral effect database for code development and validation.
- Investigation of the possible limitation of the existing best-estimate safety analysis codes

More specifically, the first "blind" phase takes aim at:

- Assessing capability of the current-leading safety analysis codes in reproducing the overall thermal-hydraulic phenomena for the DVI line break scenario.
- Investigating how much "user effects" the safety analysis codes have.

On the other hand, the subsequent "open" phase is targeting at:

- Examining how much the "user effects" can be reduced for given integral effect data.
- Assessing capability of the current-leading safety analysis codes in capturing the multi-dimensional behavior observed in the ISP-50 test, especially in the upper annulus down-comer region when the safety injection water is introduced through the DVI nozzle above the cold leg.
- Finding limitation of the safety analysis codes and thus suggesting area and/or directions where further code improvement is required.

2. Organization of the ATLAS ISP-50

2.1 Host organization

The ATLAS ISP-50 was led by KAERI in collaboration with OECD/NEA. KAERI was responsible for general coordination of the ISP-50, data provision, information on the ATLAS and the ISP-50, code calculation, receipt of submissions, results comparison, progress meetings, final workshop, and comparison report.

2.2 List of participants

A total of nineteen organizations joined the ATLAS ISP-50 program as listed in Table 2.2-1. A few organizations joined the "open" phase followed by the "blind" phase. Each signed organization has an obligation to perform an open calculation within the calculation period by using the test results which were provided by the operating agency, KAERI. All the participants are also requested to write their analysis results in an assigned section of a final comparison report.

Table 2.2-1 List of participants

Country	Organization	Participants	Code
China	CIAE[1)]	Chen Yuzhou; chenyz@ciae.ac.cn	RELAP5/MOD3.3
Czech Republic	NRI	Radim Meca; mec@ujv.cz	ATHLET
Finland	VTT	Pasi Inkinen; Pasi.Inkinen@vtt.fi Ismo Karppinen; Ismo.karppinen@vtt.fi	APROS 5.09
	FORTUM[1)]	Ahonen Aino; Aino.Ahonen@fortum.com	APROS v.5.08
Germany	GRS	Henrique Austregesilo; Henrique.Austregesilo@grs.de	ATHLET Mod 2.2 Cycle A
Hungary	KFKI/AEKI[2)]	Antal Takacs; takacs@aeki.kfki.hu	CATHARE2V1.5Bmod3.1
Italy	U. of Pisa	Marco Cherubini; m.cherubini@ing.unipi.it	RELAP5/MOD3.3
Japan	JAEA[3)]	Akira Satou; Satou.akira@jaea.go.jp	TRACE 5.0
	JNES[3)]	Hideaki Utsuno; Utsuno-hideaki@jnes.go.jp	TRACE

Russia	EDO Gidropress	I. A. Cheremisov, V. V. Schekoldin (blind) M.S. Khvostov, V. V. Schekoldin (open) Schekoldin_vv@grpress.podolsk.ru V. I. Shchekoldin V.V. Yudahin S.L. Borisov	KORSAR/GP (GP1) KORSAR/GP (GP1) KORSAR/GP (GP2) KORSAR/GP (GP3) TECH-M-97 (GP4)
Sweden	KTH	Erdenechimeg Sudvantsetseg, Fabio Veronese and Tomasz Kozlowski tomasz@safety.sci.kth.se	TRACE 5.0 patch 01
Switzerland	PSI[2)]	Annalisa Manera; Annalisa.manera@psi.ch Medhat Sharabi; Medhat.sharabi@psi.ch	RELAP5/MOD3.3
UK	HSE[3)]	John Jones; john.jones@hse.gsi.gov.uk	NA
USA	NRC	Harrington Ronald; Ronald.Harrington@nrc.gov Scott Krepel; Scott.krepel@nrc.gov	TRACE 5.200
Korea	KAERI	K. D. Kim; kdkim@kaeri.re.kr	MARS-KS
	KINS	S. H. Ahn; K175ash@kins.re.kr	MARS-KS
	KNF	T. S. Choi; tschoi@knfc.co.kr	RELAP5/MOD3.3
	KEPRI	S. J. Ha; hsj@kepri.re.kr S.Y. Kim; seyunkim@kepri.re.kr	MARS-KS
	KOPEC	C. W. Kim; cwkim@kopec.co.kr H. R. Choi; hrchoi@kopec.co.kr Y.M. Kim; kimym@kopec.co.kr	RELAP5-ME RELAP5/MOD3.3

[1)] contributed to the "blind" calculation only
[2)] joined the "open" calculation
[3)] participated as an observer

2.3 Schedule of ISP-50

Table 2.3-1 shows the final schedule of ISP-50. This schedule was determined by incorporation with comments from the participants at the kick-off meeting, but slight modification was made at the 2nd workshop.

Table 2.3-1 ISP-50 Schedule

Date	Events/Actions
February 2009	Distribution of draft specification of ISP-50
April 21, 2009	The 1st workshop to kick off ISP exercise Comments on the ISP specification Provide the facility summary report
May 2009	Freeze ISP-50 specifications
June 2009	Perform the agreed test by operating agency
August 2009	Provide detailed information on actual test conditions and procedures
December 2009	Complete blind calculation (Phase 1) by all participants
January 2010	Collect calculation results from all participants
February 2010	Provide test report and draft comparison report on blind calculations
May 25~26, 2010	The 2nd workshop to discuss the draft comparison report Distribution of experimental results
September 2010	Presentation to GAMA
End of December 2010	Complete open calculation (Phase 2) by all participants
End of February 2011	Provide final draft report
May 25~26, 2011	Final workshop
Early July 2011	Final report
Sept-Oct. 2011	Review and GAMA endorsement Submission to PRG/CSNI for approval

It was agreed in the kick-off meeting on April, 2009 that the steady state input deck of the ATLAS facility can be provided to participants who want to have it with a notification to the other participants. Thus, a code input deck for RELAP5/MOD3.3 prepared by the operating agency was delivered to eight organizations who requested the input deck. The organizations who have received the input deck from the operating agency are JNES (Japan), NRI (Czech Republic), Univ. of Pisa (Italy), GRS (Germany), KTH (Sweden), NRC (USA), CIAE (China) and PSI (Switzerland). Most Korean participants who are familiar with the ATLAS facility already have the RELAP5/MOD3.3 input deck. Such provision provided the participants who were not familiar with the ATLAS facility with the opportunity of easy participation. Nonetheless, most organizations made the best use of their own code experience and expertise to analyze the test scenario as closely as possible.

2.4 List of requested parameters

Among 1,250 measuring parameters, a total of 86 parameters were requested to participants for a comparison with the data in the first "blind" phase. As one of the main objectives of the "blind" phase was to assess capability of safety analysis codes in reproducing the overall thermal-hydraulic phenomena for the DVI line break scenario, only 86 key parameters were selected and considered to be sufficient to characterize the ISP-50 scenario. A full list of requested parameters is shown in Table 2.4-1. Information of the reference instruments in this table is found from Figure 2.4-1 through Figure 2.4-7. The shaded line indicates that the experimental data were not available or should be post-processed. In the 2nd workshop, multi-dimensional behavior in the RPV was discussed. Some participants expressed the need for additional information in order to improve their understanding and interpretation of the test and hence in order to improve their calculation results in the post-test phase. Hence, the operating agency provided additional data, including the detailed temperature distribution in the core region. In order to perform more improved comparison of calculations with the data, the requested parameter sets were expanded from 86 to 145 parameters as shown in Table 2.4-2. The organizations who showed their willingness to perform 3-D modeling for the core region can submit their calculation results either at the last column of the parameter list or in a free format. During the data collection and the quantitative comparison process by operating agency, it was found that the PCT information at different elevations was not requested. Thus, the maximum wall temperatures at each 12 elevation in the core region were additionally requested and added at the end of the list of Table 2.4-2. In most 1-D calculations, these data correspond to the heat structure temperatures of the hot channel.

Table 2.4-1 List of experimental data requested in the blind calculation

No	Instrument name	Type	Unit	Remarks
1	∑ HP-CO-0i-P	Power	Watt	Total core power, i=1~3
2	-	Power	Watt	Heat removal rate of SG1 Only reliable before the break
3	-	Power	Watt	Heat removal rate of SG2 Only reliable before the break
4	PT-UH-01	Pressure	Pa	Upper head of RPV
5	PT-PZR-01	Pressure	Pa	Pressurizer
6	PT-SGSD1-01	Pressure	Pa	Steam dome of SG1
7	PT-SGSD2-01	Pressure	Pa	Steam dome of SG2
8	PT-SIT1-02	Pressure	Pa	Safety Injection Tank-1
9	PT-SIT2-02	Pressure	Pa	Safety Injection Tank-2

10	PT-SIT3-02	Pressure	Pa	Safety Injection Tank-3
11	PT-CS-04	Pressure	Pa	Containment Simulator
12	DP-HL1IL1A-01	Pressure	Pa	DP from HL-1 inlet to IL-1A
13	DP-HL1IL1B-01	Pressure	Pa	DP from HL-1 inlet to IL-1B
14	DP-HL2IL2A-01	Pressure	Pa	DP from HL-2 inlet to IL-2A
15	DP-HL2IL2B-01	Pressure	Pa	DP from HL-2 inlet to IL-2B
16	TF-LP-02G18	Water Temp.	K	Core inlet plenum
17	Average of TF-CO-07-G14, TF-CO-07-G18, TF-CO-07-G21, TF-CO-07-G25	Water Temp.	K	Core outlet plenum
18	TF-PZR-08	Water Temp.	K	Pressurizer
19	TF-HL1-02B	Water Temp.	K	Hot leg-1
20	TF-HL2-02B	Water Temp.	K	Hot leg-2
21	TF-CL1A-03B	Water Temp.	K	Cold leg-1A
22	TF-CL1B-03B	Water Temp.	K	Cold leg-1B
23	TF-CL2A-03B	Water Temp.	K	Cold leg-2A
24	TF-CL2B-03B	Water Temp.	K	Cold leg-2B
25	TF-SGP1-01	Water Temp.	K	SG-1 inlet plenum
26	TF-SGP1-02	Water Temp.	K	SG-1 outlet plenum
27	TF-SGP2-01	Water Temp.	K	SG-2 inlet plenum
28	TF-SGP2-02	Water Temp.	K	SG-2 outlet plenum
29	TF-SGSD1-03	Temperature	K	SG-1 dome
30	TF-SGSD2-03	Temperature	K	SG-2 dome
31	TF-SIT1-03	Water Temp.	K	Active SIT-1
32	TF-SIT2-03	Water Temp.	K	Active SIT-2
33	TF-SIT3-03	Water Temp.	K	Active SIT-3
34	TF-HPSI1-03	Water Temp.	K	Active SIP-02
35	TF-CS-04	Temperature	K	Containment
36	TF-HL1-02A	Steam Temp.	K	Hot leg-1
37	TF-HL2-02A	Steam Temp.	K	Hot leg-2
38	TF-CL1A-03A	Steam Temp.	K	Cold leg-1A
39	TF-CL1B-03A	Steam Temp.	K	Cold leg-1B
40	TF-CL2A-03A	Steam Temp.	K	Cold leg-2A
41	TF-CL2B-03A	Steam Temp.	K	Cold leg-2B
42	TH-CO-01G11a1	Wall Temp.	K	Core region 1

43	TH-CO-02G11a1	Wall Temp.	K	Core region 2
44	TH-CO-03G11a1	Wall Temp.	K	Core region 3
45	TH-CO-04G11a1	Wall Temp.	K	Core region 4
46	TH-CO-05G11a1	Wall Temp.	K	Core region 5
47	TH-CO-06G11a1	Wall Temp.	K	Core region 6
48	TH-CO-07G11b1	Wall Temp.	K	Core region 7
49	TH-CO-08G11b1	Wall Temp.	K	Core region 8
50	TH-CO-09G11b1	Wall Temp.	K	Core region 9
51	TH-CO-10G11b1	Wall Temp.	K	Core region 10
52	TH-CO-11G11b1	Wall Temp.	K	Core region 11
53	TH-CO-12G11b1	Wall Temp.	K	Core region 12
54	-	Flow rate	kg/s	UH-to-DC bypass line
55	-	Flow rate	kg/s	HL-to-DC bypass line
56	QV-HL1-01A+B	Flow rate	kg/s	Hot leg-1
57	QV-HL2-01A+B	Flow rate	kg/s	Hot leg-2
58	QV-CL1A-01A+B	Flow rate	kg/s	Cold leg-1A
59	QV-CL1B-01A+B	Flow rate	kg/s	Cold leg-1B
60	QV-CL2A-01A+B	Flow rate	kg/s	Cold leg-2A
61	QV-CL2B-01A+B	Flow rate	kg/s	Cold leg-2B
62	QV-MF1-01	Flow rate	kg/s	SG-1 feed water to economizer
63	QV-MF1-02	Flow rate	kg/s	SG-1 feed water to down-comer
64	QV-MF2-01	Flow rate	kg/s	SG-2 feed water to economizer
65	QV-MF2-02	Flow rate	kg/s	SG-2 feed water to down-comer
66	QV-SIT1-01	Flow rate	kg/s	Active SIT-1
67	QV-SIT2-01	Flow rate	kg/s	Active SIT-2
68	QV-SIT3-01	Flow rate	kg/s	Active SIT-3
69	QV-HPSI1-03	Flow rate	kg/s	Active SIP-02
70	∑ (QV-CS-03+ d(LC-CS-01+ LC-CS-02)/dt)	Flow rate	kg/s	Total break flow rate 0~364s : RCS inventory based method 364 ~ 2944 s : Load cell based method
71	Integral of 70	Mass	kg	Accumulated total break mass
72	LT-RPV-04A	Water level	m	RPV down-comer
73	LT-RPV-01	Water level	m	Active core region
74	LT-PZR-01	Water level	m	Pressurizer
75	LT-IL1A-03	Water level	m	Intermediate leg-1A
76	LT-IL1B-03	Water level	m	Intermediate leg-1B
77	LT-IL2A-03	Water level	m	Intermediate leg-2A

78	LT-IL2B-03	Water level	m	Intermediate leg-2B
79	LT-SGP1-02A	Water level	m	SG-1 U-tube upward section
80	LT-SGP1-02B	Water level	m	SG-1 U-tube downward section
81	LT-SGP2-02A	Water level	m	SG-2 U-tube upward section
82	LT-SGP2-02B	Water level	m	SG-2 U-tube downward section
83	RS-RCP1A-01	speed	rpm	RCP-1A
84	RS-RCP1B-01	speed	rpm	RCP-1B
85	RS-RCP2A-01	speed	rpm	RCP-2A
86	RS-RCP2B-01	speed	rpm	RCP-2B

Table 2.4-2 List of experimental data requested in the open calculation

No	Instrument name	Type	Unit	Remarks
1	∑ HP-CO-0i-P	Power	Watt	Total core power, i=1~3
2	-	Power	Watt	Heat removal rate of SG1 Only reliable before the break
3	-	Power	Watt	Heat removal rate of SG2 Only reliable before the break
4	PT-LP-01	Pressure	Pa	Lower plenum of RPV
5	PT-PZR-01	Pressure	Pa	Pressurizer
6	PT-SGSD1-01	Pressure	Pa	Steam dome of SG1
7	PT-SGSD2-01	Pressure	Pa	Steam dome of SG2
8	PT-SIT1-02	Pressure	Pa	Safety Injection Tank-1
9	PT-SIT2-02	Pressure	Pa	Safety Injection Tank-2
10	PT-SIT3-02	Pressure	Pa	Safety Injection Tank-3
11	PT-CS-04	Pressure	Pa	Containment Simulator
12	DP-HL1CL1A	Pressure	Pa	DP from HL-1 to CL-1A Difference between PT-HL1-01 and PT-CL1A-01
13	DP-HL1CL1B	Pressure	Pa	DP from HL-1 to CL-1B Difference between PT-HL1-01 and PT-CL1B-01
14	DP-HL2CL2A	Pressure	Pa	DP from HL-2 to CL-2A Difference between PT-HL2-01 and PT-CL2A-01
15	DP-HL2CL2B	Pressure	Pa	DP from HL-2 to CL-2B Difference between PT-HL2-01 and

				PT-CL2B-01
16	DP-HL1	Pressure	Pa	DP along the HL-1 Sum of DP-HL1-01 and DP-HL1-02
17	DP-HL2	Pressure	Pa	DP along the HL-2 Sum of DP-HL2-01 and DP-HL2-02
18	DP-CL1A	Pressure	Pa	DP along the CL-1A Sum of DP-CL1A-01 and DP-CL1A-02
19	DP-CL1B	Pressure	Pa	DP along the CL-1B Sum of DP-CL1B-01 and DP-CL1B-02
20	DP-CL2A	Pressure	Pa	DP along the CL-2A Sum of DP-CL2A-01 and DP-CL2A-02
21	DP-CL2B	Pressure	Pa	DP along the CL-2B Sum of DP-CL2B-01 and DP-CL2B-02
22	DP-HL1IL1A-01	Pressure	Pa	DP from HL-1 inlet to IL-1A
23	DP-HL1IL1B-01	Pressure	Pa	DP from HL-1 inlet to IL-1B
24	DP-HL2IL2A-01	Pressure	Pa	DP from HL-2 inlet to IL-2A
25	DP-HL2IL2B-01	Pressure	Pa	DP from HL-2 inlet to IL-2B
26	TF-UH-02	Temp.	K	Middle upper head of RPV
27	TF-UH-04	Temp.	K	Highest upper head of RPV
28	TF-UP-02	Temp.	K	Upper plenum of RPV at the same elevation of the legs
29~34	TF-DC-011~016	Temp.	K	Down-comer at elevation 1
35~40	TF-DC-021~026	Temp.	K	Down-comer at elevation 2
41~46	TF-DC-031~036	Temp.	K	Down-comer at elevation 3
47~52	TF-DC-041~046	Temp.	K	Down-comer at elevation 4
53~58	TF-DC-051~056	Temp.	K	Down-comer at elevation 5
59~64	TF-DC-061~066	Temp.	K	Down-comer at elevation 6
65	TF-DC-07	Temp.	K	Down-comer at elevation 7
66	TF-LP-02G18	Water Temp.	K	Core inlet plenum
67	Average of TF-CO-07-G14, TF-CO-07-G18, TF-CO-07-G21, TF-CO-07-G25	Water Temp.	K	Core outlet plenum
68	TF-PZR-08	Water Temp.	K	Pressurizer
69	TF-HL1-02B	Water Temp.	K	Hot leg-1
70	TF-HL2-02B	Water Temp.	K	Hot leg-2
71	TF-CL1A-03B	Water Temp.	K	Cold leg-1A

72	TF-CL1B-03B	Water Temp.	K	Cold leg-1B
73	TF-CL2A-03B	Water Temp.	K	Cold leg-2A
74	TF-CL2B-03B	Water Temp.	K	Cold leg-2B
75	TF-SGP1-01	Water Temp.	K	SG-1 inlet plenum
76	TF-SGP1-02	Water Temp.	K	SG-1 outlet plenum
77	TF-SGP2-01	Water Temp.	K	SG-2 inlet plenum
78	TF-SGP2-02	Water Temp.	K	SG-2 outlet plenum
79	TF-SIT1-03	Water Temp.	K	Active SIT-1
80	TF-SIT2-03	Water Temp.	K	Active SIT-2
81	TF-SIT3-03	Water Temp.	K	Active SIT-3
82	TF-HPSI1-03	Water Temp.	K	Active SIP-02
83	TF-HL1-02A	Steam Temp.	K	Hot leg-1
84	TF-HL2-02A	Steam Temp.	K	Hot leg-2
85	TF-CL1A-03A	Steam Temp.	K	Cold leg-1A
86	TF-CL1B-03A	Steam Temp.	K	Cold leg-1B
87	TF-CL2A-03A	Steam Temp.	K	Cold leg-2A
88	TF-CL2B-03A	Steam Temp.	K	Cold leg-2B
89	TF-SGSD1-03	Temperature	K	SG-1 dome
90	TF-SGSD2-03	Temperature	K	SG-2 dome
91	TF-CS-04	Temperature	K	Containment
92	TH-CO-G1-Max	Temperature	K	Max. temp. in heater group 1
93	TH-CO-G2-Max	Temperature	K	Max. temp. in heater group 2
94	TH-CO-G3-Max	Temperature	K	Max. temp. in heater group 3
95	-	Flow rate	kg/s	Total DC-to-UH bypass line
96	-	Flow rate	kg/s	Total DC-to-HL bypass line
97	QV-HL1-01A+B	Flow rate	kg/s	Hot leg-1
98	QV-HL2-01A+B	Flow rate	kg/s	Hot leg-2
99	QV-CL1A-01A+B	Flow rate	kg/s	Cold leg-1A
100	QV-CL1B-01A+B	Flow rate	kg/s	Cold leg-1B
101	QV-CL2A-01A+B	Flow rate	kg/s	Cold leg-2A
102	QV-CL2B-01A+B	Flow rate	kg/s	Cold leg-2B
103	QV-MF1-01	Flow rate	kg/s	SG-1 feed water to economizer
104	QV-MF1-02	Flow rate	kg/s	SG-1 feed water to down-comer
105	QV-MF2-01	Flow rate	kg/s	SG-2 feed water to economizer
106	QV-MF2-02	Flow rate	kg/s	SG-2 feed water to down-comer
107	QV-SIT1-01	Flow rate	kg/s	Active SIT-1
108	QV-SIT2-01	Flow rate	kg/s	Active SIT-2

109	QV-SIT3-01	Flow rate	kg/s	Active SIT-3
110	QV-HPSI1-03	Flow rate	kg/s	Active SIP-02
111	∑ (QV-CS-03+ d(LC-CS-01+ LC-CS-02)/dt	Flow rate	kg/s	Total break flow rate 0~364s : RCS inventory based method 364 ~ 2944 s : Load cell based method
112	Integral of 70	Mass	kg	Accumulated total break mass
113	LT-RPV-02	Water level	m	RPV upper head
114	LT-RPV-04A	Water level	m	RPV down-comer
115	LT-DC-01	Water level	m	Down-comer at elevation 1
116	LT-DC-02	Water level	m	Down-comer at elevation 2
117	LT-DC-03	Water level	m	Down-comer at elevation 3
118	LT-DC-04	Water level	m	Down-comer at elevation 4
119	LT-DC-05	Water level	m	Down-comer at elevation 5
120	LT-DC-06	Water level	m	Down-comer at elevation 6
121	LT-DC-07	Water level	m	Down-comer at elevation 7
122	LT-RPV-01	Water level	m	Active core region
123	LT-CO-01	Water level	m	Active core at elevation 1
124	LT-CO-02	Water level	m	Active core at elevation 2
125	LT-CO-03	Water level	m	Active core at elevation 3
126	LT-CO-04	Water level	m	Active core at elevation 4
127	LT-CO-05	Water level	m	Active core at elevation 5
128	LT-CO-06	Water level	m	Active core at elevation 6
129	LT-CO-07	Water level	m	Active core at elevation 7
130	LT-PZR-01	Water level	m	Pressurizer
131	LT-IL1A-03	Water level	m	Intermediate leg-1A
132	LT-IL1B-03	Water level	m	Intermediate leg-1B
133	LT-IL2A-03	Water level	m	Intermediate leg-2A
134	LT-IL2B-03	Water level	m	Intermediate leg-2B
135	LT-SGP1-02A	Water level	m	SG-1 U-tube upward section
136	LT-SGP1-02B	Water level	m	SG-1 U-tube downward section
137	LT-SGP2-02A	Water level	m	SG-2 U-tube upward section
138	LT-SGP2-02B	Water level	m	SG-2 U-tube downward section
139	RS-RCP1A-01	speed	rpm	RCP-1A
140	RS-RCP1B-01	speed	rpm	RCP-1B
141	RS-RCP2A-01	speed	rpm	RCP-2A
142	RS-RCP2B-01	speed	rpm	RCP-2B
143	CPU time		sec	Current CPU time for calculation to 2000

				seconds
144	dt		sec	Current time step
145+	TH-CO-IJKL	Wall temp.	K	3-D heater rod temperature Only for participants who perform 3-D modeling for the core region
146	Maximum of TH-CO-01Gija1	Wall Temp.	K	Maximum temperature in core region 1
147	Maximum of TH-CO-02Gija1	Wall Temp.	K	Maximum temperature in core region 2
148	Maximum of TH-CO-03Gija1	Wall Temp.	K	Maximum temperature in core region 3
149	Maximum of TH-CO-04Gija1	Wall Temp.	K	Maximum temperature in core region 4
150	Maximum of TH-CO-05Gija1	Wall Temp.	K	Maximum temperature in core region 5
151	Maximum of TH-CO-06Gija1	Wall Temp.	K	Maximum temperature in core region 6
152	Maximum of TH-CO-07Gijb1	Wall Temp.	K	Maximum temperature in core region 7
153	Maximum of TH-CO-08Gijb1	Wall Temp.	K	Maximum temperature in core region 8
154	Maximum of TH-CO-09Gijb1	Wall Temp.	K	Maximum temperature in core region 9
155	Maximum of TH-CO-10Gijb1	Wall Temp.	K	Maximum temperature in core region 10
156	Maximum of TH-CO-11Gijb1	Wall Temp.	K	Maximum temperature in core region 11
157	Maximum of TH-CO-12Gijb1	Wall Temp.	K	Maximum temperature in core region 12

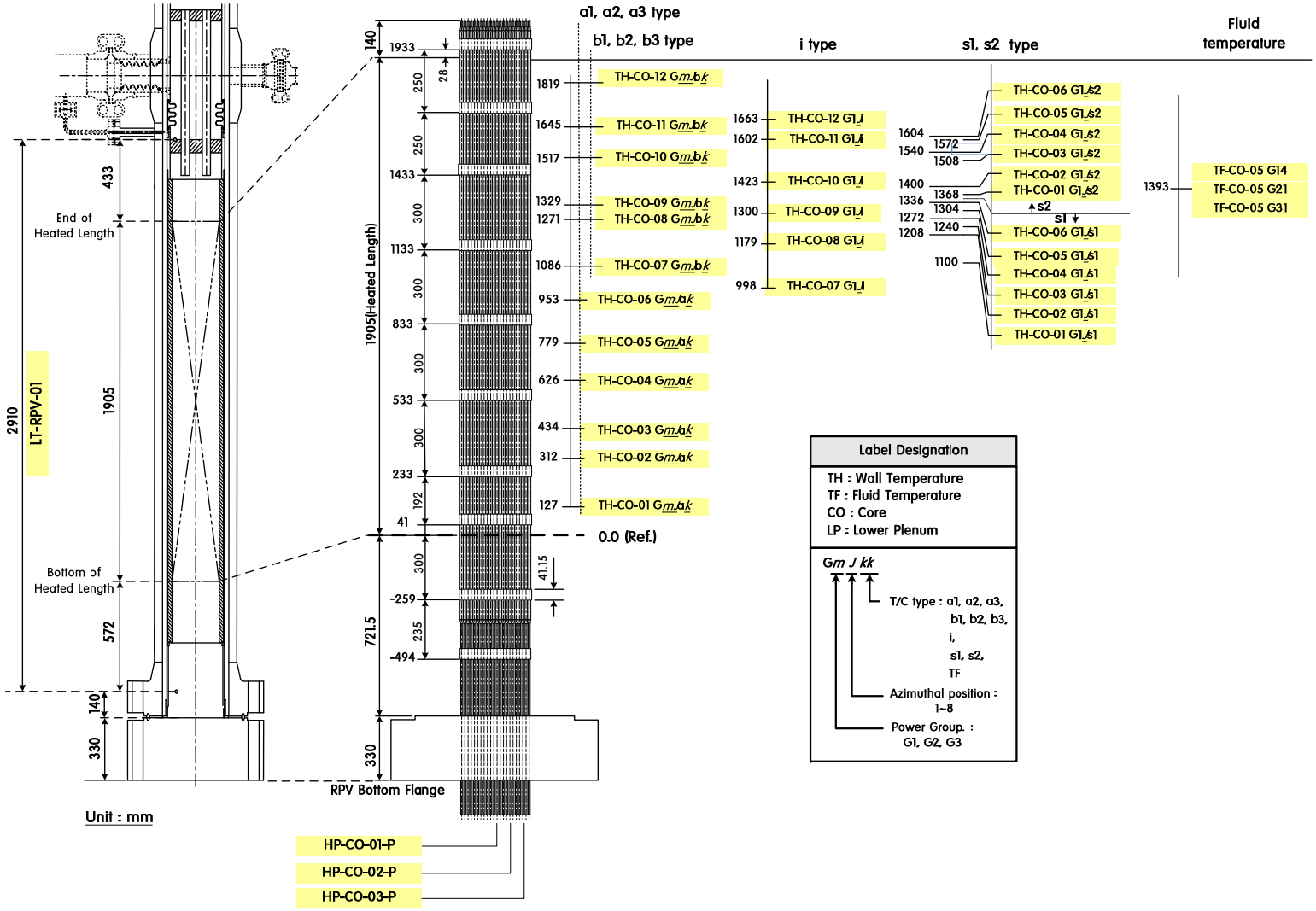

Figure 2.4-1 Detailed diagram of thermocouple for wall temperature measurement

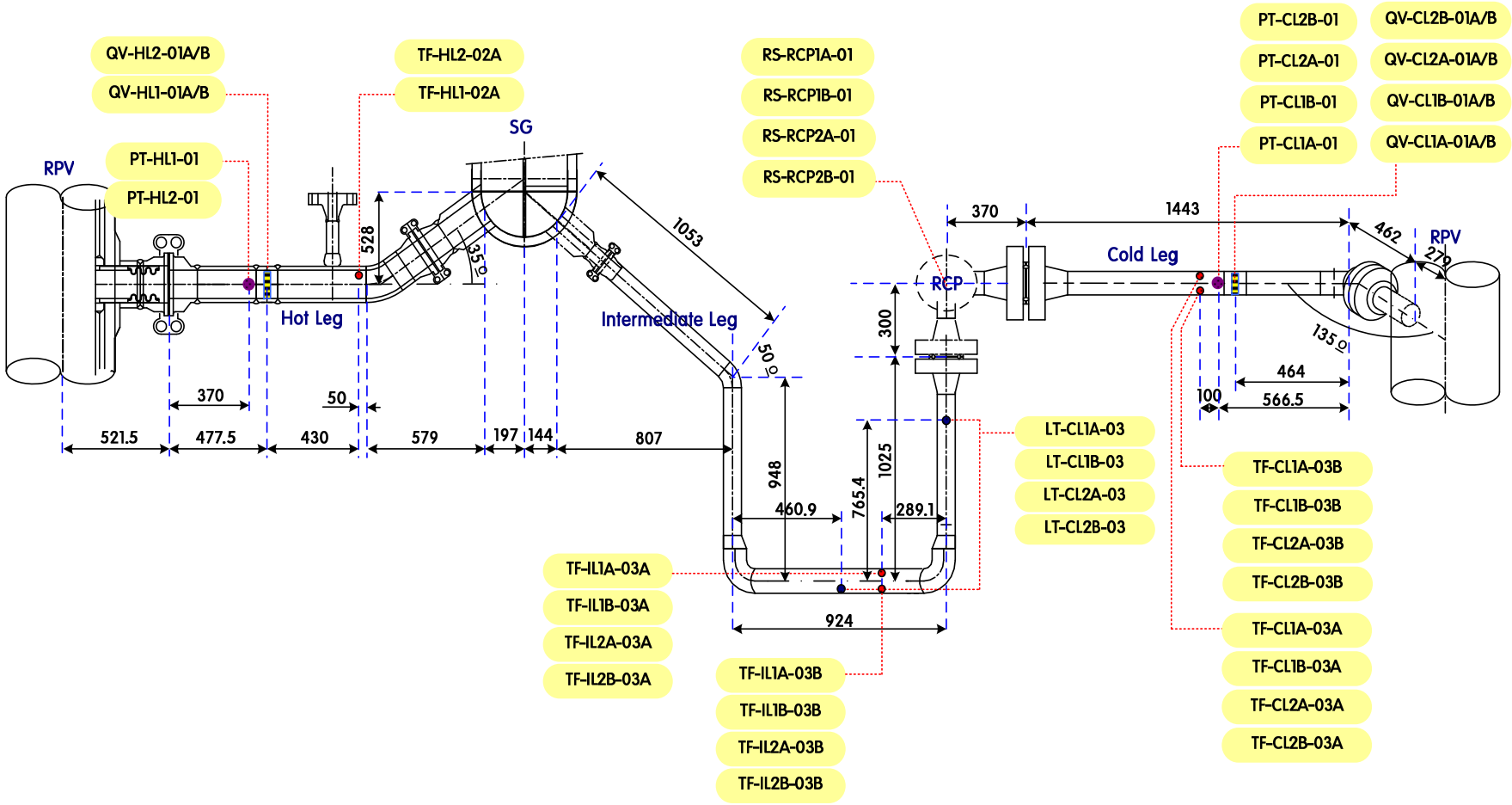

Figure 2.4-2 Major measurement locations of the primary loop

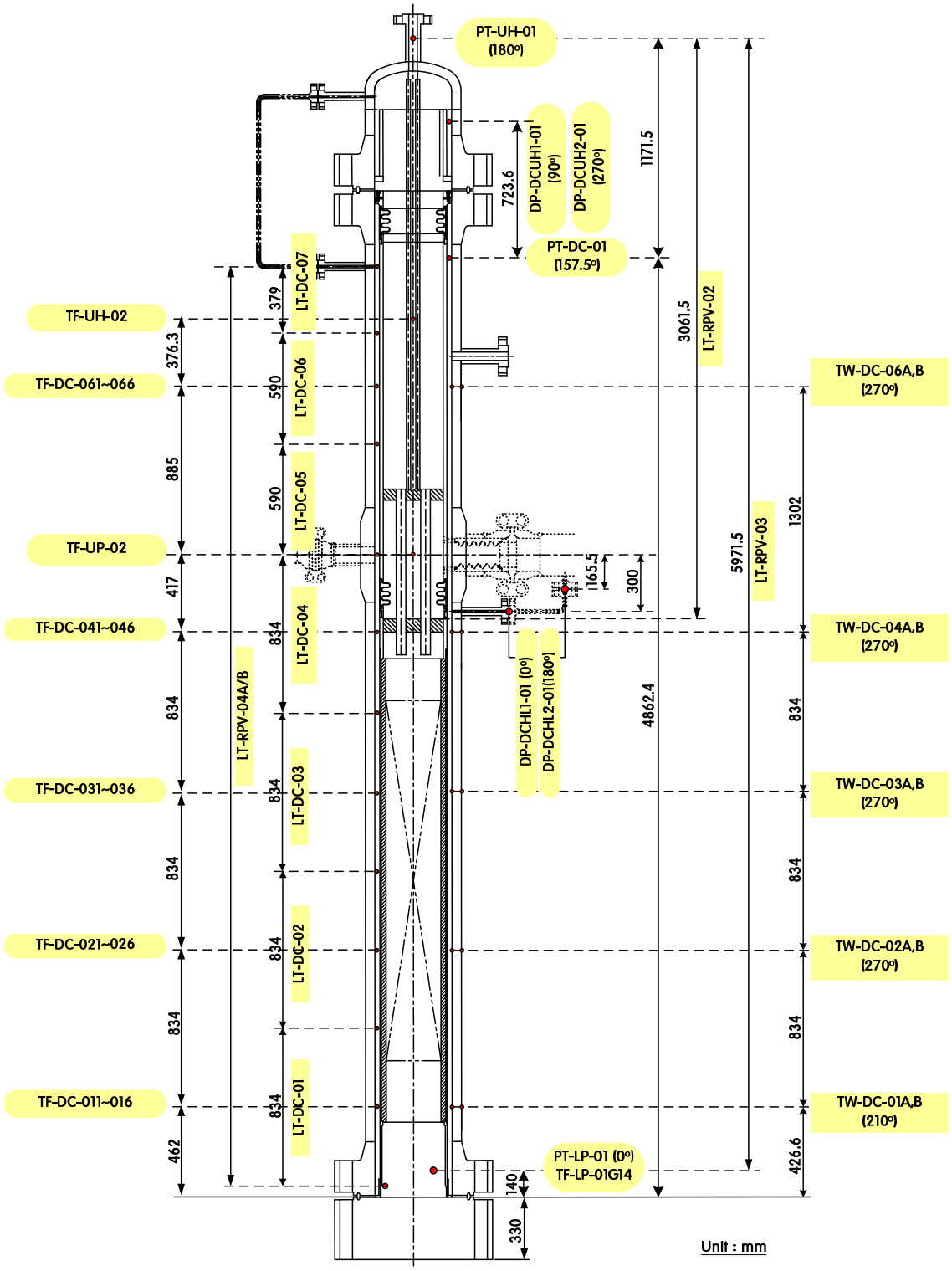

Figure 2.4-3 Major measurement locations in the reactor pressure vessel

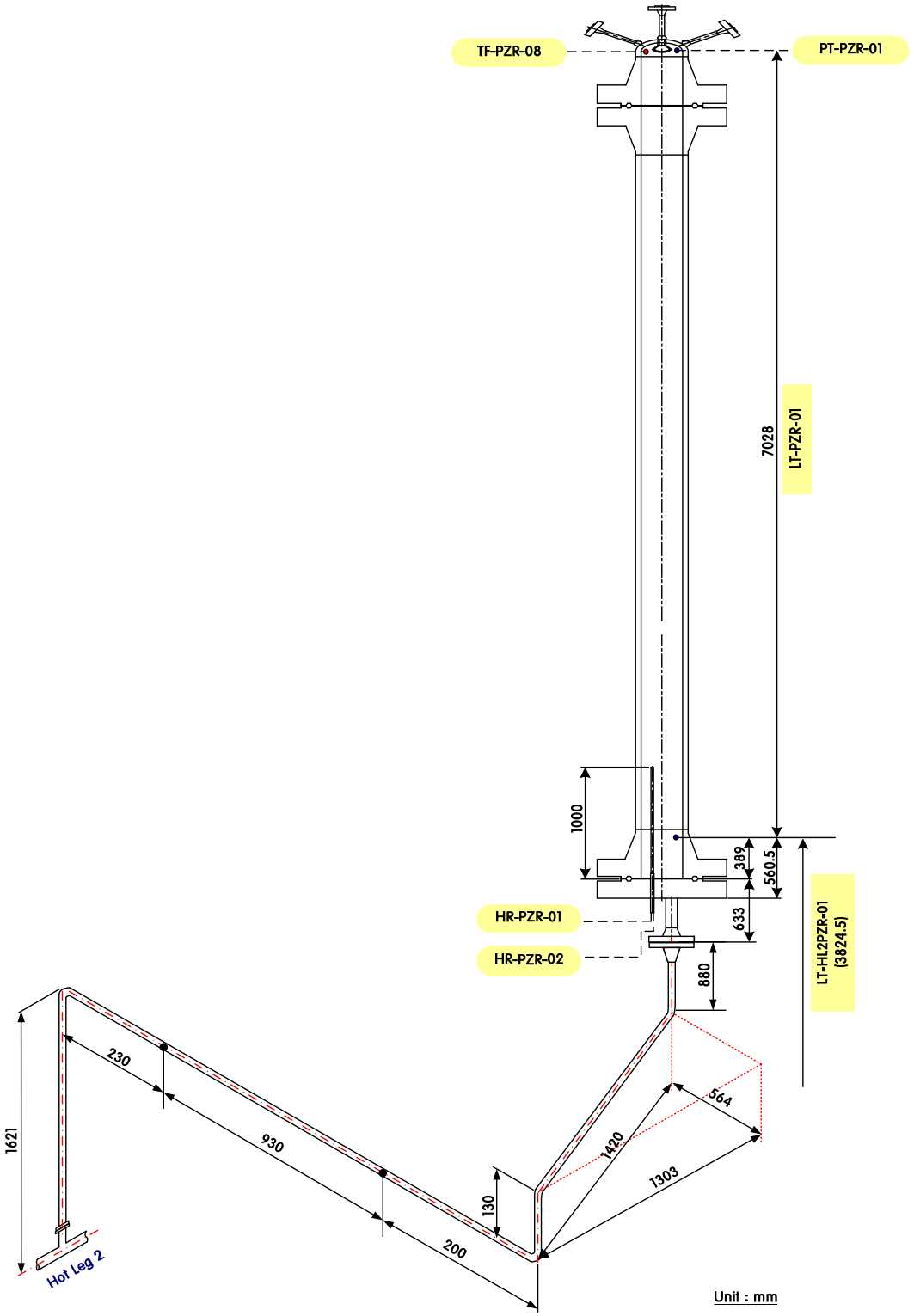

Figure 2.4-4 Major measurement locations of the pressurizer and the surge line

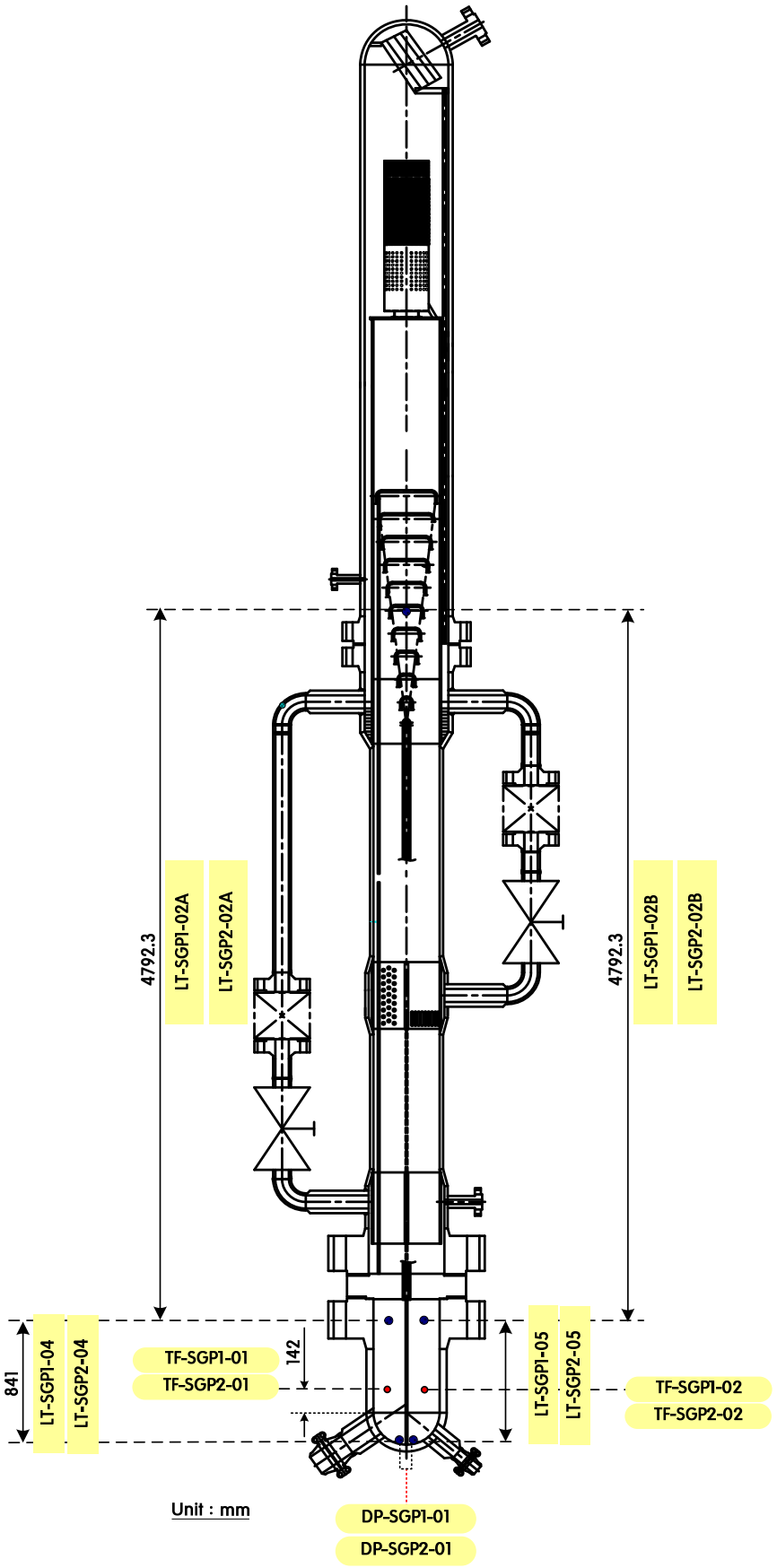

Figure 2.4-5 Major measurement locations of the primary side of the steam generator

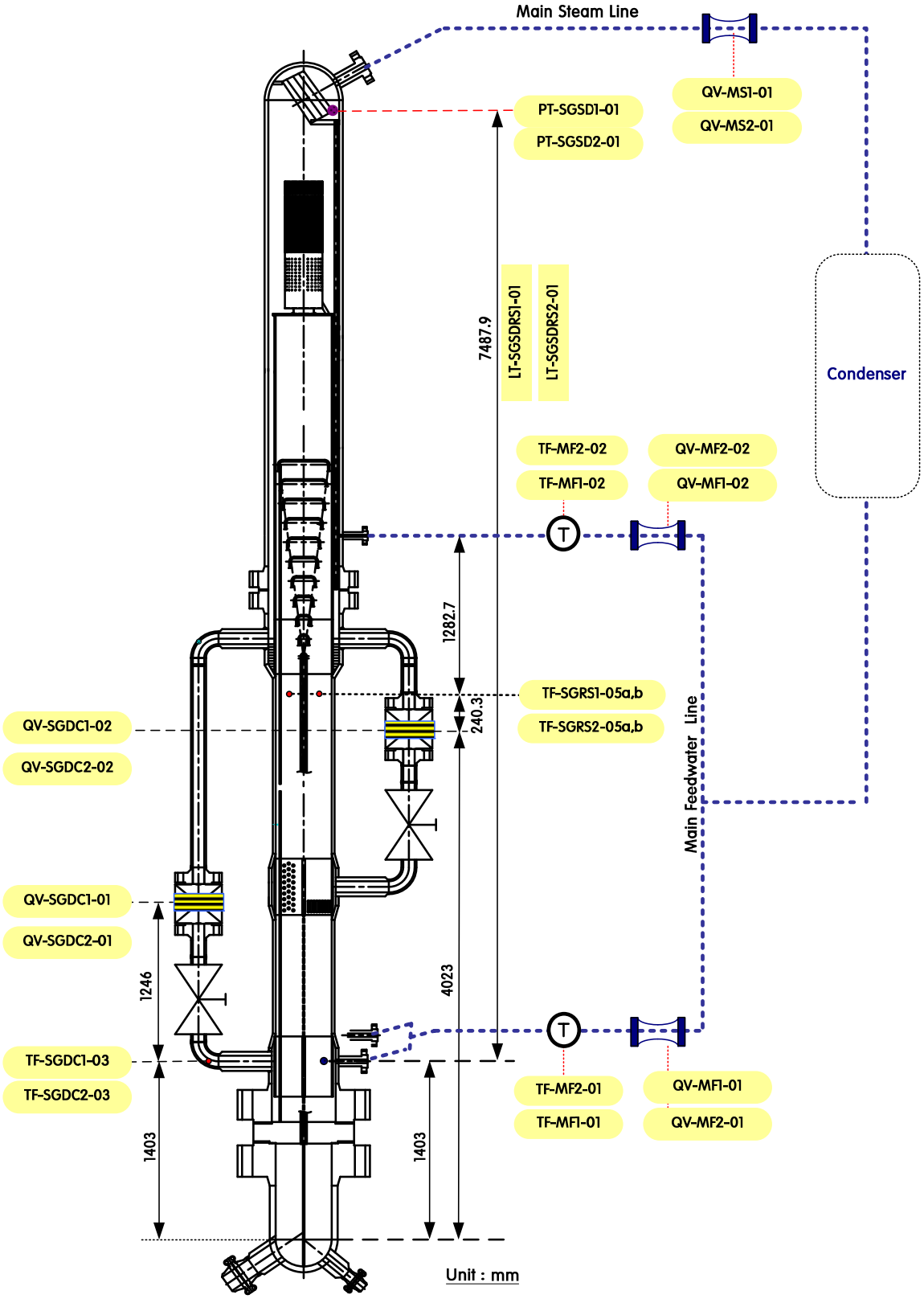

Figure 2.4-6 Major measurement locations of the secondary side of the steam generator

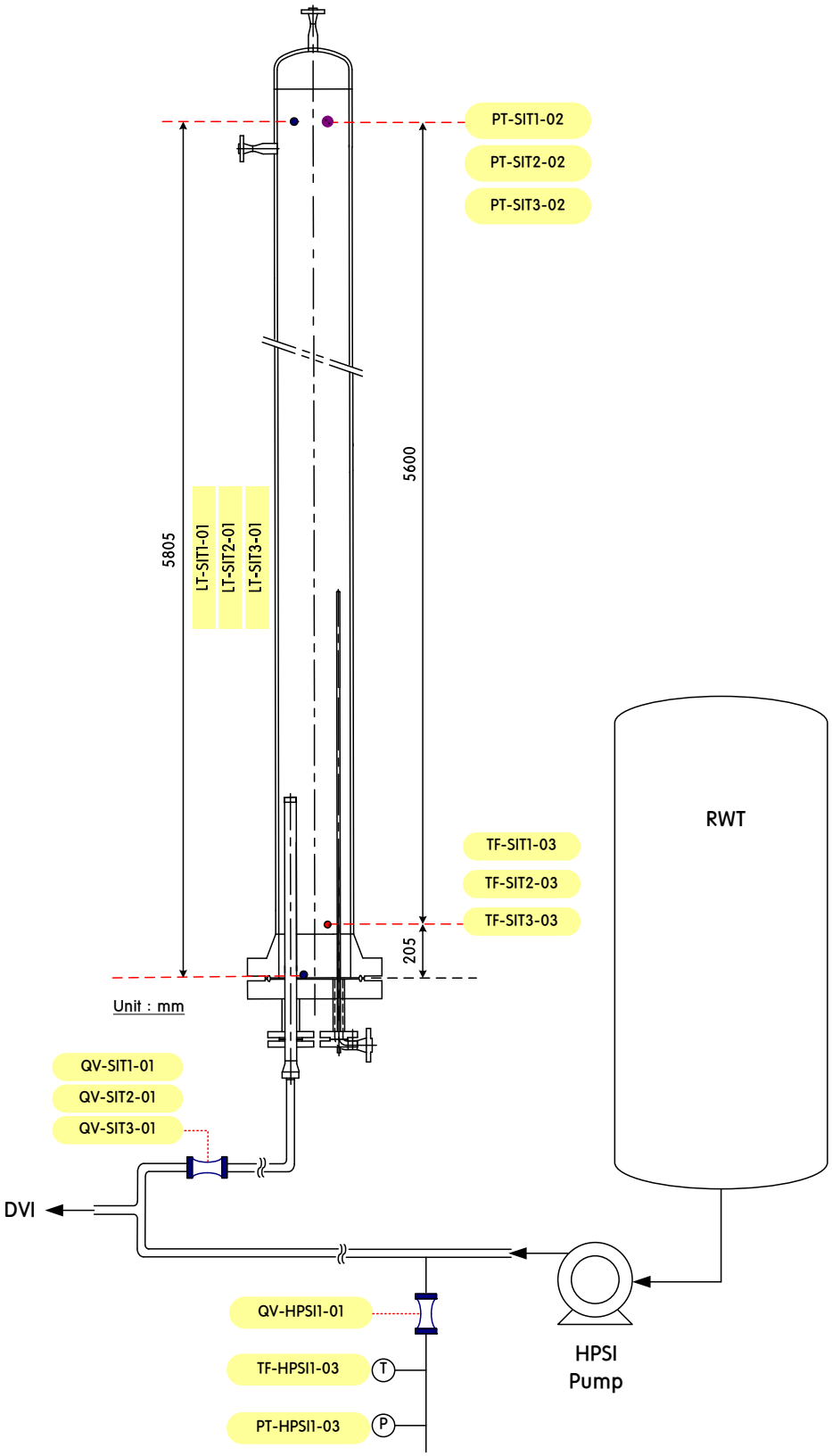

Figure 2.4-7 Major measurement locations of the safety injection tank (SIT)

2.5 Submission record

Submission records of the participants in blind and open phases are summarized in Table 2.5-1 and Table 2.5-2, respectively.

Table 2.5-1 ISP-50 Phase 1 submission record (blind calculation)

Country/ Organization	Participant	Code	Submission date
China/CIAE	Chen Yuzhou; chenyz@ciae.ac.cn	RELAP5/MOD3.3	Feb. 22, 2010
Czech Republic/NRI	Radim Meca; mec@ujv.cz	ATHLET	Jan. 16, 2010
Finland/VTT	Pasi Inkinen; Pasi.Inkinen@vtt.fi Ismo Karppinen; Ismo.karppinen@vtt.fi	APROS 5.09	Jan. 16, 2010
Finland/FORTUM	Ahonen Aino; Aino.Ahonen@fortum.com	APROS v. 5.08	Jan. 17, 2010
Germany/GRS	Henrique Austregesilo Henrique.Austregesilo@grs.de	ATHLET Mod 2.2 Cycle A	Jan. 7, 2010
Italy/U. of Pisa	Marco Cherubini; m.cherubini@ing.unipi.it	RELAP5/MOD3.3	Jan. 22, 2010
Japan/JAEA	Akira Satou; Satou.akira@jaea.go.jp	TRACE 5.0	Later
Japan/JNES	Hideaki Utsuno; Utsuno-hideaki@jnes.go.jp	TRACE	Later
Russia/EDO Gidropress	Vladimir Schekoldin Schekoldin_vv@grpress.podolsk.ru	KORSAR/GP (3 cases) TECH-M-97 (1 case)	Jan. 22, 2010 Feb. 16, 2010
Sweden/KTH	Erdenechimeg Sudvantsetseg, Fabio Veronese and Tomasz Kozlowski tomasz@safety.sci.kth.se	TRACE 5.0 patch 01	Jan. 7, 2010
USA/NRC	Harrington Ronald Ronald.Harrington@nrc.gov	TRACE 5.200	Jan. 16, 2010
Korea/KAERI	K. D. Kim; kdkim@kaeri.re.kr	MARS-KS	Jan. 5, 2010
Korea/KNF	T. S. Choi; tschoi@knfc.co.kr	RELAP5/MOD3.3	Dec. 24, 2010
Korea/KEPRI	S. J. Ha; hsj@kepri.re.kr S. Y. Kim; seyunkim@kepri.re.kr	MARS-KS	Jan. 25, 2010
Korea/KOPEC	C. W. Kim; cwkim@kopec.co.kr H. R. Choi; hrchoi@kopec.co.kr Y. M. Kim; kimym@kopec.co.kr	RELAP5-ME (KIMERA) RELAP5/MOD3.3 patch 1	Jan. 17, 2010

Table 2.5-2 ISP-50 Phase 2 submission record (open calculation)

Country/ Organization	Participant	Code	Submission date
China/CIAE	Chen Yuzhou; chenyz@ciae.ac.cn	RELAP5/MOD3.3	Mar. 10, 2011
Czech Republic/NRI	Radim Meca; mec@ujv.cz	ATHLET	Jan. 19, 2011
Finland/VTT	Pasi Inkinen; Pasi.Inkinen@vtt.fi Ismo Karppinen; Ismo.karppinen@vtt.fi	APROS 5.09	Dec. 23, 2010
Germany/GRS	Henrique Austregesilo Henrique.Austregesilo@grs.de	ATHLET Mod 2.2 Cycle A	Dec. 16, 2010
Hungary/AEKI	Antal Takacs; takacs@aeki.kfki.hu	CATHARE2V1.5Bmod3.1	Oct. 28, 2010 Dec. 16, 2010
Italy/U. of Pisa	Marco Cherubini; m.cherubini@ing.unipi.it	RELAP5/MOD3.3	Jan. 26, 2011
Russia/EDO Gidropress	Vladimir Schekoldin Schekoldin_vv@grpress.podolsk.ru	KORSAR/GP (3 cases)	Nov. 3, 2010
Sweden/KTH	Fabio Veronese and Tomasz Kozlowski tomasz@safety.sci.kth.se	TRACE 5.0 patch 02	Feb. 1, 2011
Switzerland/PSI	Medhat Sharabi; medhat.sharabi@psi.ch Jordi Freixa; jordi.freixa@psi.ch Annalisa Manera; annalisa.manera@psi.ch	RELAP5/MOD3.3	Nov. 11, 2010
USA/NRC	Harrington Ronald Ronald.Harrington@nrc.gov Scott Krepel; Scott.krepel@nrc.gov	TRACE 5.0 patch 2	Nov. 8, 2010 Dec. 30, 2010 Jan. 5, 2011
Korea/KAERI	K. D. Kim; kdkim@kaeri.re.kr	MARS-KS	Jan. 26, 2011
Korea/KNF	T. S. Choi; tschoi@knfc.co.kr	RELAP5/MOD3.3	Dec. 29, 2010
Korea/KEPRI	S. J. Ha; hsj@kepri.re.kr S. Y. Kim; seyunkim@kepri.re.kr	MARS-KS	Jan. 31, 2011
Korea/KOPEC	C. W. Kim; cwkim@kopec.co.kr H. R. Choi; hrchoi@kopec.co.kr Y. M. Kim; kimym@kopec.co.kr	RELAP5-ME (KIMERA)	Jan. 14, 2011

3. The ATLAS Facility and Test Description

3.1 Overview of the ATLAS Facility

The ATLAS is a large-scale thermal-hydraulic integral effect test facility with a reference plant of APR1400 (Advanced Power Reactor, 1400MWe), which is under construction in Korea. It has a scaling ratio of 1/2 in height and 1/288 in volume with respect to APR1400 and a summary of scaling ratios of the major parameters is shown in Table 3.1-1. The three-level scaling methodology consisting of integral scaling, boundary flow scaling, and local phenomena scaling was applied to the design of ATLAS [Ishii *et al.* 1998]. The ATLAS can simulate a wide variety of accident and transient conditions including large- and small-break LOCAs. The information on the ATLAS program, major design characteristics, scoping analyses, commissioning test results, and some test results can be found in the literatures [Baek *et al.*[2)], 2008; Baek *et al.*[3)], 2009; Choi *et al.*[4)], 2009; Cho *et al.*, 2009; Park *et al.*[1)],2007; Park *et al.*[2)],2009]. Figure 3.1-1 shows isometric configuration of the ATLAS facility.

Table 3.1-1 Summary of scaling ratios of the ATLAS

Parameters	**Scaling law**	**ATLAS design**
Length	l_{OR}	1/2
Diameter	d_{OR}	1/12
Area	d^2_{OR}	1/144
Volume	$l_{OR}\ d^2_{OR}$	1/288
Velocity	$l^{1/2}_{OR}$	$1/\sqrt{2}$
Time	$l^{1/2}_{OR}$	$1/\sqrt{2}$
Flow rate	$l^{1/2}_{OR}\ d^2_{OR}$	1/203.6
Core ΔT	ΔT_{OR}	1
Core power	$l^{1/2}_{OR}\ d^2_{OR}$	1/203.6
Heat flux	$1/l^{1/2}_{OR}$	$\sqrt{2}$
Power/volume	$1/l^{1/2}_{OR}$	$\sqrt{2}$
Pressure drop	l_{OR}	1/2
Pump head	l_{OR}	1/2
Core rod diameter	1	1
SG U-tube diameter	$l^{1/2}_{OR}$	$1/\sqrt{2}$
No. of core rods	d^2_{OR}	1/144
No. of SG U-tubes	-	1/72

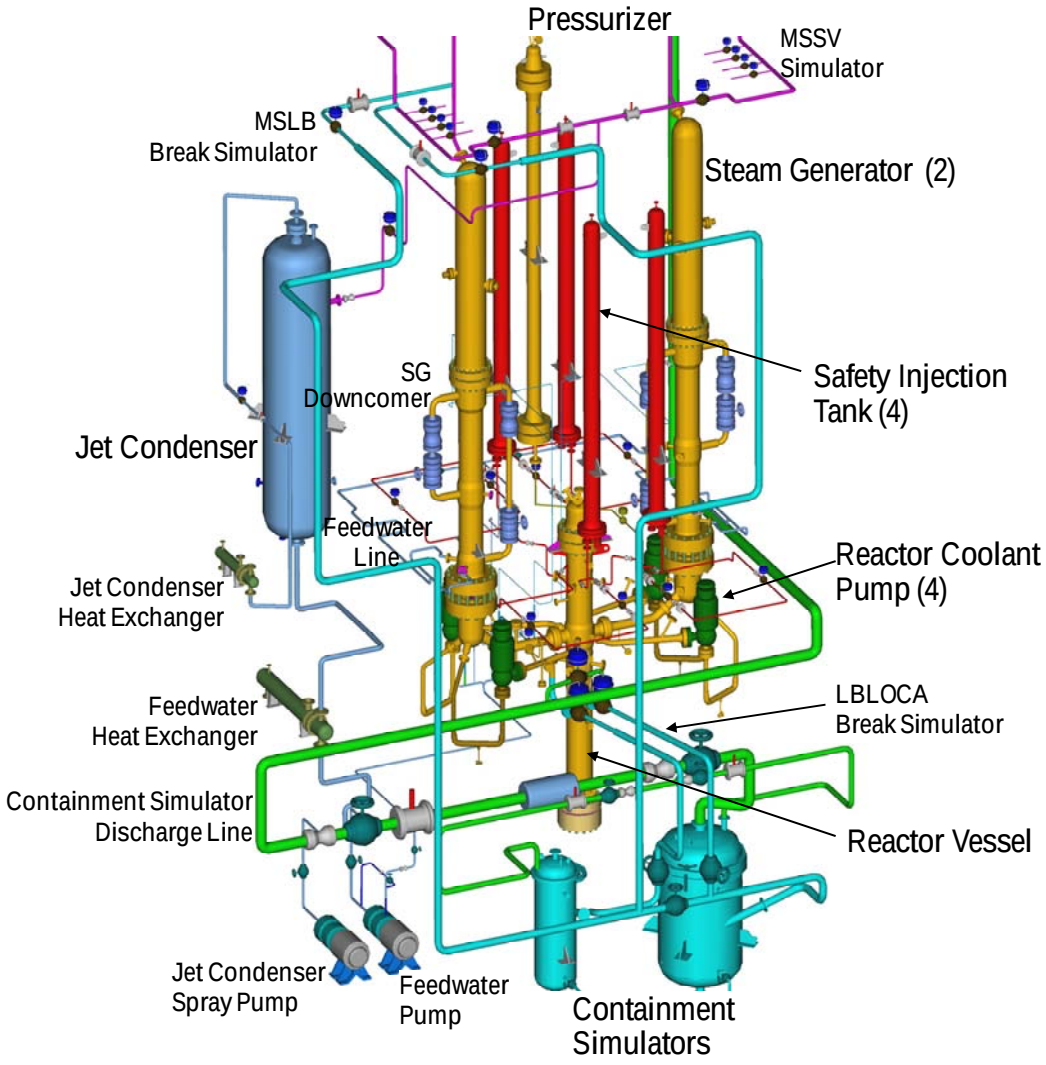

Figure 3.1-1 Isometric configuration of the ATLAS facility

3.2 Experimental procedure

The ISP-50 test on a 50% DVI line break was performed in accordance with the test prospectus described in the test specifications [Choi *et al.*[5], 2009]. Most test conditions were determined by a pre-test calculation with a best-estimate thermal hydraulic code, MARS3.1 [Jeong *et al.* 1999]. A best-estimate safety analysis methodology which is now commonly accepted in nuclear industries was applied to the transient calculation of the reference plant APR1400. Based on the obtained sequence of events during the DVI line break accident for APR1400, the initial and boundary conditions for the present integral effect test were determined by applying scaling law to the ATLAS. The pressure set points for actuation of major components were preserved as the same to the reference plant, while the delay times for an isolation of the secondary feed water or steam supply systems, and for an initiation of the

safety injection systems such as the SIP and the SIT were scaled down by a square root of two according to the time scaling ratio of the ATLAS. The detailed sequence of events applied to the present test is summarized in Table 3.2-1.

Table 3.2-1 Comparison of the sequence of a 50% DVI line break

Events	APR1400 (time, sec)	ATLAS (time,sec)	Description
Break open	0	0	
Low pressurizer pressure trip (LPP)	28.6		If pressurizer pressure < 10.72MPa
Pressurizer heater trip	LPP+0.0 sec	LPP+0.0 sec	Delay time is reduced by a square root of two
Reactor scram & RCP trip	LPP+0.5 sec	LPP+0.35 sec	
Turbine isolation	LPP+0.1 sec	LPP+0.07 sec	
Main feed water isolation	LPP+10 sec	LPP+7.07 sec	
Safety injection pump start	LPP+40 sec	LPP+28.28 sec	
Low upper down-comer pressure trip (LUDP)	LUDP	LUDP	If down-comer pressure < 4.03MPa
Safety injection tank (SIT) start	LUDP+0.0 sec	LUDP+0.0 sec	
Low flow turndown of the SIT			If water level of the SIT is less than a specified set point

The same pressure condition as the prototypic plant, APR1400 was used as an initial condition. The temperature distribution along the primary loop was also preserved. The primary inventory was heated with core heaters to its specified steady state condition and was pressurized by a pressurizer until the primary system reached a steady state condition. During the primary heat-up process, the secondary system was also heated up to a specified target hot condition by controlling the heat removal rate from the primary system. In a steady state condition, the core power generated by electrical heaters was balanced by the energy removed by the secondary system.

During the heat-up process, several crucial components influencing the boundary conditions of the test were controlled by operators. The four core bypass flow control valves were controlled to have the pre-determined stem positions to have a scaled core bypass flow rate. The initial water levels and pressures of SITs were controlled to have these specified values.

The refueling water storage tank (RWT) was filled with water to its initial level of 50% and the water inventory was electrically heated to its pre-determined temperature of 52°C, and then the water was circulated through the injection line so as to pre-heat the line up to the same temperature as the water.

The DVI line break test was initiated by opening a quick-opening break valve, OV-BS-03 at the break spool piece. A DVI line break was simulated by installing a break spool piece at one of the DVI nozzles. The configuration of the break spool piece is shown in Figure 3.2-1. It consists of a quick opening valve, a break nozzle, a case holding the break nozzle, and a few instruments. A pressure transducer and two thermocouples were installed on both upstream and downstream of the break nozzle. Detailed geometry of the break nozzle for the present DVI line break tests is shown in Figure 3.2-2. The break nozzle was designed according to the scaling law to simulate the scaled-down break discharge flow from the primary system. The break nozzle was installed vertically downward at the discharge line of the DVI nozzle. The quick opening valve was opened within 0.5 s by operators when the test was initiated. The break flow was discharged to the containment simulating system.

When the pressurizer pressure reached a specified pressure of 10.72MPa, the low pressurizer pressure (LPP) signal was automatically generated by embedded control logics. The heaters of the pressurizer and all tracing heaters in the primary system were tripped at the same time of the LPP signal. The RCP was automatically tripped with a time delay of 0.35 s after the LPP signal. The main steam and the main feed water lines were isolated with a time delay of 0.1 s and 7.1 s after the LPP signal, respectively. The isolation of the secondary system requires a simultaneous actuation of several valves in the pipe line. It was done by the programmed control logics without an operator intervention. Operation of the SIP was triggered by the LPP signal with a time delay of 28.3 s. The initiation of the SI pump requires an alignment of the valves located in the supply line. This alignment was also completed automatically by the control logic without any time delay.

When the down-comer pressure of the reactor vessel became lower than the specified pressure of 4.03MPa, the SIT started to deliver the high safety injection flow to the reactor vessel by fully opening the flow control valve. When the water level of the SIT reached a specified set point, the stem of the flow control valve was lowered to a specified position to supply a required low injection flow rate. When the water level of the SIT was decreased to a specified empty set point, the flow control valve was fully closed for the nitrogen gas not to be injected into the reactor vessel. The transient was terminated with a termination of the data logging when it was judged by operators that all the major phenomena have already happened.

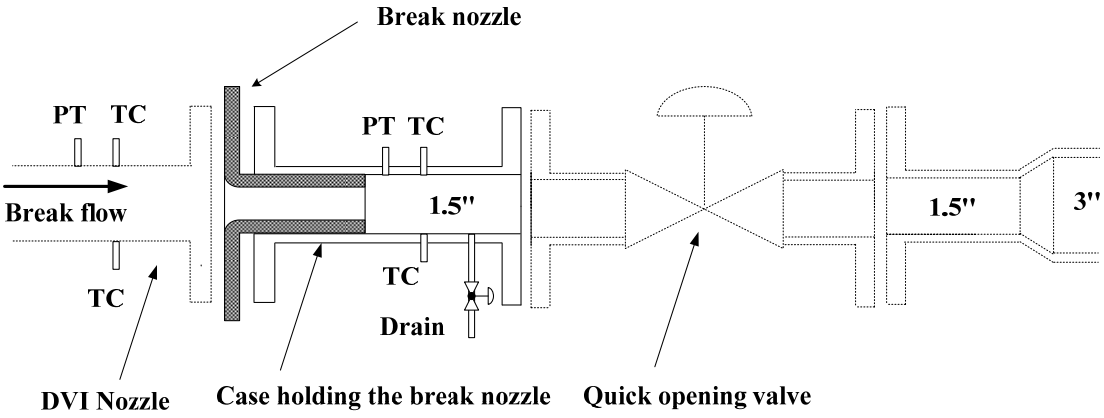

Figure 3.2-1 Configuration of the break simulation system for the DVI line break test

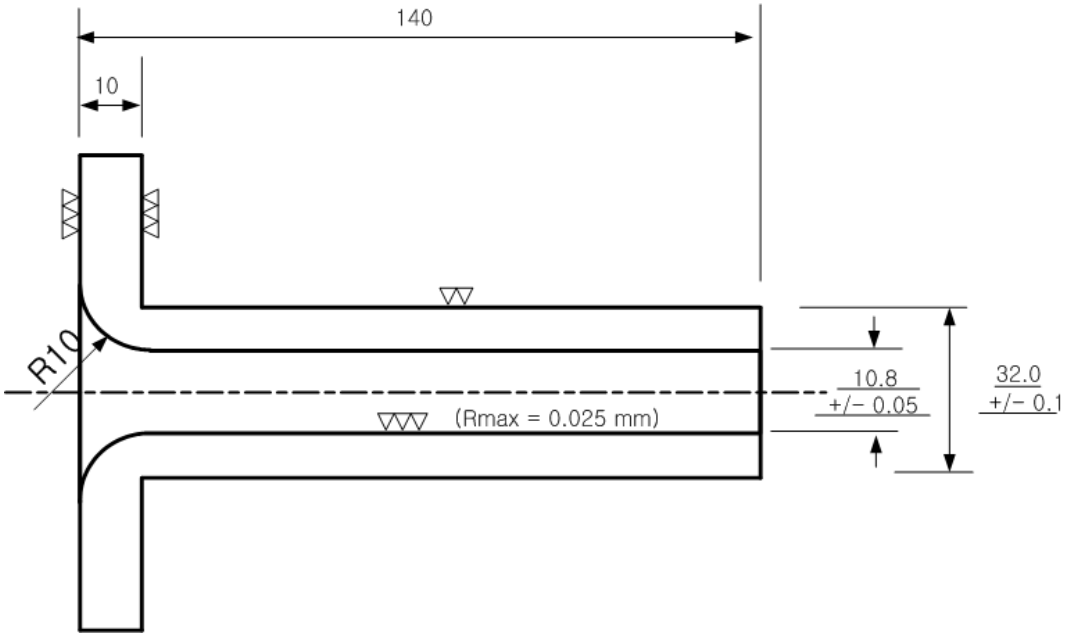

Figure 3.2-2 Detailed geometry of the break nozzle for the present DVI line break test

3.3 Actual initial conditions

When the ATLAS reached a specified initial steady state condition for a transient test through a series of heat-up processes, the primary coolant flow rate was reduced to 8% of the scaled-down value by decreasing the RCP speed to have the same temperature distribution along the primary loop. The required 8% scaled-down of the primary coolant flow rate was achieved in a natural circulation mode, indicating that four RCP speeds were close to zero. The measured flow rate at each cold leg was about 2.2kg/s. As the flow velocity was as low as about 0.5m/s, the uncertainty of the measured flow was within about 5% of the measured value. The core bypass flow rate was almost zero at the initial conditions since the primary coolant flow rate is small by scaled-down value. In the APR1400 design, 90% and 10% of total feedwater

flow rate is injected through the economizer and the down-comer at nominal full power condition, respectively. Therefore, in the ISP-50 test, the scaled feedwater flowrate was injected through the economizer and the down-comer nozzle. The nozzle location of the ATLAS can be shown in Figure 2.4-6. However, the measured feedwater flow rate to down-comer nozzle indicated negligible values due to very small flow rate in the actual initial condition. The major thermal hydraulic parameters at the initial conditions are summarized in Table 3.3-1 where specified values defined in the test specification were also included.

Table 3.3-1 Measured initial conditions for a 50% DVI line break test

Parameter	Measured value	Specified value for blind calculation	Instruments	Remarks
Primary system				
- Core power (MW)	1.636[1)]	1.56[2)]	-	[1)] including heat loss [2)] excluding heat loss
- Heat loss (kW)	83.5/57.0	-	Primary/Secondary	estimation at a steady state condition
- PZR Pressure (MPa)	15.596	15.5	PT-PZR-01	pressurizer
- Core inlet temp. (K)	563.2	563.9	TF-LP-02G18	
- Core exit temp.(K)	598.2	597.4	TF-CO-07-G14, G18, G21, G25	averaged
- Hot leg temp. (K)	597.6 598.5	-	TF-HL1-03A TF-HL2-03A	hot leg 1 hot leg 2
- Cold leg temp. (K)	565.4 565.3 565.0 565.2	-	TF-CL1A-04A TF-CL1B-04A TF-CL2A-04A TF-CL2B-04A	cold leg 1A cold leg 1B cold leg 2A cold leg 2B
- RCS flow rate (kg/s)	2.2 ± 5% 2.2 ± 5% 2.3 ± 5% 2.2 ± 5%	2.0 2.0 2.0 2.0	QV-CL1A-01B QV-CL1B-01B QV-CL2A-01B QV-CL2B-01B	cold leg 1A cold leg 1B cold leg 2A cold leg 2B
- Core bypass flow rate (kg/s)	~0.0 ~0.0		Down-comer to upper head Down-comer to hot leg	estimated value

- Pressurizer level (m)	3.32		LT-PZR-01	
Secondary system	(SG1/SG2)			
- Pressure (MPa)	7.83/7.83	7.83/7.83	PT-SGSD1-01/PT-SGSD2-01	Fig.4.1.16 of FDR*
- Steam temp. (K)	566.3/566.1 568.6/568.8	566.7/566.7	TF-MS1-01/TF-MS2-01 TF-SGSD1-03/TF-SGSD2-03	steam pipe line steam dome
- FW temp. (K)	507.6/508.4 498.7/529.5	505.4 505.4	TF-MF1-03/TF-MF2-03 TF-MF1-04/TF-MF2-04	economizer down-comer
- FW flow rate (kg/s)	0.431/0.435 0.0/0.0	0.44/0.44 0.044/0.044	QV-MF1-01/QV-MF2-01 QV-MF1-02/QV-MF2-02	economizer down-comer
- Water level (m)	2.03/1.97	2.0/2.0	LT-SGSDDC1-01/LT-SGSDDC2-01	Fig.4.1.22 of FDR*
- Heat removal(MW)	0.693/0.774	0.78/0.78	-	Approximation**
- Heat loss(kW)	28.5/28.5	-		estimation
ECCS				
- SIT pressure (MPa)	4.19/4.21/4.23	4.2/4.2/4.2	PT-SIT1,2,3-02	
- SIT temp. (K)	323.3~323.7	323.2	TF-SIT1,2,3-03	
- SIT level (%)	95.0/95.2/94.3	95.1/94.9/94.2	LT-SIT1,2,3-01 (5.32/5.33/5.28)	Tag name/meter
- RWT temp. (K)	323.3	323.2	TF-RWT-01	storage tank
Containment - Pressure (MPa)	0.1013	0.1013	atmospheric condition	open

* Detailed instrument location can be found in the latest facility description report [Kang et al[3], 2011]

** Heat removal indicates primary to secondary heat removal rate through SG, it was estimated based on energy balance of the secondary side

3.4 Actual boundary conditions

The boundary conditions for the selected test were determined from the transient calculation of the prototypic plant, APR1400. The design values of the APR1400 were scaled down according to the scaling law of the ATLAS. For instance, the emergency core cooling water flow rates provided by the SIP and the SITs were scaled down and applied to the present test. The break nozzle was carefully designed to discharge the scaled critical flow. All the boundary conditions of each control device during the test period were implemented automatically by embedded control logics, including the required delay time. There was no operator intervention during the entire test period.

3.4.1 Definition of time

When the data acquisition system (DAS) started data logging, transient time was recorded starting from -10.0 s and the actual break was activated at 193.0 s. This actual measured time is named "DAS time" throughout this report and is used to analyze experimental results. In addition, a "shifted time" is defined so that the break time is shifted to 0.0 s because most code calculations assumed that the break occurred at time zero. The "DAS time" was used as it was in the analysis of experimental data itself, but the "shifted time" was used when the data was compared with calculation results.

3.4.2 Core power

The core power was provided by three groups of electrical heaters, which can be controlled to simulate a non-uniform radial power distribution. In the present test, a uniform radial power was used for simplicity. The total core power of 1.553MW was required to reach a steady-state condition. The primary heat loss was estimated during the test and it was added to the core power to compensate for the heat loss to environment. Thus, the initial core power was 1.636MW. The heat loss added to the core power with respect to time will be explained in the next section. The transient test started at the DAS time of 193 s by opening the break valve. The initial core initial power was maintained to the DAS time of 226 s and it started to decay following the ANS73 curve multiplied by a factor 1.2. Measured core power behavior is shown in Figure 3.4-1. A tabulated core power with respect to time during the present ISP-50 test can be found in Appendix-A of this document.

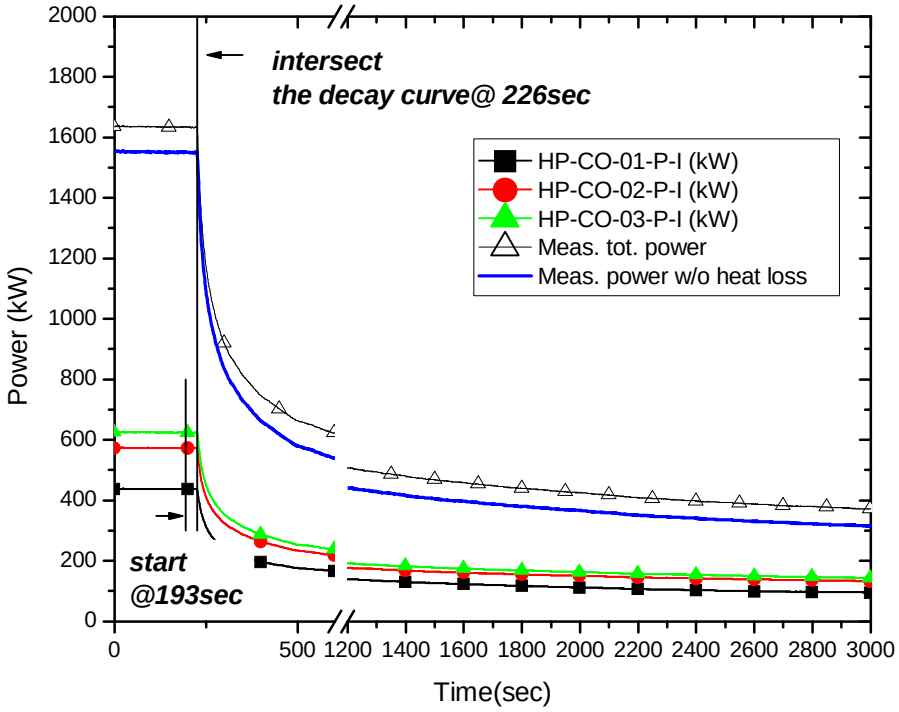

Figure 3.4-1 Measured core power behavior

3.4.3 Heat loss

The heat loss from the primary system to environment cannot be completely avoided even though the reactor pressure vessel and the primary pipelines are surrounded by thick insulation materials. The heat loss was estimated by a further simplified empirical correlation than that outlined in the literature [Kang *et al.*[1], 2009].

$$Q_{loss,1} = 0.32 \cdot (T_w - T_{atm}), \tag{3.4.1}$$

where T_w is outer wall surface temperature measured at the middle of the reactor pressure vessel, TW-DC-04A and T_{atm} is atmospheric temperature measured on the test day. The estimated primary heat loss was plotted in Figure 3.4-2. A tabulated heat loss with respect to time during the current ISP-50 test is also provided in Appendix-A of this document.

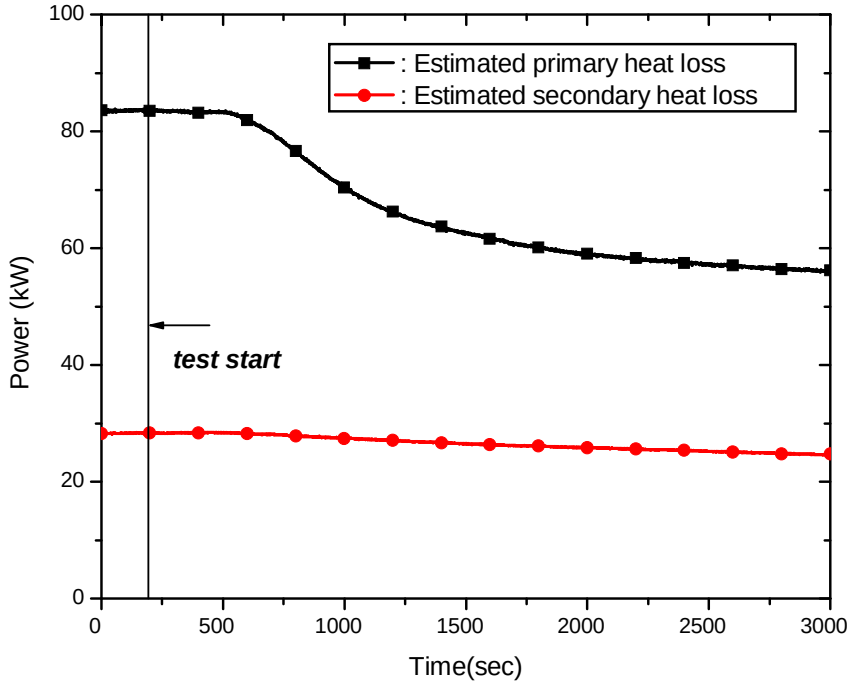

Figure 3.4-2 Estimated primary and secondary heat loss with respect to time

The heat loss from each steam generator to environment was also estimated according to the empirical correlation in the literature [Kang *et al.*[1], 2009].

$$Q_{loss,2} = 0.00077 \cdot (T_w - T_{atm})^{1.8843}, \quad (3.4.2)$$

where T_w is averaged values of the temperatures measured at the outer wall surface of the steam generator, TW-SGP1-02A, TW-SGRS1-01A, TW-SGRS1-02A, TW-SGRS1-03A, TW-SGSD1-01A, TW-SGSD1-02A and T_{atm} is atmospheric temperature. The estimated heat loss was plotted in Figure 3.4-2.

3.4.4 Safety injection flow

The safety injection system of the APR1400 has four mechanically separated hydraulic trains. They are also electrically separated by two divisions, implying that each emergency diesel generator powers two hydraulic trains. The pre-test calculation was conducted with the assumption of loss of off-site power simultaneously with the break and the worst single failure as a loss of a diesel generator, resulting in the minimum safety injection flow to the core. Furthermore, the safety injection flow to the broken DVI-4 nozzle was not credited. Therefore, the safety injection flow by the safety injection pump (SIP) was injected only through the DVI-2 nozzle opposite to the broken DVI-4 nozzle. The required safety injection flow rate was

obtained by scaling down the flow rate of the reference plant as shown in Table 3.4-1. The safety injection flow rate was programmed to be injected as a function of the primary down-comer pressure, PT-DC-01.

Table 3.4-1 Scaled-down SIP flow rate with respect to the primary pressure

Primary pressure (PT-DC-01, MPa)	SIP flow rate (kg/s)
0.1013	0.323158
0.446	0.318567
0.791	0.313965
1.136	0.309055
1.480	0.304144
2.170	0.294039
2.859	0.283579
4.238	0.260868
5.617	0.235408
6.995	0.206240
8.375	0.170933
9.754	0.123685
10.100	0.107735
10.440	0.088879
11.130	0.0

As regards the safety injection flow by the four safety injection tanks (SITs), three SITs except for the SIT connected to the broken DVI-4 nozzle were used to provide the safety injection flow into the down-comer. Isometric piping line from each SIT to the corresponding DVI nozzle was shown in Figure 3.4-3 through Figure 3.4-5. The piping line from the SIT nozzle to the inlet face of the flow control valve was fabricated with an 1-1/2″ SCH.80 (ID=38.1mm) pipe and the downstream piping line from the exit face of the control valve to the DVI nozzle was fabricated with an 1-1/2″ SCH.160 (ID=33.99mm) pipe. There were several devices along the safety injection piping line resulting in an additional pressure drop as shown in Figure 3.4-3 through Figure 3.4-5: a strainer, a flow straightener, an orifice, a 90-degree elbow, a 45-degree elbow, a flowmeter, a flow control valve, and an on-off valve.

A strainer was installed at the horizontal pipeline just downstream of the SIT and its k-factor is about 4.0. A flow straightener was installed before the flow meter as shown in

Figure 3.4-6 and its k-factor is 0.4. An orifice was installed downstream the flow control valve in order to simulate the passive fluidic device inside the SIT indirectly. The high flow condition of the SIT was obtained with the orifice and the flow control valve which was fully open. The bore diameters of the orifices are summarized in Table 3.4-2. The flow control valves are gate-type valves which have the linear characteristics. The rated flow coefficient, Cv of the control valves is summarized in Table 3.4-3.

The low flow condition of the SIT was simulated by reducing the valve position to a specified set point. The percentage of the valve position for the low flow condition was also included in Table 3.4-3.

The on-off valve was a gate-type valve of which the throat diameter was the same as the pipe diameter, thus the pressure drop across the on-off valve was small enough to be neglected. The curved section of the pipe line was joined by a 90-degree and a 45-degree socket welding elbow with a 6000 lb class. The detailed geometric information is shown in Figure 3.4-7 and Figure 3.4-8.

The flow rate was measured by a Coriolis-type mass flow meter and an estimated k-factor across the flow meter is about 1.1. This value was calculated from the pressure drop specification of the flow meter.

Table 3.4-2 A summary of bore diameters of the orifices

Orifice name	Bore diameter (mm)
OR-SIT1-01	10.5
OR-SIT2-01	10.5
OR-SIT3-01	11.2

Table 3.4-3 A summary of rated Cv of the flow control valves of the SITs

Flow control valve	Rated Cv (100% open)	Rated opening for low flow (%)
FCV-SIT1-01	5.59	18.0
FCV-SIT2-01	5.59	13.0
FCV-SIT3-01	4.69	24.0

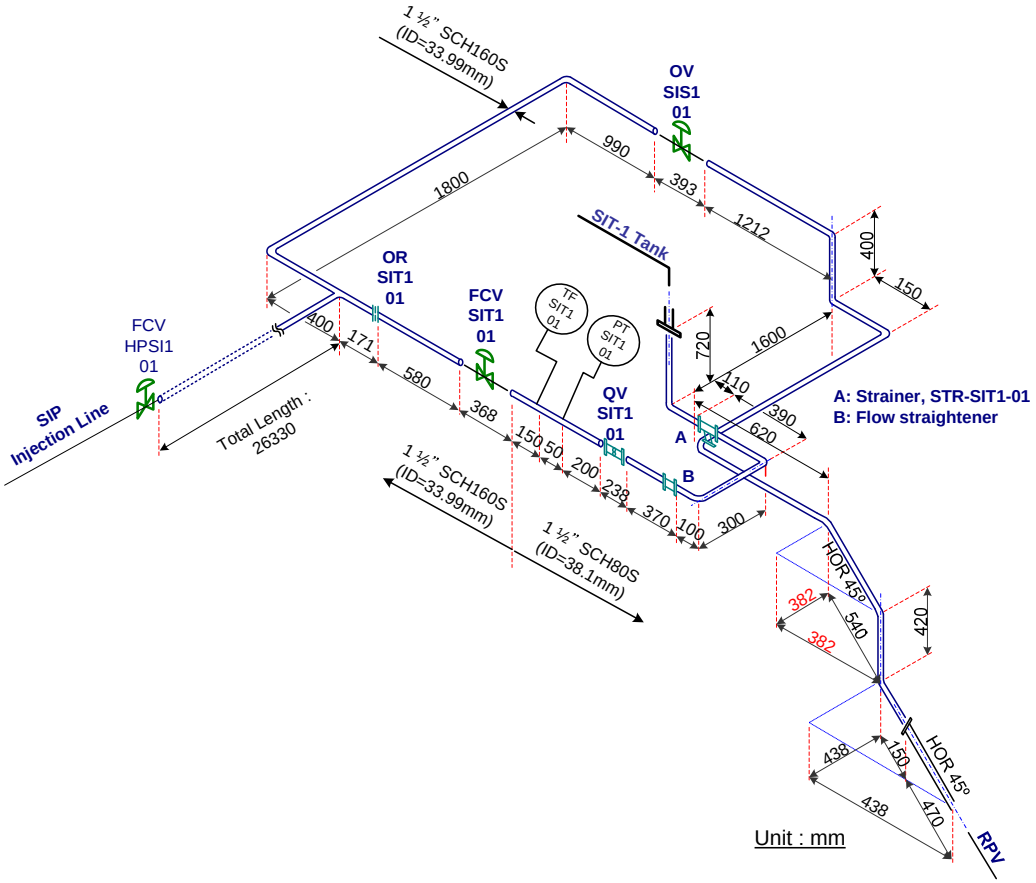

Figure 3.4-3 Safety injection line from SIT-1 to RPV

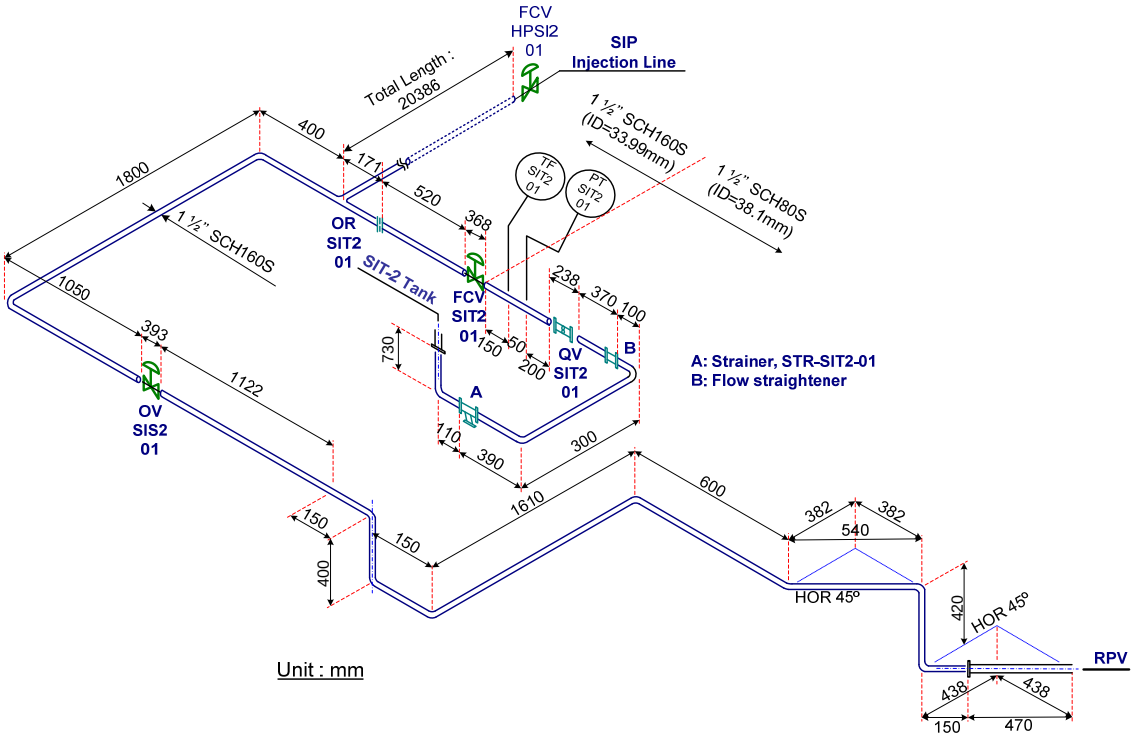

Figure 3.4-4 Safety injection line from SIT-2 to RPV

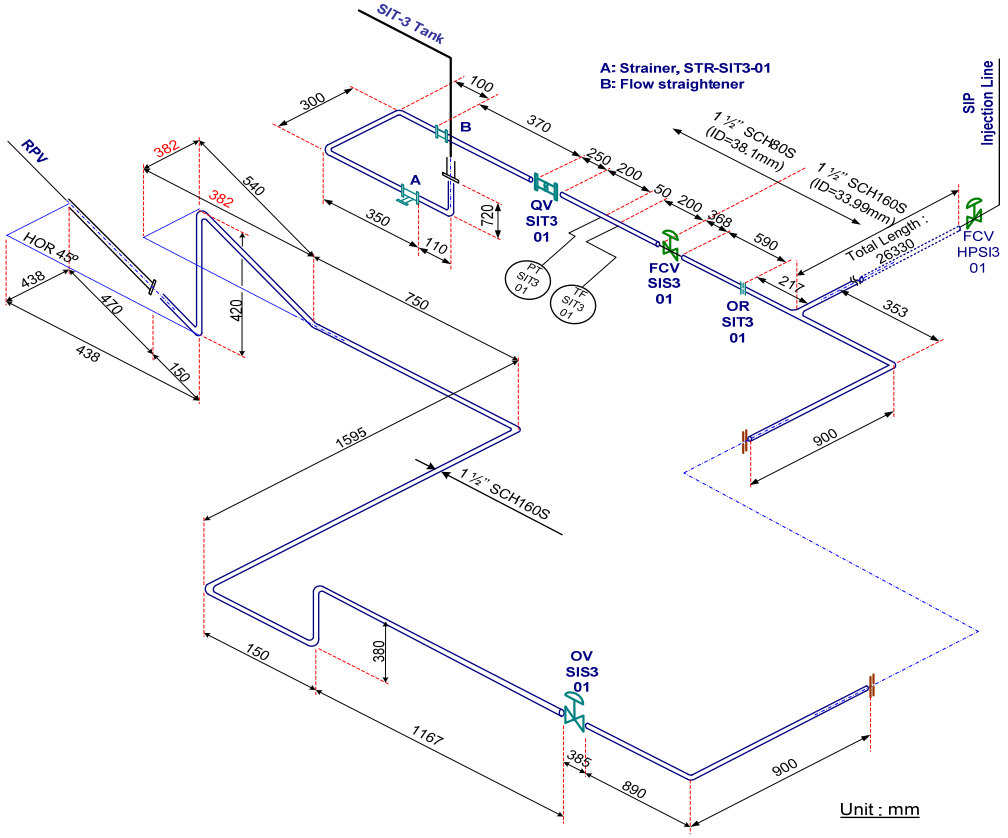

Figure 3.4-5 Safety injection line from SIT-3 to RPV

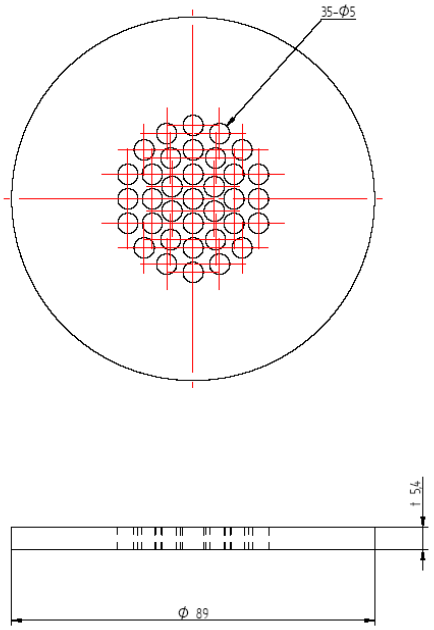

Figure 3.4-6 Detailed dimension of the flow straightener

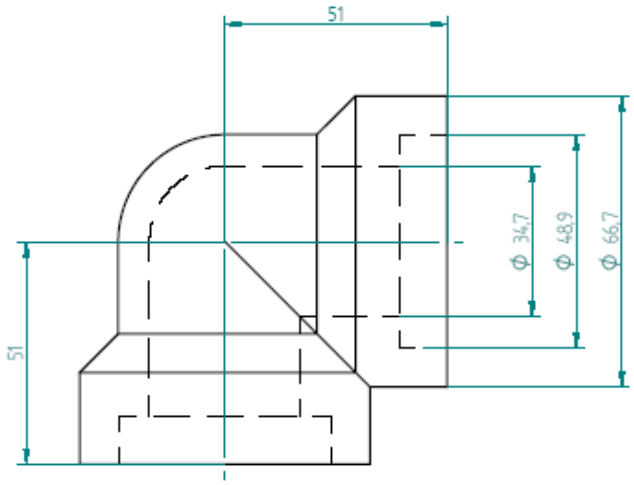

Figure 3.4-7 A dimension of a 90-degree socket welding elbow

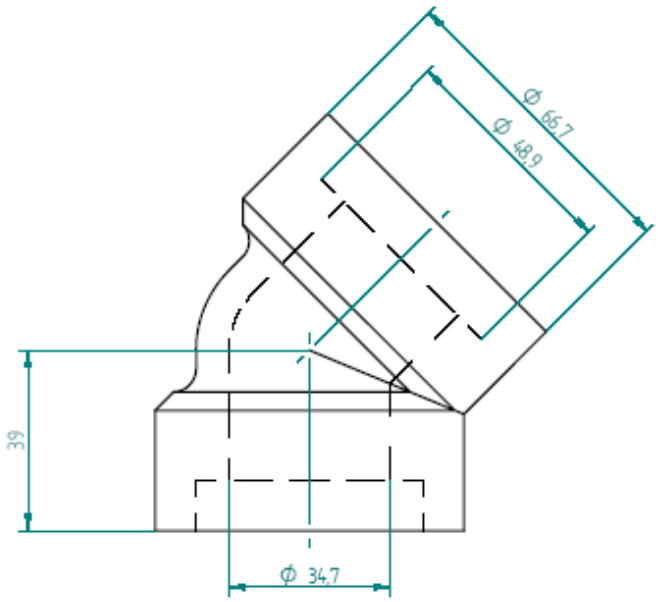

Figure 3.4-8 A dimension of a 45-degree socket welding elbow

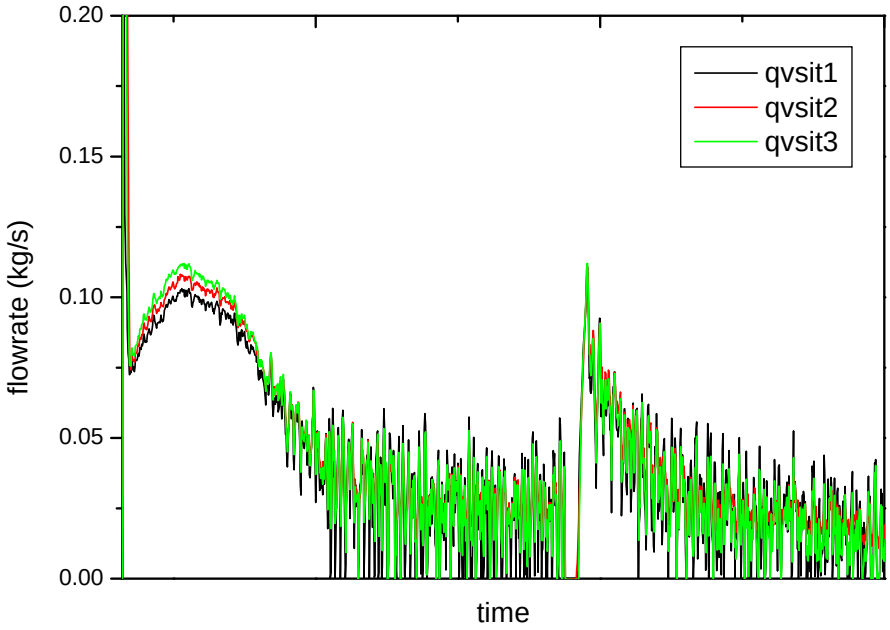

Figure 3.4-9 Safety injection flow rates from SITs

3.4.5 Containment pressure

The containment pressure is simulated by a separating vessel in the ATLAS facility. The separating vessel collects the discharged two-phase break flow and separates it into steam and water. The steam is discharged through a vent line to the atmosphere and the separated water is drained to a measuring vessel. The steam vent line was fabricated with an 8-inch SCH.10 pipe line (ID=211.56mm). Initially the steam vent line was fully opened so that the pressure of the separating vessel was maintained at atmospheric pressure. Isometric drawing of a DVI break pipe line from the broken DVI-4 nozzle to the separator nozzle is shown in Figure 3.4-10 and Figure 3.4-11. The total length of the pipe line from the exit of the OV-BS-03 to the separator nozzle is 17.269m. The free volume of the separator is 5.4m^3. The containment pressure was measured at two locations. The transmitter PT-CS-04 was located inside the separating vessel and PT-CS-03 was located at the steam vent line. The measured containment pressures with respect to time are shown in Figure 3.4-12. The measured PT-CS-03 was lower than PT-CS-04 as it was installed at the steam vent line downstream the separating vessel. PT-CS-03 is also provided in Appendix-A of this document.

Pressures at the upstream and the downstream of the break nozzle were also measured. Participants would also use the downstream pressure as a boundary condition of the containment. The measured pressure from PT-DVIBS-01 with respect to time is shown in Figure 3.4-13 and also provided in Appendix-A of this document.

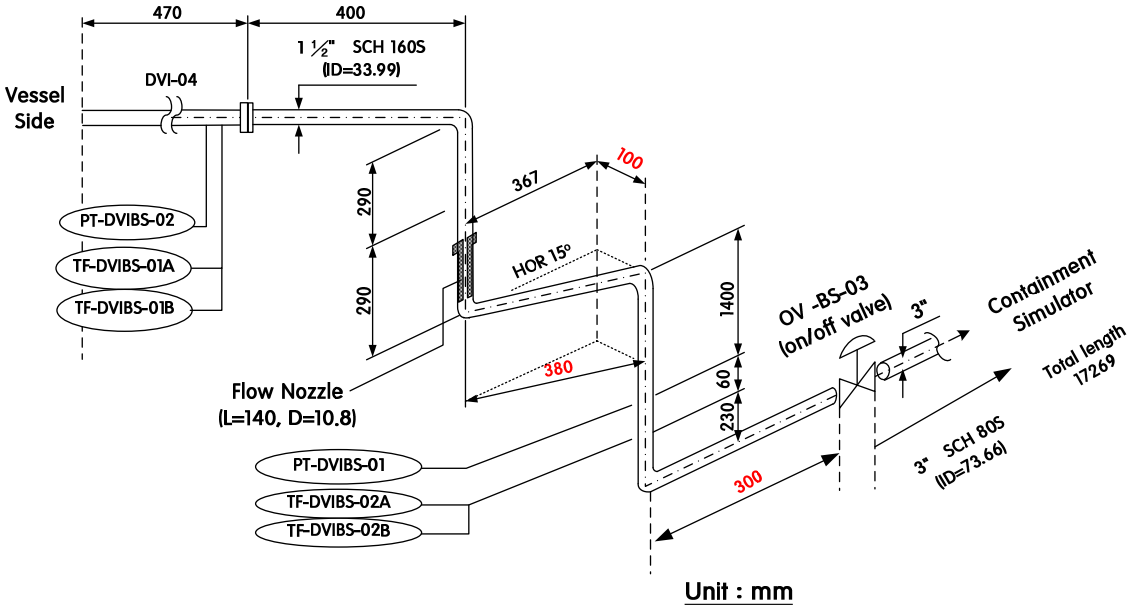

Figure 3.4-10 Isometric drawing of a DVI break pipe line

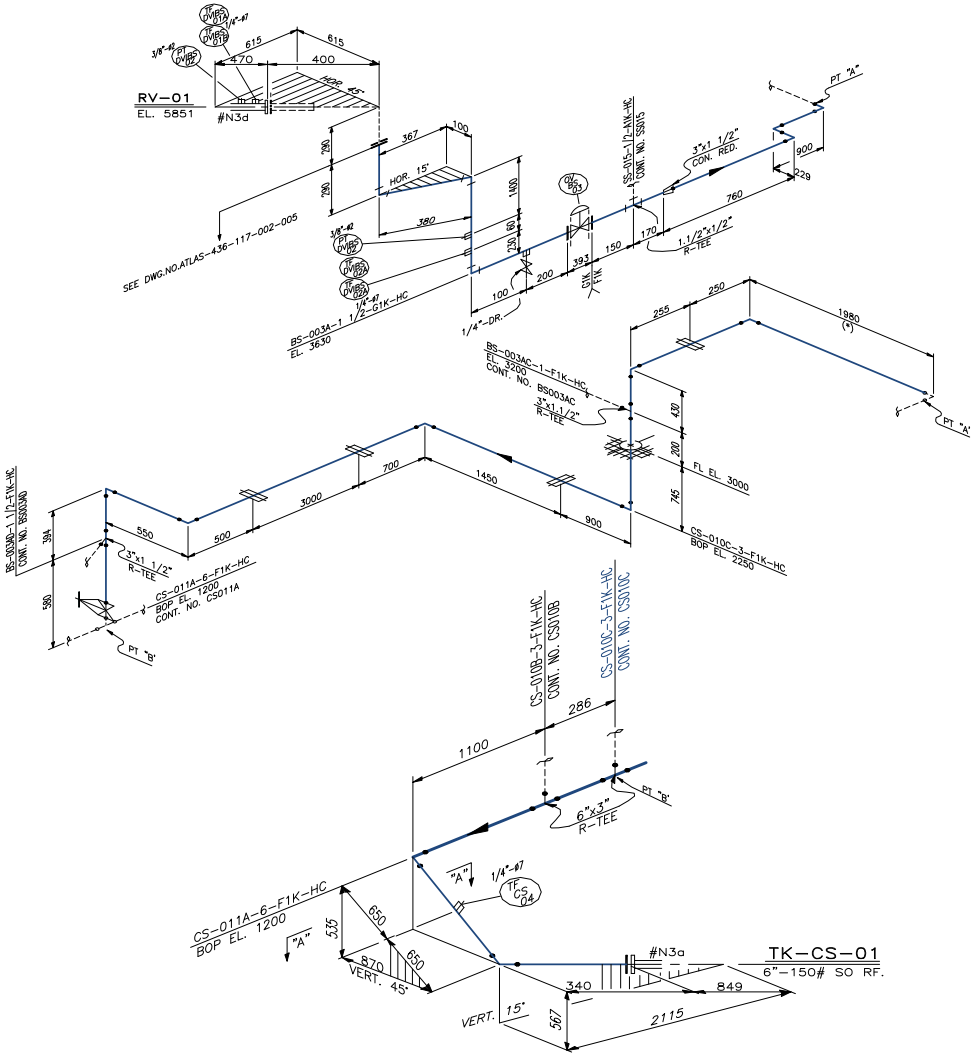

BILL OF MATERIAL

ITEM	SIZE	UNIT	Q'TY	DESCRIPTION
		F1K		
PIPE	1/2"	M	0.3	PIPE A312GR. TP316 SMLS BE SCH80S
	3"	M	13.9	PIPE A312GR. TP316 SMLS PE SCH80S
90°ELBOW	3"	EA	9	ELBOW A182GR. F316 90-LR BW SCH80S
TEE RED	1 1/2"x1/2"	EA	1	TEE A182GR. F316 REDUCING SW SCH80S
	3" x 1 1/2"	EA	2	TEE A182GR. F316 REDUCING BW SCH80S
REDUCER	3" x 1 1/2"	EA	1	REDUCER A182GR. F316 CON BW SCH80S
GATE V/V	3"	EA	1	GATE A182GR. F316 HF BW BB OS&Y ANSI 1500LB
		G1K		
PIPE	1 1/2"	M	2.6	PIPE A312GR. TP316 SMLS PE SCH160S
90°ELBOW	1 1/2"	EA	1	ELBOW A182GR. F316 90-LR SW 6000LB
FLANGE	1 1/2"	EA	3	FLANGE A182GR. F316 SW RF ANSI 2500LB
GASKET	1 1/2"	EA	3	GASKET ANSI 2500LB 4.5TH'K FLAT RING SWG SS316
B/N	M30 x 180L	SET	3	STUD BOLT(METRIC) A193GR. B7/A194GR. 2H CL 2500LB HEX. NUT HEAVY.
TUBE	1/4"	M	0.2	ASTM A269 316SS. SMLS. TH'K 0.049" BA
MPWC	1/4"	EA	1	MAIL PIPE WELD CONNECTOR 316SS. ASTM A276/ASME SA479 WBT
NEVH	1/4"	EA	1	NEEDLE VALVE 316SS.A276/A479. GRAPHITE(PACKING) 6000PSI

Figure 3.4-11 Detailed isometric drawing from the broken DVI nozzle to the separating vessel

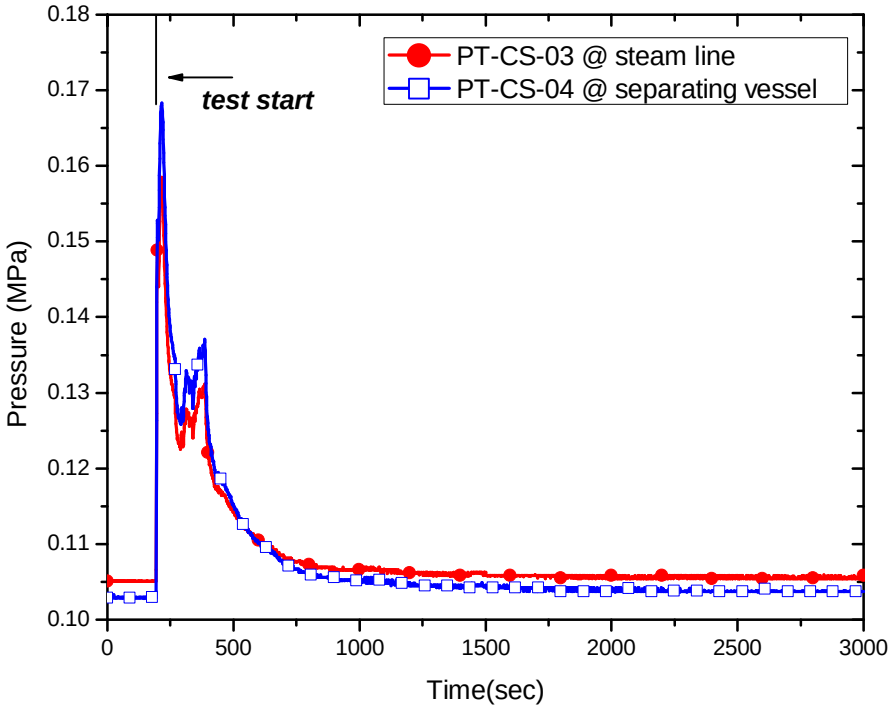

Figure 3.4-12 Measured pressure trend of the containment simulator

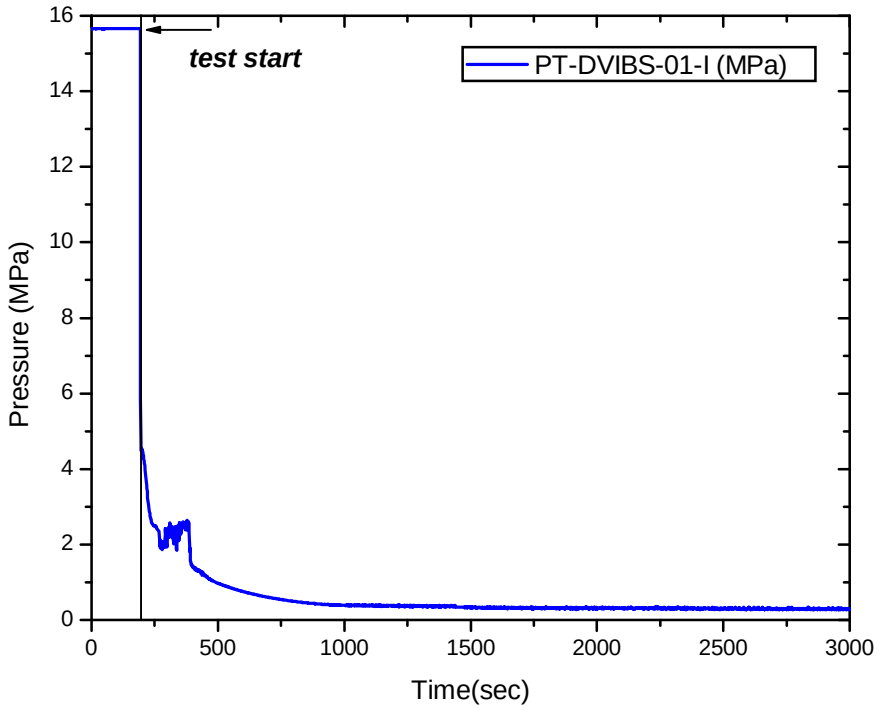

Figure 3.4-13 Measured pressure trend of the downstream of the DVI nozzle

3.5 Major phenomena observed

3.5.1 Sequence of events

The test was started by opening the break valve, OV-BS-03 at 193.0 s after steady state data were measured for 203.0 s. The major sequence of events observed during the whole test period is summarized in Table 3.5-1. For comparison convenience, the break time was shifted to 0.0 s and added in the table because most calculations started their transients at time of zero.

Table 3.5-1 Measured sequence of events

Event	Time (sec)		Remarks
	DAS[1)]	Shifted[2)]	
Data logging starts	-10.0	-203	
Break valve open	193.0	0.0	
MSSV of SG-2 open (1st opening)	217.0	24.0	PT-SGSD2-01>8.1 MPa
MSSV of SG-1 open (1st opening)	217.0	24.0	PT-SGSD1-01>8.1 MPa
Low pressurizer pressure trip (LPP)	218.0	25.0	PT-PZR-01 <10.7214 MPa
Pressurizer heater off	218.0	25.0	LPP + 0.0 sec
Main steam isolation	218.0	25.0	LPP + 0.1 sec
RCPs trip	218.0	25.0	LPP + 0.35 sec
Main feed water isolation	225.0	32.0	LPP + 7.0 sec
Core power starts to decay	226.0	33.0	
SIP-2 injection	247.0	54.0	LPP + 28.3 sec
MSSV of SG-2 open (2nd opening)	250.0	57.0	PT-SGSD2-01>8.1 MPa
MSSV of SG-1 open (2nd opening)	255.0	62.0	PT-SGSD1-01>8.1 MPa
MSSV of SG-2 open (3rd opening)	306.0	113.0	PT-SGSD2-01>8.1 MPa
MSSV of SG-1 open (3rd opening)	311.0	118.0	PT-SGSD1-01>8.1 MPa
1st loop seal clearing occurs	383.0	190.0	Only in loop 1A/1B
SIT actuation (high flow)	661.0	468.0	PT-DC-01 <4.03 MPa
2nd loop seal clearing occurs	1429.0	1236.0	Loop 2B
SIT low flow conversion	-	-	did not occur
Test stops	3126.0	2933.0	

1) DAS: actual measured time starting from -10.0 s

2) shifted : break time was shifted to zero for convenience

3.5.2 Core power and heat loss

The core power table with respect to time was obtained from a pre-test calculation by a best-estimated safety analysis code, MARS3.1. A measured core power table was shown in Figure 3.4-1 in the previous section.

The estimated heat loss of the primary and the secondary system with respect to time was shown in Figure 3.4-2 and explained in the previous section. The primary heat loss at the initial condition was about 83 kW and the secondary heat loss of each steam generator was about 29 kW. During the test, the primary heat loss was compensated by adding it to the core decay power table with respect to time.

3.5.3 Primary and secondary pressure

The measured primary and secondary pressures are shown in Figure 3.5-1. An enlarged figure between 100.0 and 600.0 s were included inside the figure for clear observation. The pressurizer pressure, PT-PZR-01 was used as a reference pressure for the primary system. It rapidly dropped to about 8.2 MPa from its initial pressure of 15.6 MPa on break. The primary pressure showed a little oscillation between 250 s and 390 s and it decreased again from 390 s. This oscillation was attributed to the secondary pressure variation caused by opening of MSSVs.

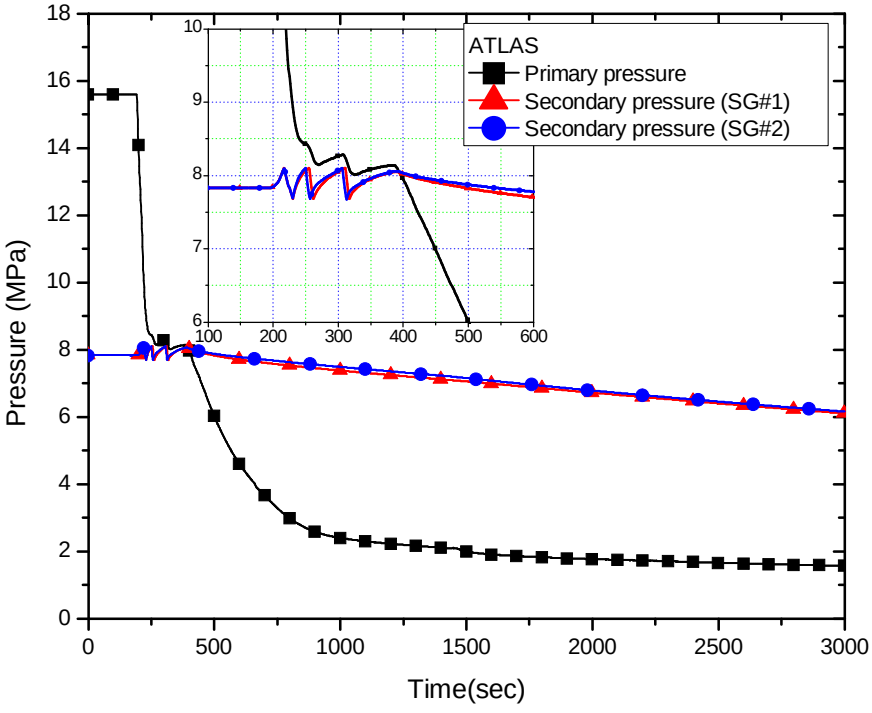

Figure 3.5-1 Measured primary and secondary pressures

On break, the secondary pressure started to increase up to the MSSV set-point, 8.1MPa. Three MSSVs were installed in parallel at each steam line. Each MSSV has the characteristics of opening and closing in response of SG's pressure for limiting SG's pressure as shown in Table 3.5-2. In the present test, OV-MSSV1-03 at the SG-1 line and OV-MSSV2-03 at the SG-2 line were opened three times at 217.0, 255.0 and 311.0 s and 217.0, 250.0 and 306.0 s, respectively because the secondary steam pressure reached the first set-point 8.1MPa. The other two MSSV banks were not activated. An increase in the secondary pressure was effectively depressed only by opening of one bank of the MSSVs. During the test, an isolation valve, OV-MS12-01 between SG-1 and SG-2 was closed at 230.0 s, which resulted in independent transient behavior of the steam pressure of each steam generator.

Table 3.5-2 Characteristics of the MSSVs of each steam line

MSSV bank	**MSSVs at SG-i (i=1 or 2)**	**Set-point for opening (MPa)**	**Set-point for Closing (MPa)**	**Throat diameter (mm) /Open area (m^2)**
Bank 1	OV-MSSVi-03	8.10	7.7	$18.85/2.79 \times 10^{-4}$
Bank 2	OV-MSSVi-02	8.31	7.9	$18.85/2.79 \times 10^{-4}$
Bank 3	OV-MSSVi-01	8.48	8.05	$32.46/8.275 \times 10^{-4}$

3.5.4 Core heater surface temperature

A total of 264 thermocouples (T/Cs) were installed at the 44 heater rods among the 390 heater rods to measure the surface temperatures of the heater rods. The thermocouples can be categorized into four groups; a-type, b-type, i-type, and s-type. Each instrumented heater rod has 6 T/Cs at different elevations. Detailed label designations of the T/Cs for four types were summarized from Table 3.5-3 to Table 3.5-5.

Table 3.5-3 Label designations of the T/Cs for wall temperature measurement of a- and b-type

Tag name	**Elevation from the bottom of heated section (mm)***	**Remarks**
TH-CO-01Gmjkk	127	m: group number, 1, 2, or 3
TH-CO-02Gmjkk	312	j: azimuthal angle
TH-CO-03Gmjkk	434	
TH-CO-04Gmjkk	626	
TH-CO-05Gmjkk	779	
TH-CO-06Gmjkk	953	

j	angle	remarks
1	0°	Hot leg #1
2	45°	
3	90°	

TH-CO-07Gmjkk	1086	4	135°		
TH-CO-08Gmjkk	1271	5	180°	Hot leg #2	
TH-CO-09Gmjkk	1329	6	225°		
TH-CO-10Gmjkk	1517	7	270°		
TH-CO-11Gmjkk	1645	8	315°		
TH-CO-12Gmjkk	1819	kk: T/C type; a1, a2, a3, b1, b2, b3			

* The offset distance between the bottom of the heated section and the bottom of the RPV is 721.6mm

Table 3.5-4 Label designations of the T/Cs for wall temperature measurement of i-type

Tag name	**Elevation from the bottom of heated section (mm)**	**Remarks**
TH-CO-07Gmjk	998	m: group number, 1 j: azimuthal angle
TH-CO-08Gmjk	1179	
TH-CO-09Gmjk	1300	
TH-CO-10Gmjk	1423	
TH-CO-11Gmjk	1602	
TH-CO-12Gmjk	1663	k: T/C type, i

J	angle	remarks
1	0°	Hot leg #1
3	90°	
5	180°	Hot leg #2
7	270°	

Arrangement of the instrumented heater rods is shown in Figure 2.4-1 and Figure 3.5-2. The hot leg-1 is located at 0 degree of the azimuthal angle and the hot leg-2 is at 180 degree. In order to investigate multi-dimensional PCT behavior in the core, the measured wall temperatures of the selected heater rods at four azimuthal angles were compared in each group: 0, 90, 180, and 270 degree.

In the heater group 1, the rods 'a3' and 'b3' in the sub-group G11 at 0 degree, 'a1' and 'b1' in G13 at 90 degree, 'a1' and 'b1' in G15 at 180 degree, and 'a1' and 'b1' in G17 at 270 degree were selected for comparison. Measured PCTs of the heater rods 'a3' and 'b3' in the sub-group G11 at 0 degree of the azimuthal angle are shown in Figure 3.5-3. Before the break, initial wall temperatures show a variation between 570 K and 620 K due to a chopped cosine axial power profile. During the transient, no temperature excursion was observed. Figure 3.5-4 shows the measured PCTs of the heater rods 'a1' and 'b1' in the sub-group G13 at 90 degree of azimuthal angle. The measured temperatures were almost the same to the sub-group G11. The other sub-groups, G15, G17 showed the similar trends, in which there was no temperature excursion as shown in Figure 3.5-5 and Figure 3.5-6. In summary, a temperature excursion was not observed in the heater group 1. It was found that there was no noticeable multi-dimensional

effect in the measured surface temperatures of the heater rods in the heater group 1.

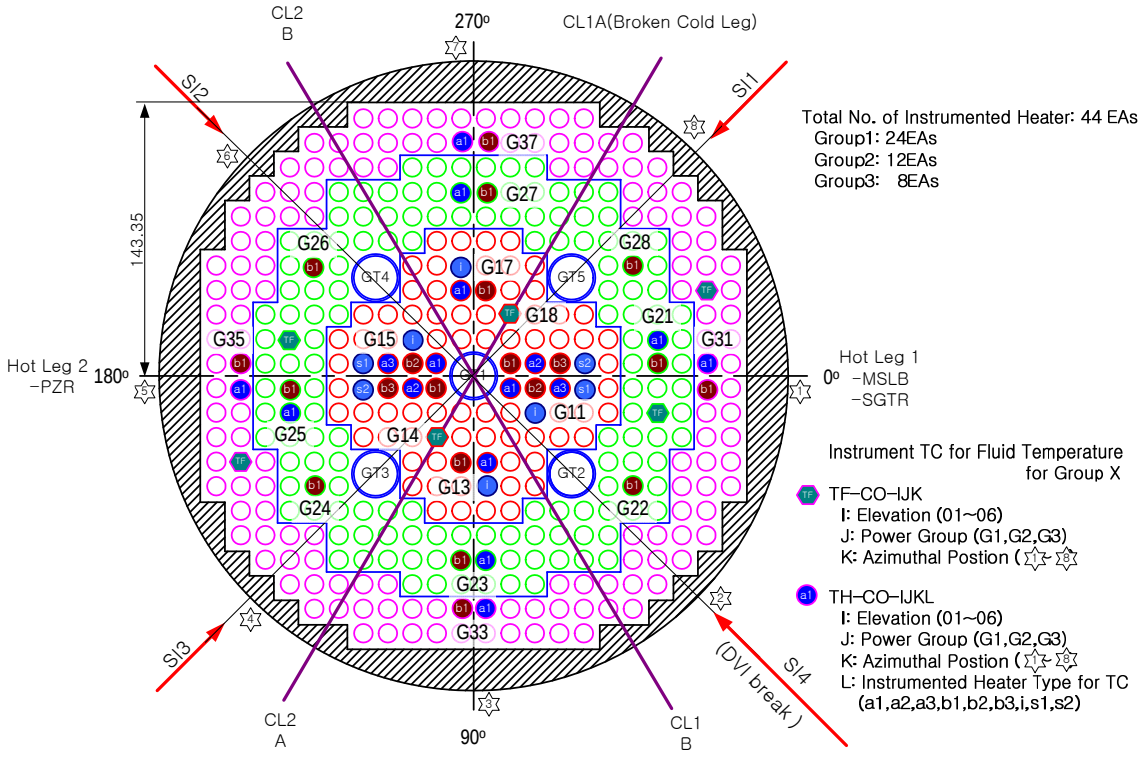

Figure 3.5-2 Arrangement of the heater rods in the core

Table 3.5-5 Label designation of the T/Cs for wall temperature measurement of s-type

Tag name	**Elevation from the bottom of heated section (mm)**	**Remarks**
TH-CO-01Gmjs1	1100	m: group number, 1 j: azimuthal angle
TH-CO-02Gmjs1	1208	
TH-CO-03Gmjs1	1240	
TH-CO-04Gmjs1	1272	
TH-CO-05Gmjs1	1304	
TH-CO-06Gmjs1	1336	
TH-CO-01Gmjs2	1368	
TH-CO-02Gmjs2	1400	
TH-CO-03Gmjs2	1508	
TH-CO-04Gmjs2	1540	
TH-CO-05Gmjs2	1572	
TH-CO-06Gmjs2	1604	

J	angle	remarks
1	00°	Hot leg #1
5	180°	Hot leg #2

On the other hand, a temperature excursion was measured in the other groups 2 and 3. In the heater group 2, two heater rods in the sub-group G21, G23, G25, and G27 which are located at 0, 90, 180, and 270 degree of the azimuthal angle, respectively, were selected. Figure 3.5-7 shows PCTs of the heater rods 'a1' and 'b1' in the sub-group G21. A temperature excursion was observed at about 384 s. The maximum PCT of about 580 K was measured at the 10th elevation. (z=1517mm from the bottom of the heated section). The higher PCT of about 585 K was observed in the sub-group G23 as shown in Figure 3.5-8. However, no temperature excursion was observed in the sub-group G25 and G27 as shown in Figure 3.5-9 and Figure 3.5-10, respectively.

Similar to the heater group 2, two heater rods were selected from G31, G33, G35, and G37 located at 0, 90, 180, and 270 degree of the azimuthal angle, respectively. The typical wall temperature trends of the heater rods in the group 3 were plotted in Figure 3.5-11 and Figure 3.5-12 for sub-group G31 and G33, respectively. Four heater rods experienced a temperature excursion at 9th, 10th, 11th, and 12th elevations. The maximum temperature was observed at the 10th elevation. Similar to the heater group 2, the heaters in the sub-group G33 showed higher temperatures than those in the sub-group G31. However, no temperature excursion was observed in the sub-group G35 and G37 as shown in Figure 3.5-13 and Figure 3.5-14, respectively. This was the same observation to the group 2.

Sixteen temperatures were measured from the 1st to the 6th elevations of the heaters, whereas twenty temperatures were obtained from the 7th to 12th elevations of the heaters. Thus, a cross-sectional maximum peak temperature was obtained and compared in Figure 3.5-15. A temperature excursion was observed at 9th, 10th, and 11th elevations. Among them, the maximum was observed at 10th elevation. Taking into account all the instrumentations of the heater wall temperature, the maximum envelope of the measured PCTs is shown in Figure 3.5-16. The measured maximum PCT was 587.7 K in the group 3.

Based on this measurement, multi-dimensional non-uniformity in the PCTs was observed in the present test. In conclusion, the heater rods located in the 4th quadrant of Figure 3.5-2 between 0 degree and 90 degree showed a higher temperature excursion than those in other quadrants. It is inferred that the observed higher temperature excursion was related to the break location, because the broken DVI nozzle is located at 45 degree. Unfortunately, water level measurement in the core region was done in a one-dimensional manner. So, water level comparison in the azimuthal direction could not be made.

More detailed contour plot of the measured heater wall temperature was shown in Figure

3.5-17. Cross sectional views of the heater wall temperature contour were also plotted from Figure 3.5-18 through Figure 3.5-20 for the same x-, y- , and z-plane, respectively. All the measured 264 wall temperatures were used to investigate the 3-D distribution of the heater wall temperature, in particular focusing on the temperature excursion period from 380 s to 386 s. A 3-dimensional interpolation method between measurement locations was utilized to estimate the wall temperature. The origin of the plot is located at the center of the core. The positive x-axis is in the direction to the hot leg 1, i.e., 0 degree of the azimuthal angle and the positive y-axis is at 270 degree of the azimuthal angle in Figure 3.5-2. The z-axis is based on the elevation from the bottom of the heated section.

It can be seen from the figures that most non-uniformity was observed around the elevation z=1517mm where the maximum PCT was observed. Although the heater rods had a chopped cosine distribution axially, the maximum temperature was observed at higher elevation than the center region. Also it can be seen that the highest temperature region at around z=1517mm is located at x near 100 mm and y near -100 mm as shown in Figure 3.5-21. This is the same observation explained in the previous paragraph. More temperature gradients in the same y-plane than in the same x-plane can be seen by comparison of Figure 3.5-19 with Figure 3.5-18. It implies that more non-uniformity in the PCT existed in the x-direction than in the y-direction

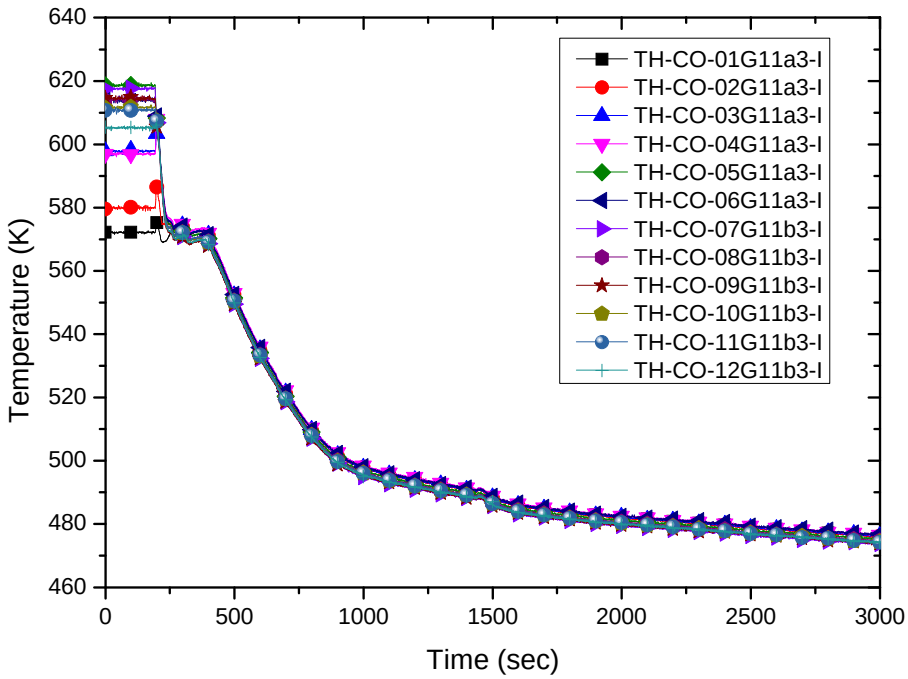

Figure 3.5-3 Measured PCT of the heaters in G11a3 and G11b3

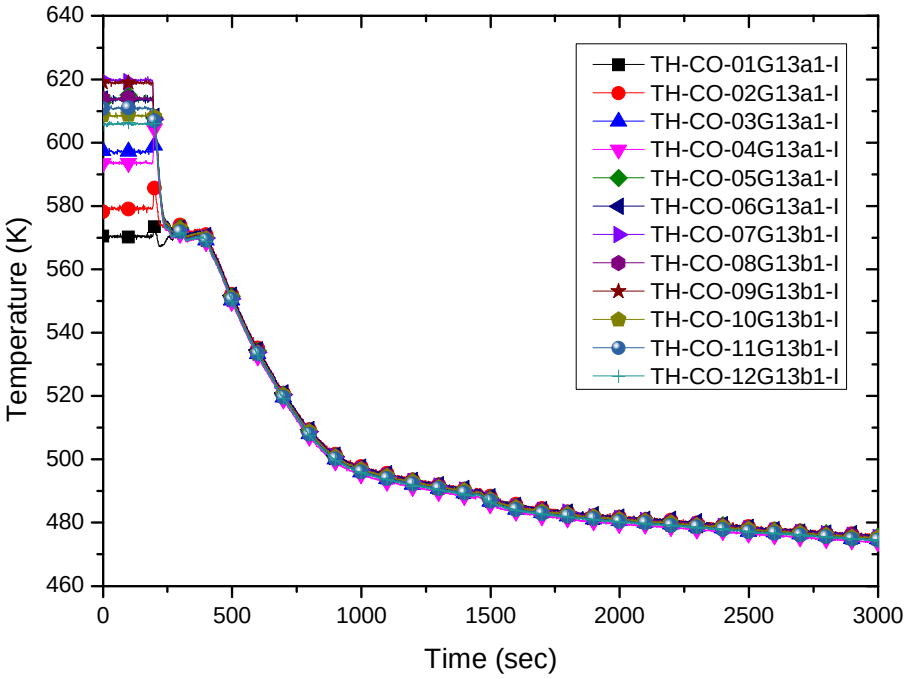

Figure 3.5-4 Measured PCT of the heaters in G13a1 and G13b1

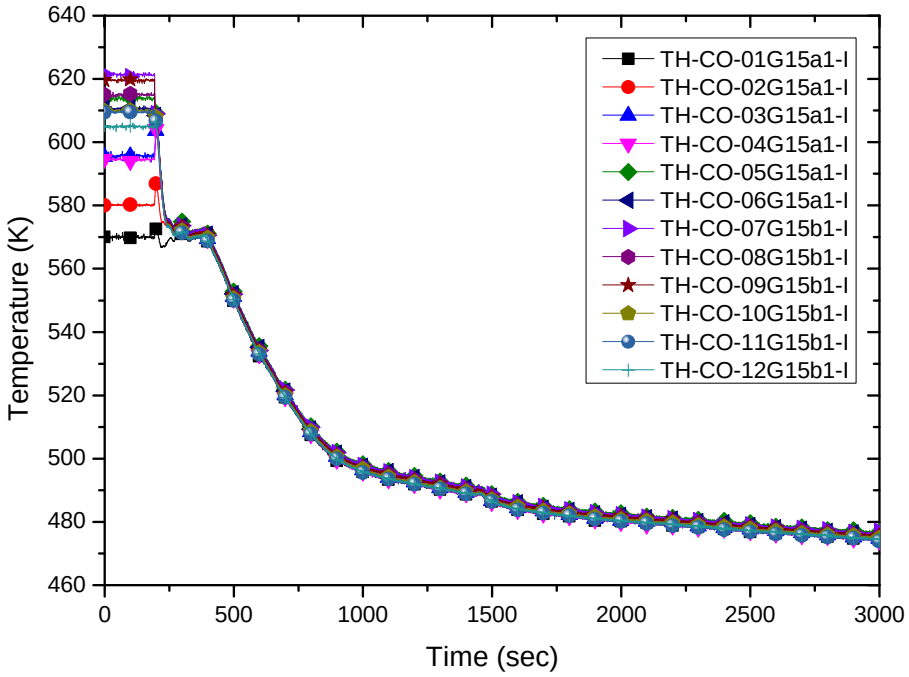

Figure 3.5-5 Measured PCT of the heaters in G15a1 and G15b1

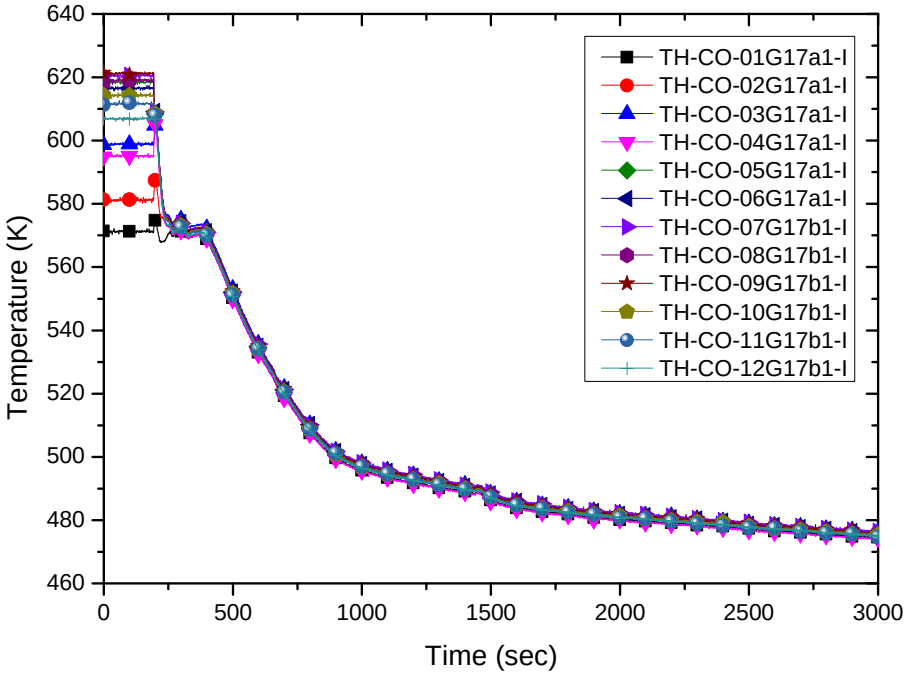

Figure 3.5-6 Measured PCT of the heaters in G17a1 and G17b1

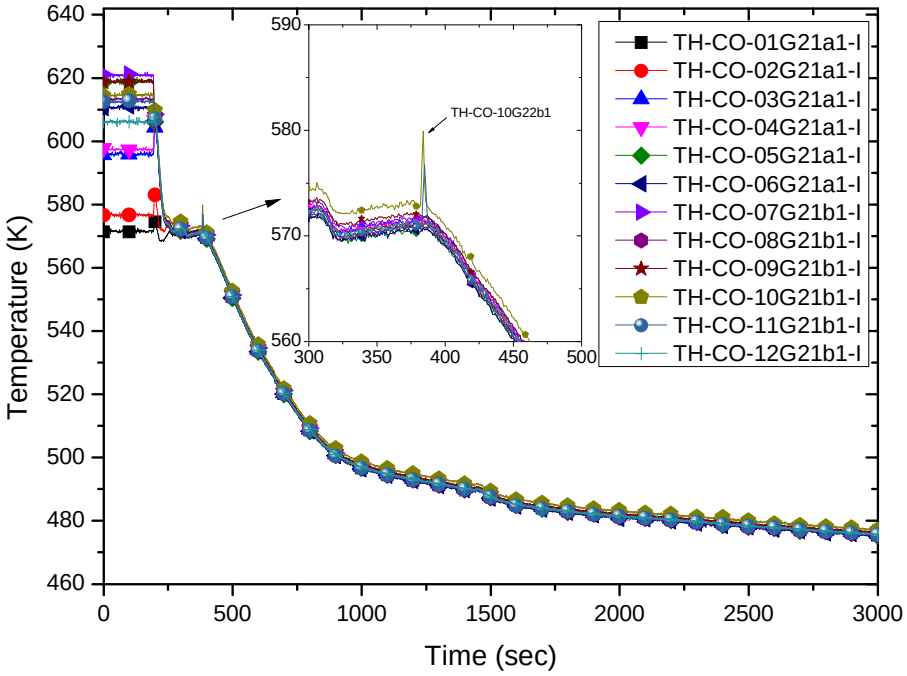

Figure 3.5-7 Measured PCT of the heaters in G21a1 and G21b1

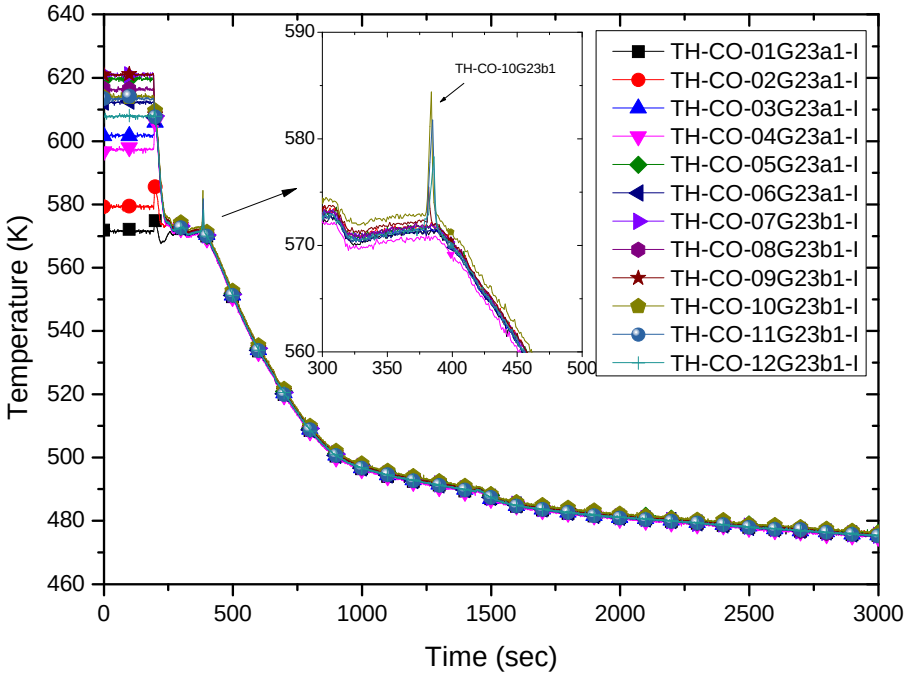

Figure 3.5-8 Measured PCT of the heaters in G23a1 and G23b1

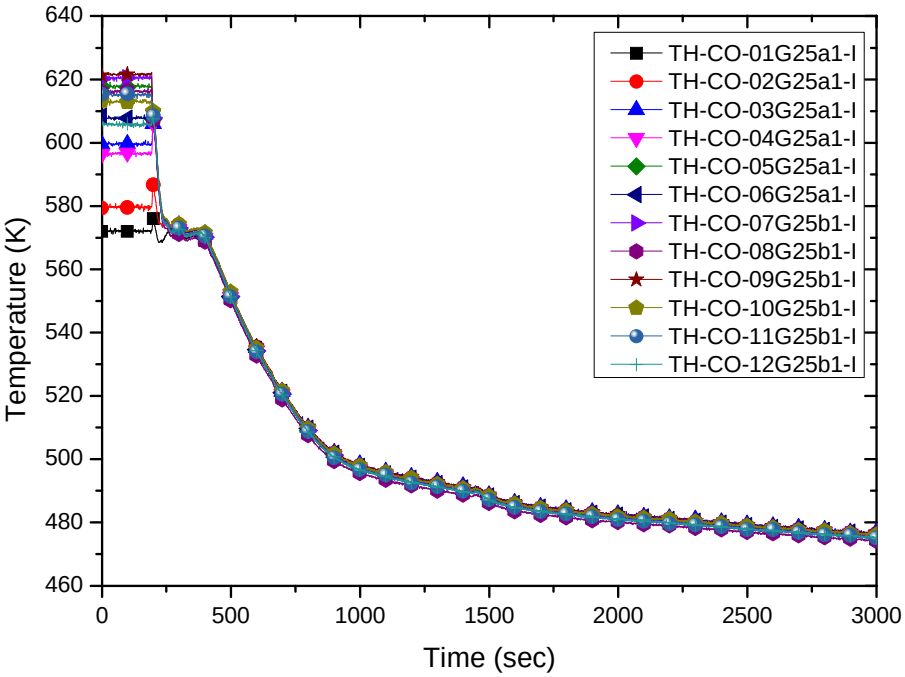

Figure 3.5-9 Measured PCT of the heaters in G25a1 and G25b1

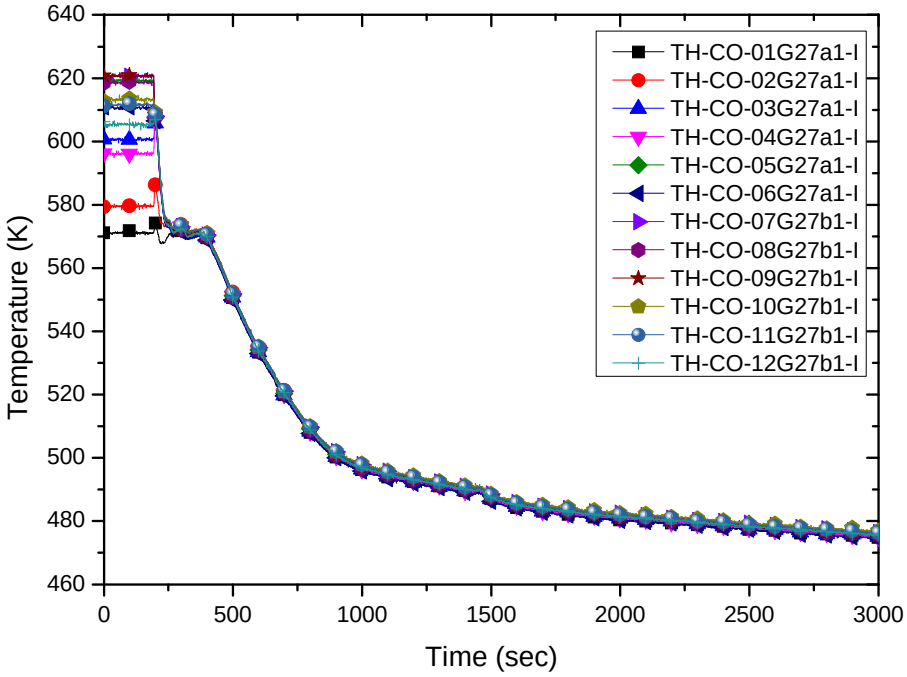

Figure 3.5-10 Measured PCT of the heaters in G27a1 and G27b1

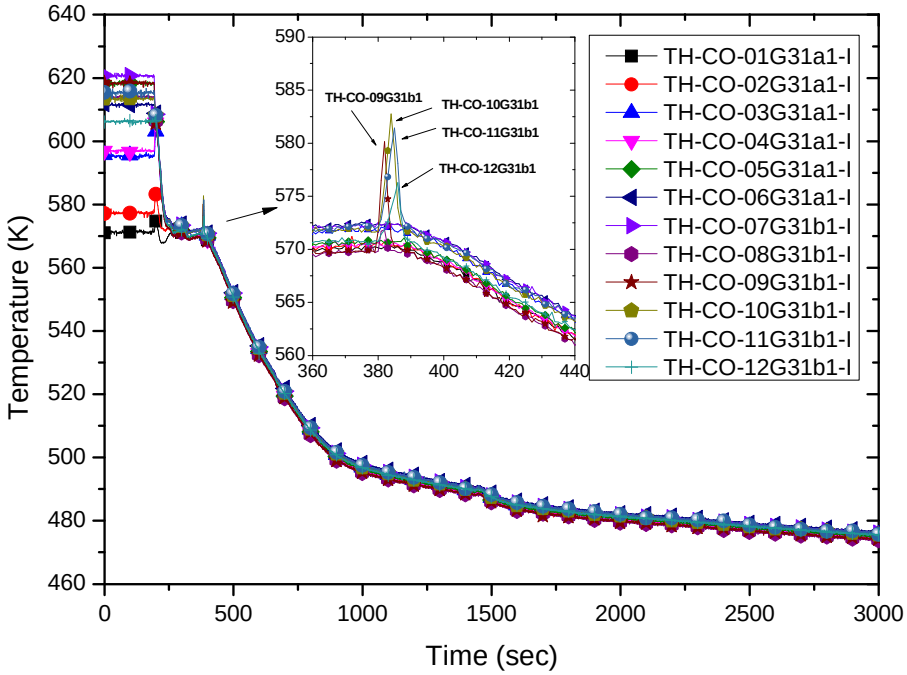

Figure 3.5-11 Measured PCT of the heaters in G31a1 and G31b1

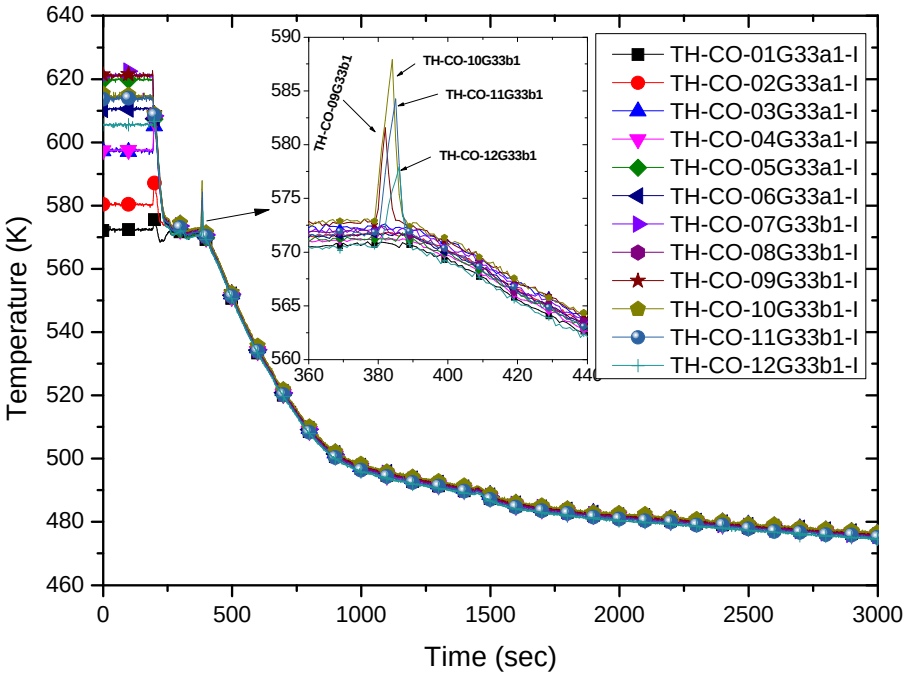

Figure 3.5-12 Measured PCT of the heaters in G33a1 and G33b1

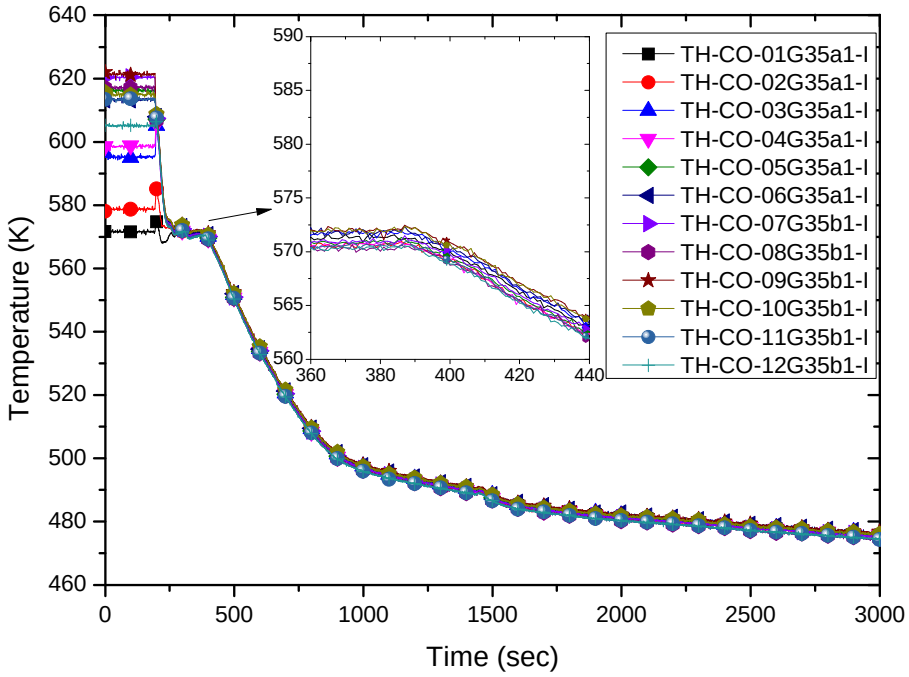

Figure 3.5-13 Measured PCT of the heaters in G35a1 and G35b1

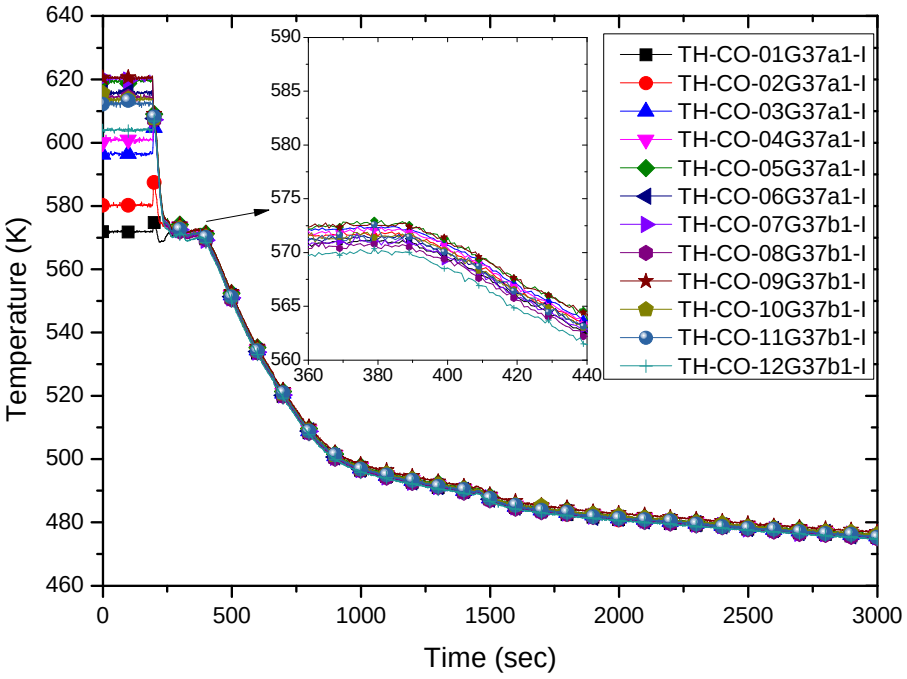

Figure 3.5-14 Measured PCT of the heaters in G37a1 and G37b1

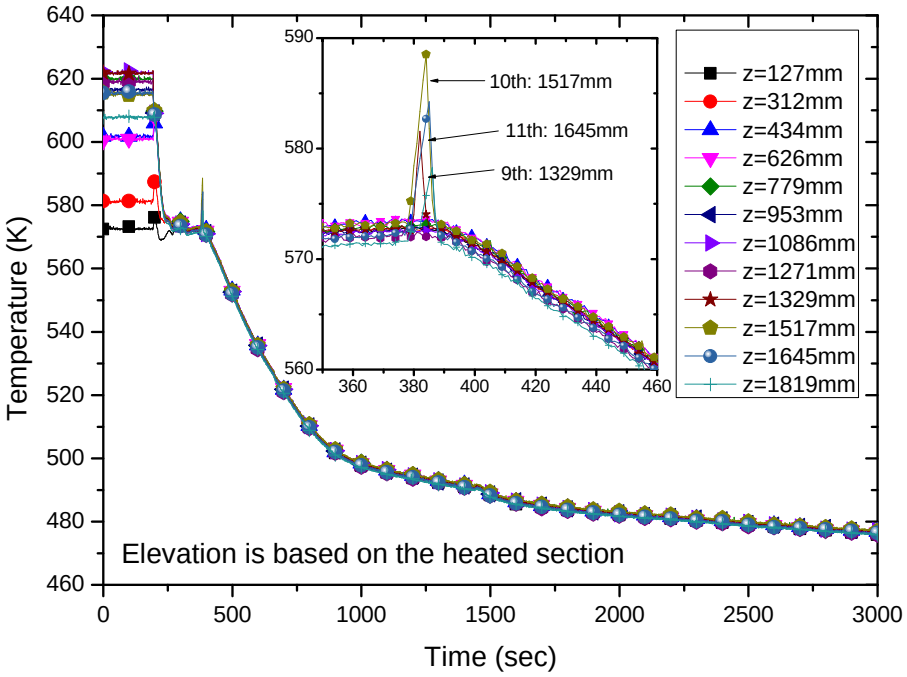

Figure 3.5-15 Measured cross sectional maximum PCT at each heater elevation

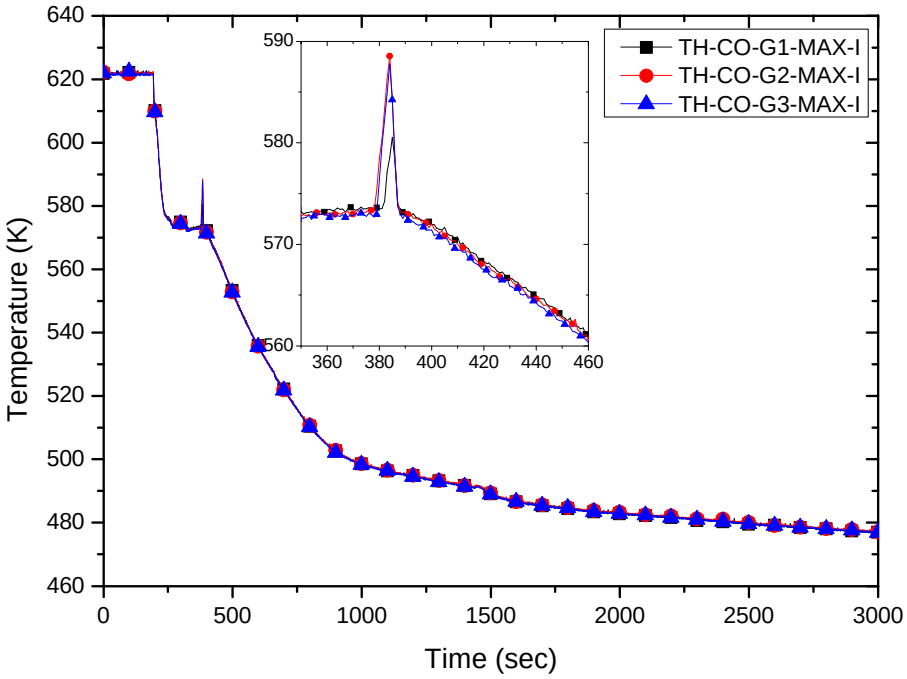

Figure 3.5-16 Maximum envelope of the measured PCTs of all instrumented heaters

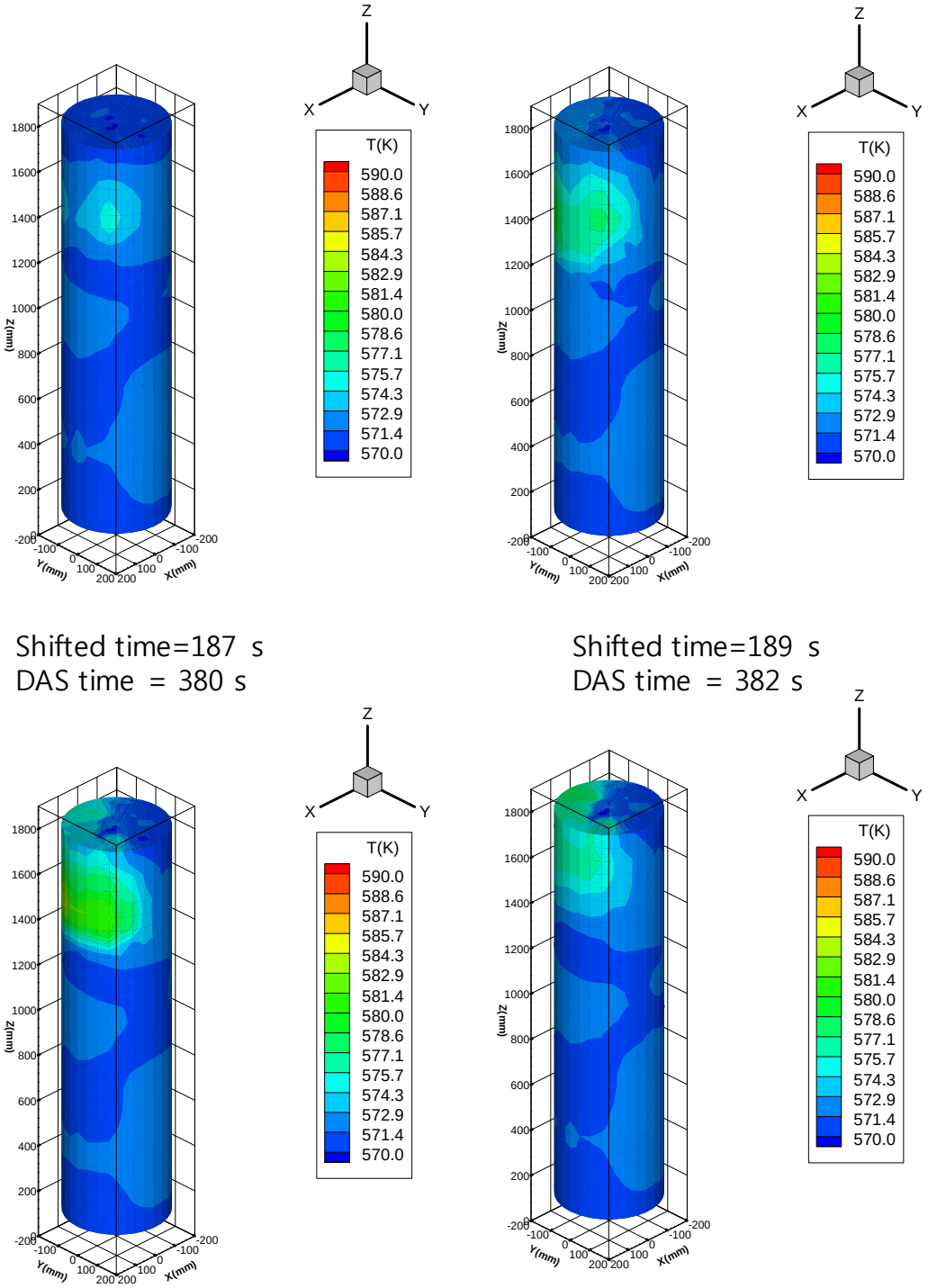

Figure 3.5-17 A measured PCT contour distribution during the PCT excursion

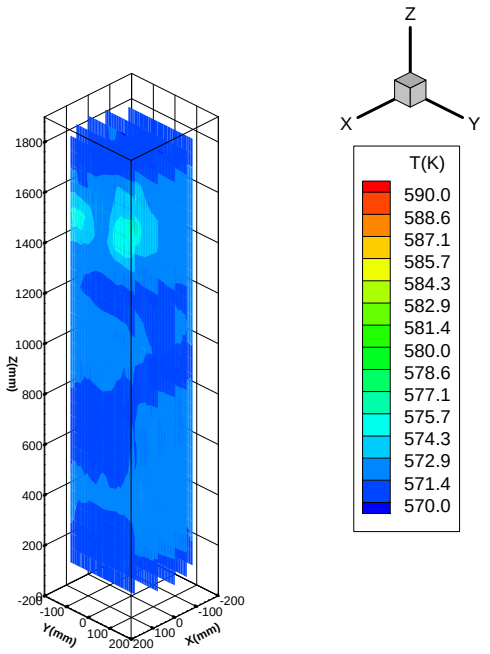

Shifted time=187 s
DAS time = 380 s

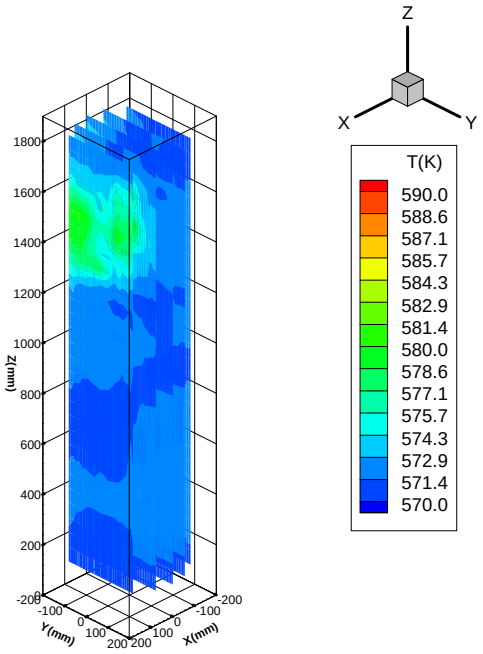

Shifted time=189 s
DAS time = 382 s

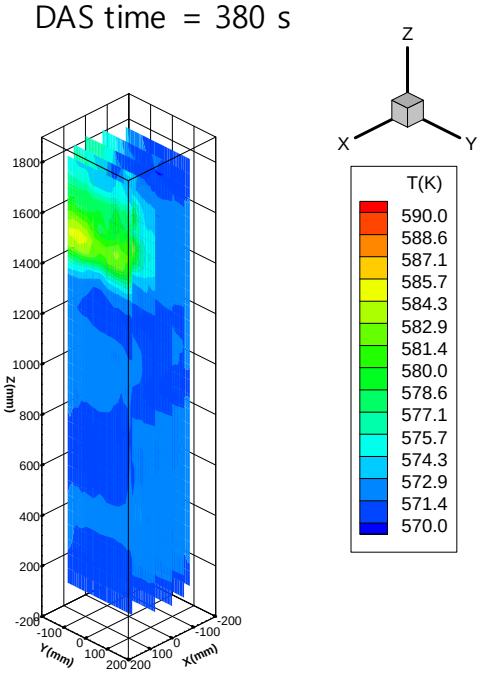

Shifted time=191 s
DAS time=384 s

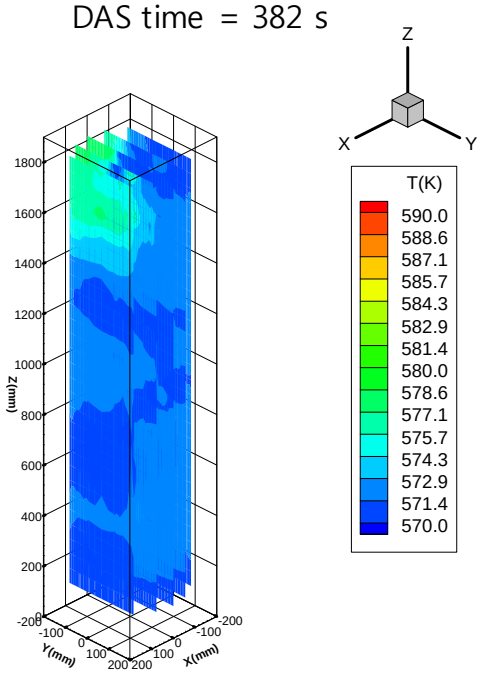

Shifted time=193 s
DAS time=386 s

Figure 3.5-18 A measured PCT contour in a x-plane during the PCT excursion

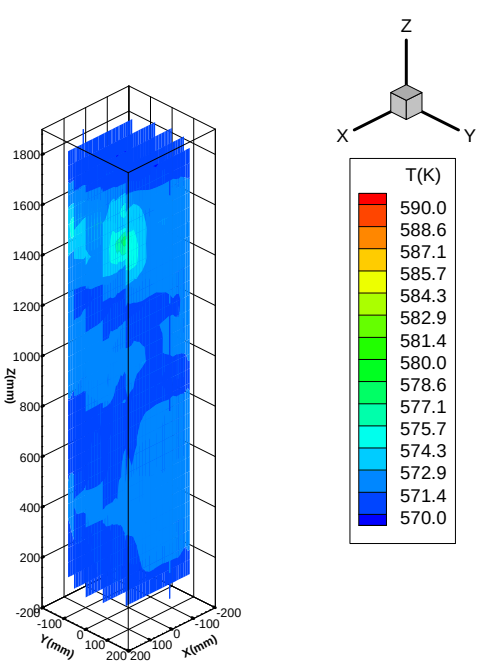

Shifted time=187 s
DAS time = 380 s

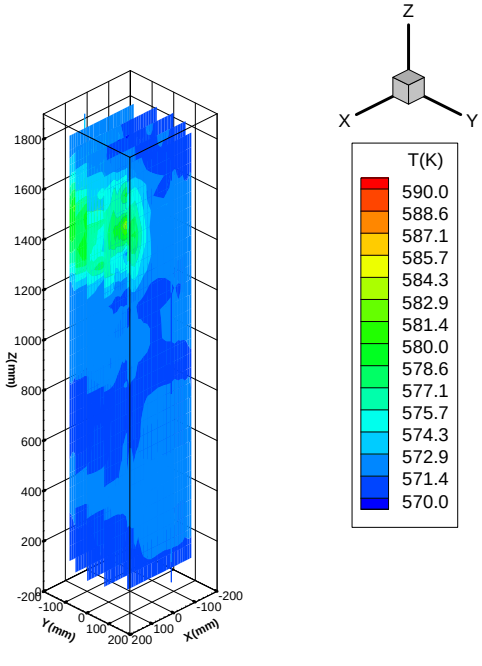

Shifted time=189 s
DAS time = 382 s

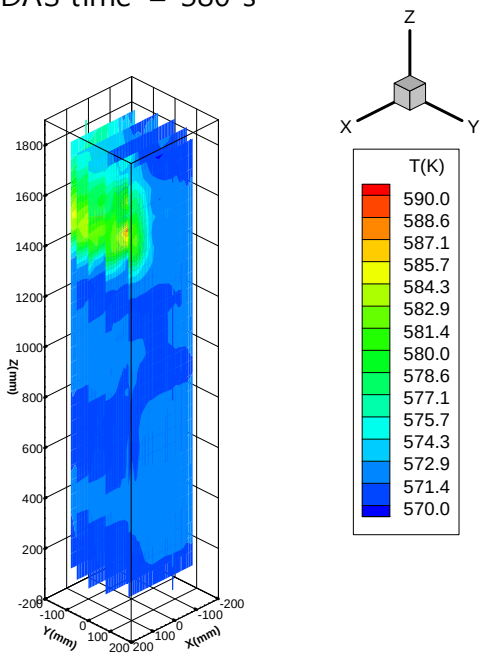

Shifted time=191 s
DAS time=384 s

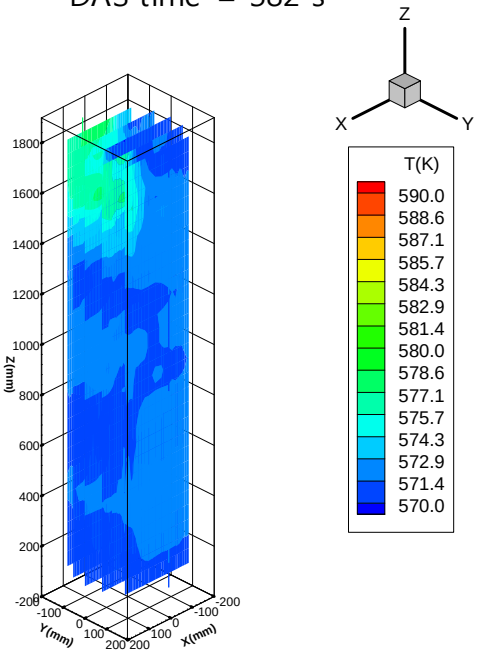

Shifted time=193 s
DAS time=386 s

Figure 3.5-19 A measured PCT contour in a y-plane during the PCT excursion

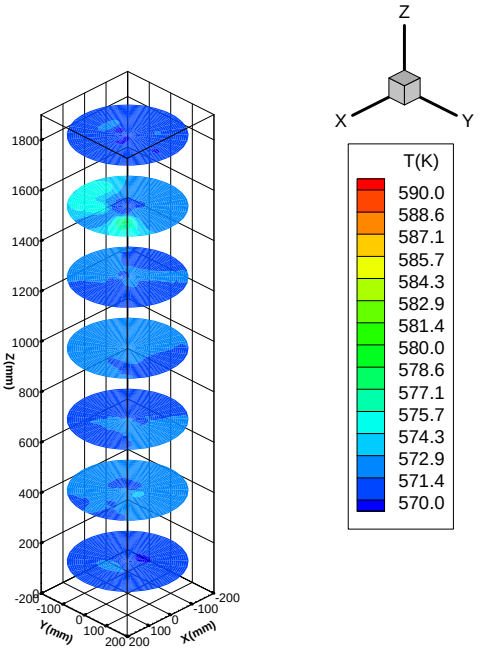

Shifted time=187 s
DAS time = 380 s

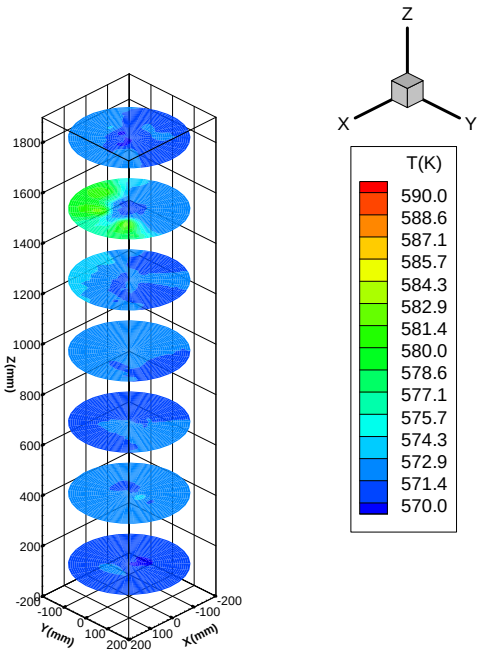

Shifted time=189 s
DAS time = 382 s

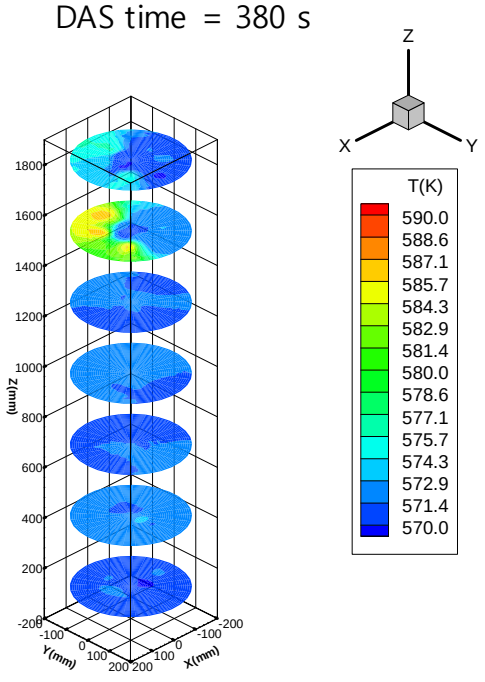

Shifted time=191 s
DAS time=384 s

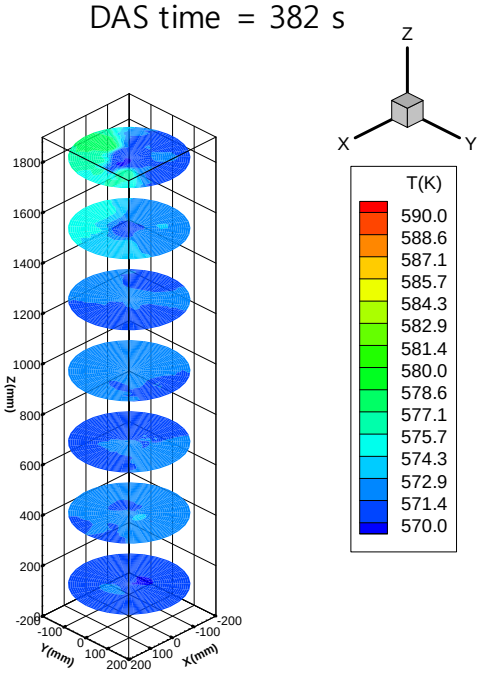

Shifted time=193 s
DAS time=386 s

Figure 3.5-20 A measured PCT contour in a z-plane during the PCT excursion

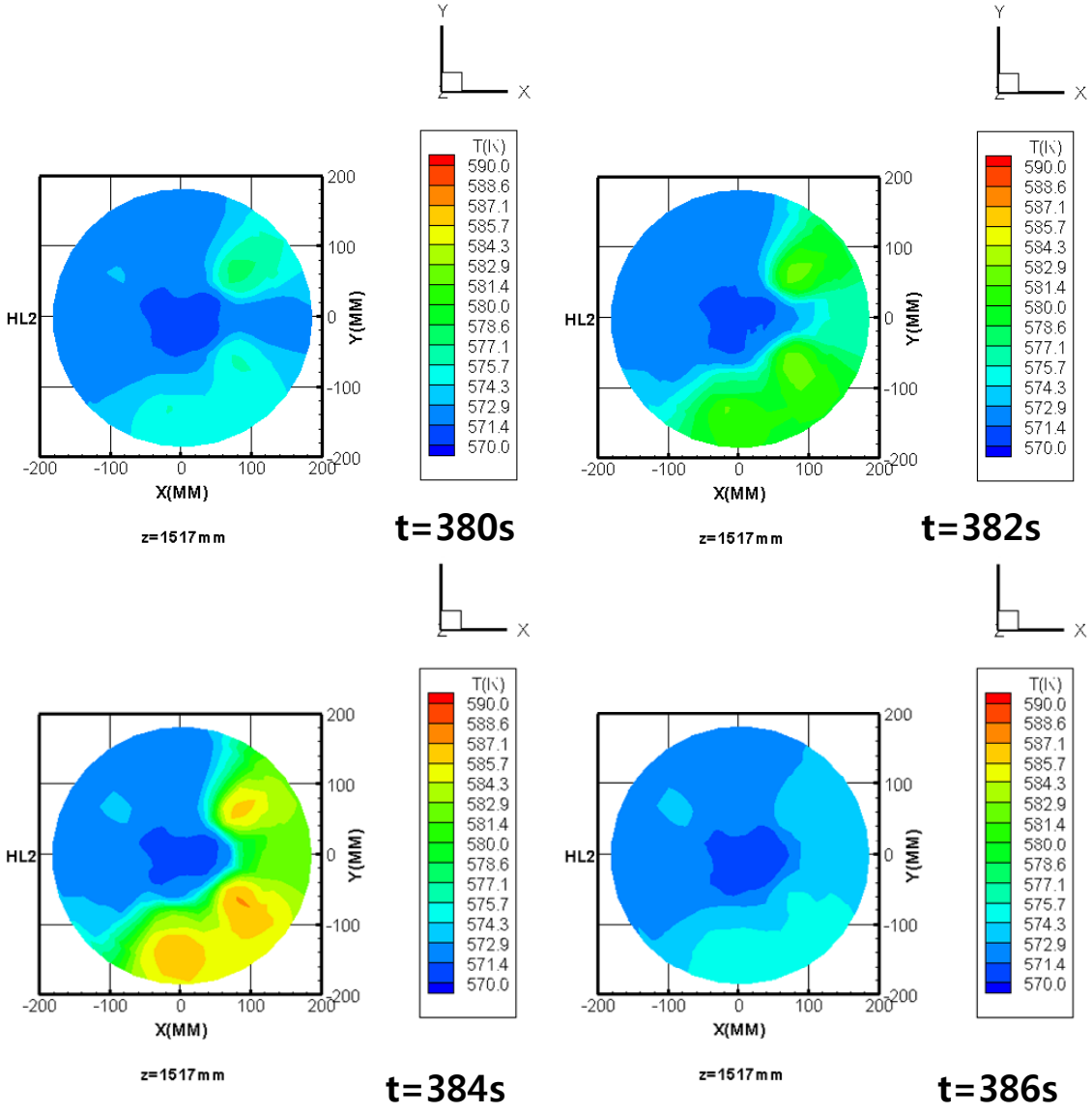

Figure 3.5-21 A measured PCT contour at the 19th elevation, z=1517mm

3.5.5 Loop flow rate and fluid velocity

In the ATLAS facility, a bi-directional flow tube (BDFT) which was developed by KAERI was installed at each leg, including the hot and cold legs [Yun *et al.*[1], 2005; Yun *et al.*[2], 2005; Kang *et al.*[2], 2009]. The location of the BDFT in each loop is shown in Figure 3.5-22. Its working principle is similar to that of the Pitot tube, wherein the dynamic pressure is measured. In the BDFT, the pressure measured at the front of the flow tube is equal to the total pressure, while that measured at the rear tube is slightly less than the static pressure of the flow field due to the suction effect downstream. The flow rate can be obtained by measuring the pressure difference between the front and rear tubes. In order to obtain the loop flow rate in each loop, a pair of a differential pressure transmitter and a level transmitter was installed at the same location. The differential pressure transmitter measures a pressure drop across the meter and the level transmitter measures the void (or liquid fraction) at the same measuring location. The DP and void fraction are used to calculate two-phase flow rate during the transient. Even though each BDFT was carefully calibrated in a single phase flow condition, it is known that the BDFT has a measurement uncertainty within ± 15 %. Detailed calibration results will be described in Section 3.6.1. As the BDFT utilizes a void fraction in an engineering conversion routine, it can produce measurement with great uncertainty if void fraction is not measured correctly.

The measured loop flow rate of each cold leg is shown from Figure 3.5-23 to Figure 3.5-26. In these figures, the measured flow rate was compared with two limiting estimations where either α=0.0 or α=1.0 was used instead of measured void fraction. This bounding analysis was done because the measured void fraction in each loop has great measurement uncertainty possibly due to harsh environment and/or incomplete water filling. In principle, two estimated flow rates bound the measured two-phase flow rates and it can be seen in those figures. From the test start to 100 s, α=0.0 was intentionally used by operators to provide more accurate boundary condition for steady state calculation. This assumption is valid during the steady state condition because the whole loops are full of water before the break. After around 100 s, the intentional forcing of α=0.0 was released by operators so that the transmitter should reads a local on-line void fraction from the field. That's why sudden decreases in flow rate were observed around 100 s for 3 loops, excluding the loop CL2A. These reductions are suspected to be due to a bias error in measuring the void fraction. The loop 2A was the only loop not to be biased among the other three loops.

On break, the loop flow rate abruptly increased because a large amount of water was discharged through the upper down-comer to the break nozzle. Then the loop flow rate decreased as the loop flow changed into two phase flow. After the first loop seal clearing at

383 s, the flow rates measured at two loops, CL-1A and CL-1B, were very close to the estimation with the assumption of α=1.0. The measured flow rate of the loop CL-2B approached the estimation with the assumption of α=1.0 at the second loop seal clearing occurred at 1429 s. On the other hand, the measured loop flow rate of CL-2A is close to the estimation with the assumption of α=0.0. It is due to the fact that the loop seal of the loop CL-2A was not cleared during the test period.

Based on the estimated mass flow rate in each loop with the assumption of either α=0.0 or α=1.0, fluid velocity of each loop was also estimated and plotted from Figure 3.5-27 to Figure 3.5-30. Similar to the flow rates, these two estimations can also be considered as an envelope velocity to include the actual fluid velocity. On break, the fluid velocity increased suddenly and decreased afterwards. After the first loop seal clearing, the two loops of CL-1A and CL-1B are occupied by steam as shown in Figure 3.5-27 and Figure 3.5-28. Thus, the estimated velocities of those two loops with assumptions of α=1.0 can be considered to be very close to the real steam velocities. In general, the CL-1A loop shows higher steam velocity than those of the loop CL-1B and CL-2B especially after around 750 s. The fluid velocity of the loop CL-2A is shown in Figure 3.5-29. As this loop is occupied by water as shown in Figure 3.5-25, the estimation with an assumption of α=0.0 gives the actual water velocity in this loop. Figure 3.5-30 clearly shows an increase in steam velocity after the second loop seal clearing.

The measured water and steam flow rate in each hot leg is shown in Figure 3.5-31 and Figure 3.5-32, respectively. Like the cold leg flow rate, the sudden drop in water flow rate at 100 s was due to the measurement bias to measure the water level in each hot leg. On break, the water flow rate rapidly decreased until the 1st loop seal clearing happened. As the core water level was depressed below the hot leg elevation before the 1st loop seal clearing as shown in Figure 3.5-43 and Figure 3.5-45, the forward water flows in the hot legs were reversed back to the RPV core. Even though there existed a little measurement bias in the flow rate, such negative water flow rates in the hot leg can be seen in Figure 3.5-43. After the 1st loop seal clearing, the water flow rate in the hot leg 2 showed almost zero value because the loop 2 was still blocked by the loop seals. On the other hand, the water flow rate in the hot leg 1 showed an oscillatory behavior. The steam flow rates showed initial peaks just after the break and then were almost zero until the 1st loop seal clearing. But, after the 1st loop seal clearing, the steam flow rates showed high oscillatory behaviors.

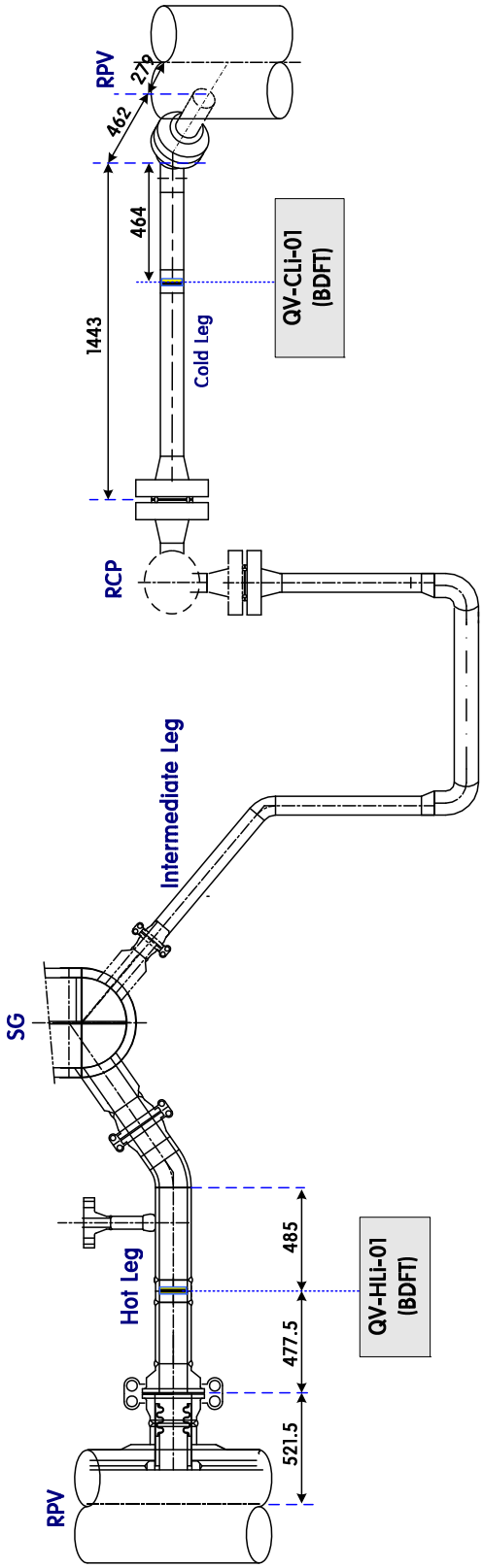

Figure 3.5-22 Location of the BDFT in the RCS loop

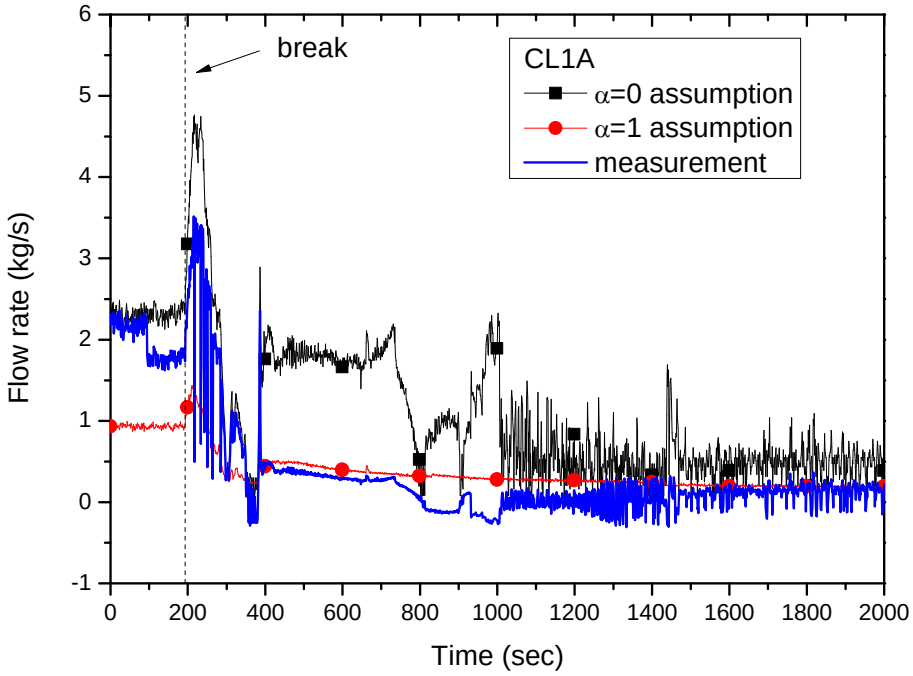

Figure 3.5-23 Cold leg flow rate in loop CL-1A

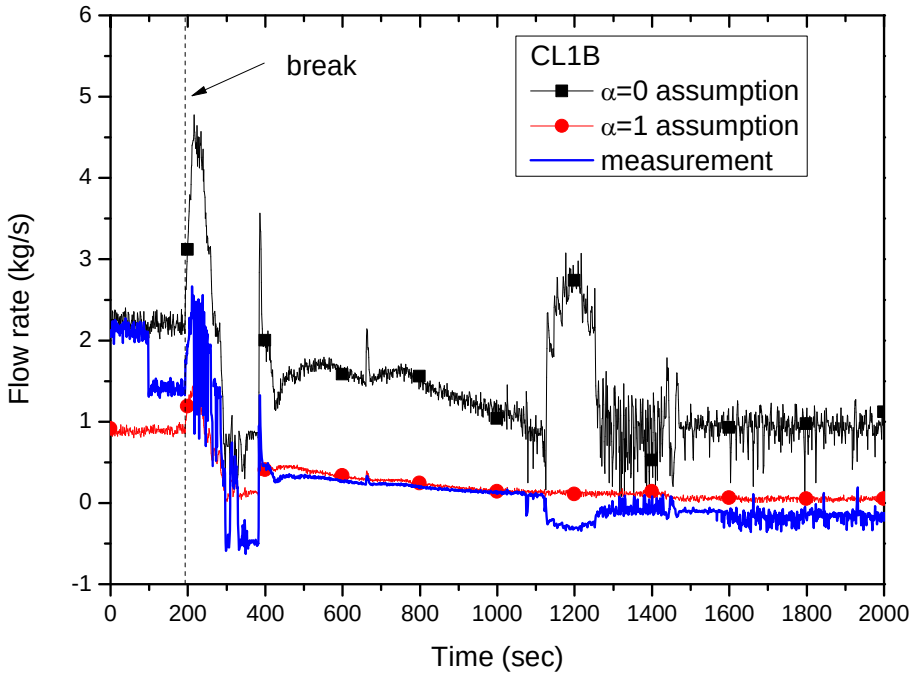

Figure 3.5-24 Cold leg flow rate in loop CL-1B

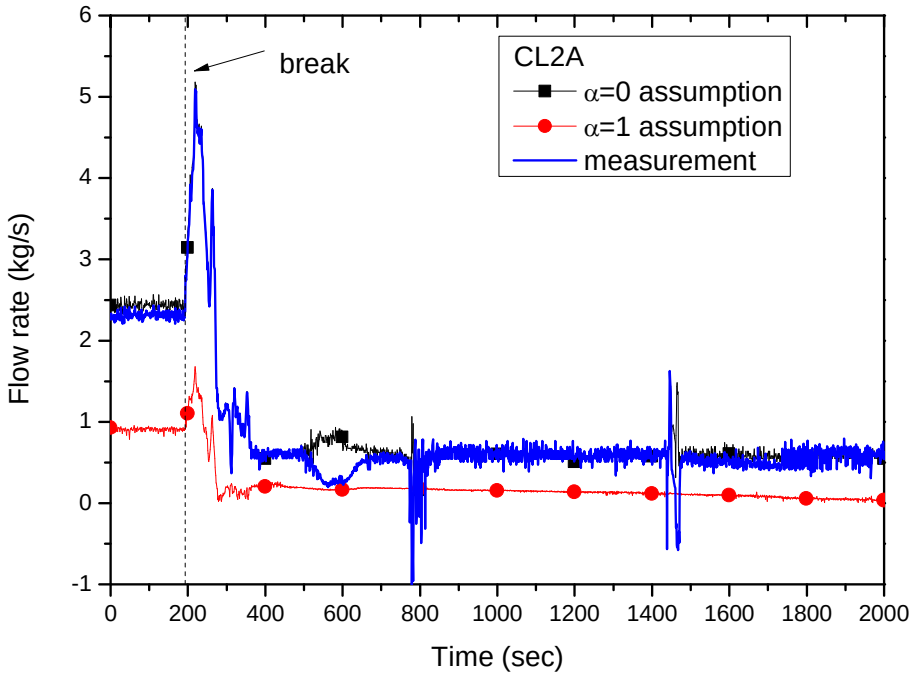

Figure 3.5-25 Cold leg flow rate in loop CL-2A

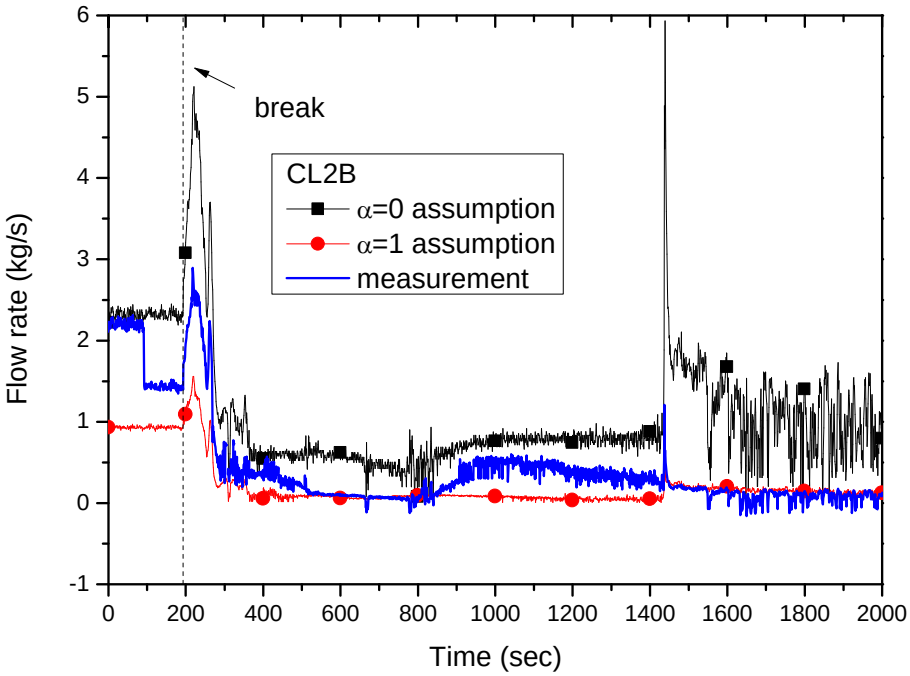

Figure 3.5-26 Cold leg flow rate in loop CL-2B

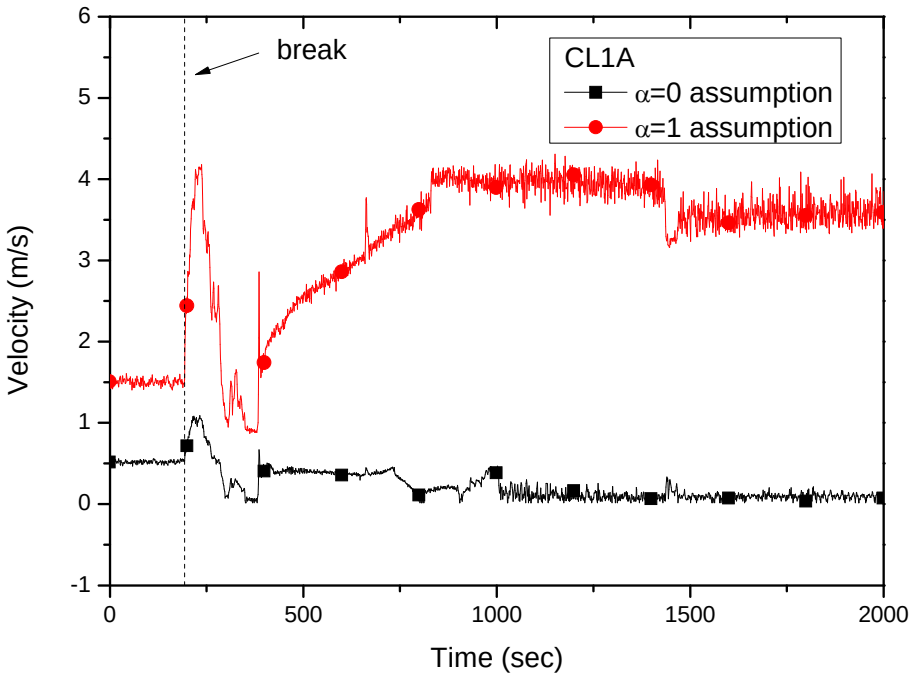

Figure 3.5-27 Cold leg fluid velocity in loop CL-1A

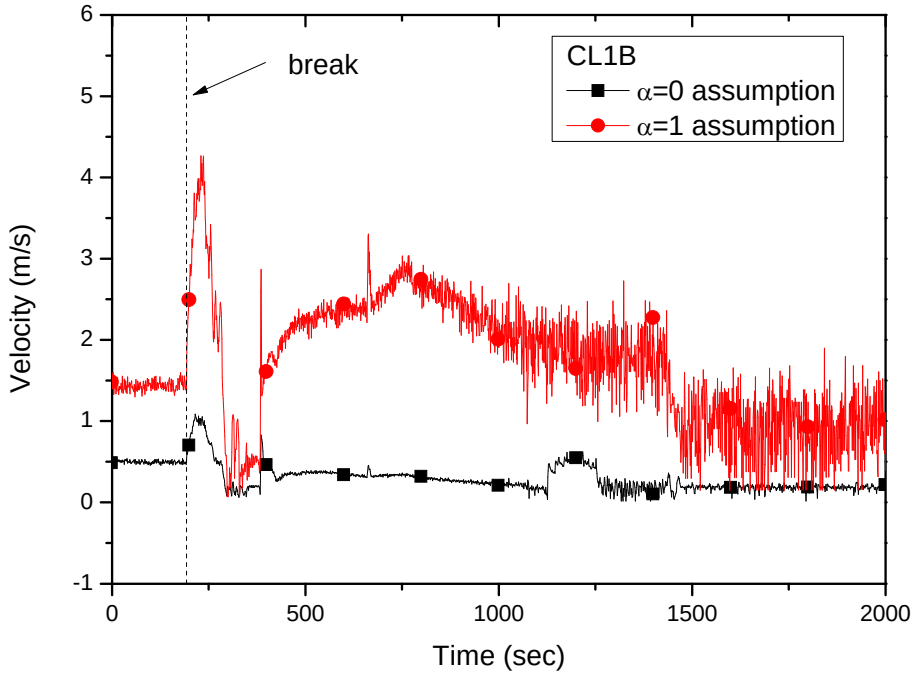

Figure 3.5-28 Cold leg fluid velocity in loop CL-1B

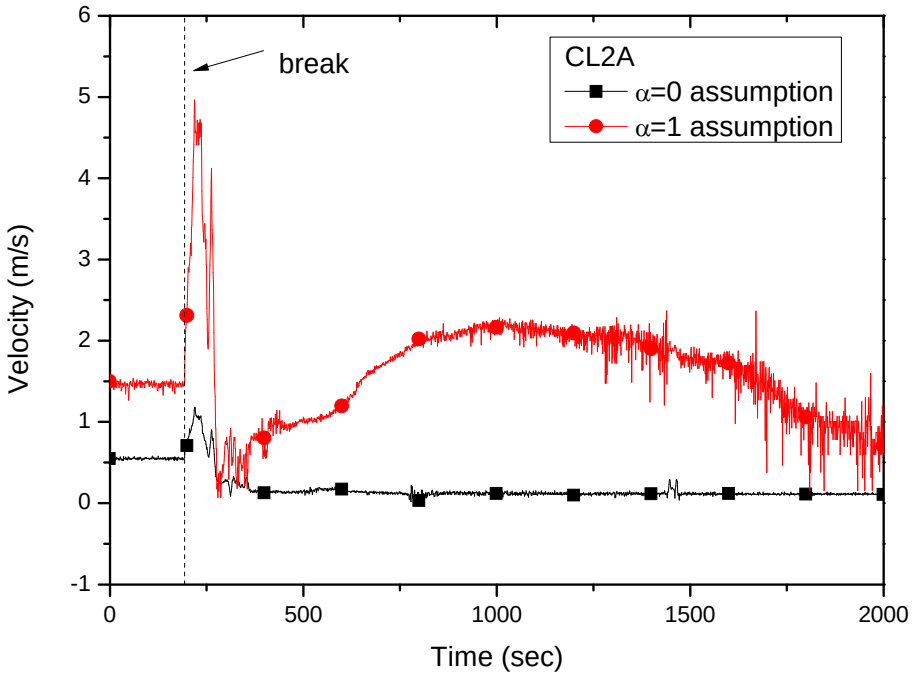

Figure 3.5-29 Cold leg fluid velocity in loop CL-2A

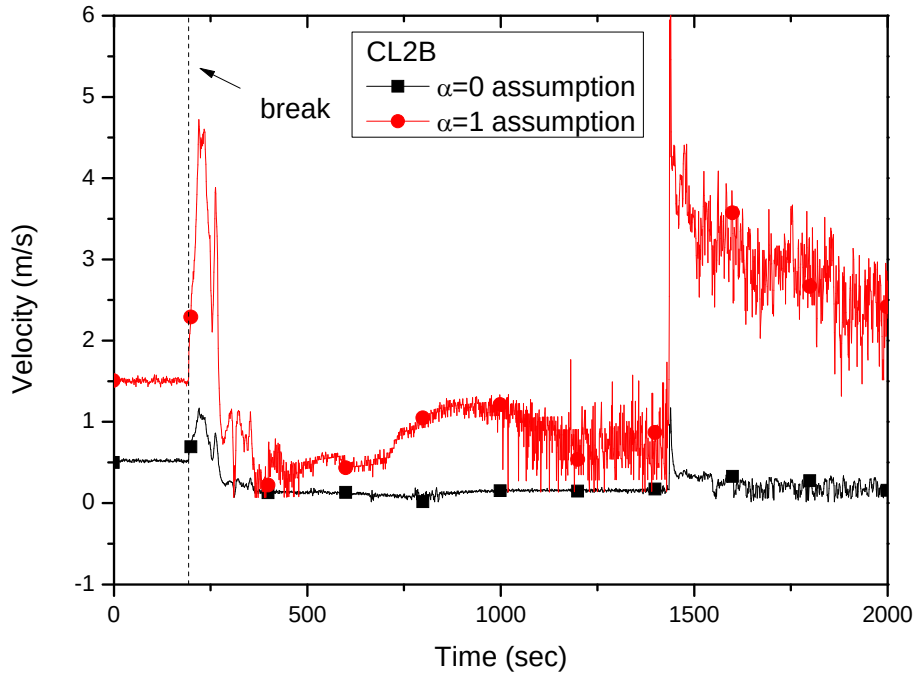

Figure 3.5-30 Cold leg fluid velocity in loop CL-2B

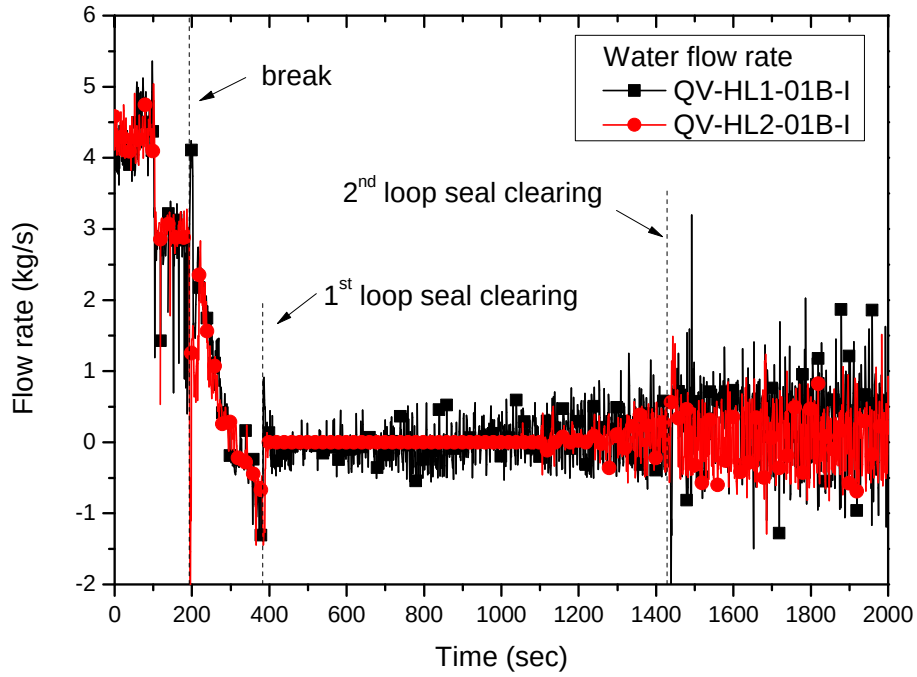

Figure 3.5-31 Measured water flow rates in hot legs

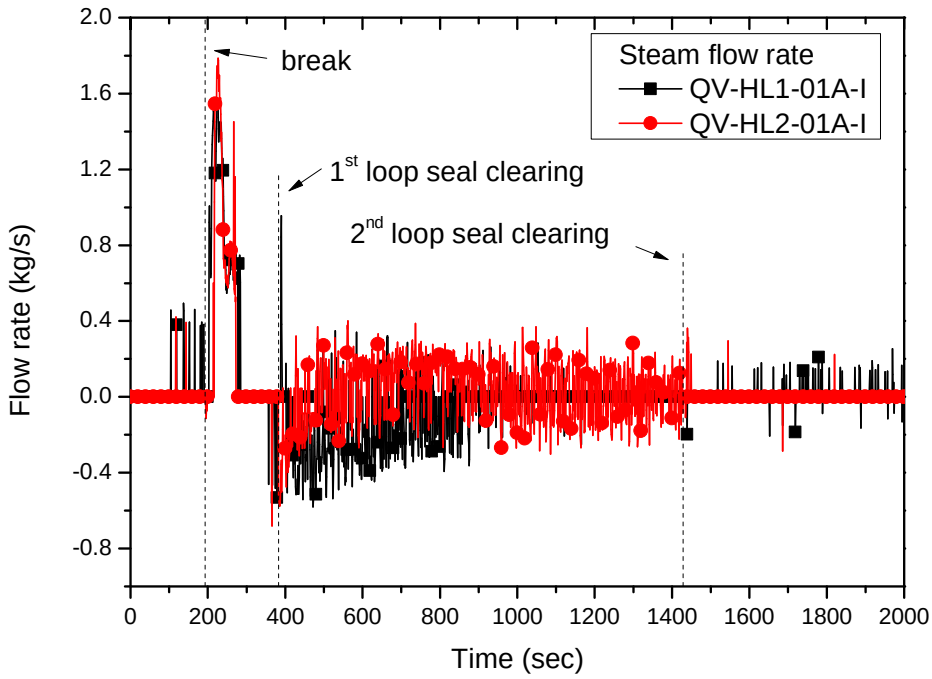

Figure 3.5-32 Measured steam flow rates in hot legs

3.5.6 Break flow

A containment simulator of the ATLAS plays a role of maintaining a pre-specified containment pressure during the transient. It also functions as a measuring system of the break flow. A configuration of the containment simulator is shown in Figure 3.5-33.

The pressures and temperatures at the upstream and the downstream of the break spool piece were measured simultaneously. Variations of the pressures both upstream and downstream of the break spool piece are shown in Figure 3.5-34 along with the temperature trends. Choking was maintained throughout the test period due to the considerable pressure difference across the break nozzle. A ratio of the downstream to the upstream pressures of the break spool piece decreases to a value less than 0.6 within a few seconds after the break. The pressure ratio continuously decreased to 0.2 at about 400 s and maintained almost constant value after 1000 s. A subcooled break flow was observed in the early period of the test, but it rapidly converted to a saturated two-phase choking flow. After keeping for a short period of time the state, the two-phase choking was changed to a single-phase steam choking flow after around 364 s and it was maintained at a single-phase choking condition during the remaining test period.

In the ISP-50 test, the total break flow rate was obtained by using the measured data of QV-CS-03, LC-CS-01 and LC-CS-02, and, as a complementary method to the load cell-based break flow measuring method, a RCS inventory-based break flow estimation method was also applied. Measured total break flow characteristics was shown in Figure 3.5-35. A separating vessel was equipped in the containment simulator to separate the two phase flow into steam flow and water flow for convenience of measuring flow rate. Once a two-phase break flow is introduced into the separating vessel, it was separated into steam and water within the separating vessel. Then the separated steam and water should be transported to each flow rate measuring system; the vortex flowmeter for steam and the load cell for water. In order to prevent water accumulation inside the separating vessel due to a swirling water flow, design optimization was made in the separating vessel to drain the separated water efficiently to the measuring vessel. The hemispheric bottom part of the separating vessel was reconstructed to be a cone-shape with an enlarged diameter and several rib-like plates were vertically installed inside the vessel to prevent the water swirling effect.

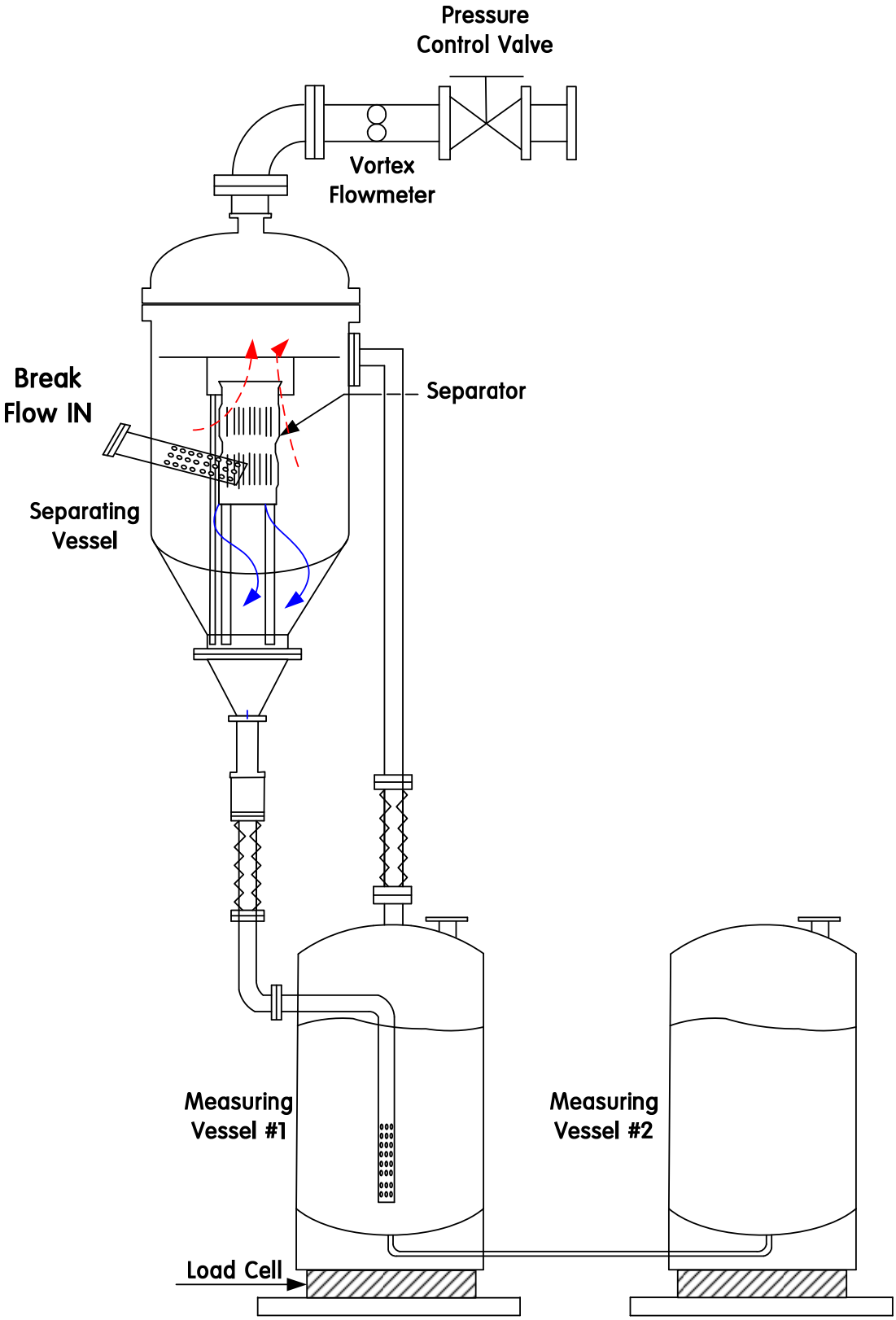

Figure 3.5-33 Containment simulator of the ATLAS

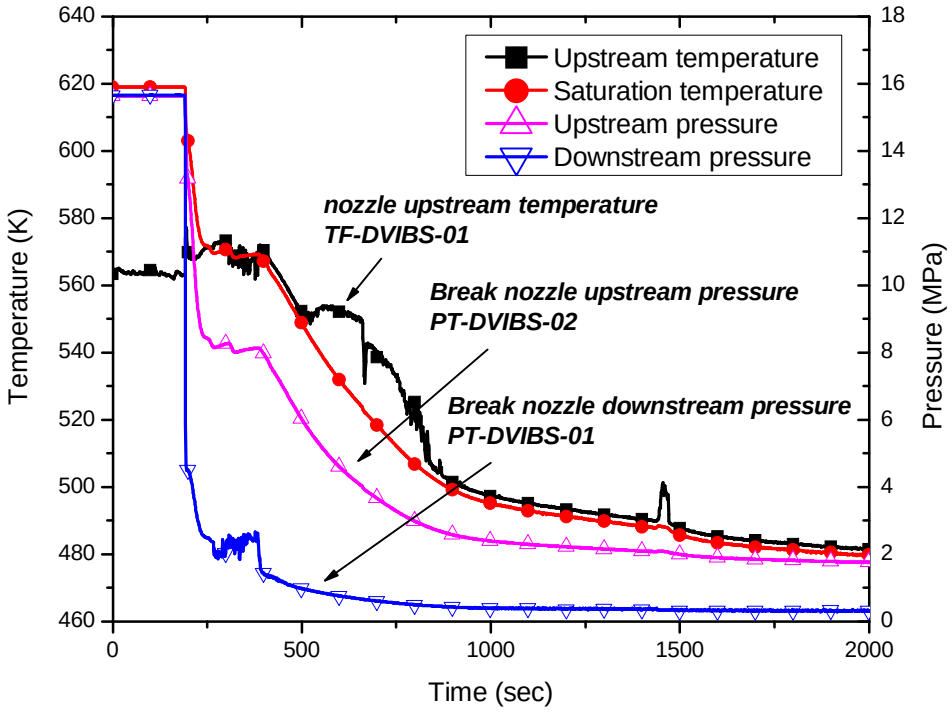

Figure 3.5-34 Pressure and temperature across the break nozzle

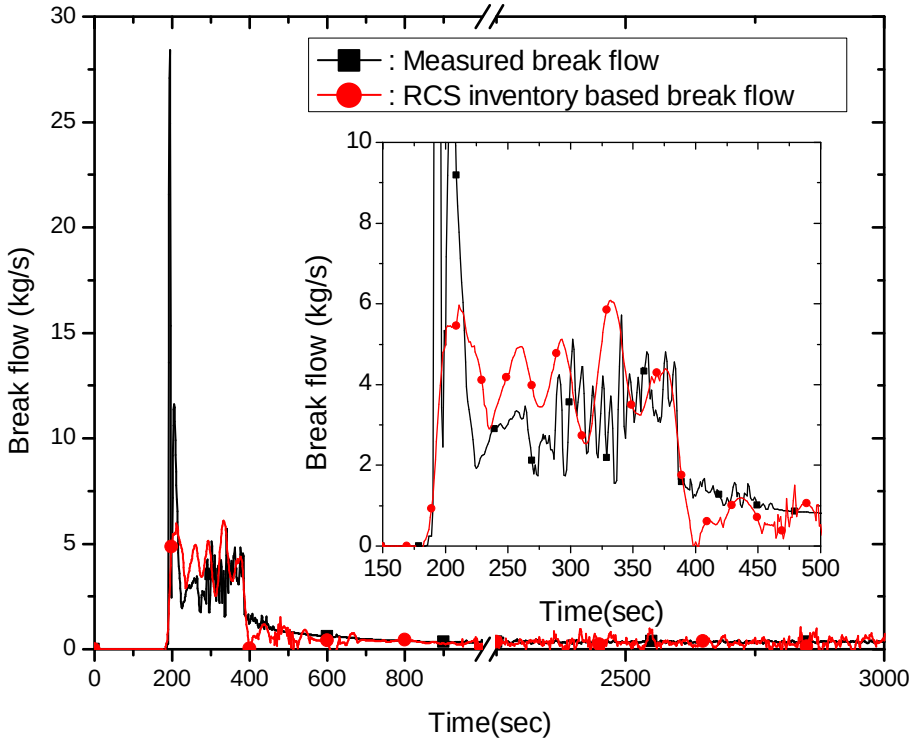

Figure 3.5-35 Measured total break flow rate comparison

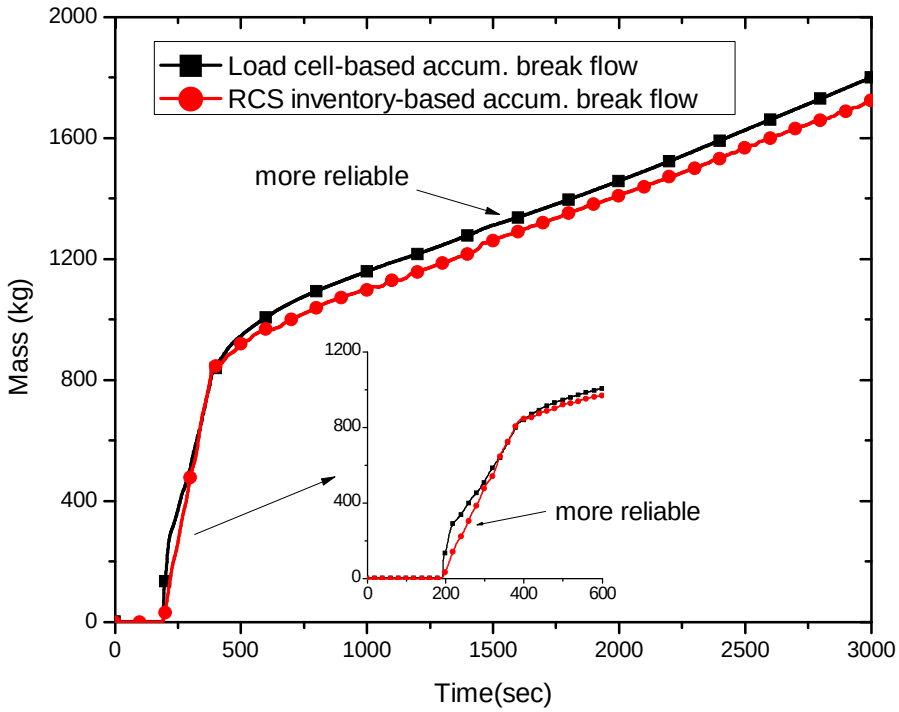

Figure 3.5-36 Accumulated break flow rate

As a complementary method to the load cell-based break flow measuring method, a RCS inventory-based break flow estimation method has been developed, which is based on a mass balance change rate in the RCS and the ECC injection flow rate during the progression of the break. The detailed description of this measurement method can be found in the literature [Choi *et al.*[4], 2009]. The RCS inventory-based break flow rate was plotted together with the load cell-based data in Figure 3.5-35. As shown in Figure 3.5-35, the break flow was relatively high and fluctuating during the earlier stage up to 364 s and maintained a low and steadier flow thereafter. The former was estimated from the RCS inventory change with a relatively higher uncertainty of 0.59 kg/s and the latter was measured by using the containment simulator (CS) with the relatively lower uncertainty of 0.07 kg/s. [Park *et al.*[3], 2010]

Overall, both measurements showed the similar trend during the entire test period except for the initial period. Initially, the load cell-based break flow rate was higher than the RCS inventory-based break flow rate. It was due to the fact that the load cell experienced an additional virtual load when a high break flow was introduced into the separating vessel, which resulted in higher break flow rate than real value. Therefore, the RCS inventory-based break flow rate can be considered to be more reliable than the load cell-based data especially in the very early period of the transient. The break flow rate was abruptly dropped to less than 1.0

kg/s at 383 s, where the first loop seal clearing occurred. When the loop seal was cleared, the upper down-comer region between the cold leg and the broken DVI nozzle was also cleared simultaneously. This clearing resulted in a change of the break flow characteristics from a single- phase water flow to a two-phase flow with high void fraction. The collapsed water level at the upper down-comer region in Figure 3.5-47 shows this phenomenon clearly. At 383 s, the water level abruptly decreased from unity to almost zero. Thereafter, the break flow rate continuously decreased during the remaining test period.

Accumulated break flow rate is plotted in Figure 3.5-36. The load cell-based data show more or less higher values than the RCS inventory-based data. The increasing gradient became smaller after the loop seal was cleared. Taking into account measurement uncertainties of two measuring methods, load cell-based and RCS inventory-based method, it has been concluded that the RCS inventory-based measurement is more reliable than the load cell-based measurement in the early blow down period up to 364 s. However, the load cell-based measurement is more reliable during the remaining test period. Therefore, a hybrid break flow data has been obtained by combining the RCS inventory-based data with the load cell-based data at time of 364 s in order to provide reliable data for break flow. Resulting figures for the break flow and the accumulated break flow are shown in Figure 3.5-37 and Figure 3.5-38. Note that the large-amplitude oscillation between 200 s and 400 s in Figure 3.5-37 comes from the uncertainty of the RCS inventory method to obtain the break flow rate.

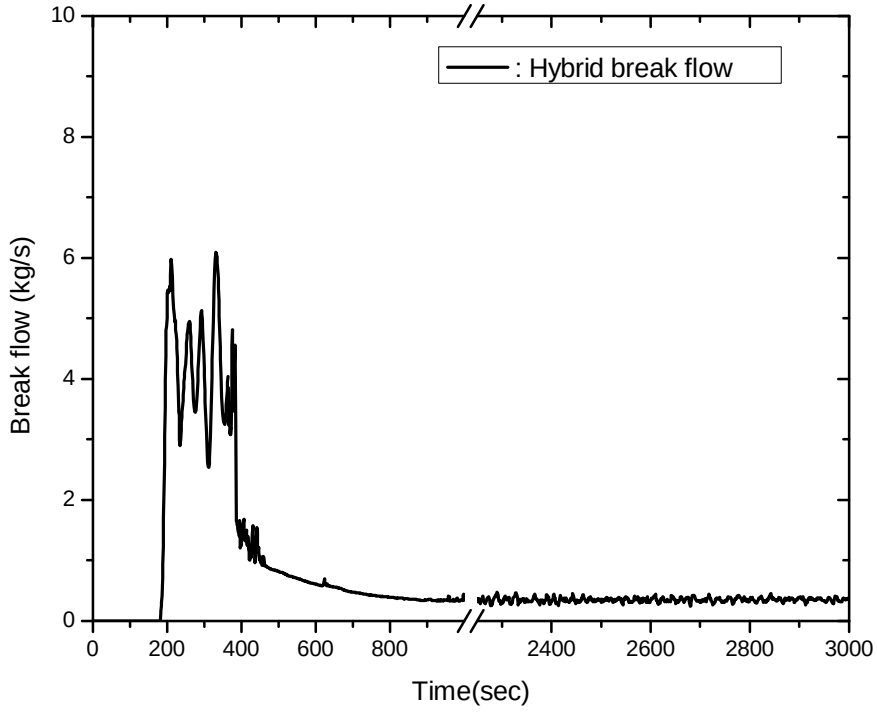

Figure 3.5-37 Final hybrid break flow rate

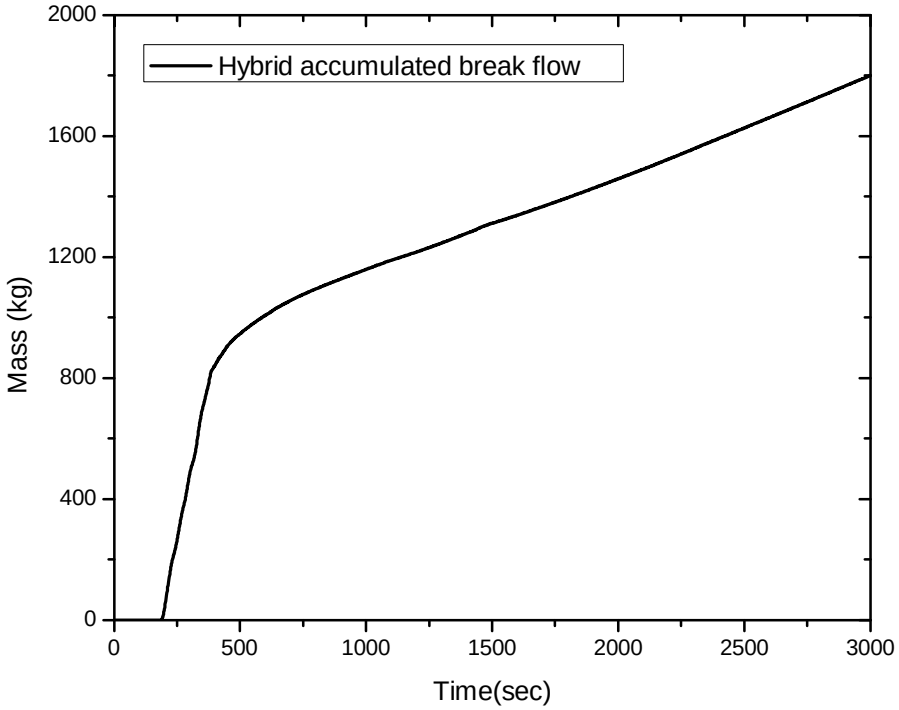

Figure 3.5-38 Final hybrid accumulated break flow

3.5.7 Safety injection flow

In the present test, two safety injection sources were used: one from a SIP and the other one from three SITs. The safety injection flow rate from the SIP was introduced into the RPV through the DVI-2 nozzle opposite to the broken nozzle. The flow rate was controlled as a function of a down-comer pressure, PT-DC-01. A functional relationship between the down-comer pressure and the flow rate in a table format is shown in Table 3.4-1 in the previous section. The flow rate was obtained by scaling down the values of the APR1400 according to the scaling law. Actuation of the SIP was triggered by a LPP signal with a delay time of 28.3 s. Actual flow rate by the SIP was plotted in Figure 3.5-39. During the period between 258 and 286 s, there was a temporary drop in the flow rate as seen in the figure. It was attributed to a spurious leakage of a control valve located at a DVI-3 line, the leaked water was not injected into the RPV because an isolation valve upstream the DVI-3 nozzle was maintained to be close during this period. Instead, the leaked flow was transported to an unused pipeline. The leaked water inventory was estimated to be about 2.1kg by extrapolating the measured safety injection flow curve in Figure 3.5-39. Thus, this inventory loss in the safety injection flow rate was deemed not to affect the transient significantly.

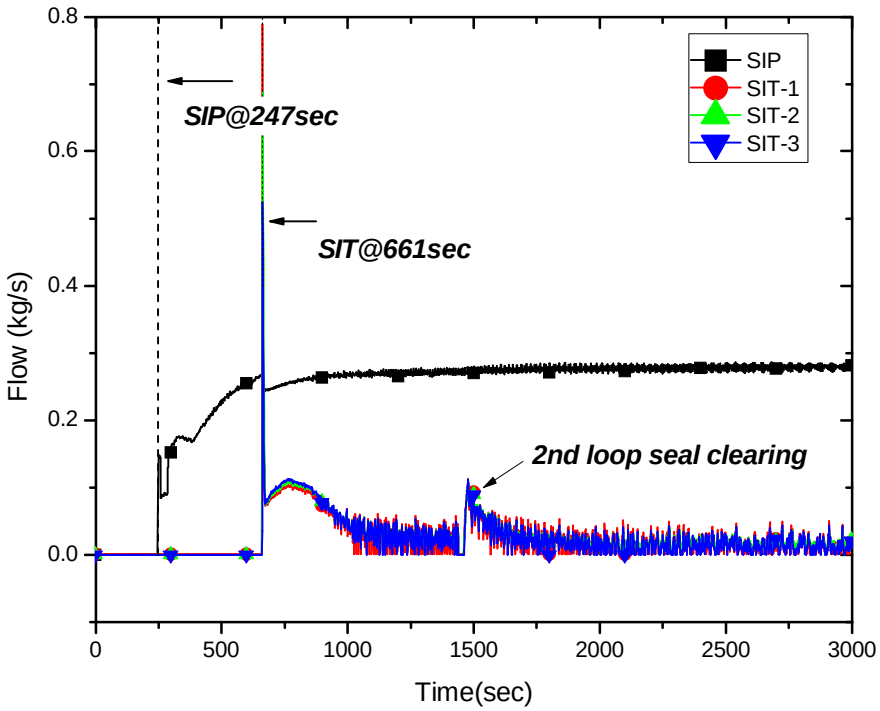

Figure 3.5-39 Measured ECC water flow rate

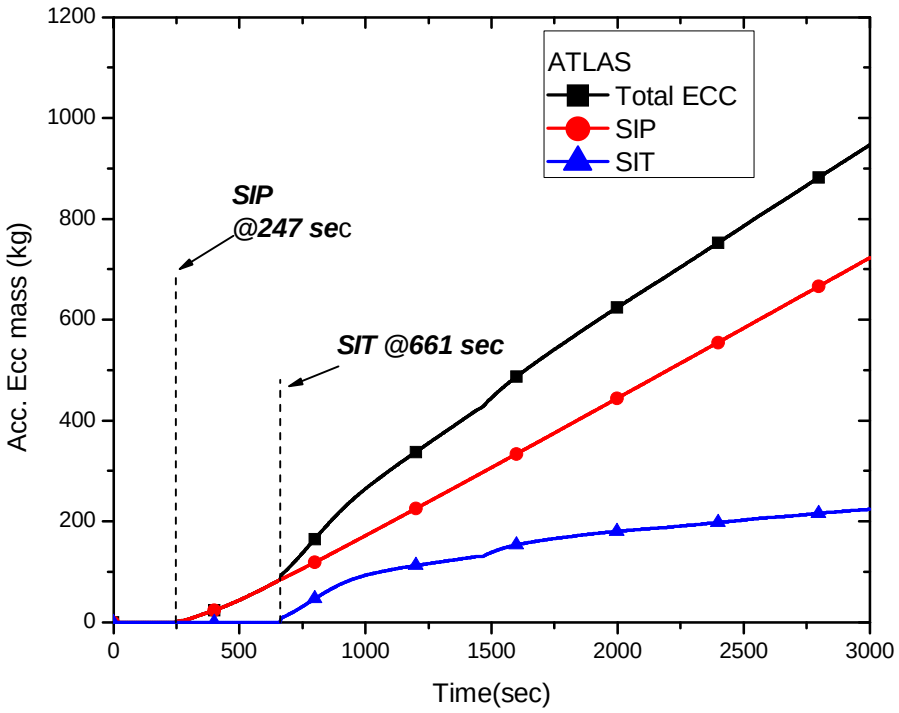

Figure 3.5-40 Accumulated ECC flow rate by one SIP and three SITs

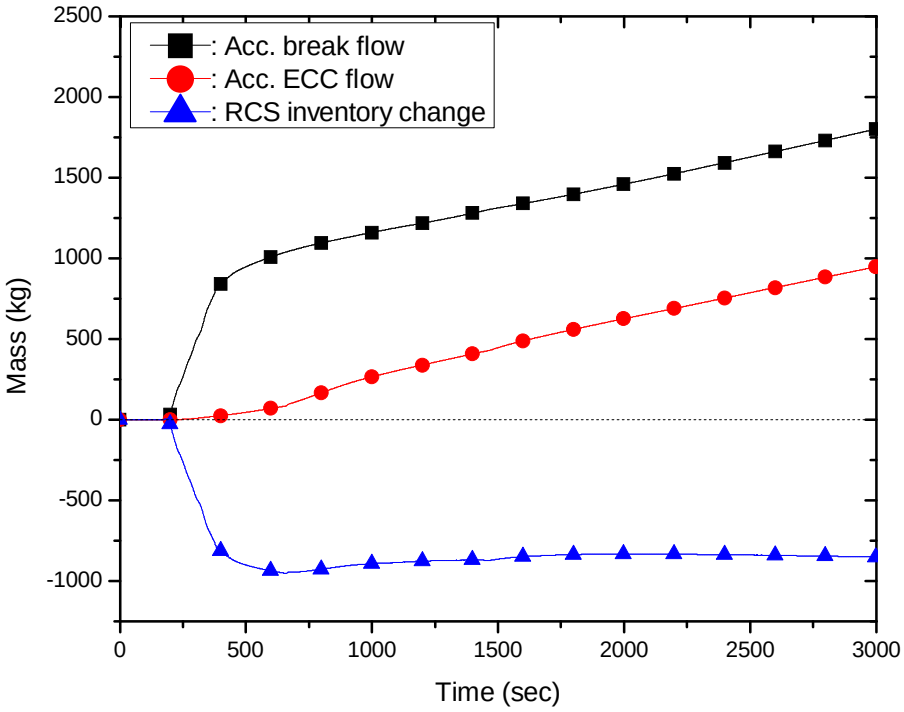

Figure 3.5-41 Primary inventory change during the test

The safety injection flow rates by three SITs were also plotted in Figure 3.5-39. Three SITs started to supply water into the corresponding intact DVI nozzles at 661 s: DVI-1, DVI-2, and DVI-3. The water flow rate injected by each SIT was almost the same with each other. The flow rate gradually decreased with respect to time, but increased again at 1429 s. This change is related to the second loop seal clearing behavior occurred at that time. Once the upper down-comer region between the DVI nozzle and the cold leg was cleared for the first time at 383 s (the first loop seal clearing), the annulus down-comer region started to be filled with water again in a very slow manner. When the water accumulated in the region reached a certain level, the water in the region was again cleared (the second loop seal clearing). At that time, the flow rate injected by the SITs suddenly increased because the region was occupied again with condensable steam. The accumulated ECC flow during the test was plotted in Figure 3.5-40. The change of the primary inventory during the test is shown in Figure 3.5-41. This graph was plotted with the measured break flow as well as the measured ECC flow. Initially, the primary inventory decreased due to the break flow but thereafter maintained almost the same value by the injected ECC water.

3.5.8 Collapsed water levels in the RPV core

The RPV was extensively instrumented to measure collapsed water levels including the core and the down-comer regions. Detailed locations of the level transmitters are shown in Figure 3.5-42. The measured collapsed water level of the core region is shown in Figure 3.5-43. It was based on a wide-range instrument, LT-RPV-01 of the core region. On break, the water level decreased to the middle of the active core region. When the first loop seal was cleared, the water level was recovered, but was maintained thereafter at around 2.0 m. The second loop seal clearing evoked another increase in the core water level as shown in Figure 3.5-43. More detailed sectional water level was plotted in Figure 3.5-45. The measuring range of the LT-RPV-01 was sub-divided into eight fine instruments: LT-LP-02, LT-CO-01, LT-CO-02, LT-CO-03, LT-CO-04, LT-CO-05, LT-CO-06, and LT-CO-07. Two-phase mixture level was measured based on these eight level transmitters. The collapsed water level of the active core region was measured by six instruments from LT-CO-01 to LT-CO-06. The center elevation of the horizontal intermediate leg is 662 mm below the top of the active core. Before the first loop seal clearing at 383 s, it can be seen from Figure 3.5-45 that water levels from LT-CO-07, LT-CO-06 and LT-CO-05 decreased to zero. This measurement indicates that two-phase mixture level was around the elevation somewhere LT-CO-04 was located. Thus, it is evident that the core was uncovered before the first loop seal clearing. The core uncovering period was estimated to be about 25 s from the figure. The first loop seal clearing resulted in recovery of all water levels. The second loop seal clearing at 1429 s also affected the core water levels but its effect was not so significant compared with the first loop seal clearing.

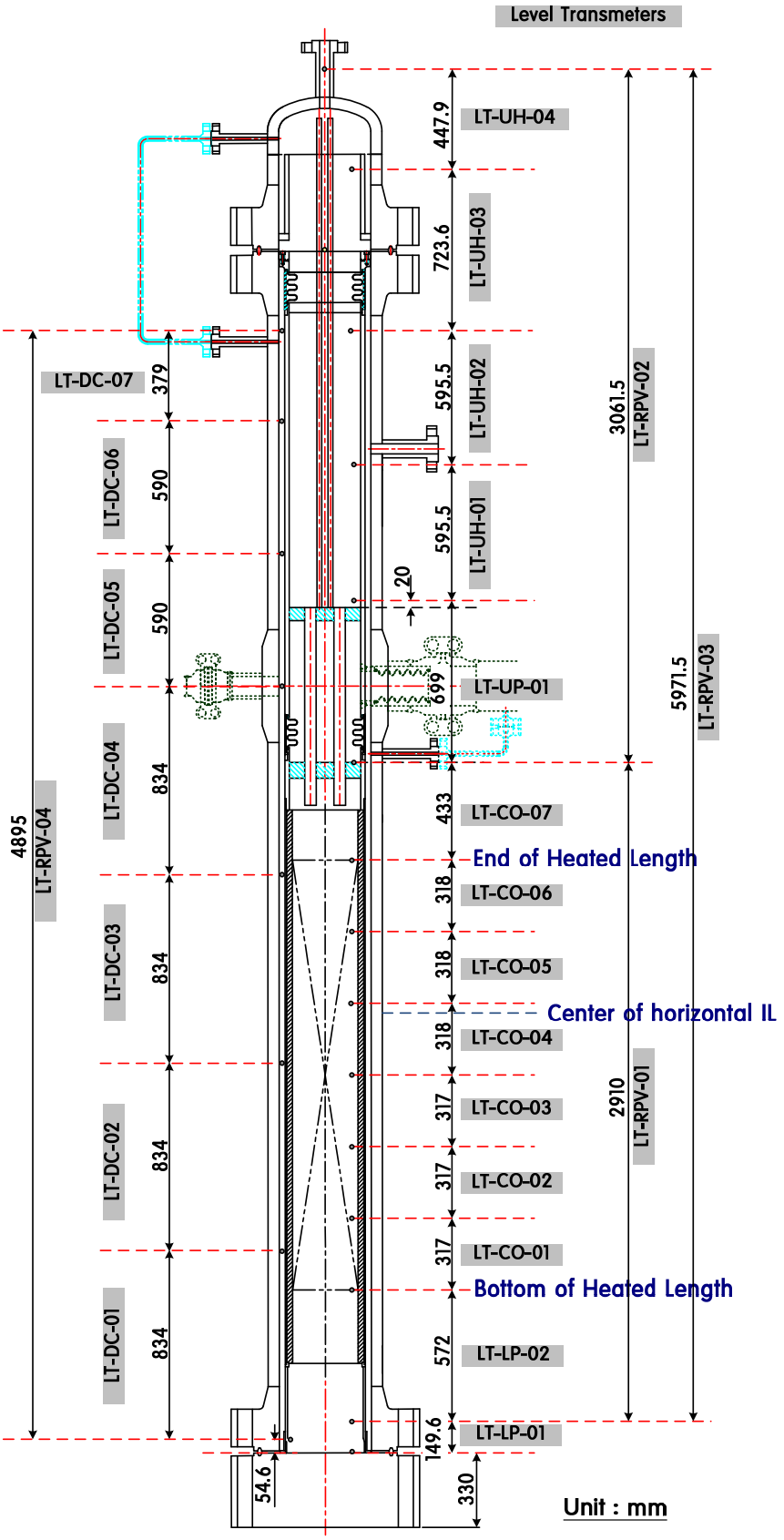

Figure 3.5-42 Level transmitters in the RPV

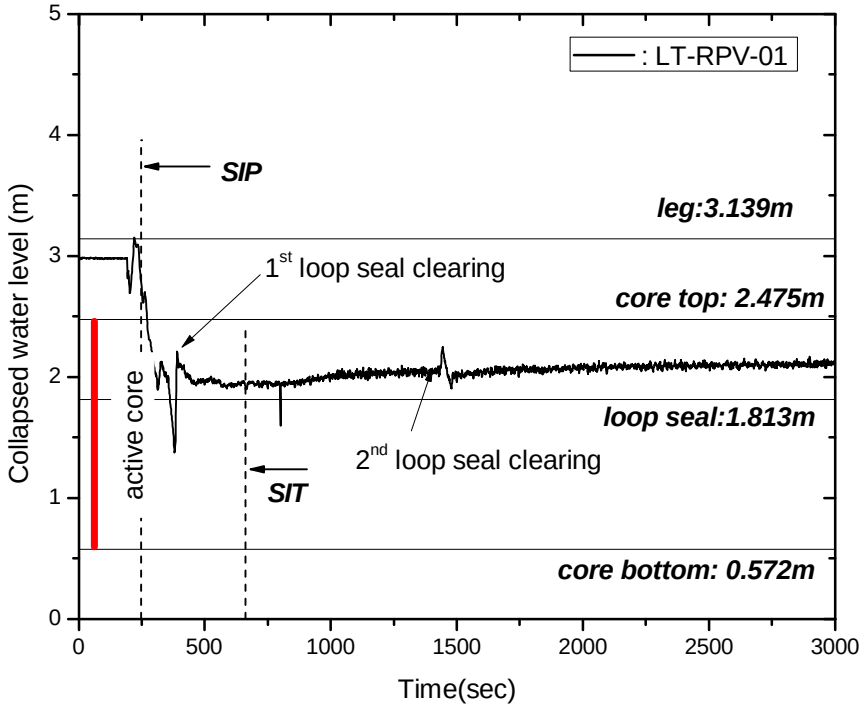

Figure 3.5-43 Measured collapsed water level of the core region

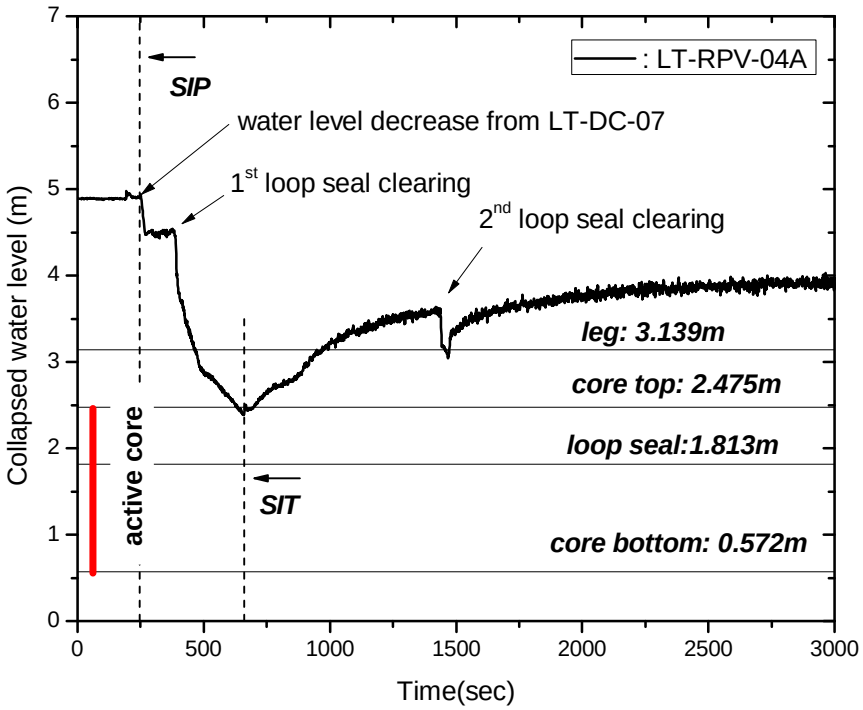

Figure 3.5-44 Measured collapsed water level of the RPV down-comer region

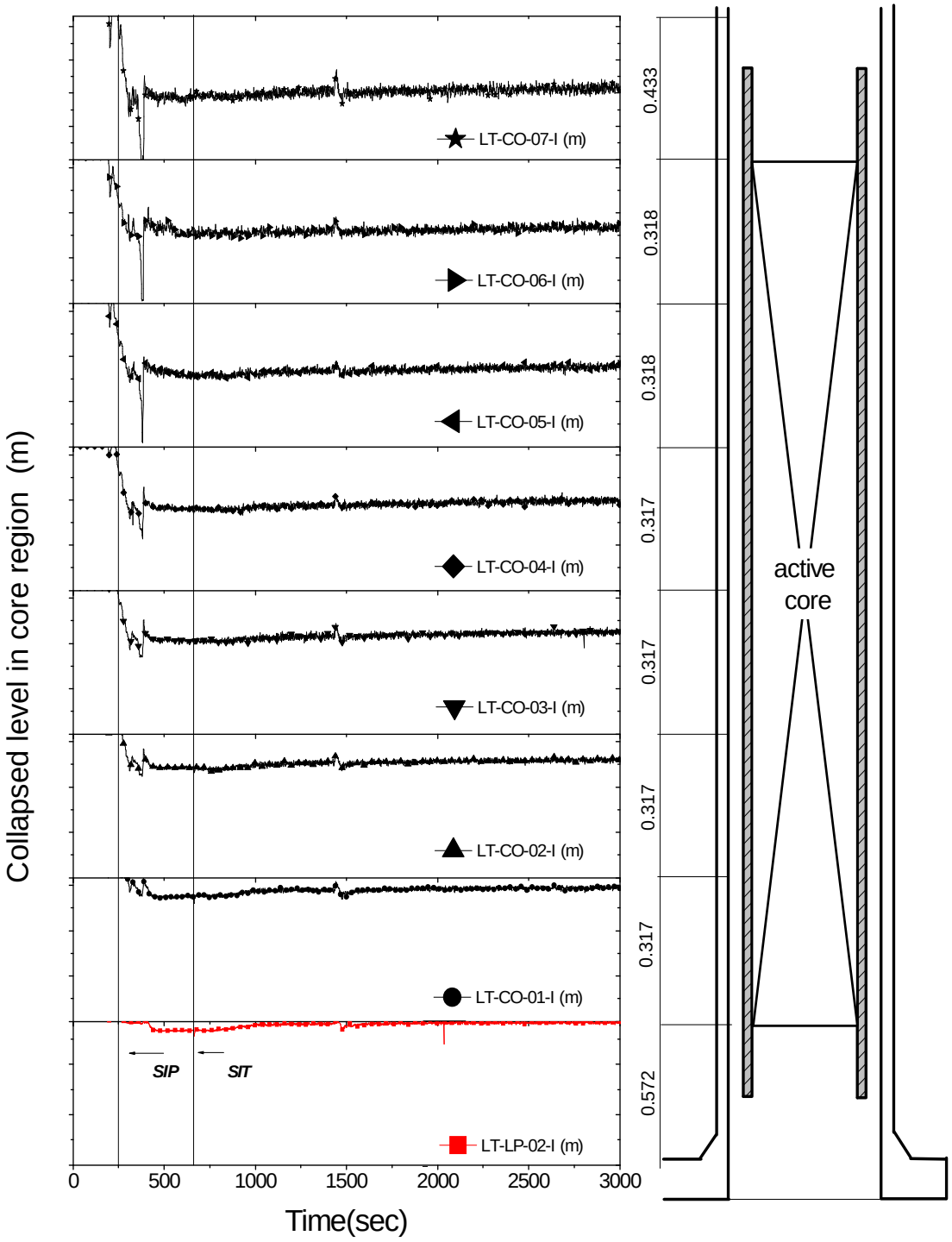

Figure 3.5-45 Sectional collapsed water level of the core region

3.5.9 Collapsed water levels in the RPV upper head

The collapsed water levels in the upper plenum and the upper head are shown in Figure 3.5-46. The detailed locations of the instruments can be found in Figure 3.5-42. On break, the water levels rapidly decreased to zero within a short time. It can be found that the RPV was drained from the top in due sequence though there were temporal increases in the water levels of LT-UH-01 and LT-UH-02. These temporal increases in the water levels were due to measurement uncertainties caused by the changes in local fluid velocity. The water level, LT-UP-01 showed an initially high depression and then a smooth decrease with respect to time.

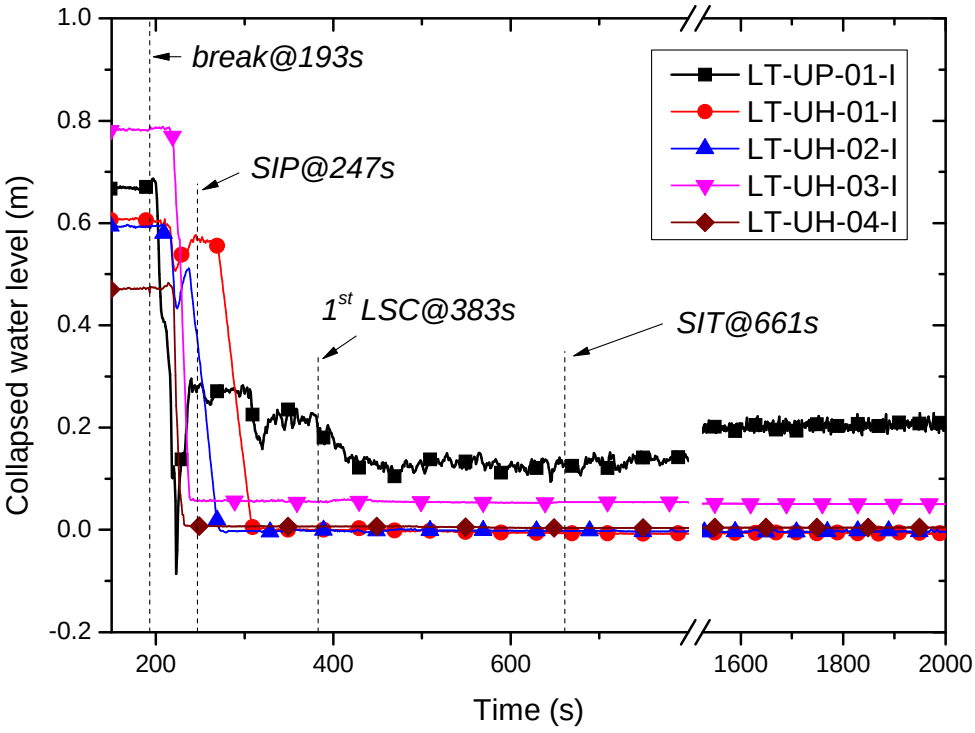

Figure 3.5-46 RPV upper head collapsed water level

3.5.10 Collapsed water levels in the RPV down-comer

The collapsed water level of the down-comer region of the RPV is shown in Figure 3.5-44. This data was based on a wide-range instrument, LT-RPV-04A of the down-comer region. It covered almost all the down-comer region excluding the upper head region. The water level from LT-RPV-04A should be equal to sum of the sectional water levels from LT-DC-01 to LT-DC-07. On break, the collapsed water level of the upper head first started to decrease and then the LT-DC-07 started to decrease. However this decrease ceased when the water level reached a certain elevation corresponding to the DVI nozzle and the collapsed water level

maintained a constant level until the occurrence of the 1st loop seal clearing. During this period, the injected ECC water from the SIP was discharged through the broken DVI nozzle, nevertheless the water level in the core continuously decreased due to boil-off.

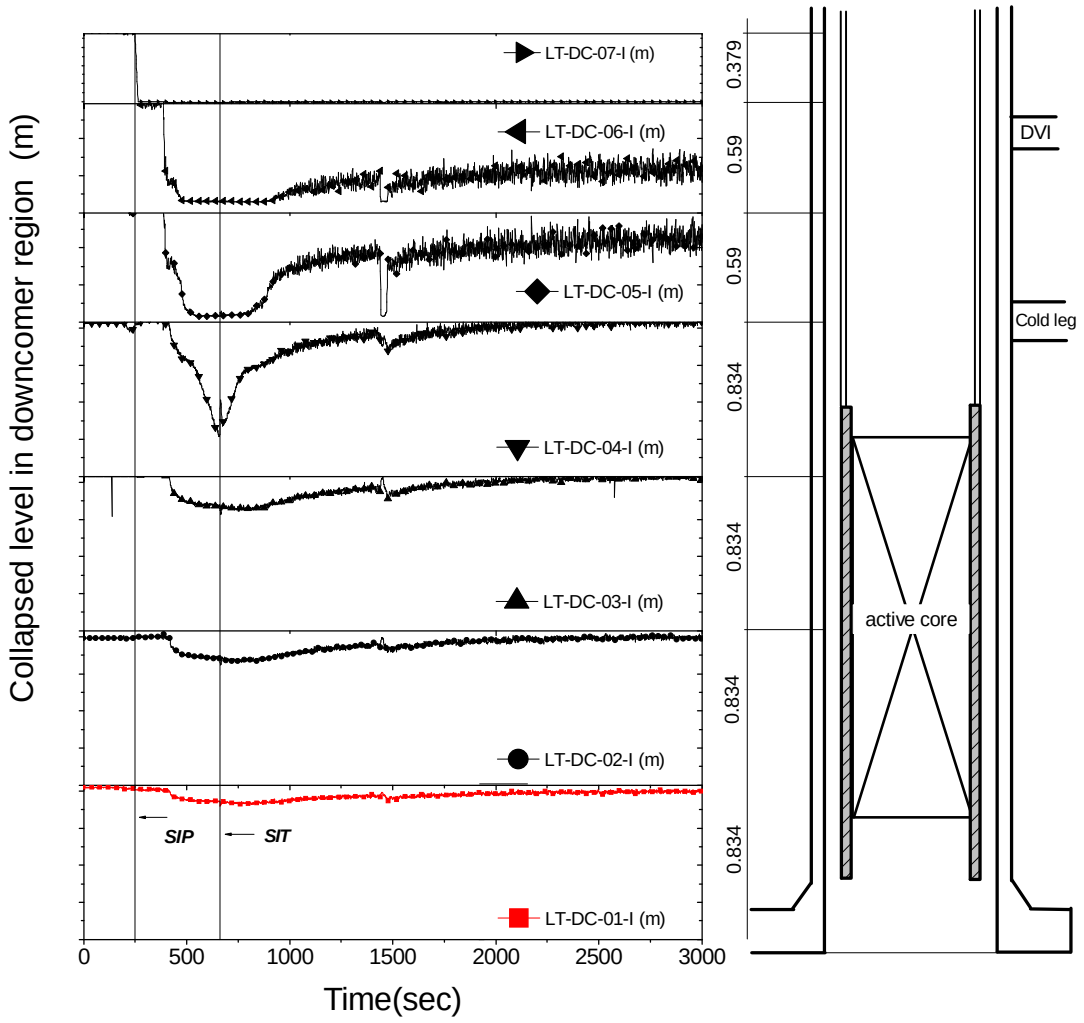

Figure 3.5-47 Sectional collapsed water level of the RPV down-comer region

It can be seen that the water level started to rapidly decrease from the time of the first loop seal clearing to the actuation of SITs. The second loop seal clearing also caused a sudden decrease in the water level. Afterwards the water level continuously increased during the remaining test period due to ECC water injection. More detailed behavior in the down-comer region can be found from Figure 3.5-47. The axial region measured by LT-RPV-04A was divided into seven level transmitters from LT-DC-01 to LT-DC-07. The first loop seal clearing evacuated most water in the down-comer region between the cold leg and the DVI nozzle. At the actuation time of the SITs, the two-phase mixture level can be inferred to be below the cold leg elevation. The second loop seal clearing again evacuated most water in the down-comer region

as shown in Figure 3.5-47. However, the evacuated down-comer region was filled with water within a very short time due to the injected safety water from the SITs. After around 2000 s, the down-comer water level was maintained at almost the same value. Two-phase mixture level was inferred to be around the DVI nozzle elevation.

3.5.11 Fluid temperatures in the RPV core

Measured fluid temperatures in the RPV during the test period were investigated. Figure 3.5-48 shows the transient behavior of core inlet and exit temperatures. The core inlet temperature is based on the measurement of the instrument, TF-LP-02G18, which is located 278mm below the heated region of the active core. The rod where the thermocouple is installed can be found in the G18 sub-group of Figure 3.5-2. The core exit temperature is an averaged value of the four measured temperatures, TF-CO-07-G14, TF-CO-07-G18, TF-CO-07-G21, and TF-CO-07-G25. These thermocouples are located 222 mm above the heated region of the active core. On break, the core exit temperature suddenly increased up to 604 K and then decreased as shown in Figure 3.5-48. On the other hand, the core inlet temperature maintained almost constant value before the first loop seal clearing. The increase in the core exit temperature in the beginning period of the break is due to a decrease in the axial water velocity along the core region. More detailed fluid temperature behavior inside the core region can be seen in Figure 3.5-49. This figure shows the axial fluid temperature profile measured inside the active core region. All nine instruments were installed at the same heater rod located in G18 sub-group. The core power was maintained at constant value during the period from the break time (t=193 s) to the decay power initiation time (t=232 s). On break, the fluid temperatures above the elevation higher than 794mm from the bottom of the heated region suddenly increased up to a certain maximum. The difference in the temperature rise along the axial locations was due to the chopped cosine power profile. The temperature rise in the middle region of the heated section was the largest because the core power in the middle of the active core was the largest there. The core fluid temperatures reached a maximum peak, and hereafter decreased. The saturation temperature based on the upper head pressure, PT-UH-01 was also plotted for comparison. The fluid temperatures were maintained in a sub-cooled condition as the upper head pressure decreased. The fluid temperatures at higher elevations were always larger than those at lower elevations, indicating that there was no flow reversal in the core region.

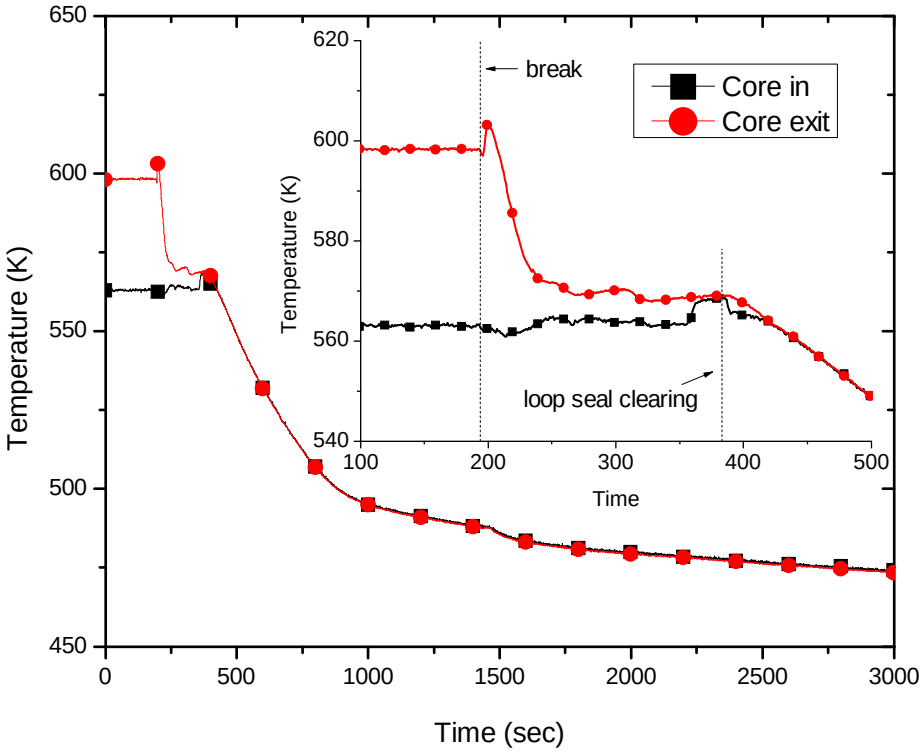

Figure 3.5-48 Core inlet and exit temperatures

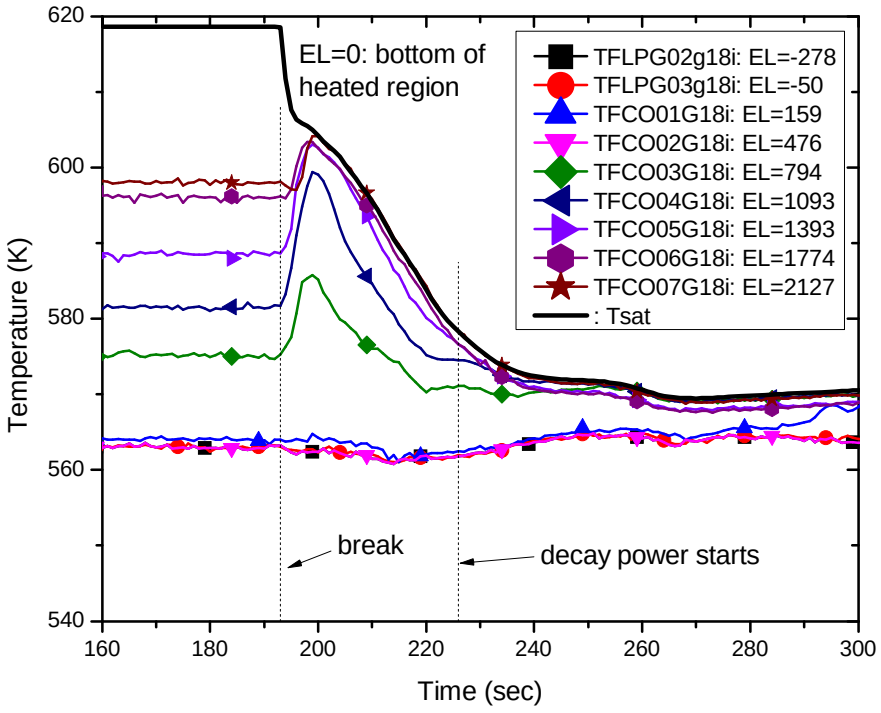

Figure 3.5-49 Core fluid temperature details

A lot of temperature sensors were installed in the RPV to measure fluid temperatures and wall temperatures. The fluid temperatures in the core upper plenum and head are shown in Figure 3.5-50. Locations of the installed temperature sensors are shown in Figure 3.5-51. Initially, the upper plenum fluid temperatures, TF-UP-01, TF-UP-02, and TF-UP-03 had almost the same value as that of the core exit temperature, TF-CO-07G18. However, the upper head temperatures, TF-UH-01, 02, 03, and 04 were a little smaller than the core exit temperature. When the break started, the upper plenum temperatures showed temporal increases caused by temporal decrease in the upward fluid velocity and then they became the same temperatures of the upper head. At around the time when the ECC water by the SIT was provided at 661 s, TF-UH-02 and TF-UH-03 increased abruptly and thereafter decreased mildly.

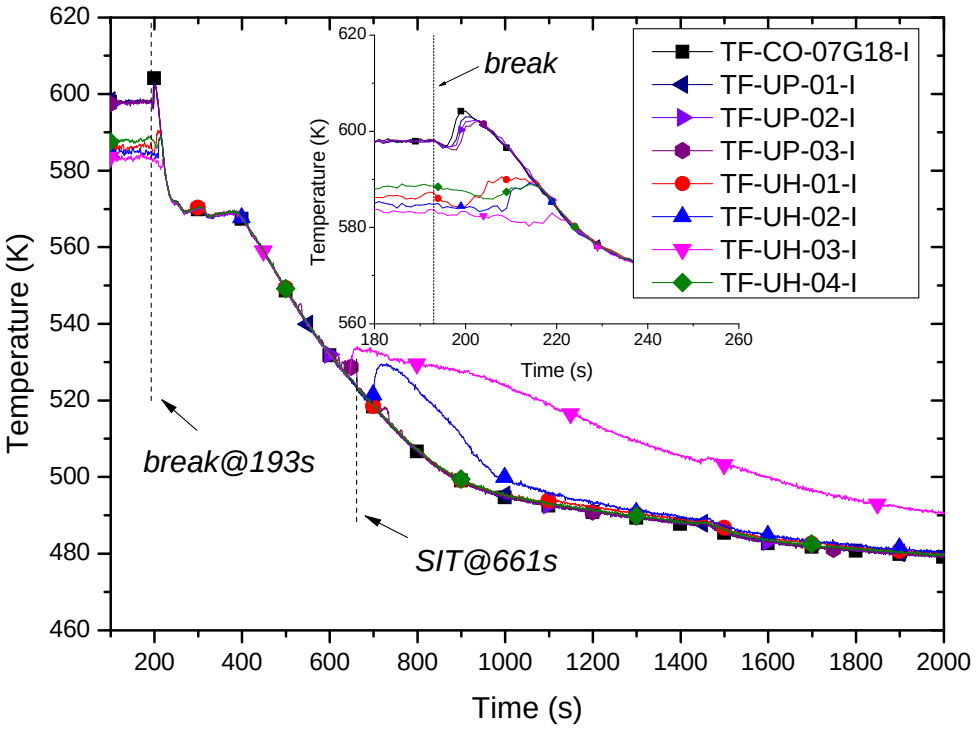

Figure 3.5-50 Core upper plenum and upper head fluid temperatures

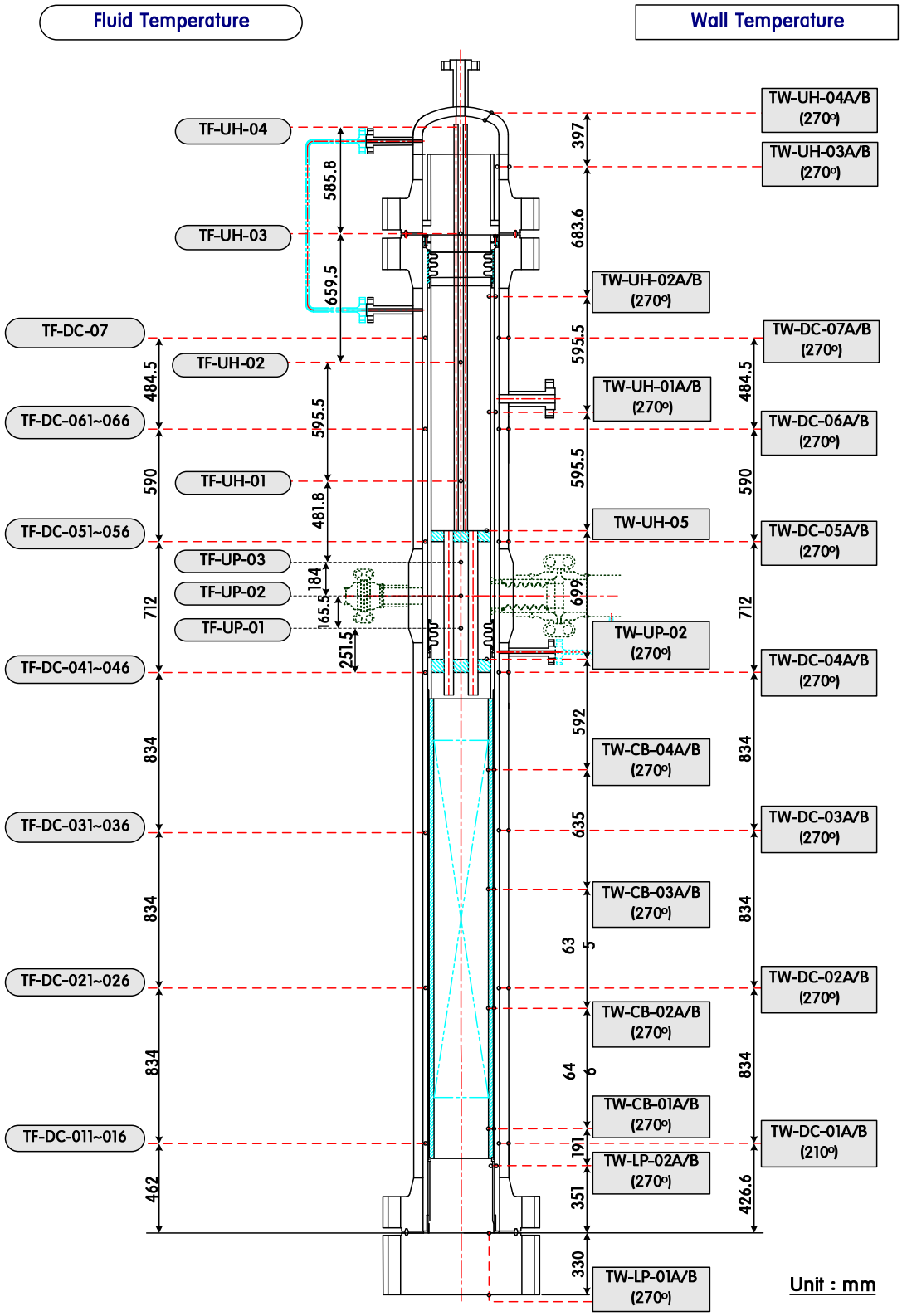

Figure 3.5-51 Locations of temperature sensors in RPV

3.5.12 Fluid temperatures in the RPV down-comer

Thermocouples were installed to measure the down-comer fluid temperatures at seven different axial levels. At each level, six thermocouples were uniformly installed in azimuthal direction except for TF-DC-07i at highest elevation where only one measurement at 300 degree of the azimuthal angle was available. Definitions of the azimuthal subsection the axial level and for the down-comer fluid temperatures analysis are shown in Figure 3.5-52 and Figure 3.5-53, respectively. An unfolded down-comer map to show six azimuthal subsections and seven axial levels can be found in Figure 3.5-54. Measured collapsed water levels at the seven axial levels were shown in Figure 3.5-47. The broken nozzle was located at level 6 between TF-DC-06i and TF-DC-07i and at the azimuthal angle of 45 degree in subsection 2.

There was no significant temperature variation at lower locations: from TF-DC-01i to TF-DC-04i. The temperatures maintained their initial values at about 566 K before the decay power started. Whereas, initial temperatures measured at higher elevations from TF-DC-05i to TF-DC-07i were about the average of the core inlet and exit temperatures, 577 K. After break, TF-DC-05i and TF-DC-06i suddenly decreased because the water at the lower down-comer region changed its flow direction and started to be discharged through the broken nozzle. TF-DC-07i located above the broken nozzle showed some oscillations just after the break. Axial distribution of the down-comer fluid temperature can be seen in Figure 3.5-55. When cold water was injected to the down-comer region from the safety injection pump, TF-DC061i and TF-DC-061i started to oscillate greatly whereas, the other temperature signals did not vary as much. This oscillation was due to complex mixing of the cold ECC water with the hot inventory in the down-comer region. In fact, the cold ECC water was introduced from the DVI nozzle 2 located opposite to the broken DVI nozzle 4. Thus, this location corresponds to the azimuthal angle of 240 degree as shown in Figure 3.5-54. Fluid temperature distribution along the azimuthal direction is plotted in Figure 3.5-56 and an enlarged figure prior to the loop seal clearing is shown in Figure 3.5-57. It is evident that temperatures measured at 5^{th} and 6^{th} elevations showed great oscillations. From the graph at 6^{th} elevation, it can be inferred that the cold ECC water propagates downward from the injection point after around 260 s.

In order to investigate the fluid temperature distribution in the down-comer region, two-dimensional contours on an expanded down-comer domain just after the break were plotted as shown in Figure 3.5-58 and Figure 3.5-59. Before the break, vertical temperature stratification was observed but the fluid temperature was uniform in the azimuthal direction. On break, great two-dimensional temperature distribution in the down-comer region was observed. The flow direction changed from downward to upward for the discharged fluid through the broken nozzle, DVI-04. Much fluid seemed to be directed to the broken nozzle.

Near the hot leg, blockage effects in the annulus down-comer region were also observed as shown in Figure 3.5-58 at time of 198 s.

When the ECC water from the SIP was injected at 247 s, the down-comer fluid temperature started to be mixed with the injected cold water. But, the substantial mixing started with some delay as shown in Figure 3.5-55. Thus, typical fluid mixing phenomena was plotted from 290 s to 305 s as shown in Figure 3.5-60. The cold water introduced from the DVI-2 nozzle can be seen in this figure.

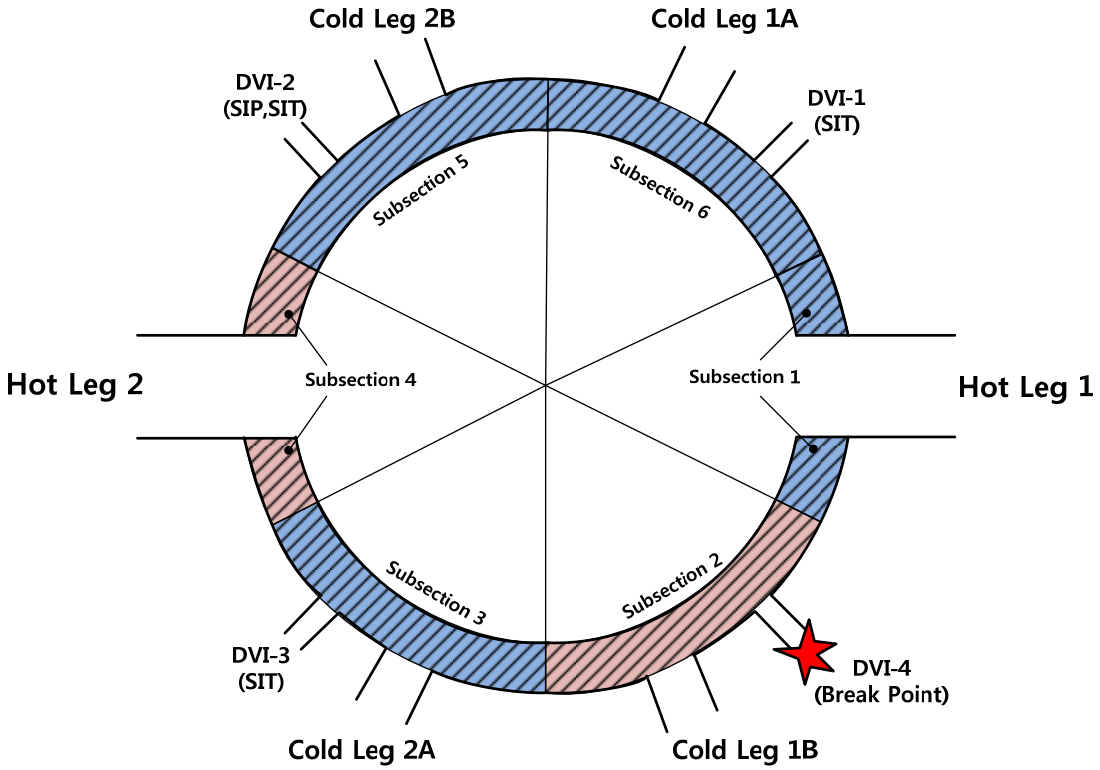

Figure 3.5-52 Definition of azimuthal subsections in the down-comer for comparison

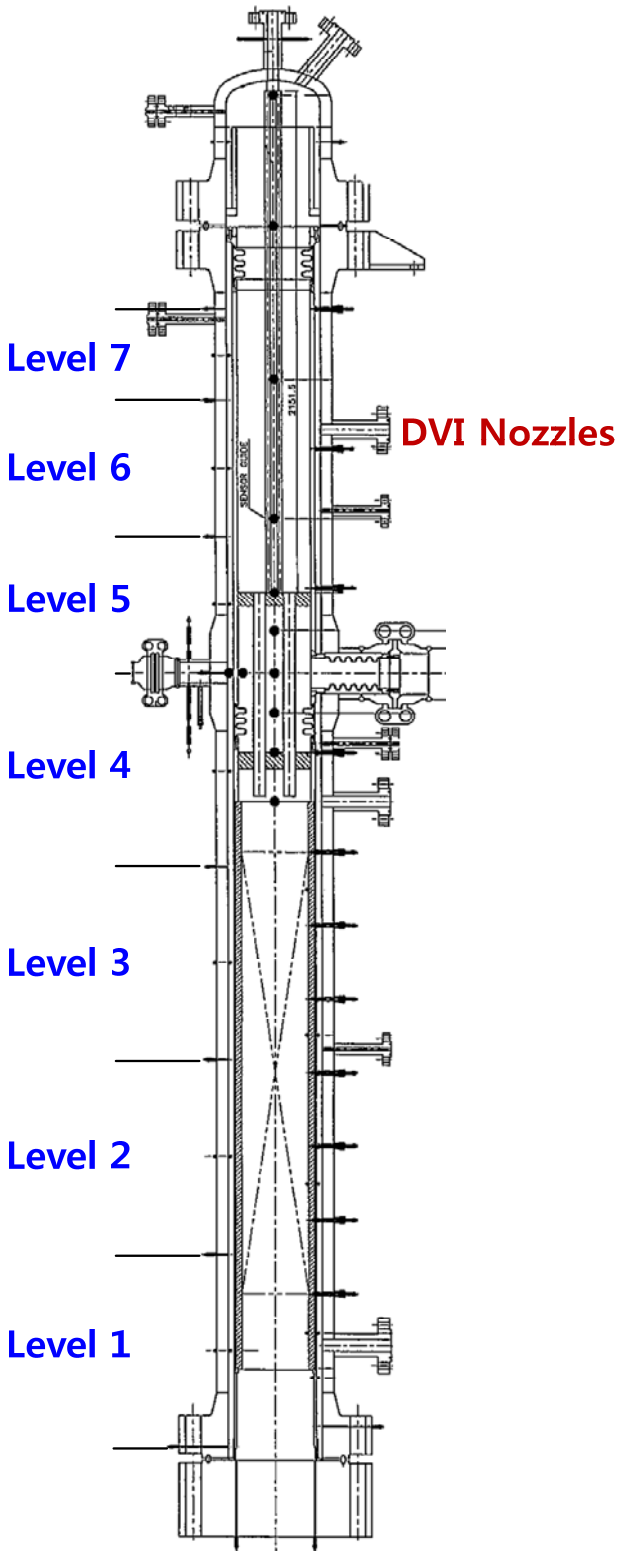

Figure 3.5-53 Definition of the down-comer levels for comparison

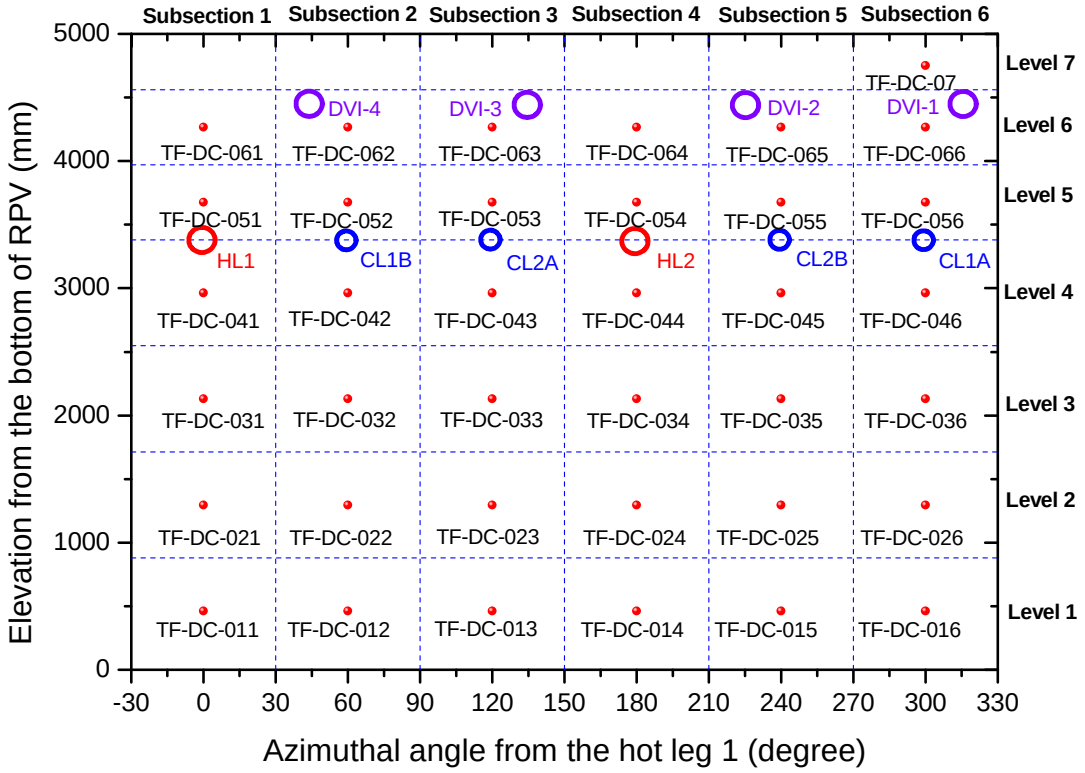

Figure 3.5-54 Detailed fluid temperature measurement locations in the down-comer

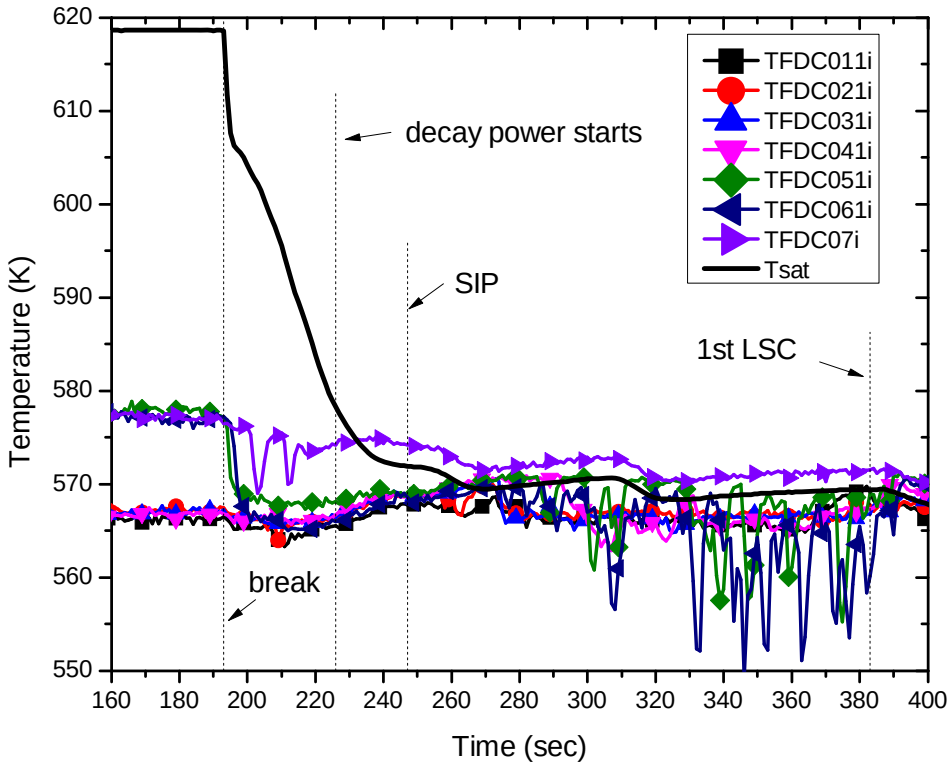

Figure 3.5-55 Axial distribution of down-comer fluid temperatures at azimuthal angle of 0.0

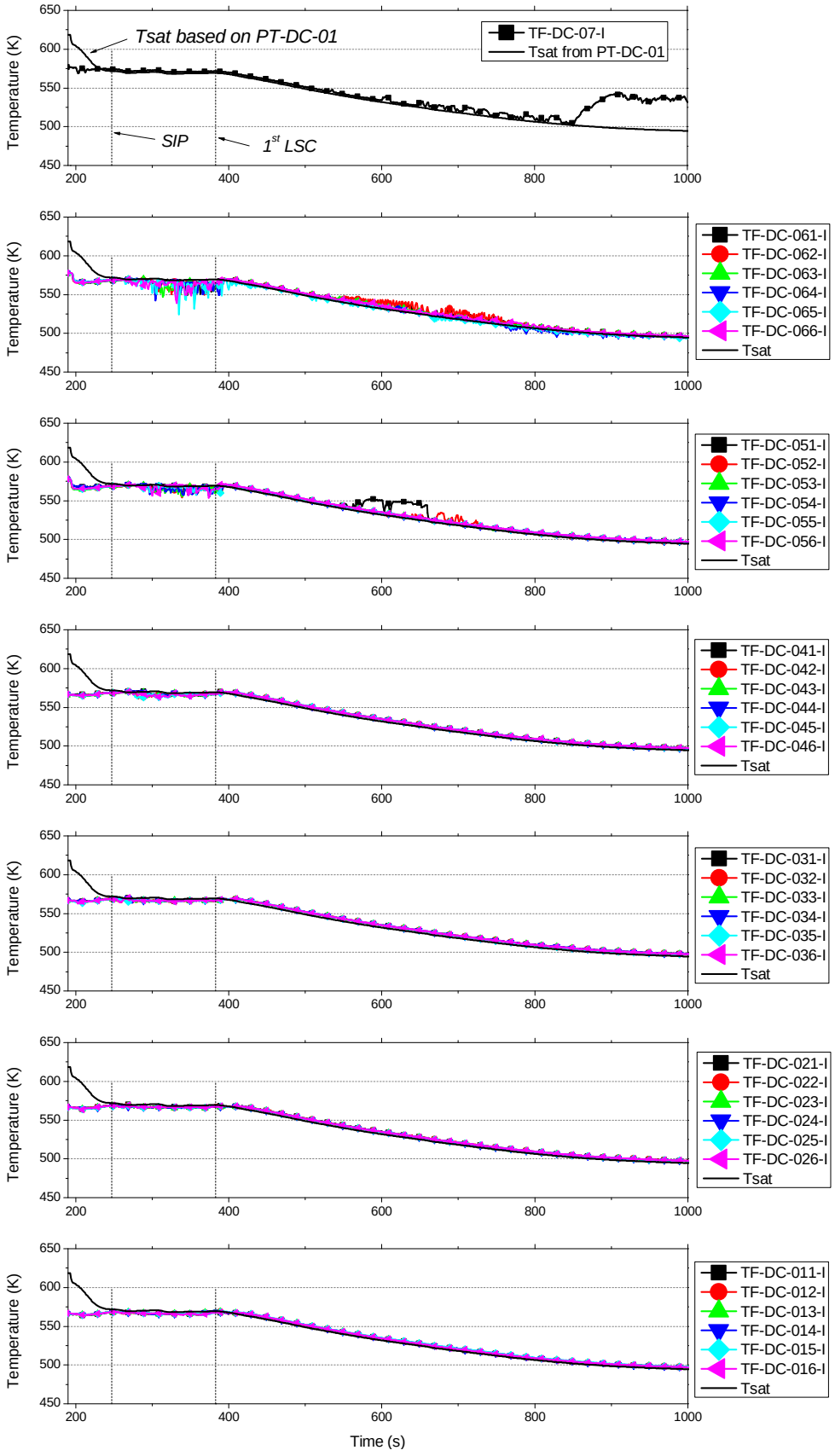

Figure 3.5-56 Azimuthal distribution of down-comer fluid temperatures up to 1000 s

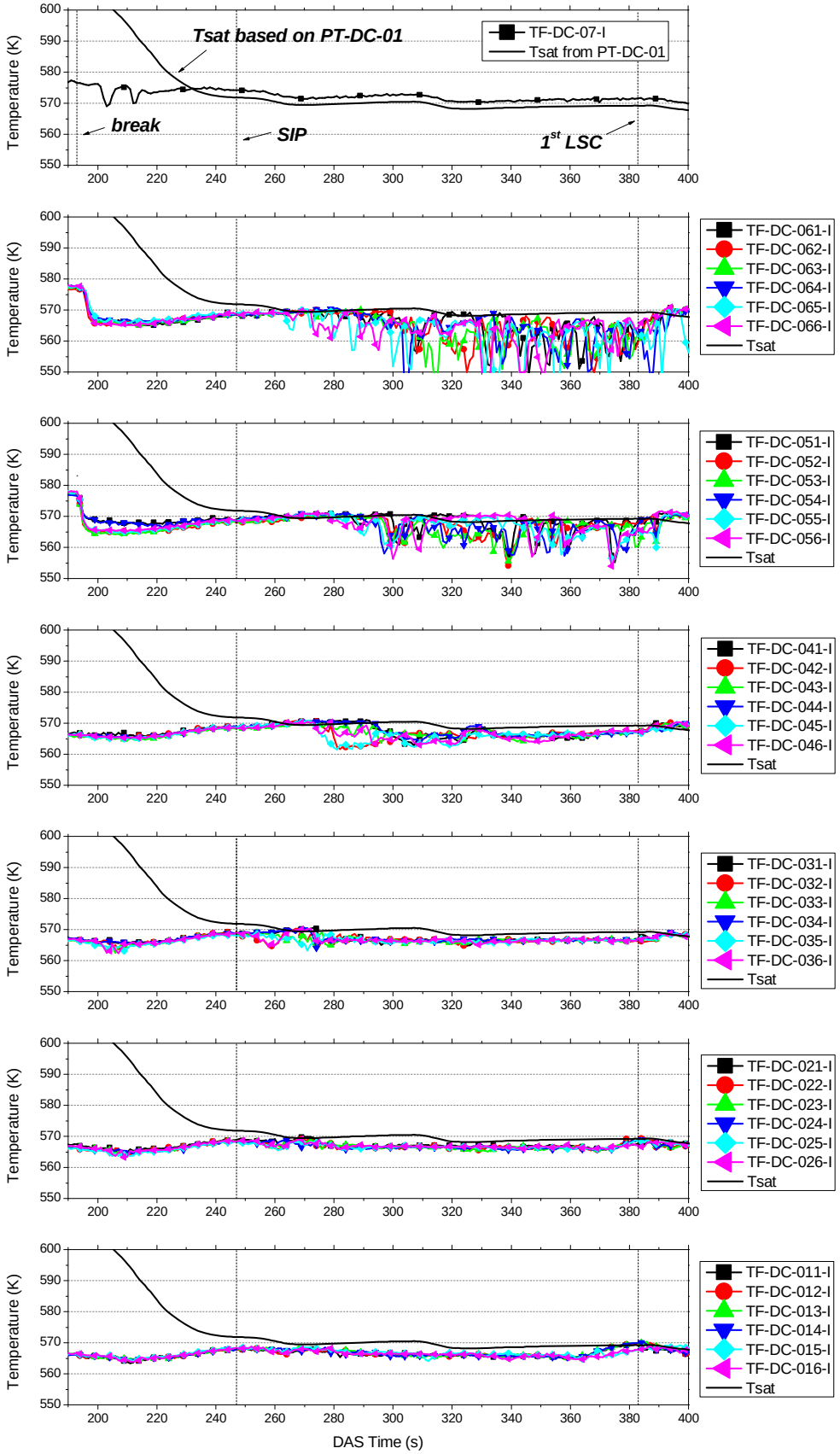

Figure 3.5-57 Azimuthal distribution of down-comer fluid temperatures up to 400 s

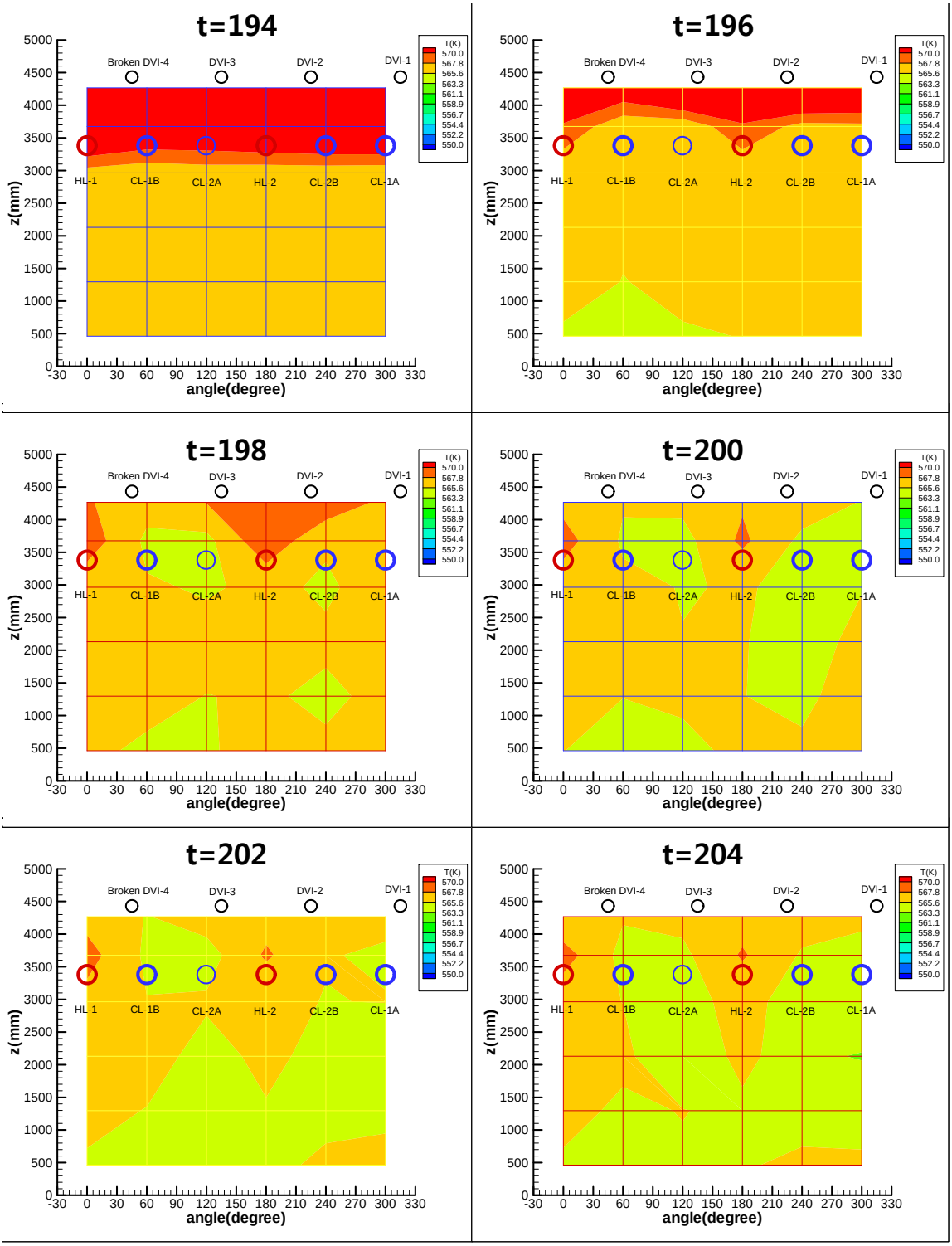

Figure 3.5-58 Fluid temperature contour in the down-comer region (1)

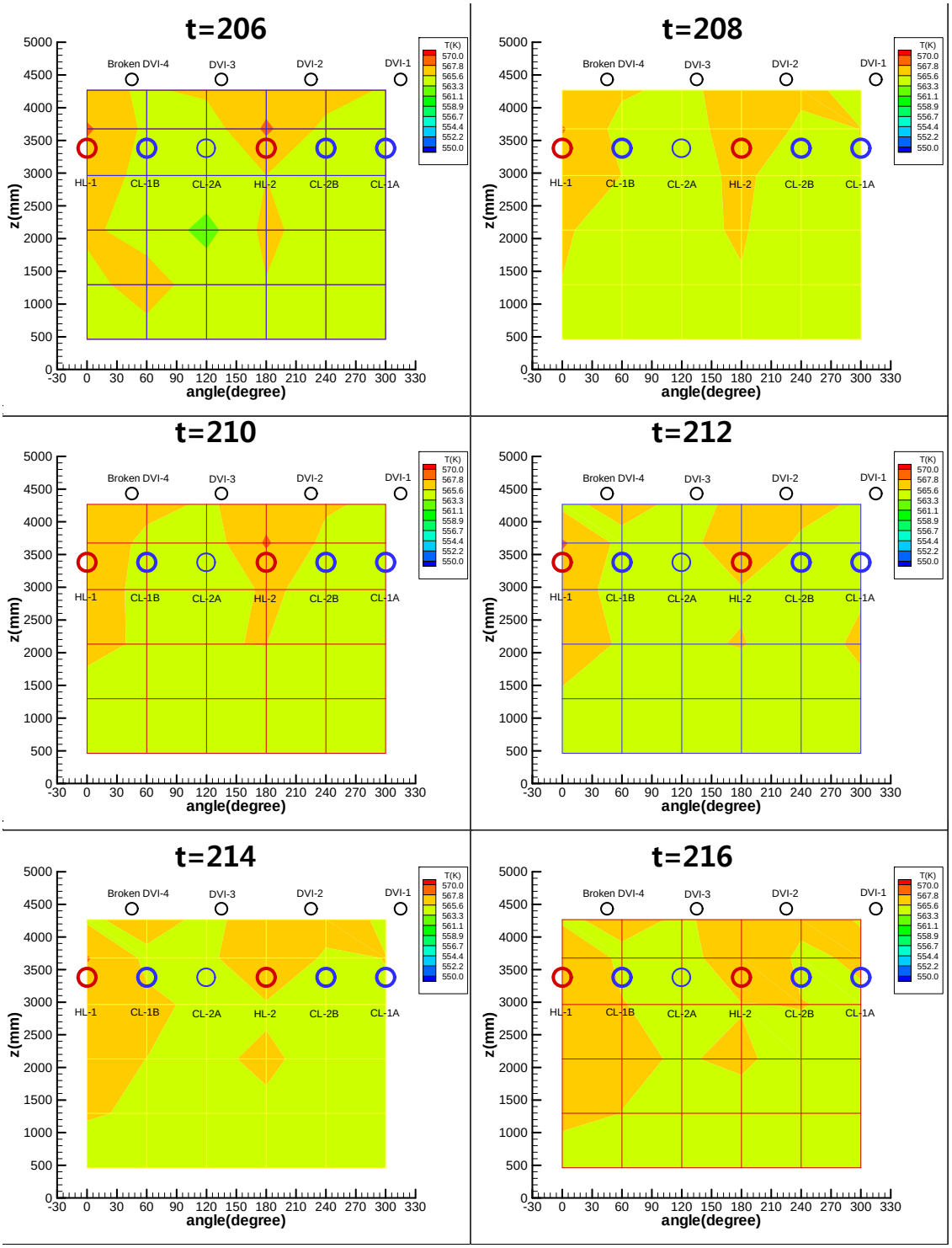

Figure 3.5-59 Fluid temperature contour in the down-comer region (2)

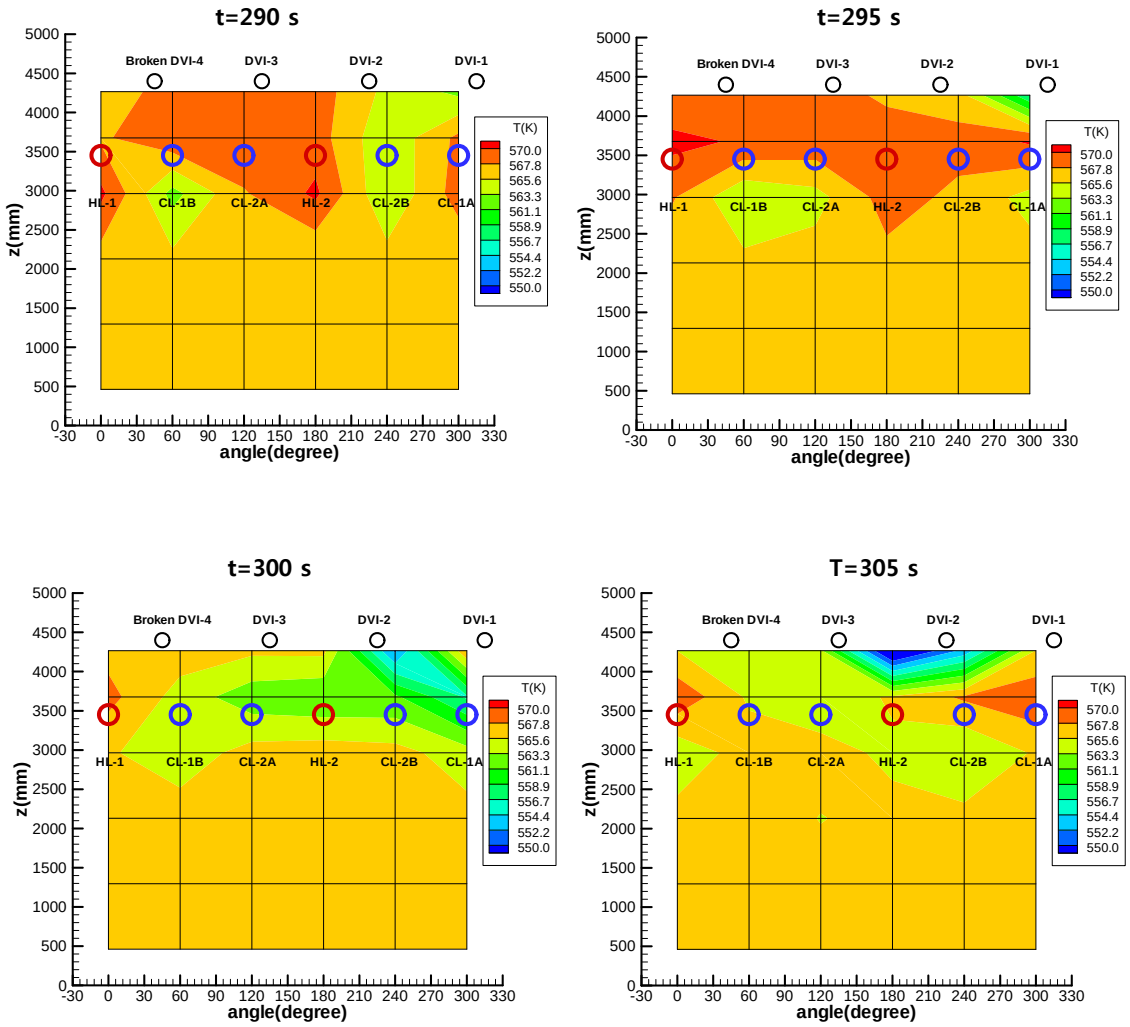

Figure 3.5-60 Fluid temperature contour in the down-comer region (3)

3.5.13 Wall temperatures in the RPV

The down-comer wall temperatures were measured at the same seven elevations where the fluid temperatures were obtained. Measured wall temperatures at the inner and the outer surface were shown in Figure 3.5-61 and Figure 3.5-62 for lower and upper down-comer regions, respectively. The character 'A' or 'B' in the tag name indicates the outer and the inner surface of the down-comer wall, respectively. The inner wall temperatures, TW-DC-05B and TW-DC-06B showed rapid decreases on break. It was due to cooling by the rising water from the lower down-comer region. The inner wall temperatures showed the similar trend to the water temperatures as shown in Figure 3.5-55. The inner wall temperature, TW-DC-04B showed much larger decrease than TW-DC-05B on break. The thermocouple, TW-DC-04B was installed just below the DC-to-HL bypass nozzle at the same azimuthal angle of 270° as shown in Figure 3.5-51. This large temperature drop was also observed in the repeatability test and it seemed

to be attributed to the DC-to-HL bypass flow induced cooling. When the ECC water by the SIP was introduced, the similar temperature drop in TW-DC-04B was also observed at around 250 s. The inner wall temperature in the upper down-comer region, for instance, TW-DC-06B, showed an initial decrease on break and it showed an oscillating behavior after the SIP injection due to the contact of cold ECC water with the hot down-comer wall as shown in Figure 3.5-62. Comparisons of the fluid and the wall temperatures at seven elevations are shown in Figure 3.5-63 and Figure 3.5-64.

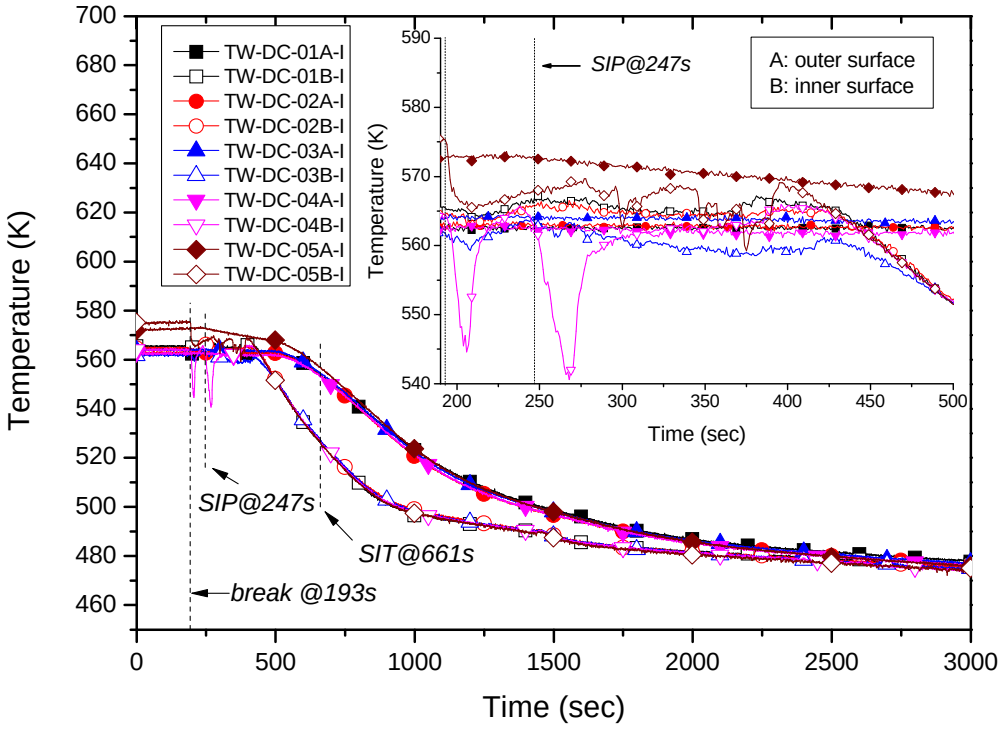

Figure 3.5-61 Measured lower down-comer wall temperatures

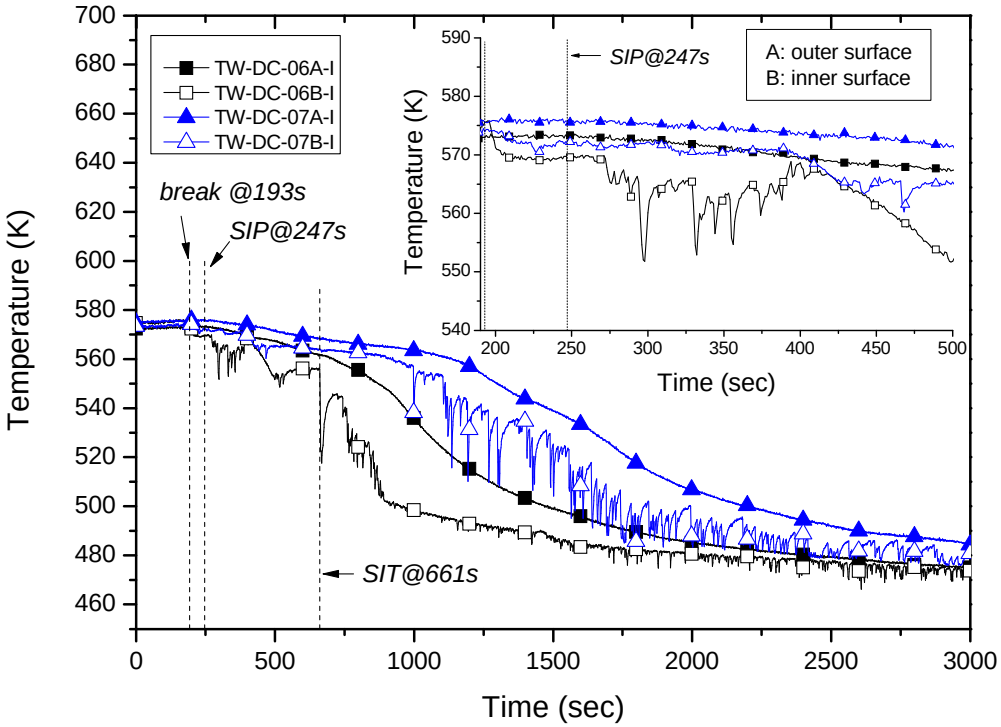

Figure 3.5-62 Measured upper down-comer wall temperatures

Several thermocouples were installed at the upper plenum and the upper head as shown in Figure 3.5-51: TW-UP-02, TW-UH-05, TW-UH-01A/B, TW-UH-02A/B, TW-UH-03A/B, and TW-UH-04A/B. The character 'A' or 'B' in the tag name indicates the down-comer side and the core side surface of the wall, respectively. Measured wall temperatures are shown in Figure 3.5-65 and Figure 3.5-66. Initially, TW-UP-02 was lower than TW-UH-05 by about 14 K, but it maintained higher temperature than TW-UH-05 from the time of about 450 s. With regard to the upper head wall temperatures, the down-comer side wall temperature, TW-UH-01A located just below the DVI nozzles was lower than the core side wall temperature, TW-UH-01B. After break, it showed a decreasing trend just like the down-comer fluid temperature. After occurrence of the first loop seal clearing at 383 s, TW-UH-01A showed the similar trend to TW-UP-02 but it rapidly decreased when the ECC water from the SIT was provided into the down-comer region at 661 s.

As for the upper head wall temperatures located somewhere between the lower nozzle of the DC-UH bypass lines, the core side wall temperature TW-UH-02B was higher than that in the down-comer side, TW-UH-02A by about 7 K before the break. However, the temperature difference disappeared in about 25 s after the break as shown in Figure 3.5-66. The upper head inner wall temperatures, TW-UH-03B and TW-UH-04B had higher temperatures than those of the outer surface before the break. However, the inner surface temperatures decreased after the break while the outer surface temperature showed a slow decrease.

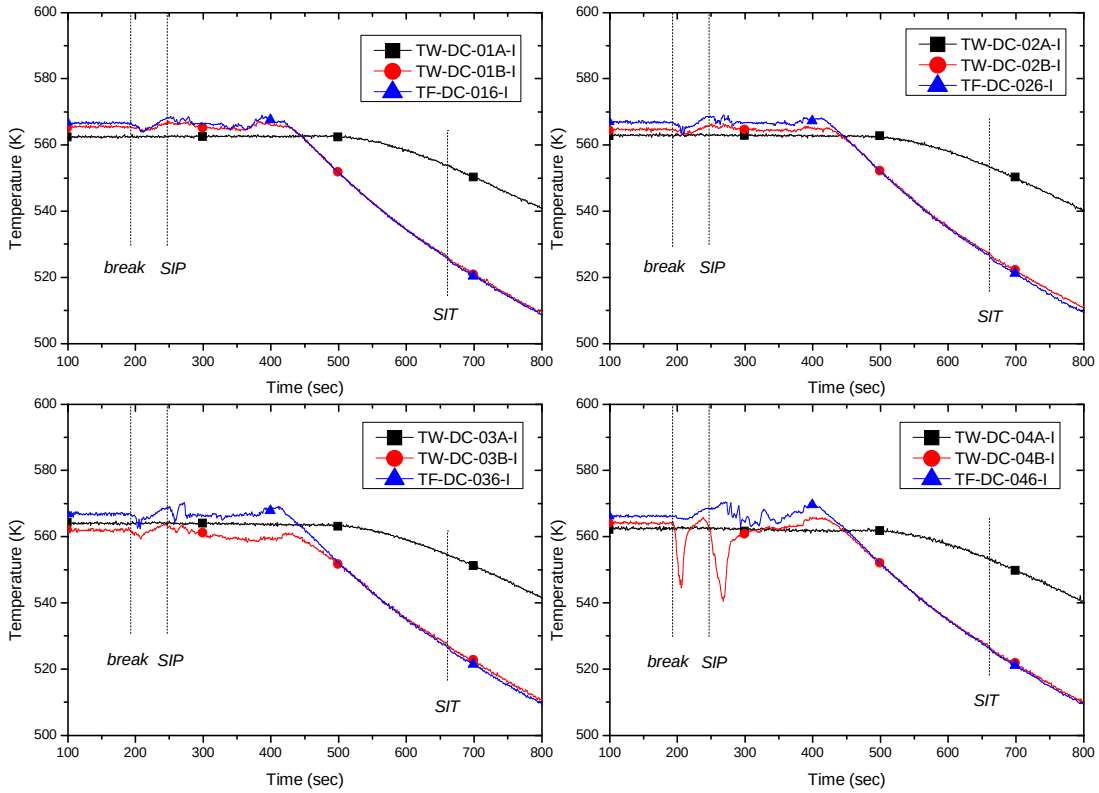

Figure 3.5-63 Lower down-comer wall and fluid temperatures

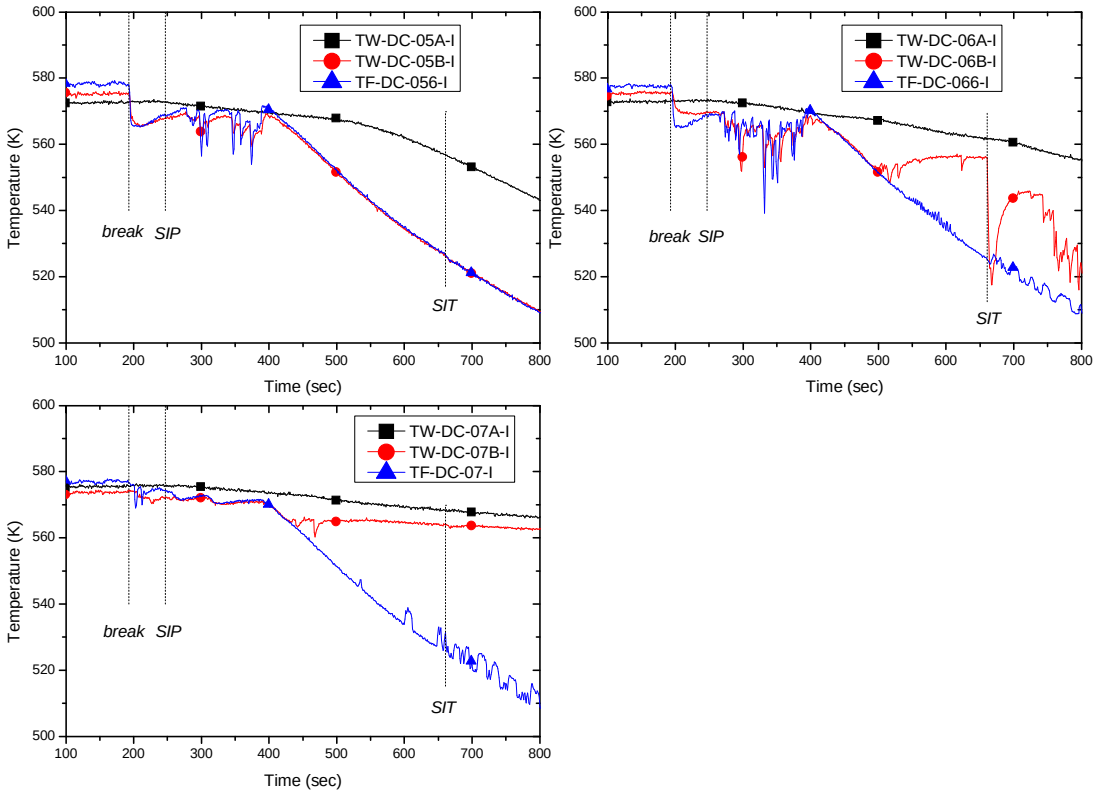

Figure 3.5-64 Upper down-comer wall and fluid temperatures

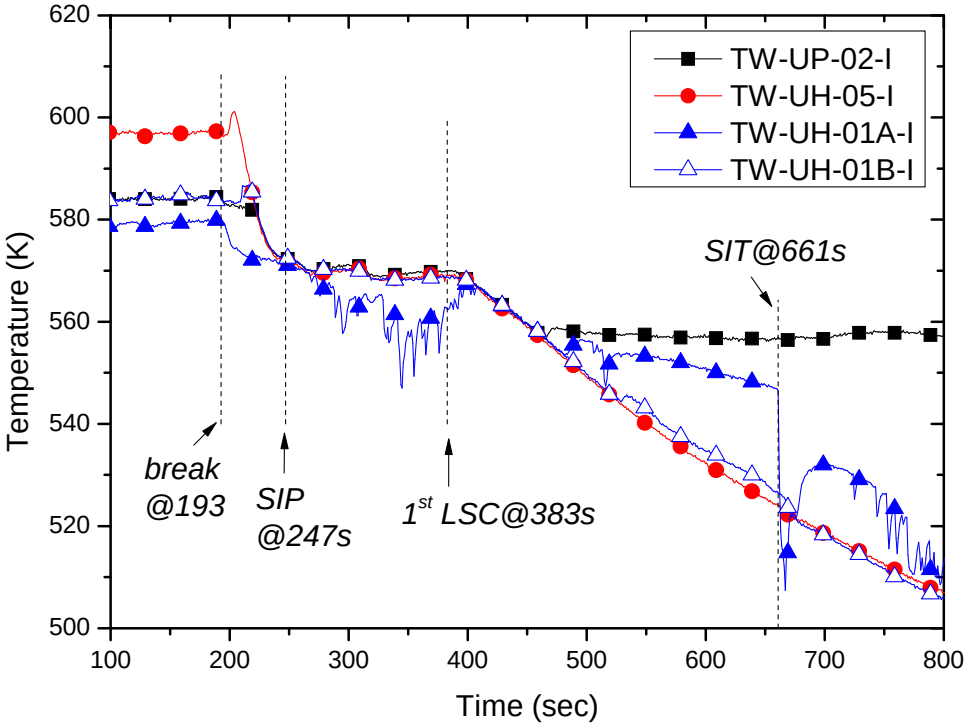

Figure 3.5-65 RPV upper plenum wall temperatures

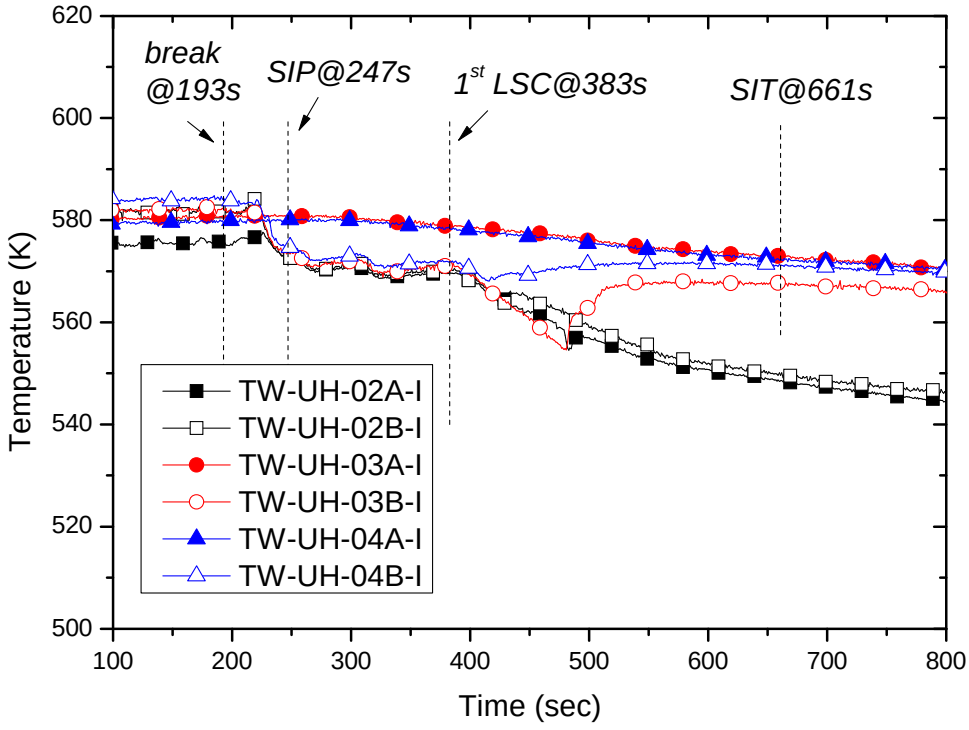

Figure 3.5-66 RPV upper head wall temperatures

3.5.14 Fluid temperatures in the RCS loop

Several thermocouples were installed at cold, hot, and intermediate legs to measure fluid temperatures as well as wall temperatures. At the same axial location, two thermocouples were installed to measure water and steam temperature separately. Steam temperature measuring thermocouple was vertically inserted from the upper wall of the loop pipe. The measuring point was adjusted to locate 10 mm below the inside upper wall of the pipe. Water temperature measuring thermocouple was also vertically inserted from the bottom wall of the loop pipe. The measuring point was located 3 mm above the inside wall of the pipe. Detailed locations of the measuring points can be seen in Figure 3.5-67 through Figure 3.5-69.

Measured steam and water temperatures in the RCS loops during the test period was plotted in Figure 3.5-70 and Figure 3.5-71, respectively. The second location along the hot leg (TF-HL1-02 and TF-HL2-02) and the fourth location along the cold leg (TF-CL1A-04, TF-CL1B-04, TF-CL2A-04, TF-CL2B-04) were selected for comparison because wall temperatures were also measured at the same locations. Inner and outer wall temperatures near TF-CL1A-04A/B in loop 1A were also plotted for a comparison. Saturation temperature based on the upper head pressure of the RPV, PT-UH-01 was also added in each figure. A highly oscillating behavior of the steam temperatures of TF-CL1A-04A and TF-CL1B-04A was measured during the test period between 500 s and 1250 s in Figure 3.5-70. But, the water temperature did not show such fluctuating behavior as shown in Figure 3.5-71. A sudden increase in TF-CL1A-04B at around 700 s indicates that water in this loop was completely evacuated by steam flow. It was found that the water temperature increased when water was evacuated by steam due to the heat transfer from the hot wall. Therefore, the increase in the water temperature can be used as an indicator of the loop seal clearing.

Water temperature distribution along each cold leg is shown from Figure 3.5-72 to Figure 3.5-75, where the sequence of water clearing can be inferred. Water clearing started from the RCP discharge side to the RPV side. In case of the cold leg 1A as shown in Figure 3.5-72, the water temperature measured at the location very close to the discharge of the RCP-1A, TF-CL1A-01B, maintained the same temperature as the wall temperature after the 1st loop seal clearing. This implies that the measuring location is emptied and the thermocouple indicates the bottom wall temperature. Temperatures measured at different locations show a little oscillatory behavior. In case of the cold leg 1B as shown in Figure 3.5-73, temperatures measured at five different locations along the cold leg are close to the wall temperature. On the other hand, water temperatures at the cold legs 2A and 2B are very close to the saturation temperature until the 2nd loop seal clearing as shown in Figure 3.5-74 and Figure 3.5-75. It is because the loop seals of the loops 2A and 2B were not cleared until the 2nd loop seal clearing.

After the 2nd loop seal clearing at the loop 2B, it can be seen from Figure 3.5-75 that the water temperature increases. But the temperatures at the loop 2A maintained the same temperature as the loop is sealed by water.

Steam temperatures measured at each cold leg are shown from Figure 3.5-76 to Figure 3.5-79. The measuring locations of the thermocouples are almost the same as those of thermocouples for water temperatures in the axial direction as shown in Figure 3.5-67 and Figure 3.5-68. During the time between the 1st and the 2nd loop seal clearing, steam temperatures measured at cold leg 1A and 1B show a great oscillation near the saturation temperature. It is due to the steam and droplet mixture flowing through the evacuated cold legs. Meanwhile, steam temperatures measured at cold leg 2A and 2B decrease smoothly. In fact, these measured temperatures are not steam temperatures, but water temperatures because these loops are occupied with water. Upon the 2nd loop seal clearing, the steam temperature in the cold leg 2B started to show the oscillatory behavior due to steam-droplet mixture as shown in Figure 3.5-79. Wall temperatures also started to increase by loss of water cooling.

Figure 3.5-80 shows the water temperatures in the hot leg 1 along the axial locations in the initial period of the test. TF-HL1-01B was located close to the RPV and TF-HL1-03B was located close to the steam generator. Figure 3.5-81 shows the water temperatures in the hot leg 2 along the same locations. By comparing these two figures, the water temperatures in the hot leg 2 showed a sudden decrease after the break. But, the water temperatures in the hot leg 1 did not show this temperature drop. It is due to the fact that sub-cooled water in the surge line of the pressurizer connected at the hot leg 2 was insurged into the hot leg.

Thermocouples TF-SGPi-01 and TF-SGPi-02 were installed inside the inlet and outlet plenum of each steam generator and measured values are shown in Figure 3.5-82. The inlet plenum temperature of SG-1 followed the saturation value but the outlet plenum temperature of SG-1 showed much higher value after the 1st loop seal clearing. It was due to reverse heat transfer from the secondary side when the steam passed through the U-tubes. On the other hand, the inlet plenum temperature of SG-2 showed higher value than that of the outlet plenum until the 2nd loop seal clearing occurred. After the 2nd loop seal clearing, it was reversed.

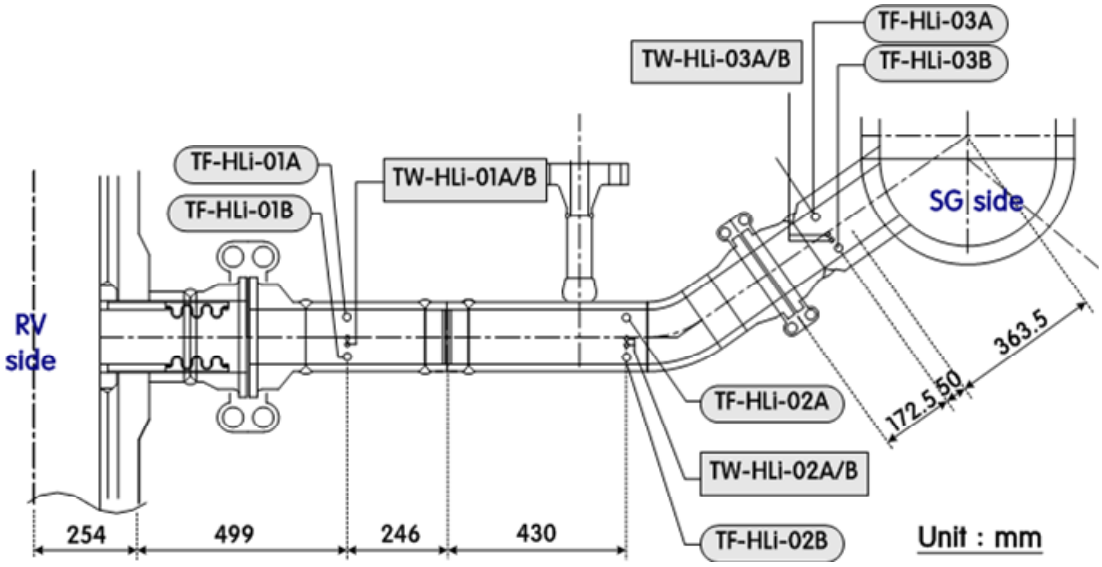

Figure 3.5-67 Detailed locations of the thermocouples to measure hot leg temperatures

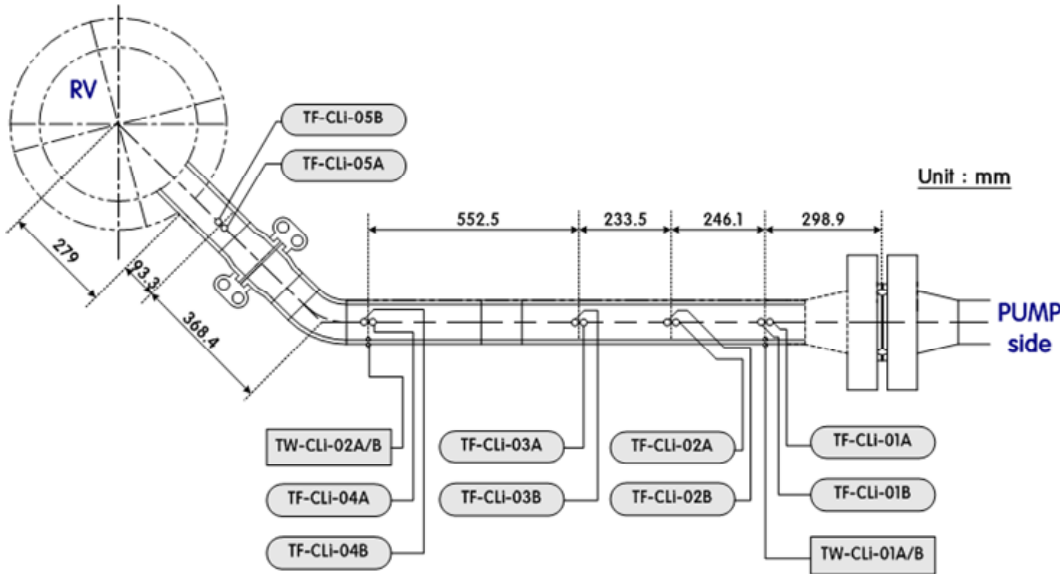

Figure 3.5-68 Detailed locations of the thermocouples to measure cold leg temperatures

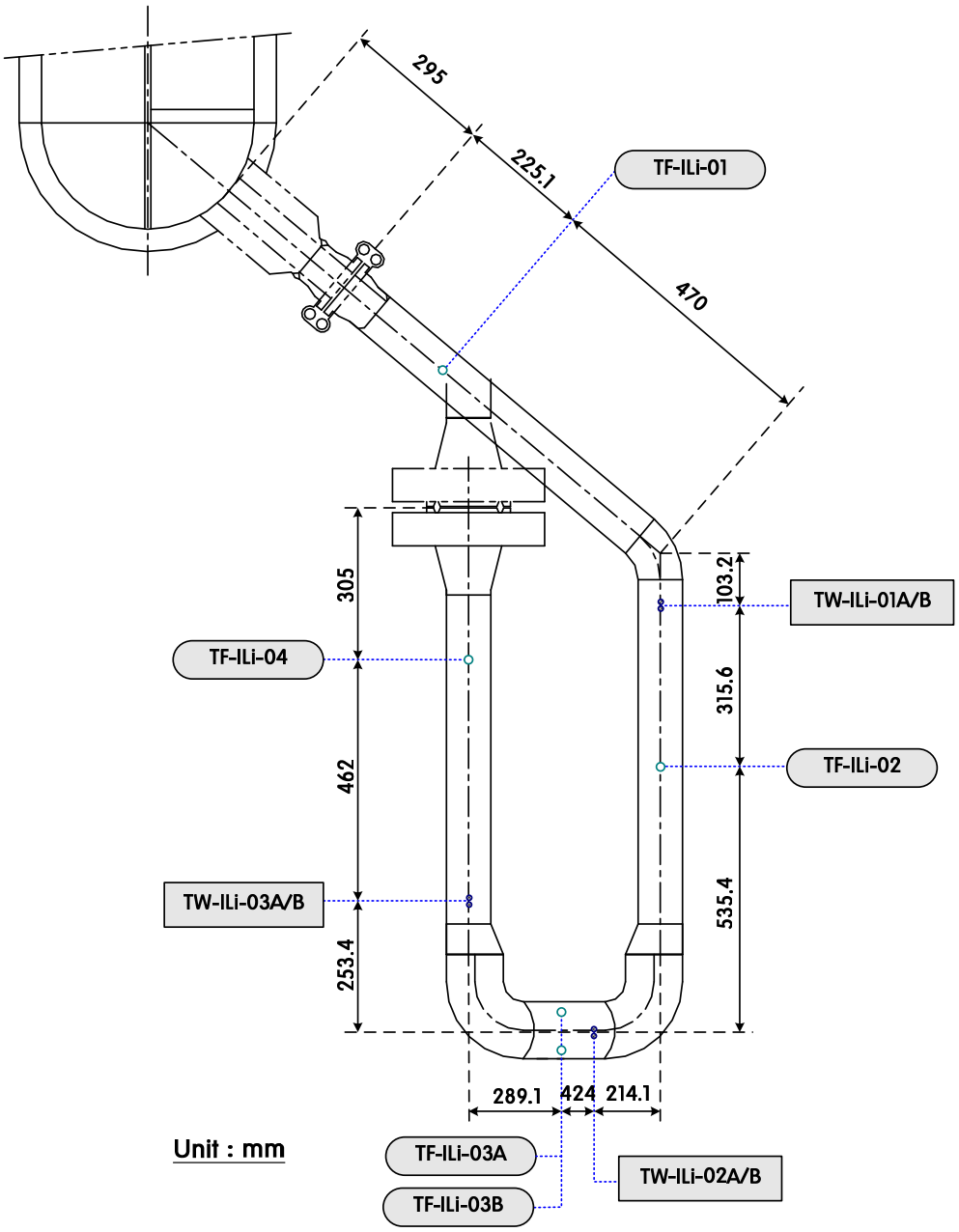

Figure 3.5-69 Detailed locations of the thermocouples to measure intermediate leg temperatures

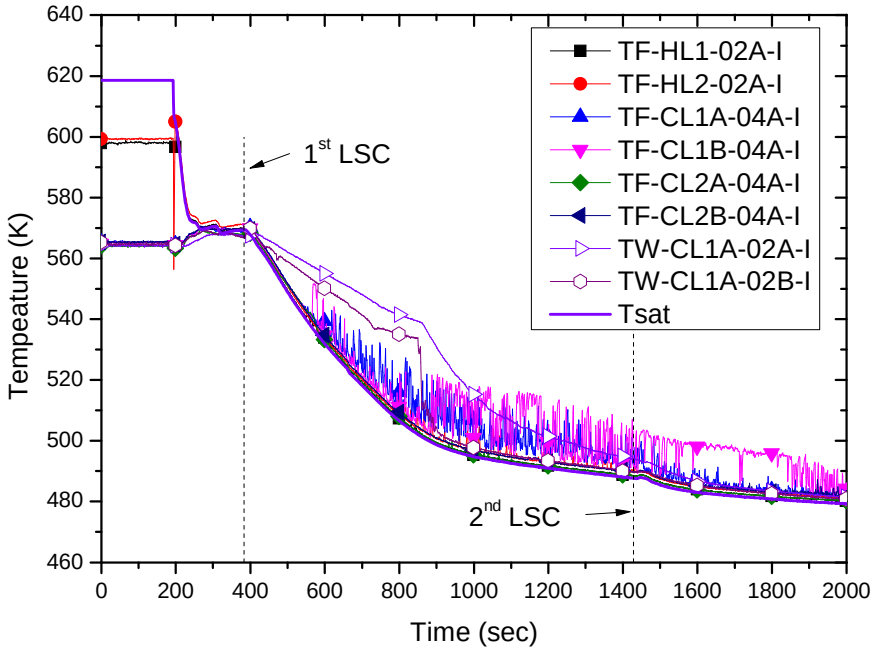

Figure 3.5-70 Loop steam temperatures

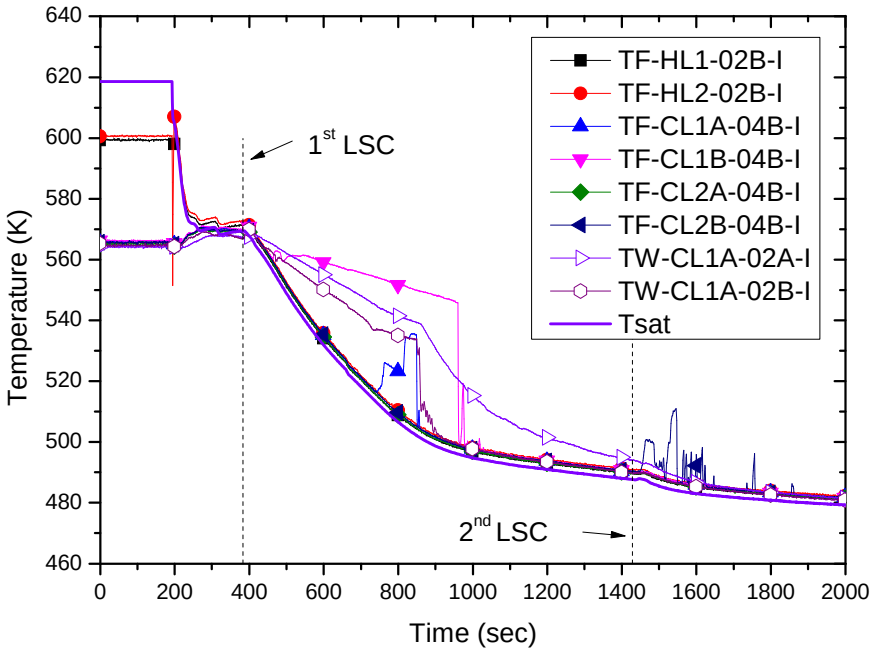

Figure 3.5-71 Loop water temperatures

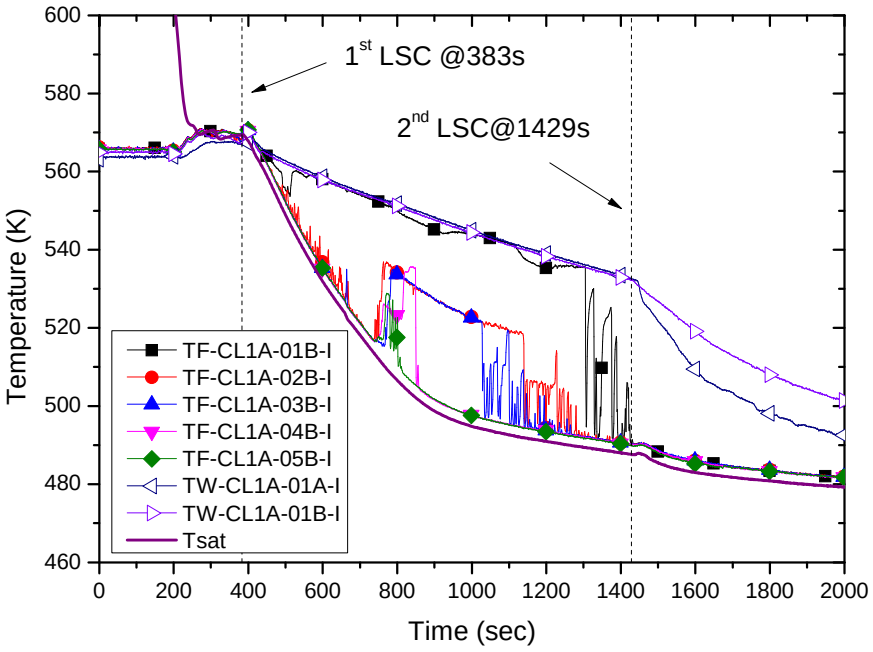

Figure 3.5-72 Water temperature distribution in the cold leg 1A

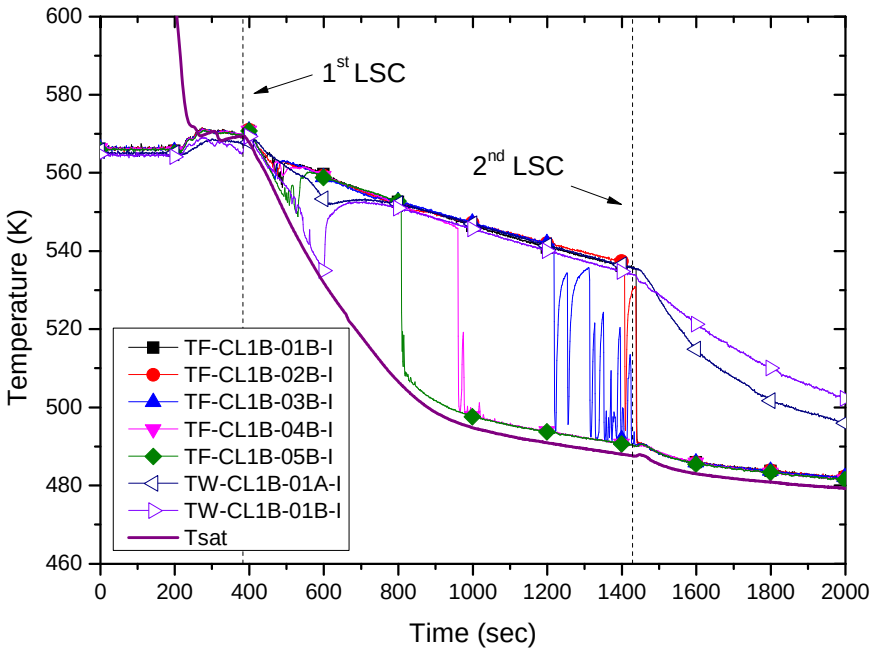

Figure 3.5-73 Water temperature distribution in the cold leg 1B

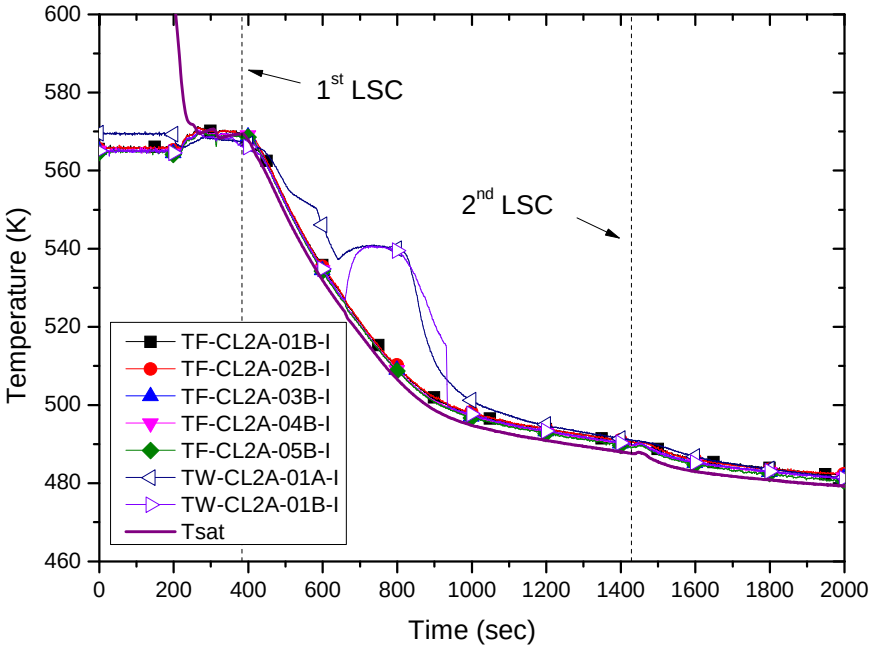

Figure 3.5-74 Water temperature distribution in the cold leg 2A

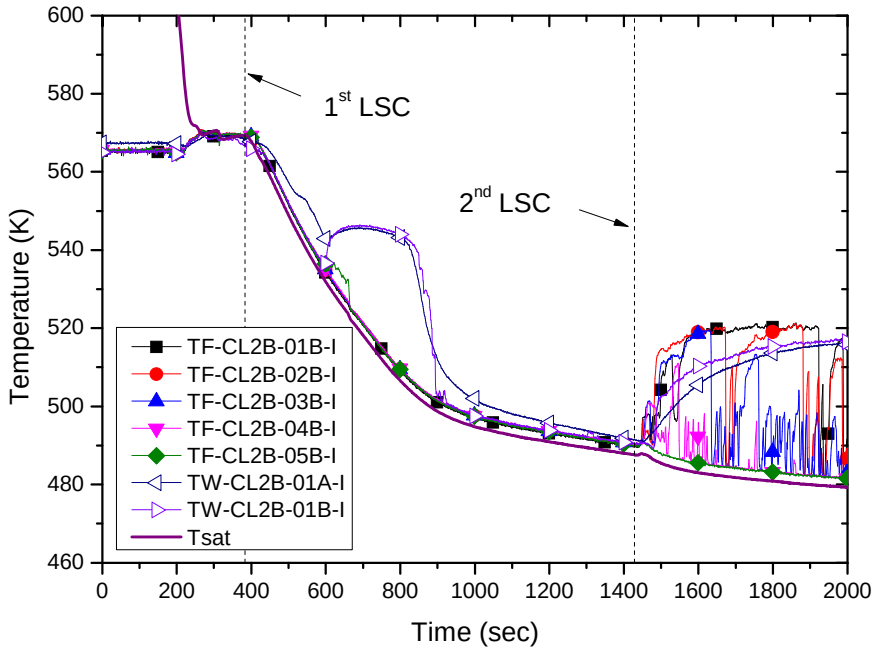

Figure 3.5-75 Water temperature distribution in the cold leg 2B

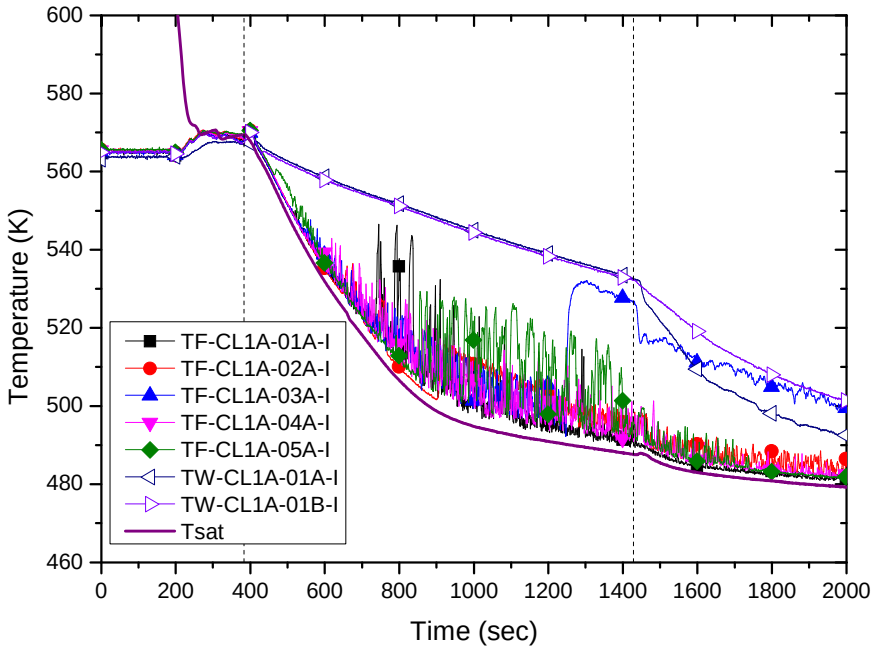

Figure 3.5-76 Steam temperature distribution in the cold leg 1A

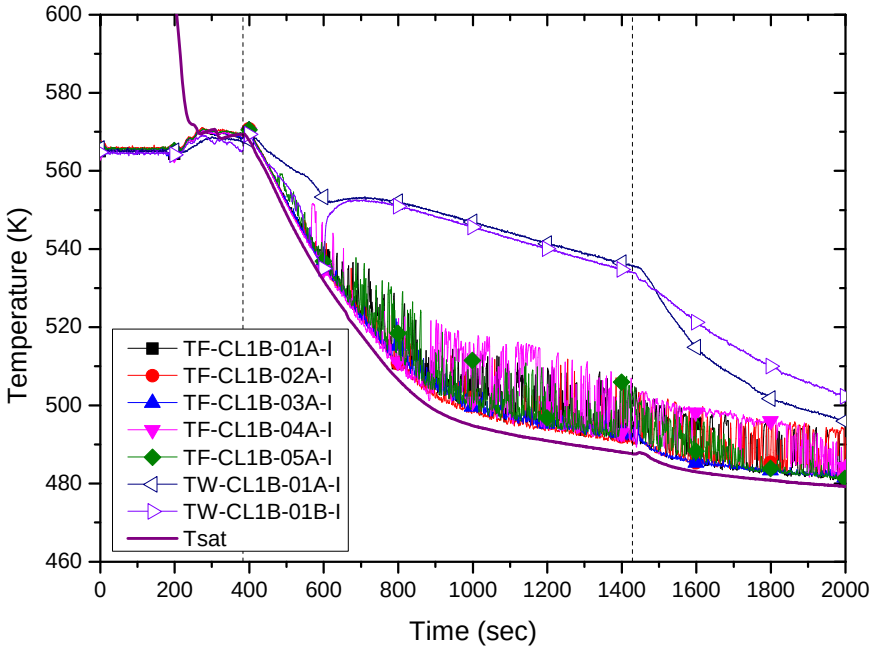

Figure 3.5-77 Steam temperature distribution in the cold leg 1B

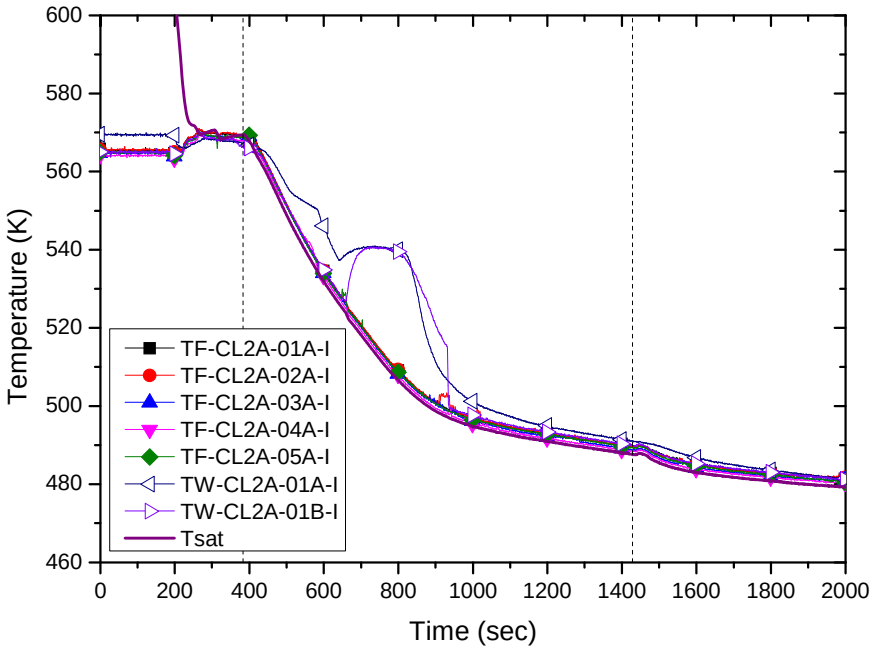

Figure 3.5-78 Steam temperature distribution in the cold leg 2A

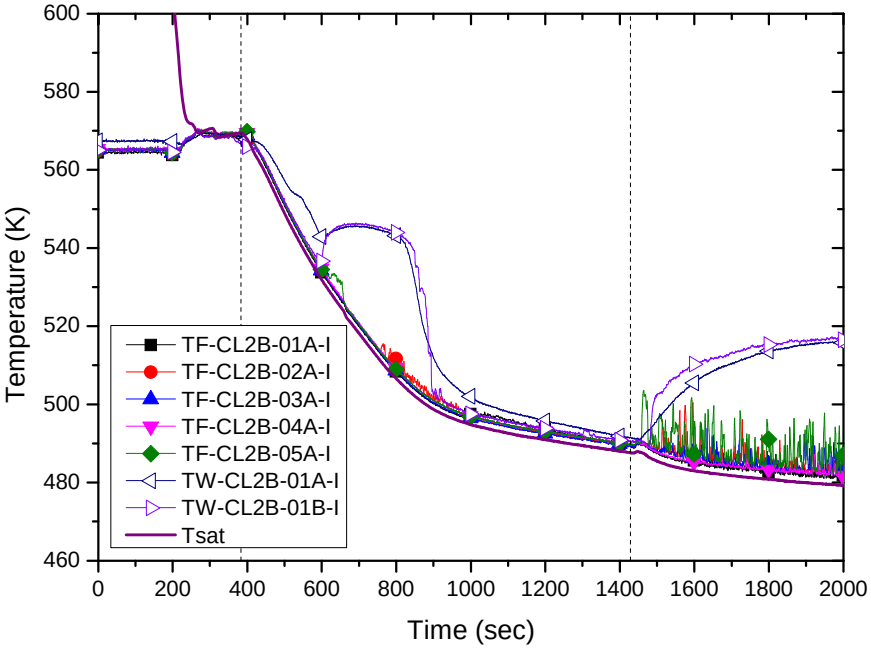

Figure 3.5-79 Steam temperature distribution in the cold leg 2B

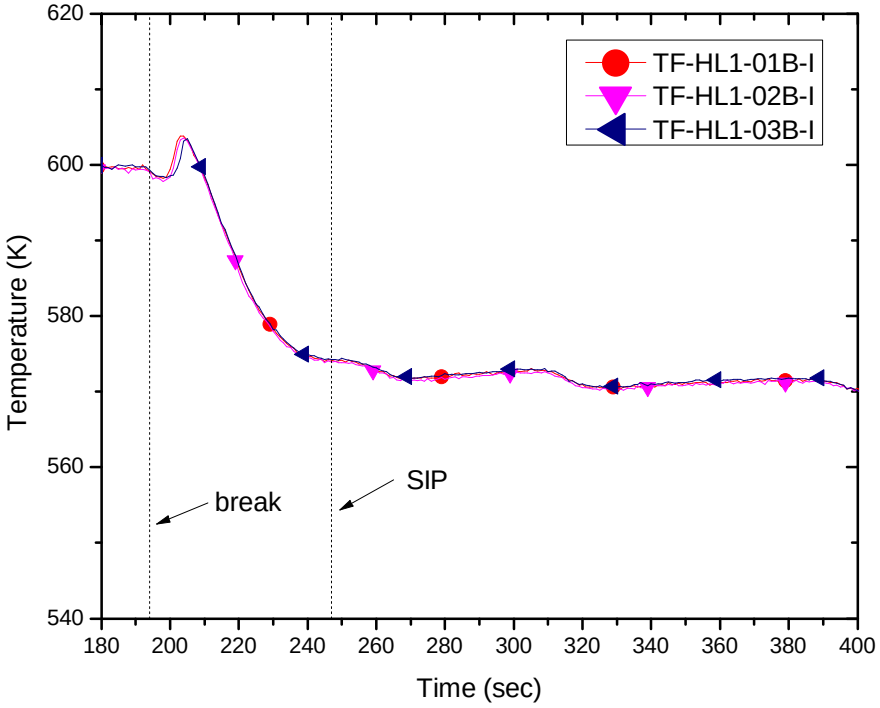

Figure 3.5-80 Water temperatures along the hot leg 1

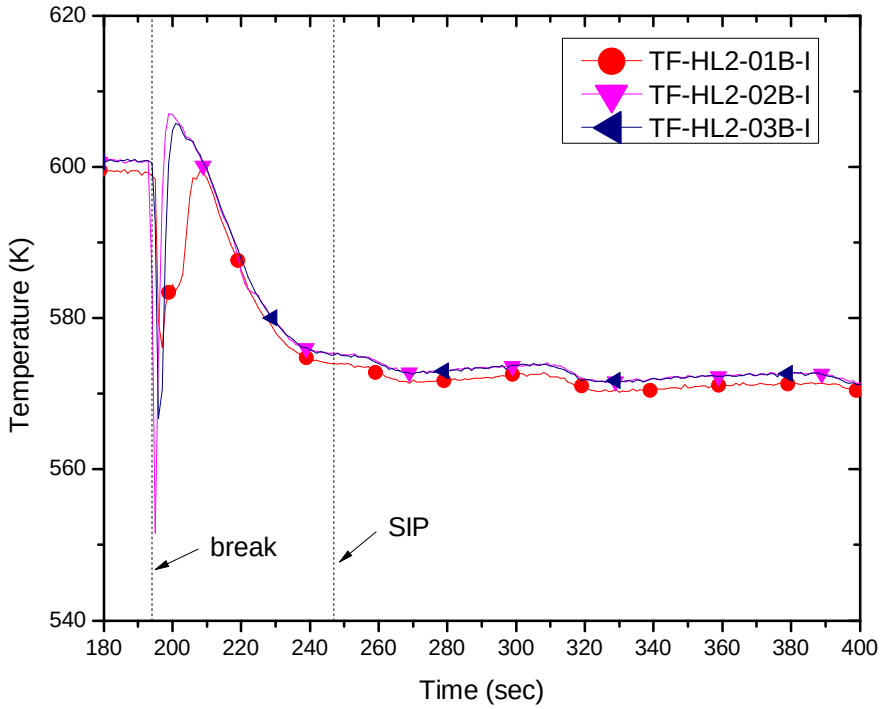

Figure 3.5-81 Water temperatures along the hot leg 2

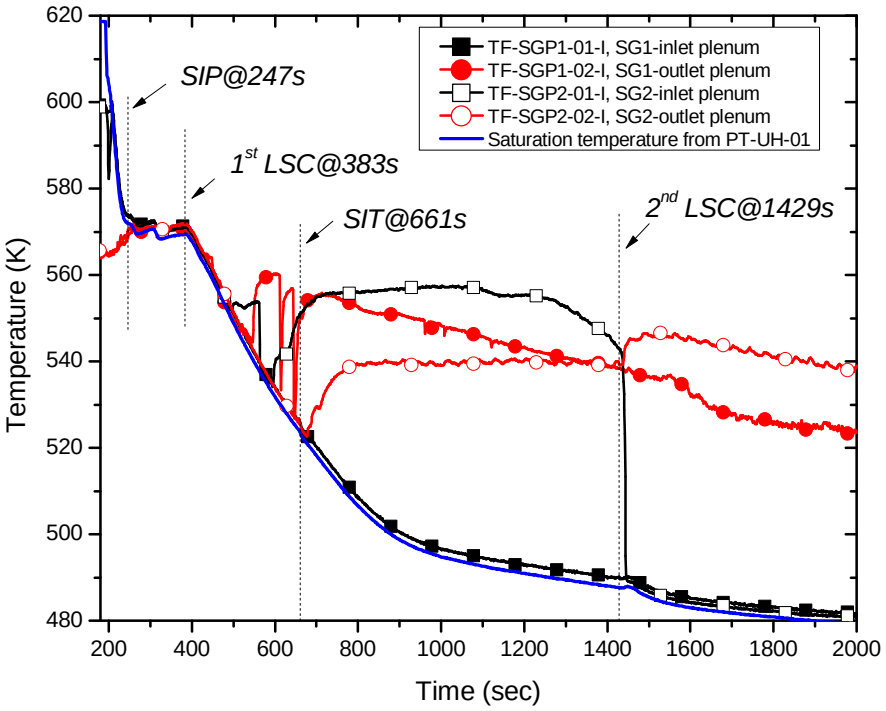

Figure 3.5-82 SG inlet/outlet plenum temperatures

3.5.15 RPV bypass flow

In the ATLAS facility the bypass flow rates were simulated to preserve the bypass behavior of the APR1400 as realistically as possible. Two external bypass flow pipelines were installed to simulate the down-comer to upper head and the down-comer to the hot leg, respectively. A schematic diagram of the bypass lines is shown in Figure 3.5-83. Detailed isometric drawings of the bypass lines are given in Figure 3.5-84 and Figure 3.5-85. The differential pressure along each bypass flow pipeline was measured. Two bypass valves FCV-RV-37 and FCV-RV-38 between the down-comer and the upper head were opened by 74% and 65%, respectively, to provide the scaled flow rate of 0.02 kg/s each, and two bypass valves FCV-RV-95 and FCV-RV-96 between the down-comer and hot legs were opened by 81% and 97%, respectively, to provide the scaled flow rate of 0.057kg/s each at a reduced 8% steady state condition where the RCS flow rate was reduced to 8% of the scaled flow rate. The opening positions of four bypass valves were determined based on the characteristics of the valves and the corresponding pipelines. The mass flow rate Q_{bypass} flowing across a valve can be determined as follows:

$$Q_{bypass} = 2.396\times10^{-5} C_v \sqrt{\rho_f \Delta P} \quad \text{[kg/s]}, \tag{3.5-1}$$

where, C_v, ρ_f, ΔP is a valve coefficient, fluid density [kg/m^3], and differential pressure [Pa]. The valve coefficient of each valve is shown in Figure 3.5-86 and Figure 3.5-87.

Before the break, the differential pressure between the down-comer and the hot leg was very close to zero, indicating there was negligible bypass flow as shown in Figure 3.5-88. The estimated bypass flow rate of each bypass line was -0.09 kg/s and -0.16 kg/s as shown in Figure 3.5-89, respectively. On break, DP-DCHL1-01 as well as DP-DCHL2-01 showed a momentary increase but they continuously reduced to negative values. This negative differential pressure implies that a portion of the forward hot leg flow was bypassed through the bypass line to the down-comer and it was discharged to the broken DVI nozzle. No significant effects of the ECC water by the SIP on this bypass flow were observed. The differential pressures from DP-DCHL1-01 and DP-DCHL2-01 became more negative until the 1st loop seal clearing occurred. It means that more hot leg flow rate was bypassed to the down-comer. It was due to the blockage of the loop seals in the intermediate legs. As will be described in the following section, the 1st loop seal clearing resulted in clearing of the intermediate legs only in the loop 1 while the loop seals in the loop 2 were remained. This asymmetric loop seal clearing caused an asymmetric behavior of the differential pressure between the hot leg 1 and 2. The differential pressure in the loop 1 drastically increased. The degree of increase in differential pressure of DP-DCHL1-01 was much greater than that of DP-DCHL2-01. Also a little fluctuation in differential pressure was measured in the bypass line of the hot leg 1. The loop seal clearing indicates that the flow passage from the hot leg through the steam generator to the cold leg (or down-comer) is driven through. Thus, the loop seal clearing in the loop 1 made the forward hot leg flow possible, resulting in decrease the bypass flow rate. It was the main reason of the drastic increase in DP-DCHL1-01. On the other hand, DP-DCHL2-01 did not show such a great change because the loop seals in the hot leg 2 were not cleared.

Regarding the down-comer to the upper head bypass, two measured differential pressures, DP-DCUH1-01 and DP-DCUH2-01 showed the similar results as shown in Figure 3.5-88. Negligible difference between two bypass lines was obtained. The bypass flow rate was also estimated by using the characteristics of the valve and the corresponding pipeline and shown in Figure 3.5-90. Before the break, the differential pressures indicated negative values around -0.7 kPa. Based on the pressure drop characteristic of the bypass pipeline, it corresponds to 0.02 kg/s, resulting in the total bypass flow rate of 0.04 kg/s, 0.5% of the total core flow rate, implying that a flow direction is from the upper head to the down-comer. However it is not clear whether the bypass flow direction is from the upper head to the down-comer or not because such a small negative pressure difference could be affected by a measurement bias. On break, the differential pressure DP-DCUH1-01 and DP-DCUH2-01 rapidly decreased to negative values until the 1st loop seal clearing occurred. It implies that

the bypass flow rate from the upper head to the down-comer increased with respect to time. This increase in the bypass flow rate can be explained by the fact that the flow passage from the hot leg through the steam generator to the cold leg (or the down-comer) was blocked due to the formation of the loop seals of the intermediate legs and thus more core inventory was bypassed through these bypass lines to the upper down-comer in order to be discharged through the broken DVI nozzle. When the 1st loop seal clearing occurred in the loop 1, this bypass flow rate became reduced which corresponds to an increase in the differential pressure. However, the loop seals in the loop 2 were not still cleared by the 2nd loop seal clearing, the bypass flow rate started to increase again which corresponds to a decrease in the differential pressure. At the 2nd loop seal clearing, such a similar change in the bypass flow rate was observed.

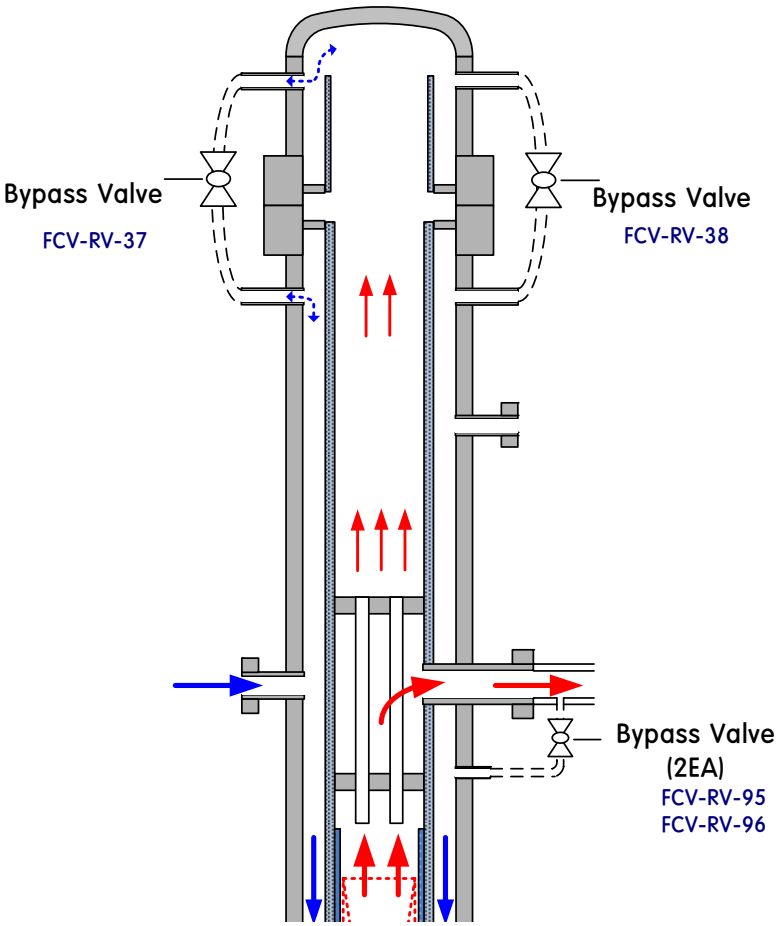

Figure 3.5-83 Schematic diagram of the RPV bypass pipelines

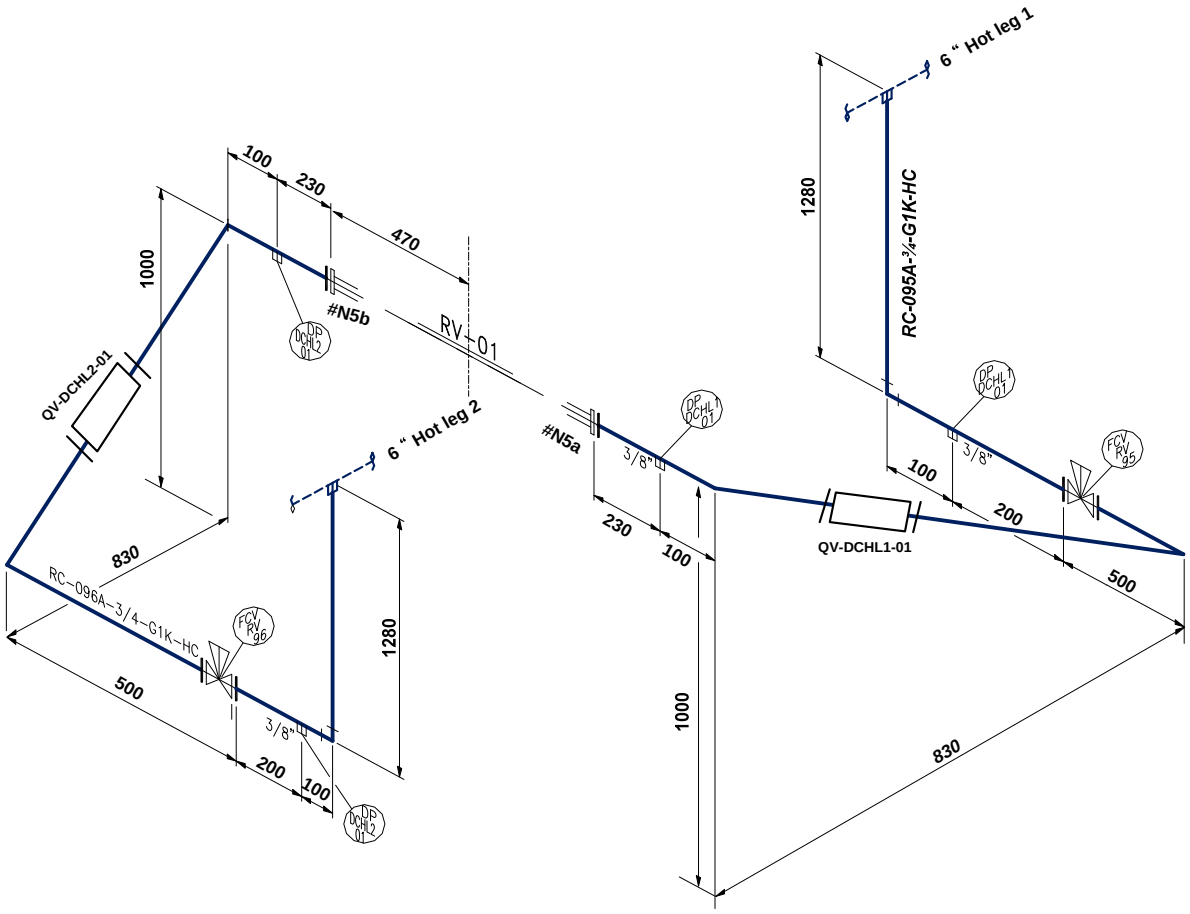

Figure 3.5-84 Isometric configuration of the down-comer to the hot leg bypass line

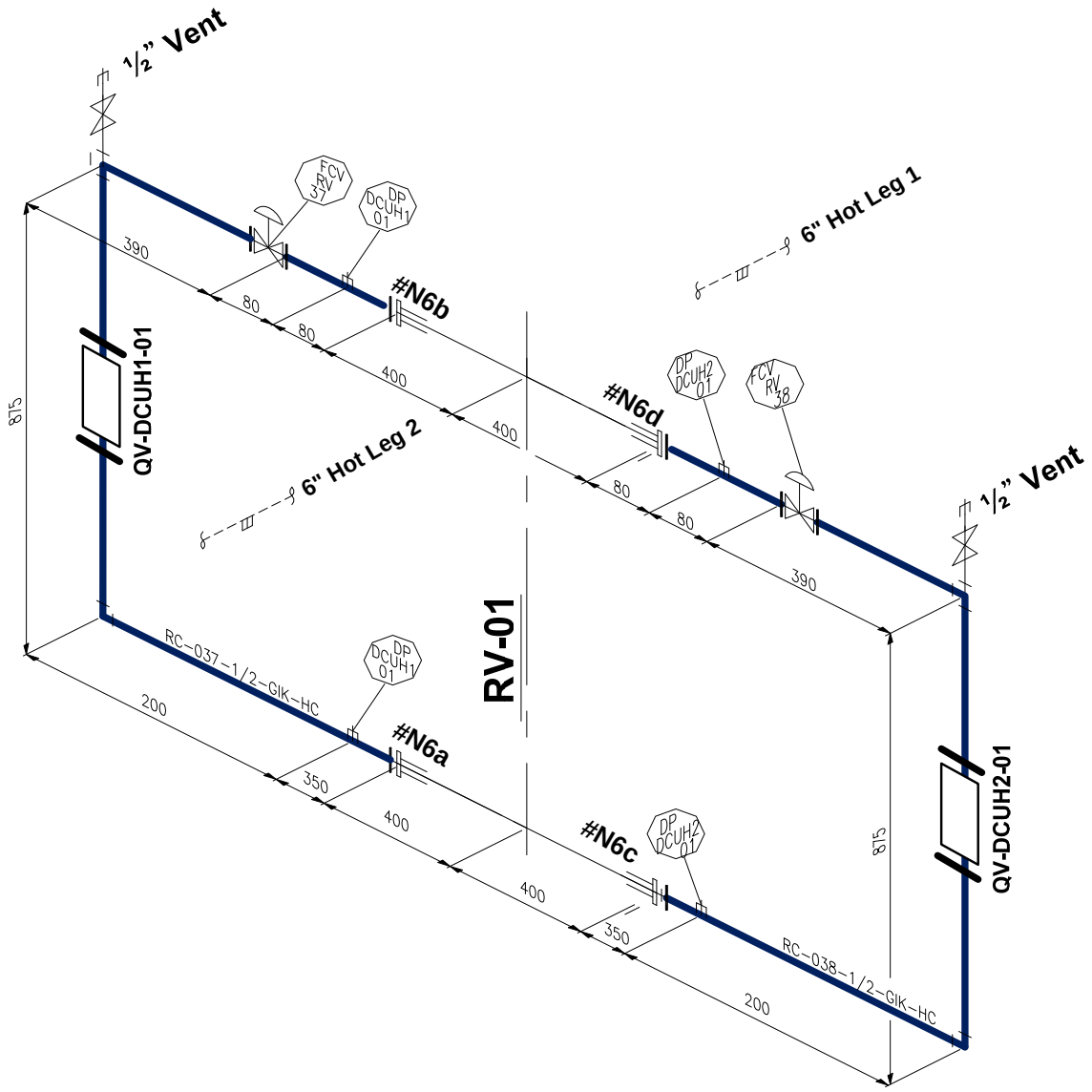

Figure 3.5-85 Isometric configuration of the down-comer to the upper head bypass line

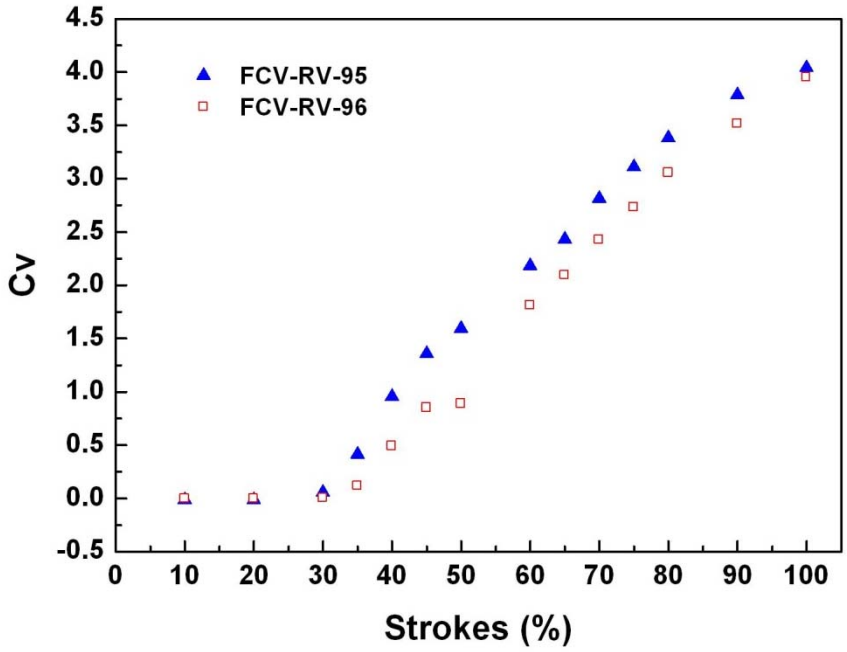

Figure 3.5-86 Down-comer to hot leg valve coefficient with respect to opening

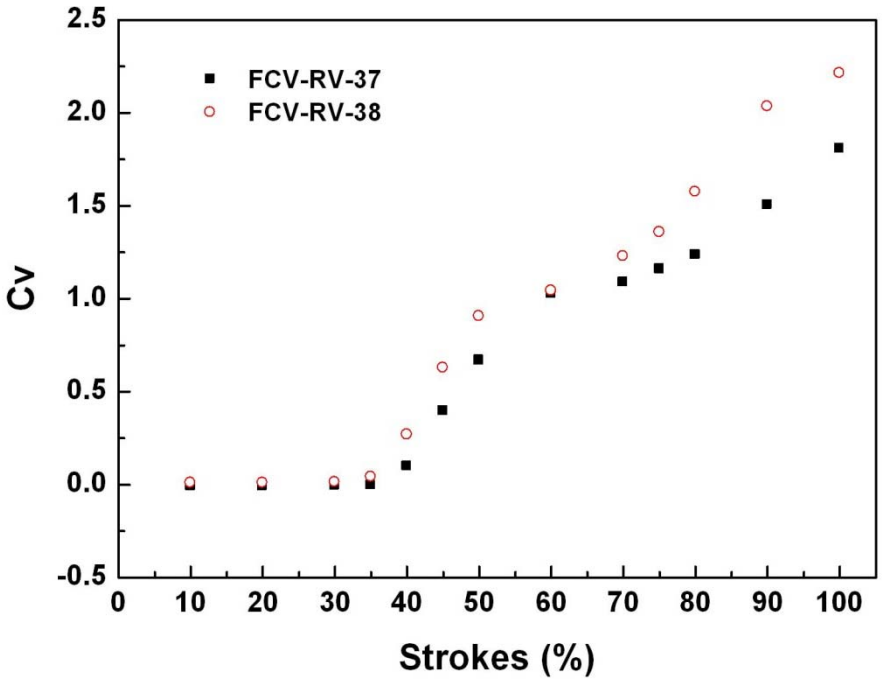

Figure 3.5-87 Down-comer to upper head valve coefficient with respect to opening

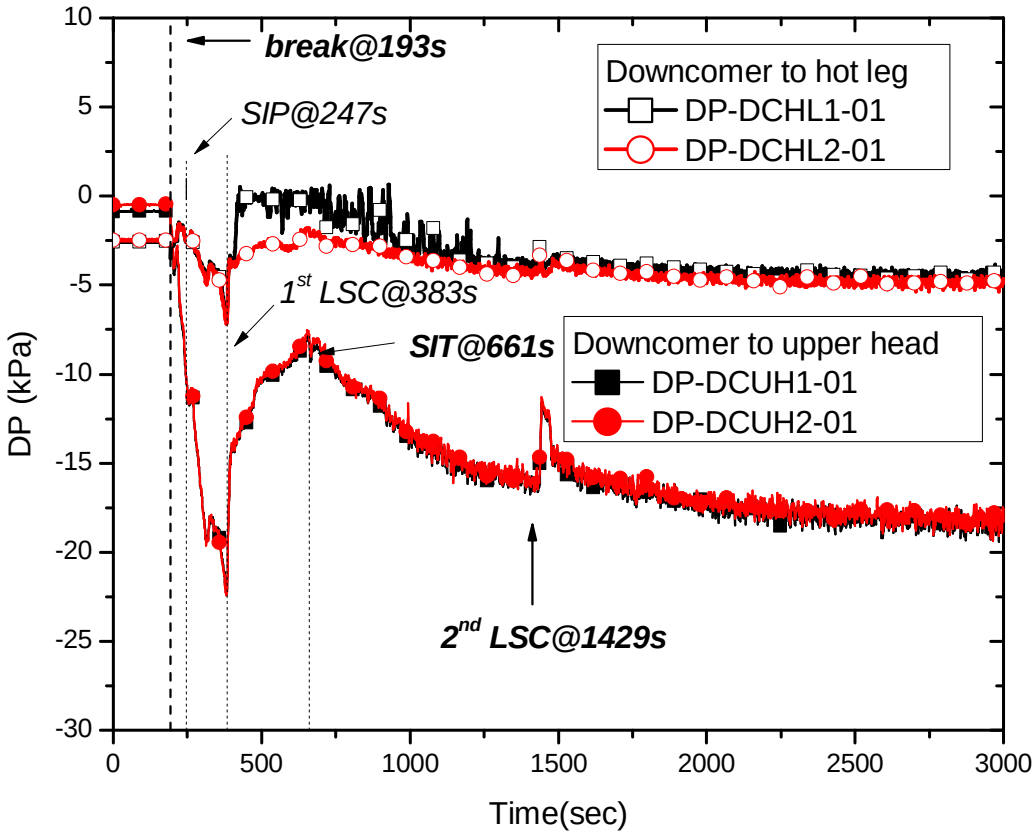

Figure 3.5-88 Differential pressure between the bypass lines

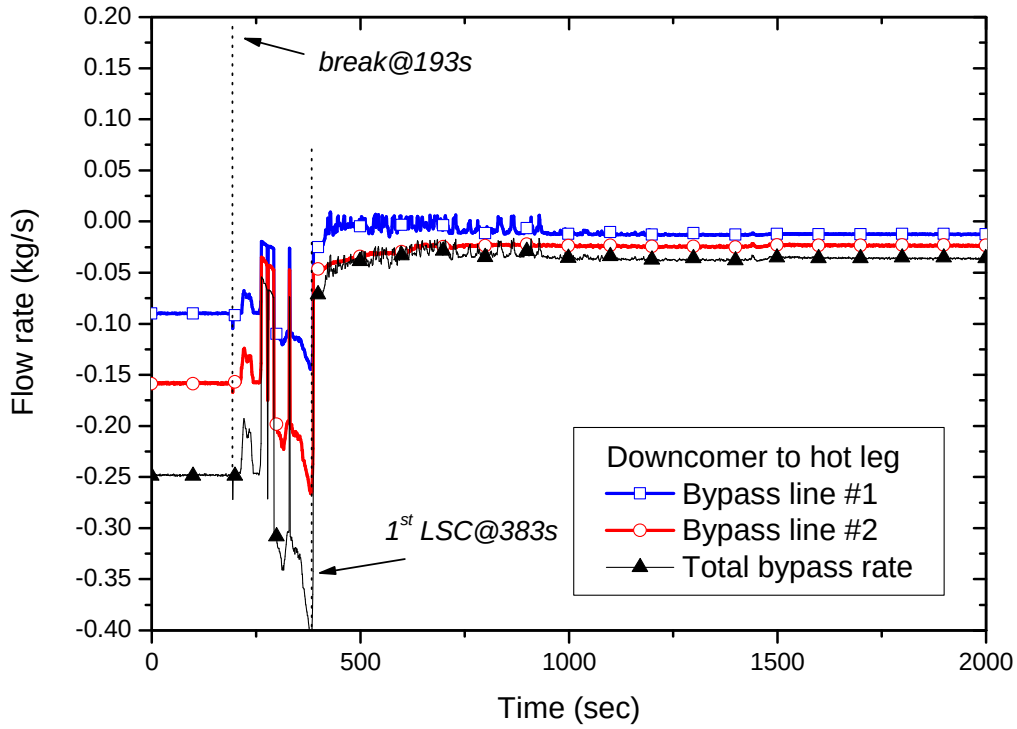

Figure 3.5-89 Bypass flow rates from down-comer to hot leg

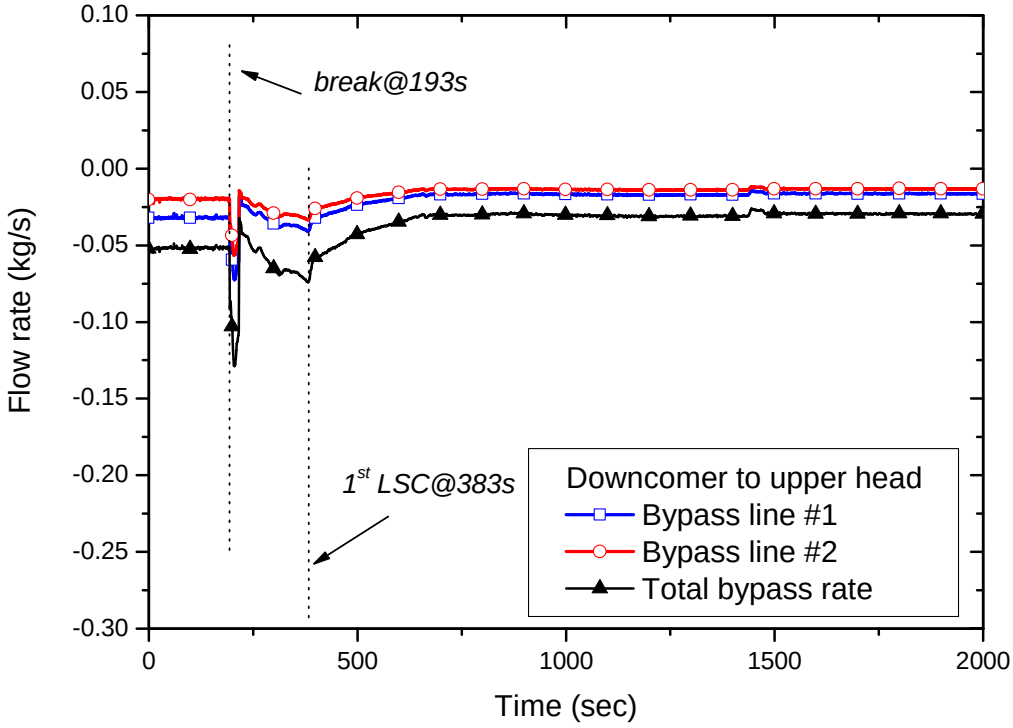

Figure 3.5-90 Bypass flow rates from down-comer to upper head

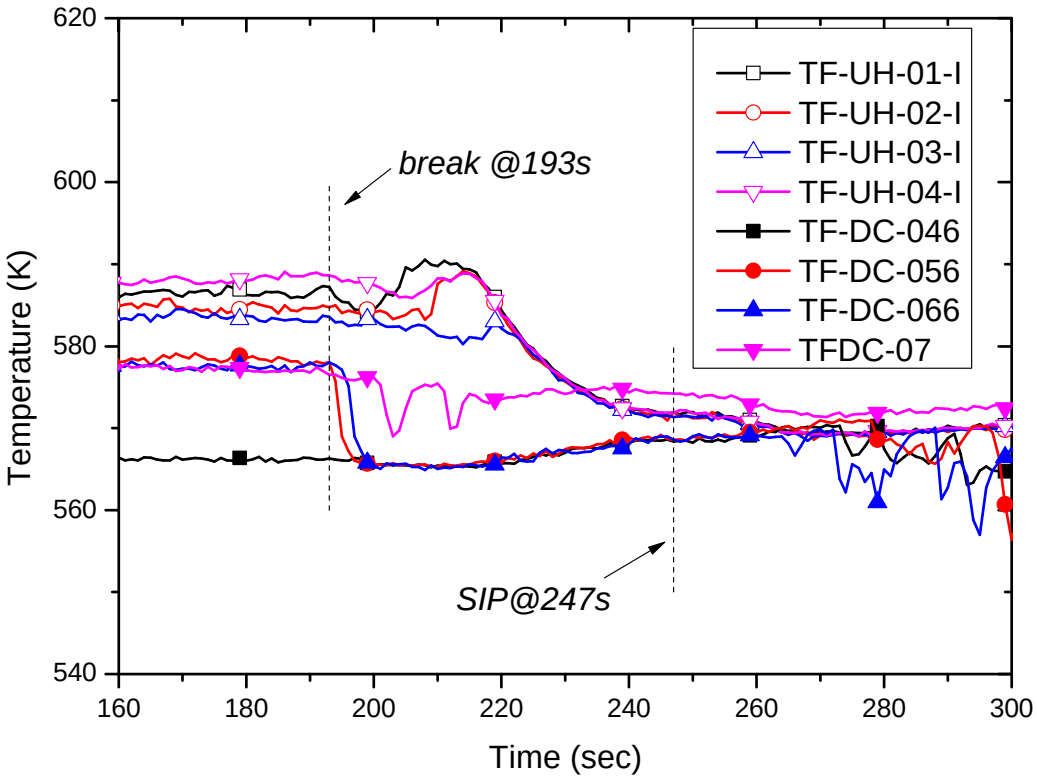

Figure 3.5-91 Comparison of the detailed temperature of the RPV upper head and the down-comer

3.5.16 Differential pressure in the RCS loop

Pressure transmitters installed along the RCS loop are shown in Figure 3.5-99. Figure 3.5-92 shows the pressure differences between the hot legs and the cold legs. Each differential pressure was obtained by subtracting PT-CLj-01 from PT-HLi-01. Even though a little negative bias was measured in the loop 1B, 2A and 2B, it is enough to see the trend of the differential pressure between each circulation loop. The differential pressure linearly increased till the 1st loop seal clearing. This increase was caused by the pressure buildup of the hot legs due to blockage of the circulation passage caused by the loop seal formed in the intermediate loop. When the differential pressure between the hot leg and the cold leg became large enough to push the water in the loop seal to the down-comer, the 1st loop seal clearing occurred and thus the differential pressure started to decrease. When the SIT started to deliver the ECC water into the down-comer, the differential pressure started to increase again. It seems that the injected ECC water by three SITs made the discharge of the inventory through the broken nozzle worse: a partial blockage of the down-comer. This was the main cause of the increase in the differential pressure between the hot leg and the cold leg after the injection of the SITs.

In order to investigate the loop flow characteristics during the test, the measured differential pressures along the hot legs were compared in Figure 3.5-93 and Figure 3.5-94. The differential pressures along the horizontal hot legs, DP-HL1-01 and DP-HL2-01 showed almost constant values. Though the differential pressures along the inclined hot legs, DP-HL1-02 and DP-HL2-02 showed initial negative bias, they included useful information on the loop flow characteristics. In particular, there existed a great asymmetric difference during the period between the 1st loop seal clearing and the 2nd loop seal clearing. Upon the 1st loop seal clearing, DP-HL2-02 showed a great decrease to negative values and it was recovered on the 2nd loop seal clearing. The decrease in DP-HL2-02 implies that the pressure of the inlet plenum of the steam generator 2 is higher than that of the hot leg 2.

This negative differential pressure was caused by the pressure buildup in the U-tubes of the steam generator 2. After the 1st loop seal clearing, the U-tubes of the both steam generators were emptied but the flow passage through the loop 2 was still blocked due to the loop seal formed in the intermediate legs and maintained such a blocked condition until the 2nd loop seal clearing. Thus, the reverse heat transfer in the U-tubes of the steam generator 2 resulted in heatup of the fluid inside the U-tubes, causing an increase in pressure. This heatup can be confirmed from the measured fluid temperatures inside the ascending and descending U-tube shown in Figure 3.5-95 and Figure 3.5-96, respectively. The suffix from A01 to A05 indicates the measurement elevation in the sequential order of higher elevation, i.e., A01 is located at the lowest elevation and A05 at the highest. As shown in Figure 3.5-95, the fluid temperature inside

the U-tubes of the steam generator 1 increased along the elevation. It indicates that the steam flowed upward during heatup by the reverse heat transfer. But, the temperatures inside the U-tubes of the steam generator 2 showed almost the same temperatures, implying that there was no flow in this loop. The fluid temperature distributions in the descending U-tubes are shown in Figure 3.5-96. The same difference observed in Figure 3.5-95 were observed but the axial temperature gradient was smaller than that of the ascending side.

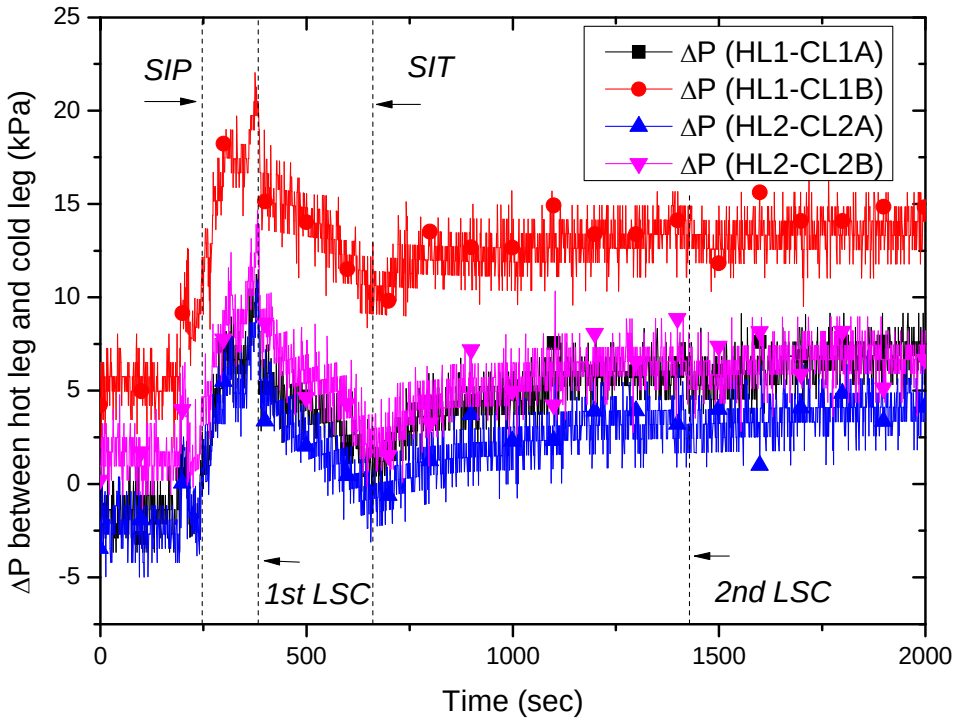

Figure 3.5-92 Pressure differences between the hot legs and the cold legs

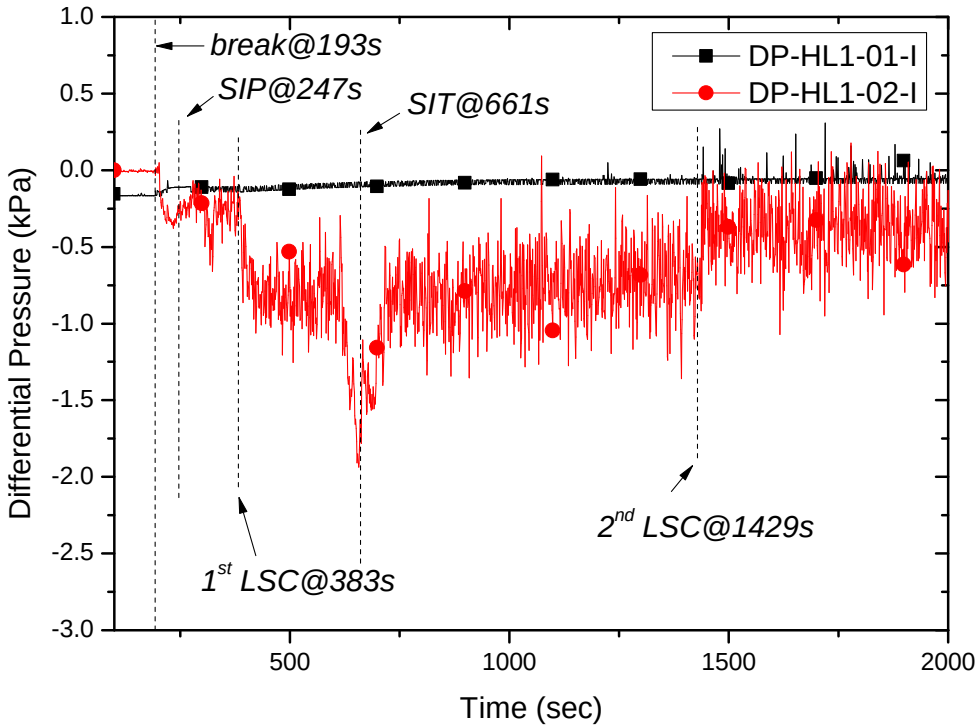

Figure 3.5-93 Differential pressures in the hot leg 1

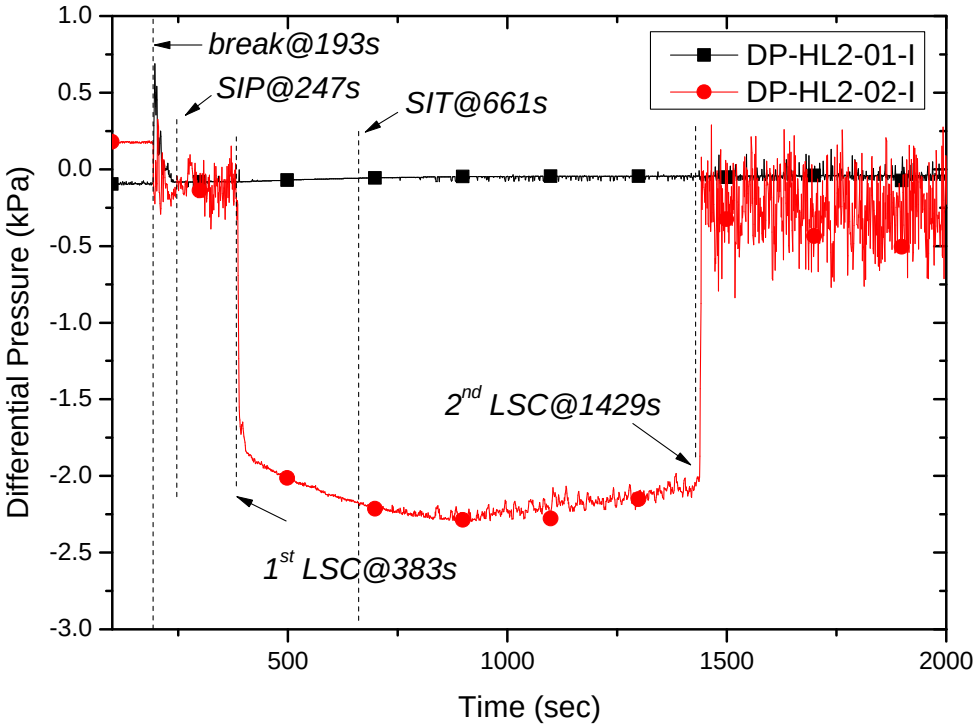

Figure 3.5-94 Differential pressures in the hot leg 2

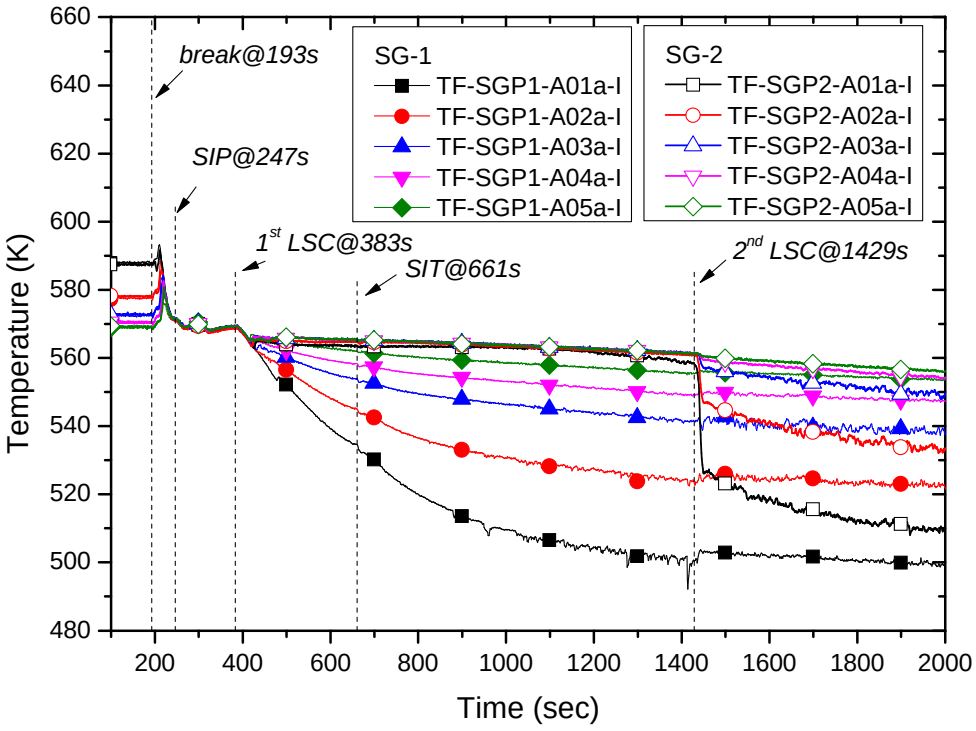

Figure 3.5-95 Primary fluid temperature distribution inside the ascending U-tube

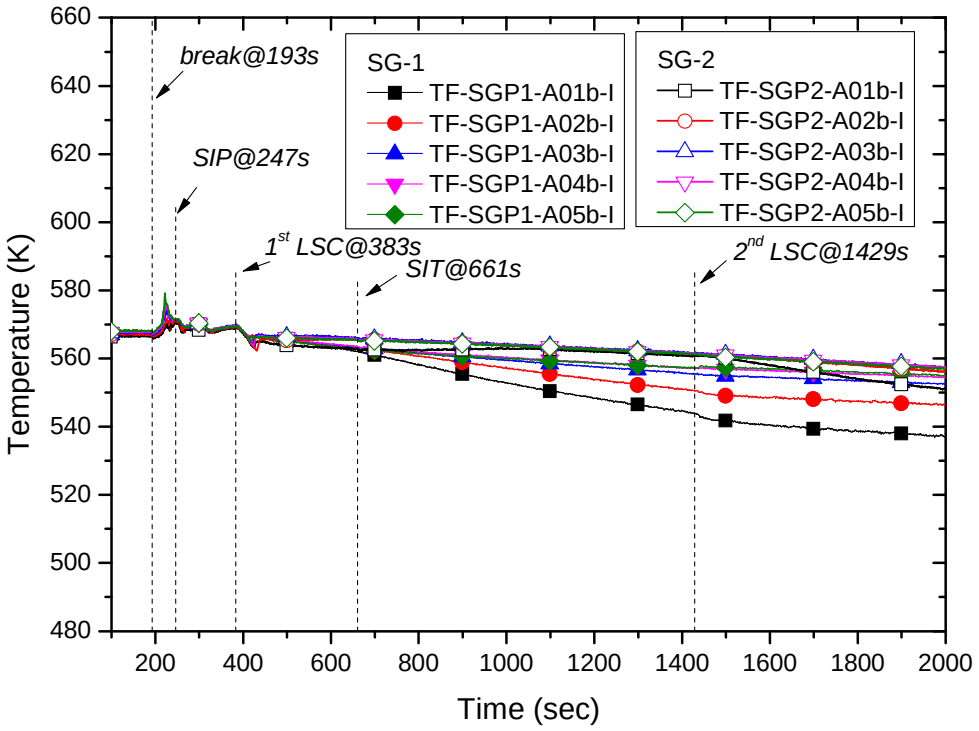

Figure 3.5-96 Primary fluid temperature distribution inside the descending U-tube

3.5.17 Water level distribution in the RCS loop

Transient behaviors of the collapsed water levels in the RCS loop, including the core, the down-comer, the hot, the intermediate, and the cold legs, the inlet and the outlet plenums of SGs and the SG U-tubes were summarized in Table 3.5-6. A RCS loop configuration of the ATLAS is shown in Figure 3.5-97. Detailed locations of the level transmitters and pressure transmitters in the RCS loop are shown in Figure 3.5-98 and Figure 3.5-99, respectively. Observed water level variation of each component of the RCS loop is described as follows:

The water level variations of the core, RPV upper head and the down-comer were explained in the previous Sections from 3.5.8 through 3.5.10. Collapsed water level distribution of each loop is shown in Figure 3.5-100, Figure 3.5-101, Figure 3.5-102, and Figure 3.5-103 for loop 1A, 1B, 2A, and 2B, respectively. It is evident that two loop seals in the loop 1 were abruptly cleared at occurrence of the 1st loop seal clearing. The water levels of the loop 1A showed the similar behavior to those of the loop 1B. Whereas the water levels in the loop 2 showed somewhat different behaviors from those in the loop 1.

Intermediate legs

First of all, the collapsed water levels in three parts of the intermediate legs were compared: vertical downward, horizontal, and vertical upward pipelines. At the 1st loop seal clearing, the collapsed water levels of the vertical downward intermediate legs in loop 1 LT-IL1A-01 and LT-IL1B-01 decreased to an empty condition and showed no change thereafter. Whereas the water levels in the vertical downward intermediate legs in loop 2 LT-IL1A-01 and LT-IL1B-01 decreased down to around 27% of the full range at the 1st loop seal clearing and started to decrease again to almost zero levels when the SITs started to inject water into the down-comer. At the 2nd loop seal clearing, LT-IL2A-01 the water level in loop 2A was recovered by relief of pressure build-up in the core but LT-IL2B-01 in the loop 2B was completely emptied.

The collapsed water levels of the horizontal intermediate legs in the loop 1 showed a sudden decrease to zero at the 1st loop seal clearing and remained empty during the remaining transient period. On the other hand, no significant changes in the collapsed water level in the horizontal intermediate leg of the loop 2A, LT-IL2A-02 was observed but the collapsed water level in the loop 2B, LT-IL2B-02 was emptied when the 2nd loop seal clearing occurred.

The collapsed water levels in the vertical upward intermediate legs were used to judge whether the loop seal clearing occurred or not. These water levels showed a sudden decrease to zero when the loop seal clearing happened. LT-IL1A-03 and LT-IL1B-03 showed a sudden drop indicating the 1st loop seal clearing. Whereas LT-IL2A-03 and LT-IL2B-03 did not show significant changes until the 2nd loop seal clearing occurred. As the pressurizer was installed at the hot leg 2, the volume of the loop 2 was larger than that of the loop 1. This difference in the volume might play a role in initiating the 1st loop seal clearing only in the loop 1.

The collapsed water level LT-IL2A-03 was around 0.8 m but LT-IL2B-03 was around 0.6 m shortly before the 2nd loop seal clearing as shown in Figure 3.5-102 and Figure 3.5-103. Such small hydrostatic head in the loop 2B initiated earlier loop seal clearing than the loop 2A. As the 2nd loop seal clearing equalized the differential pressure between the core and the cold legs instantaneously, it resulted in recovery of the water levels, LT-IL2A-01 and LT-IL2A-03. At the moment, it is not clear why the loop 2B was cleared faster than the loop 2A. It might be due to a small asymmetric pressure distribution among the loops.

Hot and cold legs

Note that before the test, the void fractions from the water level transmitters of the hot legs and cold legs were enforced to be zero by operators to achieve initial loop flow rates. At 100 s, such enforcement was released by operators and the water levels of the hot legs and cold legs dropped to about half of the initial values except for the cold leg 2A. That's the reason of the sudden drops of the measured water levels of hot legs and cold legs. So, water levels in these figures had a negative measurement error except for the cold leg 2A.

Hot legs

Collapsed water levels of the hot legs are compared in Figure 3.5-104. On break, the water levels of the hot legs decreased to around 50% of the full range and maintained the similar values between the hot legs 1 and 2. There was no recognizable difference between the two loops. Upon the 1st loop seal clearing, the water level in the hot leg 1 LT-HL1-01 decreased further to around 20% of the full range, but the water level the hot leg 2 was emptied. As only the two loop seals of the loop 1 were cleared, steam generated in the core flowed only through the loop 1 to the down-comer. This steam flow resulted in retardation of complete drain of the water in the hot leg 1. However, as there was no flow in the loop 2 because the loop 2 was still blocked by the loop seals, the water in the hot leg 2 was easily drained to be empty. This was the reason of higher water level in the hot leg 1 than that in the hot leg 2.

Cold legs

Collapsed water levels of the cold legs are compared in Figure 3.5-105. The water levels of

LT-CL1A-01 and LT-CL1B-01 suddenly dropped on the 1st loop seal clearing, but those of LT-CL2A-01 and LT-CL2B-01 showed relatively slow decreasing behaviors. It can be explained by the different hydraulic behaviors between the loop 1 and 2. In the loop 1, LT-CL1A-01 and LT-CL1B-01 suddenly decreased since the 1st loop seal clearing occurred only in the loop 1. On the contrary, in the loop 2, the water levels of the vertical downward intermediate leg, LT-IL2A-01 and LT-IL2B-01 reduced to about 26% levels. It pushed the water filled in the horizontal and the vertical upward intermediate legs, resulting in gradual decrease of the water level of the corresponding cold legs. In particular, the water level of the LT-CL2A-01 showed a partial recovery after reaching a certain minimum level. The main reason of this recovery is not clear. At around 2 minutes after the injection of SITs, LT-CL2A-01 and LT-CL2B-01 showed rapid increases. This raid increase in the water levels was due to the rising of the down-comer mixture level to the cold legs. The down-comer mixture level can be inferred from the previous figures, Figure 3.5-44 and Figure 3.5-47.

SG U-tubes

Figure 3.5-106 and Figure 3.5-107 show the water levels of the U-tubes of steam generator 1 and 2, respectively. In each figure, the water levels of the ascending and descending U-tubes were plotted. It can be seen that all the U-tubes were emptied before the 1st loop seal clearing. Overall, the water levels of the ascending U-tubes were slightly higher than those of the descending U-tubes. It was because the pressure in the hot leg side was higher than that in the cold leg side during the draining period.

SG plenums

The water levels in the inlet and the outlet plenum of the steam generators as shown in Figure 3.5-108 and Figure 3.5-109. Just before the 1st loop seal clearing, the water levels of the inlet plenums of both steam generators, LT-SGP1-04, LT-SGP2-04, showed rapid decreases. It was estimated to be due to that the water inventory in the inlet plenums of steam generators was drained to the core as the core water level was greatly depressed at that time. However, the water inventory of the inlet plenum compensated for the reduction of the hot leg inventory resulting in no significant variation of the water level in the hot legs.

After the 1st loop seal clearing, the water level of the inlet plenum of the steam generator 1 increased suddenly but the water level of the inlet plenum of the steam generator 2 decreased to zero. The water level increase in LG-SGP1-04 was due to the transfer of the water in the hot leg 1 to the inlet plenum. As the loop 2 was still blocked, the water of the hot leg and the inlet plenum of loop 2 were drained to the core. The water level of the inlet plenum of the steam generator 1 showed a linear decrease after the 1st loop seal clearing and an increase just after the actuation of SITs. The decrease was due to boiling of the water in the inlet plenum and

the increase was due to refilling in the core by the SIT injection.

At the 2nd loop seal clearing, the water level in the inlet plenum of the steam generator 1, LT-SGP1-04 showed a shallow depression and a continuous increase afterward. The water level in the inlet plenum of the steam generator 2, LT-SGP2-04 showed a sudden increase up to the similar level to that of steam generator 1.

On the other hand, the water levels of the outlet plenums of the steam generators decreased to zero a little before the 1st loop seal clearing and remained the empty condition during the remaining test period.

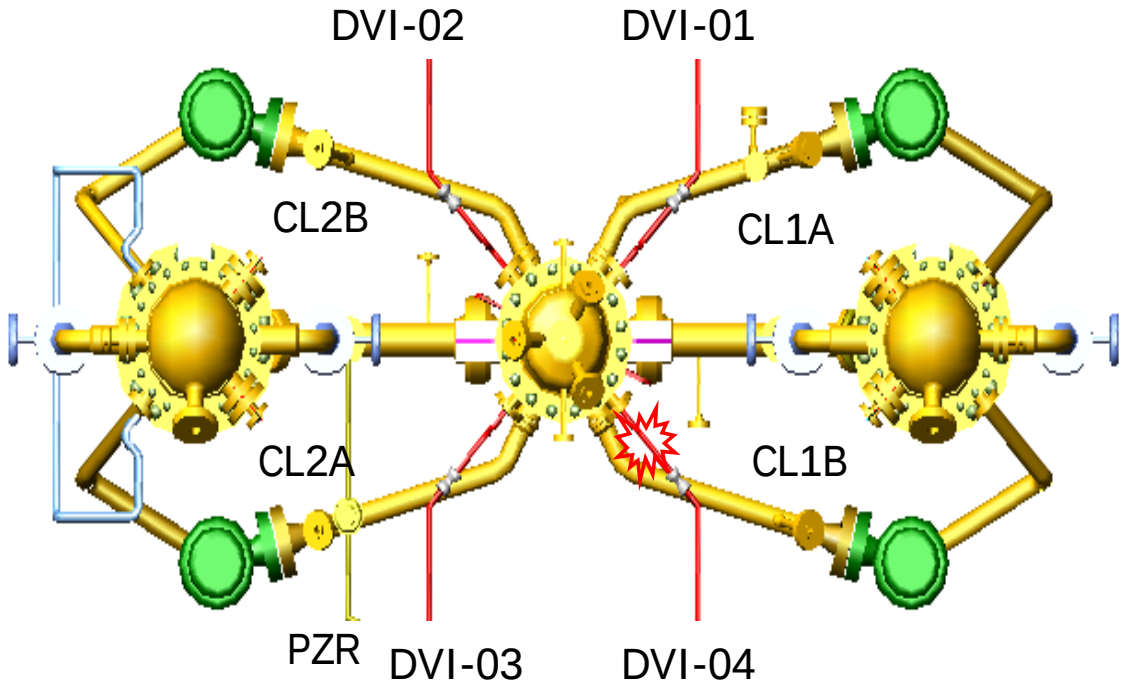

Figure 3.5-97 RCS loop configuration

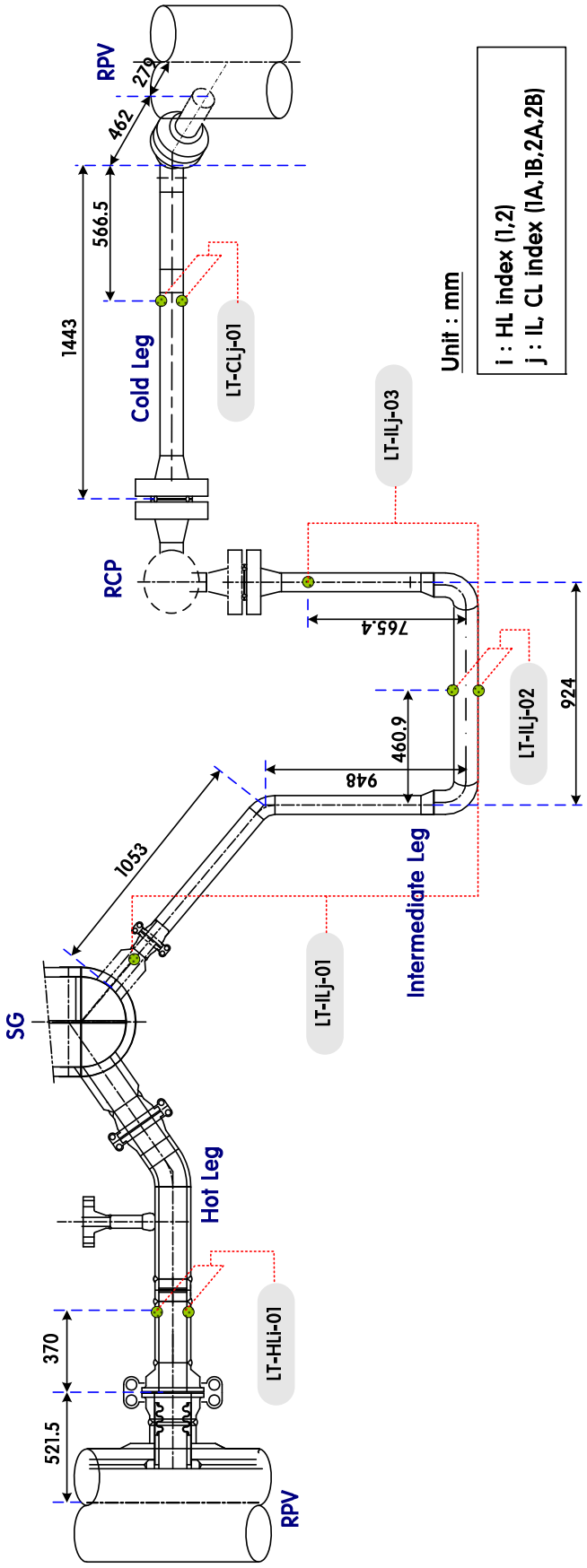

Figure 3.5-98 Level transmitters in RCS loop

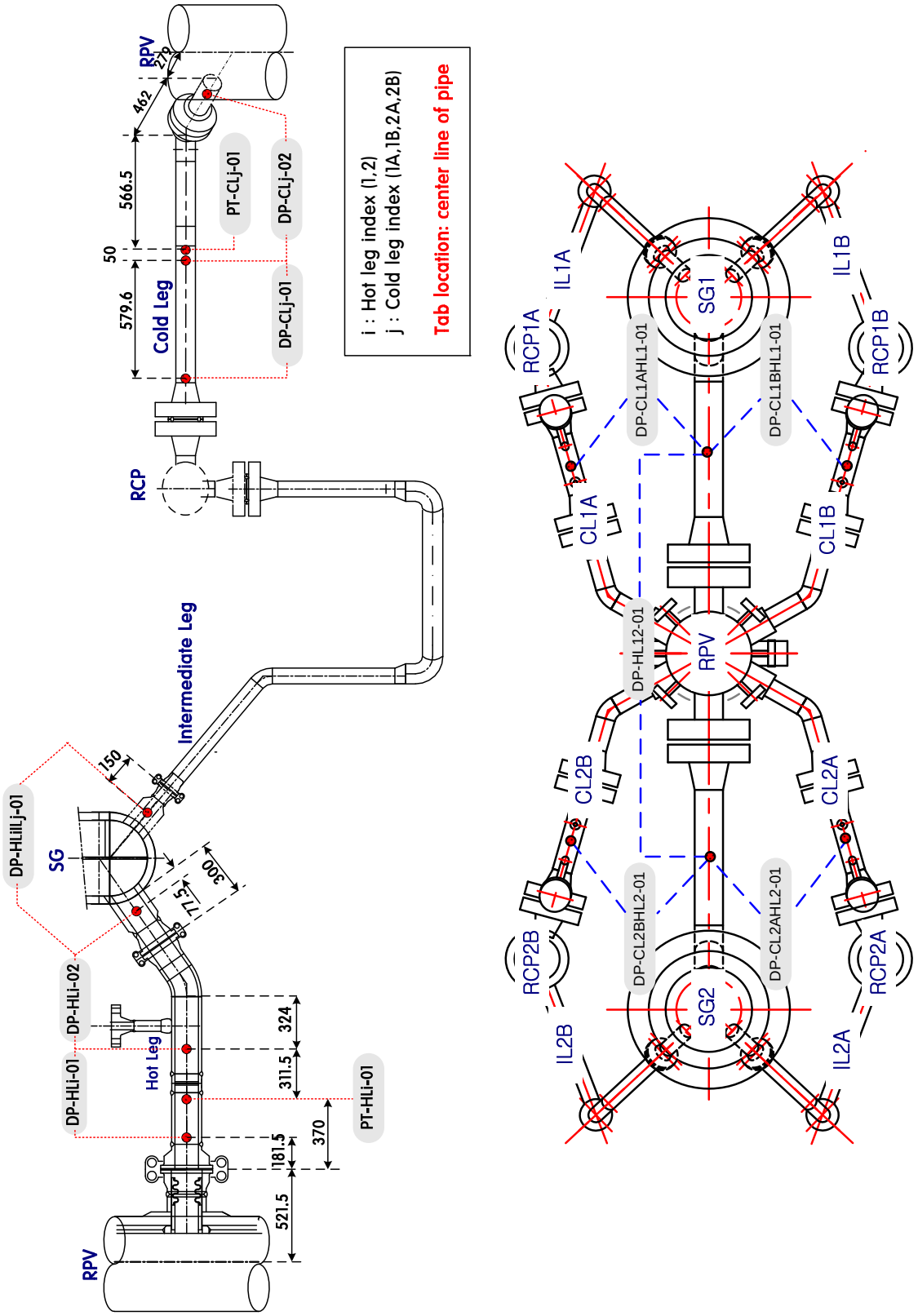

Figure 3.5-99 Pressure transmitters in RCS loop (plan view, cross view)

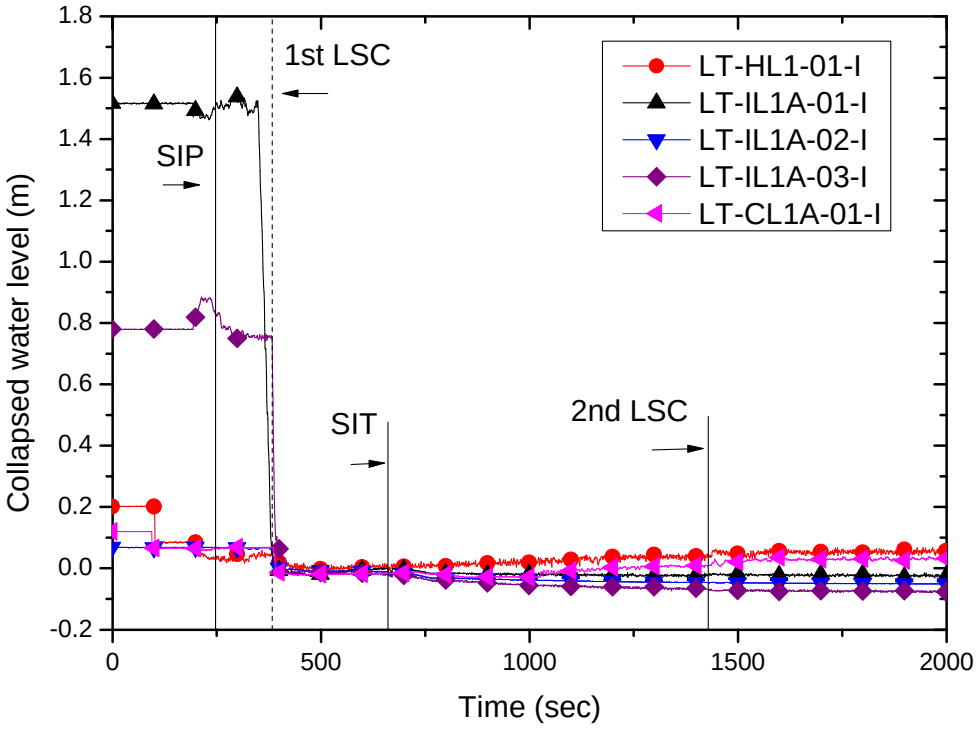

Figure 3.5-100 Water level distribution along the loop 1A

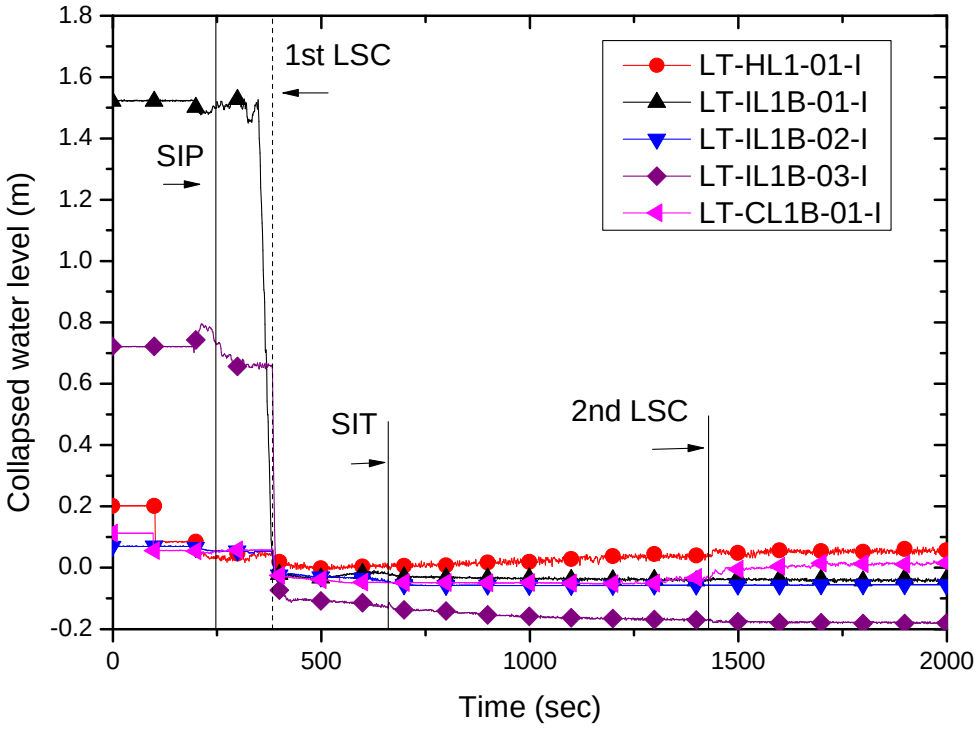

Figure 3.5-101 Water level distribution along the loop 1B

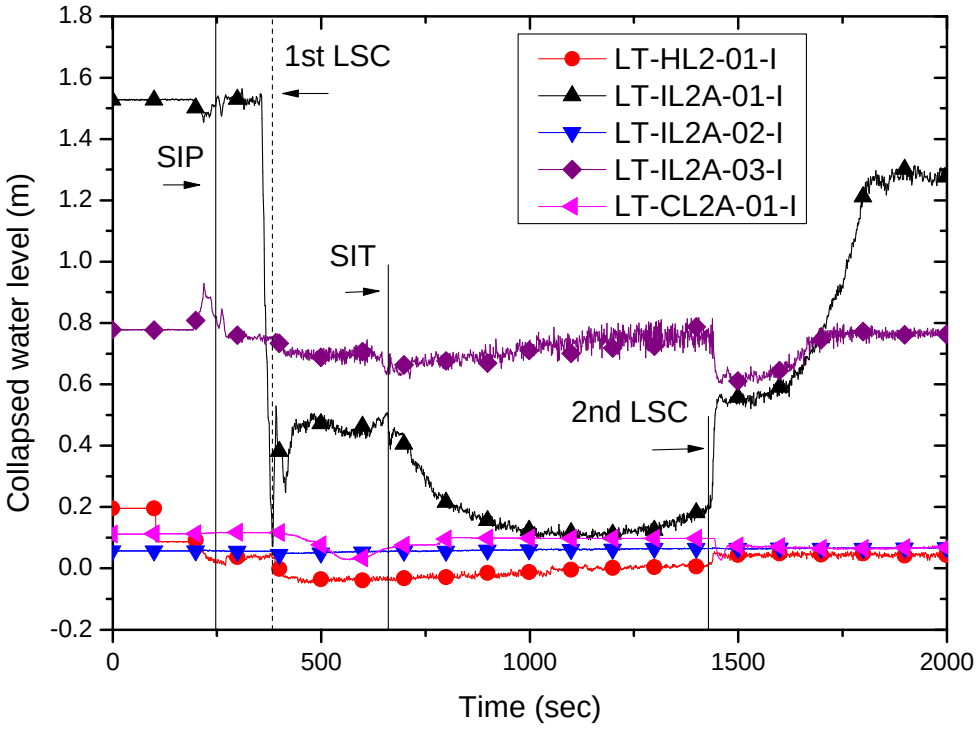

Figure 3.5-102 Water level distribution along the loop 2A

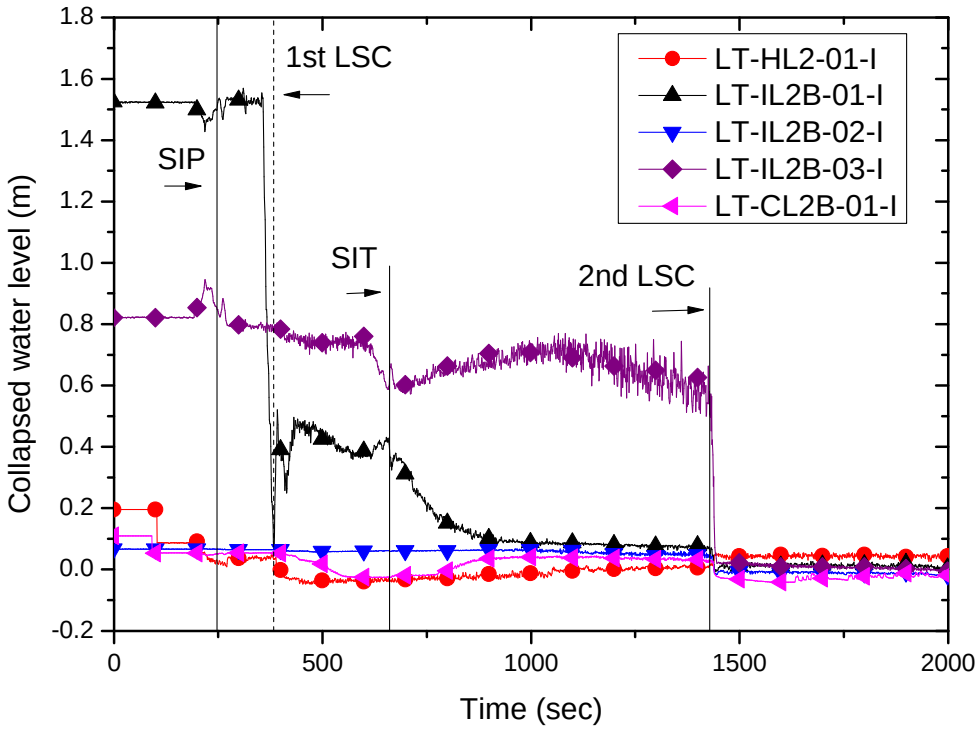

Figure 3.5-103 Water level distribution along the loop 2B

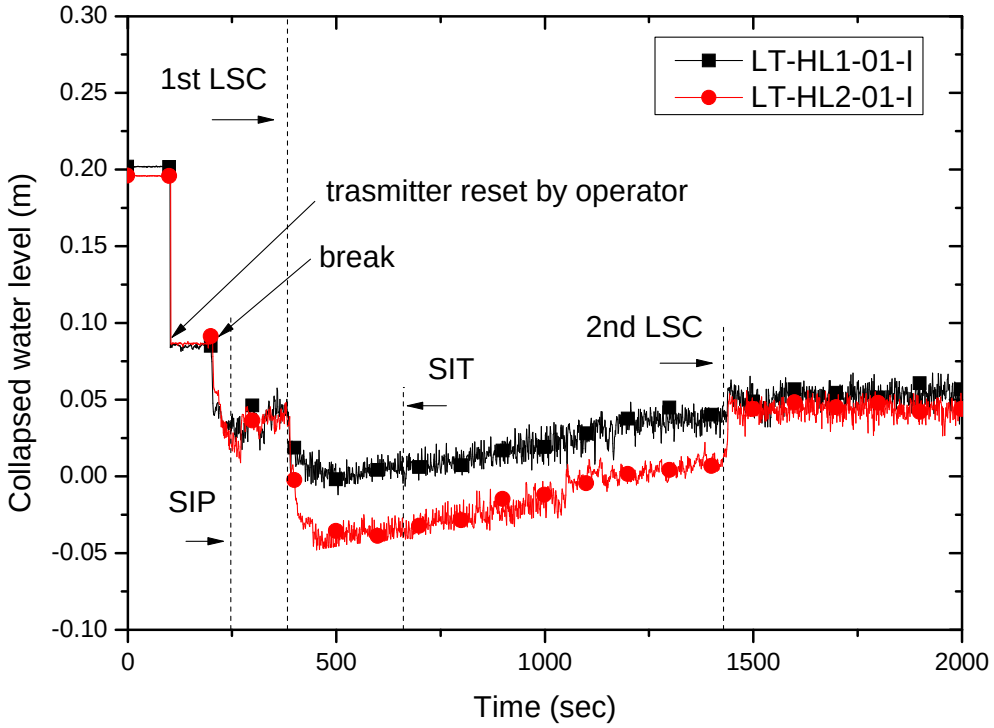

Figure 3.5-104 Comparison of water levels between the hot leg 1 and 2

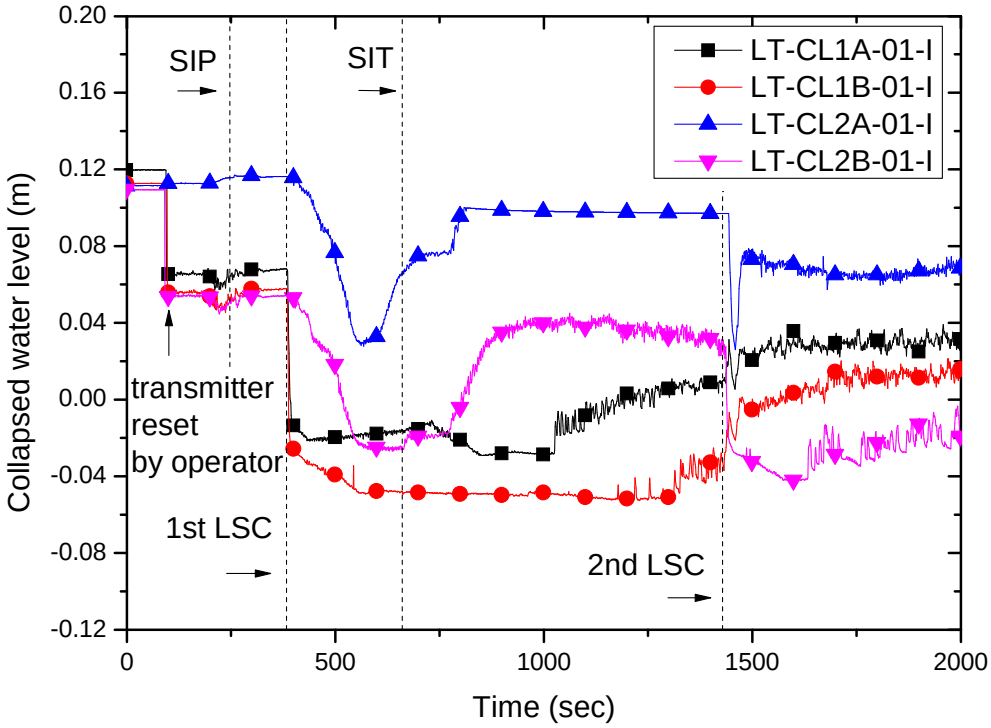

Figure 3.5-105 Comparison of water levels among the cold legs

Table 3.5-6 Collapsed water level behaviors in the RCS loop

Phase	**Before 1st LSC**	**After 1st LSC**	**After SIT injection**	**After 2nd LSC**	**Reference Figure**
Core (LT-RPV-01)	deep depression	Recovery and mixture level near HL	slight increasing	slight increasing after shallow depression	Figure 3.5-43
Down-comer (LT-RPV-04A)	near broken DVI nozzle	continuous decreasing	continuous recovery	slight increasing after shallow depression	Figure 3.5-44
Hot leg 1 (LT-HL1-01)	constant ~50%	sudden decrease to~20%	slight increasing	sudden increase to ~50%	Figure 3.5-104
Hot leg 2 (LT-HL2-01)	constant ~50%	sudden decrease to empty	slight increasing lower than HL-1	sudden increase to ~50%	Figure 3.5-104
U-tubes of SG-1 (LT-SGP1-03A,B)	continuous decreasing	empty	empty	empty	Figure 3.5-106
U-tubes of SG-2 (LT-SGP2-03A,B)	continuous decreasing	empty	empty	empty	Figure 3.5-107
Inlet plenum of SG1 (LT-SGP1-04)	sudden decrease near LSC	sudden recovery and decrease again	continuous increasing	slight increasing after shallow depression	Figure 3.5-108
Inlet plenum of SG2 (LT-SGP2-04)	sudden decrease near LSC	empty	empty	sudden increase to similar to SG-1	Figure 3.5-109
Outlet plenum of SG1 (LT-SGP1-05)	sudden and earlier decrease than inlet plenum near LSC	empty	empty	Empty	Figure 3.5-108
Outlet plenum of SG2 (LT-SGP2-05)	sudden and earlier decrease than inlet plenum near LSC	empty	empty	empty	Figure 3.5-109

Vertical downward leg Loop 1 (LT-IL1A-01)	a little reduction	empty	empty	empty	Figure 3.5-100
Vertical downward leg Loop 1 (LT-IL1B-01)	a little reduction	empty	empty	empty	Figure 3.5-101
Vertical downward leg Loop 2 (LT-IL2A-01)	a little reduction	sudden decrease to ~27%	continuous decrease to empty	Sudden and continuous increase to ~80%	Figure 3.5-102
Vertical downward leg Loop 2 (LT-IL2B-01)	a little reduction	sudden decrease to ~27%	continuous decrease to empty	empty	Figure 3.5-103
Horizontal int. leg (LT-IL1A,1B-02)	no significant change	sudden decrease to empty	empty	empty	Figure 3.5-100 ~ Figure 3.5-101
Horizontal int. leg (LT-IL2A-02)	no significant change	no significant change	no significant change	no significant change	Figure 3.5-102
Horizontal int. leg (LT-IL2B-02)	no significant change	no significant change	no significant change	empty	Figure 3.5-103
Vertical upward int. leg Loop 1 (LT-IL1A-03)	a little reduction	sudden decrease to empty	empty	Empty	Figure 3.5-100
Vertical upward int. leg Loop 1 (LT-IL1B-03)	a little reduction	sudden decrease to empty	empty	empty	Figure 3.5-101
Vertical upward int. leg Loop 2 (LT-IL2A-03)	a little reduction	a little reduction	no significant change	a little reduction and recovery	Figure 3.5-102
Vertical upward int. leg Loop 2 (LT-IL2B-03)	a little reduction	a little reduction	no significant change	sudden decrease to empty	Figure 3.5-103

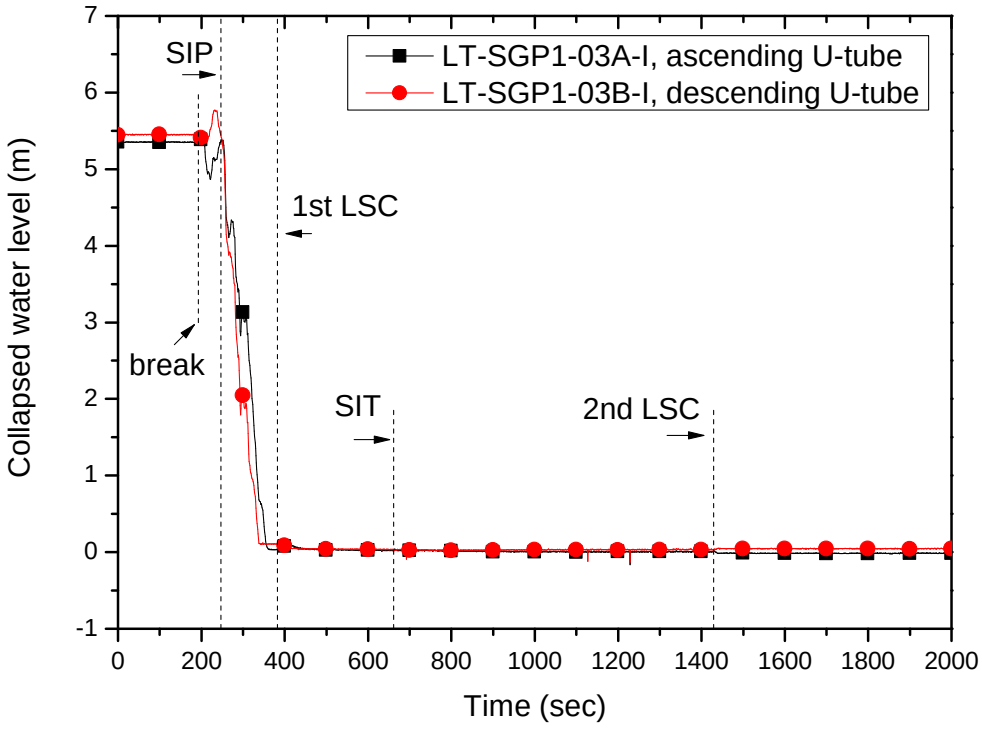

Figure 3.5-106 Water levels in the primary U-tube of steam generator 1

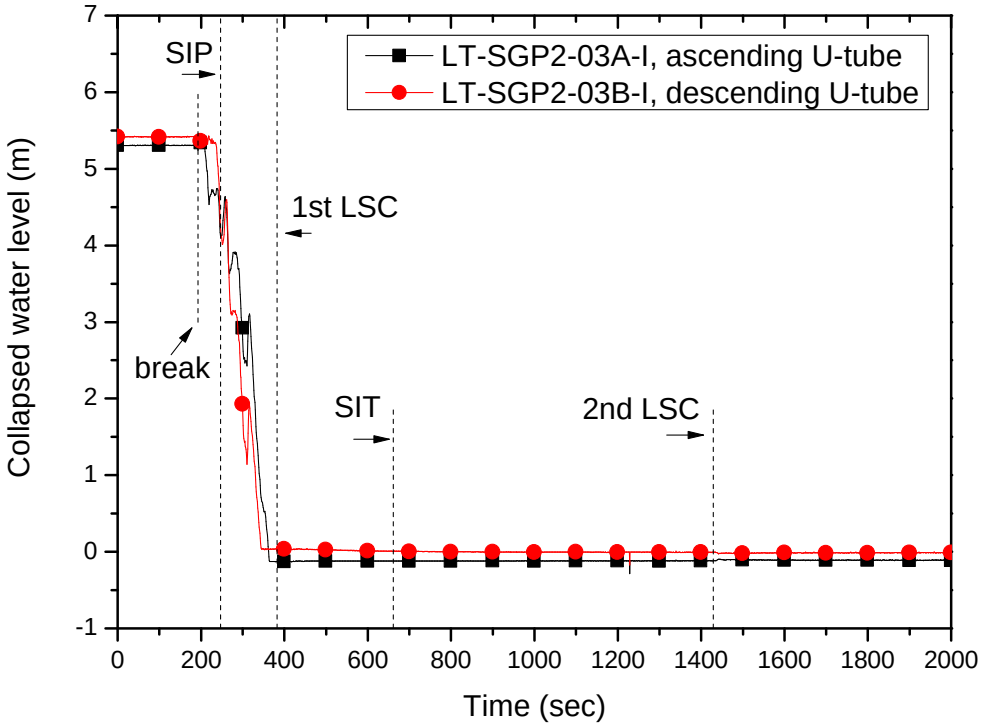

Figure 3.5-107 Water levels in the primary U-tube of steam generator 2

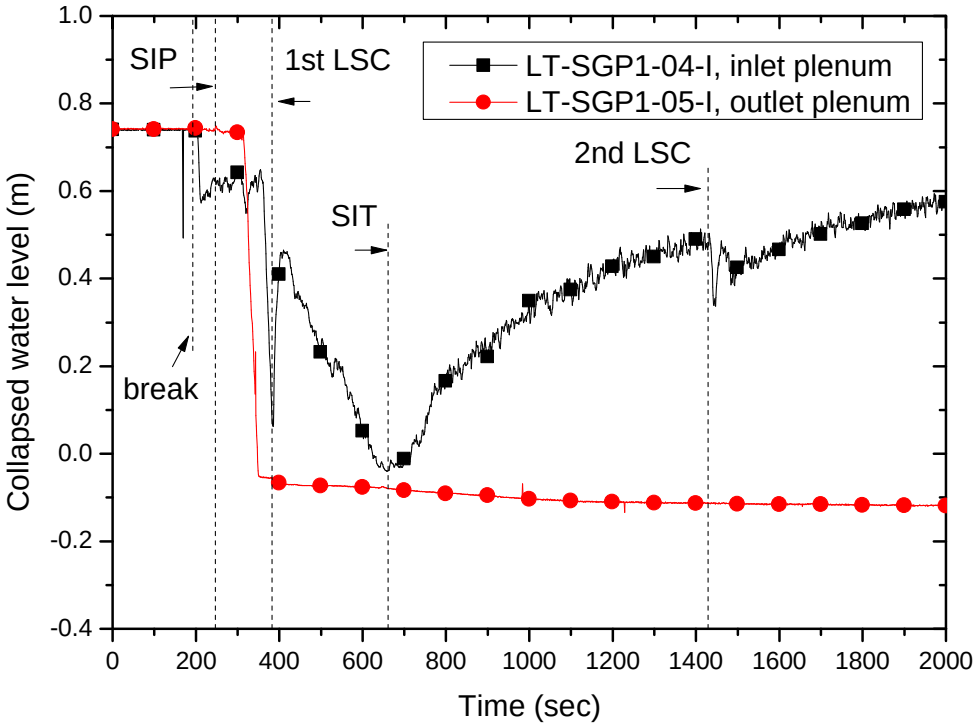

Figure 3.5-108 Water levels of inlet and outlet plenum of steam generator 1

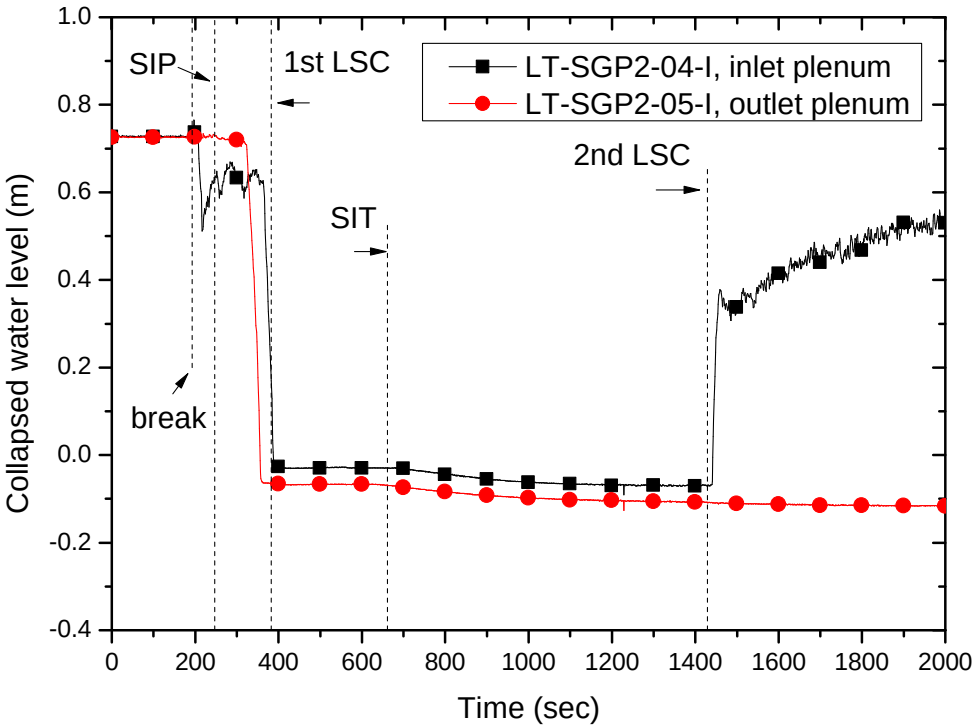

Figure 3.5-109 Water levels of inlet and outlet plenum of steam generator 2

3.5.18 Loop seal clearing

Occurrence of a loop seal clearing was detected from the level data of the vertical intermediate leg at the suction pipeline of the RCP: LT-IL1A-03, LT-IL1B-03, LT-IL2A-03, and LT-IL2B-03. In the ISP-50 test, two loop seals in the loop 1 were cleared at 383 s followed by the second loop seal clearing in the loop 2B at 1429 s as shown in Figure 3.5-110. The remaining loop seal in the loop 2A was not cleared during the test period. In the test for the same break size, named as SB-DVI-07 which was performed one year before the ISP-50 test, very similar loop seal clearing behavior was measured as shown in Figure 8.5-4. In the test SB-DVI-07, the first loop seal clearing occurred in both loops 1A and 1B at 379 s and the loop 2B was cleared at 1250 s with the loop 2A remained. Even though there was a little time difference in the occurrence of loop seal clearings between the two tests, it can be noteworthy that the location and the sequence of the loop seal clearing were well reproduced in two tests.

The potential reason of the non-uniform loop seal clearing can be inferred from the measured differential pressures between the inlet and outlet plenums of each SG as shown in Figure 3.5-111: DP-HL1IL1A, DP-HL1IL1B, DP-HL2IL2A, and DP-HL2IL2B. The pressure taps were located at the inlet and outlet nozzles of SGs as shown in Figure 3.5-99. The differential pressure between the inlet and the outlet of SGs increased with fluctuations and reached their maximum values just before the first loop seal clearing at the loop 1A and 1B. At the instant of the loop seal clearing, these differential pressures at the loop-1 showed a sharp fluctuation and after then they continuously decreased until the actuation of the SIT. After the actuation of the SIT through three intact DVI nozzles, the differential pressures measured by DP-HL1IL1A and DP-HL1IL1B returned to increase mainly due to the water accumulation in the hot leg-1 and the up-flow side of the U-tubes of the SG-01.

On the other hand, the differential pressures of the loop-2 show a different behavior as shown in Figure 3.5-111. The differential pressures measured by DP-HL2IL2A and DP-HL2IL2B decreased to the minimum level at the instant of the loop seal clearing and the minimum differential pressure was maintained until the second loop seal clearing occurred at the IL-2B at 1429 s. When the 2nd loop seal clearing occurred at IL-2B, the differential pressures DP-HL2IL2A and DP-HL2IL2B increased suddenly, it was due to an increase in the hydrostatic pressure of the inlet plenum of SG-2 caused by the water accumulation in HL-2. The measured water level in the inlet and outlet plenum of each steam generator is shown in Figure 3.5-108 and Figure 3.5-109, respectively. The exact locations of the level taps are shown in Figure 2.4-5. Also the measured water levels in the hot legs are shown in Figure 3.5-104. By comparing Figure 3.5-111 with Figure 3.5-108 and Figure 3.5-109, it can be found that the differential pressures between the inlet and outlet plenums of the steam generator were closely related to the water level not

in the outlet plenum but in the inlet plenum of steam generators. That is the reason why the same sharp increases in DP-HL2IL2A and DP-HL2IL2B were obtained at the 2nd loop seal clearing, even though the loop seal in loop 2A was not cleared at that time.

After the 1st loop seal clearing, circulation flow was initiated only in the loop-1, which resulted in the coolant accumulation in the HL-1 and the inlet plenum of the SG-1 as shown in Figure 3.5-104 and Figure 3.5-108. In particular, the water level of the inlet plenum of the SG-1 experienced a sharp increase, and then linearly decreased due to the reverse heat transfer from the 2nd side of the SG-1. With the start of the SIT injection, measured water level was increased again. On the other hand, the loop-2 was in a relatively low or no circulation flow state. Therefore, coolant was not accumulated in the HL-2 and the inlet plenum of the SG-2. The increased water inventory in the inlet plenum of SG-1 just before the second loop seal clearing could be acted as a partial blockage for the flow conduit, which could lead the second loop seal clearing to compensate the differential pressure between the core and the down-comer.

Undoubtedly, the coolant accumulation in the HL-2 was resulted by the coolant circulation through the cleared intermediate leg-2B. From the observation of the different differential pressure trend between the loop-1 and the loop-2, we can understand that the main circulation flow in the primary loop between the 1st and the 2nd loop seal clearing phase is occurred in the loop-1. During this period, the loop flow in the loop-2 is very weaker than that of the loop-1. This indicates that the system depressurization was performed mainly by the broken loop through vent of high pressure steam to the break point, but the venting capacity through the loop-1 was not enough to keep the hydrostatic head balance of the system. Therefore, the loop-2 was also cleared to result in an additional venting capacity. Due to this second loop seal clearing at loop-2B, the down-comer water level decreased, and the fluid temperature in the cold leg started to fluctuate, and the flow rate from the SIT abruptly increased.

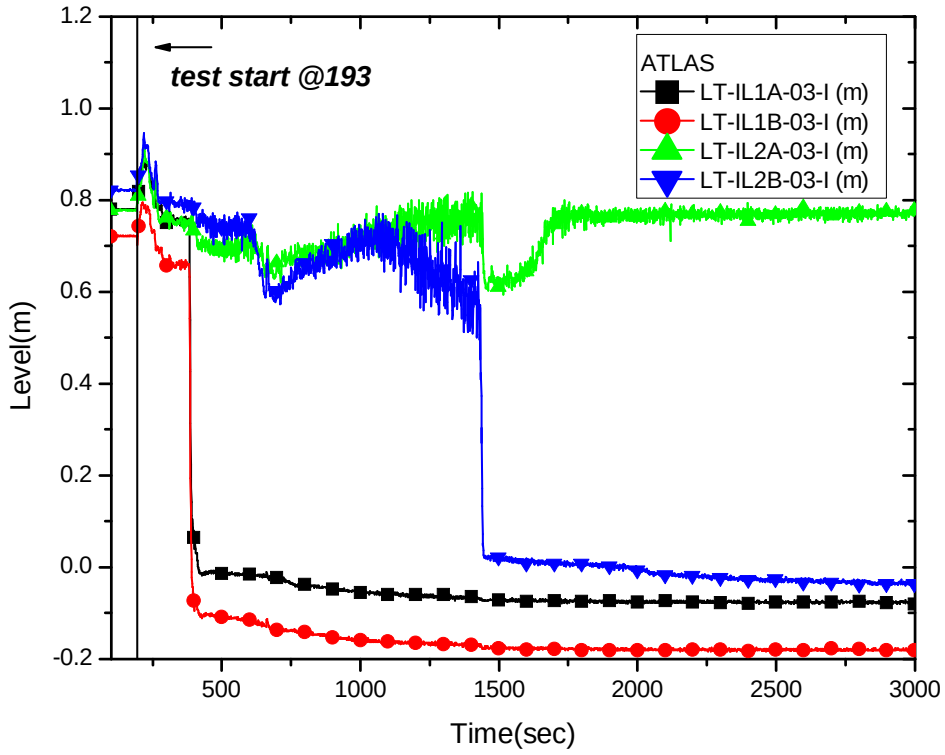

Figure 3.5-110 Collapsed water levels of the vertical intermediate legs for SB-DVI-09 (50%)

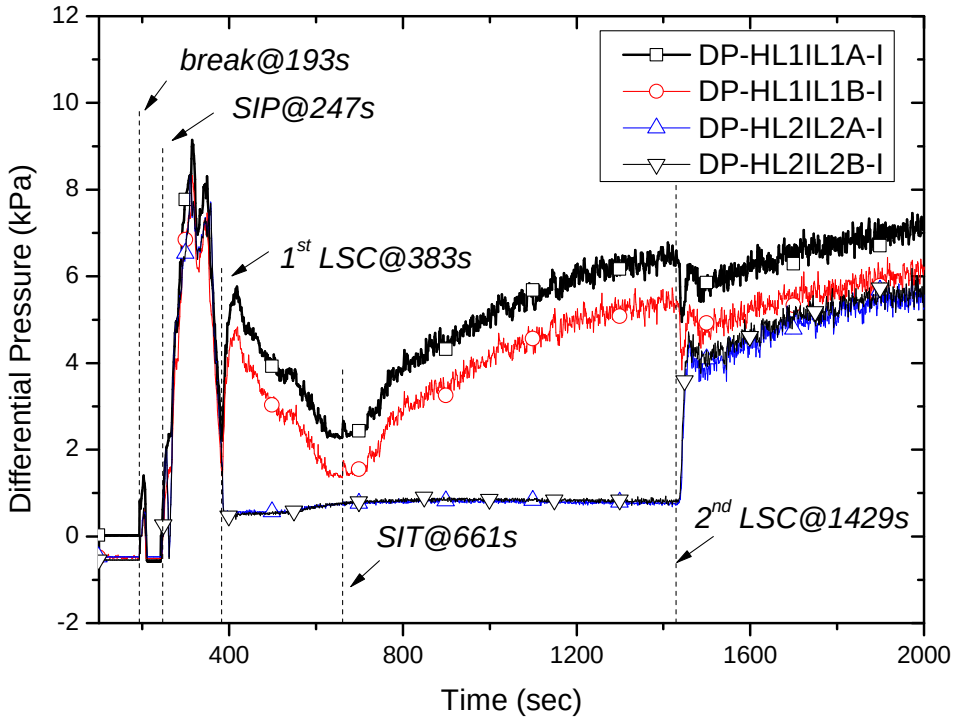

Figure 3.5-111 Differential pressure trends between the inlet and the outlet plenum of each SG

3.6 Measurement uncertainties

3.6.1 Loop flow rate

Flow rate in the RCS loop during transient period has a high priority from a viewpoint of instrumentation. There is much difficulty in measuring the loop flow rate especially in the transient period because a two-phase flow rather than a single-phase flow is expected to occur. In the ATLAS, a BiFlow flowmeter which was developed by the operating agency was installed at 2 hot legs and 4 cold legs. In principle, it can measure a flow rate in a single-phase condition as well as in a two-phase condition if a void fraction at the measuring location is available. Thus, a level transmitter was attached at the measuring location together with the BiFlow meter. However, the measured void fractions (or water level) at the legs have much uncertainties due to the small diameter of the legs. ($\mathrm{D_{HL}} = 132\mathrm{mm},\ \mathrm{D_{CL}} = 87\mathrm{mm}$) The uncertainty of the loop flow rate thus greatly depends on the accuracy of the water level of the loop.

In order to avoid the uncertainties caused by the water level measurement, the void fractions of the loops were enforced to be zero at the initial steady state condition by operators. After logging the data for around 100 s, the enforcing on the water level was released for the instrument to be ready to measure two-phase flow rate.

Applicability of the BiFlow flowmeter for the measurement of a two-phase flow rate was examined by performing a calibration test [Yun *et al.*[1], 2005; Yun *et al.*[2], 2005; Kang *et al.*[2], 2009]. The calibration test was conducted at the horizontal air/water test loop whose schematic diagram is shown in Figure 3.6-1. The horizontal air/water test loop consists of a test section, an inlet reservoir, an outlet reservoir, a water supply system, an air supply system, a water storage tank, and a data acquisition system. The test section is composed of a transparent acryl pipe whose diameter is 0.08 m similar to that of the cold leg of the ATLAS. A Coriolis mass flowmeter and a vortex flowmeter were installed at the inlet of the test section to measure the reference flow rates of water and air, respectively.

The flow regime of the calibration test was a stratified flow which is expected to be a major flow regime in the cold legs during the transient period of the ATLAS. In the calibration test, the void fraction was changed from 35% to 94%, and the velocity ranges were 0.3-1.2m/sec and 3.0-18m/sec for the water and the air flows, respectively. The two-phase flow rates measured by the BiFlow flowmeter were compared with the reference flow rates measured by the Coriolis and the vortex flowmeters. Figure 3.6-2 shows the comparison between the reference flow rates and the flow rates measured by the BiFlow flowmeter in the present calibration test. As shown in Figure 3.6-2, the BiFlow flowmeter can measure the two-phase flow rates within a ±

15 % error against the reference flow rates. It was confirmed from the calibration test that the BiFlow flowmeter can measure a two-phase flow rate with an acceptable measurement uncertainty for an anticipated flow regime in the cold legs during the transient period of the ATLAS.

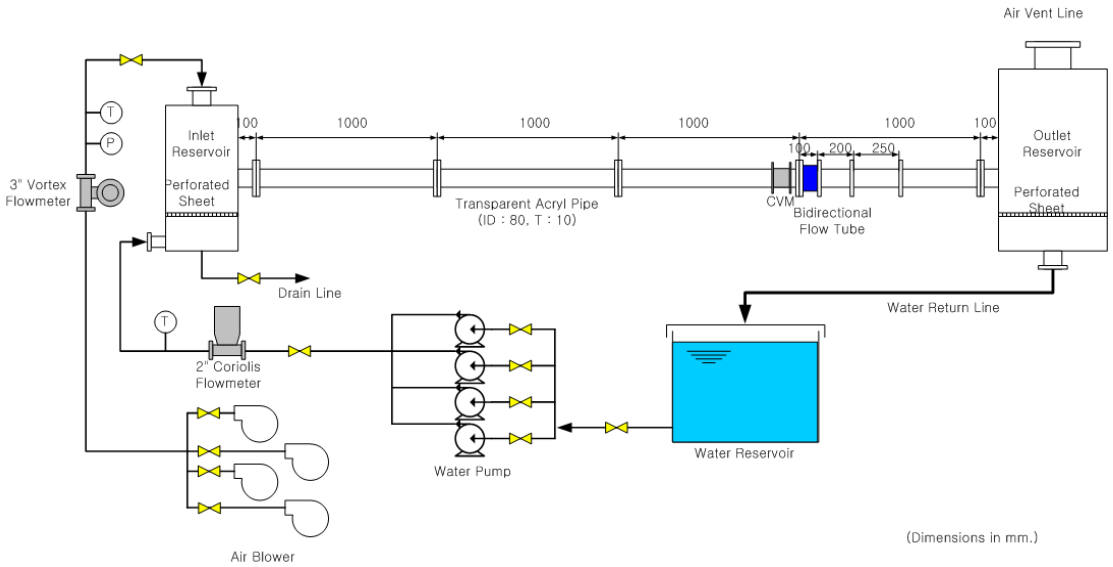

Figure 3.6-1 Schematic diagram of the horizontal test loop

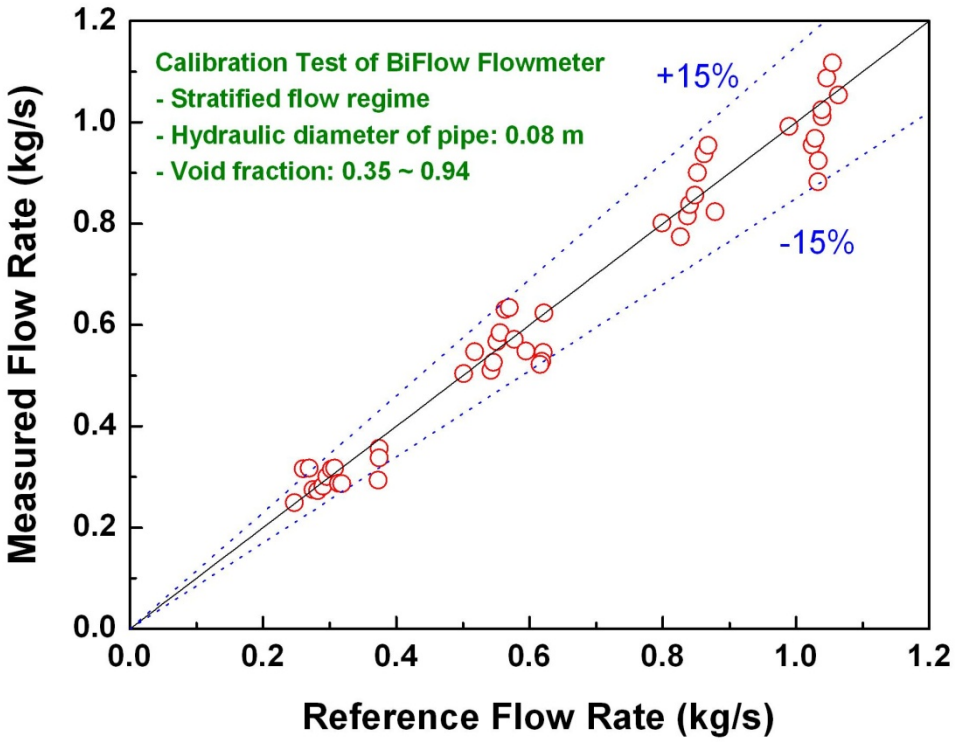

Figure 3.6-2 Comparison of the two-phase flow rates in the calibration test

3.6.2 Collapsed water level

Collapsed water levels were instrumented to investigate inventory distribution during the transient. A total of 11 instruments were installed at the major components, including RPV, DC, RCS loops, SG, and etc. The collapsed water level h can be measured from the momentum balance assuming a static condition as follows:

$$h = \frac{(\rho_c - \rho_g)gH - \Delta P_{measured}}{(\rho_h - \rho_g)g} \quad , \tag{3.6.1}$$

where ρ_c, ρ_g, ρ_h is density of water in the pressure impulse line, steam and water in the component of interest, respectively. H and g is the distance between the measurement taps, the gravitational constant, respectively. $\Delta P_{measured}$ is the measured differential pressure. The measured differential pressure is composed of pressure drops due to hydrostatic head, acceleration, friction, and geometric change as follows:

$$\Delta P_{measured} = \Delta P_{hydrocstat\ ic} + \Delta P_{accelerati\ on} + \Delta P_{friction} + \Delta P_{form} \quad . \tag{3.6.2}$$

If there is no flow, the other terms could be negligible except for the hydrostatic term, $\Delta P_{hydrostati\ c}$, and then Equation (3.6.1) is applicable ideally. However, if there exists a high flow in the component of interest, for instance during the initial phase of the test, the measured differential pressure could be affected by the neglected terms of Equation (3.6.2). The possible errors could be estimated from Equation (3.6.2). The pressure drop due to acceleration is negligible assuming a slow velocity change, but the pressure drops due to friction and geometric change increase proportional to the square of fluid velocity as follows:

$$\Delta P_{error} = \Delta P_{friction} + \Delta P_{form} = (f\frac{L}{D} + K_{form}) \cdot \frac{1}{2}\rho v^2 \quad . \tag{3.6.3}$$

The maximum errors due to friction and geometric change were estimated based on the following assumptions:

- Maximum break flow rate of 4 kg/s.
- The pressure and temperature conditions of 15.0 MPa and 600 K, respectively.

The collapsed water levels in the core, the down-comer, and the RCP suction side of the intermediate leg were analyzed and the calculation results were summarized in Table 3.6-1. During the initial phase of the test, the maximum possible uncertainties for each location were found to be 1.8%, 2.6%, and 8.6%, respectively.

Table 3.6-1 Estimation of the maximum possible uncertainty of the collapsed water level

Parameter	Core (LT-RPV-01)	Down-comer (LT-RPV-04A)	Intermediate leg RCP side, vertical (LT-IL1A-03)
Discharge coefficient-friction, $K_{friction}$	7.16	1.68	0.155 (vertical) 0.159 (horizontal)
Discharge coefficient-form, K_{form}	42.7	0	0 (vertical) 0.719 (horizontal)
Total differential pressure (kPa), ΔP_{error}	0.343	0.754	0.460
Equivalent head (m), h_{error}	0.053	0.117	0.070
LT full range (m), h	2.91	4.5174	0.8717
Uncertainty (%), h_{error}/h	1.8	2.6	8.6

3.6.3 Differential pressure

The Differential pressures (DP-HL1IL1A-01, DP-HL1IL1B-01, DP-HL2IL2A-01, and DP-HL2IL2B-01) between the inlet and outlet plenum of SGs were measured by KDG 4301 differential pressure transmitter. In the ATLAS, pressure taps for these instruments were located in the hot legs (6", SCH.160) and the corresponding intermediate legs (6", SCH.160). Therefore, velocity difference between the hot leg and the intermediate leg could cause the additional error in the measured differential pressure. From the Equation (3.6.3) of Section 3.6.2, the maximum uncertainty due to the velocity difference was estimated to be 0.0035 kPa. Therefore, the uncertainty due to the velocity difference between two measurement taps could be very small. However, considering the total error of the measured differential pressure accounting for the system error and the velocity difference error, the total uncertainty of the measured differential pressure was estimated to be 0.234 kPa.

3.6.4 Temperature

In the ATLAS system, the temperatures were measured by K-type thermocouples, and the maximum uncertainty of the temperature was estimated to be 2.4 ºC.

3.6.5 Break flow

Two-phase break flow from the break nozzle was separated in a separating vessel in the

actual test. The separated water inside the separating vessel was drained into the measuring vessel where its mass was weighed by a load cell. The separated water mass showed an increasing trend with time due to the inflow from the break system. The water mass change rate with respect to time was converted to a break water flow rate. Meanwhile the separated steam flow rate was measured by a vortex flow meter which was installed at the steam discharge line at the top of the separating vessel. The total break flow rate was calculated by summing the water and steam flow rates. This measuring concept of a break flow rate was effective for a slow transient condition, but the initial break flow of the present test was compensated by an RCS inventory-based break flow estimation method in order to avoid an additional dynamic load effect on the load cell itself by high steam flow.

As described in Section 3.5.6, the RCS inventory-based break flow estimation method has been developed as an alternative method to the load cell-based break flow rate measurement. This measurement method was used to complement the break flow data in the initial stage of the present test. It is based on the mass balance of the reactor coolant inventory in the primary system. The maximum uncertainties of break flow rates measured by this load cell-based measuring system and by the RCS inventory change were estimated to be 0.07 and 0.59 kg/s, respectively. The uncertainty of the flow rate estimated from RCS inventory change basically originates from the uncertainty of the level transmitters and is considerably higher than that measured by load cell-based measuring system. As shown in Figure 3.5-35, the break flow rate was high and fluctuating during the earlier stage up to around 364 s and it maintained a low steady flow thereafter. The break flow rate during this earlier stage was estimated from the RCS inventory-based method with relatively smaller uncertainty, and the later break flow rate thereafter was obtained by the load cell-based method with relatively lower uncertainty. Thus the obtained final break flow and the accumulated break flow mass were shown in Figure 3.5-37 and Figure 3.5-38.

4. Comparison of Blind Predictions with Data

4.1 Initial and boundary conditions

The ISP-50 participants were grouped into 4 sub-groups by taking into account the similarity of the code used as shown in Table 4.1-1.

Table 4.1-1 Grouping of the submitted participants

Group ID	Participants index	Code used	Remarks
A	KAERI, KEPRI, KTH, NRC	MARS or TRACE	4 orga'ns
B	CIAE, UNIPI, KNF, KOPEC1, KOPEC2	RELAP series	5 orga'ns
C	GP1, GP2, GP3, GP4	KORSAR/GP or TECH-M	4 orga'ns
D	GRS, NRI, FORTUM, VTT	ATHLET, APROS	4 orga'ns

The initial and boundary conditions used by all the calculations are listed in Table 4.2-1. Key parameters among the requested parameters were selected and compared with the data in order to check whether the calculations were performed in conformity with the actual test conditions. Calculated values of the submitted calculation results at an initial time were listed and reference data column number was also included in the table.

4.2 Nodalization and sequence of events

Nodalization schemes were different from participant to participant as each participant used their preferred method based on his previous experience. Table 4.2-2 shows a summary of nodalization schemes used in the present exercise. Drawings and description provided by the participants are included in the Appendix-C of this report. In the present blind phase, detailed information on the nodalization schemes used by participants was not requested. However, the nodalization information was gathered in the following open phase.

Table 4.2-3 shows the sequence of events calculated by the participants and compares them with the experimental data. In order to summarize the sequence of events in calculations and to compare them with the data, the break time for all submitted calculations and experiment was adjusted to be 0.0 s. The MSSV opening characteristics were modeled only by 8 participants among the 17 participants. The other 9 participants need to improve their calculations by considering the actual MSSV characteristics. With regard to the first opening time of the MSSVs, there existed some delay in time compared with the data. Only the GRS and UNIPI's predictions were within a reasonable accuracy.

The LPP trip times, in general, were well predicted by all calculations. The KOPEC's calculation showed more rapid depressurizations than the data. On the other hand, GP3, GP4 and FORTUM predicted slower depressurization of the primary system than the data. The RCP trip time has no special importance on the current transient because the RCP was operated in a free running condition from the beginning of the test. The initial condition of the test was achieved at a natural circulation condition. Therefore, the RCP trip time of 25 s in the present test did not cause any change in the RCS flow rate. All participants were recommended to check whether their calculations are based on the actual test condition.

The MSIV (main steam isolation valve) closure times could not be obtained from the submitted calculations due to limited parameter request. In the ISP-50 test, the MSIV was closed with a delay of 0.1 s after the LPP. All participants were recommended to check the activation of the MSIV in their calculations. The main feed water was also isolated with a delay of 7.0 s after the LPP in the test. Most calculations correctly simulated the isolation of the main feed water in connection with the LPP signal, but the KOPEC's main feed water isolation time was 19.0 s after the LPP. They need to check the trip variables in their calculations.

The core power with respect to time was provided to all participants as a boundary condition. However, the calculated core powers were not in consistent with the experimental data in most calculations. All the participants were recommended to update their calculations with the provided core power with respect to time. The provided core power with respect to time is included in Appendix-A of this report.

The actuation times of the SIP and the SITs depend on the depressurization rate of the primary system. Different participants calculated different depressurization rate of the primary system, so the actuation times differed between calculated results by different participants. In particular, the times calculated by GP3 and GP4 showed the largest difference.

Table 4.2-1 Comparison of initial conditions in blind calculations

	Experiment	Reference data column number	Group A				Group B					Group C				Group D			
			KAERI	KEPRI	KTH	USNRC	CIAE	Univ. of Pisa	KNF	KOPEC 1	KOPEC 2	EDO Gid. (GP1)	EDO Gid. (GP2)	EDO Gid. (GP3)	EDO Gid. (GP4)	GRS	NRI	FORTUM	VTT
Primary system																			
Core power, MW	1.635	D1	1.636	1.566	1.636	1.636	1.610	1.636	1.570	NA	NA	1.636	1.636	1.636	1.636	1.636	1.636	1.636	1.636
Pressure, MPa	15.62	D4	15.60	15.50	15.55	15.57	15.20	15.47	15.60	15.51	15.51	15.64	15.50	15.53	15.59	15.60	15.60	15.60	15.56
Core inlet temp., K	562.7	D16	563.15	563.80	562.58	562.42	562.50	562.05	563.16	563.80	563.80	563.60	562.75	564.50	563.45	565.61	568.68	563.10	564.60
Core exit temp., K	597.7	D17	598.15	596.92	596.11	597.46	596.92	594.83	597.30	576.52	576.51	598.00	597.44	597.84	598.35	598.88	597.87	598.06	598.47
Bypass UH-DC, kg/s	~0.0	D54	0.029	NA	0	~0	~0	-0.081	-0.041	-0.012	-0.012	0	NA	0	0	-0.039	0.344	0.046	-0.210
Bypass HL-DC, kg/s	~0.0	D55	0.018	NA	0	0	~0	0.017	0.123	0.013	0.013	0	NA	0	0	0.034	0.720	-0.018	0.131
CL flow rate, kg/s	2.2 ± 5%	D58	1.98	1.99	2.08	2.06	2.02	2.15	1.98	1.99	1.99	2.06	2.05	2.04	4.0	2.12	2.18	2.01	2.07
PZR level, m	3.36	D74	3.59	4.04	3.42	2.93	3.22	3.12	3.32	3.68	3.67	3.32	3.22	3.61	3.32	3.30	3.32	3.30	3.30
RCP speed, rpm	10~20	D83	22	216	21	20	24	0	23	234	225	NA	NA	NA	0	152	68	0	162
Secondary system																			
Pressure, MPa	7.83	D6	7.77	7.83	7.83	7.83	7.83	7.84	7.75	7.81	7.82	7.83	7.43	7.86	7.23	7.83	7.83	7.83	7.83
Steam temp., K	568.5	D29	566.14	566.60	566.67	566.67	566.64	566.72	565.98	566.48	566.55	566.50	563.33	566.79	560.15	566.72	566.53	566.43	566.46
FW temp., K	508.2	-																	
FW flow (ECO), kg/s	0.43	D62	0.455	0.400	0.463	0.468	0.431	0.539	0.433	0.400	0.400	0.434	0.430	0.457	NA	0.435	1.578	0.431	0.432
FW flow (DC), kg/s	~0.0	D63	0	0.044	0	NA	0	0	0	0.044	0.044	0	NA	0.457	0.478	0	0	0	0
SG level, m	1.97~2.03	-	-	-	-	-	-	-	-	-	-	-	-	-	-	-	-	-	-
Heat removal, kW	753.67	D2	809.51	775.05	788.73	849.57	784.00	769.66	775.41	774.99	775.13	794.30	804.49	19.60	797.30	790.57	773.58	781.81	786.17
ECC																			
SIT pressure, MPa	4.19	D8	4.19	4.03	4.19	4.19	4.19	4.19	4.21	4.23	4.23	4.20	4.20	4.20	4.20	4.19	4.19	4.19	4.20
SIP Temp., K	321.3	D34	322.04	326.15	323.25	323.25	323.30	323.00	325.25	323.15	323.15	323.10	NA	323.15	323.15	323.15	323.15	323.52	323.25
SIT Temp., K	323.5	D31	323.35	322.04	323.35	323.35	323.36	323.20	323.45	320.85	320.85	323.10	323.15	323.15	323.15	323.55	323.34	320.71	322.31
SIT level, %	~95	-	-	-	-	-	-	-	-	-	-	-	-	-	-	-	-		-
Containment																			
Pressure, MPa	0.10	D11	0.1010	0.1010	0.1050	0.1051	0.1010	0.1013	0.1051	NA	NA	0.1055	NA	NA	0.1055	0.1066	0.1051	0.000	0.1000
Remarks																			

Table 4.2-2 Summary of nodalization schemes[1)]

		Group A				Group B					Group C				Group D			
		KAERI	KEPRI	KTH	USNRC	CIAE	Univ. of Pisa	KNF	KOPEC 1	KOPEC 2	EDO Gid 1 (GP1)	EDO Gid 2 (GP2)	EDO Gid 3 (GP3)	EDO Gid 4 (GP4)	GRS	NRI	FORTUM	VTT
Code		MARS-KS	MARS-KS	TRACE 5.0 p1	TRACE 5.200	R5/M3.3	R5/M3.3	R5/M3.3	RELAP5-ME	R5/M3.3	KORSAR/GP	KORSAR/GP	KORSAR/GP	TECH-M-97	ATHLET M2.2	ATHLET	APROS v.5.08	APROS 5.09
3-D Features		NA	NA	NA	NA	NA	NA	NA	NA	NA	NA	NA	NA	NA	NA	NA	NA	NA
Node info.	Volume	NA	NA	NA	NA	NA	NA	NA	NA	NA	NA	NA	NA	NA	NA	NA	NA	486
	Junction	NA	NA	NA	NA	NA	NA	NA	NA	NA	NA	NA	NA	NA	NA	NA	NA	NA
	HS[2)]	NA	NA	NA	NA	NA	NA	NA	NA	NA	NA	NA	NA	NA	NA	NA	NA	1466
	Special noding	NA	NA	NA	NA	NA	NA	NA	NA	NA	NA	NA	NA	NA	NA	NA	34 DC nodes	NA
Special models used		NA	NA	NA	NA	NA	NA	NA	NA	NA	NA	NA	NA	NA	NA	NA	NA	NA
Remarks		2-D in down-comer																

[1)] Detailed contents of this table were provided by participants later in the open phase (see Table 5.3-2)

[2)] Heat structure

Table 4.2-3 Summary of calculated sequence of events

		Exp. (shifted time, sec)	Group A				Group B					Group C				Group D			
			KAERI	KEPRI	KTH	USNRC	CIAE	Univ. of Pisa	KNF	KOPEC 1	KOPEC 2	EDO Gid 1 (GP1)	EDO Gid 2 (GP2)	EDO Gid 3 (GP3)	EDO Gid 4 (GP4)	GRS	NRI	FORTUM	VTT
Break		0.	0.0	0.0	0.0	0.0	0.0	0.0	0.0	0.0	0.0	0.0	0.0	0.0	0.0	0.0	0.0	0.0	0.0
1st MSSV open		24.	34.1	NM[2]	NM[2]	37.7	33.1	28.0	NM[2]	X	X	NM[2]	NM[2]	NM[2]	NM[2]	26.8	52.3	41.0	41.0
LPP trip		25.	29.0	23.0	23.5	31.0	24.3	24.0	23.0	14.5	15.0	31.39	26.9	42.1	44.5	23.0	26.0	36.0	26.0
RCP trip		25.	0.0	13.9	24.0	31.5	0.0	0.0	4.0	27.0	27.0	NA	NA	NA	0.0	22.4	25.8	NA	24.0
MSIV closure		25.	32.1	25.5	23.6	28.4	24.1	NM[2]	23.1	28.7[4]	28.7[4]	32.0	NM[2]	NM[2]	NA	23.0	26.1	NA	24.0
MFW isolation		32.	38.1	31.7	30.0	38.7	29.0	31.0	29.0	34.0	34.0	38.46	34.0	49.17	51.5	29.9	34.4	42.0	31.0
Core decay		33.	30.1	25.54	30.0	31.5	~30.0[3]	24.0	30.0	NA	NA	31.0	26.0	42.0	44.5	30.9	56.8.	34.0	27.0
SIP activation		54.	57.1	52.7	50.0	60.1	49.0	52.0	51.0	58.0	58.0	60.0	55.0	70.38	73.0	502.0	56.0	64.0	56.0
SIT activation		468.	435.	433.1	224.0	387.8	456.0	401.0	379.0	357.0	332.0	615.99	684.0	658.6	364.0	502.0	NA [5]	563.0	616.0
Loop seal	CL1A	190.	108.	325.8	83.	170.	150.	149.2	159.	388.0	403.3	X.	254,	NA,	127.1,	223.1	X	X	152.0
	CL1B	190.	107.	323.2	113.	169.	150.	150.2	159.	X	X	X.	253,	NA,	127.1,	223.1	X	X	152.0
	CL2A	X[1]	105.	139.1	83.	170.	X	1502.	188.	728.4	781.1	288.0	254,	NA,	132.5,	208.8	X	125.0	169.0
	CL2B	1236	105.	141.6	83.	170.	X	150.2	X	731.6	784.3	287.0	254	NA	132.5	208.8	X	125.0	169.0
Stop		2933	1806	2000.	2932.	3000.	1460.	3000.	2000.	3000.	3000.	3000.	3000.	2905.	2998.	3006.	3000.	2007.	2806.

[1] X: not occurred
[2] NM: not modelled
[3] Time at which core power follows the decay curve
[4] No MSIV was modeled, TCV closure time
[5] unrealistic behavior

4.3 Steady state results

Comparisons of steady state results for the major thermal-hydraulic parameters are shown from Figure 4.3-2 to Figure 4.3-10. Most participants correctly initialized their codes. However, there are some parameters which have apparent difference with the test data. For instance, the core powers used by most participants were in good agreement with the measured value, but two calculations by KEPRI and KNF showed much lower value than the data by around 67 kW. It might be because they took into account of the primary heat loss in their calculations.

Calculated core exit temperatures by KOPEC 1 and 2 were much below the data. As for the core bypass flow rates, calculations showed a large variation. In the test, the core bypass flow rates were not directly measured but the bypass flow rates were estimated to be close to zero at initial steady state condition. Most calculations presented very small bypass flow rate close to zero even though there was some variation in the flow direction. But, NRI overestimated the core bypass flow rates compared with the test data.

The GP4 showed almost double the cold leg flow rate at the initial condition. It was due to the nodalization restriction of the TECH-M code. The cold leg A and B was modeled by one leg in TECH-M code. As for the initial RCP speed, three participants calculated too high initial RCP speed compared with the data. The major secondary parameters were well predicted by most participants. But, the feed water flow rate was over-predicted by NRI. GP3 and GP4 allowed the feed water injection through the down-comer nozzle, which needed to be corrected in the open calculation. As for the heat removal rate through steam generators, most calculations well agreed with the data but GP3 predicted too small heat transfer rate which might be caused by output errors.

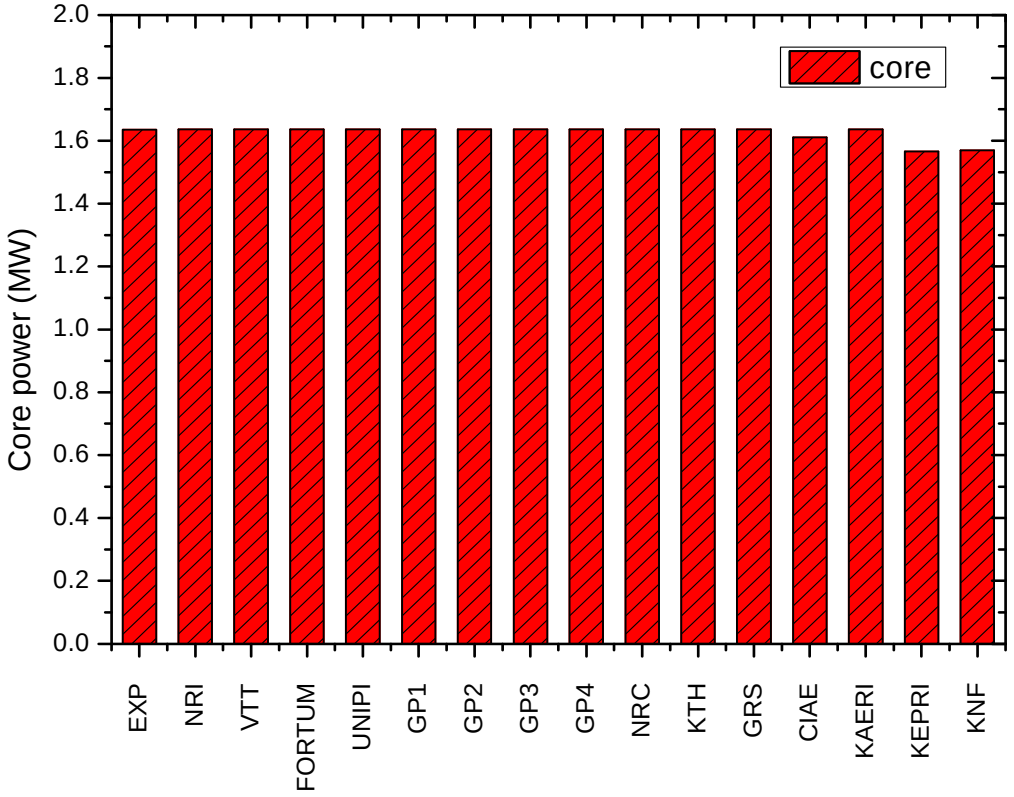

Figure 4.3-1 Comparison of the initial core power

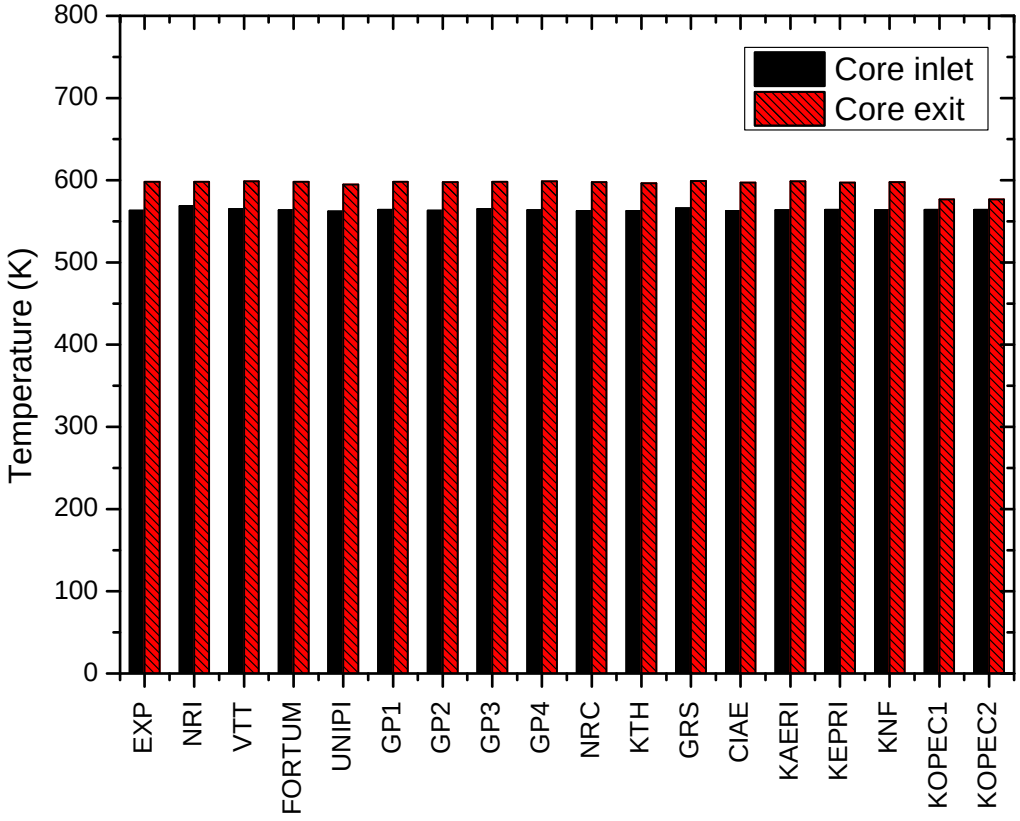

Figure 4.3-2 Comparison of the initial core temperature

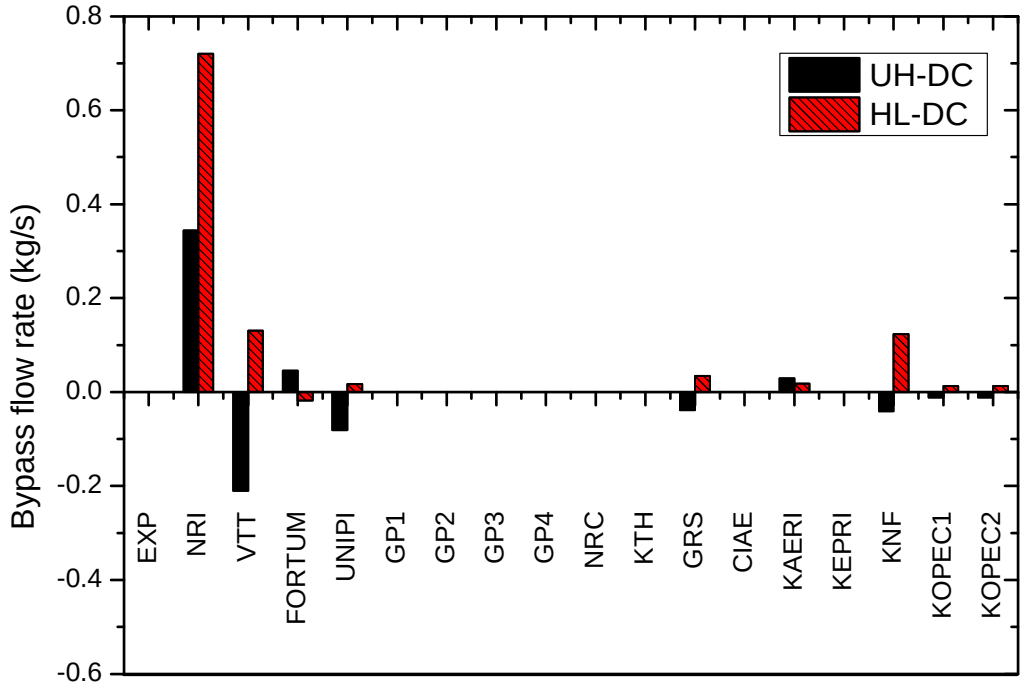

Figure 4.3-3 Comparison of the initial core bypass flow rate

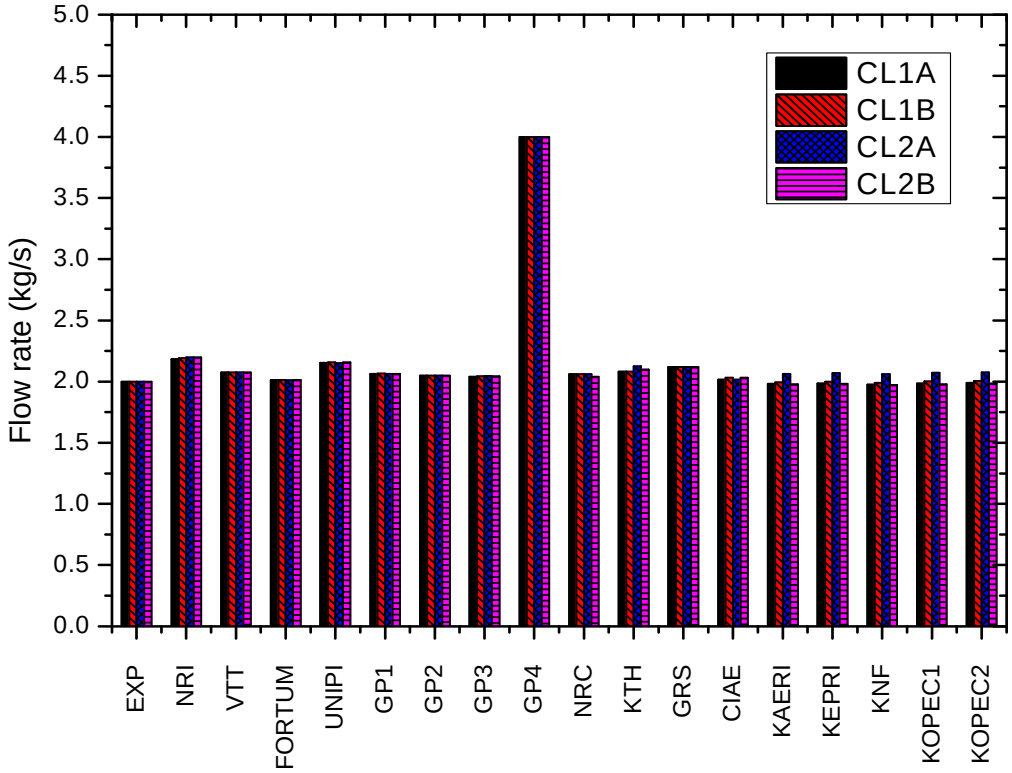

Figure 4.3-4 Comparison of the initial cold leg flow rates

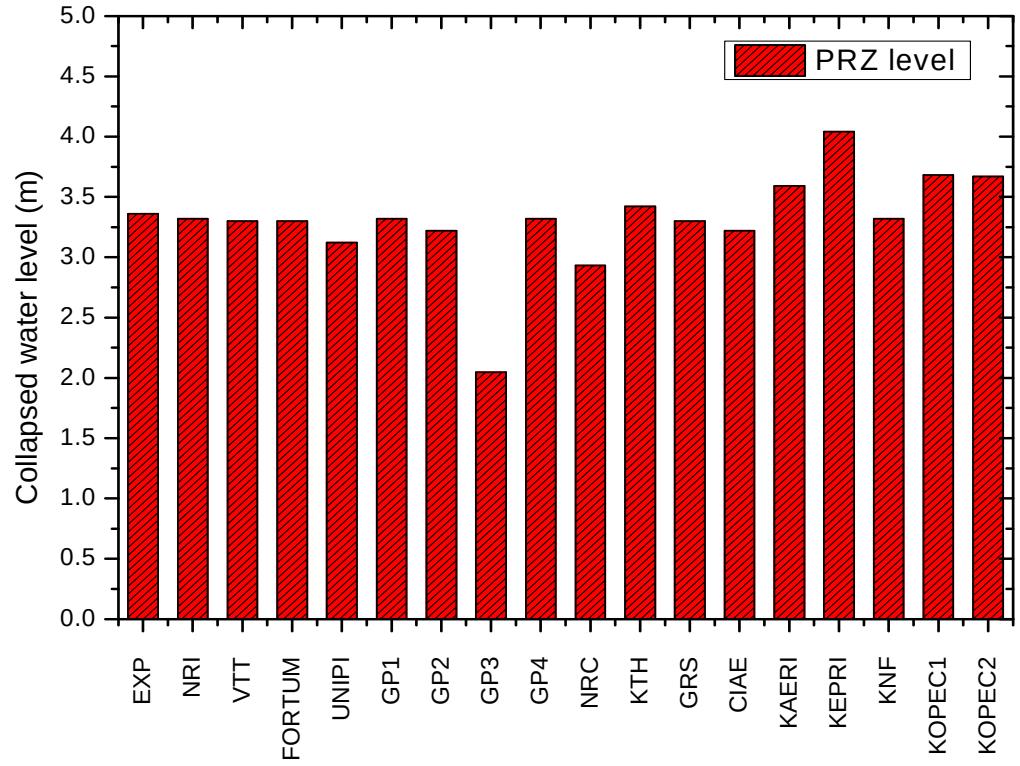

Figure 4.3-5 Comparison of the initial water level of a pressurizer

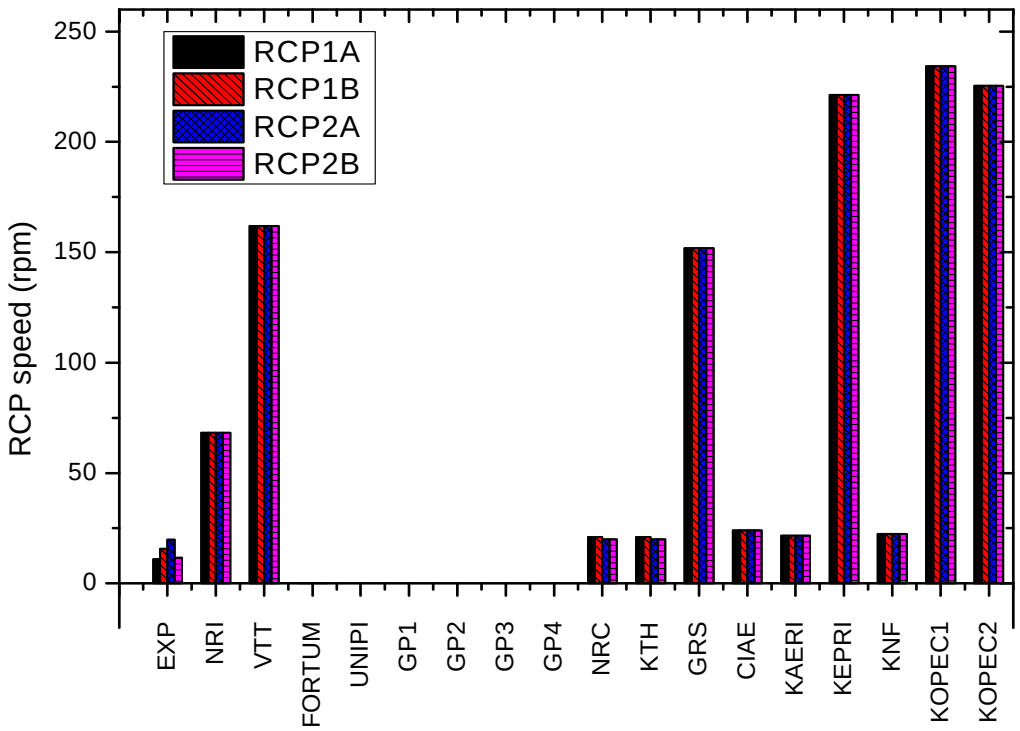

Figure 4.3-6 Comparison of the initial RCP speed

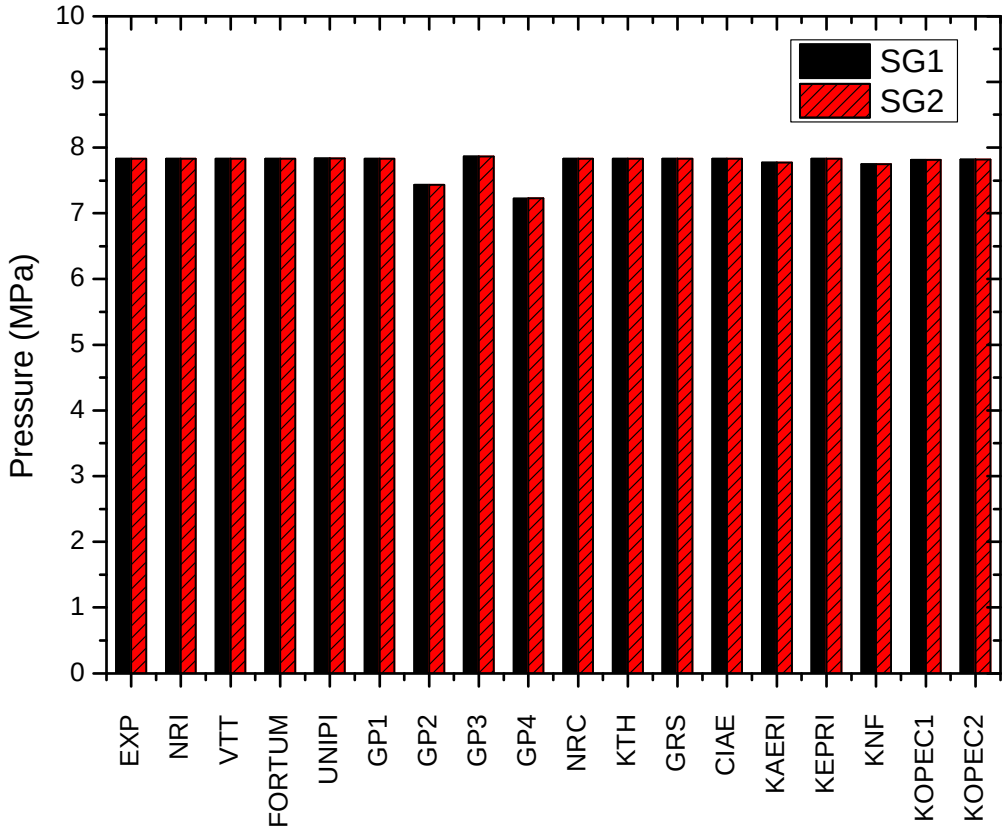

Figure 4.3-7 Comparison of the initial steam pressures

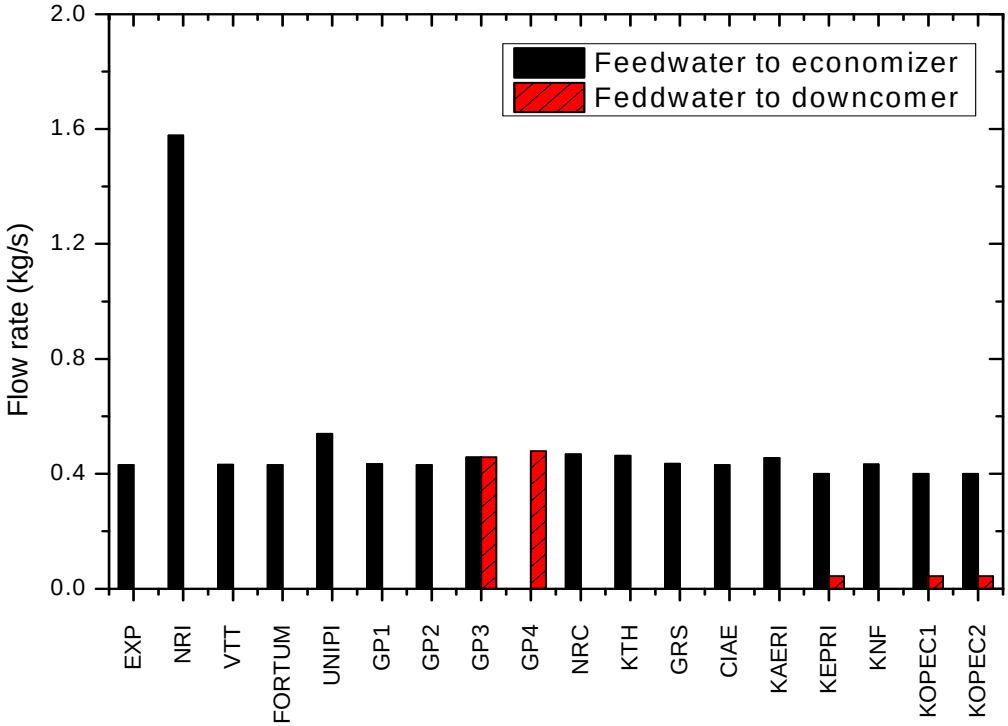

Figure 4.3-8 Comparison of the initial feed water flow rates

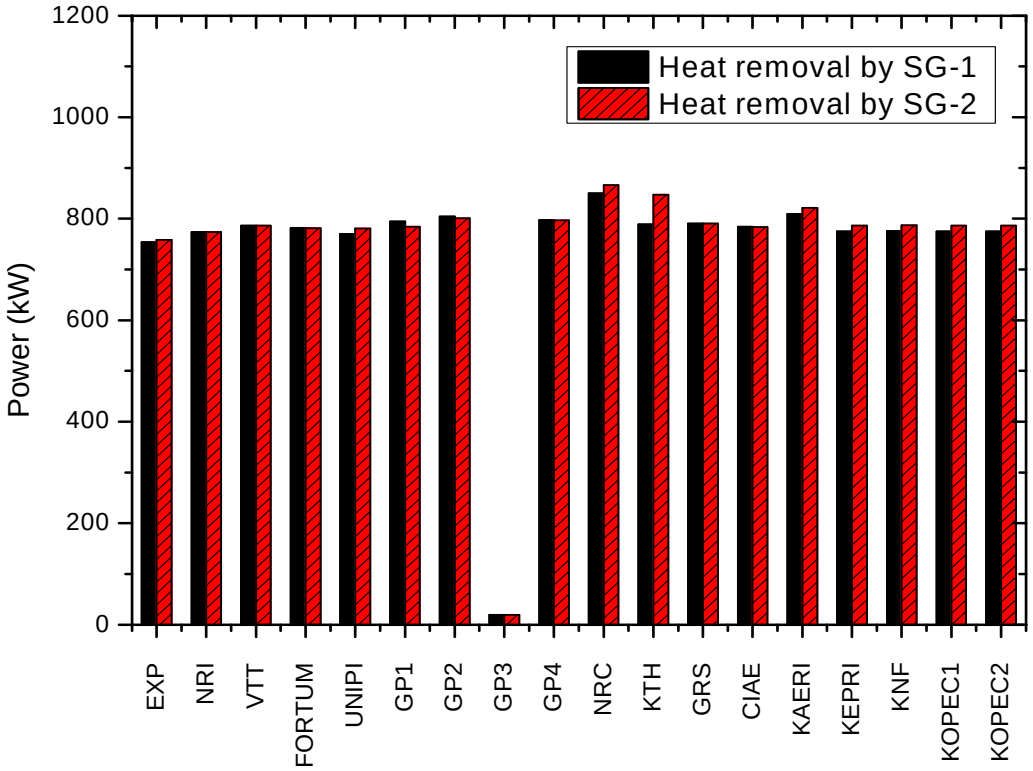

Figure 4.3-9 Comparison of the initial heat removal rate by steam generators

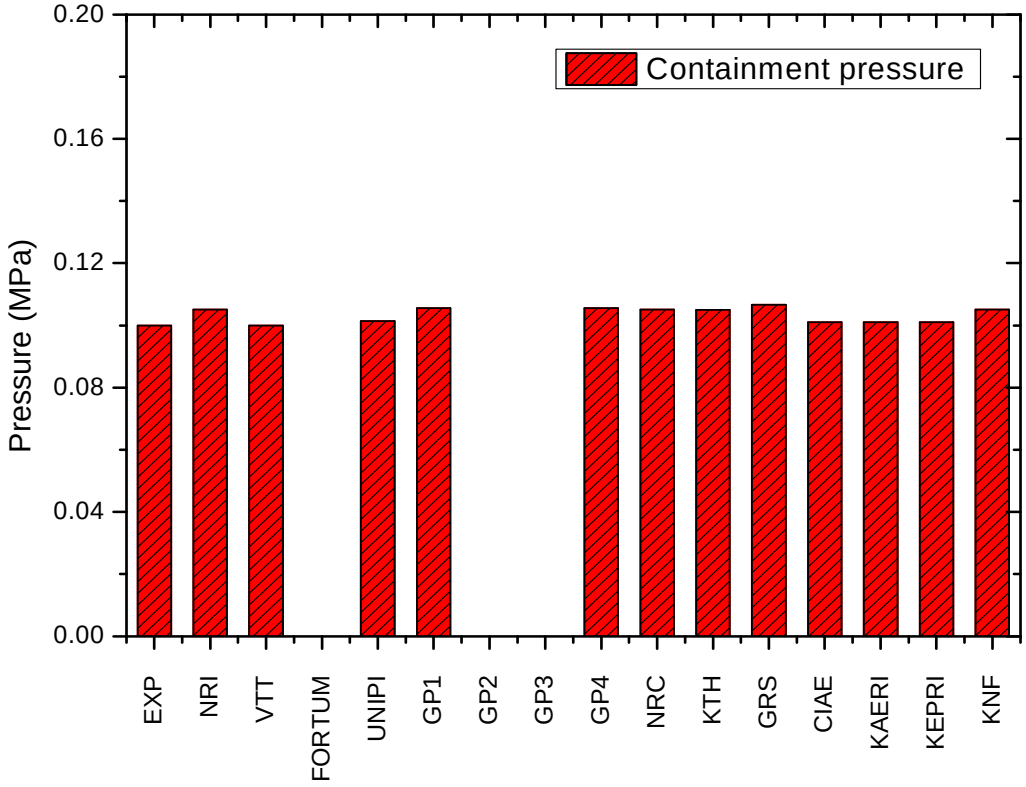

Figure 4.3-10 Comparison of the initial containment pressure

4.4 Submitted data analysis

The calculation times and number of submitted data, and time step showed some differences and it was summarized in Table 4.4-1. Most calculations assumed that the break was initiated at 0.0 s but some participants used different assumptions; KAERI, KTH, FORTUM, and VTT used the similar break initiation time to the data, 201 s, 193 s, 193 s, and 194 s, respectively. Thus their time data have been shifted to zero. Of course, the data time was also shifted for the break to start at time zero.

Table 4.4-1 Submitted data analysis

Grp	Participant	Cal. Time (sec)	Number of data	Time step (sec)	Remarks
Exp. Data		2932	3127	1.0	
A	KAERI	1799	1841	~1.0	-201 s shift to match break time
	KEPRI	1999.5	4000	0.5	D54,D55 are not available Power unit mismatch, Bypass flow path was not modeled
	KTH	2933	3127	1.0	-193 s shift to match break time
	USNRC	2999	2946	~1.0	D63, D65 not available
B	CIAE	1460	371	~4.0	D12~D15 not available Actual power table not used
	UNIPI	3000	3002	1.0	
	KNF	2000	2001	1.0	
	KOPEC1	3000	3241	0.01~10.0	D1, D11 missing
	KOPEC2	3000	1246	0.1~10.0	D1, D11 missing
C	GP1	3000	2532	1.0~2.0	D54, D55 not available
	GP2	2998	2999	1.0	D11, D13, D15, D34~D41, D54~D55, D63, D65, D71, D79~D86 missing
	GP3	2905	3396	1.0	Significant time digit missing for t<10.0 D11, D54, D55, D72, D73, D75~D86 not available
	GP4	2998	3300	0.01~6.0	
D	NRI	3000	2529	~1.0	
	GRS	3006	3065	~1.0	
	FORTUM	2007	2201	~1.0	-193 s shift to match break time
	VTT	2806	3001	~1.0	-194 s shift to match break time

4.5 Comparison of transient results

The submitted transition calculation results were qualitatively compared with the measured data. All the comparing figures are included in Appendix-B. For each requested parameter, a total of 5 figures were plotted. In the first figure were compared all the 17 calculation results with the data. The following 4 figures compared the calculation results of each divided group with the data for clear comparison. In particular, initial transient period where major thermal-hydraulic phenomena occurred has been enlarged if needed. In this section, qualitative prediction accuracy of the submitted calculations focusing on the important major thermal-hydraulic parameters is described. Note that only key parameters among the 86 submitted parameters were selected and discussed by taking into account a priority of affecting overall transient behavior.

4.5.1 Major system pressures

In the ISP-50 test, the primary system pressure rapidly dropped to about 8.2 MPa from its initial pressure of 15.6 MPa on break as shown in Figures B.4 and B.5. The measured primary system pressure showed some oscillation due to simultaneous cycle opening of one MSSV in both steam generators forming a plateau of the pressure from 50 s to 200 s and it decreased again from 200 s when the 1st loop seal clearing occurred. Most codes well predicted the initial pressure drop behavior after break. As for the prediction performance of the primary system pressure, the ATHLET code, the TRACE code, the RELAP5 code and the MARS-KS code presented relatively excellent calculation results for the depressurization behavior and the pressure plateau.

Two participants, KAERI and KEPRI, used the MARS-KS code. As for the depressurization rate and the pressure plateau, the KEPRI's calculation predicted the primary system pressure with a satisfactory accuracy as shown in Figure B.4-A. In the KAERI's calculation, the plateau of the primary system pressure was also correctly predicted and afterward pressure predictions were satisfactory despite some underestimation during the test period from 200 s to 600 s.

Two participants, NRC and KTH, used the TRACE code. In the NRC's calculation, the plateau of the primary system pressure was correctly predicted and afterward primary pressure prediction was satisfactory despite some underestimation during the test period from 200 s to 600 s. On the other hand, the KTH's calculation overestimated the value of the primary pressure plateau by 1.0 MPa and then showed remarkably rapid depressurization of the RCS compared to the experimental data.

Four participants, CIAE, KNF, UNPI, and KOPEC, performed blind calculations with the RELAP5 code. CIAE predicted the primary system pressure with an outstanding accuracy as shown in Figure B.4-B. However, initial pressure of the primary system was incorrectly predicted, which could be attributed to some mistakes in a steady-state calculation. KNF predicted the initial depressurization and the pressure plateau correctly but they underestimated the primary system pressure after 200 s of the test period. The prediction performance of the University of Pisa (UNIPI)' calculation was similar to that of KNF. UNIPI accurately predicted the initial depressurization and the pressure plateau but they also underestimated the primary system pressure after 200 s of the test period. KOPEC provided two calculation data using KIMERA and RELAP5 codes. The calculation results were depicted by KOPEC1 and KOPEC2, respectively. There was no definite difference between two calculations. Both calculations by KOPEC showed more rapid depressurization compared with the experimental data and they underestimated the primary system pressure during whole the test period.

EDO Gidropress used the KORSAR code and the TECH-M-97 code for blind calculations of the ISP-50 exercise. They submitted three calculation data (GP1, GP2 and GP3) using the KORSAR code and one calculation data (GP4) using the TECH-M-97 code. In the KORSAR calculations, they modified the nodalization and some models in each calculation of GP1, GP2 and GP3. Detail information on their specific modeling was described in Appendix C. The KORSAR code generally overestimated the primary system pressure in all three calculations as shown in Figure B.4-C. The differences of the calculation results among the GP1, GP2 and GP3 were not so significant in predicting the primary system pressure. As for a prediction performance of the primary system pressure, the TECH-M-97 code was superior to the KORSAR code. The TECH-M-97 code resulted in overestimation of the pressure plateau and underestimation of the second depressurization rate.

Two participants, GRS and NRI, used the ATHLET code for the blind calculation of the ISP-50 exercise. In general, GRS correctly predicted the primary system pressure in terms of the pressure plateau and the depressurization rate despite showing a little overestimation of the primary system pressure from 200 s to 600 s as shown in Figure B.4-D. NRI, however, underestimated the primary system pressure during the whole test period except the initial rapid depressurization. In the NRI's calculation, the pressure plateau was not clearly observed.

FORTUM and VTT performed a blind calculation with the APROS code. In regard to the primary system pressure prediction, FORTUM showed the similar performance to GRS. However, the FORTUM's calculation did not produce a clear pressure plateau. Although the VTT's calculation showed a pressure plateau, they incorrectly predicted the second depressurization of the primary system pressure from 200 s to 800 s.

In the actual ISP-50 test, due to the main feed water isolation subsequent to the reactor trip, the secondary pressure started to increase up to the MSSV set-point, 8.1MPa. Three MSSVs were installed in parallel at each steam line. Each MSSV has the following characteristics for opening and closing shown in Table 3.5-2. In the present test, OV-MSSV1-03 at the SG-1 line and OV-MSSV2-03 at the SG-2 line were opened three times at 230.0, 268.0 and 324.0 s and 230.0, 262.0 and 319.0 s, respectively because the secondary steam pressure reached the first set-point 8.1MPa as shown in Figures B.6 and B.7. The other two MSSV banks were not activated. The increase in the secondary pressure was depressed only by one bank of the MSSVs. In general, the prediction performances of the secondary system pressure by the participant's calculations were not satisfactory contrary to the primary system pressure prediction. Among the various codes, the ATHLET code, the APROS code and the RELAP5 code presented relatively better calculation results for the MSSV opening and the subsequent secondary system pressure behavior. However, opening frequency of the MSSVs was not accurately simulated in any code. In the KAERI and the NRC's calculations, the opening of the MSSVs was correctly predicted but the calculation results of the subsequent secondary system pressure showed different behaviors with the experimental data. In the EDO Gidropress, KNF, KEPRI and KTH's calculations, the opening of the MSSVs was not reproduced which could be attributed to a possible inaccurate modeling of the MSSV operation. Since the MSSV was not pertinently simulated in these calculations, the secondary system pressure maintained relatively a higher value compared with the experimental data. As shown in Figure 3.5-1, the primary pressure was higher than the secondary system pressure before the loop seal clearing. This relationship is important to consider steam condensation in the SG U-tubes.

In the ISP-50 test, when the primary pressure reached 4.03 MPa, three SITs started to supply water through the corresponding three intact DVI nozzles at the shifted time of 468 s: DVI-1, DVI-2, and DVI-3. Pressures of the SITs used in the test were plotted from Figures B.8 through B.10. Great deviations from the data were obtained in most calculations. In particular, the activation time of each SIT showed a significant difference compared with the data. Incorrect prediction of the primary pressure trend was the major source of this difference.

In the ISP-50 test, the containment pressure increased up to 0.175 MPa from its initial pressure of 0.102 MPa on break as shown in Figure B.11. As for the prediction performance of the containment pressure, the calculations performed by NRI, EDO Gidropress, NRC and KNF showed relatively excellent simulations. The other calculations did not show any variations of the containment pressure during the whole test period. They simply used a constant containment back-pressure in their calculations.

4.5.2 Differential pressure and fluid temperature of primary side of SG

In the ISP-50 test, differential pressures between inlet and outlet plenums of the steam generators showed different behaviors in the SG-1 and the SG-2. In the SG-1, the differential pressures maintained some values after the initial peak on break. On the other hand, in the SG-2, the differential pressures were not formed after the initial peak on break. Comparison of the calculations with the data is shown from Figures B.12 through B.15. The calculation results performed by NRI, UNIPI and KTH presented a reverse differential pressure behavior contrary to the experimental data. Meanwhile, the TECH-M-97's calculation showed a highly oscillating behavior of the differential pressures. As for the differential pressure prediction for the SG-1, the NRC's calculation showed outstanding accuracy. However, they incorrectly predicted the differential pressures of the SG-2. The KOPEC's calculations presented too high initial peaks in the differential pressures for both steam generators. The other calculations showed relatively reasonable prediction performance for the initial differential pressure peaks but they did not correctly predict the afterward pressure behaviors in the SG-1.

Fluid temperatures of the inlet and outlet plenums of the steam generators are compared from Figures B.25 through B.28. As discussed in Section 3.5.14, the loop seal clearing significantly affected the fluid temperatures. But most calculations were not acceptable to predict the fluid temperature behaviors of the inlet and outlet plenums of steam generators.

4.5.3 Major fluid temperatures

The core inlet and exit temperatures were requested as important thermal-hydraulic parameters and compared in Figures B.16 and B.17, respectively. Until the time 200 s when the second depressurization started, most calculations showed reasonable predictions of the core inlet and exit temperatures. In this initial period, the KTH's calculation presented the worst prediction. After 200 s, the predictions showed a wide range of variations and the deviation from the data increased with time. On the whole, the largest discrepancy was observed in the calculation of GP4, which overestimated the fluid temperatures and showed a highly fluctuating behavior especially after about 300 s. In general, the core temperatures were underestimated by KTH, NRI, KOPEC1, and KOREC2 and overestimated by GP1, GP2, GP3, FORTUM, and VTT overestimated the core temperatures. In particular, the GRS's calculation showed an excursion in the core exit temperature during 400 s and 1100 s. It seemed that the core was uncovered during this period. The calculations by NRC, UNIPI, KEPRI, and KNF showed a relatively good agreement with the experimental data.

The pressurizer temperature was excellently estimated by KAERI among the submitted

calculations as shown in Figure B.18. The UNIPI's calculation also showed acceptable prediction accuracy. However, the other calculations significantly underestimated the experimental data. The calculated pressurizer temperatures showed great deviation up to more than 200°C at 1200 s. The thermocouple TF-PZR-08 was located at the top of the pressurizer as shown in Figure 2.4-4 and it showed higher temperature than a saturation value during transient. It was found from the experimental data that other thermocouples inside the pressurizer also showed the similar superheated steam temperatures. However, the submitted calculation results did not predict the superheated steam temperature correctly.

Each calculated hot leg fluid temperatures showed the similar trend to the core outlet temperature as shown in Figures B.19 and B.20. The GP4 and GRS's calculation results showed rapid excursion in water temperatures. The same excursions in water temperatures were predicted in the hot legs, indicating that the hot legs were occupied by steam. The other calculations especially by KOPEC1, KOPEC2, NRI, and KTH predicted lower hot leg temperatures than the data. On the other hand, the results by VTT, GP4, and GRS showed higher temperatures than the data. Comparison of each cold leg fluid temperature is shown from Figures B.21 through B.24. The best prediction of the hot leg and the cold leg temperatures were obtained in the calculations by CIAE, KEPRI, and KAERI. The measured cold leg temperatures show asymmetrically different behaviors depending on the loop. A sudden increase in the fluid temperature indicates that the water in the cold leg is emptied by steam flow.

The steam dome temperatures shown in Figures B.29 and B.30 were predicted in the range of 20°C deviation in most calculations. However, GP4 predicted greatly lower steam dome temperatures than the corresponding saturation temperatures for the most calculation period, especially after 400 s. This unreasonable prediction of the steam dome temperature was observed more severely in SG2 than in SG1. The SIT liquid temperatures were simulated relatively well for most calculations within +/- 3.5°C except for FORTUM and KTH shown from Figures B.31 and B.33. The FORTUM's calculation showed a relatively large decrease in the temperature of SIT-1, SIT-2, and SIT-3 starting from their injection time, and the KTH's calculation showed an increase in temperatures of the SIT-1 and SIT-3. As for the temperature of SIP-2 shown in Figure B.34, the water temperature of SIP-2 experienced a small fluctuation at the initial injection period in the experiment. The KEPRI's calculation showed about 6°C higher value than the other calculations. Containment fluid temperature was compared in Figure B.35. The initial containment fluid temperature was calculated relatively well except for KOPEC2, KTH, CIAE and VTT, which underestimated the data. The experimental data were overestimated by KOPEC2 and KTH, but underestimated by CIAE and VTT. Steam temperatures of the main RCS loops were compared through Figures B.36 through B.41. Experimental data

was obtained from the thermocouples installed just below the top wall of the RCS pipelines. When the RCS loop is occupied with water, steam temperatures show the same values as the water temperatures. But, if phase separation occurs, the sensors indicate steam temperatures.

4.5.4 Loop flow and break flow

As shown in Figure B.54, all the predictions under-estimated the bypass flow rates through upper head to down-comer bypass lines. The calculations from KAERI, NRI, NRC and VTT predicted the same flow direction to the data but the others predicted the opposite flow directions except for the zero bypass flow rate of EDO Gidropress. In particular, the NRI's prediction was as much as 50% high with respect to experimental flow rate and the NRC's prediction showed quite large fluctuating behavior. As shown in Figure B.55, all the predictions under-estimated the bypass flow rates through hot leg to down-comer bypass lines except for the NRI's prediction. Only the predictions from NRI and UNIPI reproduced the same flow direction to the data. In particular, the predictions by GRS, KAERI, and KNF were in opposite flow directions to the data and those by EDO Gidropress resulted in zero bypass flow rate.

In the ATLAS facility the flow rates in two hot legs and four cold legs were measured by using the BiFlow flow meters. As shown in Figures B.56 through B.61, all the predictions estimated the experimental data well in overall sense. However, the NRI's prediction was higher than the experimental data for hot leg 1. Several predictions from KAERI, KEPRI, etc, show fluctuations during the later period for hot legs 1 and 2, and are higher than the experimental data for cold legs 2A and 2B.

In the ATLAS facility the flow rates through main feed lines were measured by using the Coriolis flow meters. As shown in Figures B.62 through B.65, all the predictions estimated the experimental data well in overall sense. Although some of the initial flow rates were incorrectly given by KOPEC1 and KOPEC2 shown in Figures B.62-B and B.64-B, by GP3, GP4 shown in Figures B.62-C and B.64-C, and by NRI shown in Figures B.62-D and B.64-D, which seems not to affect the transient behavior.

In the ATLAS facility the flow rates from three SITs and one SIP were measured by using the Coriolis flow meters. As shown in Figures B.66 through B.68, most of the predictions of the flow rates from three SITs over-estimated the experimental data except for the negative flow rates predicted by NRI. The amount of over-predictions is different from one another. As shown in Figure B.69, all the predictions of the flow rate from a SIP are slightly higher than the experimental data in overall sense except for the predictions from KEPRI and GRS.

In the ATLAS facility the total break flow rate were calculated by using the experimental data of QV-CS-03, LC-CS-01 and LC-CS-02. In order to obtain reliable break flow rate, the RCS inventory-base method was also utilized, which is based on the measured water level data as described in Section 3.5.6. As shown in Figure B.70, most of the predictions of the total break flow rate over-estimated the experimental data for an initial period of about 200 s and they agreed well after about 200 s except for the predictions from KOPEC1, KOPEC2 and KTH. As shown in Figure B.71, the predictions from KAERI, KNF, GP4, and UNIPI predicted the experimental data very well except for the initial period. However, the predictions from KOPEC1, KOPEC2, VTT over-estimated the experimental data and the others under-estimates them.

4.5.5 Collapsed water level of the down-comer and the core

In the experiment, the collapsed water level of the down-comer experienced a sudden drop with the opening of the break valve. This water level maintained a constant value until the loop seal clearing. Afterward, it significantly decreased until the SIT injection started. With a start of the SIT injection, the collapsed water level slowly increased again. This general trend can be observed in all calculations as shown in Figure B.72. However, the decreasing and the increasing rates of the water levels were different depending on the participant. For instance, the NRI's calculation showed the best prediction among the calculations. The NRC's calculation was very close to the data. GRS also predicted the data well until the loop seal clearing, but overestimated the decreasing rate. Other calculations were not successful to predict the recovery of the down-comer water level, resulting in under-prediction of the down-comer water level.

With regard to the core water level, temporary core level depression was observed when the loop seal clearing occurred in the experiment. After that, the core water level maintained a constant level during the remaining test period. In general, most calculations showed a very fluctuating results and great deviations, from the data. Great user effects were found and no calculations predicted the data well with satisfactory accuracy. Such fluctuating calculation results for the core water level can be seen in Figure B.73. The GP1 and GP2's results showed a temporary core water level depression as shown in Figure B.73-C, but their depression magnitude and the duration time were not appropriately simulating the test results. Meanwhile, the pressurizer water level was predicted relatively well in all calculations as shown in Figure B.74.

The water in the vertical intermediate leg-1A and -1B was cleared then the first loop seal clearing occurred in the test as shown in Figures B.75 and B.76. The water in the leg-2A was not cleared during the test period and the second loop seal clearing occurred only in the leg-2B as

shown in Figures B.77 and B.78. The CIAE's prediction showed a relatively good agreement with the data even though it showed a little time deviation in the occurrence time. The GRS, GP4, KAERI, KEPRI and NRC's calculations predicted that the collapsed water levels of all the intermediate legs were cleared and they showed significant fluctuations. The NRI's calculation did not predict water level clearing at any intermediate leg during their whole calculation period. GP1, FORTUM predicted the water level clearing at the intermediate leg-2A and -2B only. The collapsed water levels in the intermediate legs are closely related to the loop seal clearing phenomena and also the collapsed water level behavior of the core and the down-comer.

The collapsed water levels in the U-tube region were relatively well predicted in most calculations as shown from Figures B.79 through B.82. The water levels of the downward section were decreased more rapidly than those of the upward section both in the experiment and in the calculations. In the KTH's calculation, the water level of the upward section showed a little fluctuation and finally increased after about 350 s.

4.5.6 Core heater surface temperature

The core heater surface temperatures represented by the wall temperature in active core regions were compared between the data and the calculations from Figures B.42 and B.53. The active core region was instrumented with thermocouples at 12 elevations from the core inlet to the core outlet to measure the core heater surface temperatures. In this section, the core wall temperatures were compared for 3 representative regions along the core, e.g. region 2, region 7, and region 12.

In the lower region (region 2), most calculations showed quite well predictions, but 2 cases (GP1 and GP2) showed PCTs occurred at about 250 s and other 4 cases (NRI, KOPEC1, KOPEC2, and KTH) show, quite large under-predictions after 200~400 s.

In the middle region (region 7), 5 cases (GP1, GP2, GP3, GP4, and GRS) showed one or two PCTs around 200~800 s and other 4 cases (NRI, KOPEC1, KOPEC2, and KTH) showed quite large under-predictions after 200~400 s. But the other 8 cases (CIAE, FORTUM, KAERI, KEPRI, KNF, NRC, UNIPI, and VTT) showed quite well predictions for all the period.

In the higher region (region 12), 8 cases (CIAE, GP1, GP2, GP3, GP4, GRS, KNF, and KTH) showed one or two PCTs at around 200~1400 s and other 4 cases (NRI, KOPEC1, KOPEC2, and KTH) showed quite large under-predictions after around 400 s. In this region, most of the PCTs showed quite long quenching times. But the other 6 cases (FORTUM, KAERI, KEPRI, NRC, UNIPI,

and VTT) showed quite well predictions for all the period.

4.5.7 RCP speed

Initial steady state condition for the test was obtained at a natural circulation condition. The impellers of the RCPs were let to rotate freely without any operator control. Measured speed of the RCPs was about 10 rpm. By considering the uncertainty of the rotational speed measurement, especially in a low range, the actual rotational speed can be assumed to be zero in the test. The calculated initial RCP speed showed some variations as summarized in Table 4.2-1. The difference between the calculation and the data seems to be attributed to either incorrect implementation of the pump characteristics of the actual RCPs which was provided by the operating agency or a different pressure drop characteristics along the RCS loop. Comparison of the calculated speed of each RCP with the data was shown from Figure B.83 through B.86. Most calculated RCP speeds linearly decreased to zero from its initial value by the RCP trip signal. But, some calculations by CIAE, KEPRI, and KNF showed an initial speed-up and then decrease to zero.

4.6 Summary and comments

In this chapter, the submitted calculations were evaluated qualitatively by comparing initial and boundary conditions, steady state results, major sequence of events, and transient behaviors of the key parameters with the data. It seemed that the actual initial and boundary conditions were not fully understood and they were not well implemented into the code calculations in the present "blind" phase. It is because most participants are not so much familiar with the ATLAS facility as well as the actual test conditions. On the whole, the code's predictions were reasonable only in the beginning of the transient. The prediction accuracy became greater during the course of the transient. As expected, the most disagreement was originated from the break flow and collapsed water levels in the core and down-comer. The prediction accuracy on the secondary pressure was not so good out of our expectation. The loop seal clearing phenomena in the four intermediate legs were not well reproduced in the most calculations.

It is difficult to evaluate each participant's prediction accuracy only by comparing the calculation results for selected parameters with the data. However, comparing all the requested parameters with the data will give us an overall qualitative assessment on the participant's calculation and code prediction capability. All figures are included in Appendix-B. More quantitative evaluation on the submitted results will be described in the following chapter.

5. Comparison of Open Predictions with Data

5.1 Inventory distribution of the code models

The primary and the secondary side inventories are considered as one of the most influential factors of the code models to affect a transient calculation. These inventories of the code models should be as close as those of the test facility to minimize the transient distortion. A component-wise inventory is also as important as the total inventory. Inventory distributions of the participants' code models are compared with the geometric data of the ATLAS as shown in Table 5.1-1. Detailed geometric information of the ATLAS facility can be found in the latest facility description report [Kang *et al.*[3], 2011]. The primary system was divided into several major components and their internal volumes were compared with the measured ones. As for the secondary system, the steam generator itself and the steam pipe lines to the turbine isolation valve were separated. Percentile error (ε) distribution was summarized in Table 5.1-2.

Component-wise percentile errors of the primary system are plotted from Figure 5.1-1 to Figure 5.1-4. In the group A, for instance, KTH showed a +40% error in modeling the core region but each RCP's volume was modeled with a small volume by -60%. In general, the percentage errors of KTH and NRC, who used the TRACE code, were the very similar. On the other hand, participants in group B showed the very similar errors and the excellent agreement with the data, but KOPEC modeled the cold leg with larger volume than the data by 60%. In group C, the AEKI's CATHARE model showed larger volumes especially in DC and PZR. The other GP models were all similar with each other. Participants in group D showed excellent agreement in volume distribution.

Compared with the primary inventory, the secondary inventory showed much larger errors. In general, the steam generator was modeled with a small volume and the steam line was also modeled with small volume compared with the data. Comparison of total volumes of the primary and the secondary system is shown in Figure 5.1-5.

Subsequent to the qualitative comparison, nodalization quantification was performed according to the method used in the BEMUSE Phase II [OECD/NEA, 2005]. The present quantification is not a rigorous one because only the primary and the secondary inventories were used as quantities. As the first step, the acceptable errors (AE) for the quantification process were determined. 2% and 5% were used for AEs for the primary and the secondary inventories, respectively. In fact, the AEs affect the final quantification output, the global acceptability factor, Q_A. The effects of the AE, especially of the secondary inventory, were investigated and compared in Figure 5.1-6. The percentile error, E was defined as the ratio

$$E = \frac{\left|(\exp value \pm \exp error) - calc\ value\right|}{\left|(\exp value \pm \exp error)\right|}$$

The percent error, E becomes zero if the |(exp value ± exp error) – calc. value| is lower than the experimental error. Secondly, weighing factors for taking into consideration the importance of the parameters with respect to the present SBLOCA transient were determined. Taking into account the phenomena of the SBLOCA, the relative importance of the secondary inventory was assumed to be half that of the primary inventory. Thus, the weighting factors, W_i, of 1.0 and 0.5 were used for the primary and the secondary inventory, respectively. Then, the single acceptability factor, Q_i was obtained by the following formula:

$$Q_i = \frac{E}{AE} \cdot W_i$$

where normalized weighting factors were used. Finally, the global acceptability factor, Q_A can be obtained by summing the whole single acceptability factors

$$Q_A = \sum_i Q_i$$

Detailed calculation results are summarized in Table 5.1-3 and sensitivity results on the acceptable errors of the secondary inventory were plotted in Figure 5.1-6. In the literature, Q_A<1.0 is required as an acceptable criterion. Around 50% calculations fulfilled the global acceptability with the AE of 5%. If the acceptable error level increases, more calculations fall into the acceptable region. In fact, Q_A is affected by two factors, AE and W_i, and an proper choice of those factors are important for meaningful quantification process. In the present quantification, two factors were determined by considering the relative importance of each inventory during the typical SBLOCA scenario though they look more or less subjective.

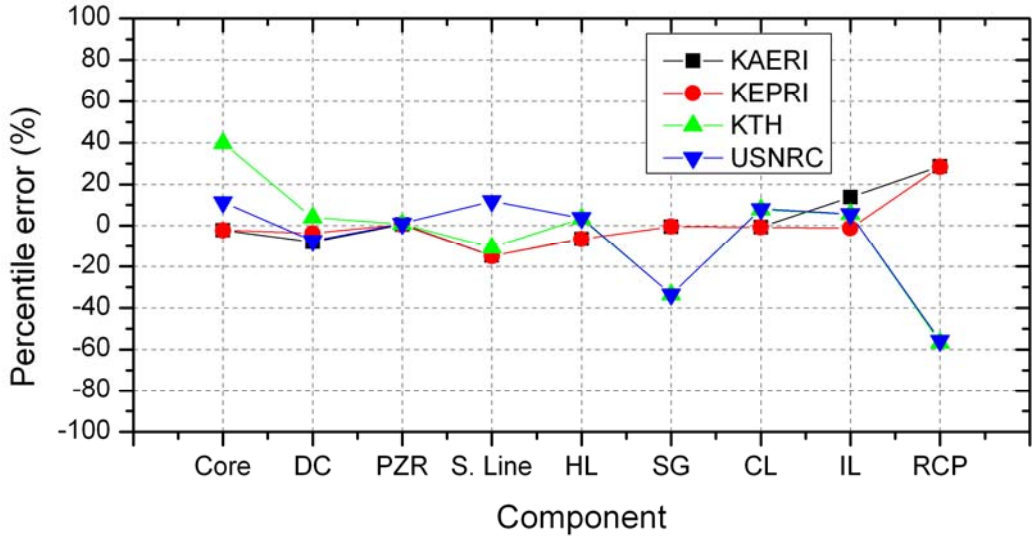

Figure 5.1-1 Component-wise inventory distribution errors (Group A)

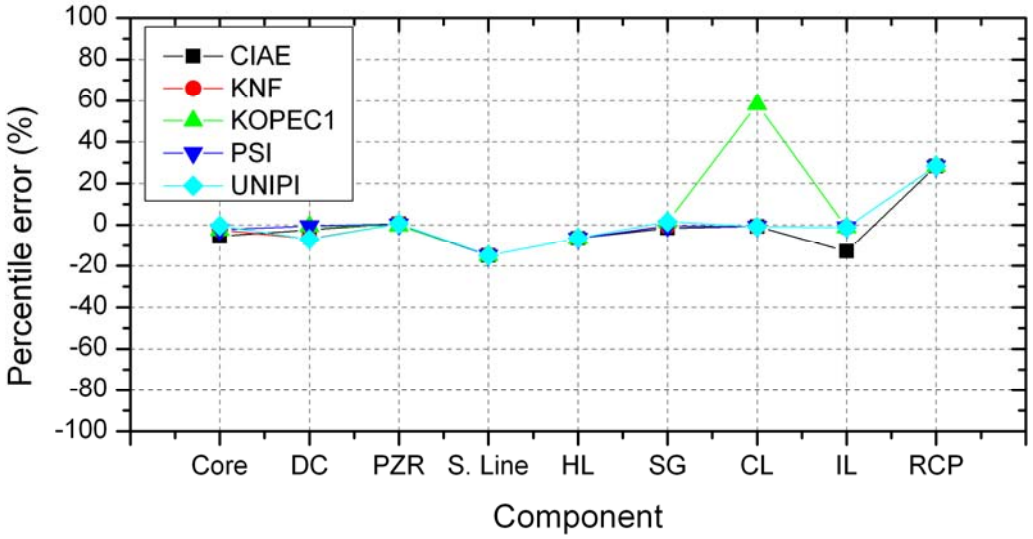

Figure 5.1-2 Component-wise inventory distribution errors (Group B)

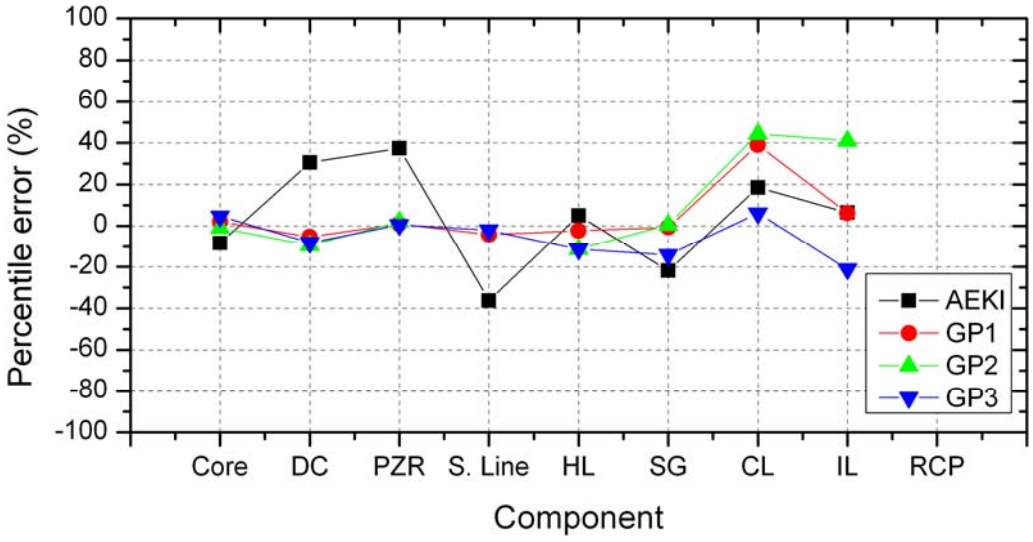

Figure 5.1-3 Component-wise inventory distribution errors (Group C)

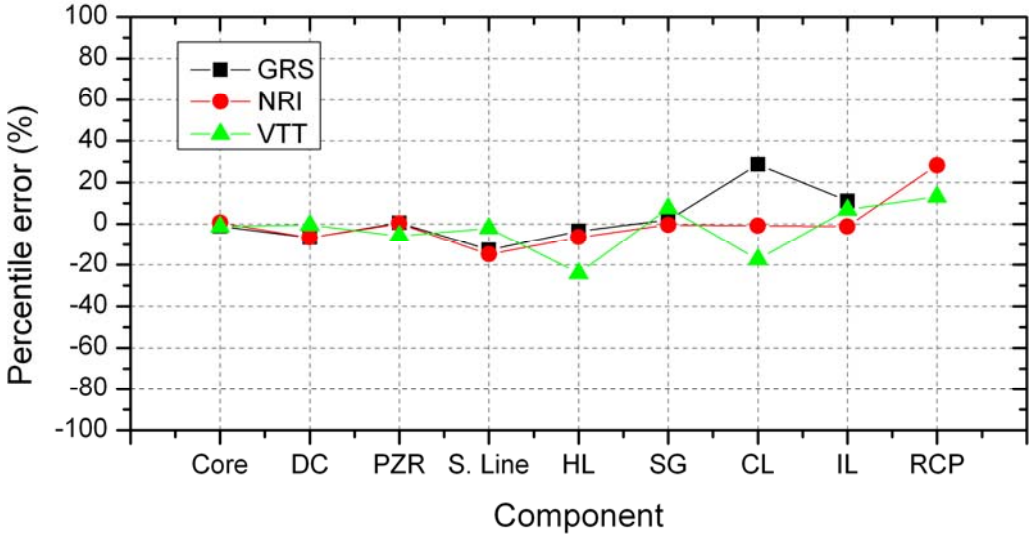

Figure 5.1-4 Component-wise inventory distribution errors (Group D)

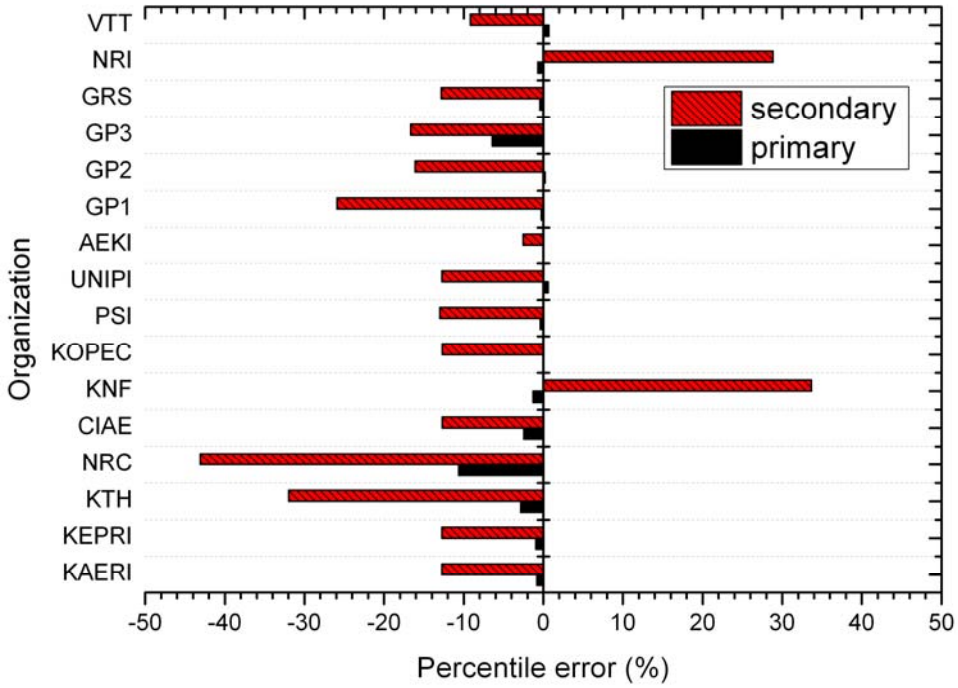

Figure 5.1-5 Comparison of the participants' inventory distribution

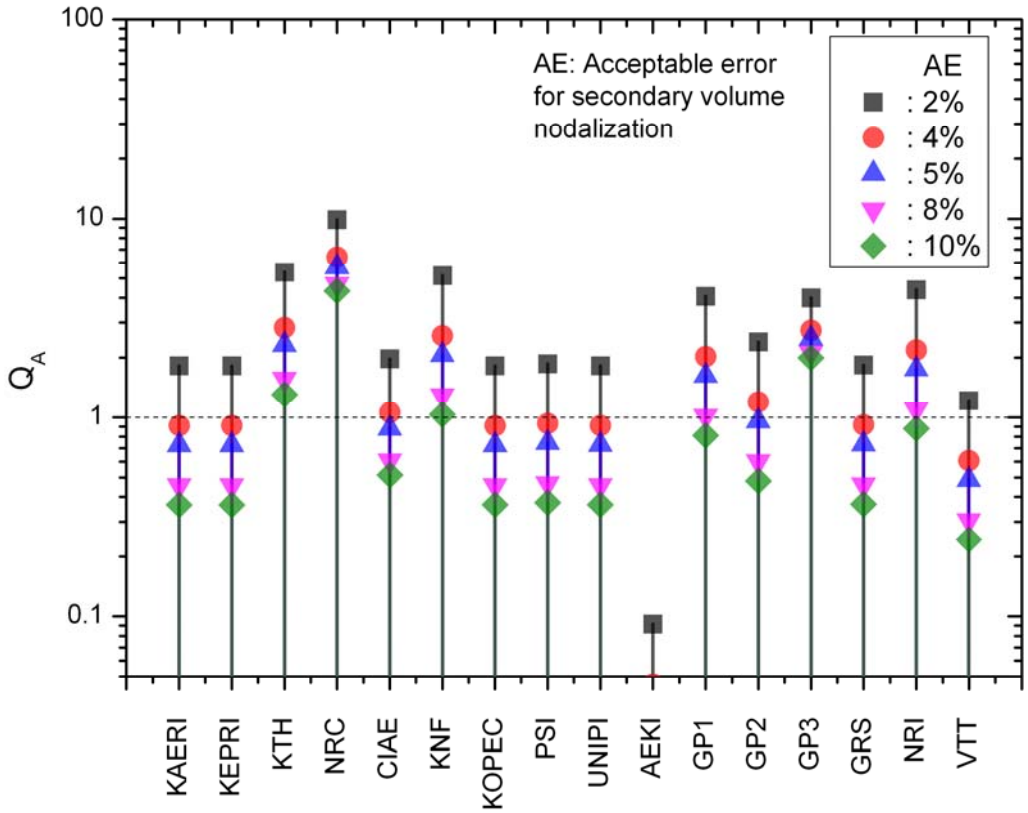

Figure 5.1-6 Comparison of Q_A for nodalization quantification

Table 5.1-1 Summary of the inventory distributions of the code models

	Exp.	Group A				Group B					Group C				Group D		
		KAERI	KEPRI	KTH	USNRC	CIAE	KNF	KOPEC1	PSI	UNIPI	AEKI	GP1	GP2	GP3	GRS	NRI	VTT
Core (m^3)	0.3840	0.3756	0.3754	0.537	0.4275	0.3627	0.3749	0.3749	0.3750	0.3823	0.352	0.3919	0.3802	0.4017	0.3793	0.3860	0.3790
Down-comer (m^3)	0.1790	0.1649	0.1724	0.186	0.1660	0.1749	0.1670	0.1780	0.1780	0.1663	0.2336	0.1693	0.1621	0.1644	0.1670	0.1671	0.1780
Pressurizer (m^3)	0.2720	0.2735	0.2734	0.274	0.2748	0.2734	0.2734	0.2711	0.2730	0.2734	0.374	0.2748	0.2776	0.2735	0.2735	0.2726	0.2560
PZR surge line (m^3)	0.0047	0.0040	0.0040	0.0042	0.0053	0.004	0.0040	0.0040	0.0040	0.0040	0.003	0.0045	Note [e]	0.0046	0.0041	0.0040	0.0046
Hot leg (1 of 2) (m^3)	0.0262	0.0245	0.0245	0.0271	0.0272	0.0245	0.0245	0.0245	0.0245	0.0245	0.0275	0.0256	0.0232	0.0232	0.0253	0.0245	0.0199
SG (1 of 2) (m^3)	0.3066	0.3051	0.3051	0.204	0.2039	0.3018	0.3051	0.3111	0.3050	0.3111	0.24	0.3043	0.3083	0.2630	0.3123	0.3051	0.3300
Cold leg (1 of 4) (m^3)	0.0115	0.0114	0.0114	0.0124	0.0124	0.01141	0.0114	0.0182	0.0114	0.0114	0.01363	0.0160	0.0166	0.0122	0.0148	0.0114	0.0095
Int. leg (1 of 4) (m^3)	0.0161	0.0183	0.0159	0.0170	0.0170	0.01404	0.0159	0.0159	0.0159	0.0159	0.01714	0.0171	0.0227	0.0127	0.0179	0.0159	0.0172
RCP (1 of 4) (m^3)	0.0053	0.0068	0.0068	0.0023	0.0023	0.0068	0.0068	0.0068	0.0068	0.0068	0.0[c]	Note [f]	Note [f]	Note [f]	0.0 [g]	0.0068	0.0060
Primary sum (m^3)	1.6366	1.6234	1.6211	1.590	1.4628	1.5966	1.6152	1.6359	1.6300	1.6464 [b]	1.6359	1.6327	1.640	1.5315	1.6299	1.6253	1.6479
SG (1 of 2) (m^3)	1.3330	1.1706	1.1706	0.965	0.7352	1.1706	1.1706	1.1706	1.17	1.171	1.3421	0.9867	1.1697	1.1722	1.1692	1.1706	1.2417
Steam line (1 of 2) (m^3)	0.0862[a]	0.0682	0.0681	0	0.0729	0.0682	0.6581	0.0681	0.064	0.0681	0.0411[d]	0.0650	0.0420	0.0214	0.0682	0.6580	0.0475
Secondary sum (m^3)	2.8385	2.4775	2.4775	1.931	1.6161	2.4776	3.7938	2.4776	2.47	2.477	2.7664	2.1034	2.3810	2.3660	2.4748	3.6573	2.5784

Note [a] : This value is from the exit nozzle of SG to the turbine isolation valve

[b] : V=1.6341m^3 excluding core guide tubes, core-upper plenum bypass, downcomer-upper head bypass

[c] : 0D pump in model

[d] : Estimated value

[e] : This volume was included in PZR

[f] : This volume was included in Int. leg

[g] : RCP is a junction-related model in ATHLET. Therefore its volume was assigned partially to the IL (suction), partially to the cold leg (discharge)

Table 5.1-2 Summary of percentile errors of the inventory distributions of the code models

	Group A				Group B					Group C				Group D		
	KAERI	KEPRI	KTH	USNRC	CIAE	KNF	KOPEC1	PSI	UNIPI	AEKI	GP1	GP2	GP3	GRS	NRI	VTT
Core	2.20%	-2.24%	39.84%	11.33%	-5.55%	-2.37%	-2.37%	-2.34%	-0.44%	-8.33%	2.06%	-0.99%	4.61%	-1.22%	0.52%	-1.30%
Down-comer	-7.88%	-3.69%	3.91%	-7.29%	-2.29%	-6.70%	-0.56%	-0.56%	-7.09%	30.50%	-5.42%	-9.44%	-8.16%	-6.70%	-6.65%	-0.56%
Pressurizer	0.53%	0.51%	0.74%	1.03%	0.51%	0.51%	-0.33%	0.37%	0.51%	37.50%	1.03%	2.06%	0.55%	0.55%	0.22%	-5.88%
PZR surge line	-14.68%	-14.89%	-10.64%	11.91%	-14.89%	-14.89%	-14.89%	-14.89%	-14.89%	-36.17%	-4.26%	-	-2.13%	-12.77%	-14.89%	-2.13%
Hot leg (1 of 2)	-6.45%	-6.49%	3.44%	3.74%	-6.49%	-6.49%	-6.49%	-6.49%	-6.49%	4.96%	-2.29%	-11.45%	-11.45%	-3.44%	-6.49%	-24.05%
SG (1 of 2)	-0.48%	-0.49%	-33.46%	-33.50%	-1.57%	-0.49%	1.47%	-0.52%	1.47%	-21.72%	-0.75%	0.55%	-14.22%	1.86%	-0.49%	7.63%
Cold leg (1 of 4)	-0.78%	-0.87%	7.83%	8.09%	-0.78%	-0.87%	58.26%	-0.87%	-0.87%	18.52%	39.13%	44.35%	6.09%	28.70%	-0.87%	-17.39%
Int. leg (1 of 4)	13.85%	-1.24%	5.59%	5.65%	-12.80%	-1.24%	-1.24%	-1.24%	-1.24%	6.46%	6.21%	40.99%	-21.12%	11.18%	-1.24%	6.83%
RCP (1 of 4)	28.68%	28.30%	-56.60%	-55.85%	28.30%	28.30%	28.30%	28.30%	28.30%	-	-	-	-	-	28.30%	13.21%
Primary sum	-0.81%	-0.95%	-2.85%	-10.62%	-2.44%	-1.31%	-0.04%	-0.40%	0.6%	-0.04%	-0.24%	0.21%	-6.42%	-0.41%	-0.69%	0.69%
SG (1 of 2)	-12.18%	-12.18%	-27.61%	-44.85%	-12.18%	-12.18%	-12.18%	-12.23%	-12.15%	0.68%	-25.98%	-12.25%	-12.06%	-12.29%	-12.18%	-6.85%
Steam line (1 of 2)	-20.94%	-21.00%	-100.0%	-15.43%	-20.88%	663.46%	-21.00%	-25.75%	-21.00%	-52.32%	-24.59%	-51.28%	-75.17%	-20.88%	663.34%	-44.90%
Secondary sum	-12.72%	-12.72%	-31.97%	-43.06%	-12.71%	33.66%	-12.71%	-12.98%	-12.74%	-2.54%	-25.90%	-16.12%	-16.65%	-12.81%	28.85%	-9.16%

Note : percentile error (ε) = (model – data)/data

Table 5.1-3 Nodalization quantification based on inventory information

		Quantity		Remarks
		Primary sum (m^3)	Secondary sum (m^3)	
Acceptable Error, AE		2%	5%	Assumption
EXP	Y_E	1.6366	2.8385	[m^3]
	Error(±)	0.0327	0.0568	~ 2 %
Weighting factor, Wi		1.0	0.5	relative importance
KAERI	Calculation	1.6234	2.4775	[m^3]
	Percentile Error, E	0%	10.94%	
	Qi	0.0	0.729	
	Q_A	0.729		
KEPRI	Calculation	1.6211	2.4775	[m^3]
	Percentile Error, E	0.0%	10.94%	
	Qi	0.0	0.729	
	Q_A	0.729		
KTH	Calculation	1.59	1.931	[m^3]
	Percentile Error, E	0.86%	30.58%	
	Qi	0.288	2.039	
	Q_A	2.327		
NRC	Calculation	1.4628	1.6161	[m^3]
	Percentile Error, E	8.80%	41.90%	
	Qi	2.933	2.793	
	Q_A	5.726		
CIAE	Calculation	1.5966	2.4776	[m^3]
	Percentile Error, E	0.45%	10.93%	
	Qi	0.151	0.728	
	Q_A	0.880		
KNF	Calculation	1.6152	3.7938	[m^3]
	Percentile Error, E	0.0%	31.03%	
	Qi	0.0	2.069	
	Q_A	2.069		
KOPEC	Calculation	1.6359	2.4776	[m^3]
	Percentile Error, E	0.0%	10.93%	
	Qi	0.0	0.729	
	Q_A	0.729		

PSI	Calculation	1.63	2.47	[m³]
	Percentile Error, E	0.0%	11.21%	
	Qi	0.0	0.747	
	Q_A	0.747		
UNIPI	Calculation	1.6464	2.477	[m³]
	Percentile Error, E	0.0%	10.95%	
	Qi	0.0	0.730	
	Q_A	0.730		
AEKI	Calculation	1.6359	2.7664	[m³]
	Percentile Error, E	0.0%	0.55%	
	Qi	0.0	0.037	
	Q_A	0.037		
GP1	Calculation	1.6327	2.1034	[m³]
	Percentile Error, E	0.0%	24.38%	
	Qi	0.0	1.626	
	Q_A	1.626		
GP2	Calculation	1.64	2.381	[m³]
	Percentile Error, E	0.0%	14.40%	
	Qi	0.0	0.960	
	Q_A	0.960		
GP3	Calculation	1.5315	2.366	[m³]
	Percentile Error, E	4.51%	14.94%	
	Qi	1.504	0.996	
	Q_A	2.500		
GRS	Calculation	1.6299	2.4748	[m³]
	Percentile Error, E	0.0%	11.03%	
	Qi	0.0	0.736	
	Q_A	0.736		
NRI	Calculation	1.6253	3.6573	[m³]
	Percentile Error, E	0.0%	26.32%	
	Qi	0.0	1.755	
	Q_A	1.755		
VTT	Calculation	1.6479	2.5784	[m³]
	Percentile Error, E	0.0%	7.31%	
	Qi	0.0	0.487	
	Q_A	0.487		

5.2 Initial and boundary conditions

Similar to the blind case, the ISP-50 participants in the open calculation were grouped into 4 sub-groups by taking into account the similarity of the code used as shown in Table 5.2-1. The PSI of Switzerland who joined the open calculation was included in Group B because they used the RELAP5/MOD3.3 code. KOPEC which performed two calculations in the previous blind phase submitted one calculation with RELAP5-ME code in the open phase. Gidropress which used two codes – KORSAR/GP and TECH-M-97- in the previous blind phase also submitted only one calculation with TECH-M-97 code in this open phase.

Table 5.2-1 Grouping of the submitted participants

Group ID	Participants index	Code used	Remarks
A	KAERI, KEPRI, KTH, USNRC	MARS or TRACE	4 orga'ns
B	CIAE, KNF, KOPEC, PSI, UNIPI	RELAP series	5 orga'ns
C	AEKI, GP1, GP2, GP3	CATHARE, KORSAR/GP	4 orga'ns
D	GRS, NRI, VTT	ATHLET, APROS	3 orga'ns

The initial and boundary conditions used by all the calculations are listed in Table 5.3-1. The same parameters used in the previous blind calculation were used for comparison against the data. The reference data column number was also included in Table 5.3-1. Note that the reference data column number for a given parameter is different from that in the blind case because the number of requested parameters was increased from 86 to 144.

5.3 Nodalization scheme and sequence of events

A summary of nodalization schemes of the submitted calculations is listed in Table 5.3-2. Most calculations were performed by one dimensional modeling, but multi-dimensional modeling on the down-comer and the reactor pressure vessel was done by some participants. Most participants applied two-dimensional modeling to the down-comer region. When multiple channels were used to take into account the effects of cross flow between two adjacent channels, this modeling can be treated as two-dimensional. The number of azimuthal sections showed a variation from 4 to 8 depending on calculations. As for the reactor pressure vessel, KTH and USNRC applied a 3-D vessel component in order to predict the 3-D behavior of the peak cladding temperature.

Number of nodalization is summarized in Table 5.3-2 where a wide range of variation can be found. Comparison of the number of volumes, nodes and heat structures is shown in Figure

5.3-1. KTH used the greatest number of volumes, 863 volumes, to model the ATLAS facility with the TRACE code. Whereas, USNRC who used the same TRACE code used only 94 volumes. It is because the number of volumes used to model the core with the VESSEL component was not taken into account in the table. UNIPI used 823 volumes with RELAP5/MOD3.3 code. VTT used 592 volumes with the APROS code. On average, the number of volumes used by the other participants ranges around 100 and 300. Number of heat structures also showed a great variation. KTH used the minimum number of heat structures but VTT used the maximum of 1866. Details of nodalization of the submitted calculations can be found in the reports prepared by the participants and they were included in Appendix-F.

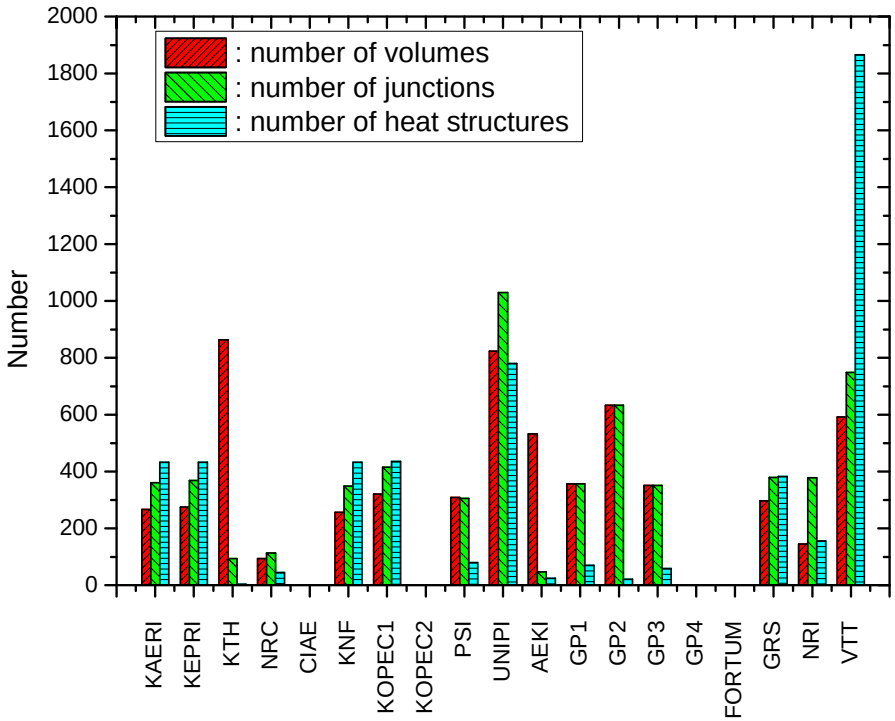

Figure 5.3-1 Comparison of number of nodes

Note [1)] Number of detailed nodes was inferred from the participants' reports in some cases

Table 5.3-3 summarizes the sequence of events calculated by the participants in the open calculation. In order to make the comparison with the data convenient, the submitted calculation times and experimental times were adjusted for the break time to be 0.0 s. Detailed sequence of events in open calculations needs to be compared with the previous blind calculation as well as the experimental values. Table 5.3-4 through Table 5.3-7 summarize the comparison of the calculated sequence of events from Group A to Group D. Note that only the timing of sequence of events is compared in this section. Agreement in timing of a certain

event does not always imply quantitative agreement in physical phenomena.

5.3.1 Group A

Four organizations were grouped in 'A' and three used the MARS-KS code and one used TRACE 5.300 code. In group A, the KAERI's calculation showed much improved agreement in timing of the 1st MSSV opening, the LPP trip, and the SIT activation compared with the blind calculation. However, the prediction of main feed water isolation time was worsened. It is noteworthy that the prediction of the loop seal clearing timing was much improved and the loop remained sealed during the test period was also accurately predicted.

The KEPRI's calculation also showed much improved agreement in the timing of the 1st MSSV opening, the LPP trip, and the SIT activation compared with the blind calculation. The prediction of main feed water isolation time, however, was more or less worsened. The prediction of the loop seal clearing timing was much improved but all loop seals were cleared at the same time. Prediction of the loop 2A remained sealed all the time was failed even in the open phase.

KTH showed better agreement in predicting the timing of the 1st MSSV opening and the SIT activation compared with the blind calculation. However, the prediction of the timing of main feed water isolation, the LPP trip, the SIP actuation, and the SIT actuation was worsened. As for the prediction of the loop seal clearing, KTH showed greatly worsened results. Only the loop seal in the loop 2A was cleared, whereas the other loop seals were not cleared, which is the opposite result to the experimental observation.

The USNRC's calculation did not show a significant difference in terms of the timing of major sequence of events between the blind and the open calculations. And the prediction of SIT actuation time was a little bit improved. Note that the loop seal 2A remained blocked during the test period was correctly predicted.

5.3.2 Group B

Five organizations were grouped in 'B' and they all used the RELAP5/Mod3.3 code series. KOPEC used a little modified version of RELAP5/Mod3.3 code series, named RELAP5-ME. PSI was a new comer joined in the open phase.

The CIAE's calculation showed a little improvement in the prediction of the timings of the LPP and the RCP trips. And the prediction of the 1st MSSV opening, the MFW isolation, the core

decay heat, and the SIP activation was much the same as the blind case, but the prediction of the timing of the SIT activation and loop seal clearing was worsened a little, but the difference was not so great. On the whole, the prediction of the sequence of events was comparable to the blind case. However, the loop seal clearing happened two times and the second loop seal clearing removed the water seals in the loop 2A and 2B.

The KNF's calculation showed a little better improvement in the prediction of timing of the SIT activation and the loop seal clearings of the loop 1A and 1B. However, the prediction of the 1st MSSV opening, the LPP trip, the RCP trip, the MFW isolation, the core decay heat, and the SIP activation was worsened a little compared with that in the blind calculation. On the whole, the prediction of the sequence of events was more or less similar to the blind case.

As for the KOPEC's calculation, it showed a little improvement in the prediction of the timings of the LPP trip and the SIT activation. In particular, the prediction of the loop seal clearing timing showed a great difference compared to the blind data.

The UNIPI's calculation shows a little improvement in the prediction of the timing of the core decay start and quite a large improvement for the SIT activation and the loop seal clearing of the CL1A. However, the prediction of the timings of the 1st MSSV open, the LPP trip, the RCP trip, the MFW isolation, and the SIP activation was very similar to the blind case. The prediction of the loop seal clearing timings were worsened on the contrary.

PSI participated only for the open calculation. In general, the PSI's calculation showed good agreement in timing with the data except the RCP trip, the core decay heat, and the loop seal clearing of the loop 2B. It is noteworthy that the PSI's prediction for the loop seal clearings was quite a good agreement with the data except for the loop 2B, whose occurring time was much earlier.

5.3.3 Group C

A Hungarian participant, KFKI/AEKI joined the ISP-50 late with the CATHARE code and was grouped in 'C' together with calculations by Russian codes. The KFKI/AEKI's calculation results showed a reasonable agreement with the experimental data except for the timing of the 1st MSSV opening and the loop seal clearing. The predicted timing of the 1st MSSV opening showed a 40 s delay. The calculated loop seal clearing timings of broken loop were delayed 1200 s. On the other hand, the loop seals of intact loop were cleared in 1076 s earlier than the data.

The GP1's calculation showed much improved agreement in the timing of the 1st MSSV opening, the MFW isolation, the SIT and the SIP activation compared with the blind calculation. The timing of the core power decay, however, showed a larger distortion than that of the blind calculation. The loop seals showed a different behavior. In the blind calculation, the loop seals of the broken loop were not cleared. In the intact loop, however, the loop seals were all cleared around 287~288 s. In the open calculation, only one of the loop seal 1A in the broken loop was not cleared.

The GP2's open calculation showed the prediction similar to that of the blind calculation. The prediction of the SIT activation timing, however, was considerably improved. In the blind calculation, the entire loop seals were cleared around 253~254 s. In the open calculation, however, the loop seals in the broken loop were not cleared, and the timings of the clearing of the intact loop were more delayed than those of the blind calculation.

The GP3's calculation showed a little bit improved trend in the timing of the 1st MSSV opening, the LPP trip, the MFW isolation, the core decay, the SIP activation compared with the blind calculation. It is noteworthy that the prediction of the SIT activation timing was much improved. However, the entire loop seals were not cleared in both blind and open calculations.

5.3.4 Group D

Calculations by the ATHLET or APROS codes were grouped in 'D'. In group D, FORTUM did not participate in the open calculation with good reason. In the blind calculation all the major events were predicted later than the experimental data except for the loop seal clearing.

The GRS's calculation showed improved agreement in the timing of the 1st MSSV opening, the MSIV closure, and the SIP activation compared with the blind calculation. However, the prediction of loop seal clearing was different with each other. While all the loop seals were cleared in the blind calculation, two loop seals of 1B and 2A were cleared in the open calculation.

The NRI's calculation showed better agreement in the timing of the 1st MSSV opening, the MSIV closure, the core decay, the SIP activation, and the loop seal clearing than those in the blind calculation.

The VTT's calculation showed improved agreement in the timing of the 1st MSSV opening, the MSIV closure, the core decay, the SIT activation, and the loop seal clearing compared with the blind calculation.

Table 5.3-1 Comparison of initial conditions in open calculations

	Experiment	Reference data column number	Group A				Group B					Group C				Group D		
			KAERI	KEPRI	KTH	USNRC	CIAE	KNF	KOPEC1	PSI	Univ. of Pisa	AEKI	EDO Gid. (GP1)	EDO Gid. (GP2)	EDO Gid. (GP3)	GRS	NRI	VTT
Primary system																		
Core power, MW	1.635	D1	1.635	1.566	1.636	1.553	1.613	1.636	1.633	1.638	1.636	1.636	1.636	1.635	1.636	1.636	1.636	1.64
Pressure, MPa	15.67	D4	15.67	15.59	15.39	15.63	15.15	15.66	15.66	15.53	15.67	15.76	15.67	15.67	15.52	15.63	15.60	15.6
Core inlet temp., K	562.7	D66	563.1	563.8	562.9	562.7	562.5	564.6	563.0	562.3	561.9	566.7	563.8	565.0	564.8	565.0	562.9	562.3
Core exit temp., K	597.7	D67	598.2	598.5	598.3	598.5	597.3	598.2	596.4	597.4	596.6	597.7	599.0	598.8	597.8	598.4	597.2	595.5
Bypass DC-UH, kg/s	~0.0	D95	0.0158	-0.008	0.0	0.0	0.0	-0.0185	-0.0089	-0.0336	-0.1073	0.0027	0.1105	0.0	0.0	-0.033	0.567	-0.03
Bypass DC-HL, kg/s	~0.0	D96	0.0178	0.0	0.0	0.0	0.0	0.0322	0.0011	0.0	0.0	NA	0.3478	0.0	0.0	7.5e-6	0.48	0.08
CL flow rate, kg/s	2.2 ± 5%	D99	1.9988	2.0068	1.9568	1.8469	2.017	2.0657	2.1098	2.0032	2.0306	2.2657	2.0412	2.0590	2.0433	2.11	2.18	2.1
PZR level, m	3.36	D130	3.587	4.112	3.23	3.42	3.22	3.323	3.365	3.252	3.309	3.242	3.234	3.360	3.745	3.307	3.32	3.3
RCP speed, rpm	15 ± 5	D139	22.2	223.9	21.5	200.5	24.0	263.9	30.0	23.3	11.6	0.0	0.0	0.0	0.0	10.7	18.9	19.2
Secondary system																		
Pressure, MPa	7.83	D6	7.775	7.831	7.830	7.830	7.832	7.832	7.787	7.861	7.831	7.831	7.830	7.728	7.862	7.83	7.83	7.83
Steam temp., K	568.5	D89	566.1	566.6	566.7	566.7	566.6	568.5	566.2	566.9	566.7	566.7	566.5	565.9	566.8	566.7	566.2	566.4
Avg. FW temp., K	508.2	-		505.4	508.0	508.4		-	505.4	-	-	508.0	-	-	-	508.2	507.2	508.2
FW flow (ECO), kg/s	0.43	D103	0.455	0.3998	0.473	0.432	0.431	0.433	0.4639	0.4206	0.4326	0.4600	0.4382	0.4059	0.4566	0.432	0.431	0.42
FW flow (DC), kg/s	~0.0	D104	0.0	0.0444	0.0	0.0	0.0	0.0	0.0	0.0	0.0	0.0	0.0	0.0	0.0	0.0	0.0	0
SG level, m	1.97~2.03	-		4.08	3.44	1.83		-	5.91	-	-	2.61	-	-	-	2.07	4.76	2.70
Heat removal, kW	753.67	D2	815.8	781.17	815.46	777.06	784.17	810.82	816.97	750.92	772.94	813.18	791.96	796.80	817.54	786	730	775
ECC																		
SIT pressure, MPa	4.19	D8	4.19	4.23	4.19	4.20	4.21	4.21	4.23	4.17	4.19	4.19	4.17	4.20	4.20	4.19	4.23	4.23
SIP Temp., K	321.3	D82	323.3	320.9	325.1	323.3	323.3	323.3	323.2	320.2	323.0	323.2	322.9	323.1	323.2	323.2	323.2	321.3
SIT Temp., K	323.5	D79	323.4	324.3	323.4	323.4	323.3	323.5	320.9	323.2	323.2	323.4	323.5	323.1	323.2	323.6	323.2	324.1
SIT level, %	~95	-		95	95	95	-	-	~95	-	-	~95	-			-	95	95
Containment																		
Pressure, MPa	0.10	D11	0.1013	0.1013	0.1029	0.1088	0.1013	0.1028	0.1029	0.1444	0.1013	0.1	0.1013	0.1000	0.0	0.1032	0.10	0.100

Table 5.3-2 Summary of nodalization schemes in open calculation

	Group A				Group B					Group C				Group D		
	KAERI	KEPRI	KTH	USNRC	CIAE	KNF	KOPEC1	PSI	Univ. of Pisa	AEKI	EDO Gid 1 (GP1)	EDO Gid 2 (GP2)	EDO Gid 3 (GP3)	GRS	NRI	VTT
Code	MARS-KS	MARS-KS	TRACE 5.0 p.1	TRACE 5.0 p.2	RELAP5/M3.3	R5/M3.3	RELAP5-ME	RELAP5/M3.3	RELAP5/M3.3	CATHARE2V1.5B mod3.1	KORSAR/GP	KORSAR/GP	KORSAR/GP	ATHLET M2.2	ATHLET	APROS 5.09
Node information																
No. of Volume	267	275	863	94	NA	256	321	309	823	532	357	633	351	297	145	592
No. of Junction	360	368	97	114	NA	349	415	305	1029	47	357	633	351	379	378	749
No. of Heat Structure	433	433	4	44	NA	433	435	80	780	24	70	21	59	382	155	1866
Downcomer[1)] axi x rad x azi	2-D 10 x 6	2-D 10x6	2-D	2-D 19x1x8	2-D 10x1x6	2-D 10x1x6	2-D 10x1x6	2-D 10x1x6	2-D 23x1x4	1-D	2-D 17x1x4	1-D 16x1x1	2-D 22x1x4	2-D 11x1x4	2-D 14x1x6	2-D 24x1x6
RPV[1)] axi x rad x azi	1-D	1-D	3-D 19 x3x6	3-D 19x4x8		1-D	1-D	1-D	1-D	1-D	1-D 12x1x1	1-D 12x1x1	1-D 12x1x1	1-D	1-D	1-D 24x1x1
Others									RPV 4 parallel channels					RPV 3 parallel channels		

Note [1)] Number of detailed nodes was inferred from the participants' reports in some cases

Table 5.3-3 Summary of calculated sequence of events in open calculation

		Exp. (shifted time, sec)	Group A				Group B					Group C				Group D		
			KAERI	KEPRI	KTH	USNRC	CIAE	KNF	KOPEC1	PSI	Univ. of Pisa	AEKI	EDO Gid 1 (GP1)	EDO Gid 2 (GP2)	EDO Gid 3 (GP3)	GRS	NRI	VTT
Break		0.	0.0	0.0	0.0	0.0	0.0	0.0	0.0	0.0	0.0	0.0	0.0	0.0	0.0	0.0	0.0	0
1st MSSV open		24.	28.0	29.0	49.2	37.0	33.1	6.0	21.0	28.0	28.1	64.0	32.0	34.0	17.0	23.4	33.0	33.0
LPP trip		25.	25.0	26.0	37.1	34.0	25.1	28.0	29.0	25.0	26.4	29.1	26.0	27.0	29.0	23.0	28.5	28.0
RCP trip		25.	25.0	26.4	37.1	34.0	37.1	0.0	29.0	52.0	0.0	30.14	0.0	0.0	0.0	23.0	28.9	28.35
MSIV closure		25.	32.1	26.1	37.2	33.3	24.1	29.1	28.8	25.0	230.0	30.1	26.5	NM[4]	NM[4]	23.0	28.6	28.0
MFW isolation		32.	32.1	33.5	44.2	41.1	29.1	35.0	35.0	31.0	33.4	37.1	33.1	34.1	36.1	30.0	35.5	35.0
Core decay		33.	29.0	26.5	32.1	34.0	29.1	29.0	35.0	26.0	38.1	30.1	26.4	27.3	29.4	28.5	33.0	34.0
SIP activation		54.	86.0	54.3	65.2	62.1	49.0	57.0	58.0	54.0	54.7	57.6	54.3	55.3	57.3	52.0	57.3	56.3
SIT activation		468.	452	453.4	426.4	416.8	433.0	475.0	399.0	469.0	469.0	460.9	477.0	508.3	464.0	494.0	500.2	485.0
Loop seal clear	CL1A	190.	170	172	X	188	145	180.0	1710.0	183.0	185.0	1400	X	X	X	X	X(281)[3]	165
	CL1B	190.	170	172	X	188	145	180.0	X	183.0	X	1400	420	X	X	217	X(400)[3]	165
	CL2A	X[1]	X	172	204	X	1472	181.0	142.0	X[2]	184.0	160	390	280	X	192	X	182
	CL2B	1236	170	172	X	188	1472	X	142.0	168.0	184.0	160	X	280	X	X	X	182
Stop		2933	1999	2000	3300	1999	1500	2000	2000	3000	2500	3000	2933	3000	3000	2807	2933	2000

Note

[1] X: not occurred

[2] Loop seal clearing occurred at 168 s but, after about 25 s it returned to water plugging

[3] Loop seal clearing was reported in the participant's report, but it did not occur according to the submitted data

[4] NM: not modeled

Table 5.3-4 Detailed comparison of calculated sequence of events of Group A

	Exp. (shifted time, sec)	Group A															
		KAERI				KEPRI				KTH				USNRC			
		Blind		Open		Blind		Open		Blind		Open		Blind		Open	
		cal.	diff.	cal.	diff.	cal.	diff.	cal.	diff.	cal.	diff.	cal.	diff.	cal.	diff.	cal.	diff.
Break	0.	0.0	0.0	0.0	0.0	0.0	0.0	0.0	0.0	0.0	0.0	0.0	0.0	0.0	0.0	0.0	0.0
1st MSSV open	24.	34.1	+10.1	28.0	+4.0	X	bad	29.0	+5.0	X	bad	49.2	+25.2	37.7	+13.3	37.0	+13.0
LPP trip	25.	29.0	+4.0	25.0	0.0	23.0	-2.0	26.0	+1.0	23.5	-1.5	37.1	+12.1	31.0	+6.0	34.0	+9.0
RCP trip	25.	0.0	-	25.0	0.0	13.9	-11.1	26.4	+1.4	24.0	-1.0	37.1	+12.1	31.5	+6.5	34.0	+9.0
MSIV closure	25.	32.1	+7.1	32.1	+7.1	25.5	+0.5	26.1	+1.1	23.6	-1.4	37.2	+12.2	28.4	+3.4	33.3	+8.3
MFW isolation	32.	38.1	+6.1	32.1	+0.1	31.7	+0.3	33.5	+1.5	30.0	-2.0	44.2	+12.2	38.7	+6.7	41.1	+9.1
Core decay	33.	30.1	-2.9	29.0	-4.0	25.54	-7.46	26.5	-6.5	30.0	-0.9	32.1	-0.9	31.5	-1.5	34.0	+1.0
SIP activation	54.	57.1	+3.1	86.0	+32.0	52.7	-1.3	54.3	+0.3	50.0	-4.0	65.2	+11.2	60.1	+6.1	62.1	+8.1
SIT activation	468.	435.	-33.0	452	-16.0	433.1	-34.9	453.4	-14.6	224.0	-244.0	426.4	-41.6	387.8	-80.2	416.8	-51.2
Loop seal clear CL1A	190.	108.	-82.0	170	-20.0	325.8	+135.8	172	-18	83	-107	X	bad	170	-20	188	-2.0
Loop seal clear CL1B	190.	107.	-83.0	170	-20.0	323.2	+133.8	172	-18	113	-77	X	bad	169	-21	188	-2.0
Loop seal clear CL2A	X[1)]	105.	bad	X	good	139.1	bad	172	bad	83	-107	204	bad	170	bad	X	good
Loop seal clear CL2B	1236	105	-1131.	170	-1066	141.6	-1094.	172	-1064	83	-107	X	bad	170	-1066	188	-1048
Stop	2933	1806	-	1999	-	2000	-	2000	-	2932	-	3300	-	3000	-	1999	-

Note

[1)] X: not occurred

Table 5.3-5 Detailed comparison of calculated sequence of events of Group B

	Exp. (shifted time, sec)	Group B																			
		CIAE				KNF				KOPEC1				KOPEC2		PSI		UNIPI			
		Blind		Open		Blind		Open		Blind		Open		Blind		Open		Blind		Open	
		cal.	diff.	cal.	diff.	cal.	diff.	cal.	diff.	cal.	diff.	cal.	diff.	cal.	diff.	cal.	diff.	cal.	diff.	cal.	diff.
Break	0.	0.0	0.0	0.0	0.0	0.0	0.0	0.0	0.0	0.0	0.0	0.0	0.0	0.0	0.0	0.0	0.0	0.0	0.0	0.0	0.0
1st MSSV open	24.	33.1	+9.1	33.1	+9.1	X	X	6.0	-18.0	X	X	21.0	-3.0	X	X	28.0	+4.0	28.0	+4.0	28.1	+4.1
LPP trip	25.	24.3	-0.7	25.1	+0.1	23.0	-2.0	28.0	+3.0	14.5	-10.5	29.0	+4.0	15.0	-10.0	25.0	0.0	24.0	-1.0	26.4	+1.4
RCP trip	25.	0.0	-25.0	37.1	+12.1	4.0	-21.0	0.0	-25.0	27.0	+2.0	29.0	+4.0	27.0	+2.0	52.0	+27.0	0.0	-25.0	0.0	-25.0
MSIV closure	25.	24.1	-0.9	24.1	-0.9	23.1	-1.9	29.1	+4.1	28.7[2]	+3.7	28.8	+3.8	NA	-	25.0	0.0	NM	-	230.0	+205.0
MFW isolation	32.	29.0	-3.0	29.1	-2.9	29.0	-3.0	35.0	+3.0	34.0	+2.0	35.0	+3.0	34.0	+2.0	31.0	-1.0	31.0	-1.0	33.4	+1.4
Core decay	33.	~30.	-3.0	29.1	-2.9	30.0	-3.0	29.0	-4.0	NA	-	35.0	+2.0	NA	-	26.0	-7.0	24.0	-9.0	38.1	+5.1
SIP activation	54.	49.0	-5.0	49.0	-5.0	51.0	-3.0	57.0	+3.0	58.0	+4.0	58.0	+4.0	58.0	+4.0	54.0	0.0	52.0	-2.0	54.7	+0.7
SIT activation	468.	456.0	-12.0	433.0	-35.0	379.0	-89.0	475.0	+7.0	357.0	-111.0	399.0	-69.0	332.0	-136.0	469.0	+1.0	401.0	-67.0	469.0	+1.0
Loop seal clear CL1A	190.	150.	-40.0	145.0	+45.0	159.	-31.0	+180.0	-10.0	388.0	+198.0	1710.0	+1520.0	403.3	+213.3	183.0	-7.0	149.2	-40.8	185.0	-5.0
Loop seal clear CL1B	190.	150.	-40.0	145.0	+45.0	159.	-31.0	+180.0	-10.0	X	bad	X	bad	X	bad	183.0	-7.0	150.2	-39.8	X	bad
Loop seal clear CL2A	X[1]	X	good	1472.0	bad	188.	bad	+181.0	bad	728.4	bad	142.0	bad	781.1	bad	X[3]	good	X[4]	good	184.0	bad
Loop seal clear CL2B	1236	X	bad	1472.0	+236.0	X	bad	X	bad	731.6	-504.4	142.0	-1094.0	784.3	-451.7	168.0	-1068.0	150.2	-1085.8	184.0	-1052.0
Stop	2933	1460		1500		2000.		2000		3000.		2000		3000.		3000		3000.		2500	

Note [1] X: not occurred

[2] No MSIV was modeled, TCV closure time

[3] Loop seal clearing occurs at 168 s but, after about 25 s it returned to water plugging

[4] Loop seal clearing occurs at 150 s but, after about 550 s it returned to water plugging

Table 5.3-6 Detailed comparison of calculated sequence of events of Group C

	Exp. (shifted time, sec)	Group C															
		AEKI		GP1				GP2				GP3				GP4	
		Open		Blind		Open		Blind		Open		Blind		Open		Blind	
		cal.	diff.	cal.	diff.	cal.	diff.	cal.	diff.	cal.	diff.	cal.	diff.	cal.	diff.	cal.	diff.
Break	0.	0.0	0.0	0.0	0.0	0.0	0.0	0.0	0.0	0.0	0.0	0.0	0.0	0.0	0.0	0.0	0.0
1st MSSV open	24.	64.0	+40.0	NA	-	+32.0	8.0	NA	-	34.0	+10.0	NA	-	17.0	-7.0	NA	-
LPP trip	25.	29.1	+4.1	31.39	6.4	+26.0	1.0	26.9	+1.9	27.0	+2.0	42.1	+17.1	29.0	+4.0	44.5	+19.5
RCP trip	25.	0.0	-25.0	NA	-	0.0	-25.0	NA	-	0.0	-25.0	NA	-	0.0	-25.0	0.0	-25.0
MSIV closure	25.	30.1	+5.1	32.0	7.0	+26.5	1.5	NM	-	NM	-	NM	-	NM	-	NA	-
MFW isolation	32.	37.1	+5.1	38.46	6.5	+33.1	1.1	34.0	+2.0	34.1	+2.1	49.17	+17.2	36.1	+4.1	51.5	+19.5
Core decay	33.	30.1	-2.9	31.0	-2.0	+26.4	-6.6	26.0	-7.0	27.3	-5.7	42.0	+9.0	29.4	-3.6	44.5	+11.5
SIP activation	54.	57.6	+3.6	60.0	6.0	+54.3	0.3	55.0	+1.0	55.3	+1.3	70.38	+16.4	57.3	+3.3	73.0	+19.0
SIT activation	468.	460.9	-7.1	615.99	148.0	+477.0	9.0	684.0	+216.0	508.3	+40.3	658.6	+190.6	464.0	-4.0	364.0	-104.0
Loop seal clear CL1A	190.	1400.0	+1210.0	X	bad	X	bad	254	+64.0	X	bad	X	bad	X	bad	127.1	-62.9
Loop seal clear CL1B	190.	1400.0	+1210.0	X	bad	420	+230	253	+64.0	X	bad	X	bad	X	bad	127.1	-62.9
Loop seal clear CL2A	X[1)]	160.0	bad	288.0	bad	390	bad	254	bad	200	bad	X	good	X	good	132.5	bad
Loop seal clear CL2B	1236	160.0	-1076.0	287.0	-949.0	X	bad	254	-982.0	200	-1036	X	bad	X	bad	132.5	-1103.5
Stop	2933	3000	67.0	3000.	67.0	2933	0.0	3000.	67.0	3000	67.0	2905.	-28.0	3000	67.0	2998.	65.0

Note [1)] X: not occurred

Table 5.3-7 Detailed comparison of calculated sequence of events of Group D

		Exp. (shifted time, sec)	Group D													
			FORTUM		GRS				NRI				VTT			
			Blind		Blind		Open		Blind		Open		Blind		Open	
			cal.	diff.	cal.	diff.	cal.	diff.	cal.	diff.	cal.	diff.	cal.	diff.	cal.	diff.
Break		0.	0.0	0	0.0	0.0	0.0	0.0	0.0	0.0	0.0	0.0	0.0	0.0	0	0.0
1st MSSV open		24.	41.0	+17.0	26.8	+2.8	23.4	-0.6	52.3	+28.3	33.0	+9.0	41.0	+17.0	33.0	+9.0
LPP trip		25.	36.0	+11.0	23.0	-2.0	23.0	-2.0	26.0	+1.0	28.5	+3.5	26.0	+1.0	28.0	+3.0
RCP trip		25.	NA	-	22.4	-2.6	23.0	-2.0	25.8	+0.8	28.9	+3.9	24.0	-1.0	28.35	+3.35
MSIV closure		25.	NA	-	23.0	-2.0	23.0	-2.0	26.1	+1.1	28.6	+3.6	24.0	-1.0	28.0	+3.1
MFW isolation		32.	42.0	+10.0	29.9	-2.1	30.0	-2.0	34.4	+2.4	35.5	+3.5	31.0	-1.0	35.0	+3.0
Core decay		33.	34.0	+1.0	30.9	-2.1	28.5	-4.5	56.8.	+22.8	33.0	0.0	27.0	-6.0	34.0	+1.0
SIP activation		54.	64.0	+10.0	502.0	+448.0	52.0	-2.0	56.0	+2.0	57.3	+3.3	56.0	+2.0	56.3	+2.3
SIT activation		468.	563.0	+95.0	502.0	+34.0	494.0	+26.0	NA [3]	NA	500.2	+32.2	616.0	+148.0	485.0	+17.0
Loop seal clear	CL1A	190.	X	bad	223.1	+33.1	X	bad	X	bad	281	+91	152.0	-38	165	-25
	CL1B	190.	X	bad	223.1	+33.1	217	+27	X	bad	400	+210	152.0	-38	165	-25
	CL2A	X[1]	125.0	bad	208.8	bad	192	bad	X	good	X	good	169.0	bad	182	bad
	CL2B	1236	125.0	-1111	208.8	-1027.2	X	bad	X	bad	X	bad	169.0	-1067	182	-1054
Stop		2933	2007.	-926	3006.	+73	2807	-126	3000.	+67	2933	0	2806.	-127	2000	-933

Note [1] X: not occurred

5.4 Steady state results

Comparisons of steady state results for the major thermal-hydraulic parameters are shown from Figure 5.4-1 to Figure 5.4-18. In these figures, the steady state results obtained in the previous blind phase were also plotted together with the open phase results for comparison.

Figure 5.4-1 shows the initial core power. Depending on whether the primary heat loss was taken into account in the code model, difference in the calculated core power was observed. For instance, KEPRI excluded the additional power for compensating the primary heat loss in his model, resulting in around 1.56 MW. It is interesting that NRC and KNF changed their modeling strategy in the open calculation. NRC included the additional core power for the primary heat loss in the blind calculation but excluded it in the open calculation. KNF took the opposite strategy between two calculations. How the heat loss effects can be treated in the code model is open to dispute. However, most participants were in favor of inclusion of the additional core power for heat loss compensation in their model.

Comparison of the initial primary pressure is shown in Figure 5.4-2. In the open calculation, the PT-LP-01 was used as a representative primary pressure instead of PT-UH-01 in the previous calculation. Therefore, pressure from PT-LP-01 has higher value than that for PT-UH-01. However, a few organizations produced lower primary pressures than those in the blind case. Calculated primary pressures show a variation from 15.39 MPa (KHT) to 15.76 MPa (AEKI).

Comparisons of the core inlet and exit temperature are shown in Figure 5.4-3 and Figure 5.4-4, respectively. The submitted core inlet temperatures are close to the measured data and the minimum is 561.9 K by UNIPI and the maximum is 566.7 K by AEKI. NRI and VTT presented better values than the blind case. As for the core exit temperature, most calculations are in very good agreement with the data. The improvement by KOPEC1 is remarkable.

Down-comer-to-upper head and down-comer-to-hot leg bypass flow rate are compared in Figure 5.4-5 and Figure 5.4-6, respectively. In the ISP-50 test, two bypass flow rates could not be measured accurately but they were estimated to be very close to zero. In particular, the down-comer-to-upper head flow rate is inferred to be negative according to experimental observation. Detailed comparison of the temperature distribution inside the upper head and the upper down-comer region was described in Section 3.5. Note that many organizations – KEPRI, KNF, KOPEC1, PSI, UNIPI, GRS, VTT – predicted negative down-comer-to-upper head flow rate. NRI's calculation showed a little higher down-comer-to-upper head flow rate than that in the case of open calculation. On the other hand, the predicted down-comer-to-hot leg

bypass flow rate was always positive which is consistent with experimental observation. Most calculations agree well with the data in the open phase. But, GP1 predicted enhanced bypass flow rate in the open phase compared with the blind phase.

Comparison of cold leg flow rate is shown in Figure 5.4-7. Only the flow rate in the cold leg 1A was plotted as the other three loops showed the similar flow rate trend. Considering the uncertainty of the measured cold leg flow rate, most calculations are in good agreement with the data. KTH and NRC predicted reduced cold leg flow rates compared with those in the blind phase. AEKI has the maximum flow rate among the calculations.

Initial water levels of the pressurizer are compared in Figure 5.4-8. Calculated water levels varied wide, but the difference among predictions was much reduced in the open calculation. KEPRI and GP3's model predicted the highest water level of the pressurizer.

Great difference in prediction of the RCP speed was still observed in the open calculation as shown in Figure 5.4-9. KEPRI predicted the similar high RCP speed as in the blind phase. NRC and KNF predicted much higher RCP speeds than those of the blind case. However, KOPEC1, GRS, NRI, and VTT showed better agreement than the blind calculations.

The secondary pressure and temperature are compared in Figure 5.4-10 and Figure 5.4-11, respectively. There was no significant difference between the blind and the open calculations. Overall, KAERI's prediction was a little lower than the data. Better agreement can be observed in the predictions by KNF and GP2. The feed water flow rates through the economizer and the down-comer are compared in Figure 5.4-12 and Figure 5.4-13, respectively. Most predictions of the economizer flow are in good agreement with the data. In particular, the NRI's prediction was much improved compared with the blind case. Incorrect predictions of the down-comer feed water flow rate in the blind phase were improved except for the KEPRI's calculation. Figure 5.4-14 compares the heat removal rate by the steam generator (SG-1). Most calculations predicted higher heat removal rates except for PSI and NRI.

The initial pressure of the SIT-1 was well predicted in most calculations as shown in Figure 5.4-15. The coolant temperature of the SIP-1 was also correctly predicted by most participants as shown in Figure 5.4-16. On the other hand, the water temperature of the SIT-1 was well predicted by all the models as shown in Figure 5.4-17. Finally, the containment pressure comparison is shown in Figure 5.4-18. Though the prediction by PSI shows a little higher value than the data, most predictions are well consistent with the data.

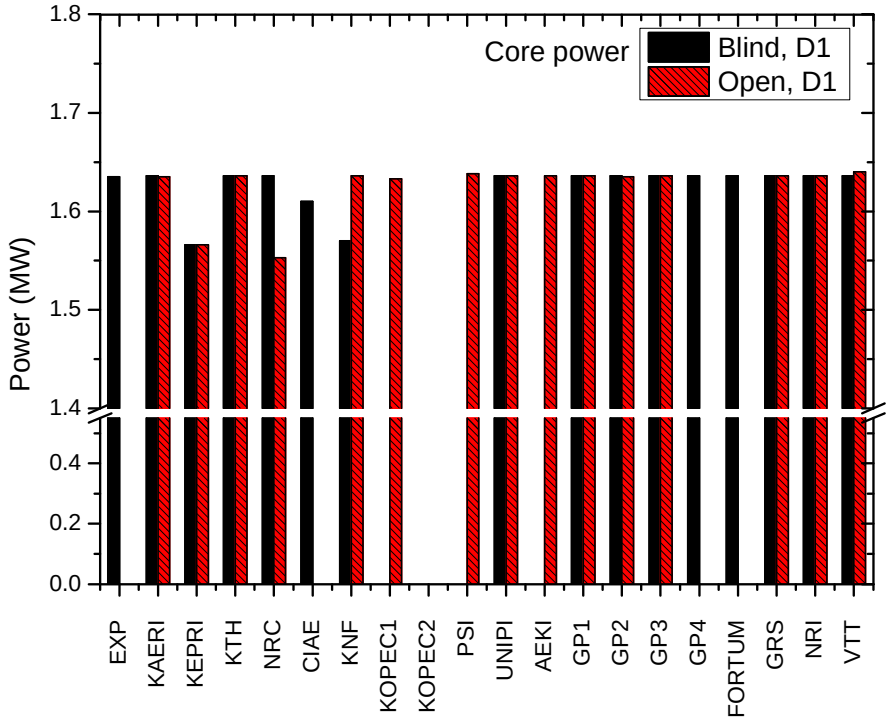

Figure 5.4-1 Comparison of the initial core power

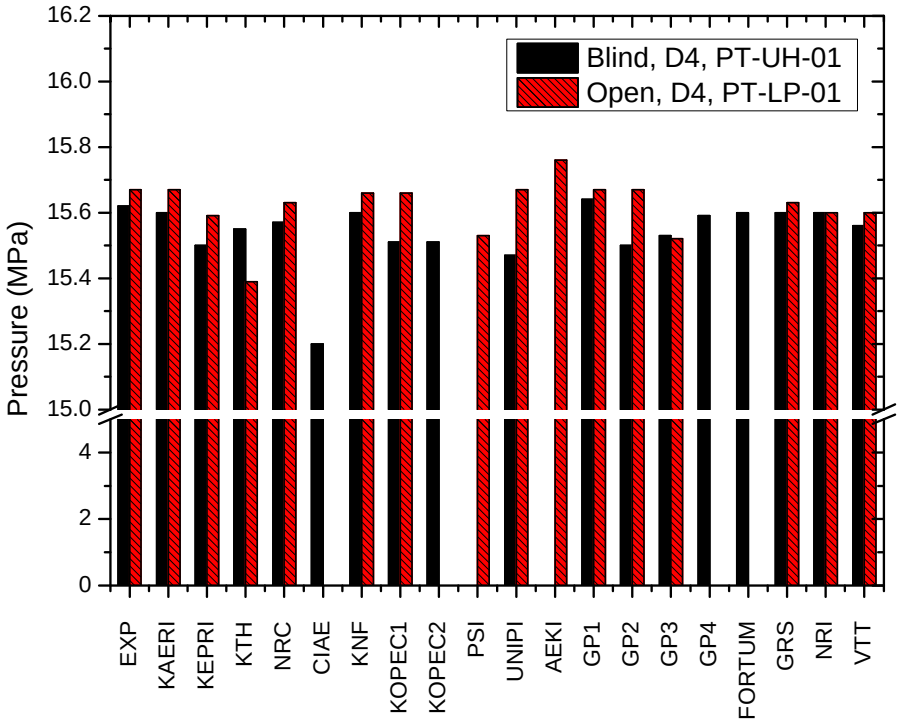

Figure 5.4-2 Comparison of the initial primary pressure

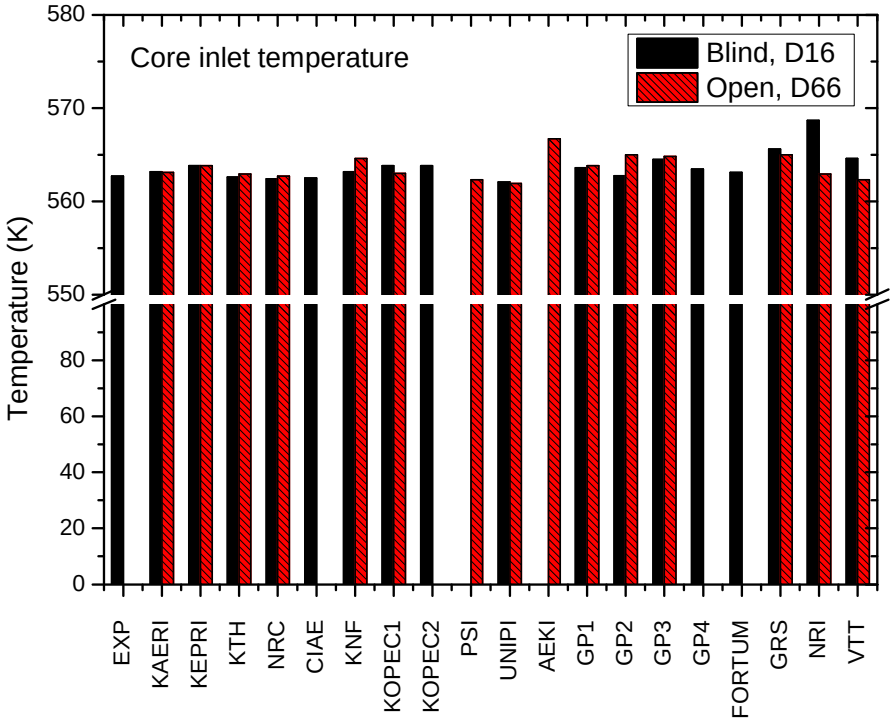

Figure 5.4-3 Comparison of the initial core inlet temperature

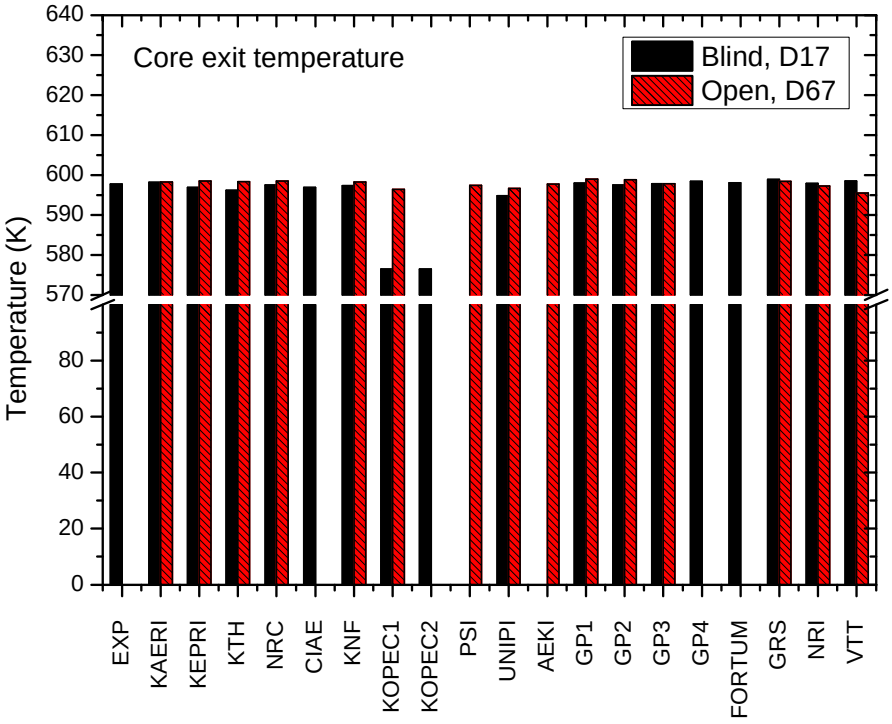

Figure 5.4-4 Comparison of the initial core exit temperature

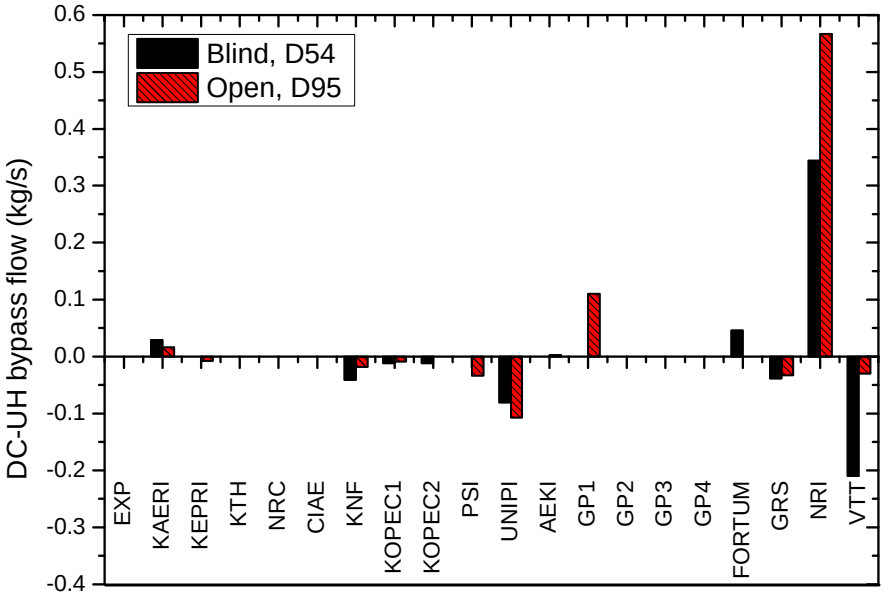

Figure 5.4-5 Comparison of the initial down-comer-to-upper head bypass flow

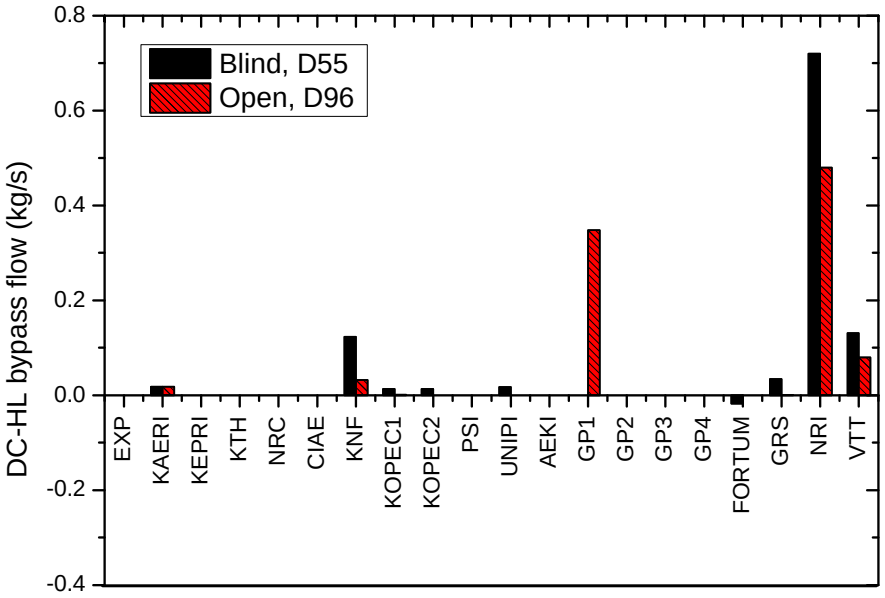

Figure 5.4-6 Comparison of the initial down-comer-to-hot leg bypass flow

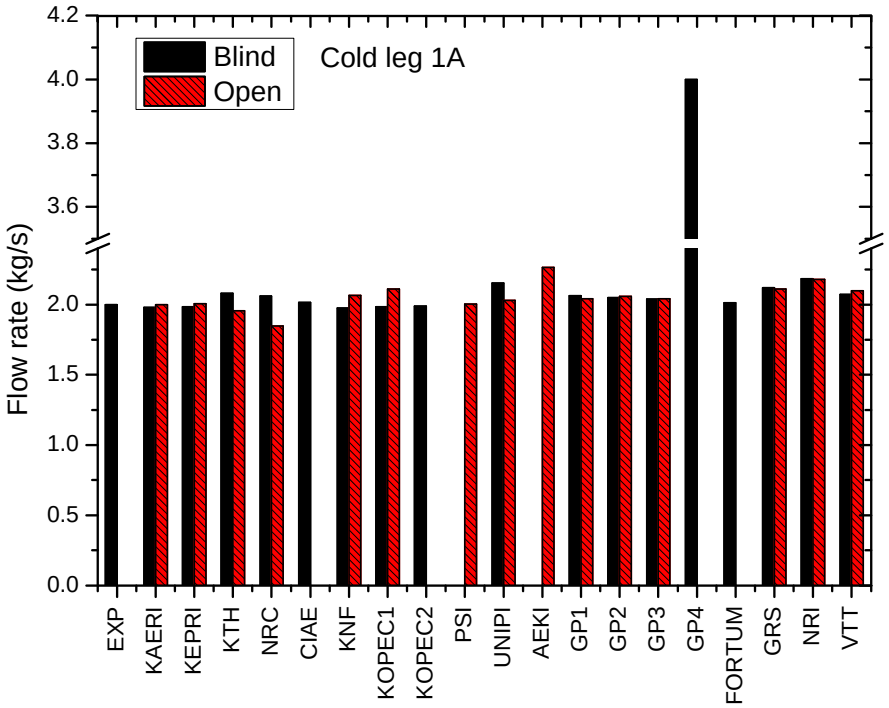

Figure 5.4-7 Comparison of the initial cold leg flow rate

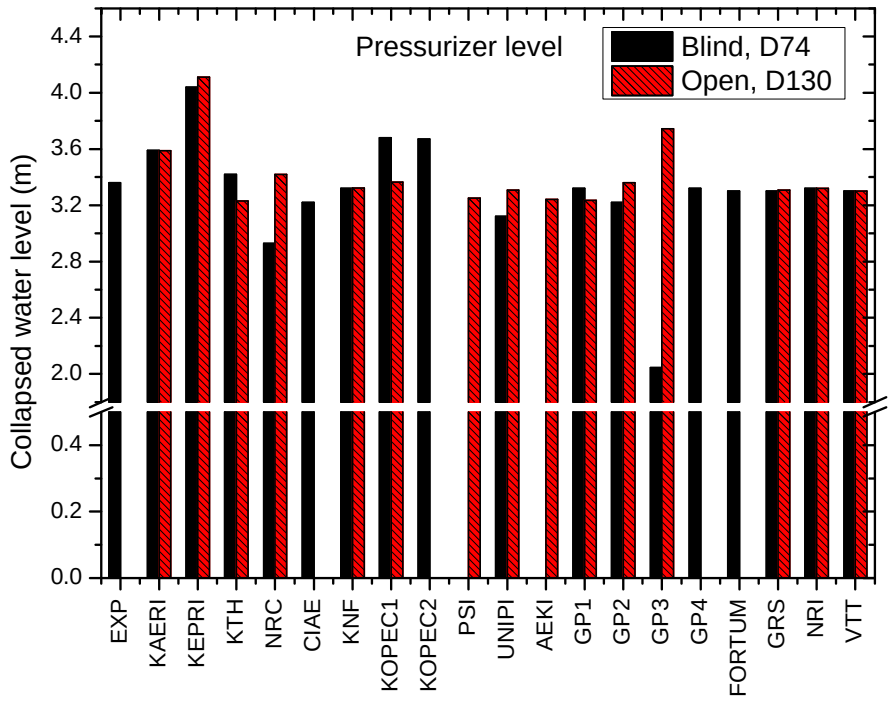

Figure 5.4-8 Comparison of the initial water level of the pressurizer

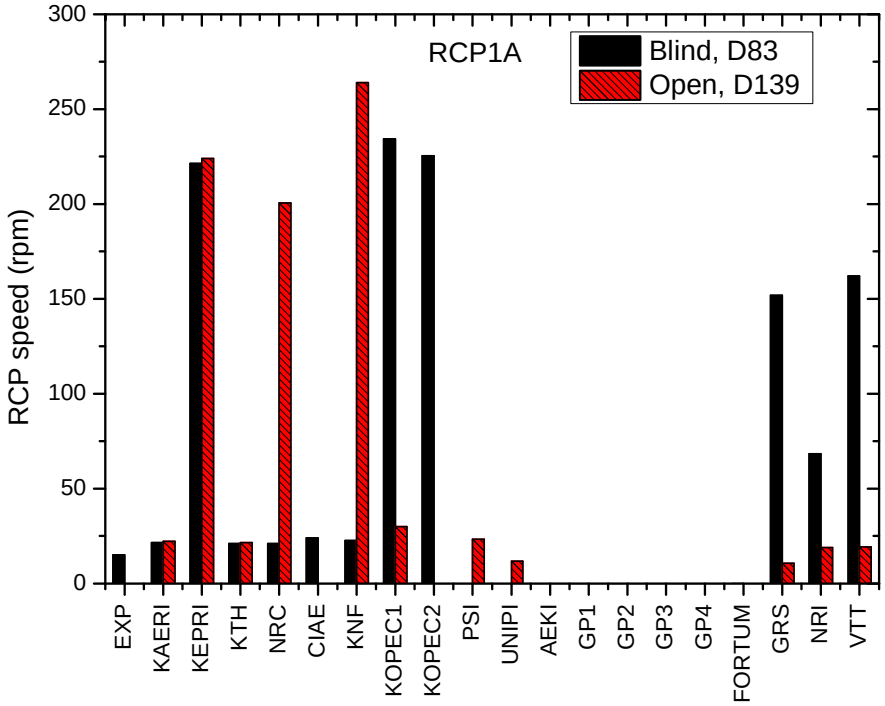

Figure 5.4-9 Comparison of the initial RCP speed

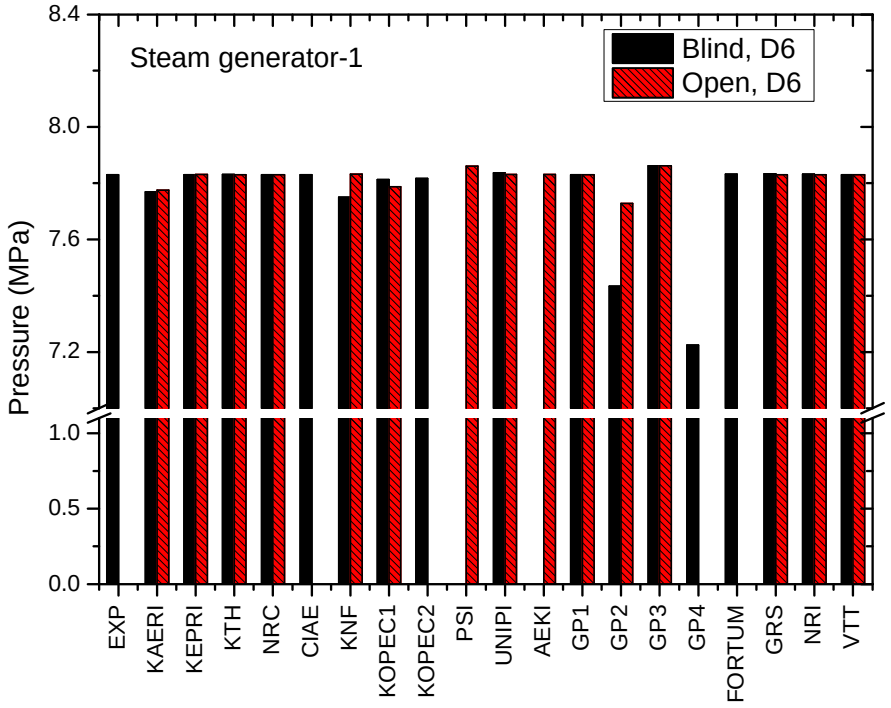

Figure 5.4-10 Comparison of the initial steam generator (SG-1) pressure

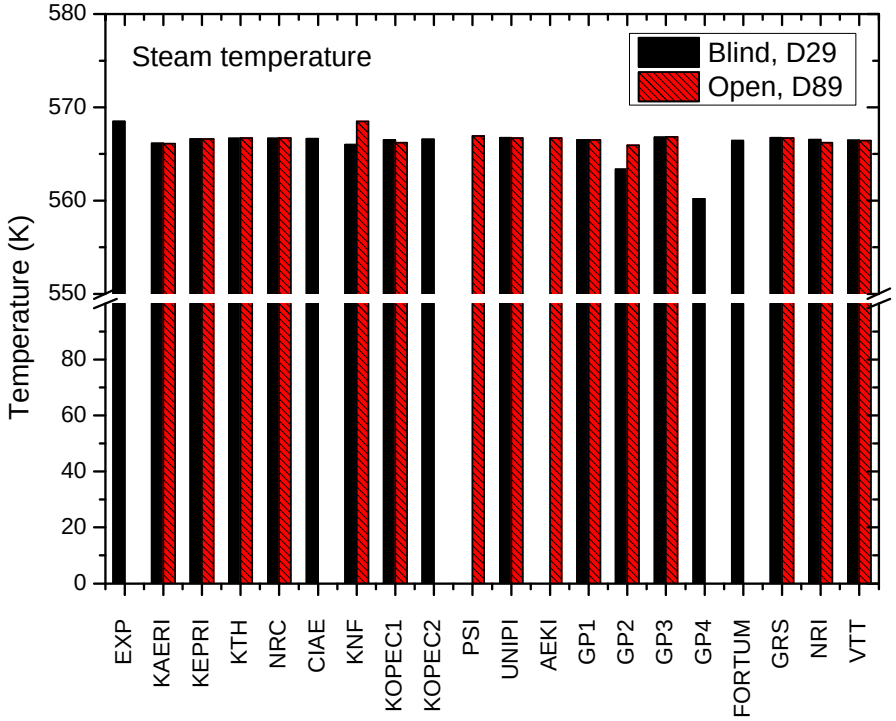

Figure 5.4-11 Comparison of the initial steam generator (SG-1) temperature

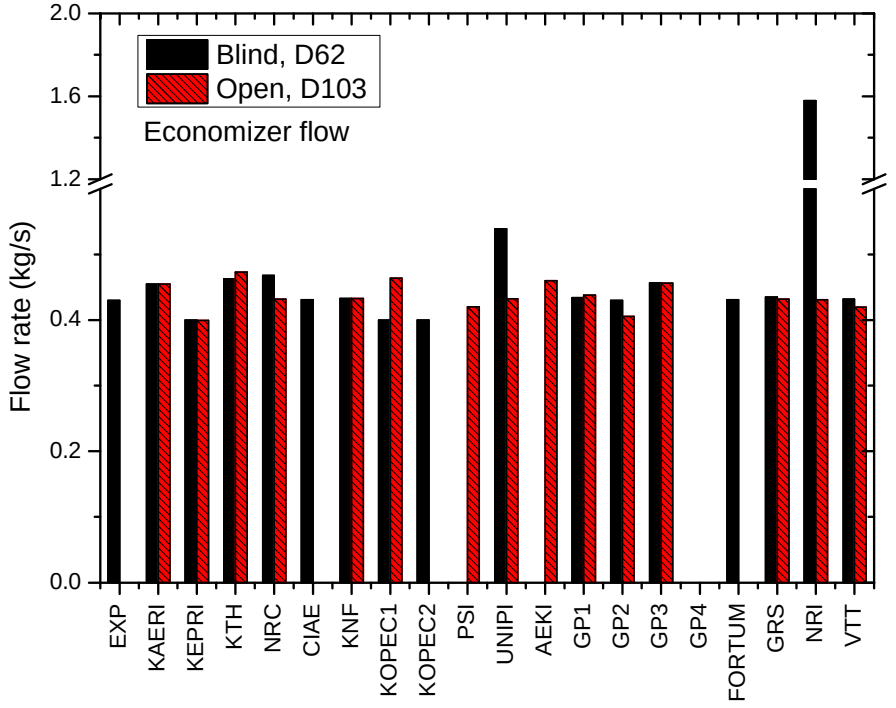

Figure 5.4-12 Comparison of the initial feed water flow rate to the economizer

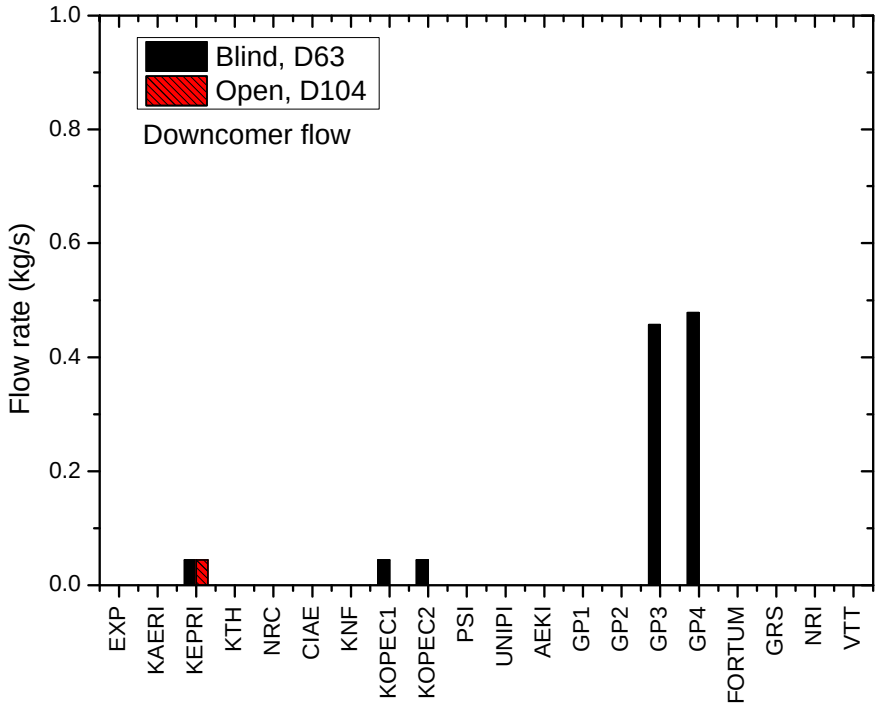

Figure 5.4-13 Comparison of the initial feed water flow rate to the down-comer

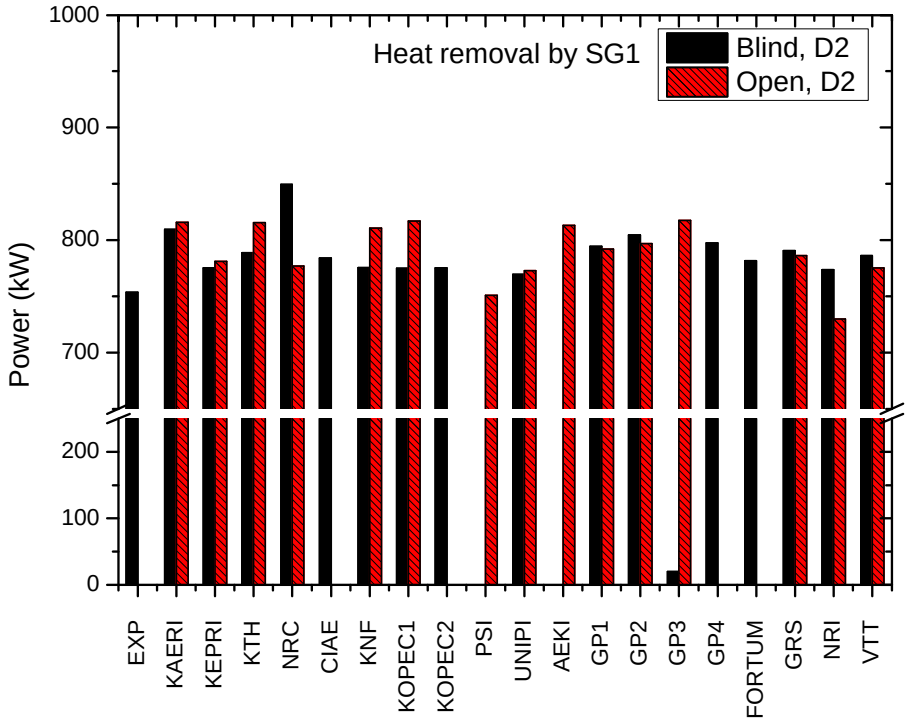

Figure 5.4-14 Comparison of the initial heat removal rate by steam generator 1 (SG-1)

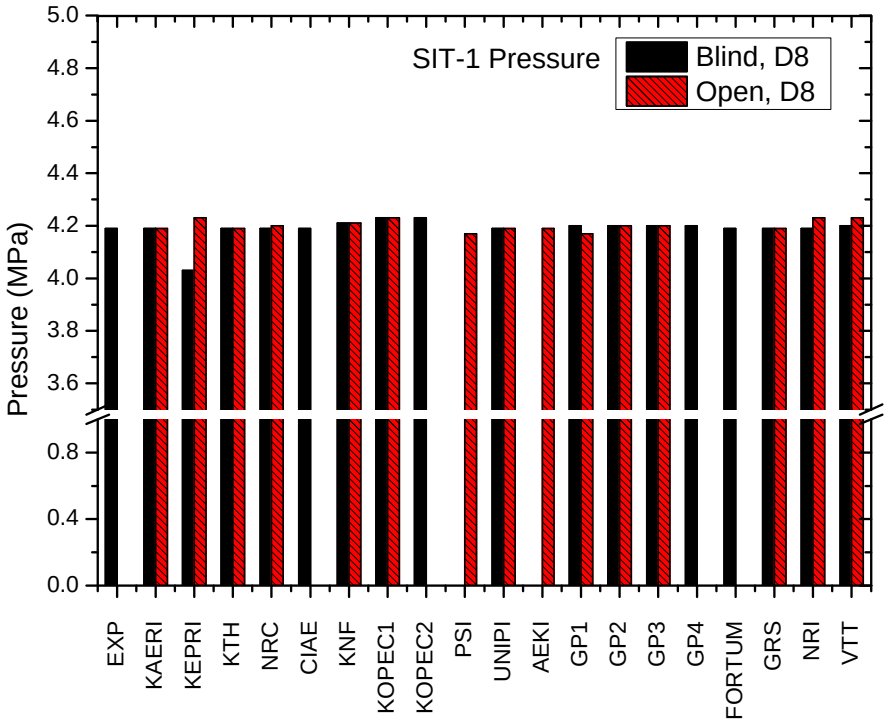

Figure 5.4-15 Comparison of the initial SIT-1 pressure

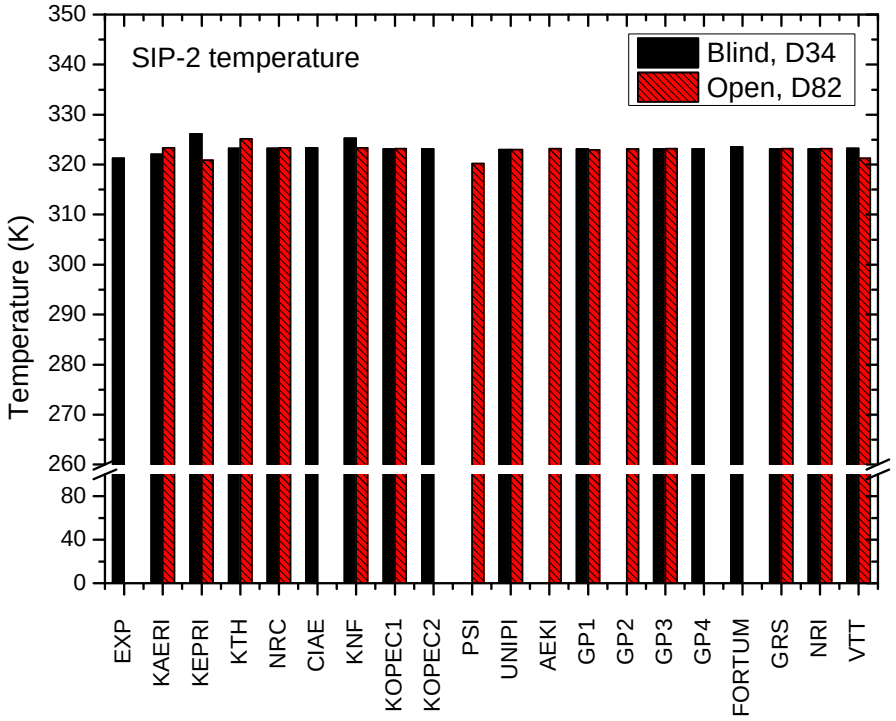

Figure 5.4-16 Comparison of the initial SIP-2 temperature

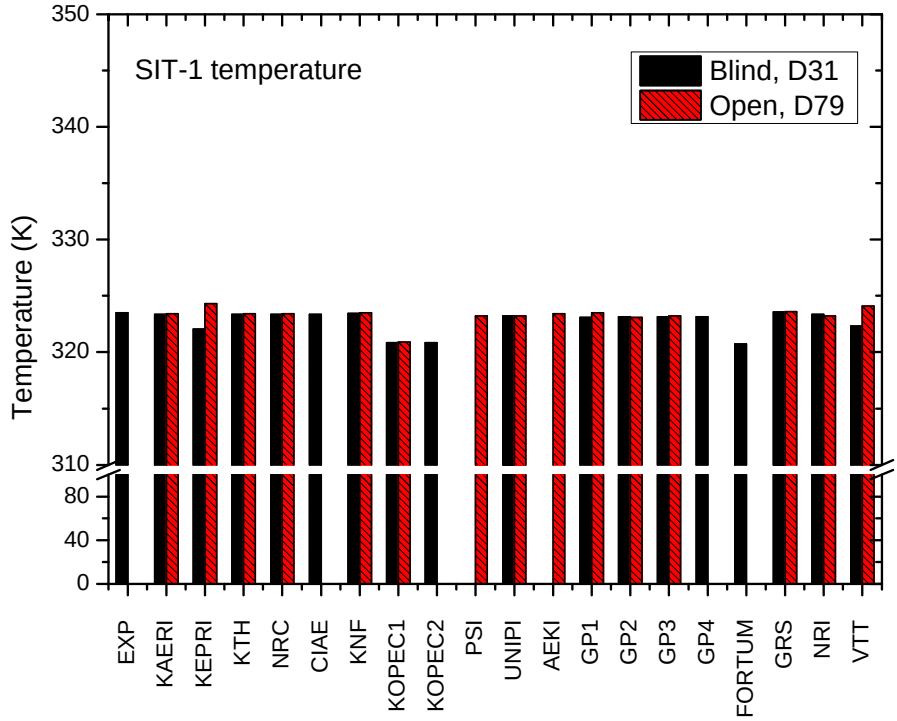

Figure 5.4-17 Comparison of the initial SIT-1 temperature

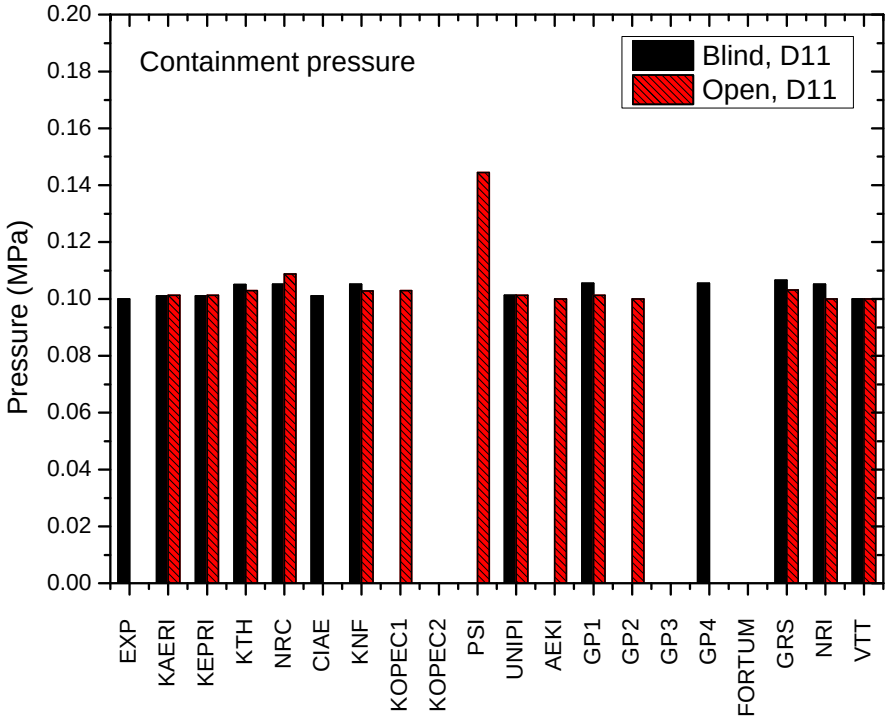

Figure 5.4-18 Comparison of the initial containment pressure

5.5 Submitted data analysis

A total of 16 code calculations were submitted to the operating agency. Detailed information of the submitted data is summarized in Table 5.5-1. Total calculation time, number of data, time step and break time were analyzed and compared with each other. Most participants succeeded in performing transient analysis up to 2000 s as requested in the ISP specification [Choi *et al.*[5], 2009], but a few participants submitted their results analyzed up to a little shorter calculation time than requirement.

Table 5.5-1 Submitted data analysis

Grp.	Parti'pant	Cal. Time[1] (sec)	CPU time[2] (sec)	Number of data	Time step (sec)	Break time (sec)	Remarks
Exp. Data		2932		3127	1.0	193	-193 s shift
A	KAERI	1999	2732	2000	1.0	193	-193 s shift
	KEPRI	2000	53642	4000	0.5	204	-204 s shift
	KTH	3300	10471	3487	1.0	0	
	USNRC	1999	38703	1995	1.0	0	
B	CIAE	1484	1938[3]	375	4.0	0	
	KNF	2192	729	2001	0.01~0.08	192	-192 s shift
	KOPEC1	2000	4551	2181	0.01	0.0	
	PSI	3000	2830	1251	0.003~0.2	0.04	
	UNIPI	2500	3450	2507	0.001~0.3	0.044	
C	AEKI	3000	470	2778	1.0	0.0	
	GP1	2933		2933	1.0	193	-193 s shift
	GP2	3000		6001	0.5~20	0.0	
	GP3	3000		3001	1.0	0.0	
D	GRS	3000	6630	3461	1.0	193	-193 s shift
	NRI	2933	18560	2660	1.0	0.0	
	VTT	2000	6628	2011	1.0	0.0	

[1] The calculation time includes the steady state time before break

[2] The CPU time is based on calculations for 1800 s

[3] The CPU time is based on calculations for 1484 s

5.6 Comparison of transient results

The submitted transition calculation results in "open" phase were qualitatively compared with the measured data in the similar manner of the "blind" phase. All the comparing figures are included in Appendix-D. For each requested parameter, four figures comparing the divided group's calculations with the data were prepared for clear comparison. In this section, qualitative prediction improvement of "open" phase compared with "blind" phase is described, focusing on the important major thermal-hydraulic parameters. Not all the submitted parameters were discussed, but only key parameters were discussed in this section by taking into account a priority of affecting overall transient behavior and were discussed.

5.6.1 Major system pressures

Compared with the blind calculation results, the prediction performance of the primary system pressure was remarkably improved in all the open calculations as shown in Figures D.4 and D.5. The calculations by KTH, NRC, and KOPEC slightly underestimated the primary pressure after 300 s of the calculation time. Whereas the GP2's calculation showed a slight overestimation. Among the submitted calculations, the NRI's calculation showed the largest difference from the data in terms of initial depressurization and the pressure plateau prediction as shown in Figures D.4-D and D.5-D.

As for the secondary pressure, great improvement was also obtained in the open phase as shown in Figures D.6 and D.7, but the prediction accuracy of the secondary system pressure was not as great as the prediction of the primary pressure. Among the various codes used, ATHLET, APROS, and KORSAR (GP1) presented relatively good accuracy in predicting the MSSV opening characteristics as well as the subsequent secondary system pressure behavior. However, no calculations simulated the opening frequency of the MSSVs accurately. As for the MSSV opening behavior, AEKI which used the CATHARE code presented the best prediction accuracy. Contrary to the blind calculations, the opening of the MSSVs was reproduced in the EDO Gidropress, KNF, KEPRI and KTH's open calculations. In the KOPEC, KEPRI, GP3 and AEKI's calculations, the secondary system pressure maintained a relatively higher value compared to the experimental data.

Comparisons of the active three SIT's pressures are shown from Figures D.8 through D.10. Compared with the blind calculations, the prediction accuracy of the SITs pressure was greatly improved. Above all, the actuation timing of the SIT was remarkably improved and this improvement was due to better prediction of the primary pressure. As for the actuation timing of the SIT, the KOPEC, KTH, and NRC's calculations showed relatively earlier injection timings of

the SITs compared to the experimental data. The NRI and the GP3's calculations underestimated but the GP2's calculation overestimated the pressure behavior of the SITs, respectively.

Comparison of the containment pressure is shown in Figure D.11. As for the prediction performance of the containment pressure, the participant's open calculations showed relatively better simulations compared with the blind calculations. However, KAERI, KEPRI, CIAE, UNIPI, GP1, GP2 and VTT simply applied a constant containment back-pressure condition in their calculations.

5.6.2 Differential pressure of the primary loop

Calculated differential pressure between the hot leg and the cold leg of each loop was compared with the data as shown from Figures D.12 through D.15. Difference between "blind" and "open" phase cannot be discussed, because these parameters were not requested in "blind" phase. Measured differential pressure continuously increased until the loop seal clearing and thereafter decreased and maintained almost constant value. As shown from Figures D.12-B through D.15-B, all participants in group B showed very good agreement with the data, but the differential pressure between HL-1 and CL-1B was underestimated. The other participants in the other groups also showed reasonable prediction accuracy, but AEKI and VTT showed a negative increasing trend of the differential pressure after break. This prediction is not consistent with the typical behavior of the differential pressure prior to loop seal clearing phenomena. Therefore, the sign of the differential pressure seemed to be reversed in their calculations. Any significant difference among the individual loop was not obtained. Note that KEPRI predicted very high differential pressure compared with the other calculations.

Comparison of differential pressure along the hot and the cold leg is shown from Figures D.16 through D.21. Note that these parameters were not also requested in "blind" phase. Measured differential pressure along the hot leg and the cold leg of each loop maintained almost constant value. As for the differential pressure along the hot leg, most calculations showed a little bit overestimation. Most calculations showed fluctuations in predicting the differential pressure along the cold leg. The NRI and the UNIPI calculations highly overestimated the differential pressure along the cold leg. The GP2 calculation presented the negative sign of the differential pressure in the CI-1A. Despite some oscillations, the GRS and the VTT calculations showed relatively good agreement with measured differential pressure along the cold leg.

5.6.3 Differential pressure and fluid temperature of primary side of SG

Prediction of differential pressure between inlet and outlet plenum of each steam generator is compared in this section. The calculation results are shown from Figure D.22 through D.25. In general, the open calculation results on the differential pressures between the inlet and outlet plenums of the steam generators were improved compared with the blind calculations. Note that the blind calculation results can be seen from Figures B.12 through B.15. However, the calculation result performed by NRC presented a reverse differential pressure behavior contrary to the experimental data. And the VTT calculation showed zero differential pressure after 300 s of the calculation time. As for the differential pressure along the cold legs, the NRC and the KNF's calculations presented some oscillations during the initial and the later test period. The UNIPI's calculation showed extremely high values only for the cold leg-2A. The GP2's calculation presented highly fluctuating differential pressure behaviors for the all cold legs. In terms of the prediction accuracy, the NRI presented the worst calculation results.

Calculated fluid temperatures of the inlet and outlet plenums of the steam generators are compared from Figures B.25 through B.28 and from Figures D.75 through D.78 for "blind" and "open" phase, respectively. In general, better agreement can be seen by comparing each pair of calculation. The inlet plenum temperature of the SG-1 was reasonable in most open calculations as shown in Figure D.7. However, for the outlet plenum of the SG-1 and the inlet and outlet plenum of the SG-2, the calculated results showed a different behavior with the data. The calculated water temperatures of all participants except for NRC, GRS, and VTT showed a similar trend between at the inlet and at the outlet plenum for both SGs. It is noteworthy that this trend could be observed in the results especially in the group B, who calculated using the RELAP5 code, and group C, who used the CATHARE2 and KORSAR/GP codes. In the experiment, even though the water temperature in the outlet plenum showed a lower value at the initial steady state condition, it maintained a relatively higher value, especially after the loop seal clearing phase. The results from NRC and GRS showed a relatively good agreement in that point. The VTT's calculation showed a better trend than those of NRC and GRS. However, the temperature fluctuation in the inlet plenum of intact SG-2 was not predicted by all participants. This difference is closely related to the asymmetric loop seal clearing phenomenon.

5.6.4 Loop Seal Clearing

NRC, PSI, and KAERI presented relatively reasonable prediction results on the loop seal clearing. Especially, from the calculated collapsed water levels of NRC and PSI, the non-uniform loop seal clearing phenomena could be observed obviously. Many participants predicted the first loop seal clearing only, and no participants predicted the second loop seal clearing

occurred at loop 2B in the ISP-50 test. In order to predict the second loop seal clearing behavior correctly, several thermal hydraulic models such as a break flow model, a steam generation rate model, a droplet entrainment model, and 3-D node simulation in the down-comer region could be required to investigate the differential pressure distribution in the RPV and to quantify the accumulated water inventory in the hot leg and the SG inlet plenum.

NRC presents the most accurate results on the collapsed water level in the intermediate leg-1A, and -1B. With respect to the timings of the 1st loop seal clearing occurred in loop-1 are predicted with excellent accuracy. However, in the loop-2, NRC's prediction results show a different loop seal clearing trend and they do not predict the 2nd loop seal clearing. All of the loop seal were cleared at around 200 s nearly same with the experimental data. However, the loop seals of IL-1A and -2A were refilled at around 1100 s and 900 s, respectively. GP4 presents similar results. In their results, all of the intermediate legs were cleared at around 140 s and the loop seal refill was not observed. Even though all of the calculation results of NRC for the differential pressure between SG inlet and outlet plenum show a relatively nice agreement with the experimental data, the loop seal clearing behavior in the loop-2 shows a remarkable difference with the experimental data.

The prediction results of KOREC1 and KOPEC2 show several fluctuations of the collapsed water level in the all of the intermediate leg. However, the largest water level fluctuation was found in the loop-1A. GP1, GP2, and FORTUM's results show that the loop-1 was not cleared, but the loop-2 was all cleared at around 300 s, 280 s, and 130 s, respectively. Especially for GP2, intermittent collapsed water level fluctuation was found at loop-1A and -1B. NRI predicted the all of the loop seals were not cleared during the whole test period. As for GRS, the loop-1A and -2A were cleared with several fluctuations.

5.6.5 Major fluid temperatures

In "open" phase, the fluid temperatures in the upper head (D26 and D27) and the upper plenum (D28) were additionally requested in order to have better understanding of the thermal-hydraulic phenomenon. Comparison results are shown through Figures D.26 and D.28. In general, the fluid temperatures were predicted well by all participants except for GRS, VTT who presented over-estimated the upper head fluid temperature corresponding to the TF-UH-04 from about 400 s after the break as shown in Figure D.27-D.

Comparison of the core inlet and exit temperatures with the data is shown in Figures D.66 and D.67, respectively. Most participants showed great improvement in agreement with the data compared with the "blind" calculations in Figures B.16 and B.17. However, NRC and NRI

presented a little bit lower values, especially for the inlet plenum temperature, than the experimental data. The NRI's calculation for the outlet plenum temperature showed over-estimated values up to 800 s, and after then it showed a good agreement with the data. For the pressurizer water temperature, the PSI showed the best and correct estimation result. The other participants except for NRC presented a highly lower value than the experimental data. The NRC's calculation showed a little bit higher value during the whole period of the test.

Calculated pressurizer temperature in "open" phase is compared in Figure D.68. The prediction accuracy was more or less similar to that in "blind" phase. Several calculations showed the similar value to the saturation temperature, the submitted calculation results did not predict the superheated steam temperature correctly.

Comparisons of hot leg temperatures are shown from Figures D.69 through D.70. All participants except for NRC, NRI, KOPEC, AEKI, and GP2 showed good prediction results for the fluid temperatures in the hot leg. NRC and NRI predicted slightly lower values for the steam and water temperatures than the experimental data. However, KOPEC predicted an over-estimated value for the hot leg-1 temperature from 300 s to 1720 s, and for the hot leg-2 larger fluctuation was observed from 330 s to 620 s. The AEKI's calculation showed a higher trend than that of the experimental data from 250 s to 900 s. The calculation results from the GP2 showed an over-estimated steam temperature than the experimental data in the hot leg-1, and showed a large fluctuation in the hot leg-2 from 400 s to 1400 s.

Comparisons of cold leg temperatures are shown from Figures D.71 through D.74. The experimental data for the fluid temperature in the cold leg showed a complicated behavior. As described in the literature [Kang *et al.*[1], 2009], the fluid temperatures in the loop were measured by two vertically separated thermocouples installed in the upper (named as –A) and lower (named as –B) part of the horizontal loop piping. In the broken cold leg, there were several fluctuations for the water temperature, and especially for the cold leg-1B the measured water temperature showed a differently higher trend than that of the others. This seems to be mainly due to the vertical measuring point of the thermocouples installed in each cold leg and the flow pattern during the experiment. Moreover, it needs to be considered that the presented temperature data were measured by bare thermocouples. It means that the installed thermocouples are easily affected by the entrainment and deposition of dispersed droplet at the tip of the thermocouples. Considering this facts, it seemed that the measured fluid temperatures for the loop piping could not be exactly identified as the only water or steam phase temperature.

Generally, the predicted water temperatures in the cold leg showed a relatively good

agreement with the experimental data. However, the NRI's calculation showed a higher trend in the cold leg-1A, -2A, and -2B. The GRS's prediction result for the water temperature in the cold leg-1B showed a good agreement with the experimental data, but the nearly same trend could be observed in the cold leg-2A, which means that the calculated water temperature in the cold leg-2A showed an over-estimated value from 300 s to 500 s. For the steam temperature in the cold leg, almost participants presented an over-estimated trend. On the other hand, the calculation results of NRI and KTH showed a little bit lower value than the experimental data. The NRC's calculation presented an over-estimated value from about 350 s to 940 s, and after then suddenly dropped below the experimental value. GP1 and GRS showed a good agreement with the data in the cold leg-1A and 2B, but they showed an over-estimated trend with frequent fluctuations in the cold leg-1B and -2A. On the other hand, the GP2 showed a good agreement in the broken loop, but the cold leg steam temperatures in the intact loop showed a higher value than the experimental data.

Comparisons of steam temperatures at the steam dome are shown in Figures D.89 and D.90. The steam temperatures at the steam-dome were well predicted by all participants. However, KEPRI and KOPEC predicted relatively larger deviations from the test data compared with the other participants. Temperature fluctuations due to the MSSV's action at the initial stage of the accident were well predicted by all participants. In the experiment, the initial steam temperature in the containment was about 367 K. This temperature showed a sudden increase with the break up to 393 K due to the increasing of the static pressure in the containment, and then it decreased with time. However, this temperature showed a large fluctuation from 290 s to 900 s. The best calculation result for the steam temperature in the containment was presented by PSI who predicted the small fluctuation at the initial stage of the accident and after then the large fluctuation. However, the timing of the large fluctuation was different from that of the experimental data. Other participants such as the NRC, GP1, and VTT predicted different steady state temperatures. The calculation result of KTH showed a decreasing trend with time. The other participants predicted a constant value during the transient similar with the steady state temperature.

ECC water temperatures from SITs and SIP are compared from Figures D.79 and D.82. Compared with the blind calculation, no significant differences were found in most calculations because the fluid temperatures of ECC system were used set as boundary conditions. Regarding the SIT temperature, KEPRI and KOPEC used 1°C higher and 2°C lower value than the data, respectively. As for the SIP-2 fluid temperature, KEPRI corrected his boundary condition to match the experimental data.

5.6.6 Down-comer fluid temperature and water level

The test data showed that multi-dimensional behaviors of the down-comer temperatures were observed from level 4 to level 6 as shown in Figure 3.5-57. The multi-dimensional behavior of the down-comer fluid temperatures started at around 50 s after break (or 243 s from DAS time) and continued until around 340 s. In the ISP-50 data, there are six data measured for each level from level 1 to level 6 azimuthally and one data, for level 7.

Most participants submitted 2-dimensional down-comer fluid temperatures in their submittals. It was AEKI that adopted a one-dimensional down-comer modeling. Thus, AEKI submitted only seven axial down-comer fluid temperatures with respect to time. Calculated two-dimensional temperature distribution of each participant was plotted and included in Appendix-E. Multi-dimensional results both in axial and azimuthal directions were found in most submitted calculations. In the view point of the multi-dimensional effect, temperature distributions along the azimuthal direction would be more meaningful. In this section, the multi-dimensional effects were considered according to the azimuthal direction for each level in the down-comer. There was just one data for level 7, i.e. lumped data, so it was not considered for the azimuthal effect.

Among the submitted calculations, KTH, AEKI and GP2 showed no azimuthal variation in the down-comer fluid temperatures as shown in Figures E.5 and E6, E19 and E20, E23 and E24, respectively. Their data seemed to be obtained from one-dimensional modeling. In particular, the GP2's calculation showed that fluid temperature at level 6 continuously decreased down to 400 K until the loop seal clearing at 200 s when the fluid temperature was recovered. This continuous temperature drop seemed to be caused by injection of cold ECC water at level 6. However, it is strange that temperature at level 5 maintained a constant value around 565 K. The injected cold ECC water seemed not to be mixed at all.

The other calculations showed multi-dimensional effects although there were some different trends between them. As the injection location of the cold ECC water by the SIP was at the subsection 5 (azimuthal angle of 240 degree), the fluid temperature at subsection 5 should be the lowest among the other subsections especially at level 6. This phenomenon was well predicted by most participants, but NRC, CIAE, KNF, KOPEC1, and VTT showed incorrect predictions. Their lowest temperatures at level 6 were found at subsection 6, 4, 6, 6, and 4, respectively. It is uncertain whether this disagreement was caused by azimuthal velocity term or by incorrect down-comer modeling. In addition, it can be found that most calculations showed clear azimuthal stratifications at every level. It implies that the injected ECC water was not mixed well with adjacent azimuthal cells. In the ISP-50 test, great mixing was observed

especially at level 5 and 6 as shown in Figure 3.5-57. NRC was the only participant who carried out three-dimensional calculation in the core. In terms of ECC mixing, NRC predicted the most similar temperature behavior to the measured data.

In the ISP-50 test, the down-comer water levels were measured by two broad range (LT-RPV-04A, B) and 7 narrow range DP transmitters (LT-DC-01 ~ 07). Initially, the down-comer region was filled with the water. On break, the water in the upper head was first drained and then the water level corresponding to the LT-DC-07 started to decrease. However this decrease ceased at a certain elevation corresponding to the DVI nozzle and the collapsed water level maintained a constant level until the occurrence of the 1st loop seal clearing. During this period, the injected ECC water from the SIP was discharged through the broken DVI nozzle and the water level in the core continuously decreased due to boil-off. This constant water level suddenly decreased with the 1st loop seal clearings occurred in the 1A and 1B loops at 190 s. After the loop seal clearing, which is closely related to the collapsed water level in the core and the down-comer regions, the whole down-comer region became a two phase mixture condition and the collapsed water level continuously decreased far below the cold leg level up to the minimum 2.4 m at 465 s after the break. After then, it experienced a continuous increase with the activation of the SITs.

Comparison of calculated water level in the upper head is shown in Figure D.113, where LT-RPV-02 was used as a reference data. Note that LT-RPV-02 indicates the core water level in the second upper half of the core region as shown in Figure 3.5-42. Most calculations predicted the exponentially decreasing trend of the water level in the upper head reasonably well, but GP1 showed a little milder decrease than the data. The GP3's prediction was not available. Among the collected calculations, NRI showed great difference from the others. They predicted an early recovery of the core water level as shown in Figure D.113-D.

An accumulated down-comer water level, LT-RPV-04A was compared with the data in Figure D.114. Though the general trend was in consistent with the data, most calculations underestimated the down-comer water level except for the NRI's. The NRI's result overestimated the down-comer collapsed water level during the whole test period, especially after the loop seal clearing. It should be noted that the down-comer collapsed water level of NRI showed a slow and slight change after 250 s, which was caused by the fact that the four loop seals were not cleared. On the other hand, in the case of the GP3, even though all of the loop seals were not cleared like NRI, the collapsed water level showed a steep decrease at 160 s. The GP3's result showed an underestimated trend during the whole period of simulation. NRC showed the best agreement with the experimental data among the submitted calculation.

All the participants presented the narrow range collapsed water levels in the down-comer corresponding to the LT-DC-01 ~ -07. The collapsed water levels from the 7 narrow range DP transmitters were compared one by one from Figure D.115 to Figure D.121. In addition, a quick-look comparison plot for each sub-group can be seen in Figure E.33 to Figure E.36 of Appendix E. From the narrow range collapsed water level, the difference between the collapsed water level and the two phase water level could be estimated. In the experiment, the upper down-comer region corresponding to the LT-DC-07 was evacuated just after break. However, the other region of the down-comer was filled with two phase mixture. Volumetric void fractions measured by the narrow range DP transmitters showed an increasing tendency with the vertical height from the bottom of the down-comer. Especially the upper down-comer regions above the cold leg level corresponding to the LT-DC-05 and -06 showed relatively larger void fractions than those of the lower regions. The collapsed water levels near the cold leg level, the LT-DC-04 and -05, showed large fluctuations according to the sequence of events such as the loop seal clearing, SIP, and SIT injection, whereas the lower down-comer regions, LT-DC-01 and -02 did not show much variation during the test period.

Detailed comparison of the calculated sectional down-comer water level was done from group to group. In the group A as shown in Figure E.33, NRC presented a relatively reasonable prediction. KTH predicted the smallest water level depression, whereas KAERI predicted the largest water level depression among the others according to LT-DC-04. In particular, the KTH's calculation showed an unrealistic rapid decrease in the lowest down-comer water level, LT-DC-01 while the upper parts of the down-comer were still filled with water. The main cause of this is not clear. In the group B as shown in Figure E.34, all calculations underestimated the water level, especially LT-DC-04. Water level recovery observed at around 468 s due to ECC injection by SITs was not properly reproduced in any case. In particular, LT-DC-03 by UNIPI was greatly underestimated. Comparison of the calculations belongs to the group C was shown in Figure E.35. GP1 predicted the similar trend, but AEKI presented much lower water level, especially LT-DC-04. In the GRS's and VTT's calculation, the collapsed water levels in the upper down-comer region corresponding to the LT-DC-04 ~ 07 showed a complete collapse, which meant the void factions of those regions were equal to 1, especially after the loop seal clearing as shown in Figure E.36. On the other hand, the NRI's prediction showed a milder decrease and increase in the water level, LT-DC-03 ~ 05.

5.6.7 Loop flow and break flow rate

In the ATLAS facility the bypass flow rates through upper head to down-comer and through hot leg to down-comer bypass lines were estimated to be 0.0 kg/s. As shown in Figure D.95, all the predictions estimated the bypass flow rates through upper head to down-comer bypass

lines properly except for the positive bypass flow rate of NRI of Group D. The NRI's prediction was high as 5.5 kg/s in maximum. As shown in Figure D.96, the predictions from KAERI, KTH, NRC, KOPEC, AEKI, GP2, and GP3 estimated the bypass flow rates through hot leg to down-comer bypass lines properly. However, the prediction from KEPRI showed a negative peak. The predictions from KNF, GRS, and VTT estimated slightly negative flow rates and those from PSI and GP1 estimated significantly negative flow rates. The prediction from UNIPI estimated slightly positive flow rate and that from NRI estimated significantly positive flow rate.

In the present ISP-50 test, the flow rates in two hot legs and four cold legs were measured by using the BiFlow flow meters. As shown in Figures D.97 and D.98, all the predictions estimated the flow rates in two hot legs well in overall sense except for the high flow rates during the initial 100 s and some fluctuations around zero. The flow rate was as high as 8 kg/s in maximum during the initial 100 s. The fluctuations of flow rates in hot leg-1 were shown in KAERI, KEPRI, KTH, and NRC of Group A (from around 500 s), KNF (from around 650 s), KOPEC (from around 1,300 s), and PSI (from around 800 s) of Group B, and VTT (from around 900 s) of Group D. The fluctuations of flow rates in hot leg-2 were similar to those in hot leg-1 except for the data from Group B, which showed different initiation of the fluctuations (KNF from around 800 s, KOPEC from around 1,100 s, PSI from around 900 s). As shown in Figures D.99 through D.102, all the predictions estimated the flow rates in four cold legs well in overall sense except for the high flow rates during the initial 100 s and some difference in cold leg-2A and -2B. The flow rate was as high as 4 kg/s in maximum during the initial 100 s. The measured flow rates in cold leg-2A and -2B were around 0.6 kg/s from around 400 s and 500 s, respectively, while all the code predictions showed lower flow rates than the experimental data.

The flow rates through main feed water lines were measured by using the Coriolis flow meters in the test. In general, all the calculations predicted the experimental data well as shown in Figures D.103 through D.106. However, two minor differences were found. In the case of KEPRI of Group D, some portion of feed water was supplied through the down-comer of SG, while it was not supplied during the test. In the case of NRI of Group D, the feed water flow rate decreased linearly to zero from the start, while it was decreased abruptly to zero during the test.

The flow rates from three SITs and a SIP were also measured by using the Coriolis flow meters in the test. Most predictions on the flow rates from three SITs was in good agreement with the test data except for the initial high flow rates predicted by KOPEC of Group B as shown in Figures D.107 through D.109. As shown in Figure D.110, all the predictions on the flow rate from a SIP showed good agreement with the experimental data in general.

In the ISP-50 test, the total break flow rate was calculated by using the measured data of QV-CS-03, LC-CS-01 and LC-CS-02. In order to obtain reliable break flow rate, the RCS inventory-base method was also utilized, which is based on the measured water level data as described in Section 3.5.6. The break flow rate increased and decreased rapidly after the break, reached a plateau with a short duration, and then decreased again. In the plateau region, a large-amplitude oscillation was seen in the experimental data as shown in Figure 3.5-37. As shown in Figure D.111, KAERI and KEPRI of Group A, CIAE, KNF, KOPEC, PSI, and UNIPI of Group B, GP2 and AEKI of Group C, and VTT of Group D predicted the measured break flow rates well during the initial period of 200 s, but KTH and NRC of Group A, GP1 and GP3 of Group C, and GRS of Group D under-predicted the experimental data during this period. Especially NRI of Group D predicted the break flow rate much lower during the plateau than the experimental data. As shown in Figure D.112, KAERI and KEPRI of Group A, UNIPI and KOPEC of Group B, GP2 of Group C, and VTT of Group D predicted the experimental data very well. However, CIAE, KNF and PSI of Group B predicted the experimental data slightly lower, and KTH and NRC of Group A, AEKI, GP1 and GP3 of Group C, and GRS of Group D predicted the experimental data significantly lower. It should be noted that NRI of Group D predicted the experimental data much lower.

5.6.8 Core water level

In the ISP-50 test, the core water levels were measured by a broad range (LT-RPV-01) and 7 narrow range DP transmitters (LT-CO-01 ~ 07). The former was plotted in Figure D.122 and the latter was plotted one by one from Figure D.123 to Figure D.129. The broad range collapsed water level gradually decreased just before the loop seal clearing, and it increased steeply with the loop seal clearing. After this fluctuation, the core collapsed water level maintained almost constant value. KEPRI showed the deepest water level depression among the others. The KTH's calculation result for LT-RPV-01 needs to be reviewed. In group B, KOPEC predicted a delayed depression of the core water level and UNIPI underestimated the water level. In group C, AEKI showed the best prediction result among them on average, though the water level depression was not properly predicted. GP1 and GP3 overestimated and GP2 underestimated the water level. In group D, VTT showed the best prediction capability among them. NRI overestimated and GRS underestimated the water level compared with the data.

The void fraction distribution can be observed from the narrow range level data. On break, the two-phase water level was formed throughout the core region, and the distribution of the void faction showed a nearly same trend with that of the down-comer region. The upper part regions of the core corresponding to the LT-CO-05, -06 and -07 showed larger volumetric void factions than those of the lower part regions corresponding to the LT-CO-01, -02, and -03.

Detailed quick-look comparison plot for each sub-group can be seen from Figure E.37 to Figure E.40 in Appendix-E. In group A, KAERI showed the best prediction result. In general, NRC showed an over-prediction but KTH showed under-prediction. In group B, most calculations were similar to the data but a great oscillation was observed in the UNIPI's calculation. In group C, AEKI showed better prediction results than GP1. In general, participants in group D presented very similar trend to the data. The upper core region corresponding to the LT-CO-07 of KAERI and KNF experienced an empty condition during the simulation. The KTH predicted a zero broad range collapsed water level after the loop seal clearing along with a low initial water level.

5.6.9 Core heater surface temperature

Measured core heater surface temperatures represented by the wall temperatures in active core regions were compared with the calculations. The active core region was instrumented at 12 elevations from the core inlet to the core outlet to measure the core heater surface temperatures. Also, calculation of the wall temperatures at 12 elevations were requested and submitted to the operating agency. As most participants applied 1-D modeling to the core, the submitted temperatures were considered as a cross-sectional maximum temperature at each elevation. Detailed comparison of the predicted PCT with the test data is shown from Figures D.146 through D.157 of Appendix-D.

At low locations below the 5th elevation, most participants showed quite good predictions and no increases in the PCT were obtained except for KEPRI. In the KEPRI's calculation, a temperature excursion at around 170 s was obtained which was 20 s earlier than the data. Such a temperature excursion was predicted at almost all elevations from the 2nd to the 12th elevation as shown from Figures D.147-A through D.157-A. KEPRI also predicted the 2nd PCT between 400 s and 600 s from 10th to 12th elevations as shown from Figures D.155-A through D. 157-A. The higher the elevation was, the broader the width of the PCT was.

At high locations above the 6th elevation, several kinds of increases in the PCT were predicted from calculation to calculation. In the group A, KAERI and NRC also predicted a little peak at the 11th and the 12th elevations as shown in Figures D.156-A and D.157-A. The peak predicted by KAERI was earlier than the data by 25 s, but the peak by NRC at the 12th elevation was very close to the data in timing and magnitude. As described in the previous paragraph, KEPRI predicted much higher PCT than the data at higher locations than 10th elevation. The maximum PCT was 638K at 11th elevation. No temperature excursion was obtained in the KTH's calculation.

The most noticeable prediction result for the PCT in the group B can be found from the KOPEC's calculation. KOPEC predicted a very high a temperature excursion from around 300 s and the maximum PCT was 870 K as shown in Figures D.92-B and D.155-B. KOPEC also showed earlier PCTs than the data by around 80 s at higher locations than 6th elevation. KOPEC calculated the widest and the highest PCT among all participants. On the other hand, PSI predicted very similar PCT behavior to the test data with respect to the occurrence timing as shown from Figure D.151-B through D.156-B, but the axial location where the maximum was predicted was lower than the data. In general, a wide PCT ranging from the 6th to 11th elevation was obtained. CIAE predicted a temperature excursion at the 11th and the 12th elevations, but the peak value was much greater than the test data and the timing was much delayed compared with the data. KNF also predicted a temperature excursion at the 12th elevation as shown in Figure D.157-B, but the timing was much later than the experimental data.

Table 5.6-1 Summary of the radial PCT submission results

Group	Organization	G1(inner)	G2(inter.)	G3(outer)	Remarks
A	KAERI	S	S	S	G1~G2=G3
	KEPRI	S	NA	NA	Only G1 submitted
	KTH	S	S	S	G1=G2=G3
	NRC	S	S	S	G1~G2~G3
B	CIAE	NA	NA	NA	Not submitted
	KNF	S	S	S	G1=G2=G3
	KOPEC	S	NA	NA	Only G1 submitted
	PSI	S	S	S	G1=G2=G3
	UNIPI	S	S	S	G1=G2=G3
C	AEKI	S	S	S	G1=G2=G3
	GP1	S	S	S	G1~G2~G3
	GP2	S	S	NA	G1=G2, G3 not submitted
	GP3	S	S	S	G1=G2=G3
D	GRS	S	S	S	G1~G2=G3
	NRI	S	S	S	G1=G2=G3
	VTT	S	S	S	G1=G2=G3

S: submitted

NA: not available

In the group C, GP1 produced double peaks in the PCT at locations higher than the 6th elevation especially in the temperature plateau period. The peaks were much higher than the data. The first peak was earlier than the data by around 70 s and the second one was similar to the data in timing. On the other hand, GP2 predicted much higher PCT with great time delay as shown from Figure D.154-C through D.157-C. The other Russian calculation, GP3 did not show any temperature excursion. In the group D, no calculation showed a temperature excursion.

In addition to 12 regions' axial maximum PCTs of the core, the radial maximum temperatures corresponding to the 3 radial core groups, e.g. G1 (inner), G2 (intermediate), and G3 (outer), were requested in the open calculation. The submission results are summarized in Table 5.6-1. Among the participants, CIAE did not submit the maximum temperatures of three core groups, GP2 presented only the maximum temperatures of G1 and G2. KEPRI and KOPEC only submitted the data of G1. The others provided maximum PCT results for the three groups. From the analysis on the submitted data, it is found that most calculation results are identical with each other. Thus it was difficult to find a radial PCT distribution. It is due to the fact that most calculations are based on one-dimensional modeling in the core region.

The ISP-50 data showed that there was a small PCT for each core group during the transient. The time and the magnitude of the PCT for each core group were: 192 s and 580.5 K for G1; 191 s and 588.5 K for G2; 191 s and 587.7 K for G3. Comparison of the calculated radial PCT with the data is shown from Figure D.92 through D.94 in Appendix-D. As for the maximum temperature of the core group G1, TH-CO-G1-Max, three calculations by KEPRI, KOPEC, and GP1 showed quite large deviations from the measured PCTs and four by KAERI, KNF, PSI, and UNIPI showed a little deviations in magnitude and the occurrence time. The other calculations showed very similar trends with the test data without any temperature excursion during the transient. But, the NRC's and NRI's calculations slightly under-predicted the test data after around 900 s. As for the other core groups G2, G3, the similar findings can be obtained because the calculation data are either similar or identical to each other as shown in Table 5.6-1.

Calculated initial wall temperature distribution was compared with the test data in Figures E.41 through E.44. In the group A, KEPRI, KTH, and NRC showed very good agreement but the KAERI's calculation showed lower values than the data. The calculation in the group B showed more or less similar axial distribution though the KOPEC's calculation was a little higher than the data. In the group C, AEKI showed very good agreement with the data but the GP1's calculation was a little lower than the data. In the group D, most calculation showed good predictions.

5.6.10 Other water levels

All the participants properly predicted the collapsed water level in the pressurizer, even though the GP2's calculation presented a relatively slow water level decrease just after the break. The collapsed water level data for the intermediate leg corresponding to the LT-IL1A-03 ~ LT-IL2B-03 were requested to observe the loop seal clearing behavior during the simulation. In the ISP-50 test, all intermediate legs except for the 2A loop were cleared at 190 s for the 1A and 1B loop, and at 1236 s for the 2B loop, respectively. The calculation results revealed that an accurate prediction on the timing and the place where the loop seal clearing occurred was very difficult. In the KEPRI's, AEKI's, and VTT's calculations, all loops were cleared. On the contrary, in the GP3's and the NRI's prediction, all loop seals were not cleared during the whole test period. The best prediction result was obtained by KAERI, NRC, and PSI who predicted the timely clearing time at the 1A and the 1B loop seals, even though the loop seal clearing occurrence at the 2B loop were calculated to be 1066 s, 1048 s, and 1068 s faster than that of the experiment, respectively. KTH predicted no loop seal clearings at the loop-1A and -1B. The clearing was observed only at the 2A loop seal at the 204 s after the break.

The collapsed water levels of the U-tube at the two SGs were well predicted by all participants. However, the KTH's calculations showed a slightly slower decreasing trend than the experiment. The other participants, generally, showed a little bit faster decreasing trends than the experiment.

5.6.11 RCP speed

No difference among 4 RCP speeds was observed in the calculations. Most calculations predicted the similar initial RCP speed to the test data, except for KEPRI, NRC, and KNF. The three participants initialized their codes at the condition of much higher RCP speed than the data. It implies that the pressure drop along the primary coolant circuit is over-estimated in the code model. In the transient period, the KEPRI's calculation showed an initial speed up to 470 rpm on break and a continuous decrease to zero. The increase in the RCP speed is due to the increased cold leg flow rate from 2.0 kg/s to 3.6 kg/s from the break to the RCP trip. During this period, the RCP speed increased following the RCP's homologous curve. The NRC's calculation showed that the RCP maintained a constant speed of 200 rpm and started to decrease linearly from 33 s. The RCP trip time agrees with the initiation time of the core power decay as shown in Table 3.5-1. The KNF's calculation also showed the similar trend as the NRC's calculation, but the RCP speed started to decrease from the beginning of the break. The other calculations predicted almost zero RCP speeds which are very close to the test data.

5.6.12 CPU time

The CPU time and the time step were requested to examine the calculation performance of the submitted calculations. The CPU time with respect to the calculation time is shown from Figures D.143-A through D.143-D for each group, respectively. The CPU time for calculation up to 1800 s are compared in Figure 5.6-1. The actual CPU time was tabulated in Table 5.5-1 in the previous section. Great difference in the CPU time was found among the calculations. KEPRI, KTH, NRC, and NRI spent more than 10,000 s for their calculations. The relatively long CPU time by NRC seems to be caused by their 3-D modeling in the core region. It is interesting that KEPRI spent the longest time of 53,642 s in spite of his 1-D modeling of the whole system. KNF and AEKI showed the fastest calculation time among the participants. As shown in Table 5.3-2, AEKI used the CATHARE code and the number of volumes and junctions was very small. It seems to be the main cause of their fast calculation time. On the other hand, KNF showed an excellent calculation performance, indicating that they optimized their code input very well.

The time step during the calculation was also requested to investigate the calculation performance and plotted in Figure D.144-A through D.144-D for each group, respectively. The time step did not show a significant variation during the whole calculation time. As discussed in the previous paragraph, KEPRI had the minimum time step of around 5E-4 during the whole calculation time. That is why KEPRI spent the longest CPU time. On the other hand, AEKI had the maximum time step of 1.0 s as shown in Figure D.144-C. NRI also showed relatively long time step though the time step varied with respect to time. The other calculations showed time steps between 1E-3 and 0.1 s.

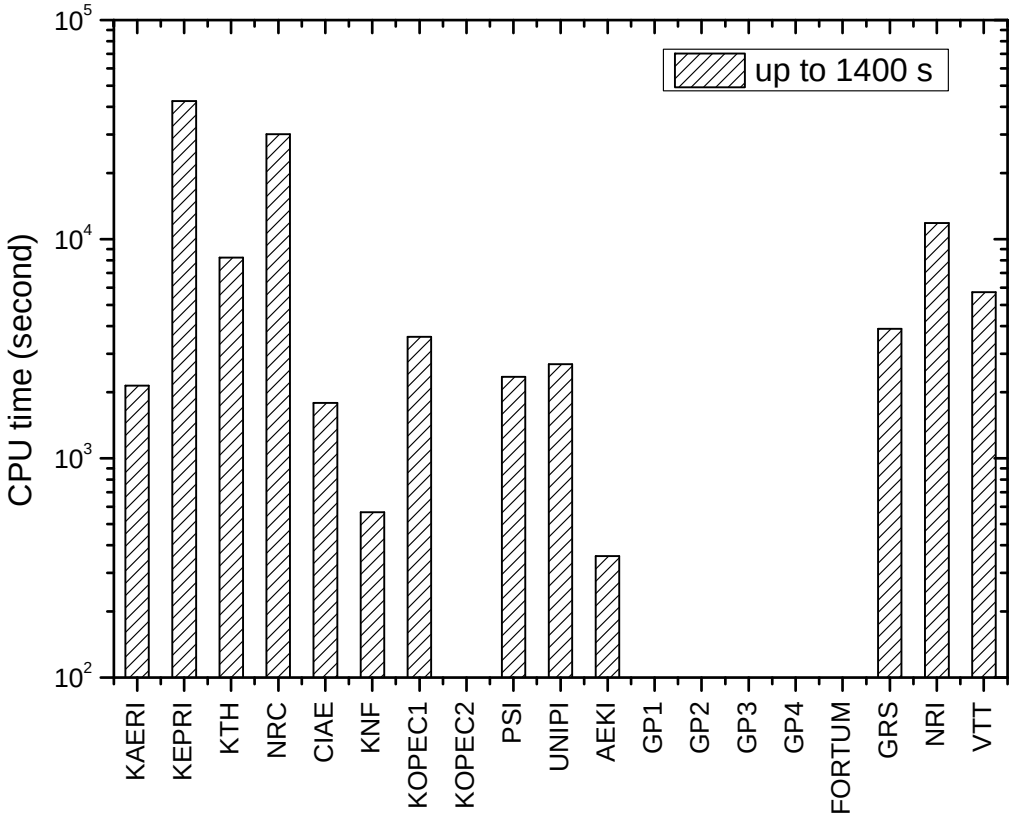

Figure 5.6-1 Comparison CPU time for calculation up to 1400 s

6. Overall Evaluation of the Calculations

6.1 Calculations of group-A

KAERI performed an open calculation with the MARS-KS code. The initial conditions of the KAERI's calculation were in good agreement with the experimental results. The plateau of the primary system pressure was correctly predicted during the whole test period. In the blind calculation, however, pressure was underestimated during the test period from 200 sec to 600 sec. As for the secondary pressure of the steam generators, the KAERI's calculation showed an improved prediction performance compared with the blind calculation. However, the KAERI's calculation underestimated the secondary pressure of the steam generators after 1000 sec of calculation time. The KAERI's calculation showed an outstanding accuracy in prediction of the accumulated mass of break flow. Overall trend of the break flow rate was well predicted. In the blind calculation, the KAERI's calculation predicted the experimental data with a satisfactory accuracy even though they slightly overestimated the accumulated mass during the initial calculation period up to 200 sec. The KAERI's prediction on the collapsed water level in core region was highly unsatisfactory. Contrary to the blind calculation, the KAERI's open calculation underestimated the core level during the whole test period. Overall trend of the collapsed water level in core region was well predicted. As for the collapsed water level in down-comer, the KAERI's blind and open calculations similarly underestimated the collapsed water level in down-comer during the whole test period except the initial calculation period less than 190 sec. Flow rate of SIP was correctly predicted in terms of injection timing and flow rate variation. The KAERI's blind calculation presented loop seal clearing phenomena in all the intermediate legs. On the other hand, the KAERI's open calculation predicted correctly the loop seal clearing phenomena at the intermediate leg 1A, 1B, 2B where loop seal clearing phenomena were observed in the ATLAS test. The prediction performance of loop seal clearings timing was also improved compared with the blind calculation. Contrary to the experimental data, the peak cladding temperature was not observed in the KAERI's blind calculation. The KAERI's open calculation, however, predicted the peak cladding temperature with a satisfactory accuracy even though the peak cladding temperature was calculated to be occurred earlier than the experimental data. In overall sense, the KAERI's calculation correctly predicted the wall temperature variations of core during the whole test period.

In conclusion, compared with the blind calculation the KAERI's open calculation presented an improved prediction performance especially for the pressures, core wall temperatures, loop seal clearings, and accumulated mass of break flow. However, prediction performance for the collapsed water level in core region was worsened.

KEPRI performed an open calculation with the MARS-KS code, whose result was depicted as

KEPRI in Group A. The actual core power which does not take into account an additional heat loss was used in the calculation. They predicted the initial trends of primary system pressure and the plateau very accurately in the open calculation on the contrary that they slightly underestimated the primary pressure around 300 s. The KEPRI's calculation over-predicted the secondary system pressure during the test period after 250 sec of calculation time. While the characteristics of the MSSVs were not modeled in the blind calculation, the actuation of the MSSVs was predicted in the open calculation even though their on-off frequency was higher than the experimental data. The flow from the active SIP began earlier than the experiment but overall trends were similar in both calculation and experiment. In terms of flow rate variation, the open calculation showed improved prediction performance compared with the blind calculation. In the blind calculation, the calculated wall temperatures in the active core regions were very accurate for all the twelve regions. However, the prediction accuracy of the peak cladding temperature was worsened in the open calculation. The prediction of the collapsed water level in the core region was improved in the open calculation. The collapsed water levels in down-comer were underestimated in both blind and open calculations. In the actual test, the loop seals in loop 1A and 1B were cleared at 190 s and the loop seal in loop 2B was cleared at 1236 s after the break initiation. The loop seal in loop 2A was not cleared. However, the KEPRI's calculation resulted in the loop seal clearings in all the intermediate legs in both blind and open calculations. The timing of loop seal clearings was improved in the open calculation. The prediction performance of the total break flow rate was improved in the open calculation and the KEPRI's calculation correctly predicted the accumulated mass of break flow.

In overall sense, compared with the blind calculation the KEPRI's open calculation presented an improved prediction performance especially for the pressures, SIP flow rate, water level in the core region, and accumulated mass of break flow. However, prediction performance for the wall temperatures in core region was worsened. And prediction accuracy of loop seal clearings needs to be improved.

KTH performed an open calculation with the TRACE 5.0 patch 01 code. The initial conditions of the KTH's calculation were in good agreement with the experimental results. The KTH's calculation showed highly improved prediction accuracy of the primary pressure compared with the blind calculation. They predicted the initial trends of primary system pressure and the plateau very accurately in the open calculation while the blind calculation overestimated the value of the primary pressure plateau by 1.0 MPa and then showed remarkably rapid depressurization of the RCS compared to the experimental data. As for the secondary system pressure, the KTH's calculation predicted the experimental data with an acceptable accuracy even though the first opening of the MSSV was delayed by about 25 sec compared to the experiment. In the blind calculation, they overestimated the overall trends and maintained a higher value during the whole test period, which could be attributed to an inaccurate modeling

of the MSSV operation. During the initial stage up to 250 sec, the KTH's calculation underestimated the break flow rate and the accumulated mass of break flow was underestimated during the whole test period. As for the accumulated mass of break flow, the discrepancy between the experimental data and the calculation result was larger in the open calculation. The KTH's calculation predicted the collapsed water level in the core region with a very poor accuracy. They underestimated the initial water level in core region and the water level in core region was underestimated during the whole test period. It could be attributed to an inappropriate calculation of the initial core water level in the steady state simulation. However, the prediction performance of the collapsed water level in down-comer was improved in the open calculation. The KTH's calculation showed an improved prediction accuracy of the wall temperatures in the active core region compared with the blind calculation. The peak cladding temperature, however, was not observed in the KTH's open calculation. As for the loop seal clearing phenomena, the prediction performance was worsened in the open calculation. In the blind calculation, they presented the loop seal clearing in all the intermediate legs. In the open calculation, the loop seal clearing phenomena at the intermediate leg 1A, 1B, 2B were not observed. On the other hand, the loop seal was cleared at the intermediate leg 2A where loop seal clearing phenomenon was not observed in the ATLAS test.

In conclusion, compared with the blind calculation the KTH's open calculation presented an improved prediction performance especially for the pressures and the wall temperatures in the core region. However, prediction performance for the collapsed water level in core region and the loop seal clearing phenomena were highly worsened.

NRC used the TRACE 5.0 patch 2 code for an open calculation of the ISP-50 exercise. The actual core power which does not take into account an additional heat loss was used in the calculation. The plateau of the primary system pressure was correctly predicted and afterward pressure predictions were satisfactory despite some underestimation during the test period after 300 sec of calculation time. Compared with the blind calculation, the prediction accuracy of the secondary pressures of the steam generators was improved in the open calculation. However the NRC's calculation steadily underestimated the secondary pressures of the steam generators after 250 s of calculation time. During the initial stage up to 250 sec, the NRC's calculation underestimated the break flow rate and the accumulated mass of break flow was underestimated during the whole test period. As for the accumulated mass of break flow, the discrepancy between the experimental data and the calculation result was similar in both blind and open calculations. The prediction performance of the collapsed water level in core region was highly improved in the open calculation. And also the prediction performance of the collapsed water level in down-comer was improved in the open calculation. The NRC's blind calculation presented loop seal clearing phenomena in all the intermediate legs. On the other hand, the NRC's open calculation predicted correctly the loop seal clearing phenomena at the

intermediate leg 1A, 1B, 2B. The prediction performance of loop seal clearings timing was also improved compared with the blind calculation. Among the Group-A calculations, the NRC's calculation shows the best prediction accuracy of the loop seal clearing phenomena. In the NRC's blind calculation, the peak cladding temperature was not clearly observed. The NRC's open calculation predicted the peak cladding temperature with an outstanding accuracy in terms of the timing of the peak cladding temperature occurrence. The overall trends of the core wall temperatures were little bit underestimated during the whole test period.

In overall sense, compared with the blind calculation the NRC's open calculation presented an improved prediction performance especially for the pressures, water level in the core region, core wall temperature, and loop seal clearing phenomena.

6.2 Calculations of group-B

In the Group B, there were five participants, e.g. CIAE, KNF, KOPEC, PSI, and UNIPI. For the blind calculations five calculations by four participants were submitted, e.g. CIAE, KNF, KOPEC1, KOPEC2, and UNIPI. And five calculations by five participants were submitted for the open calculation, e.g. CIAE, KNF, KOPEC, PSI, and UNIPI. KOPEC2 didn't submit calculation result at this time and PSI participated only for the open calculation.

CIAE used the RELAP5/MOD3.3 code for a blind calculation of the ISP-50 exercise. Before beginning of the decay curve initiation, the CIAE's calculation overestimated the core power up to above 1.8 MW and there were some discrepancies of the core power with the experimental data during the test period from 200 to 800 s. However, the plateau of the primary system pressure was correctly predicted and afterward pressure predictions were satisfactory despite some underestimation of the initial primary system pressure. As for the secondary system pressure, the CIAE's calculation presented relatively accurate calculation results for the MSSV opening and the subsequent secondary system pressure behavior. The heat removal rates of the steam generators were calculated comparatively higher than the experimental data during the initial period up to 200 s. The CIAE's calculation underestimated the accumulated mass of break flow with an acceptable discrepancy. However, collapsed water levels in the core and the down-comer were incorrectly predicted. Initial water level in the core was incorrectly simulated and the water level in the down-comer was underestimated during the whole test period except for the test period from 100 to 400 s. Even though there was some delay for complete loop seal clearing, CIAE predicted the loop seal clearing phenomena in the intermediate leg 1A and 1B with a reasonable accuracy. However, late loop seal clearing observed in the intermediate leg 2B was not simulated properly. Contrary to the experimental data, in the CIAE's calculation, the peak cladding temperatures were observed in the core region 10, 11 and 12. Except for this discrepancy, the prediction performance of the core thermal behavior was

very excellent at the other core region.

For the open calculation, the CIAE's calculation estimated the total core power very well. The primary pressure and the plateau were reasonably predicted, even though the primary pressure was slightly overestimated until the end of plateau and under-estimated after the plateau. The secondary system pressure was slightly overestimated and showed good prediction performance for the MSSV's openings. The heat removal rates of the steam generators were calculated relatively higher than the experimental data during the initial period up to 200 s. They predicted the accumulated mass of break flow with some over-estimation until 200 s and under-estimation after then. And the collapsed water level in the active core was correctly predicted and the collapsed down-comer level was underestimated. The time of the SIT actuation got worse a little rather than the blind case. For the SIP actuation, calculation result of the open calculation was similar to that of the blind case. Loop seal clearings of the intermediate legs 1A and 1B were observed to be well predicted with deviation of 45 s earlier than the experimental data and that of the 2Bwas predicted with deviation of 236 s later than the experimental data. But loop seal clearing of the 2A was simulated improperly, e.g. no loop seal clearing was observed in the test, but loop seal was cleared at 1472 s in the open calculation. As for the wall temperature in the active core, contrary to the experimental data, the peak cladding temperatures were not observed from region 1 to region 10 except regions 11 and 12. Except these deviations for the PCTs, the wall temperature in the core showed quite good agreement with the experimental data. In the overall sense, except for the LPP and the RCP trips, the open calculation of the CIAE was found to be a little improved rather than the blind case.

KNF used the RELAP5/MOD3.3 code for a blind calculation of the ISP-50 exercise. The KNF's calculation slightly underestimated the total core power. The plateau of the primary system pressure was correctly predicted and afterward pressure predictions were satisfactory despite some underestimation after 200 s of calculation time. As for the secondary system pressure, the KNF's calculation overestimated the overall trends and maintained a higher value than the data during the whole test period, which could be attributed to an inaccurate modeling of the MSSV operation. The heat removal rates of the steam generators were calculated relatively higher than the experimental data during the initial period up to 200 sec. The KNF's calculation predicted the accumulated mass of break flow with an outstanding accuracy. However, collapsed water levels in the core and the down-comer were incorrectly predicted. Calculated water level in the core highly oscillated and water level in the down-comer was underestimated during the whole test period except the initial calculation period less than 200 s. The KNF's calculation predicted the loop seal clearing phenomena in the intermediate leg 1A and 1B accurately. Late loop seal clearing observed in the intermediate leg 2B was not simulated properly. As for the wall temperature in the core, contrary to the experimental data, the peak

cladding temperature was not observed in the KNF's calculation. Even though the KNF's calculation slightly underestimated the wall temperature depending on the locations, the KNF's calculation could be considered to correctly predict the wall temperature variations of core during the whole test period.

For the open calculation, the KNF's calculation estimated the total core power very well. The primary pressure was reasonably predicted, even though the plateau of the primary pressure was slightly overestimated. The secondary system pressure was slightly overestimated and showed more frequent MSSV's openings. The heat removal rates of the steam generators were calculated relatively higher than the experimental data during the initial period up to 200 s. They predicted the accumulated mass of break flow with some underestimation. And the collapsed water level in the active core was correctly predicted and the collapsed down-comer level was underestimated. The time of the SIT actuation improved very much rather than the blind case. For the SIP actuation, calculation result of the open calculation was similar to that of the blind case. Loop seal clearings of the intermediate legs 1A and 1B were observed quite close to the experimental data, but those of the 2A and 2B were not simulated properly. As for the wall temperature in the active core, contrary to the experimental data, the peak cladding temperatures were observed at different times with small deviations. Except these deviations for the PCTs, the wall temperature in the core showed very good agreement with the experimental data. In the overall sense, the open calculation of the KNF was found to be a little improved rather than the blind case except for the SIT actuation time and the loop seal clearings of the intermediate legs 1A and 1B

KOPEC performed two blind calculations with the RELAP5-ME and the RELAP5/MOD3.3, whose results are depicted as KOPEC1 and KOPEC2 in Group B, respectively. The total core powers could not be compared because they were not included in their submitted data file. The initial heat removal rates through SG1 and 2 on break showed the rapidest increase among the other calculations especially during the early period up to 20 s. The main cause of this cannot be identified at the moment. It is recommended that KOPEC need to investigate this calculation result. The initial depressurization rate of the primary pressure was much higher than the experimental data in their two calculations, resulting in lower primary pressure than the experimental data during the whole test period. The plateau region of the primary pressure was not correctly reproduced. The predicted secondary pressures showed a rapid increase on break and then they dropped to near 7.9 MPa. Then the secondary pressured showed much milder decrease than the experimental data. The MSSVs seemed not to be correctly modeled. The pressure trends of three SITs showed very large underestimation after actuation of them. But the flow rates of three SITs were highly overestimated. And the initiation times of all the SITs were earlier than the experimental data by about 50~100 s. The flow injection by the active SIP began at the same time as the experiment but the flow rates were slightly over-predicted

compared with the experimental data. The calculated wall temperatures in the active core regions were slightly underestimated until 300~400 s for all the twelve regions, but after then the deviations became larger with time. The prediction of the collapsed water level in the down-comer showed a similar trend but it was underestimated the experimental data for all the period with large oscillations after around 700 s. The prediction of the collapsed water level in the active core region showed large oscillations against the experimental data. The calculated loop seal clearings showed different trends with respect to the experimental data. In loop 1A, the calculations showed a similar loop seal clearing but the loop 1A became filled with water after second loop clearings during the later period. In the other loops 1B, 2A, and 2B, there were no manifest loop seal clearings but instant and/or intermittent clearings for one or two times were predicted. The calculation result for the total break flow rate showed relatively good prediction performance until 400 s and after then it showed great overestimation of the experimental data. The accumulated mass of the break flow showed under-prediction until around 400 s, after then it showed quite large over-prediction.

For the open calculation, KOPEC submitted just one calculation using the RELAP5-ME code same as the KOPEC1 blind calculation. The total core power was estimated well and the pressurizer pressure was quite well predicted except slightly shorter plateau and underestimation during 170~900 s. The initial heat removal rates through SG1 and 2 on break showed relatively higher values than the experimental data. The calculated secondary pressures showed larger values than experimental data during the transient period with more frequent MSSV's openings. The actuation time of the SITs was improved a little. The accumulated mass of break flow was very accurately predicted. As for the wall temperature in the active core, contrary to the experimental data, the peak cladding temperatures were observed at different times with quite large deviations. Except these deviations for the PCTs, the wall temperature in the core showed very good agreement with the experimental data. The collapsed water levels in the active core were predicted accurately and the collapsed down-comer levels were slightly underestimated. The loop seal clearing of the intermediate leg 1A occurred with large time delay and on the other hand, for the intermediate leg 2B, it occurred much earlier than the ISP-50 test. And the loop seal clearings of the intermediate legs 1B and 2A were not simulated properly. The calculation results for the total break flow rate and the accumulated mass of the break flow showed good prediction performance. In the overall sense, the open calculation of the KOPEC was found to be a little improved rather than the blind case except for the SIT actuation time and the loop seal clearings of the intermediate legs 1A and 1B

University of Pisa (Italy) performed a blind calculation with the RELAP5/MOD3.3 code and it was named UNIPI. The total core power was well simulated. Heat removal rates through steam generators 1 and 2 were high during the initial period before about 150 s and they showed a couple of peaks. They also predicted the initial trends of primary system pressure and the

plateau accurately but they under-predicted the primary system pressure after the plateau. They predicted the secondary system pressure very accurately during the initial period and slightly over-predicted during a later period. The prediction on the flow rates from three SITs was very similar to the experimental data, and the SIT pressure decreased similarly. However, the injection time was earlier than the ISP-50 test. The flow rate by the SIP was calculated to be slightly higher than the experimental data. The calculated wall temperatures in the active core regions were very accurate for all the twelve regions. The collapsed down-comer water level showed very good agreement with the experimental data during an initial period of about 200 s but after then it decreased more rapidly and recovered more slowly than the experimental data. The collapsed core water level was similar to the experimental data. The calculated total break flow rate overestimated the experimental data during an initial period of about 150 s and it agreed well with the experimental data after about 200 s. The accumulated mass of the break flow was well predicted except for the initial period. The UNIPI's calculation showed the loop seal clearing phenomena clearly in the regions of 1A, 2A and 2B but the locations and clearing times were different from the ISP-50 test. During the experiment the regions of 1A and 1B were cleared around 200 s, the region of 2B was cleared around 1250 s, and the region of 2A was not cleared. The orientation of loop configuration and safety injection needs to be checked carefully and it is recommended that the reason should be clarified why the regions of 1B and 2A were filled with water again. The UNIPI's calculation predicted the core power, pressures, core heater surface temperatures (PCTs), and accumulated mass of the break flow very well, but it had large discrepancy on the prediction of the loop seal clearing phenomena, break flow rate, and loop flow rate. The SIP injection time needs to be checked. Since the lower collapsed water levels contributed to the poor prediction on the peak cladding temperature for the later phases, it needs to be reviewed more in detail.

For the open calculation, the total core power was well simulated. Heat removal rates through steam generators 1 and 2 were high during the initial period before about 150 s and they showed more peaks than the blind case. They also predicted the initial trends of primary system pressure and the plateau accurately. They predicted the secondary system pressure quite accurately during the initial period and slightly overestimated during a later period similar to the blind case. The prediction on the flow rates from three SITs was very similar to the experimental data, and the SIT pressure decreased similarly. However, the prediction for the injection time of the SIT was highly improved compared with the blind case. The flow rate by the SIP was calculated to be slightly higher than the experimental data. The calculated wall temperatures in the active core regions were very accurate for all the twelve regions except peak cladding temperatures. The collapsed down-comer water level showed very good agreement with the experimental data during an initial period of about 200 s but after then it decreased more rapidly and recovered more slowly than the experimental data. The collapsed core water level showed similar trend like as the collapsed down-comer level. The calculated

total break flow rate and total accumulated mass were very close to the experimental data with slight underestimation till 600 s. For the loop seal clearings, 1A was very close to the experimental data; 1B, not cleared; 2A, cleared at around 180 s; 2B, cleared much earlier than the experimental data. In the overall sense, the open calculation of the UNIPI was found to be a little improved qualitatively except for the SIT actuation time.

PSI used the RELAP5/MOD3.3 code for an open calculation of the ISP-50 exercise. Before beginning of the decay curve initiation, the PSI's calculation slightly underestimated the core power up to around 330 s and thereafter was good agreement with the experimental data. The plateau of the primary system pressure was correctly predicted. As for the secondary system pressure, the PSI's calculation overestimated with some discrepancy for the MSSV opening and the subsequent secondary system pressure behavior. The heat removal rates of the steam generators were calculated to be comparatively higher than the experimental data during the initial period up to 200 s but showed similar trends with others' calculations. The total break flow rate seemed to be good agreement with the experimental data and the accumulated mass of the break flow was underestimated slightly, e.g. ~ 8.5% at around 1600 s. The collapsed water level of the active core was correctly predicted with a slight overestimation and those of 7 down-comer elevations seemed to be very close to the experimental data except two elevations, e.g. 4 and 5 elevations where the collapsed water levels were underestimated a little. As for the loop seal clearings, two loops (1A, 1B) were correctly predicted with respect to the experimental data and one loop (2A) was calculated to follow overall trend of no clearing except for nearly clearing period during 25 s at around 170 s of the calculation time. The prediction of loop seal clearing in the 2B preceded the experimental data about 1000 s. Even though there was some deviation for the behavior of the loop seal clearings, PSI predicted the loop seal clearing phenomena with a reasonable accuracy. For the peak cladding temperature, two peaks were observed with higher temperatures and at earlier times in each group. It is noteworthy that the second peaks were very close to those of the experimental data for the three groups. Except for the peak cladding temperatures, the prediction of the maximum core temperatures were very excellent for the three groups. In the overall sense, the PSI's calculation predicted quite a good agreement with the experimental data for all the major parameters.

6.3 Calculations of group-C

In the Group-C, AEKI participates only in the open calculation, and GP1, GP2, and GP3 participate in both the blind and open calculation, and finally GP4 participates only in the blind calculation. The AEKI performed an open calculation with the CATHARE2V1.5B mod3.1 code, and the GP1, GP2, GP3 used a Russian code, KORSAR/GP, and the GP4 used another code, TECH-M-97.

The AEKI accurately simulated the core power during the transient. The primary pressure shows a good agreement with the experiment. For the secondary pressures, even though fluctuations due to the MSSV's action were simulated nicely, slower decreasing rates for both SGs than the experimental data were observed. For the fluid temperatures in the down-comer sub-sections show an under-estimated trend especially after 500 s of the break. Generally, the fluid temperatures and the flow rates show a good agreement with the experimental data, even though the hot and cold leg temperatures show an over-estimated value. For the collapsed water levels in the down-comer and core regions show a relatively good agreement. However, in the intermediate, the collapsed water levels show a very different trend. Contrary to the experimental data, the loop seals were cleared 1,400 s and 160 s for the loop-1 and loop-2, respectively. The cladding temperatures show a nice agreement with the experimental data except for the fact that there is no excursion on the cladding temperatures.

As three results of GP1, GP2, and GP3 show a similar thermal-hydraulics trends, they will be discussed together and only their difference will be discussed. The total core power was well simulated in both the blind and the open calculations. The heat removal rates of the blind calculation through steam generators 1 and 2 show over-estimated values during the initial period up to 150 s, and the rates show similar trends in the open calculation, which show a more fluctuating nature than the blind calculation. They predict a more accurate trend for the primary and the secondary pressures than those of the blind calculation. In the blind calculation, they presented a longer plateau and a higher pressure trends after the loop seal clearing. They also over-predicted the secondary system pressure quite a lot. The main reason of this over-prediction is that they did not model the MSSV in the blind phase. In the open calculation, they improved their model to show how important SG MSSV model is. Thus, they showed a great agreement with the experimental data for the primary pressure. Description of their input deck upgrade was summarized in Table 5 of their report in Appendix-F. For the secondary pressure, they also show a better agreement than the blind calculation, even though the GP2 and the GP3 show a lower decreasing rate than that of the experimental data.

The containment pressure was not simulated in the blind calculation, and this bad agreement could be observed also in the open calculation. The simulation on the flow rates and pressures of three SITs show a relatively good agreement with the experimental data. The actuation times of the SITs show more accurate values in the open calculation than the blind calculation. The fluid temperatures in the down-comer and the core regions show a more enhanced trend in the open calculation, even though the GP2 shows an abrupt fluctuation in the down-comer region around the loop seal clearing period. The fluid temperatures in the loops also show a better agreement with the experimental data in the open calculation.

However, the GP2 and the GP3 show an over-estimated trend yet in the open calculation, especially in the hot and cold legs. The steam temperatures in the steam dome show a nice agreement with the experimental data in the open calculation. Moreover, the initial temperature and pressure fluctuations due to the MSSV actions are simulated nicely in the open calculation. The predictions on the cladding temperatures in the active core regions are very inaccurate for all the twelve regions. However, in the open calculation, the cladding temperatures show a more enhanced trend than those of the blind calculation, even though there are several large temperature fluctuations in the calculation results. In the blind calculation, the core regions of 1 through 12 were overheated for the GP1 and GP2 analyses and the core regions of 7 through 12 were reheated for the GP1, GP2 and GP3 analyses. However, the degree and the number of fluctuations of the cladding temperature are reduced remarkably in the open calculation.

The prediction of GP1 on the collapsed down-comer level was very poor during the whole test period. The prediction on the collapsed core level was also very poor. The active core region was almost fully uncovered around 200 s and it was recovered and fluctuated. The uncovery of core region was the reason why the core heater wall was overheated. The predictions of GP2 on the collapsed down-comer level estimated the experimental data lower during an initial period of about 200 s but they agreed well during 200-400 s. However, after that the collapsed down-comer level decreased longer and recovered more slowly than the experimental data. The prediction on the collapsed core level was very poor. The active core region was almost fully uncovered around 200 s and it was recovered and fluctuated. Unfortunately the predictions of GP3 were not available. The predictions on the total break flow rate estimated the experimental data very well except for the higher plateau during 100 – 200 s. The predictions on the accumulated mass estimated the experimental data slightly lower.

In the blind predictions of GP1, the loop seal clearing phenomena were observed clearly in the regions of 2A and 2B around 290 s, but the locations and clearing time were different from those of the experiment. During the experiment the 1A and 1B loops were cleared around 190 s, the 2B loop was cleared at 1,236 s and the 2A loop was not cleared. In the open calculation, the loop seal clearing times become worse than those of the blind calculation, and the locations at which the loop seal clearing occurred were changed to 1B and 2A loops. The orientation of loop configuration and safety injection should be checked carefully and the reason why the 1A and 1B loops are not cleared should be clarified. The blind predictions of GP2 showed a similar trend of the loop seal clearing phenomena with the blind case of GP1 except for the clearing time of around 250 s and the partial clearing and filling of the 1A and 1B loops. However, in the open calculation, the loop-1 is not cleared. On the contrary, the loop-2 is cleared at 280 s after the break. The GP3 fails to predict the loop seal clearing during

the whole period of simulation.

In overall sense, the open calculations performed by GP group predicts the core power, pressures, and accumulated break mass more accurately, but it has large discrepancy on the prediction of the PCTs, loop seal clearing phenomena, break flow rate, and loop flow rate.

The results of GP4 are discussed separately from the other calculations of GP1, GP2 and GP3 because they participate only in the blind calculation. The core power decayed about 20 s later than the experimental data. Heat removal rates through the steam generators 1 and 2 were high during the initial period up to 150 s. They predicted the initial trends of the primary system pressure correctly, but the plateau was a little over-estimated and the pressure decrease rate was higher than that of the experimental data before 600 s. It over-predicted the secondary system pressure quite a lot and it increased more rapidly after 400 s. The SIT pressure started to decrease faster but its decreasing rate was slower than the experimental data. The injection time of GP4 was faster than that during the experiment but the predictions on the SIP flow rate estimated the experimental data lower except for the initial high flow rate.

The predictions on the wall temperatures in the active core regions were accurate for regions of 1 through 6 but the core regions of 7 through 12 were overheated in the GP4's analysis. The predictions of GP4 on the collapsed levels of down-comer and core estimated the experimental data very poor during the whole test period. They predicted a much lower collapsed levels and the core heater wall was overheated. The predictions on the total break flow rate estimated the experimental data very well except for the higher plateau during 50 – 150 s. The predictions on the accumulated mass estimated the experimental data very well except for the earlier period.

The predictions of GP4 showed the loop seal clearing phenomena clearly in all regions. During the experiment the regions of 1A and 1B were cleared around 200 s, the region of 2B was cleared around 1,250 s and the region of 2A was not cleared. The predictions of GP4 are similar to the experimental data for the regions of 1A and 1B but they are different for the regions of 2A and 2B. The GP4's calculation also predicted the core power, pressures, and accumulated break mass very well, but it had large discrepancy on the prediction of the core heater surface temperatures (PCTs), loop seal clearing phenomena, break flow rate, and loop flow rate. SG1 steam dome pressure and active SIT-01 flow rate were not simulated well. As the collapsed water level of down-comer contributed to the poor prediction on the peak cladding temperature, it should be reviewed more in detail.

6.4 Calculations of group-D

FORTUM used the APROS (v. 5.08) code for a blind calculation and it was named as FORTUM in this report. The APROS (v. 5.08) was developed in cooperation by Fortum Nuclear Services LTD and VTT Technical Research Centre of Finland. However, an open calculation results were not provided by FORTUM and only the blind calculation result was discussed in this section.

Total core power decay was applied well as a boundary condition. General trend of the primary system pressure agreed reasonably well with the data, but, in detail, the pressure plateau before the loop seal clearing was not observed and the decreasing rate of the primary pressure after the loop seal clearing was relatively lower than that of the experiment. The SG steam-dome pressure showed a good agreement with the experimental data, although the number of on-off cycles of the MSSVs on both SG-1 and SG-2 were observed in 6 times.

The down-comer liquid level decreased relatively earlier than the experimental data, due to the time difference of the loop seal clearing. In the experiment, the loop seal clearing was started in about 190 s from the break. On the other hand, in the calculation, the loop seal clearing started at about 125 s. The temporary depression of the core collapsed water level associated with the loop seal clearing was partly simulated: the first liquid level depression was calculated well but the second depression was not simulated. Moreover, the loop seal clearing was occurred in different loop. The intermediate legs 1A, 1B, and 2B were cleared in the experiment, but 2A and 2B legs were cleared in the calculation.

The break flow rate was over-predicted, especially in the initial maximum value, and then it decreased with the loop seal clearing. In this initiation period until the loop seal clearing, the break flow was overestimated. The break flow rate showed a sudden decrease with an occurrence of the loop seal clearing at about 125 s. After 300 s, the break flow rate showed a good agreement with the experimental data. The cladding temperatures were slightly overestimated. The cladding temperature excursion around the loop seal clearing, however, was not observed. The SIP and SIT flow rates were simulated well, but the injection time of the SIT was delayed in about 96 s due to the higher primary pressure response. The overall calculation results show a relatively good agreement with the experiment.

GRS submitted both blind and open calculation results with the ATHLET (Mod 2.2 Cycle A) code and it was named as GRS. The ATHLET was being developed by GRS for the analysis of the whole spectrum of leaks and transients in light water reactors. In the present section the open calculation result was discussed mainly and compared with the blind calculation results.

The total core power decay was applied well as a boundary condition. The primary system pressure was predicted well and showed an excellent agreement with the experimental data.

Timing of the pressure plateau was calculated with a good accuracy. In the open calculation the SG secondary pressure until about 200 s was calculated well, although the number of on-off cycle of the MSSVs on both SG-1 and SG-2 was 6 times. The SG secondary pressure showed a little bit lower value than the data throughout the test.

In the open calculation the down-comer liquid level showed a little underestimated trend, especially after the loop seal clearing. In the blind calculation the down-comer liquid level showed an underestimated trend, especially after the loop seal clearing. Both in the blind and open calculations the core water level showed a lower value than the experimental data during the whole test period and it showed a fluctuating nature until about 200 s. In the open calculation, the loop seal clearing was observed in the intermediate leg-1B and -2A. The timing of the loop seal clearing showed improved results than that of the blind calculation: it was delayed in only 27 s. In the blind calculation, dissimilar to the experiment, the loop seal clearing was observed in the intermediate leg-1A and -2A and temporal water level fluctuations in the intermediate leg-1B and -2B were observed. The timing of the loop seal clearing showed a relatively good agreement with that of the data: it was delayed in only 33.1 s.

In the open calculation the break flow rate was calculated to be lower than the experimental data. During the pressure plateau before the loop seal clearing, the calculated break flow rate showed a little lower value than the experimental data, and then it experienced a sudden decrease with an occurrence of the loop seal clearing. In the blind calculation the break flow rate was calculated nicely except for the initial stage. The initial maximum break flow rate was calculated as 8.3 kg/s. During the pressure plateau before the loop seal clearing, the calculated break flow rate showed a good agreement with the experimental data.

In the open calculation the cladding temperature excursion around the loop seal clearing observed in the experiment was not predicted. In the blind calculation the cladding temperature showed a large increase at several vertical levels. It was observed that this cladding temperature excursion was closely related to the core collapsed water level. Both the SIP and SIT injections were well simulated in the open calculation. However, in the blind calculation the SIP injection was delayed in about 450 s, but the SIT flow was simulated well. In overall sense, compared with the blind calculation the GRS's open calculation presented an improved prediction performance especially for the pressures, the SIP flow rate, and the collapsed water levels in the down-comer and core regions.

NRI (Czech Republic) submitted both blind and open calculation results with the AHELET code and the result has been named as NRI for convenience. The total core power decay was applied well as a boundary condition. However, in the blind calculation the core power was simulated to start to decay at 56.8 s, 23.8 s later than the experiment. In the open calculation the primary system pressure was predicted well and showed an excellent agreement with the experimental data. Timing of the pressure plateau was calculated with a good accuracy.

However, in the blind calculation the primary system pressure in the initial blowdown stage was well predicted until about 20 s, but after then the calculated primary pressure was greatly underestimated throughout the whole calculation time. Also the pressure plateau was not predicted in the calculation of the blind calculation. In the open calculation the SG secondary pressure was calculated well during the whole period, although the number of on-off cycle of the MSSVs on both SG-1 and SG-2 was 2 times. In the blind calculation the SG secondary pressures were well predicted in both SGs, although the MSSV operation was not well predicted. In the blind calculation the MSSV on SG-1, for example, cycled only one time whereas it did four times in the experiment.

In the open calculation both the water level of core and down-comer showed higher values than the experimental data during the whole test period. However, in the blind calculation the down-comer liquid level was reasonably consistent with the data until 1,500 s, after then it underestimated the data. Moreover, a degree of the underestimation increased with the time. As for the collapsed water level in the core in the blind calculation, the temporary level depression associated with the loop seal clearing was not obtained in calculation. In the open calculation the loop seal clearing occurred at the loop-1A and 1B. In the blind calculation the loop seal clearing was not predicted in calculation. There was no variation of the collapsed water levels in the four vertical intermediate legs.

In the open calculation the break flow rate was calculated to be lower than the experimental data. During the pressure plateau before the loop seal clearing, the calculated break flow rate showed a little lower value than the experimental data, and then it experienced a sudden decrease with an occurrence of the loop seal clearing. In the blind calculation the break flow rate was over-predicted, especially in the initial transient period, and then it maintained a slightly higher level than the experimental data. The calculated break flow rate, however, showed a reasonable agreement with the experimental data after 195 s both in the blind and open calculations.

In the open calculation the cladding temperature excursion around the loop seal clearing observed in the experiment was not predicted. In the blind calculation the calculated cladding temperatures underestimated the data. This was due to the lower calculated primary pressure than the experimental data. The cladding temperature excursion around the loop seal clearing observed in the experiment was not predicted. Both the SIP and SIT injections were well simulated in the open calculation. However, in the blind calculation the SIP flow was injected more than 10 %, and a SIT injection flow rate different from the provided boundary condition was also simulated. In overall sense, compared with the blind calculation the NRI's open calculation presented an improved prediction performance especially for the core power, the pressures, the SIP flow rate, and the loop seal clearing.

VTT submitted both blind and open calculation results with the APROS (v. 5.09) code and

the results has been named as VTT for convenience. The total core power decay was applied well as a boundary condition. In the open calculation the primary system pressure was predicted well and showed an excellent agreement with the experimental data. Timing of the pressure plateau was calculated with a good accuracy. However, in the blind calculation the primary system pressure showed a relatively good agreement with the experimental data until the loop seal clearing but the primary pressure was over-predicted after the loop seal clearing. In the open calculation the SG secondary pressure until about 200 s was calculated well, although the number of on-off cycle of the MSSV on both SG-1 and SG-2 was 6 times. The SG secondary pressure showed a little bit lower value than the experimental data throughout the test. However, in the blind calculation the SG secondary pressure was over-estimated and the difference in the secondary pressure between the calculation and the experiment increased with the time. With the unsuitable simulation of the set-point of the MSSV action, the secondary pressure showed a different behavior until 200 s in the blind calculation. As a higher opening pressure of the MSSV resulted in an over-estimation of the MSSV flow rate in the blind calculation, the MSSV of SG-1, for example, cycled only 2 times whereas it did 4 times in the experiment.

Both in the blind and open calculations the phenomena of down-comer liquid level drop and core liquid level swell around the loop seal clearing showed a good agreement with the experimental data. However, in the blind calculation the down-comer collapsed water level after the loop seal clearing maintained a higher value than the experimental data. Both in the blind and open calculations the loop seal clearing was observed in all the intermediate legs. However, the timing of the occurrence of the loop seal clearing was improved during the open calculation. The loop seal clearing of the loop-1 and loop-2 started at about 165 s and 182 s, respectively, in the open calculation, but the loop seal clearing of the loop-1 and loop-2 started at about 152 s and 169 s, respectively, in the blind calculation.

In the open calculation the break flow rate was predicted well. However, in the blind calculation the break flow rate was over-predicted, especially in the initial maximum value, and then it decreased steeply with the loop seal clearing. Especially in this period, however, the break flow rate was overestimated. The break flow rate showed a sudden decrease with an occurrence of the loop seal clearing at about 152 s in the loop-1.

In the open calculation the cladding temperature excursion around the loop seal clearing observed in the experiment was not predicted. In the blind calculation the cladding temperature showed a good agreement with the experimental data except for the time period between the loop seal clearing and the SIT injection. In this time period, the cladding temperature showed an overestimated value due to the effect of the primary pressure. The cladding temperature excursion around the loop seal clearing was observed.

Both the SIP and SIT injections were well simulated in the open calculation. However, in the blind calculation the injection time of the SIT was delayed in about 150 s due to the primary

pressure response, although the SIP and SIT flow rates were simulated reasonably. In overall sense, compared with the blind calculation the VTT's open calculation presented an improved prediction performance especially for the pressures, the SIP flow rate, and the break flow rates.

7. Accuracy Quantification

7.1 FFTBM methodology

Qualitative comparison of the submitted calculation results against the measured data was described in the previous chapter of this report. In addition, in order to give more clear quantification of the prediction performance, a methodology proposed by Prof. F. D'Auria at the University of Pisa (DCMN), FFTBM (Fast Fourier Transform Based Method) was adopted in the present ISP-50 exercise [Ambrosini *et al.*, 1990, D'Auria *et al.*, 1994, Kunz *et al.*, 2002, Prosek *et al.*, 2006]. It is an integral method using the Fast Fourier Transform (FFT) in order to represent the code discrepancies in the frequency domain. This method has been successfully applied to the past international standard problems (ISPs) or standard problem exercises (SPEs) organized by CSNI or IAEA in order to quantify the prediction accuracy of the codes used in the program [D'Auria *et al.*, 1989]. A good review can be found in the literature [Prosek *et al.*, 2002].

Both experimental signal and error signal are required for calculation. Suppose that we have N consecutive sampled values, the error signal in the discrete time domain can be expressed:

$$\Delta F(t_k) = F_{cal}(t_k) - F_{exp}(t_k), \qquad t_k = k\tau, \qquad k = 0,1,2,\dots,N-1, \tag{7.1.1}$$

where $F_{cal}(t_k)$ and $F_{exp}(t_k)$ are calculated and experimental signals sampled at evenly spaced intervals in time, respectively. The number of discrete signal should be a power with base equal to 2, that is, $N=2^{m+1}$ to apply FFT and sampling theorem must be fulfilled. By applying FFT on the discrete experimental signal and the error signal, we can obtain the discrete Fourier transform of the N points F_k in the frequency domain.

$$\tilde{F}_{exp}(f_n) = \tau \sum_{k=0}^{N-1} F_{exp,k} e^{2\pi i k n/N}, \tag{7.1.2}$$

$$\Delta\tilde{F}(f_n) = \tau \sum_{k=0}^{N-1} \Delta F_k e^{2\pi i k n/N}, \tag{7.1.3}$$

where $f_n = n/N\tau$.

The accuracy quantification for an individual parameter is based on amplitude of discrete experimental and error signals obtained by FFT at frequencies, f_n, where (n=0, 1, ..., 2^m) and m is the exponent ranging from m=8 to m=11. According to the sampling theorem, sampling frequency is calculated by

$$\frac{1}{\tau} = f_s = 2 f_{\max} = \frac{N}{T_d} = \frac{2^{m+1}}{T_d}, \tag{7.1.4}$$

where f_{max} is the maximum frequency component of the signal. These spectra of amplitude together with frequencies are used for calculation of average amplitude (AA) and weighted frequency (WF) that characterize code accuracy. The AA is defined as the sum of error function amplitudes normalized to the sum of experimental signal amplitude as follows:

$$AA = \frac{\sum_{n=0}^{2^m} \left| \Delta \tilde{F}(f_n) \right|}{\sum_{n=0}^{2^m} \left| \tilde{F}_{\exp}(f_n) \right|}, \tag{7.1.5}$$

and the WF is defined as sum of frequencies multiplied by error function amplitudes, normalized to the sum of error function amplitude

$$WF = \frac{\sum_{n=0}^{2^m} \left| \Delta \tilde{F}(f_n) \right| \cdot f_n}{\sum_{n=0}^{2^m} \left| \Delta \tilde{F}(f_n) \right|}, \tag{7.1.6}$$

A cut-off frequency (f_{cut}) is introduced to cut off spurious contribution to accuracy quantification. The overall accuracy of the code calculation can be obtained by defining average performance indices, total weighted AA and total WF as follows:

$$AA_{tot} = \sum_{i=1}^{N_{var}} (AA)_i \cdot (w_f)_i, \tag{7.1.7}$$

$$WF_{tot} = \sum_{i=1}^{N_{var}} (WF)_i \cdot (w_f)_i, \tag{7.1.8}$$

$$\sum_{i=1}^{N_{var}} (w_f)_i = 1 \tag{7.1.9}$$

where, N_{var} is the number of the variable analyzed, and $(AA)_i$, $(WF)_i$, and $(w_f)_i$ are AA, WF and weighting factors for i-th analyzed variable, respectively. The weighting factor can be further sub-divided into three components by considering the following contributions:

① Experimental accuracy $(w_{exp})_i$: this factor takes into account experimental uncertainty due to intrinsic characteristics of instruments, the measurement method, and different evaluation procedures used to compare experimental measures and the code predictions.

② Safety relevance $(w_{saf})_i$: this factor is related to safety relevance. Higher importance is assigned to those calculated variables such as pressure, PCT and etc which are relevant for safety and design.

③ Primary pressure nodalization $(w_{norm})_i$: this is a factor to normalize the AA value calculated for the selected variables with respect to the AA value calculated for the primary pressure. This has been introduced in order to consider the physics relations existing between different quantities.

The weighting factor for the i-th variable is therefore defined as:

$$(w_f)_i = \frac{(w_{exp})_i (w_{saf})_i (w_{norm})_i}{\sum_{i=1}^{N_{var}} (w_{exp})_i (w_{saf})_i (w_{norm})_i}, \quad (7.1.10)$$

where $(w_{exp})_i$ is the contribution related to the experimental accuracy, $(w_{saf})_i$ is the contribution related to safety and $(w_{norm})_i$ the contribution of primary pressure normalization.

7.2 Application to the ISP-50 calculations

In order to apply the FFTBM to the present ISP-50 calculation, we have to decide several parameters used in the method, including the parameter selection (N_{var}), the analysis time frame selection (T_d), the number of points (N), the cut-off frequency (f_{cut}), and the weighting factor selection.

7.2.1 Selection of parameters

A total of 86 thermal-hydraulic parameters were requested in the blind phase of the ISP-50 and they have been submitted to the operating agency as shown in Table 2.4-1. In the following open phase of the ISP-50, the number of requested parameters was extended up to 145 in order to perform more detailed comparison, especially focusing on 3-D behavior.

The full FFTBM method requires 20-25 parameters selected representing relevant thermal-hydraulic aspects. In order to apply the FFTBM to the ISP-50 calculation, major parameters should be selected among the submitted parameters. By personal communication with Prof. D'Auria's group in the blind phase, 22 parameters among the submitted 86

parameters were selected to characterize all the relevant phenomena that were measured during the experiment. Similar parameters which would affect the analysis results and the parameters which have much measurement uncertainties have been avoided in this selection process. In the subsequent open phase, the parameters used in the blind phase were used as it is for FFTBM calculation except for the cladding temperature in the middle region. The cladding temperature at 7th elevation was replaced with that at 10th elevation as the maximum PCT was observed at 10th elevation in the ISP-50 test. As reference data, the cross sectional maximum temperatures at 2nd, 10th, and 12th elevations were used for comparison with the calculations. The final selected parameters are listed in Table 7.2-1.

Table 7.2-1 Weighting factor components for the analyzed parameters

Parameters			Instrument Name	Weighting factor			
	blind	open		w_{exp}	w_{saf}	w_{norm}	w_f
Core power	D1	D1	∑ HP-CO-0i-P	0.8	0.8	0.5	0.32
Pressurizer pressure	D5	D5	PT-PZR-01	1.0	1.0	1.0	1.00
SG1 steam dome pressure	D6	D6	PT-SGSD1-01	1.0	0.6	1.1	0.66
SIT-01 pressure	D8	D8	PT-SIT1-02	1.0	0.6	1.1	0.66
Core inlet temperature	D16	D66	TF-LP-2G18	0.8	0.8	2.4	1.536
Core exit temperature	D17	D67	averaged	0.8	0.8	2.4	1.536
Clad temp. at region 2	D43	D147[2)]	max. at reg. 2	0.9	1.0	1.2	1.08
Clad temp. at region 10[1)]	D48	D155[2)]	max. at reg. 10	0.9	1.0	1.2	1.08
Clad temp. at region 12	D53	D157[2)]	max. at reg. 12	0.9	1.0	1.2	1.08
Hot leg 1 flow rate	D56	D97	QV-HL1-01A+B	0.5	0.8	0.5	0.20
Hot leg 2 flow rate	D57	D98	QV-HL2-01A+B	0.5	0.8	0.5	0.20
Active SIT-01 flow rate	D66	D107	QV-SIT1-01	0.5	0.8	0.5	0.20
Active SIP-02 flow rate	D69	D110	QV-HPSI1-03	0.5	0.8	0.5	0.20
Total break flow rate	D70	D111	calculated	0.5	0.8	0.5	0.20
Accumulated break mass	D71	D112	Integral of D70	0.8	0.9	0.9	0.648
Down-comer level	D72	D114	LT-RPV-04A	0.8	0.9	0.6	0.432
Active core region level	D73	D122	LT-RPV-01	0.8	0.9	0.6	0.432
Pressurizer level	D74	D130	LT-PZR-01	0.8	0.9	0.6	0.432
Collapsed water level IL1A	D75	D131	LT-IL1A-03	0.8	0.9	0.6	0.432
Collapsed water level IL1B	D76	D132	LT-IL1B-03	0.8	0.9	0.6	0.432
Collapsed water level IL2A	D77	D133	LT-IL2A-03	0.8	0.9	0.6	0.432

Collapsed water level IL1B	D78	D134	LT-IL2B-03	0.8	0.9	0.6	0.432

1) Clad temperature at region 7 was used in the blind phase
2) These temperatures were additionally requested and the submitted data were assumed as cross sectional maximum when one-dimensional code was used.

7.2.2 Selection of weighting factors

Weighting factors are used to consider the different importance from the viewpoint of safety analysis and to calculate overall accuracy of the calculation, i.e., the total average amplitude (AA_{tot}). The weighting factors are determined by engineering judgement. In the present analysis, the weighting factors used in Table 1 of the literature [Prosek *et al.*, 2002] were used as listed in Table 7.2-1.

7.2.3 Selection of time interval and number of data

Number of data (N) should be a power with base equal to 2 to perform FFT calculation. A number larger than 512 was suggested in the previous assessment. Experimental data were acquired with a time interval of 1.0 s, but submitted calculations show a variation of a time interval ranging from 0.01 to 10.0 s summarized in Table 4.4-1. Selection of the number of data also depends on the time interval of analysis. Experimental data were obtained up to 2932 s. Most participants provided the calculation time up to the similar time to the data. The number of data needs to be large enough to include a high frequency effect on the final AA_{tot} but does not need to be so large to include higher frequencies than the cut-off frequency. So, the number of data was determined by taking into account the time of internal.

As for the time of internal for the present analysis, the transient behavior of the DVI line break scenario should be identified from the viewpoint of phenomenology. According to the PIRT (Phenomena Identification Ranking Table) performed for the DVI line break, the transient behavior can be categorized into 4 phases: pre-trip phase, post-trip phase, refill phase, and long term cooling phase [Chung *et al.*, 2003].

1) Pre-trip phase: This phase begins with occurrence of the break and ends with reactor trip. Upon occurrence of the break, the reactor begins a fast depressurization, which triggers the reactor trip. It is expected that flashing will start throughout the hottest part of the primary system.
2) Post-trip phase: Once the reactor trips, the heat source decreases rapidly and the rate of depressurization increases more. But sufficient flashing occurs soon throughout the primary system and the most part of primary side approach the saturation condition.

The pressure remains on a plateau during this phase. The pump coastdown leads to the loss of forced circulation and two-phase natural circulation. The flow becomes two-phase flow and a bubble begins to migrate to the top of primary loop. The discharge flows are chocking with two-phase condition until the liquid sealing is cleared completely. Since the break is DVI where location is higher than the level of loop, the two-phase choking continues longer even after the loop seal clearing. Pressure balance is broken by the discharge of steam after the seal clearing. The pressure decreases again and reaches to the set point of SIT pressure. This phase ends with the start of SIT injection. During this phase, the mass inventory decrease significantly and there is a strong possibility of the uncovering of core top. If the steam leakage path is sealed by the injected SI flow, the steam of upper plenum will be accumulated and pushdown the core liquid level. It will result in the core uncover and consequent heating seriously. These processes were addressed as one of significant phenomena and predicted in the CEFLASH code.

3) Refill phase: In this phase, the SITs actuate and a large amount of safety injection water is injected to the down-comer and refills the core. The uncovered part of core rewets quickly and remains cooled as long as SIT is actuating. Fluidic device installed within SIT can make it's duration even longer with controlling the flow by vortex motion. When SIT start, highly subcooled SI water condenses the steam of down-comer rapidly. It reduces down-comer pressure and sucks the core water down.
4) Long term cooling phase: After the using up of SIT water, the core cooling is maintained with one SI pump flow. If the flow is enough to cover the whole primary heat source, the long term cooling is maintained and cooled down eventually to activate residual heat removal (RHR) to remove decay heat of core and other residual source of heat structures. There is still a possibility of bypass although steam velocity is much lower than LBLOCA case. Another process is a gradual heat-up of down-comer water by the residual stored heat of the structure.

Although most submitted calculations assumed that the break was initiated at 0.0 s, but a few calculations used the similar break time around 193.0 s to that measured in the test. In order to perform the FFTBM analysis in the same time domain, the break times in calculations as well as in the test were shifted to 0.0 s. Based on the PIRT results and observed phenomena in the ISP-50 test, three time intervals have been selected to perform the FFTBM as shown in Table 7.2-2. Submitted calculations showed some differences in the time when the core power started to decay, even though the core power began to decay at 33 s. Thus, the shortest time of 24 s was selected as the first time of interval relevant to pre-trip phase among the calculated times when the core power stated to decay. This time frame focuses on the prediction accuracy comparison during the initial blowdown period. In this time frame, all the FFTBM assessments

were carried out at the constant power condition. Despite very short time widow of 24 s, we sampled 512 data for FFT calculation according to suggestion in the literature [Prosek *et al.*, 2002], resulting in a maximum frequency up to 10.66 Hz. The sampling process was done by a linear interpolation of the calculation and the experimental data.

The second time of interval was selected as the time up to which the SITs were activated. This time of sequences also showed more or less small variations in the submitted results. So, the smallest value among those submitted calculations was selected as the second time interval. In this time frame, all the important thermal-hydraulic phenomena are expected to occur, including interaction of the break flow with the ECC flow by SIP and SITs. Also, the loop seal clearing was expected to happen. A total of 1024 data in the second time of interval was sampled by a linear interpolation of the calculation and the experimental data in order to take into account slightly higher frequencies than the cut-off frequency.

The third time of internal was selected to cover entire phenomena relevant to the DVI line break scenario. Most meaningful phenomena took place less than 2000 s even though the test was carried out up to 2932 s. So, the 2000 s was selected as the third time frame of the present FFTBM assessment. This period corresponds to the refill and long term cooling phases defined at the PIRT activity. In this third time of interval, a total of 4096 data was sampled in order to include high frequency contribution up to 1.0 Hz.

Table 7.2-2 Selected time of interval for the present FFTBM analysis

Time of interval	Phase relevant to PIRT	Phenomena observed	Number of data	Max. frequency $f_{max} = 0.5\ f_s$ (Hz)
0~24 s	Pre-trip	Before the core power decay Core power decay at 33 s in the test	512	10.66
0~300 s	Post-trip	Before the SIT injection SIP injection at 54 s in the test SIT injection at 468 s in the test 1st loop seal clearing at 190 s in the test	1024	1.71
0~2000 s	Refill and long term cooling	All the interesting phenomena are included in this time frame	4096	1.02

7.2.4 Cut-off frequency selection

It seems that the effects of the cut-off frequency on the total average amplitude are not so significant. The high frequency errors are more acceptable than the errors caused by low frequency components. Therefore, the cut-off frequency was decided to be close to the maximum frequency, 1.0 Hz. Sensitivity study on the impact of the cut-off frequency on the AA was carried out, but its impact was small if we took 1.0 Hz as a cut-off frequency.

7.3 Accuracy evaluation results for ISP-50 blind calculations

Application of FFTBM to the present ISP-50 blind calculation was performed to evaluate accuracy of the submitted calculation results. The results of FFTBM application are shown from Table 7.3-1 to Table 7.3-15. Evaluations for GP2 and GP3 were not performed as many parameters were not provided. For each participant, three cases with different time frames were calculated. In the first time frame between 0 s to 24 s, 19 parameters out of the selected 22 parameters were used because the SIP and the SIT were not available during this period. The parameters relevant to the SIP and the SIT were excluded in FFTBM calculation. In the second time frame between 0 s to 300 s, the SIT was not activated in the ISP-50 test so that 2 parameters relevant to the SIT were excluded in FFTBM calculation. In the whole time frame calculation, the selected 22 parameters were used to get the final $\mathrm{AA_{tot}}$. For all cases, the cut-off frequency was set to 1.0 Hz. A summary of results of FFTBM application to the ISP-50 can be seen in Table 7.3-16 and Figure 7.3-1

.

In the literature, the accuracy of a given calculation is characterized by the following criteria: [Prosek *et al.*, 2002]

$\mathrm{AA_{tot}} = 0.3$	: very good prediction
$0.3 < \mathrm{AA_{tot}} < 0.5$	: good prediction
$0.5 < \mathrm{AA_{tot}} < 0.7$	: poor prediction
$\mathrm{AA_{tot}} > 0.7$	: very poor prediction

In the first time frame, most calculations resulted in very good prediction of the data except for the KOPEC's calculations. The obtained $\mathrm{AA_{tot}}$ were significantly lower than the acceptable criterion ranging between 0.1 and 0.15. The best prediction was found in the calculations by GP1 (AA=0.108) and FORTUM (AA=0.108). If we looked at the detailed results for each parameter, major discrepancy was originated from incorrect prediction of the total break flow. The flow rate of the hot leg 2 also greatly contributed to the major discrepancy. Especially, the KOPEC's calculations (KOPEC1 and KOPEC2) showed significantly large AAs for the hot leg flow

rates. This result is consistent with the qualitative comparison result shown in Figures B.56-B and B.57-B. Their calculated hot leg flow rates showed a very rapid increase and reached up to around 30 kg/s in the first time frame. However, the break flow rate was not greatly affected by the high loop flow rate. It is recommended that the reason of the abnormally higher hot leg flow rates needs to be investigated so that their calculation need to be improved in the following "open" phase. This overestimation of the hot leg flow rates in the KOPEC's calculations resulted in the worst prediction among the submitted calculations in the first time frame.

In the second time frame, the effect of the SIP injection flow was added to the first time frame. But, the impact of the SIT on the prediction accuracy was still excluded. Most significant thermal-hydraulic phenomena occurred in this time frame. Compared with the first time frame results, most calculations still showed good prediction in this time period. Just like in the first time frame, most disagreements were originated from the hot leg flow rates and the break flow. However, disagreements of the collapsed water levels of the vertical intermediate legs also contributed to large AA in most calculations (KAERI, KEPRI, KTH, NRC, UNIPI, GP4, GRS, FORTUM and VTT). In particular, the water levels in loop 2 resulted in higher AA values than those in loop 1 in many calculations, implying that asymmetric loop seal clearing phenomena observed in the test was not properly predicted in the codes. Among the participants, the CIAE's prediction accuracy of the water level was outstanding.

The third time frame includes most meaningful transient phenomena in the present test. Compared with the previous second time frame, the influence of the SIT injection on the transient behavior was taken into account in this time frame. Qualitatively, the degree of disagreement became wide with respect to time in most calculations as found in the comparison figures in Appendix-B. Disagreement in the early time frame seemed to be amplified with respect to time. Thus, in this third time frame, most calculations showed very poor prediction results according to the criterion of AA.

Incorrect predictions on the hot leg flow rates, the break flow rates, and the collapsed water levels in the vertical intermediate legs in the second time frame were also maintained in the third time frame. In addition, disagreements in the predictions of the SIT flow rate, the SG1 steam dome pressure, the core and the down-comer water levels were added to the final AA. In particular, predictions of the SIT flow rate were very poor in most calculations. In the ISP-50 test, the SIT flow rate showed a fluctuating behavior due to inherent condensation phenomenon at the injection location and this behavior was not properly reproduced in the codes. The SG1 steam dome pressure was also not well predicted in most calculations. CIAE, UNIPI, NRI, GRS, and FORTUM presented relatively better predictions compared with the other

participants. GP4 produced the worst prediction on the SG1 steam dome pressure, AA=1.922. As seen in Figure B.6, the predicted SG1 steam dome pressure by GP4 showed a significantly large peak compared with the data. The calculation results on the collapsed water level in the active core and the down-comer regions were also beyond the acceptable range in most calculations. The VTT's prediction accuracy on the water levels was remarkable among the participants. NRI presented relatively better prediction on the down-comer water level than the prediction on the active core water level. Another disagreement was observed from the predictions on the collapsed water levels in the vertical intermediate legs, implying that the prediction of the loop seal clearing was not reproduced in the codes.

By comparing with the qualitative comparison analysis in the previous chapter, the current FFTBM application results showed very good consistency with them. Overall rank among the calculations by all participants can be found in Figure 7.3-1.

Table 7.3-1 Calculated total accuracy of the KAERI's blind calculation

Number	Parameter	Time of interval					
		0 ~ 24 s		0~ 300 s		0 ~ 1800* s	
		N=512		N=1024		N=4096	
		AA	WF	AA	WF	AA	WF
1	Core power	0.003	0.127	0.023	0.067	0.022	0.089
2	Pressurizer pressure	0.058	0.257	0.088	0.041	0.095	0.107
3	SG1 steam dome pressure	0.036	0.142	0.067	0.103	0.184	0.091
4	SIT-01 pressure	excl.	excl.	excl.	excl.	0.15	0.09
5	Core inlet temperature	0.003	0.2	0.025	0.091	0.032	0.099
6	Core exit temperature	0.01	0.171	0.025	0.082	0.033	0.107
7	Clad temp. at region 2	0.021	0.079	0.04	0.116	0.03	0.061
8	Clad temp. at region 7	0.013	0.221	0.022	0.051	0.038	0.124
9	Clad temp. at region 12	0.008	0.107	0.028	0.107	0.04	0.083
10	Hot leg 1 flow rate	0.394	0.096	1.36	0.173	3.02	0.243
11	Hot leg 2 flow rate	1.466	0.224	1.521	0.187	3.729	0.25
12	Active SIT-01 flow rate	excl.	excl.	excl.	excl.	1.503	0.167
13	Active SIP-02 flow rate	excl.	excl.	0.379	0.129	0.264	0.139
14	Total break flow rate	0.601	0.135	0.865	0.141	1.012	0.146
15	Accumulated break mass	0.401	0.134	0.107	0.009	0.047	0.02
16	Down-comer level	0.014	0.137	0.372	0.074	0.545	0.085
17	Active core region level	0.17	0.144	0.253	0.08	0.41	0.143
18	Pressurizer level	0.115	0.091	0.122	0.14	0.134	0.127
19	Collapsed water level IL1A	0.151	0.115	0.542	0.072	0.609	0.062
20	Collapsed water level IL1B	0.068	0.213	0.508	0.033	0.622	0.041
21	Collapsed water level IL2A	0.14	0.144	1.407	0.089	1.546	0.094
22	Collapsed water level IL2B	0.168	0.083	1.39	0.084	0.8	0.067
	Total (AA_{tot}, WF_{tot})	**0.1**	**0.158**	**0.25**	**0.084**	**0.333**	**0.098**

*excl : excluded in this time of interval

*Maximum calculation is limited to 1800 s

Table 7.3-2 Calculated total accuracy of the KEPRI's blind calculation

Number	Parameter	Time of interval					
		0 ~ 24 s		0~ 300 s		0 ~ 2000 s	
		N=512		N=1024		N=4096	
		AA	WF	AA	WF	AA	WF
1	Core power	0.04	0.009	0.082	0.058	0.083	0.103
2	Pressurizer pressure	0.041	0.141	0.068	0.085	0.072	0.064
3	SG1 steam dome pressure	0.027	0.179	0.098	0.081	0.241	0.091
4	SIT-01 pressure	excl.	excl.	excl.	excl.	0.104	0.121
5	Core inlet temperature	0.004	0.109	0.026	0.082	0.028	0.111
6	Core exit temperature	0.007	0.172	0.017	0.098	0.03	0.101
7	Clad temp. at region 2	0.021	0.042	0.036	0.14	0.029	0.073
8	Clad temp. at region 7	0.005	0.163	0.017	0.136	0.031	0.086
9	Clad temp. at region 12	0.004	0.139	0.019	0.117	0.029	0.091
10	Hot leg 1 flow rate	0.742	0.072	1.351	0.166	2.983	0.221
11	Hot leg 2 flow rate	1.646	0.119	1.519	0.161	3.652	0.219
12	Active SIT-01 flow rate	excl.	excl.	excl.	excl.	1.173	0.185
13	Active SIP-02 flow rate	excl.	excl.	0.825	0.073	0.474	0.077
14	Total break flow rate	0.569	0.19	0.636	0.171	0.772	0.186
15	Accumulated break mass	0.292	0.148	0.062	0.032	0.045	0.085
16	Down-comer level	0.101	0.019	0.235	0.099	0.45	0.107
17	Active core region level	0.304	0.077	0.422	0.045	0.546	0.084
18	Pressurizer level	0.225	0.09	0.235	0.178	0.232	0.188
19	Collapsed water level IL1A	0.274	0.064	0.53	0.079	0.599	0.081
20	Collapsed water level IL1B	0.393	0.037	0.611	0.06	0.619	0.061
21	Collapsed water level IL2A	0.291	0.07	1.601	0.11	1.874	0.101
22	Collapsed water level IL2B	0.225	0.062	1.565	0.105	0.831	0.069
	Total (AA_{tot}, WF_{tot})	**0.134**	**0.113**	**0.271**	**0.101**	**0.34**	**0.1**

*excl : excluded in this time of interval

Table 7.3-3 Calculated total accuracy of the KTH's blind calculation

Number	Parameter	Time of interval					
		0 ~ 24 s		0~ 224[1)] s		0 ~ 2000 s	
		N=512		N=1024		N=4096	
		AA	WF	AA	WF	AA	WF
1	Core power	0.003	0.127	0.039	0.061	0.035	0.07
2	Pressurizer pressure	0.048	0.123	0.255	0.127	0.197	0.016
3	SG1 steam dome pressure	0.03	0.176	0.23	0.078	0.306	0.092
4	SIT-01 pressure	excl.	excl.	excl.	excl.	0.456	0.044
5	Core inlet temperature	0.007	0.185	0.079	0.144	0.125	0.054
6	Core exit temperature	0.004	0.263	0.077	0.134	0.113	0.051
7	Clad temp. at region 2	0.062	0.096	0.115	0.186	0.146	0.112
8	Clad temp. at region 7	0.009	0.073	0.066	0.149	0.096	0.05
9	Clad temp. at region 12	0.017	0.163	0.05	0.098	0.123	0.071
10	Hot leg 1 flow rate	1.101	0.06	1.039	0.117	3.77	0.234
11	Hot leg 2 flow rate	2.122	0.172	0.985	0.131	1.735	0.175
12	Active SIT-01 flow rate	excl.	excl.	excl.	excl.	3.612	0.148
13	Active SIP-02 flow rate	excl.	excl.	0.504	0.127	0.313	0.113
14	Total break flow rate	0.749	0.159	1.045	0.154	1.181	0.17
15	Accumulated break mass	0.688	0.133	0.18	0.033	0.058	0.014
16	Down-comer level	0.148	0.101	0.444	0.079	0.44	0.093
17	Active core region level	0.08	0.165	0.229	0.072	0.436	0.095
18	Pressurizer level	0.22	0.048	0.188	0.064	0.199	0.064
19	Collapsed water level IL1A	0.151	0.115	0.644	0.032	0.629	0.048
20	Collapsed water level IL1B	0.067	0.215	0.474	0.047	0.658	0.059
21	Collapsed water level IL2A	0.141	0.144	1.422	0.09	1.581	0.098
22	Collapsed water level IL2B	0.168	0.083	1.375	0.083	0.825	0.07
	Total (AA_{tot}, WF_{tot})	**0.147**	**0.149**	**0.298**	**0.111**	**0.417**	**0.07**

*excl : excluded in this time of interval

[1)] 2nd time interval was limited to the SIT activation time of 224 s

Table 7.3-4 Calculated total accuracy of the NRC's blind calculation

Number	Parameter	Time of interval					
		0 ~ 24 s		0~ 300 s		0 ~ 2000 s	
		N=512		N=1024		N=4096	
		AA	WF	AA	WF	AA	WF
1	Core power	0.003	0.127	0.006	0.164	0.007	0.192
2	Pressurizer pressure	0.045	0.189	0.079	0.085	0.085	0.051
3	SG1 steam dome pressure	0.03	0.175	0.095	0.111	0.385	0.103
4	SIT-01 pressure	excl.	excl.	excl.	excl.	0.163	0.066
5	Core inlet temperature	0.002	0.163	0.016	0.117	0.051	0.093
6	Core exit temperature	0.012	0.168	0.019	0.097	0.042	0.082
7	Clad temp. at region 2	0.075	0.021	0.086	0.103	0.083	0.132
8	Clad temp. at region 7	0.094	0.014	0.117	0.088	0.115	0.119
9	Clad temp. at region 12	0.035	0.038	0.045	0.093	0.047	0.127
10	Hot leg 1 flow rate	0.736	0.114	1.184	0.105	1.949	0.214
11	Hot leg 2 flow rate	1.384	0.134	1.438	0.104	2.257	0.201
12	Active SIT-01 flow rate	excl.	excl.	excl.	excl.	1.355	0.171
13	Active SIP-02 flow rate	excl.	excl.	0.397	0.115	0.321	0.117
14	Total break flow rate	0.512	0.199	0.708	0.154	0.832	0.187
15	Accumulated break mass	0.205	0.144	0.189	0.1	0.146	0.068
16	Down-comer level	0.009	0.222	0.128	0.077	0.28	0.134
17	Active core region level	0.396	0.027	0.442	0.044	0.53	0.079
18	Pressurizer level	0.2	0.093	0.194	0.133	0.213	0.13
19	Collapsed water level IL1A	0.19	0.092	0.159	0.113	1.298	0.095
20	Collapsed water level IL1B	0.101	0.143	0.179	0.119	0.324	0.091
21	Collapsed water level IL2A	0.18	0.113	1.049	0.125	1.277	0.15
22	Collapsed water level IL2B	0.206	0.068	1.189	0.095	0.768	0.074
	Total (AA_{tot}, WF_{tot})	**0.121**	**0.115**	**0.218**	**0.103**	**0.32**	**0.107**

*excl : excluded in this time of interval

Table 7.3-5 Calculated total accuracy of the CIAE's blind calculation

Number	Parameter	Time of interval					
		0 ~ 24 s		0~ 300 s		0 ~ 1460* s	
		N=512		N=1024		N=4096	
		AA	WF	AA	WF	AA	WF
1	Core power	0.124	0.116	0.093	0.121	0.108	0.096
2	Pressurizer pressure	0.048	0.155	0.044	0.095	0.054	0.099
3	SG1 steam dome pressure	0.026	0.16	0.069	0.069	0.07	0.06
4	SIT-01 pressure	excl.	excl.	excl.	excl.	0.07	0.052
5	Core inlet temperature	0.002	0.166	0.013	0.061	0.022	0.074
6	Core exit temperature	0.007	0.118	0.009	0.076	0.016	0.072
7	Clad temp. at region 2	0.009	0.103	0.016	0.115	0.017	0.067
8	Clad temp. at region 7	0.004	0.22	0.008	0.087	0.016	0.078
9	Clad temp. at region 12	0.002	0.133	0.007	0.075	0.216	0.007
10	Hot leg 1 flow rate	0.681	0.048	0.896	0.119	1.299	0.144
11	Hot leg 2 flow rate	1.519	0.109	0.955	0.128	1.049	0.141
12	Active SIT-01 flow rate	excl.	excl.	excl.	excl.	0.951	0.167
13	Active SIP-02 flow rate	excl.	excl.	0.313	0.109	0.243	0.117
14	Total break flow rate	0.544	0.197	0.626	0.169	0.713	0.172
15	Accumulated break mass	0.254	0.154	0.052	0.049	0.065	0.08
16	Down-comer level	0.014	0.137	0.126	0.104	0.405	0.072
17	Active core region level	0.13	0.123	0.227	0.078	0.309	0.078
18	Pressurizer level	0.081	0.13	0.088	0.121	0.113	0.108
19	Collapsed water level IL1A	0.151	0.115	0.341	0.04	0.419	0.051
20	Collapsed water level IL1B	0.068	0.213	0.361	0.052	0.517	0.053
21	Collapsed water level IL2A	0.14	0.144	0.158	0.107	0.361	0.193
22	Collapsed water level IL2B	0.168	0.083	0.196	0.107	0.734	0.129
	Total (AA_{tot}, WF_{tot})	**0.093**	**0.144**	**0.112**	**0.085**	**0.196**	**0.08**

*excl : excluded in this time of interval

*Maximum calculation is limited to 1460 s

Table 7.3-6 Calculated total accuracy of the KNF's blind calculation

Number	Parameter	Time of interval					
		0 ~ 24 s		0~ 300 s		0 ~ 2000 s	
		N=512		N=1024		N=4096	
		AA	WF	AA	WF	AA	WF
1	Core power	0.045	0.029	0.049	0.084	0.047	0.104
2	Pressurizer pressure	0.046	0.064	0.061	0.129	0.075	0.048
3	SG1 steam dome pressure	0.047	0.107	0.089	0.098	0.227	0.107
4	SIT-01 pressure	excl.	excl.	excl.	excl.	0.179	0.05
5	Core inlet temperature	0.002	0.198	0.019	0.112	0.036	0.064
6	Core exit temperature	0.005	0.115	0.015	0.123	0.029	0.042
7	Clad temp. at region 2	0.033	0.036	0.046	0.163	0.053	0.114
8	Clad temp. at region 7	0.005	0.187	0.015	0.172	0.034	0.091
9	Clad temp. at region 12	0.006	0.256	0.041	0.159	0.321	0.018
10	Hot leg 1 flow rate	0.595	0.057	1.024	0.147	2.995	0.248
11	Hot leg 2 flow rate	2.359	0.091	1.307	0.124	3.171	0.234
12	Active SIT-01 flow rate	excl.	excl.	excl.	excl.	1.19	0.149
13	Active SIP-02 flow rate	excl.	excl.	0.349	0.135	0.266	0.133
14	Total break flow rate	0.728	0.168	0.659	0.176	0.808	0.19
15	Accumulated break mass	0.454	0.145	0.055	0.025	0.036	0.046
16	Down-comer level	0.015	0.137	0.239	0.114	0.502	0.088
17	Active core region level	0.305	0.097	0.498	0.107	0.58	0.071
18	Pressurizer level	0.082	0.113	0.09	0.111	0.111	0.095
19	Collapsed water level IL1A	0.077	0.226	0.347	0.057	0.451	0.052
20	Collapsed water level IL1B	0.175	0.082	0.451	0.055	0.517	0.053
21	Collapsed water level IL2A	0.092	0.22	0.421	0.132	1.575	0.108
22	Collapsed water level IL2B	0.073	0.192	0.293	0.098	0.594	0.129
	Total (AA_{tot}, WF_{tot})	**0.122**	**0.14**	**0.158**	**0.121**	**0.331**	**0.079**

*excl : excluded in this time of interval

Table 7.3-7 Calculated total accuracy of the KOPEC-1's blind calculation

Number	Parameter	Time of interval					
		0 ~ 24 s		0~ 300 s		0 ~ 2000 s	
		N=512		N=1024		N=4096	
		AA	WF	AA	WF	AA	WF
1	Core power[1)]	excl.	excl.	excl.	excl.	excl.	excl.
2	Pressurizer pressure	0.166	0.109	0.114	0.066	0.177	0.075
3	SG1 steam dome pressure	0.048	0.057	0.055	0.081	0.261	0.104
4	SIT-01 pressure	excl.	excl.	excl.	excl.	0.531	0.073
5	Core inlet temperature	0.018	0.107	0.021	0.111	0.252	0.09
6	Core exit temperature	0.063	0.036	0.053	0.085	0.179	0.074
7	Clad temp. at region 2	0.039	0.111	0.04	0.153	0.225	0.107
8	Clad temp. at region 7	0.076	0.087	0.06	0.1	0.194	0.106
9	Clad temp. at region 12	0.076	0.088	0.056	0.073	0.2	0.1
10	Hot leg 1 flow rate	6.766	0.06	6.644	0.133	4.898	0.15
11	Hot leg 2 flow rate	11.63	0.068	6.815	0.136	5.816	0.153
12	Active SIT-01 flow rate	excl.	excl.	excl.	excl.	5.03	0.126
13	Active SIP-02 flow rate	excl.	excl.	0.403	0.127	0.324	0.125
14	Total break flow rate	0.369	0.157	0.581	0.148	0.819	0.165
15	Accumulated break mass	0.059	0.128	0.081	0.03	0.215	0.084
16	Down-comer level	0.031	0.192	0.331	0.083	0.516	0.07
17	Active core region level	0.071	0.1	0.373	0.031	0.75	0.087
18	Pressurizer level	0.156	0.144	0.149	0.164	0.165	0.146
19	Collapsed water level IL1A	0.268	0.065	0.632	0.028	1.767	0.077
20	Collapsed water level IL1B	0.387	0.037	0.998	0.079	1.895	0.081
21	Collapsed water level IL2A	0.289	0.075	0.437	0.069	1.352	0.11
22	Collapsed water level IL2B	0.223	0.069	0.375	0.075	1.338	0.101
	Total (AA_{tot}, WF_{tot})	**0.403**	**0.091**	**0.385**	**0.091**	**0.672**	**0.096**

*excl : excluded in this time of interval

1) core power was excluded because it was not submitted

Table 7.3-8 Calculated total accuracy of the KOPEC-2's blind calculation

Number	Parameter	Time of interval					
		0 ~ 24 s		0~ 300 s		0 ~ 2000 s	
		N=512		N=1024		N=4096	
		AA	WF	AA	WF	AA	WF
1	Core power[1)]	excl.	excl.	excl.	excl.	excl.	excl.
2	Pressurizer pressure	0.168	0.114	0.148	0.094	0.177	0.075
3	SG1 steam dome pressure	0.047	0.073	0.052	0.063	0.242	0.104
4	SIT-01 pressure	excl.	excl.	excl.	excl.	0.547	0.071
5	Core inlet temperature	0.018	0.108	0.038	0.119	0.258	0.09
6	Core exit temperature	0.063	0.035	0.05	0.053	0.182	0.074
7	Clad temp. at region 2	0.039	0.11	0.049	0.162	0.23	0.107
8	Clad temp. at region 7	0.076	0.087	0.063	0.114	0.195	0.105
9	Clad temp. at region 12	0.077	0.088	0.06	0.093	0.2	0.1
10	Hot leg 1 flow rate	6.866	0.061	6.723	0.133	4.808	0.147
11	Hot leg 2 flow rate	11.66	0.07	6.851	0.137	5.693	0.151
12	Active SIT-01 flow rate	excl.	excl.	excl.	excl.	4.174	0.214
13	Active SIP-02 flow rate	excl.	excl.	0.419	0.126	0.323	0.126
14	Total break flow rate	0.289	0.183	0.522	0.156	0.856	0.183
15	Accumulated break mass	0.037	0.135	0.041	0.02	0.223	0.084
16	Down-comer level	0.035	0.168	0.365	0.088	0.465	0.071
17	Active core region level	0.071	0.1	0.382	0.048	0.709	0.083
18	Pressurizer level	0.13	0.163	0.13	0.177	0.147	0.153
19	Collapsed water level IL1A	0.268	0.065	0.535	0.046	1.665	0.073
20	Collapsed water level IL1B	0.387	0.037	0.967	0.079	1.716	0.076
21	Collapsed water level IL2A	0.294	0.08	0.6	0.069	1.178	0.102
22	Collapsed water level IL2B	0.228	0.076	0.54	0.073	1.198	0.093
	Total (AA_{tot}, WF_{tot})	**0.402**	**0.093**	**0.398**	**0.094**	**0.634**	**0.097**

*excl : excluded in this time of interval

1) core power was excluded because it was not submitted

Table 7.3-9 Calculated total accuracy of the UNIPI's blind calculation

Number	Parameter	Time of interval					
		0 ~ 24 s		0~ 300 s		0 ~ 2000 s	
		N=512		N=1024		N=4096	
		AA	WF	AA	WF	AA	WF
1	Core power	0.006	0.12	0.076	0.037	0.069	0.044
2	Pressurizer pressure	0.054	0.061	0.102	0.097	0.084	0.066
3	SG1 steam dome pressure	0.026	0.186	0.062	0.091	0.127	0.091
4	SIT-01 pressure	excl.	excl.	excl.	excl.	0.173	0.081
5	Core inlet temperature	0.003	0.112	0.024	0.106	0.046	0.096
6	Core exit temperature	0.008	0.16	0.024	0.083	0.039	0.08
7	Clad temp. at region 2	0.007	0.088	0.034	0.11	0.047	0.097
8	Clad temp. at region 7	0.005	0.257	0.025	0.087	0.04	0.083
9	Clad temp. at region 12	0.006	0.221	0.024	0.084	0.053	0.079
10	Hot leg 1 flow rate	0.739	0.084	1.007	0.109	1.454	0.179
11	Hot leg 2 flow rate	2.529	0.123	1.415	0.121	1.785	0.17
12	Active SIT-01 flow rate	excl.	excl.	excl.	excl.	1.191	0.16
13	Active SIP-02 flow rate	excl.	excl.	0.365	0.11	0.27	0.124
14	Total break flow rate	0.666	0.147	0.675	0.155	0.795	0.166
15	Accumulated break mass	0.358	0.137	0.051	0.029	0.03	0.054
16	Down-comer level	0.011	0.185	0.241	0.093	0.565	0.072
17	Active core region level	0.093	0.139	0.316	0.062	0.47	0.089
18	Pressurizer level	0.179	0.054	0.162	0.087	0.179	0.086
19	Collapsed water level IL1A	0.151	0.115	0.412	0.047	0.495	0.057
20	Collapsed water level IL1B	0.068	0.213	0.707	0.088	1.072	0.072
21	Collapsed water level IL2A	0.14	0.144	1.007	0.11	0.884	0.095
22	Collapsed water level IL2B	0.168	0.083	1.217	0.099	0.778	0.073
	Total (AA_{tot}, WF_{tot})	**0.118**	**0.144**	**0.22**	**0.089**	**0.267**	**0.086**

*excl : excluded in this time of interval

Table 7.3-10 Calculated total accuracy of the GP1's blind calculation

Number	Parameter	Time of interval					
		0 ~ 24 s		0~ 300 s		0 ~ 2000 s	
		N=512		N=1024		N=4096	
		AA	WF	AA	WF	AA	WF
1	Core power	0.003	0.127	0.017	0.084	0.019	0.091
2	Pressurizer pressure	0.098	0.146	0.212	0.1	0.137	0.024
3	SG1 steam dome pressure	0.031	0.18	0.191	0.081	0.182	0.077
4	SIT-01 pressure	excl.	excl.	excl.	excl.	0.219	0.041
5	Core inlet temperature	0.003	0.131	0.05	0.115	0.042	0.043
6	Core exit temperature	0.011	0.212	0.046	0.12	0.04	0.032
7	Clad temp. at region 2	0.005	0.149	0.219	0.054	0.182	0.057
8	Clad temp. at region 7	0.012	0.275	0.742	0.121	0.513	0.026
9	Clad temp. at region 12	0.011	0.214	0.488	0.13	0.528	0.021
10	Hot leg 1 flow rate	0.76	0.06	1.22	0.124	1.232	0.157
11	Hot leg 2 flow rate	1.146	0.25	1.258	0.15	1.499	0.169
12	Active SIT-01 flow rate	excl.	excl.	excl.	excl.	2.091	0.227
13	Active SIP-02 flow rate	excl.	excl.	0.442	0.121	0.307	0.124
14	Total break flow rate	0.368	0.259	0.575	0.155	0.656	0.18
15	Accumulated break mass	0.048	0.087	0.141	0.08	0.097	0.096
16	Down-comer level	0.13	0.015	0.588	0.045	0.662	0.058
17	Active core region level	0.041	0.207	0.72	0.051	0.64	0.051
18	Pressurizer level	0.199	0.063	0.186	0.073	0.192	0.072
19	Collapsed water level IL1A	0.102	0.17	0.855	0.105	1.578	0.077
20	Collapsed water level IL1B	0.121	0.119	0.982	0.101	1.582	0.076
21	Collapsed water level IL2A	0.091	0.222	0.65	0.17	1.34	0.064
22	Collapsed water level IL2B	0.12	0.116	0.732	0.166	0.776	0.072
	Total (AA_{tot}, WF_{tot})	**0.08**	**0.166**	**0.383**	**0.105**	**0.444**	**0.059**

*excl : excluded in this time of interval

Table 7.3-11 Calculated total accuracy of the GP4's blind calculation

Number	Parameter	Time of interval					
		0 ~ 24 s		0~ 300 s		0 ~ 2000 s	
		N=512		N=1024		N=4096	
		AA	WF	AA	WF	AA	WF
1	Core power	0.003	0.127	0.099	0.032	0.088	0.034
2	Pressurizer pressure	0.12	0.18	0.136	0.055	0.144	0.065
3	SG1 steam dome pressure	0.086	0.011	0.3	0.123	1.922	0.1
4	SIT-01 pressure	excl.	excl.	excl.	excl.	0.183	0.078
5	Core inlet temperature	0.003	0.154	0.024	0.102	0.134	0.065
6	Core exit temperature	0.023	0.172	0.051	0.121	0.451	0.047
7	Clad temp. at region 2	0.052	0.057	0.056	0.119	0.06	0.052
8	Clad temp. at region 7	0.024	0.16	0.126	0.185	0.548	0.042
9	Clad temp. at region 12	0.022	0.119	0.138	0.136	0.557	0.014
10	Hot leg 1 flow rate	1.436	0.128	2.06	0.19	1.82	0.2
11	Hot leg 2 flow rate	1.401	0.145	1.934	0.217	2.072	0.197
12	Active SIT-01 flow rate	excl.	excl.	excl.	excl.	1.107	0.149
13	Active SIP-02 flow rate	excl.	excl.	0.433	0.159	0.333	0.167
14	Total break flow rate	0.733	0.153	0.857	0.207	1.053	0.237
15	Accumulated break mass	0.458	0.152	0.12	0.049	0.051	0.062
16	Down-comer level	0.014	0.137	0.471	0.098	0.882	0.093
17	Active core region level	0.666	0.07	0.744	0.058	0.849	0.067
18	Pressurizer level	0.202	0.149	0.195	0.064	0.197	0.064
19	Collapsed water level IL1A	0.151	0.115	0.451	0.036	0.516	0.05
20	Collapsed water level IL1B	0.068	0.213	0.415	0.047	0.574	0.05
21	Collapsed water level IL2A	0.14	0.144	1.286	0.098	1.589	0.096
22	Collapsed water level IL2B	0.168	0.083	1.272	0.093	0.776	0.071
	Total (AA_{tot}, WF_{tot})	**0.155**	**0.133**	**0.317**	**0.107**	**0.546**	**0.068**

*excl : excluded in this time of interval

Table 7.3-12 Calculated total accuracy of the FORTUM's blind calculation

Number	Parameter	Time of interval					
		0 ~ 24 s		0~ 300 s		0 ~ 2000 s	
		N=512		N=1024		N=4096	
		AA	WF	AA	WF	AA	WF
1	Core power	0	0.28	0.013	0.202	0.012	0.2
2	Pressurizer pressure	0.082	0.195	0.119	0.107	0.144	0.1
3	SG1 steam dome pressure	0.03	0.176	0.09	0.082	0.115	0.091
4	SIT-01 pressure	excl.	excl.	excl.	excl.	0.156	0.051
5	Core inlet temperature	0.003	0.184	0.022	0.101	0.047	0.098
6	Core exit temperature	0.011	0.181	0.02	0.1	0.057	0.102
7	Clad temp. at region 2	0.011	0.04	0.011	0.055	0.053	0.084
8	Clad temp. at region 7	0.01	0.279	0.02	0.144	0.061	0.117
9	Clad temp. at region 12	0.009	0.168	0.018	0.082	0.057	0.096
10	Hot leg 1 flow rate	0.618	0.079	1.019	0.122	1.525	0.194
11	Hot leg 2 flow rate	1.455	0.194	1.309	0.132	2.273	0.202
12	Active SIT-01 flow rate	excl.	excl.	excl.	excl.	4.562	0.234
13	Active SIP-02 flow rate	excl.	excl.	0.386	0.114	0.311	0.12
14	Total break flow rate	0.343	0.123	0.606	0.095	0.667	0.102
15	Accumulated break mass	0.172	0.131	0.094	0.117	0.073	0.067
16	Down-comer level	0.014	0.136	0.18	0.051	0.378	0.102
17	Active core region level	0.059	0.163	0.257	0.085	0.432	0.124
18	Pressurizer level	0.152	0.122	0.152	0.12	0.175	0.114
19	Collapsed water level IL1A	0.151	0.115	0.786	0.108	1.531	0.082
20	Collapsed water level IL1B	0.068	0.213	0.91	0.103	1.511	0.088
21	Collapsed water level IL2A	0.14	0.144	1.368	0.092	1.589	0.095
22	Collapsed water level IL2B	0.168	0.083	1.331	0.088	0.778	0.069
	Total (AA_{tot}, WF_{tot})	**0.086**	**0.165**	**0.249**	**0.101**	**0.397**	**0.103**

*excl : excluded in this time of interval

Table 7.3-13 Calculated total accuracy of the GRS's blind calculation

Number	Parameter	Time of interval					
		0 ~ 24 s		0~ 300 s		0 ~ 2000 s	
		N=512		N=1024		N=4096	
		AA	WF	AA	WF	AA	WF
1	Core power	0.002	0.16	0.012	0.09	0.013	0.124
2	Pressurizer pressure	0.023	0.052	0.073	0.095	0.05	0.032
3	SG1 steam dome pressure	0.028	0.158	0.066	0.091	0.095	0.083
4	SIT-01 pressure	excl.	excl.	excl.	excl.	0.091	0.039
5	Core inlet temperature	0.007	0.055	0.02	0.081	0.035	0.106
6	Core exit temperature	0.003	0.104	0.017	0.106	0.251	0.019
7	Clad temp. at region 2	0.013	0.034	0.013	0.052	0.024	0.087
8	Clad temp. at region 7	0.01	0.105	0.018	0.123	0.471	0.014
9	Clad temp. at region 12	0.006	0.055	0.017	0.105	0.468	0.009
10	Hot leg 1 flow rate	0.629	0.112	1.144	0.102	1.143	0.162
11	Hot leg 2 flow rate	1.798	0.135	1.313	0.107	1.256	0.148
12	Active SIT-01 flow rate	excl.	excl.	excl.	excl.	1.437	0.199
13	Active SIP-02 flow rate	excl.	excl.	1.0	0.1	0.653	0.074
14	Total break flow rate	0.713	0.165	0.767	0.154	0.874	0.174
15	Accumulated break mass	0.378	0.141	0.155	0.09	0.119	0.088
16	Down-comer level	0.012	0.166	0.145	0.13	0.633	0.075
17	Active core region level	0.087	0.166	0.434	0.075	0.74	0.057
18	Pressurizer level	0.121	0.077	0.114	0.095	0.136	0.084
19	Collapsed water level IL1A	0.151	0.115	0.475	0.039	0.555	0.05
20	Collapsed water level IL1B	0.067	0.215	0.897	0.107	1.592	0.077
21	Collapsed water level IL2A	0.141	0.144	1.087	0.118	1.642	0.093
22	Collapsed water level IL2B	0.168	0.083	0.696	0.053	1.003	0.104
	Total (AA_{tot}, WF_{tot})	**0.102**	**0.1**	**0.222**	**0.093**	**0.411**	**0.067**

*excl : excluded in this time of interval

Table 7.3-14 Calculated total accuracy of the NRI's blind calculation

Number	Parameter	Time of interval					
		0 ~ 24 s		0~ 300 s		0 ~ 2000 s	
		N=512		N=1024		N=4096	
		AA	WF	AA	WF	AA	WF
1	Core power	0.003	0.127	0.152	0.023	0.13	0.024
2	Pressurizer pressure	0.055	0.081	0.142	0.088	0.18	0.08
3	SG1 steam dome pressure	0.029	0.176	0.08	0.067	0.062	0.068
4	SIT-01 pressure	excl.	excl.	excl.	excl.	0.328	0.082
5	Core inlet temperature	0.011	0.034	0.042	0.128	0.237	0.098
6	Core exit temperature	0.02	0.133	0.035	0.104	0.208	0.096
7	Clad temp. at region 2	0.027	0.203	0.058	0.137	0.233	0.106
8	Clad temp. at region 7	0.031	0.122	0.04	0.088	0.208	0.094
9	Clad temp. at region 12	0.019	0.146	0.036	0.104	0.208	0.096
10	Hot leg 1 flow rate	0.785	0.061	0.934	0.102	1.904	0.119
11	Hot leg 2 flow rate	1.401	0.123	1.134	0.128	1.126	0.174
12	Active SIT-01 flow rate	excl.	excl.	excl.	excl.	1.37	0.119
13	Active SIP-02 flow rate	excl.	excl.	0.336	0.109	0.273	0.121
14	Total break flow rate	0.443	0.223	0.65	0.166	0.744	0.193
15	Accumulated break mass	0.811	0.14	0.711	0.096	0.383	0.072
16	Down-comer level	0.01	0.2	0.09	0.067	0.205	0.141
17	Active core region level	0.07	0.1	0.324	0.034	0.586	0.092
18	Pressurizer level	0.192	0.06	0.163	0.079	0.178	0.076
19	Collapsed water level IL1A	0.102	0.17	0.802	0.103	1.522	0.079
20	Collapsed water level IL1B	0.121	0.119	0.927	0.099	1.53	0.078
21	Collapsed water level IL2A	0.091	0.222	0.175	0.1	0.384	0.191
22	Collapsed water level IL2B	0.12	0.116	0.146	0.148	0.947	0.108
	Total (AA_{tot}, WF_{tot})	**0.124**	**0.127**	**0.213**	**0.101**	**0.405**	**0.098**

*excl : excluded in this time of interval

Table 7.3-15 Calculated total accuracy of the VTT's blind calculation

Number	Parameter	Time of interval					
		0 ~ 24 s		0~ 300 s		0 ~ 2000 s	
		N=512		N=1024		N=4096	
		AA	WF	AA	WF	AA	WF
1	Core power	0.003	0.124	0.054	0.043	0.05	0.053
2	Pressurizer pressure	0.084	0.078	0.102	0.107	0.133	0.057
3	SG1 steam dome pressure	0.03	0.175	0.066	0.046	0.211	0.097
4	SIT-01 pressure	excl.	excl.	excl.	excl.	0.177	0.04
5	Core inlet temperature	0.005	0.084	0.024	0.115	0.041	0.062
6	Core exit temperature	0.008	0.121	0.021	0.123	0.048	0.08
7	Clad temp. at region 2	0.015	0.052	0.014	0.098	0.041	0.074
8	Clad temp. at region 7	0.005	0.116	0.019	0.122	0.054	0.091
9	Clad temp. at region 12	0.004	0.107	0.019	0.124	0.056	0.095
10	Hot leg 1 flow rate	0.579	0.078	2.159	0.193	2.061	0.211
11	Hot leg 2 flow rate	1.624	0.128	2.093	0.183	2.206	0.216
12	Active SIT-01 flow rate	excl.	excl.	excl.	excl.	6.627	0.278
13	Active SIP-02 flow rate	excl.	excl.	0.3	0.126	0.239	0.122
14	Total break flow rate	0.655	0.194	0.677	0.189	0.807	0.206
15	Accumulated break mass	0.312	0.143	0.039	0.047	0.046	0.07
16	Down-comer level	0.138	0.014	0.229	0.044	0.507	0.107
17	Active core region level	0.072	0.212	0.225	0.086	0.351	0.105
18	Pressurizer level	0.356	0.1	0.25	0.058	0.247	0.061
19	Collapsed water level IL1A	0.127	0.137	0.407	0.061	0.513	0.051
20	Collapsed water level IL1B	0.231	0.063	0.458	0.049	0.551	0.042
21	Collapsed water level IL2A	0.143	0.142	1.368	0.11	1.783	0.096
22	Collapsed water level IL2B	0.082	0.172	1.351	0.104	0.822	0.065
	Total (AA_{tot}, WF_{tot})	**0.113**	**0.11**	**0.251**	**0.1**	**0.384**	**0.084**

*excl : excluded in this time of interval

Table 7.3-16 Summary of the results of FFTBM to ISP-50 blind calculation

Group	Participant/Code		Time of interval					
			0 ~ 24 s		0~ 300 s		0 ~ 2000 s	
			N=512		N=1024		N=4096	
			AA_{tot}	WF_{tot}	AA_{tot}	WF_{tot}	AA_{tot}	WF_{tot}
A	KAERI	MARS-KS	0.1	0.158	0.25	0.084	0.333	0.098
	KEPRI	MARS-KS	0.134	0.113	0.271	0.101	0.34	0.1
	KTH	TRACE 5.0 p. 01	0.147	0.149	0.298	0.111	0.417	0.07
	USNRC	TRACE 5.200	0.121	0.115	0.218	0.103	0.32	0.107
B	CIAE	R5/M3.3	0.093	0.144	0.112	0.085	0.196	0.08
	KNF	R5/M3.3	0.122	0.14	0.158	0.121	0.331	0.079
	KOPEC1	RELAP-ME	0.403	0.091	0.385	0.091	0.672	0.096
	KOPEC2	R5/M3.3	0.402	0.093	0.398	0.094	0.634	0.097
	UNIPI	R5/M3.3	0.118	0.144	0.22	0.089	0.267	0.086
C	GP1	KORSAR	0.08	0.166	0.383	0.105	0.444	0.059
	GP2	KORSAR	-	-	-	-	-	-
	GP3	KORSAR	-	-	-	-	-	-
	GP4	TECH-M-97	0.155	0.133	0.317	0.107	0.546	0.068
D	FORTUM	APROS	0.086	0.165	0.249	0.101	0.397	0.103
	GRS	ATHLET M2.2	0.102	0.1	0.222	0.093	0.411	0.067
	NRI	ATHLET	0.124	0.127	0.213	0.101	0.405	0.098
	VTT	APROS	0.113	0.11	0.251	0.1	0.384	0.084

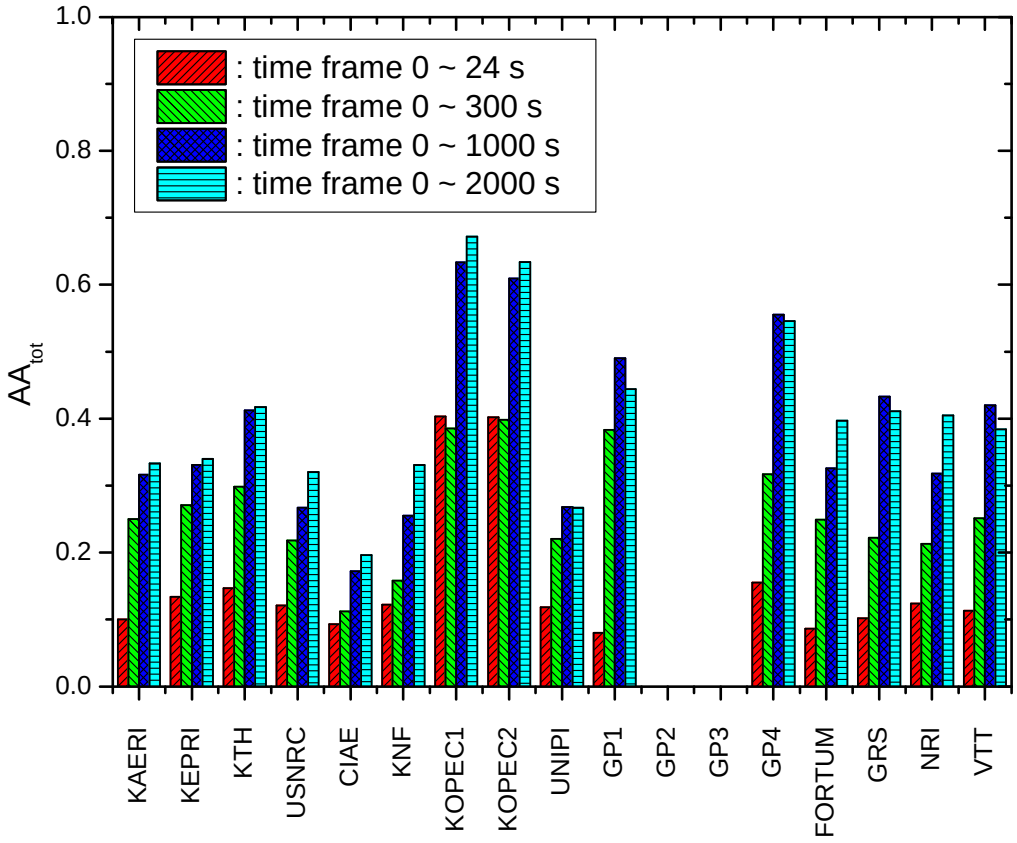

Figure 7.3-1 Comparison of the prediction accuracy of the participants based on FFTBM

7.4 Accuracy evaluation results for ISP-50 open calculations

The same methodology used in the blind calculation was applied to the open calculation in order to investigate how much the open calculation results were improved compared with those of the blind calculation. The results of the FFTBM application are shown from Table 7.4-1 to Table 7.4-16. Note that one parameter for the FFTBM calculation was changed in this open calculation. In the blind case, the cladding temperature at region 7 was selected as the 8th parameter to represent the PCT behavior as shown in the previous section. However, the peak cladding temperature was observed at region 10 in the actual test. Thus, it is considered that the temperature at region 10 is a more appropriate one than the temperature at region 7 to represent the PCT behavior. Hence, the cladding temperature at region 10 replaced the 8th parameter in the present open calculation. Therefore, three cladding temperatures at regions of 2, 10, and 12 were selected and compared with the experimental data. Many experimental data are available even at the same elevations. In the ISP-50 test, 16 cladding temperatures were measured at the same elevation in the lower region of the core and 20 cladding temperatures were obtained in the upper region of the core. As most calculations were based on

one-dimensional modeling of the core and only one cladding temperature at each elevation was collected, the submitted cladding temperature was regarded as the cross sectional maximum. Thus, the cross sectional maximum temperature was obtained from many measured data and it was compared with the submitted calculation.

Prediction accuracy was evaluated at three time frame, taking into account the different transient phases. The calculated AA and WF for each selected parameter of each calculation is shown from Table 7.4-1 to Table 7.4-16. The total AA and WF of each calculation is summarized in Table 7.4-17. Calculated AA_{tot} results at three time frames are plotted in Figure 7.4-1. As the time frame becomes longer, AA_{tot} becomes larger. But, most calculations showed very good prediction accuracy. The largest AA_{tot} (0.379) was obtained by GP2, but the difference from the other calculations was very small to be neglected. The smallest AA_{tot} (0.201) was obtained by CIAE. In the FFTBM, it is widely accepted that only AA_{tot} can have a physical meaning as an index for accuracy quantification and WF_{tot} can be neglected. Thus, comparison of AA_{tot} between the blind and the open calculations was performed and shown in Table 7.4-18. For convenience, improvement of the prediction accuracy was defined as

$$I = (AA_{tot,open} - AA_{tot,blind}) / AA_{tot,blind} .$$

Negative value of I indicates an improvement in prediction accuracy based on FFTBM and positive I means a worse in prediction accuracy. This 'I' value was included in the comparison table and plotted in Figure 7.4-2. This comparison is also plotted from Figure 7.4-3 to Figure 7.4-5 for each time frame, respectively. It can be seen from these figures that better prediction accuracy than the blind calculations was obtained in the most open calculations.

In the first time frame (0 s to 24 s) as shown in Figure 7.4-3, the calculated AA_{tot} showed more or less the similar values as the blind cases. But, the KOPEC1's calculation showed a significant improvement among the other calculations. In the open phase, all the calculations showed excellent prediction accuracy where AA_{tot} values were less than 0.1. Comparison of the second time frame is shown in Figure 7.4-4. Great improvement can be seen from the figure. Most calculations have AA_{tot} values near 0.2. The CIAE's calculation showed 20.5% worse prediction than the blind case because a little worse prediction of the pressurizer pressure was obtained. Though the 'I' value seems to be great, but the obtained AA_{tot} value of 0.135 still represents an excellent prediction. Comparison results of the third time frame are shown in Figure 7.4-5. It is noteworthy that KOPEC1 showed an improvement of 44.6%. They are GP1, GRS, NRI, and VTT that showed improvement around 25%. Meanwhile, KEPRI, NRC, CIAE, and UNIPI showed a little worse calculation results compared with the blind calculations.

In case of KEPRI, the open calculation resulted in higher PCTs and more oscillating SIT flow rates than those in the blind phase. The prediction of the loop seal clearing phenomena was also more or less worsened, causing 5.6% deterioration in AA_{tot} value. The NRC's calculation showed improved predictions of the most parameters in the open phase. However, more oscillating prediction of the hot leg and the SIT flow rates in later phase of the transient than the blind calculation counterbalanced the improvement, resulting in 8.8% deterioration in AA_{tot} value. CIAE presented the best prediction accuracy in the blind and the open calculation. The 2.6% worse in AA_{tot} value is not a big deal. Finally, the UNIPI's calculation showed 4.1% worse than the blind calculation. A little worse result in predicting the hot leg flow rates caused this worse. Average improvement for each time interval was 19%, 16%, and 12%, respectively.

Detailed distribution of AA for each calculation is shown from Figure 7.4-6 to Figure 7.4-21. As seen in these figure, the parameters which were not predicted well are hot leg flow rate, SIT flow rate and the collapsed water level in the intermediate legs. This finding was also mentioned in the previous blind calculation. Though a little improvement was observed in the open phase, these parameters are still dominant factors to degrade the total prediction accuracy. Relatively, the critical flow was well predicted. It seems that most participants used their own expertise to obtain the same break flow rate as the data. It was also found that prediction of the behavior of the collapsed water levels was much improved. This improvement can also be found in the comparison table of sequence of events summarized from Table 5.3-4 and Table 5.3-7.

Table 7.4-1 Calculated total accuracy of the KAERI's open calculation

Number	Parameter	Time of interval					
		0 ~ 24 s		0~ 300 s		0 ~ 1800* s	
		N=512		N=1024		N=4096	
		AA	WF	AA	WF	AA	WF
1	Core power	0.002	0.158	0.004	0.192	0.007	0.201
2	Pressurizer pressure	0.157	0.168	0.153	0.036	0.131	0.035
3	SG1 steam dome pressure	0.008	0.031	0.063	0.114	0.107	0.097
4	SIT-01 pressure	excl.	excl.	excl.	excl.	0.090	0.075
5	Core inlet temperature	0.002	0.174	0.016	0.065	0.023	0.093
6	Core exit temperature	0.004	0.192	0.007	0.077	0.017	0.097
7	Clad temp. at region 2	0.007	0.203	0.011	0.071	0.016	0.133
8	Clad temp. at region 10	0.007	0.143	0.018	0.098	0.023	0.128
9	Clad temp. at region 12	0.005	0.222	0.015	0.185	0.022	0.109
10	Hot leg 1 flow rate	0.357	0.099	1.374	0.155	2.997	0.257
11	Hot leg 2 flow rate	1.600	0.111	1.486	0.159	3.537	0.262
12	Active SIT-01 flow rate	excl.	excl.	excl.	excl.	1.585	0.168
13	Active SIP-02 flow rate	excl.	excl.	0.426	0.114	0.329	0.108
14	Total break flow rate	0.544	0.193	0.593	0.186	0.709	0.204
15	Accumulated break mass	0.264	0.149	0.035	0.079	0.023	0.099
16	Down-comer level	0.014	0.137	0.179	0.107	0.426	0.101
17	Active core region level	0.252	0.173	1.028	0.083	0.776	0.061
18	Pressurizer level	0.395	0.096	0.284	0.075	0.272	0.074
19	Collapsed water level IL1A	0.150	0.116	0.266	0.104	0.376	0.100
20	Collapsed water level IL1B	0.068	0.211	0.357	0.086	1.138	0.117
21	Collapsed water level IL2A	0.140	0.145	0.460	0.083	0.870	0.100
22	Collapsed water level IL2B	0.167	0.084	1.131	0.104	1.000	0.133
	Total (AA_{tot}, WF_{tot})	**0.110**	**0.160**	**0.210**	**0.096**	**0.322**	**0.108**

*excl : excluded in this time of interval

*Maximum calculation is limited to 1800 s

Table 7.4-2 Calculated total accuracy of the KEPRI's open calculation

Number	Parameter	Time of interval					
		0 ~ 24 s		0~ 300 s		0 ~ 2000 s	
		N=512		N=1024		N=4096	
		AA	WF	AA	WF	AA	WF
1	Core power	0.040	0.009	0.078	0.064	0.079	0.107
2	Pressurizer pressure	0.044	0.162	0.047	0.086	0.053	0.100
3	SG1 steam dome pressure	0.027	0.180	0.083	0.148	0.231	0.098
4	SIT-01 pressure	excl.	excl.	excl.	excl.	0.068	0.088
5	Core inlet temperature	0.004	0.122	0.012	0.061	0.020	0.108
6	Core exit temperature	0.003	0.235	0.009	0.062	0.019	0.125
7	Clad temp. at region 2	0.006	0.173	0.019	0.130	0.024	0.130
8	Clad temp. at region 10	0.008	0.084	0.038	0.145	0.107	0.057
9	Clad temp. at region 12	0.007	0.162	0.015	0.109	0.135	0.037
10	Hot leg 1 flow rate	0.765	0.069	1.097	0.133	2.976	0.258
11	Hot leg 2 flow rate	1.713	0.155	1.284	0.143	3.619	0.262
12	Active SIT-01 flow rate	excl.	excl.	excl.	excl.	1.727	0.252
13	Active SIP-02 flow rate	excl.	excl.	0.395	0.074	0.287	0.096
14	Total break flow rate	0.548	0.188	0.632	0.201	0.796	0.239
15	Accumulated break mass	0.295	0.150	0.041	0.020	0.061	0.092
16	Down-comer level	0.011	0.187	0.164	0.092	0.448	0.086
17	Active core region level	0.075	0.211	0.450	0.045	0.788	0.112
18	Pressurizer level	0.247	0.093	0.261	0.176	0.252	0.183
19	Collapsed water level IL1A	0.268	0.065	0.518	0.055	0.555	0.067
20	Collapsed water level IL1B	0.387	0.037	0.559	0.056	1.323	0.121
21	Collapsed water level IL2A	0.286	0.071	1.085	0.140	0.904	0.070
22	Collapsed water level IL2B	0.220	0.064	1.078	0.132	1.000	0.116
	Total (AA_{tot}, WF_{tot})	**0.123**	**0.141**	**0.213**	**0.096**	**0.359**	**0.108**

*excl : excluded in this time of interval

Table 7.4-3 Calculated total accuracy of the KTH's open calculation

Number	Parameter	Time of interval					
		0 ~ 24 s		0~ 224[1)] s		0 ~ 2000 s	
		N=512		N=1024		N=4096	
		AA	WF	AA	WF	AA	WF
1	Core power	0.003	0.127	0.013	0.102	0.013	0.133
2	Pressurizer pressure	0.101	0.185	0.084	0.037	0.073	0.023
3	SG1 steam dome pressure	0.030	0.175	0.053	0.069	0.056	0.061
4	SIT-01 pressure	excl.	excl.	excl.	excl.	0.118	0.060
5	Core inlet temperature	0.003	0.133	0.015	0.056	0.027	0.087
6	Core exit temperature	0.021	0.143	0.017	0.034	0.028	0.062
7	Clad temp. at region 2	0.011	0.165	0.010	0.083	0.024	0.078
8	Clad temp. at region 10	0.013	0.177	0.020	0.080	0.032	0.069
9	Clad temp. at region 12	0.018	0.166	0.018	0.062	0.027	0.062
10	Hot leg 1 flow rate	0.497	0.086	1.220	0.090	2.137	0.199
11	Hot leg 2 flow rate	1.153	0.141	1.548	0.085	2.808	0.187
12	Active SIT-01 flow rate	excl.	excl.	excl.	excl.	2.126	0.233
13	Active SIP-02 flow rate	excl.	excl.	0.421	0.107	0.340	0.105
14	Total break flow rate	0.312	0.134	0.628	0.110	0.686	0.127
15	Accumulated break mass	0.208	0.117	0.243	0.091	0.206	0.086
16	Down-comer level	0.008	0.252	0.173	0.071	0.341	0.172
17	Active core region level	0.738	0.010	0.757	0.024	0.905	0.088
18	Pressurizer level	0.145	0.072	0.126	0.078	0.140	0.089
19	Collapsed water level IL1A	0.325	0.054	0.635	0.057	1.210	0.162
20	Collapsed water level IL1B	0.450	0.032	0.698	0.048	1.523	0.102
21	Collapsed water level IL2A	0.343	0.059	1.267	0.143	0.999	0.069
22	Collapsed water level IL2B	0.275	0.051	0.810	0.122	1.000	0.133
	Total (AA_{tot}, WF_{tot})	**0.137**	**0.134**	**0.241**	**0.068**	**0.353**	**0.087**

*excl : excluded in this time of interval

[1)] 2nd time interval was limited to the SIT activation time of 224 s

Table 7.4-4 Calculated total accuracy of the NRC's open calculation

Number	Parameter	Time of interval					
		0 ~ 24 s		0~ 300 s		0 ~ 2000 s	
		N=512		N=1024		N=4096	
		AA	WF	AA	WF	AA	WF
1	Core power	0.051	0.007	0.055	0.023	0.056	0.049
2	Pressurizer pressure	0.072	0.191	0.068	0.075	0.097	0.065
3	SG1 steam dome pressure	0.030	0.175	0.065	0.070	0.095	0.079
4	SIT-01 pressure	excl.	excl.	excl.	excl.	0.215	0.082
5	Core inlet temperature	0.001	0.239	0.013	0.102	0.062	0.092
6	Core exit temperature	0.016	0.148	0.017	0.091	0.061	0.089
7	Clad temp. at region 2	0.009	0.129	0.020	0.130	0.059	0.102
8	Clad temp. at region 10	0.008	0.082	0.026	0.134	0.064	0.109
9	Clad temp. at region 12	0.010	0.047	0.022	0.152	0.064	0.109
10	Hot leg 1 flow rate	0.483	0.098	1.245	0.123	3.290	0.256
11	Hot leg 2 flow rate	1.014	0.147	1.287	0.121	4.108	0.260
12	Active SIT-01 flow rate	excl.	excl.	excl.	excl.	1.492	0.200
13	Active SIP-02 flow rate	excl.	excl.	0.411	0.113	0.331	0.112
14	Total break flow rate	0.373	0.233	0.658	0.144	0.861	0.186
15	Accumulated break mass	0.129	0.166	0.214	0.099	0.170	0.073
16	Down-comer level	0.014	0.137	0.095	0.081	0.252	0.129
17	Active core region level	0.126	0.151	0.217	0.088	0.714	0.114
18	Pressurizer level	0.101	0.123	0.104	0.125	0.119	0.102
19	Collapsed water level IL1A	0.151	0.115	0.277	0.117	0.390	0.109
20	Collapsed water level IL1B	0.068	0.213	0.256	0.077	1.091	0.116
21	Collapsed water level IL2A	0.140	0.144	0.188	0.131	0.774	0.131
22	Collapsed water level IL2B	0.168	0.083	1.078	0.106	1.000	0.116
	Total (AA_{tot}, WF_{tot})	**0.076**	**0.143**	**0.162**	**0.106**	**0.348**	**0.104**

*excl : excluded in this time of interval

Table 7.4-5 Calculated total accuracy of the CIAE's open calculation

Number	Parameter	Time of interval					
		0 ~ 24 s		0~ 300 s		0 ~ 1460* s	
		N=512		N=1024		N=4096	
		AA	WF	AA	WF	AA	WF
1	Core power	0.134	0.116	0.098	0.126	0.114	0.099
2	Pressurizer pressure	0.047	0.149	0.258	0.098	0.230	0.100
3	SG1 steam dome pressure	0.026	0.160	0.067	0.070	0.063	0.054
4	SIT-01 pressure	0.000	0.000	0.000	0.000	0.065	0.071
5	Core inlet temperature	0.002	0.166	0.018	0.052	0.026	0.084
6	Core exit temperature	0.005	0.153	0.010	0.082	0.016	0.070
7	Clad temp. at region 2	0.006	0.198	0.017	0.091	0.021	0.082
8	Clad temp. at region 10	0.008	0.135	0.022	0.115	0.027	0.106
9	Clad temp. at region 12	0.006	0.109	0.013	0.071	0.111	0.016
10	Hot leg 1 flow rate	0.640	0.050	0.881	0.120	1.333	0.153
11	Hot leg 2 flow rate	1.489	0.110	0.973	0.130	1.090	0.140
12	Active SIT-01 flow rate	0.000	0.000	0.000	0.000	0.947	0.168
13	Active SIP-02 flow rate	0.000	0.000	0.314	0.109	0.248	0.116
14	Total break flow rate	0.545	0.196	0.618	0.171	0.702	0.174
15	Accumulated break mass	0.253	0.154	0.051	0.061	0.069	0.082
16	Down-comer level	0.014	0.137	0.156	0.073	0.369	0.065
17	Active core region level	0.111	0.185	0.217	0.060	0.331	0.073
18	Pressurizer level	0.078	0.133	0.086	0.121	0.111	0.108
19	Collapsed water level IL1A	0.151	0.115	0.341	0.046	0.422	0.054
20	Collapsed water level IL1B	0.068	0.213	0.369	0.051	0.514	0.053
21	Collapsed water level IL2A	0.140	0.144	0.174	0.099	0.394	0.175
22	Collapsed water level IL2B	0.168	0.083	0.264	0.090	0.659	0.131
	Total (AA_{tot}, WF_{tot})	**0.092**	**0.149**	**0.135**	**0.084**	**0.201**	**0.085**

*excl : excluded in this time of interval

*Maximum calculation is limited to 1460 s

Table 7.4-6 Calculated total accuracy of the KNF's open calculation

Number	Parameter	Time of interval					
		0 ~ 24 s		0~ 300 s		0 ~ 2000 s	
		N=512		N=1024		N=4096	
		AA	WF	AA	WF	AA	WF
1	Core power	0.002	0.176	0.020	0.082	0.023	0.089
2	Pressurizer pressure	0.039	0.195	0.058	0.047	0.059	0.059
3	SG1 steam dome pressure	0.038	0.162	0.076	0.129	0.083	0.116
4	SIT-01 pressure	excl.	excl.	excl.	excl.	0.091	0.094
5	Core inlet temperature	0.004	0.077	0.015	0.067	0.027	0.096
6	Core exit temperature	0.008	0.167	0.011	0.042	0.023	0.103
7	Clad temp. at region 2	0.025	0.056	0.025	0.117	0.022	0.060
8	Clad temp. at region 10	0.005	0.113	0.018	0.111	0.025	0.093
9	Clad temp. at region 12	0.004	0.197	0.013	0.084	0.062	0.081
10	Hot leg 1 flow rate	0.506	0.065	1.180	0.138	2.552	0.204
11	Hot leg 2 flow rate	2.135	0.100	1.306	0.123	3.015	0.213
12	Active SIT-01 flow rate	excl.	excl.	excl.	excl.	1.691	0.157
13	Active SIP-02 flow rate	excl.	excl.	0.320	0.144	0.257	0.139
14	Total break flow rate	0.499	0.190	0.562	0.169	0.668	0.193
15	Accumulated break mass	0.268	0.154	0.045	0.098	0.062	0.080
16	Down-comer level	0.014	0.139	0.145	0.101	0.339	0.097
17	Active core region level	0.099	0.198	0.253	0.067	0.690	0.110
18	Pressurizer level	0.129	0.102	0.112	0.086	0.125	0.082
19	Collapsed water level IL1A	0.102	0.170	0.313	0.071	0.453	0.077
20	Collapsed water level IL1B	0.121	0.119	0.406	0.062	1.185	0.113
21	Collapsed water level IL2A	0.091	0.222	1.131	0.114	0.876	0.064
22	Collapsed water level IL2B	0.120	0.116	0.208	0.111	1.000	0.116
	Total (AA_{tot}, WF_{tot})	**0.097**	**0.140**	**0.159**	**0.087**	**0.302**	**0.096**

*excl : excluded in this time of interval

Table 7.4-7 Calculated total accuracy of the KOPEC-1's open calculation

Number	Parameter	Time of interval					
		0 ~ 24 s		0~ 300 s		0 ~ 2000 s	
		N=512		N=1024		N=4096	
		AA	WF	AA	WF	AA	WF
1	Core power	0.001	0.263	0.036	0.061	0.034	0.065
2	Pressurizer pressure	0.033	0.236	0.074	0.093	0.066	0.036
3	SG1 steam dome pressure	0.021	0.215	0.071	0.122	0.289	0.100
4	SIT-01 pressure	excl.	excl.	excl.	excl.	0.125	0.043
5	Core inlet temperature	0.002	0.207	0.018	0.108	0.024	0.067
6	Core exit temperature	0.010	0.198	0.017	0.083	0.022	0.050
7	Clad temp. at region 2	0.025	0.056	0.038	0.121	0.034	0.074
8	Clad temp. at region 10	0.005	0.152	0.071	0.114	0.372	0.026
9	Clad temp. at region 12	0.007	0.190	0.023	0.110	0.210	0.016
10	Hot leg 1 flow rate	0.565	0.069	1.020	0.144	1.498	0.217
11	Hot leg 2 flow rate	2.001	0.195	1.390	0.149	3.004	0.258
12	Active SIT-01 flow rate	excl.	excl.	excl.	excl.	1.589	0.217
13	Active SIP-02 flow rate	excl.	excl.	0.393	0.125	0.289	0.128
14	Total break flow rate	0.575	0.209	0.643	0.203	0.823	0.233
15	Accumulated break mass	0.254	0.147	0.058	0.024	0.025	0.023
16	Down-comer level	0.014	0.137	0.230	0.095	0.445	0.099
17	Active core region level	0.101	0.163	0.246	0.086	0.679	0.121
18	Pressurizer level	0.073	0.124	0.097	0.129	0.116	0.101
19	Collapsed water level IL1A	0.151	0.115	0.732	0.113	1.063	0.082
20	Collapsed water level IL1B	0.067	0.215	0.874	0.105	1.569	0.064
21	Collapsed water level IL2A	0.141	0.144	1.082	0.108	0.856	0.064
22	Collapsed water level IL2B	0.168	0.083	1.073	0.101	1.000	0.116
	Total (AA_{tot}, WF_{tot})	**0.096**	**0.169**	**0.229**	**0.103**	**0.372**	**0.071**

*excl : excluded in this time of interval

Table 7.4-8 Calculated total accuracy of the PSI's open calculation

Number	Parameter	Time of interval					
		0 ~ 24 s		0~ 300 s		0 ~ 2000 s	
		N=512		N=1024		N=4096	
		AA	WF	AA	WF	AA	WF
1	Core power	0.005	0.069	0.073	0.061	0.066	0.065
2	Pressurizer pressure	0.034	0.162	0.033	0.084	0.038	0.086
3	SG1 steam dome pressure	0.026	0.199	0.064	0.110	0.116	0.091
4	SIT-01 pressure	excl.	excl.	0.000	0.000	0.046	0.102
5	Core inlet temperature	0.003	0.210	0.015	0.092	0.023	0.111
6	Core exit temperature	0.005	0.208	0.008	0.124	0.016	0.132
7	Clad temp. at region 2	0.009	0.133	0.013	0.085	0.016	0.096
8	Clad temp. at region 10	0.007	0.154	0.025	0.121	0.028	0.095
9	Clad temp. at region 12	0.004	0.187	0.012	0.099	0.019	0.120
10	Hot leg 1 flow rate	0.462	0.073	1.020	0.116	2.028	0.180
11	Hot leg 2 flow rate	1.639	0.123	1.262	0.119	2.254	0.173
12	Active SIT-01 flow rate	excl.	excl.	0.000	0.000	0.893	0.210
13	Active SIP-02 flow rate	excl.	excl.	0.259	0.106	0.217	0.120
14	Total break flow rate	0.624	0.183	0.630	0.181	0.745	0.203
15	Accumulated break mass	0.312	0.146	0.041	0.094	0.085	0.083
16	Down-comer level	0.015	0.128	0.102	0.085	0.340	0.092
17	Active core region level	0.084	0.215	0.259	0.073	0.713	0.109
18	Pressurizer level	0.091	0.134	0.100	0.103	0.127	0.095
19	Collapsed water level IL1A	0.151	0.115	0.282	0.089	0.418	0.090
20	Collapsed water level IL1B	0.067	0.215	0.386	0.078	1.133	0.113
21	Collapsed water level IL2A	0.141	0.144	0.536	0.061	0.775	0.122
22	Collapsed water level IL2B	0.168	0.083	1.103	0.098	1.000	0.116
	Total (AA_{tot}, WF_{tot})	**0.091**	**0.166**	**0.160**	**0.098**	**0.262**	**0.110**

*excl : excluded in this time of interval

Table 7.4-9 Calculated total accuracy of the UNIPI's open calculation

Number	Parameter	Time of interval					
		0 ~ 24 s		0~ 300 s		0 ~ 2000 s	
		N=512		N=1024		N=4096	
		AA	WF	AA	WF	AA	WF
1	Core power	0.001	0.347	0.003	0.262	0.006	0.227
2	Pressurizer pressure	0.034	0.205	0.046	0.086	0.049	0.087
3	SG1 steam dome pressure	0.012	0.293	0.064	0.114	0.109	0.095
4	SIT-01 pressure	excl.	excl.	excl.	excl.	0.101	0.107
5	Core inlet temperature	0.003	0.108	0.012	0.073	0.029	0.110
6	Core exit temperature	0.010	0.164	0.010	0.063	0.027	0.097
7	Clad temp. at region 2	0.003	0.206	0.016	0.090	0.031	0.107
8	Clad temp. at region 10	0.004	0.115	0.023	0.100	0.037	0.114
9	Clad temp. at region 12	0.009	0.212	0.015	0.065	0.032	0.095
10	Hot leg 1 flow rate	0.545	0.081	1.062	0.107	1.643	0.234
11	Hot leg 2 flow rate	1.423	0.115	1.279	0.106	2.003	0.236
12	Active SIT-01 flow rate	excl.	excl.	excl.	excl.	1.289	0.193
13	Active SIP-02 flow rate	excl.	excl.	0.307	0.153	0.240	0.152
14	Total break flow rate	0.305	0.279	0.513	0.193	0.607	0.210
15	Accumulated break mass	0.030	0.160	0.031	0.090	0.017	0.083
16	Down-comer level	0.011	0.185	0.149	0.101	0.605	0.082
17	Active core region level	0.065	0.182	0.272	0.056	0.594	0.119
18	Pressurizer level	0.054	0.167	0.069	0.131	0.099	0.099
19	Collapsed water level IL1A	0.151	0.115	0.294	0.088	0.441	0.089
20	Collapsed water level IL1B	0.067	0.215	0.951	0.104	1.469	0.043
21	Collapsed water level IL2A	0.141	0.144	0.996	0.116	0.868	0.067
22	Collapsed water level IL2B	0.168	0.083	0.877	0.104	1.000	0.116
	Total (AA_{tot}, WF_{tot})	**0.067**	**0.173**	**0.187**	**0.094**	**0.278**	**0.108**

*excl : excluded in this time of interval

Table 7.4-10 Calculated total accuracy of the AEKI's open calculation

Number	Parameter	Time of interval					
		0 ~ 24 s		0~ 300 s		0 ~ 2000 s	
		N=512		N=1024		N=4096	
		AA	WF	AA	WF	AA	WF
1	Core power	0.003	0.124	0.007	0.175	0.009	0.172
2	Pressurizer pressure	0.063	0.142	0.061	0.090	0.046	0.075
3	SG1 steam dome pressure	0.030	0.176	0.048	0.103	0.146	0.102
4	SIT-01 pressure	excl.	excl.	excl.	excl.	0.069	0.093
5	Core inlet temperature	0.008	0.032	0.018	0.099	0.030	0.107
6	Core exit temperature	0.011	0.191	0.015	0.076	0.019	0.099
7	Clad temp. at region 2	0.019	0.072	0.026	0.106	0.019	0.082
8	Clad temp. at region 10	0.005	0.090	0.026	0.113	0.023	0.083
9	Clad temp. at region 12	0.009	0.201	0.017	0.070	0.019	0.123
10	Hot leg 1 flow rate	0.723	0.067	1.157	0.105	1.195	0.152
11	Hot leg 2 flow rate	1.740	0.175	1.581	0.125	1.484	0.148
12	Active SIT-01 flow rate	excl.	excl.	excl.	excl.	1.012	0.180
13	Active SIP-02 flow rate	excl.	excl.	0.361	0.128	0.262	0.132
14	Total break flow rate	0.501	0.191	0.650	0.132	0.723	0.148
15	Accumulated break mass	0.177	0.173	0.136	0.106	0.156	0.090
16	Down-comer level	0.072	0.027	0.195	0.098	0.344	0.096
17	Active core region level	0.211	0.037	0.294	0.113	0.737	0.123
18	Pressurizer level	0.074	0.084	0.078	0.115	0.102	0.117
19	Collapsed water level IL1A	0.151	0.115	0.706	0.108	0.675	0.048
20	Collapsed water level IL1B	0.067	0.215	0.824	0.103	1.335	0.094
21	Collapsed water level IL2A	0.141	0.144	1.323	0.097	0.889	0.062
22	Collapsed water level IL2B	0.168	0.083	1.304	0.092	1.000	0.116
	Total (AA_{tot}, WF_{tot})	**0.099**	**0.122**	**0.243**	**0.100**	**0.265**	**0.101**

*excl : excluded in this time of interval

Table 7.4-11 Calculated total accuracy of the GP1's open calculation

Number	Parameter	Time of interval					
		0 ~ 24 s		0~ 300 s		0 ~ 2000 s	
		N=512		N=1024		N=4096	
		AA	WF	AA	WF	AA	WF
1	Core power	0.003	0.127	0.032	0.058	0.031	0.065
2	Pressurizer pressure	0.041	0.175	0.036	0.090	0.033	0.088
3	SG1 steam dome pressure	0.030	0.178	0.059	0.098	0.077	0.097
4	SIT-01 pressure	excl.	excl.	excl.	excl.	0.050	0.100
5	Core inlet temperature	0.003	0.104	0.011	0.088	0.016	0.124
6	Core exit temperature	0.011	0.122	0.011	0.098	0.014	0.116
7	Clad temp. at region 2	0.025	0.033	0.026	0.117	0.026	0.119
8	Clad temp. at region 10	0.006	0.176	0.204	0.060	0.177	0.067
9	Clad temp. at region 12	0.009	0.166	0.096	0.071	0.081	0.079
10	Hot leg 1 flow rate	0.586	0.071	0.997	0.115	1.176	0.165
11	Hot leg 2 flow rate	1.632	0.131	1.206	0.121	1.354	0.149
12	Active SIT-01 flow rate	excl.	excl.	excl.	excl.	2.993	0.271
13	Active SIP-02 flow rate	excl.	excl.	0.295	0.157	0.235	0.151
14	Total break flow rate	0.297	0.263	0.594	0.160	0.747	0.199
15	Accumulated break mass	0.075	0.076	0.170	0.097	0.073	0.040
16	Down-comer level	0.016	0.122	0.103	0.069	0.305	0.139
17	Active core region level	0.088	0.131	0.257	0.094	0.735	0.113
18	Pressurizer level	0.098	0.127	0.104	0.111	0.133	0.100
19	Collapsed water level IL1A	0.135	0.129	0.790	0.108	1.525	0.083
20	Collapsed water level IL1B	0.086	0.168	0.338	0.066	1.191	0.110
21	Collapsed water level IL2A	0.124	0.163	1.052	0.111	0.953	0.100
22	Collapsed water level IL2B	0.152	0.092	0.257	0.111	1.000	0.116
	Total (AA_{tot}, WF_{tot})	**0.078**	**0.130**	**0.192**	**0.093**	**0.324**	**0.106**

*excl : excluded in this time of interval

Table 7.4-12 Calculated total accuracy of the GP2's open calculation

Number	Parameter	Time of interval					
		0 ~ 24 s		0~ 300 s		0 ~ 2000 s	
		N=512		N=1024		N=4096	
		AA	WF	AA	WF	AA	WF
1	Core power	0.005	0.069	0.052	0.077	0.048	0.088
2	Pressurizer pressure	0.074	0.078	0.066	0.069	0.067	0.068
3	SG1 steam dome pressure	0.029	0.101	0.062	0.107	0.079	0.093
4	SIT-01 pressure	excl.	excl.	excl.	excl.	0.099	0.044
5	Core inlet temperature	0.005	0.078	0.016	0.089	0.022	0.122
6	Core exit temperature	0.004	0.205	0.014	0.111	0.021	0.118
7	Clad temp. at region 2	0.022	0.041	0.019	0.098	0.018	0.113
8	Clad temp. at region 10	0.008	0.078	0.022	0.122	0.483	0.014
9	Clad temp. at region 12	0.007	0.141	0.014	0.093	0.370	0.008
10	Hot leg 1 flow rate	0.943	0.054	1.182	0.101	1.185	0.148
11	Hot leg 2 flow rate	2.068	0.145	1.505	0.119	1.426	0.167
12	Active SIT-01 flow rate	excl.	excl.	excl.	excl.	0.949	0.161
13	Active SIP-02 flow rate	excl.	excl.	0.319	0.162	0.244	0.146
14	Total break flow rate	0.390	0.224	0.592	0.184	0.731	0.220
15	Accumulated break mass	0.116	0.118	0.043	0.033	0.034	0.094
16	Down-comer level	0.252	0.492	0.427	0.322	0.820	0.250
17	Active core region level	0.065	0.181	0.335	0.088	0.735	0.115
18	Pressurizer level	0.549	0.126	0.367	0.038	0.343	0.041
19	Collapsed water level IL1A	0.081	0.214	0.819	0.104	1.575	0.083
20	Collapsed water level IL1B	0.145	0.100	0.945	0.099	1.516	0.046
21	Collapsed water level IL2A	0.070	0.289	1.140	0.119	0.887	0.064
22	Collapsed water level IL2B	0.100	0.140	1.134	0.112	1.000	0.116
	Total (AA_{tot}, WF_{tot})	**0.115**	**0.136**	**0.251**	**0.104**	**0.379**	**0.092**

*excl : excluded in this time of interval

Table 7.4-13 Calculated total accuracy of the GP3's open calculation

Number	Parameter	Time of interval					
		0 ~ 24 s		0~ 300 s		0 ~ 2000 s	
		N=512		N=1024		N=4096	
		AA	WF	AA	WF	AA	WF
1	Core power	0.003	0.127	0.037	0.053	0.037	0.061
2	Pressurizer pressure	0.062	0.137	0.064	0.051	0.061	0.062
3	SG1 steam dome pressure	0.012	0.225	0.065	0.061	0.182	0.093
4	SIT-01 pressure	excl.	excl.	excl.	excl.	0.113	0.094
5	Core inlet temperature	0.006	0.074	0.019	0.061	0.028	0.112
6	Core exit temperature	0.010	0.161	0.015	0.059	0.025	0.093
7	Clad temp. at region 2	0.006	0.197	0.012	0.071	0.024	0.090
8	Clad temp. at region 10	0.006	0.204	0.020	0.085	0.030	0.086
9	Clad temp. at region 12	0.007	0.257	0.013	0.087	0.025	0.076
10	Hot leg 1 flow rate	0.616	0.070	0.942	0.119	1.259	0.169
11	Hot leg 2 flow rate	2.254	0.104	1.215	0.103	1.552	0.150
12	Active SIT-01 flow rate	excl.	excl.	excl.	excl.	3.944	0.263
13	Active SIP-02 flow rate	excl.	excl.	0.347	0.140	0.273	0.136
14	Total break flow rate	0.678	0.166	0.736	0.155	0.860	0.173
15	Accumulated break mass	0.354	0.148	0.118	0.091	0.109	0.083
16	Down-comer level	0.029	0.113	0.202	0.088	0.454	0.097
17	Active core region level	0.058	0.170	0.334	0.086	0.770	0.111
18	Pressurizer level	0.103	0.127	0.117	0.221	0.124	0.207
19	Collapsed water level IL1A	0.119	0.146	0.845	0.106	1.549	0.082
20	Collapsed water level IL1B	0.103	0.140	0.971	0.102	1.490	0.042
21	Collapsed water level IL2A	0.108	0.187	0.216	0.109	0.780	0.119
22	Collapsed water level IL2B	0.137	0.102	0.179	0.156	1.000	0.116
	Total (AA_{tot}, WF_{tot})	**0.107**	**0.158**	**0.171**	**0.086**	**0.352**	**0.100**

*excl : excluded in this time of interval

Table 7.4-14 Calculated total accuracy of the GRS's open calculation

Number	Parameter	Time of interval					
		0 ~ 24 s		0~ 300 s		0 ~ 2000 s	
		N=512		N=1024		N=4096	
		AA	WF	AA	WF	AA	WF
1	Core power	0.003	0.142	0.004	0.190	0.007	0.203
2	Pressurizer pressure	0.023	0.140	0.035	0.068	0.039	0.070
3	SG1 steam dome pressure	0.003	0.279	0.070	0.078	0.067	0.081
4	SIT-01 pressure	excl.	excl.	excl.	excl.	0.089	0.069
5	Core inlet temperature	0.006	0.052	0.018	0.059	0.023	0.087
6	Core exit temperature	0.004	0.111	0.009	0.064	0.019	0.095
7	Clad temp. at region 2	0.008	0.068	0.009	0.090	0.017	0.113
8	Clad temp. at region 10	0.006	0.090	0.015	0.110	0.022	0.114
9	Clad temp. at region 12	0.006	0.145	0.010	0.119	0.020	0.134
10	Hot leg 1 flow rate	0.759	0.105	1.182	0.106	1.273	0.155
11	Hot leg 2 flow rate	2.231	0.162	1.615	0.164	1.549	0.177
12	Active SIT-01 flow rate	excl.	excl.	excl.	excl.	2.317	0.229
13	Active SIP-02 flow rate	excl.	excl.	0.374	0.140	0.282	0.140
14	Total break flow rate	1.162	0.277	1.221	0.259	1.456	0.283
15	Accumulated break mass	0.300	0.154	0.128	0.093	0.114	0.083
16	Down-comer level	0.012	0.165	0.148	0.103	0.336	0.094
17	Active core region level	0.076	0.170	0.525	0.091	0.655	0.109
18	Pressurizer level	0.047	0.133	0.046	0.148	0.082	0.107
19	Collapsed water level IL1A	0.151	0.115	0.749	0.114	1.544	0.084
20	Collapsed water level IL1B	0.067	0.215	0.452	0.043	1.171	0.109
21	Collapsed water level IL2A	0.141	0.144	1.136	0.110	0.878	0.064
22	Collapsed water level IL2B	0.168	0.083	0.429	0.068	1.000	0.116
	Total (AA_{tot}, WF_{tot})	**0.109**	**0.127**	**0.206**	**0.094**	**0.310**	**0.107**

*excl : excluded in this time of interval

Table 7.4-15 Calculated total accuracy of the NRI's open calculation

Number	Parameter	Time of interval					
		0 ~ 24 s		0~ 300 s		0 ~ 2000 s	
		N=512		N=1024		N=4096	
		AA	WF	AA	WF	AA	WF
1	Core power	0.001	0.311	0.013	0.101	0.014	0.140
2	Pressurizer pressure	0.064	0.087	0.129	0.073	0.091	0.041
3	SG1 steam dome pressure	0.014	0.167	0.051	0.055	0.072	0.077
4	SIT-01 pressure	excl.	excl.	excl.	excl.	0.130	0.068
5	Core inlet temperature	0.006	0.199	0.018	0.133	0.047	0.085
6	Core exit temperature	0.009	0.223	0.039	0.096	0.029	0.037
7	Clad temp. at region 2	0.010	0.092	0.021	0.051	0.041	0.087
8	Clad temp. at region 10	0.013	0.188	0.033	0.129	0.040	0.048
9	Clad temp. at region 12	0.014	0.176	0.032	0.128	0.035	0.041
10	Hot leg 1 flow rate	0.661	0.100	0.851	0.129	0.907	0.187
11	Hot leg 2 flow rate	1.784	0.238	1.041	0.191	1.057	0.210
12	Active SIT-01 flow rate	excl.	excl.	excl.	excl.	0.999	0.155
13	Active SIP-02 flow rate	excl.	excl.	0.324	0.126	0.217	0.135
14	Total break flow rate	0.559	0.205	0.717	0.137	0.812	0.161
15	Accumulated break mass	0.811	0.140	0.710	0.096	0.422	0.085
16	Down-comer level	0.120	0.018	0.374	0.093	0.514	0.049
17	Active core region level	0.069	0.122	0.409	0.082	0.809	0.110
18	Pressurizer level	0.147	0.083	0.130	0.103	0.153	0.087
19	Collapsed water level IL1A	0.102	0.170	0.855	0.105	1.550	0.082
20	Collapsed water level IL1B	0.121	0.119	0.982	0.101	1.490	0.042
21	Collapsed water level IL2A	0.091	0.222	0.232	0.102	0.785	0.118
22	Collapsed water level IL2B	0.120	0.116	0.181	0.154	1.000	0.116
	Total (AA_{tot}, WF_{tot})	**0.127**	**0.159**	**0.216**	**0.104**	**0.316**	**0.077**

*excl : excluded in this time of interval

Table 7.4-16 Calculated total accuracy of the VTT's open calculation

Number	Parameter	Time of interval					
		0 ~ 24 s		0~ 300 s		0 ~ 2000 s	
		N=512		N=1024		N=4096	
		AA	WF	AA	WF	AA	WF
1	Core power	0.003	0.124	0.009	0.126	0.010	0.136
2	Pressurizer pressure	0.057	0.125	0.067	0.072	0.082	0.068
3	SG1 steam dome pressure	0.030	0.176	0.076	0.090	0.081	0.087
4	SIT-01 pressure	excl.	excl.	excl.	excl.	0.137	0.103
5	Core inlet temperature	0.003	0.150	0.017	0.113	0.040	0.102
6	Core exit temperature	0.012	0.179	0.017	0.116	0.039	0.110
7	Clad temp. at region 2	0.009	0.175	0.011	0.099	0.036	0.110
8	Clad temp. at region 10	0.006	0.162	0.019	0.096	0.038	0.106
9	Clad temp. at region 12	0.009	0.238	0.016	0.153	0.038	0.127
10	Hot leg 1 flow rate	0.703	0.055	1.332	0.087	2.252	0.182
11	Hot leg 2 flow rate	1.527	0.116	1.693	0.089	2.565	0.171
12	Active SIT-01 flow rate	excl.	excl.	excl.	excl.	1.138	0.190
13	Active SIP-02 flow rate	excl.	excl.	0.387	0.129	0.288	0.128
14	Total break flow rate	0.535	0.200	0.588	0.189	0.699	0.206
15	Accumulated break mass	0.261	0.149	0.032	0.028	0.025	0.072
16	Down-comer level	0.022	0.088	0.169	0.105	0.598	0.105
17	Active core region level	0.090	0.173	0.225	0.071	0.645	0.115
18	Pressurizer level	0.090	0.126	0.100	0.111	0.120	0.099
19	Collapsed water level IL1A	0.111	0.156	0.387	0.040	0.507	0.061
20	Collapsed water level IL1B	0.112	0.129	0.396	0.043	1.194	0.111
21	Collapsed water level IL2A	0.100	0.202	1.281	0.104	0.900	0.062
22	Collapsed water level IL2B	0.129	0.108	1.266	0.098	1.000	0.116
	Total (AA_{tot}, WF_{tot})	**0.090**	**0.160**	**0.211**	**0.099**	**0.298**	**0.106**

*excl : excluded in this time of interval

Table 7.4-17 Summary of the results of FFTBM to ISP-50 open calculation

Group	Participant/Code		Time of interval					
			0 ~ 24 s		0~ 300 s		0 ~ 2000 s	
			N=512		N=1024		N=4096	
			AA_{tot}	WF_{tot}	AA_{tot}	WF_{tot}	AA_{tot}	WF_{tot}
A	KAERI1	MARS-KS	0.110	0.160	0.210	0.096	0.322[1)]	0.108
	KEPRI	MARS-KS	0.123	0.141	0.213	0.096	0.359	0.108
	KTH	TRACE 5.0 p. 02	0.137	0.134	0.241	0.068	0.353	0.087
	USNRC	TRACE 5.0 p. 02	0.076	0.143	0.162	0.106	0.348	0.104
B	CIAE	R5/M3.3	0.092	0.149	0.135	0.084	0.201[1)]	0.085
	KNF	R5/M3.3	0.097	0.140	0.159	0.087	0.302	0.096
	KOPEC1	RELAP-ME	0.096	0.169	0.229	0.103	0.372	0.071
	PSI	R5/M3.3	0.091	0.166	0.160	0.098	0.262	0.110
	UNIPI	R5/M3.3	0.067	0.173	0.187	0.094	0.278	0.108
C	AEKI	CATHARE2V1.5B mod3.1	0.099	0.122	0.243	0.100	0.265	0.101
	GP1	KORSAR	0.078	0.130	0.192	0.093	0.324	0.106
	GP2	KORSAR	0.115	0.136	0.251	0.104	0.379	0.092
	GP3	KORSAR	0.107	0.158	0.171	0.086	0.352	0.100
D	GRS	ATHLET M2.2	0.109	0.127	0.206	0.094	0.310	0.107
	NRI	ATHLET	0.127	0.159	0.216	0.104	0.316	0.077
	VTT	APROS	0.090	0.160	0.211	0.099	0.298	0.106

[1)] Maximum calculation time is limited to 1460 s

Table 7.4-18 Improvement of AA_{tot} between blind and open calculation

Grp.	Partic'nt	Time of interval								
		0 ~ 24 s			0~ 300 s			0 ~ 2000 s		
		N=512			N=1024			N=4096		
		blind	open	I(%)[1)]	blind	open	I(%)[1)]	blind	open	I(%)[1)]
A	KAERI	0.1	0.110	**10.0**	0.25	0.210	**-16.0**	0.333	0.322	**-3.3**
	KEPRI	0.134	0.123	**-8.2**	0.271	0.213	**-21.4**	0.34	0.359	**5.6**
	KTH	0.147	0.137	**-6.8**	0.298	0.241	**-19.1**	0.417	0.353	**-15.3**
	USNRC	0.121	0.076	**-37.2**	0.218	0.162	**-25.7**	0.32	0.348	**8.8**
B	CIAE	0.093	0.092	**-1.1**	0.112	0.135	**20.5**	0.196	0.201	**2.6**
	KNF	0.122	0.097	**-20.5**	0.158	0.159	**0.6**	0.331	0.302	**-8.8**
	KOPEC1	0.403	0.096	**-76.2**	0.385	0.229	**-40.5**	0.672	0.372	**-44.6**
	KOPEC2	0.402	-	**-**	0.398	-	**-**	0.634	-	**-**
	PSI	-	0.091	**-**	-	0.160	**-**	-	0.262	**-**
	UNIPI	0.118	0.067	**-43.2**	0.22	0.187	**-15.0**	0.267	0.278	**4.1**
C	AEKI	-	0.099	**-**	-	0.243		-	0.265	**-**
	GP1	0.08	0.078	**-2.5**	0.383	0.192	**-49.9**	0.444	0.324	**-27.0**
	GP2	-	0.115	**-**	-	0.251	**-**	-	0.379	**-**
	GP3	-	0.107	**-**	-	0.171	**-**	-	0.352	**-**
	GP4	0.155	-	**-**	0.317	-	**-**	0.546	-	**-**
D	FORTUM	0.086	-	**-**	0.249	-	**-**	0.397	-	**-**
	GRS	0.102	0.109	**6.9-**	0.222	0.206	**-7.2**	0.411	0.310	**-24.6**
	NRI	0.124	0.127	**2.4**	0.213	0.216	**1.4**	0.405	0.316	**-22.0**
	VTT	0.113	0.090	**-20.4**	0.251	0.211	**-15.9**	0.384	0.298	**-22.4**

[1)] Improvement, I is defined by (open-blind)/blind in percentile

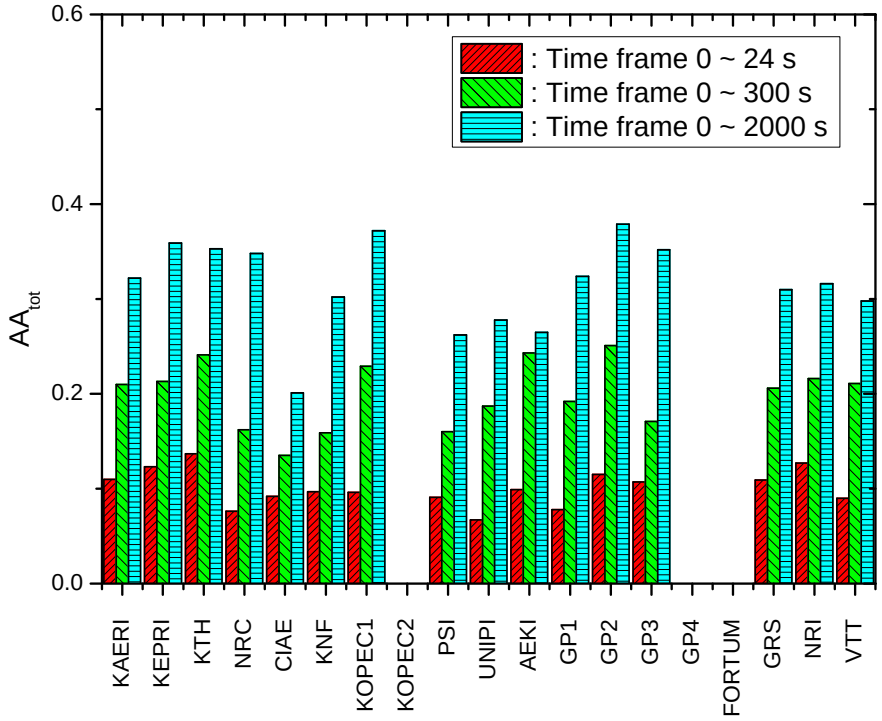

Figure 7.4-1 Comparison of the open prediction accuracy of the participants based on FFTBM

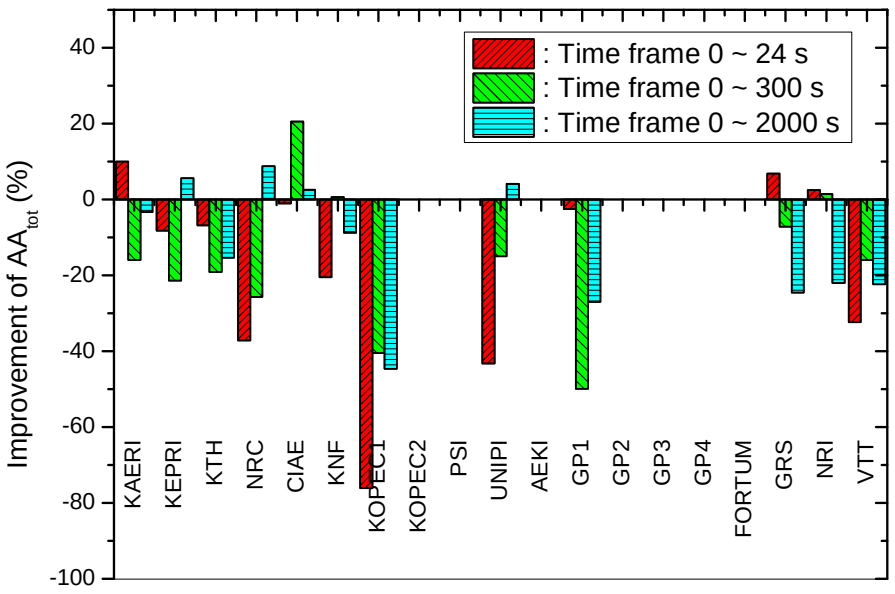

Figure 7.4-2 Comparison of improvement of prediction accuracy

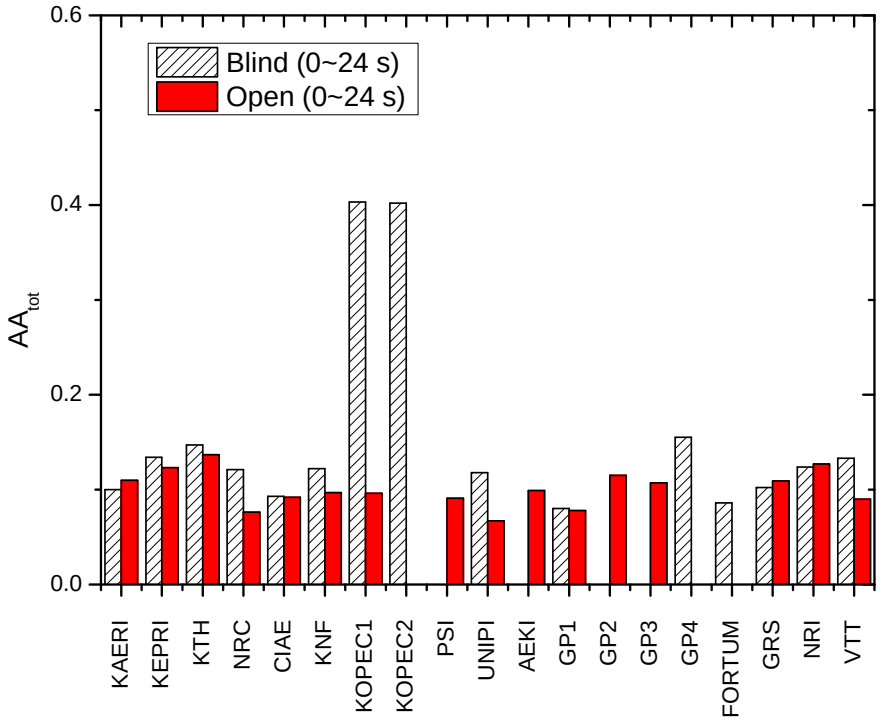

Figure 7.4-3 Comparison of the prediction accuracy of the participants in the 1st time frame

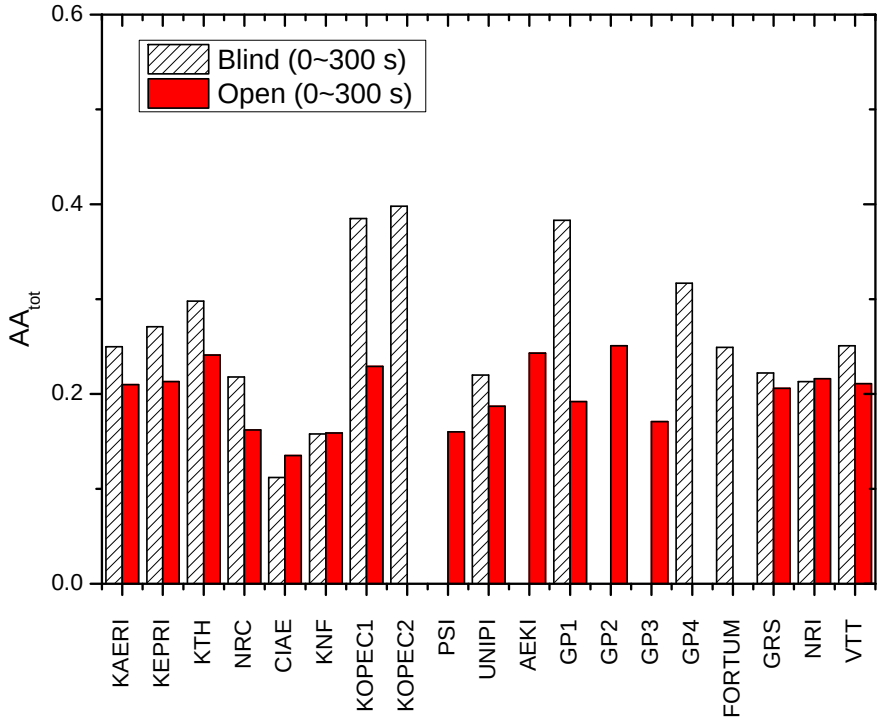

Figure 7.4-4 Comparison of the prediction accuracy of the participants in the 2nd time frame

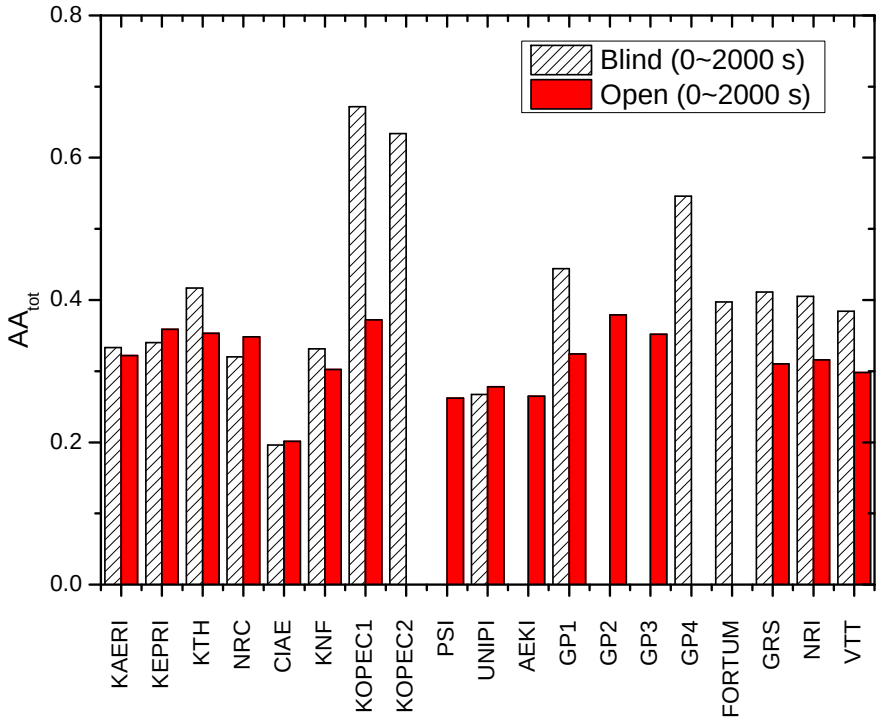

Figure 7.4-5 Comparison of the prediction accuracy of the participants in the 3rd time frame

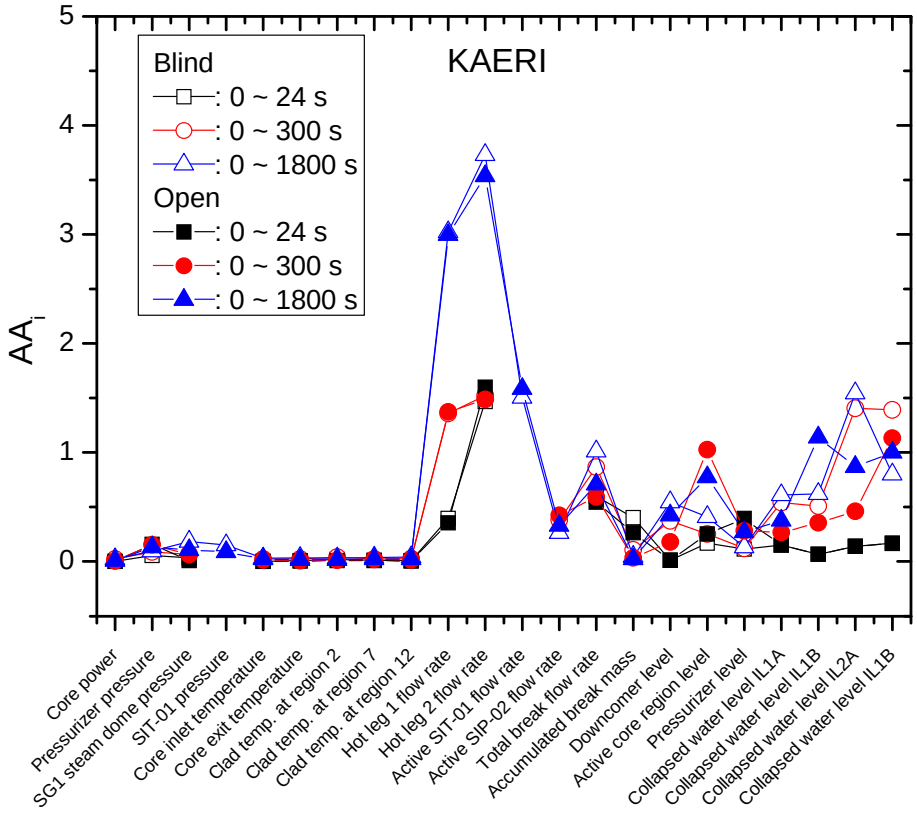

Figure 7.4-6 Comparison of accuracy by KAERI between blind and open phase

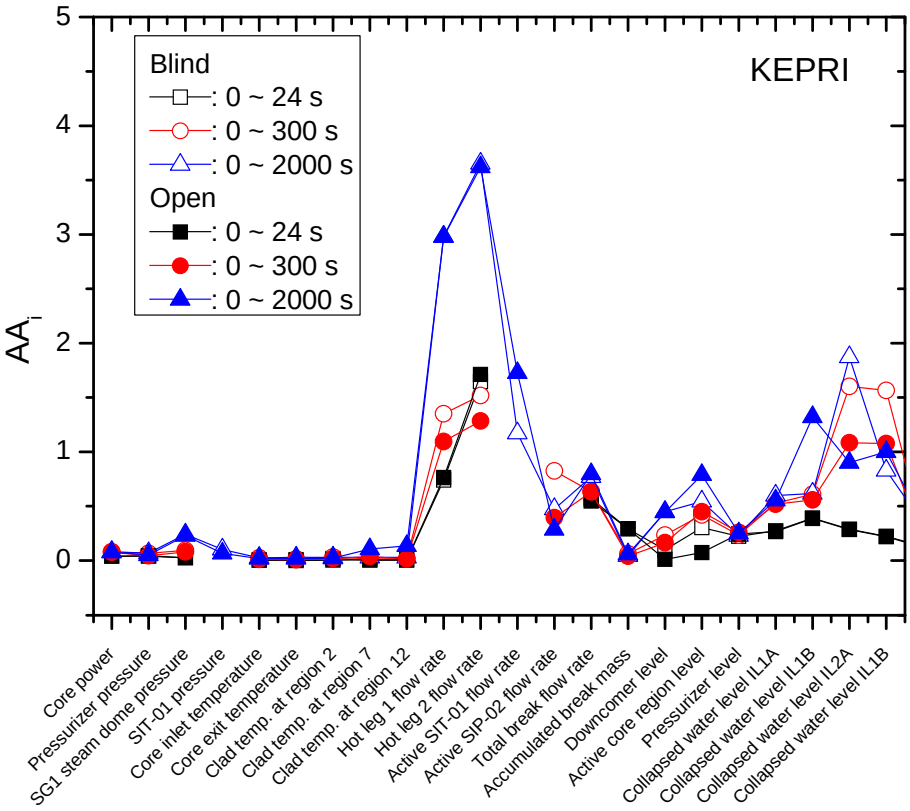

Figure 7.4-7 Comparison of accuracy by KEPRI between blind and open phase

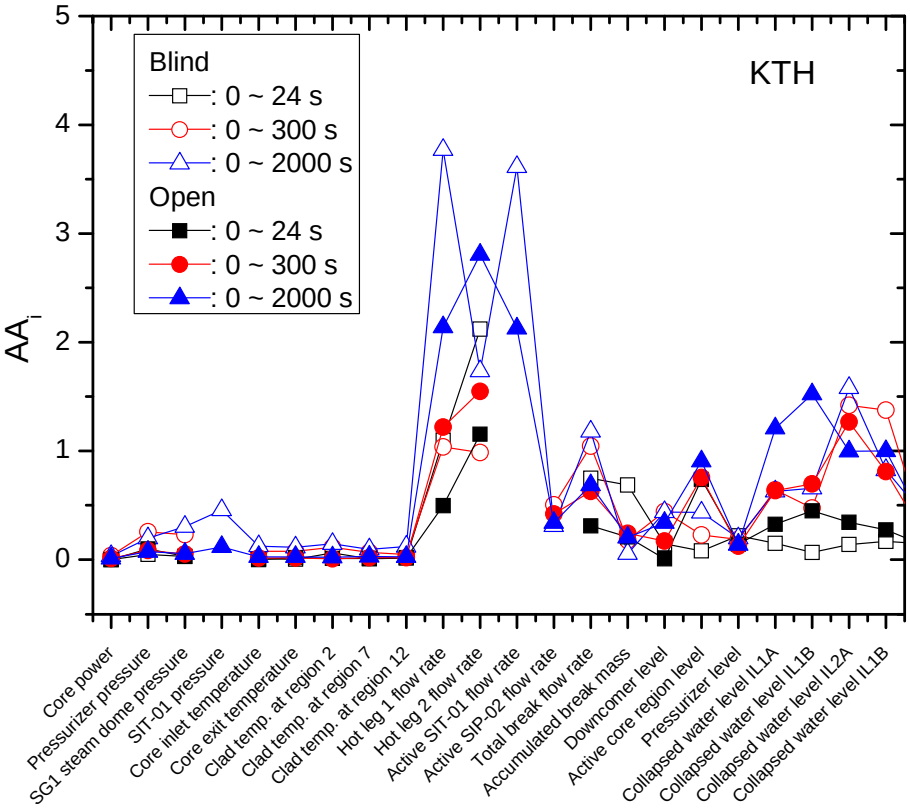

Figure 7.4-8 Comparison of accuracy by KTH between blind and open phase

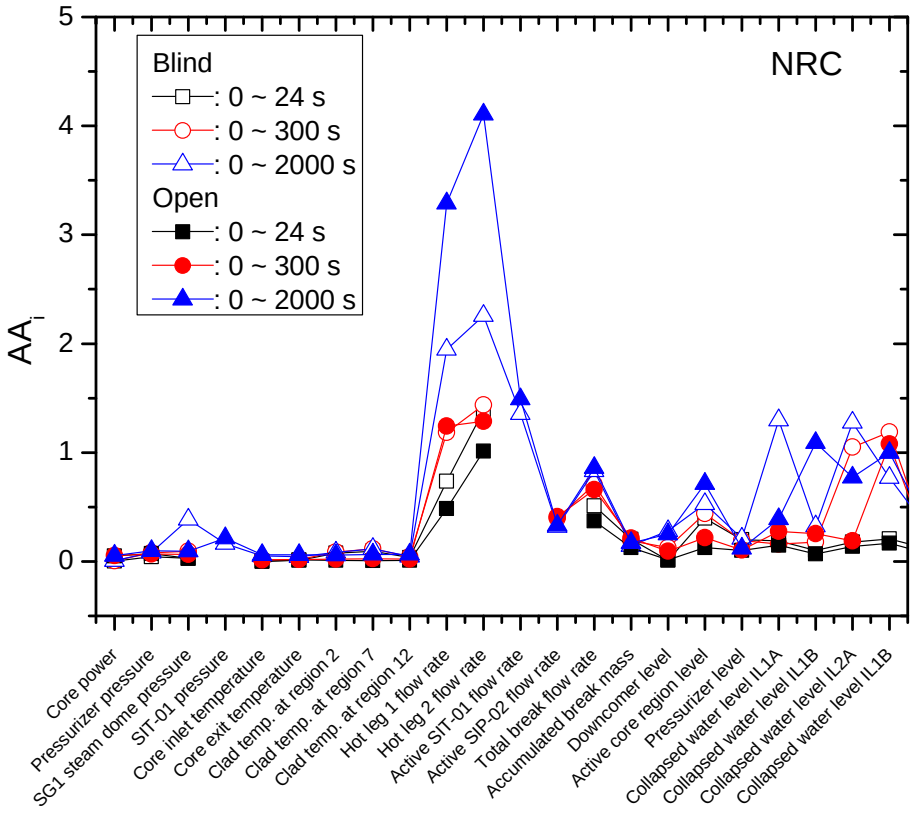

Figure 7.4-9 Comparison of accuracy by NRC between blind and open phase

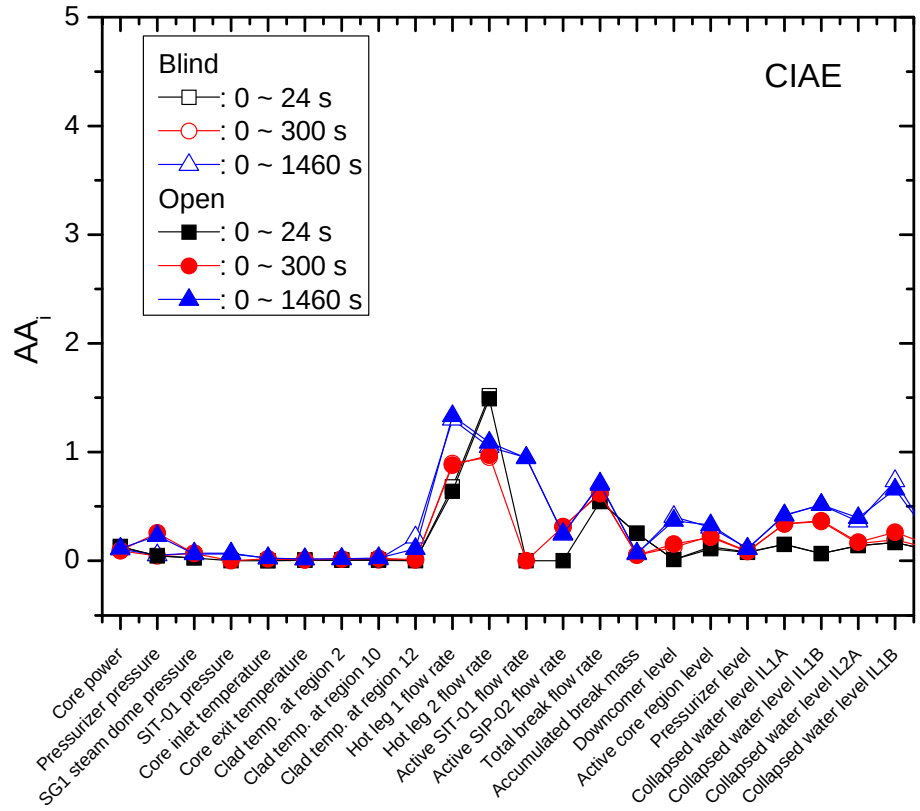

Figure 7.4-10 Comparison of accuracy by CIAE between blind and open phase

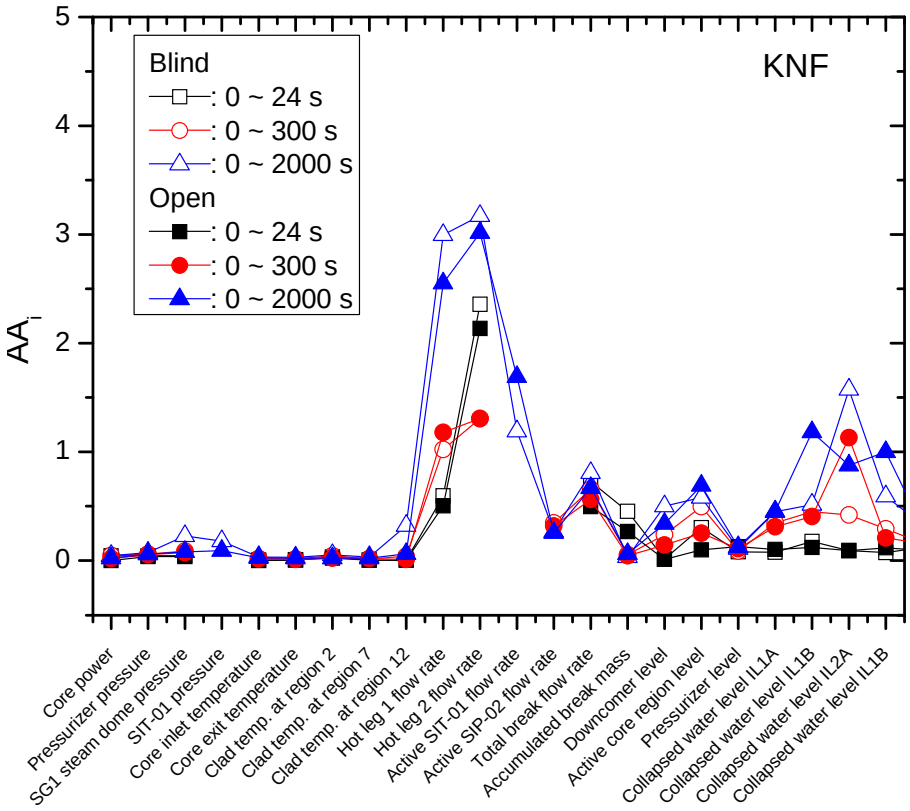

Figure 7.4-11 Comparison of accuracy by KNF between blind and open phase

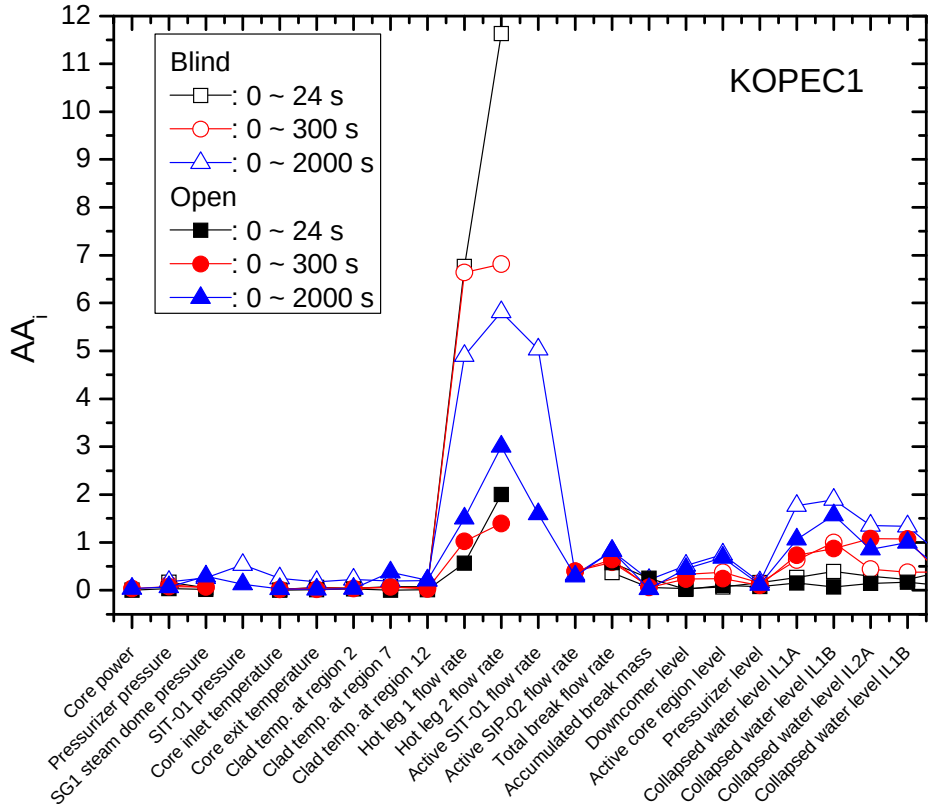

Figure 7.4-12 Comparison of accuracy by KOPEC1 between blind and open phase

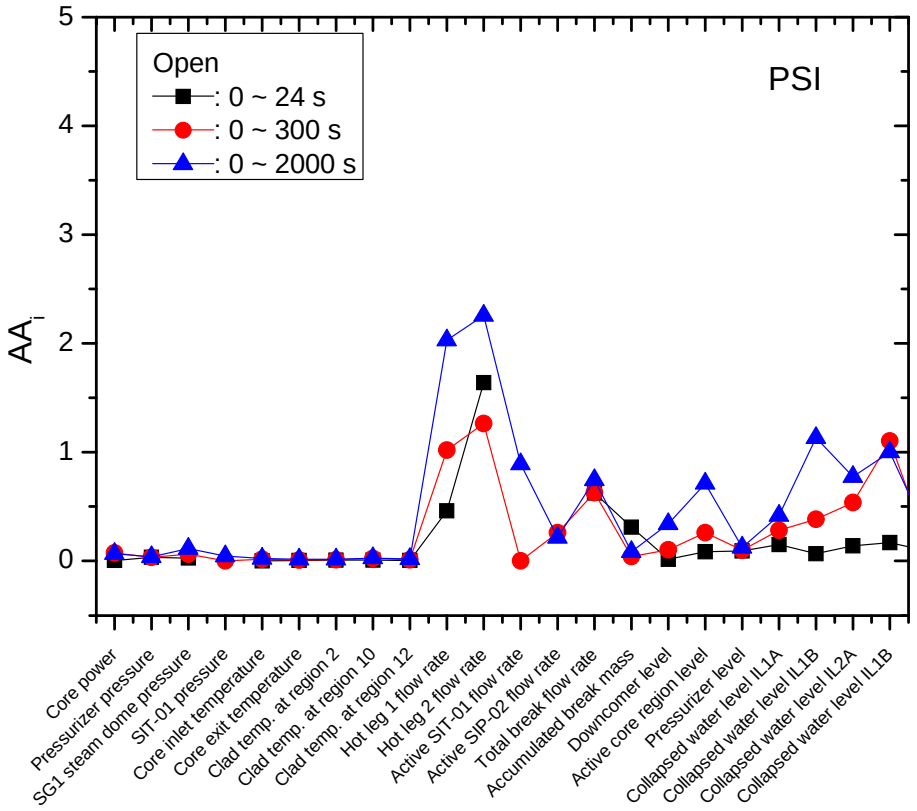

Figure 7.4-13 Comparison of accuracy by PSI between blind and open phase

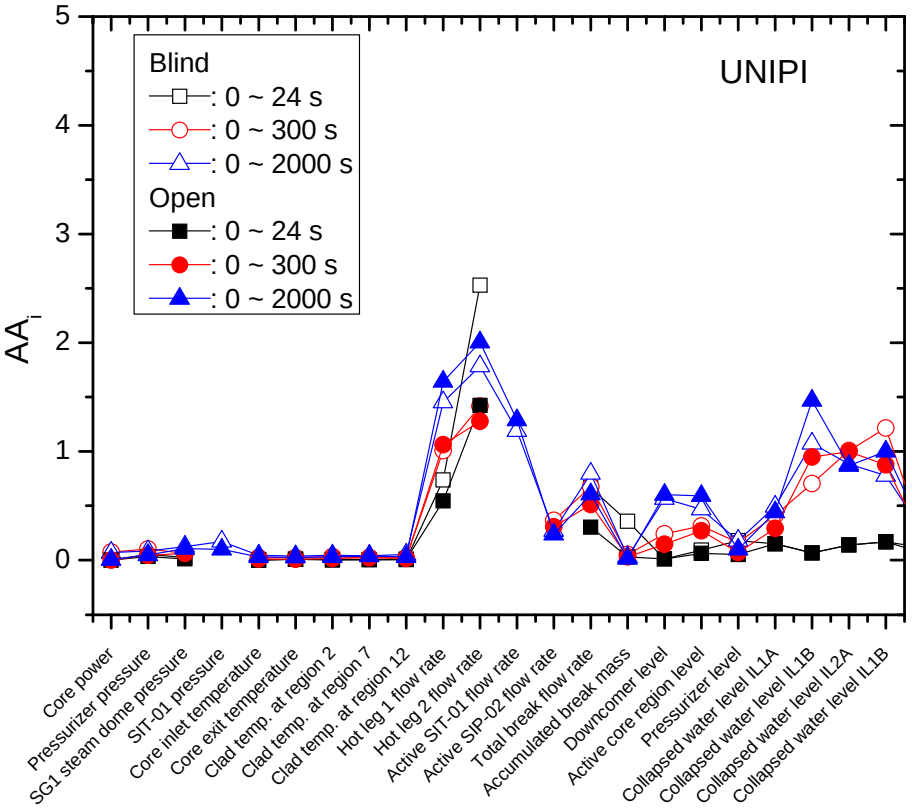

Figure 7.4-14 Comparison of accuracy by UNIPI between blind and open phase

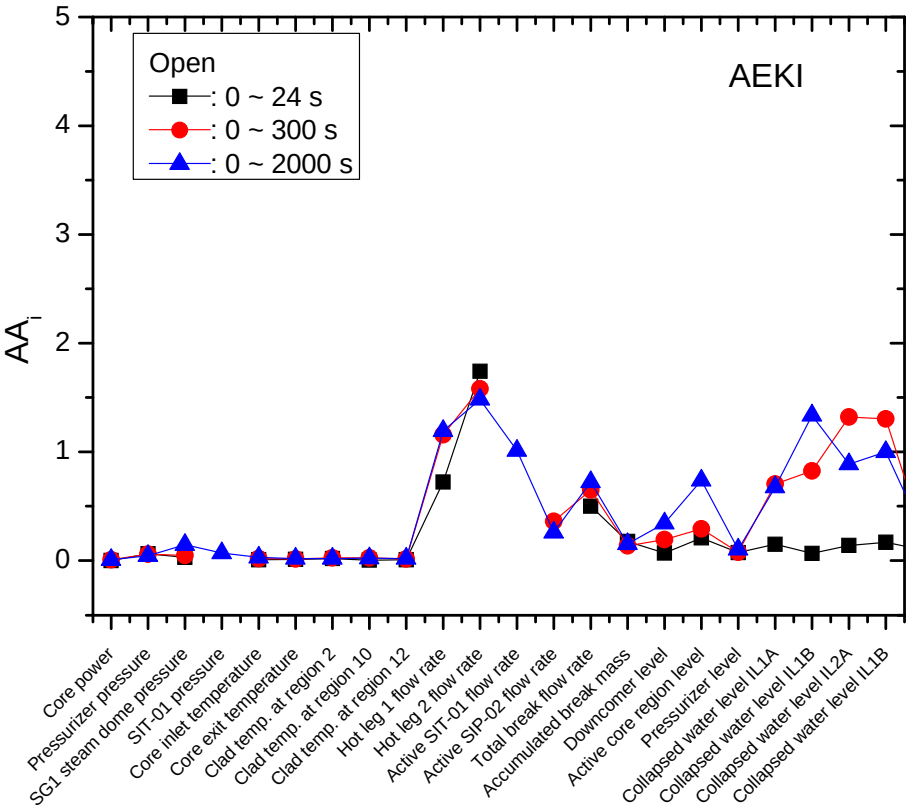

Figure 7.4-15 Comparison of accuracy by AEKI between blind and open phase

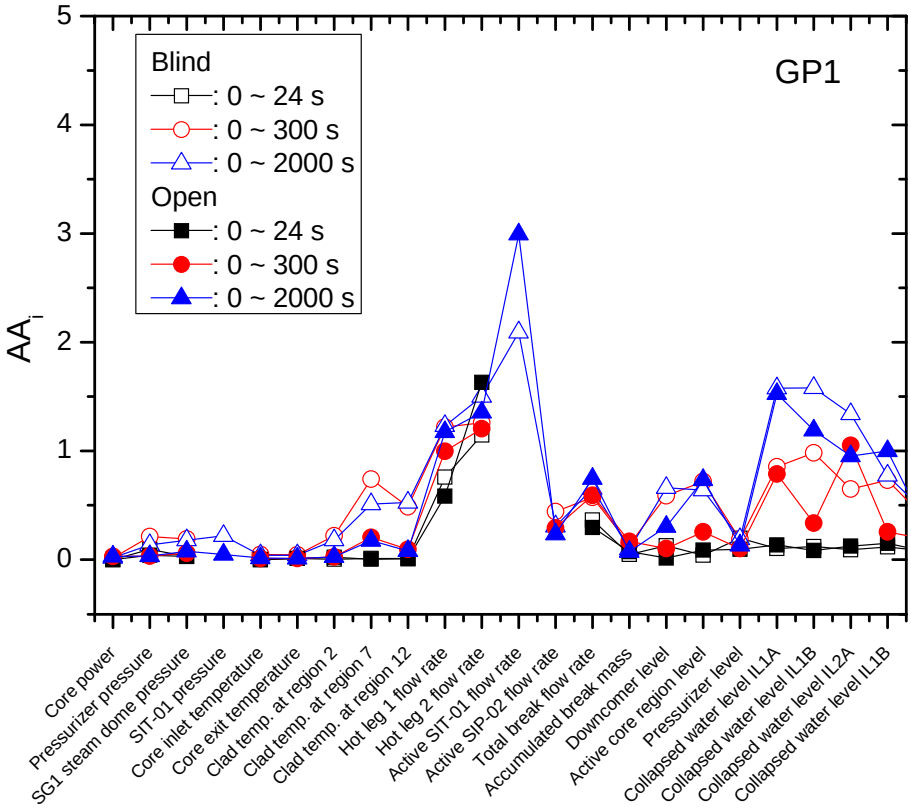

Figure 7.4-16 Comparison of accuracy by GP1 between blind and open phase

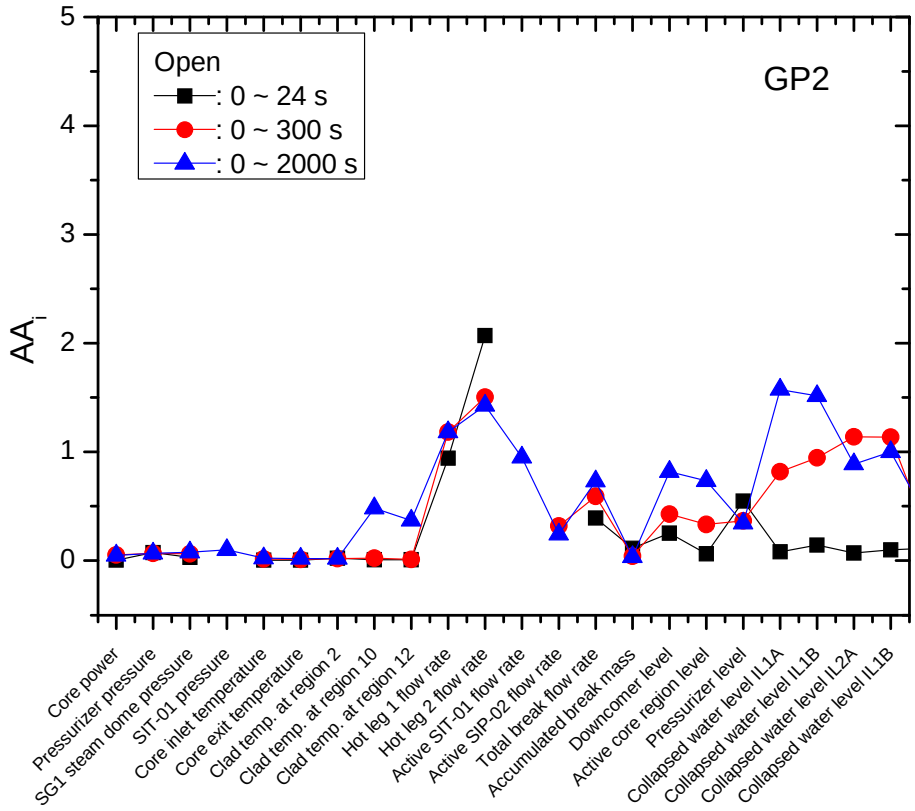

Figure 7.4-17 Comparison of accuracy by GP2 between blind and open phase

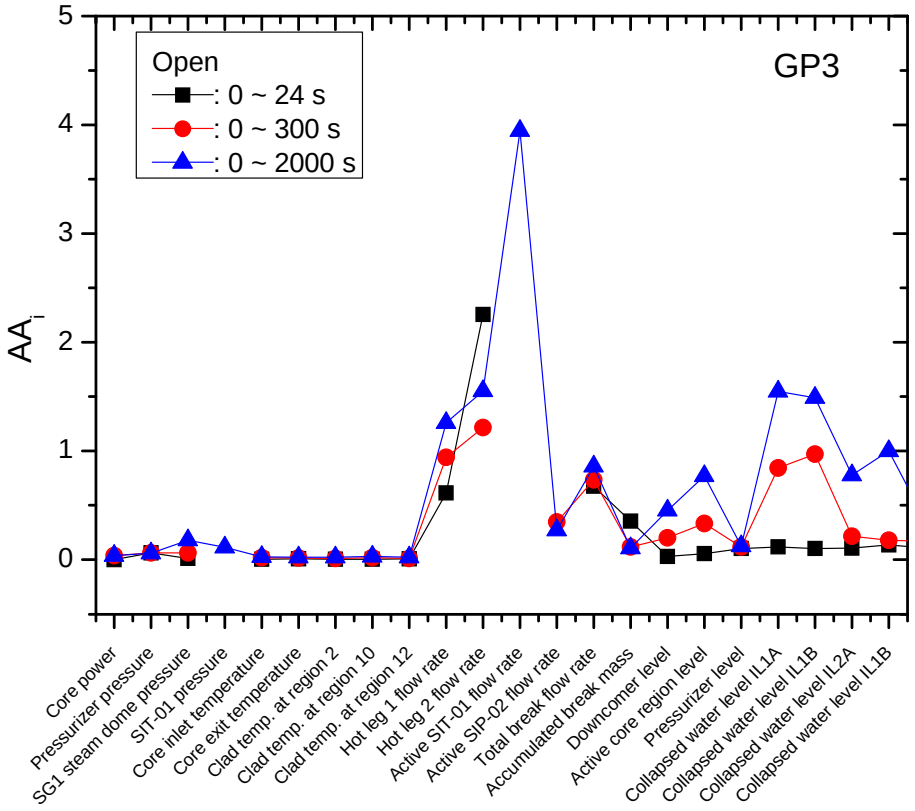

Figure 7.4-18 Comparison of accuracy by GP3 between blind and open phase

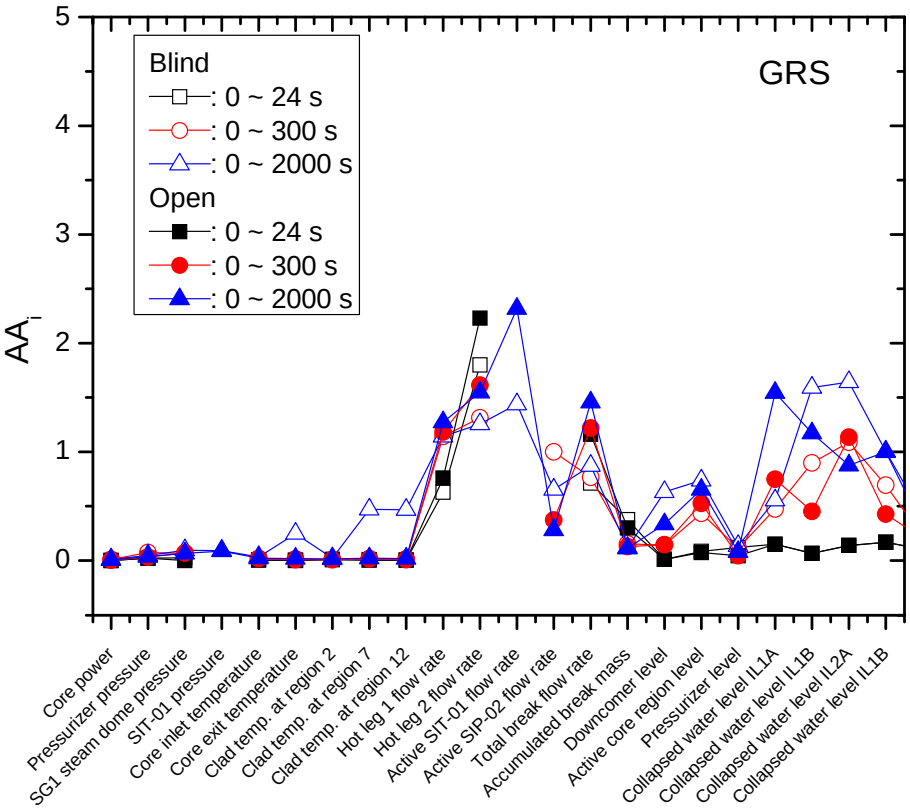

Figure 7.4-19 Comparison of accuracy by GRS between blind and open phase

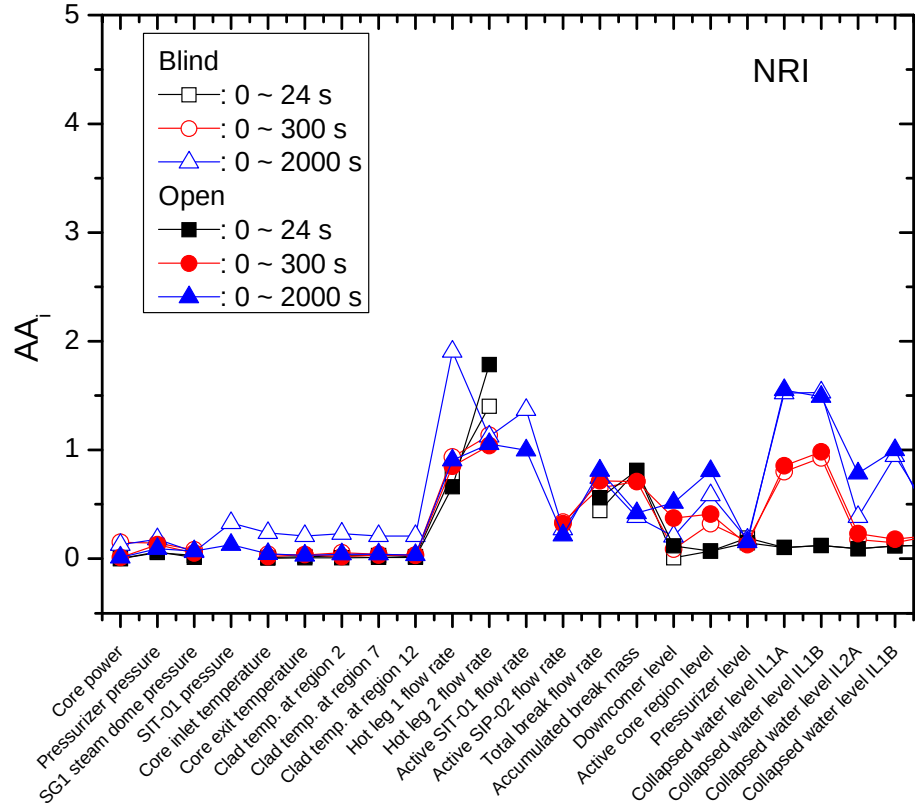

Figure 7.4-20 Comparison of accuracy by NRI between blind and open phase

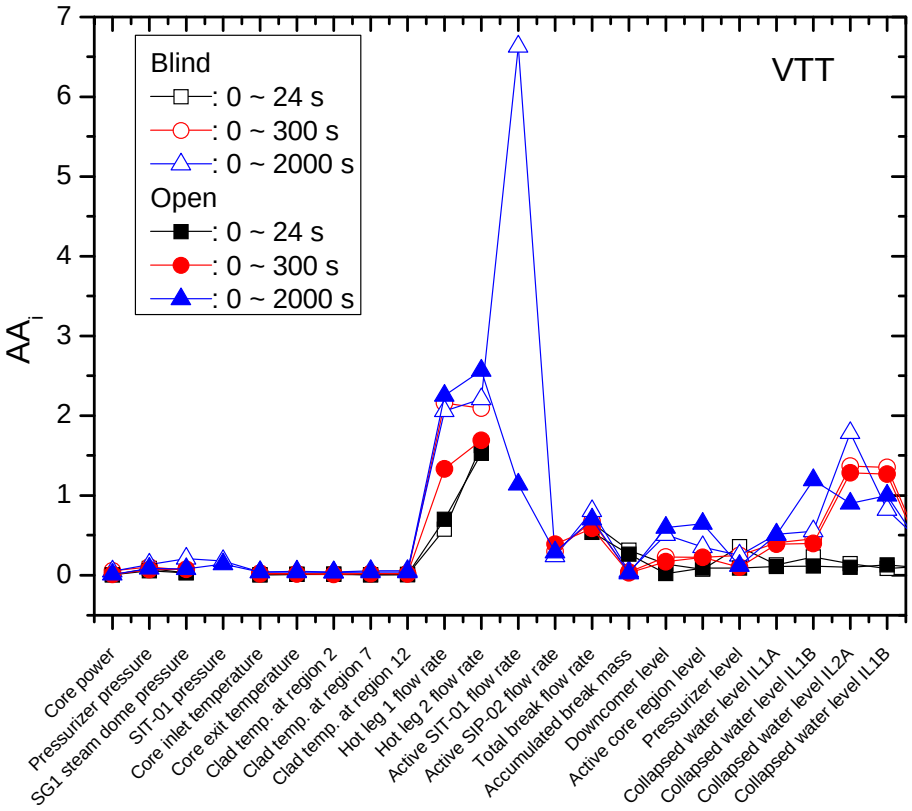

Figure 7.4-21 Comparison of accuracy by VTT between blind and open phase

8. Discussion on Key Thermal-Hydraulic Phenomena

8.1 Two-phase break flow

The break flow rate is the most influencing factor governing the transient behavior. It was confirmed experimentally that choking occurred during the discharge of the single-phase liquid, two-phase mixture, and the single-phase steam throughout the test. Such three phases of the break flow can also affect multi-dimensional phenomena in the down-comer region.

Generally the break flow rate decreased rapidly after the break opening, reached a plateau with a short duration, and then decreased again in every simulation. Most calculations showed the trends of subcooled liquid choking, saturated two-phase choking, and single-phase steam choking. However, some differences were found case by case.

As shown in Figure D.111, KAERI and KEPRI of Group A, CIAE, KNF, KOPEC, PSI and UNIPI of Group B, GP2 and AEKI of Group C, and VTT of Group D predicted the measured break flow rates well during the initial period of 200 s, but KTH and NRC of Group A, GP1 and GP3 of Group C, and GRS of Group D under-predicted the experimental data during this period. Especially NRI of Group D predicted the break flow rate much lower during the plateau than the experimental data. Regarding the accumulated total break flow as shown in Figure D.112, predictions by KAERI and KEPRI of Group A, UNIPI and KOPEC of Group B, GP2 of Group C, and VTT of Group D were excellent. However, CIAE, KNF and PSI of Group B showed slightly lower prediction than the data, whereas KTH and NRC of Group A, AEKI, GP1 and GP3 of Group C, and GRS of Group D showed much lower prediction than the data. It should be noted that NRI of Group D produced significantly lower prediction than the data.

Table 8.1-1 shows the brief summary of the break flow rate and the accumulated mass. The peak flow rate, the mean flow rate at the plateau, and the transition time from the two-phase to single-phase flow, and the accumulated masses at the transition time and at 1,600 s were compared with the experimental data. Comparison results showed that KAERI of Group A, KOPEC and UNIPI of Group B, GP2 of Group C, and VTT of Group D predicted both the break flow rate and the accumulated mass very accurately. Each code has different critical flow models. The reported critical flow models are listed in Table 8.1-1, including the discharge coefficient used to fit their simulation results to the experimental data. Also their prediction results were classified into "agreed," "underestimated," "slightly underestimated," and "highly underestimated" as there isn't any "overestimated" results in Table 8.1-1. Through the (long) break nozzle with L/D = 12, fluid should have become near to be saturated at the tip of the nozzle even for the subcooled liquid at the nozzle inlet, which allowed a good critical flow rate

calculation by the employed critical flow models. The Ransom-Trapp model, modified CATHARE model, and Moody model with a discharge coefficient of 0.95 were properly used to agree with the experimental data reasonably well by KAERI, EDO Gid2(GP2), and VTT, respectively. In case of GP2, the hydraulic resistance of break nozzle was increased during the open calculation to correct the overestimation during the blind calculation. Also the Henry-Fauske model with a default discharge coefficient of 1.0 was properly used to agree with the experimental data reasonably well by both KOPEC and UNIPI. They simulated all the break line from the break nozzle to the containment simulator. However, KEPRI, CIAE, KNF, and PSI used discharge coefficients of 0.82 ~ 0.85 and they underestimated the break flow rates considerably even though they used the same Henry-Fauske model. Also the other critical flow models used by KTH, USNRC, AEKI, GP1, GP3, and NRI simulated the mean flow rates at the plateau lower than the experimental data.

Table 8.1-1 Summary of the break flow rate and accumulated mass

	Experiment	Group A				Group B					Group C				Group D		
		KAERI	KEPRI	KTH	USNRC	CIAE	KNF	KOPEC1	PSI	Univ. of Pisa	AEKI	EDO Gid 1 (GP1)	EDO Gid 2 (GP2)	EDO Gid 3 (GP3)	GRS	NRI	VTT
Peak flow rate (kg/s)	5.79	7.05	7.23	4.86	6.03	7.00	7.12	6.77	7.64	5.61	6.80	5.34	5.22	7.13	7.98	7.21	7.04
Mean flow rate at the plateau (kg/s)	4.12	3.60	3.89	2.57	2.59	4.22	3.65	4.63	3.67	3.94	3.75	2.96	3.76	3.04	2.93	2.09	3.96
Transition end time (second)	195	206	197	240	209	185	193	160	192	198	165	210	232	194	231	NA	194
Mass at transition time (kg)	825.4	819.2	836.3	680.1	670.6	816.2	796.2	793.2	789	811.4	679	702	884	699.6	768.9	NA	826.2
Mass at 1,600 s (kg)	1393.8	1403.1	1331.7	1094.2	1160.3	NA	1316.5	1401.4	1280	1400.1	1194.2	1315.7	1410	1266.1	1237.2	798.8	1423.9
Critical flow model used	-	R-T[1)]	H-F[2)] Cd:0.85	Note[4)]	Note[4)]	H-F Cd=0.83	H-F Cd:0.85	H-F[3)] Cd:1.0	H-F[2)] Cd:0.82	H-F [3)] Cd:1.0	Note[5)]	Modified CATHARE model	Modified CATHARE model	Modified CATHARE model	CDR1D with Cd:1.0	CDR1D with Cd:1.0	Moody model Cd:0.95
Simulation capability [6)]	-	G	SU	U	U	U	SU	G	U	G	U	SU	G	U	U	HU	G

[1)] Ransom-Trapp model (subcooled Cd= 0.9, two-phase Cd=1.2, superheated Cd=0.95)
[2)] Henry-Fauske model
[3)] Henry-Fauske model, piping from the break nozzle to the break valve was modeled
[4)] Burnell model (subcooled), Ransom-Trapp model (two-phase), isentropic expansion (single-phase vapor)
[5)] Gros d`Aillon correlation
[6)] G: Good Prediction, U: Underestimation, SU: Slight Underestimation, HU: High Underestimation

8.2 Multi-dimensional heater wall temperature behavior in the core

Since the multi-dimensional heater wall temperature behavior in the core was observed in the experiment, the 3-dimensional core modeling was used only by NRC with TRACE 5.0 Patch 2 among the participants. In parallel with that, the operating agency also performed additional 3-dimensional simulations with MARS-3D and TRACE 5.0 Patch 1 as a counterpart calculation. In order to model the core region, the "MULTID"' and "VESSEL" components were used in the MARS-3D and TRACE, respectively. Two calculations by the operating agency were preliminary ones as enough resources could not be allocated to perform the work. Detailed modeling information was included in Appendix-F.

It was found that there was no temporary temperature excursion in the MARS-3D and the TRACE calculation by operating agency. However, the TRACE calculation by NRC predicted a temporary temperature excursion in the heater groups 2 and 3, which was the similar results found in the experiment. However, this multi-dimensional effect in the prediction of the surface temperature of the heater rods was somewhat different from that of the experiment. In the experiment, a temperature excursion was observed only in the heater rods located in the 4^{th} quadrant of the cross sectional view (azimuthal angle between 0 degree and 90 degree) of the heater wall temperature distribution. However the TRACE calculation showed a temperature excursion in almost all azimuthal angles of the heater groups 2 and 3 except for the heater group G27.

Figure 8.2-1 and Figure 8.2-2 show that the TRACE predictions of the heater wall temperatures in the sub-group G33 at the azimuthal angle of 90 degree by NRC and the operating agency, respectively. Experimental DAS time was used as a reference time scale; the break starts at 193 s in DAS time. We can see a temperature excursion at about 380 seconds in the TRACE calculation by NRC. In the experiment, four heater rods produced temperature excursions at 9^{th}, 10^{th}, 11^{th}, and 12^{th} elevations, however, this TRACE calculation only resulted in a temperature excursion at 12^{th} elevation. Contrary to the NRC's calculation, the TRACE calculation by the operating agency did not show any temperature excursion. Another 3-D calculation result by MARS-3D was shown in Figure 8.2-3. No temperature excursion was predicted in the MARS-3D calculation. Therefore, the multi-dimensional non-uniformity in the heater wall temperatures was investigated only in the TRACE calculation by NRC.

More detailed contour plots of the heater wall temperature predictions by NRC are shown in Figure 8.2-4 and Figure 8.2-5. As NRC presented the heater wall temperatures at the same locations as the measurement, all predicted wall temperatures were interpolated to represent the 3-D distribution, in particular focusing on the temperature excursion period from 379.5 s to

384.5 s based on DAS time. It can be seen from these figures that most non-uniformity was observed at the top of the heaters; z=1819mm which is the highest measurement location. The temperature excursion started from 379.5 s and peak value was shown at 383.5 s. The decrease of the heater wall temperature occurred within 1 s; from 383.5 s to 384.5 s. The non-uniformity of the heater wall temperature was predicted in the wider region than that of the experimental result. Figure 8.2-6 shows the cross sectional view for the z-plane at z=1819mm. It is not clear that the temperature excursion in the 4th quadrant is higher than those in the other quadrants. Although the non-uniformity of the heater wall temperatures showing a temporary temperature excursion was predicted by the TRACE calculation by NRC at the similar time as the experiment, the elevation and the distribution of the non-uniformity of the heater wall temperatures were different from those in the experiment.

More investigation on multi-dimensional behavior in the core was done with a limited 3-D calculation results conducted by NRC and the operating agency. The main cause of the heater wall temperatures observed in the side region of the core rather than in the center region might be due to non-uniform mass flux distribution in the core region. If the mass flux in the center region is higher than that in the side region, a temperature excursion can be observed in the side region first. Unfortunately, there is no local data about the mass flux distribution in the core to support this reason. However, as the NRC's 3-D calculation succeeded in capturing the temperature excursion in the side region, the NRC's computational results were further investigated by the help of NRC.

Initial cross sectional mass flux distribution in the core by the TRACE code is shown in Figure 8.2-7. It can be seen from the figure that there are some asymmetries at the beginning of the problem, most notably in Ring 4. NRC modeled the core region with four Rings in a radial direction and the detailed information can be found in Appendix-F. NRC concluded that this may be attributed to the inherent instability of the model. However, once the transient initiates and the DVI break opens, the flow in Ring 4 becomes negative. This is an interesting result and may have an impact on the results—other data from the calculation suggests that the water in the Ring 4 area completely vaporizes first, followed by Ring 3, Ring 2, and then Ring 1. The Ring 1 fuel spends only about one second in the dryout phase, while the Ring 3 fuel spends about 3 seconds in the dryout phase (with Ring 2 only slightly shorter). Ring 4 has a void fraction of 1.0 for about 5 seconds. The radial heater wall temperature distribution cannot completely be attributed to the existence of the guide tubes cooling the interior of the core, since the current NRC model does not have any thermal coupling between the guide tubes and the core, essentially modeling the flow path of the guide tubes as a separate PIPE component that is not included in the volume/flow area of the core. At the moment, it is hard to reach any definite conclusions, though there was the possibility that the specific locations of the flow areas

through the FAP might result in flow dynamics that differ somewhat from a full-scale plant configuration. NRC modeled the FAP flow areas as faithfully as possible, with the flow orifices connecting to Ring 1 as well as four of the eight azimuthal sectors of Ring 2. NRC also modeled Ring 4 separately because including it in Ring 3 would have led to a fuel-to-water ratio that was much lower than it should be for the core region, but it is possible that this modeling resulted in some unexpected phenomena.

A cross sectional mass flux distribution by the TRACE code at the time of the temperature excursion is shown in Figure 8.2-8. Compared with the initial distribution, very low mass flux very close to zero was obtained over the whole cross section when the maximum heater wall temperature was obtained at 383.5 s. The side core region showed the smaller mass flux than the center region, resulting in temperature excursion. After the loop seal clearing, the mass flux increased again as shown in Figure 8.2-9. It is interesting that the center region showed an increasing positive upward mass flux, while the side region showed an increasing negative downward mass flux.

As a complementary calculation, the operating agency performed an independent 3-D calculation for the core region with the MULTI-D component of the MARS code. The calculated mass flux distribution at the 11^{th} measuring location, z=1645mm is shown in Figure 8.2-10. Before the break, a peak positive mass flux is obtained at the core center region, while lower mass flux is predicted in the azimuthal angles of 0, 90, 180, and 270 degrees. This non-uniform mass flux distribution is very similar to the TRACE's calculation. After the break, however, the mass flux greatly decreases and shows a nearly uniform distribution even though a little higher mass flux is still predicted in the center region. Mass flux distribution around at the time of the loop seal clearing is shown in Figure 8.2-11. A slight negative mass flux over the whole cross section is predicted, which is different from the TRACE's calculation.

In the both 3-D calculations by NRC and the operating agency, a strong 3-D behavior was obtained. In particular, a non-uniform parabolic mass flux profile over the cross section of the core was predicted by two codes. The center region where the mass flux is high was effectively cooled, whereas the side region where the mass flux is either relatively low or negative was not adequately cooled, resulting in a temperature excursion. This can be a good explanation of the temperature excursion first measured at the heater group 3 in the ISP-50 test. Unfortunately, there is no experimental data to confirm this reasoning, but it can be concluded that the 3-dimenaional flow distribution in the core region can significantly affect the core wall temperature behavior.

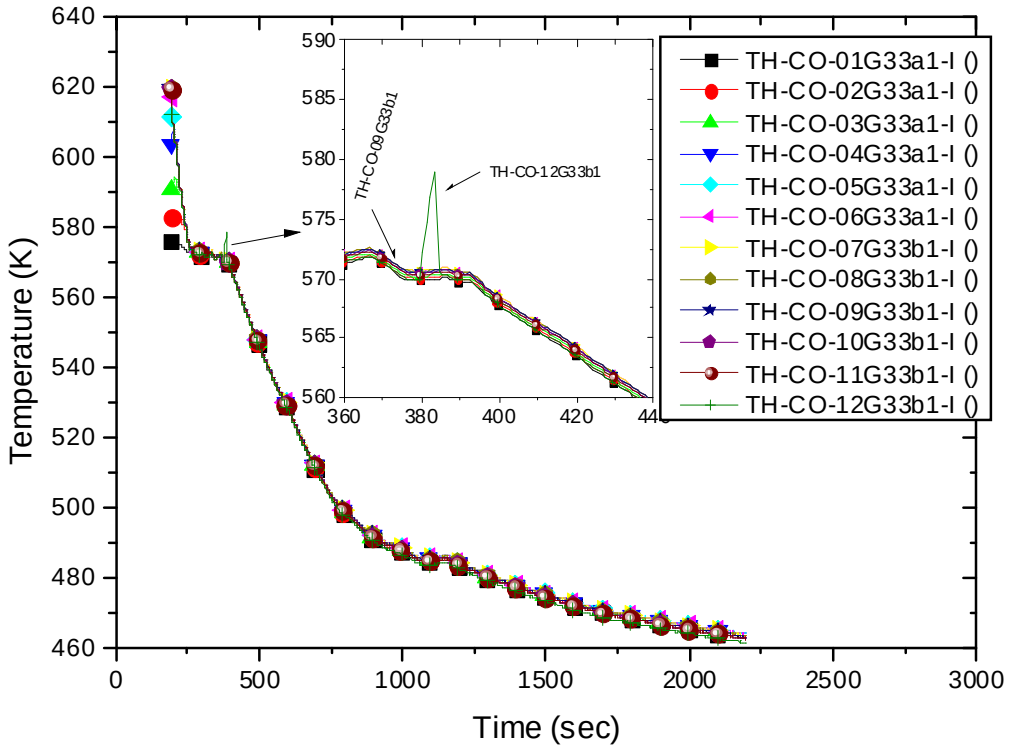

Figure 8.2-1 TRACE predictions of the wall surface temperatures of the heaters in G33a1 and G33b1 by NRC

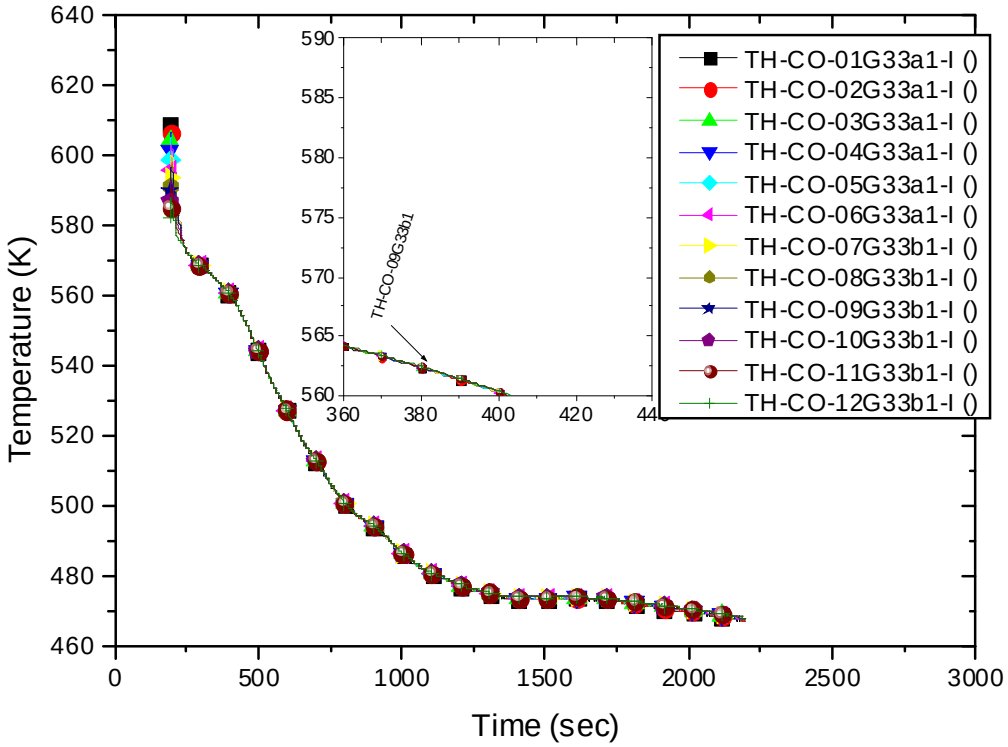

Figure 8.2-2 TRACE predictions of the wall surface temperatures of the heaters in G33a1 and G33b1 by operating agency

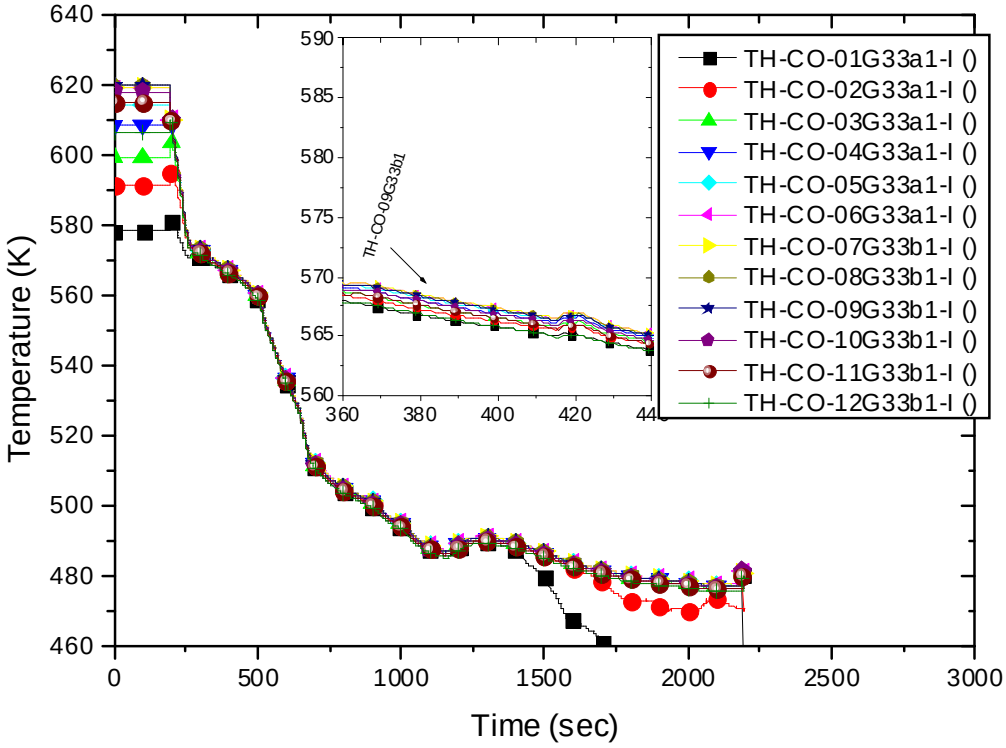

Figure 8.2-3 MARS-3D prediction of the wall surface temperatures of the heaters in G33a1 and G33b1

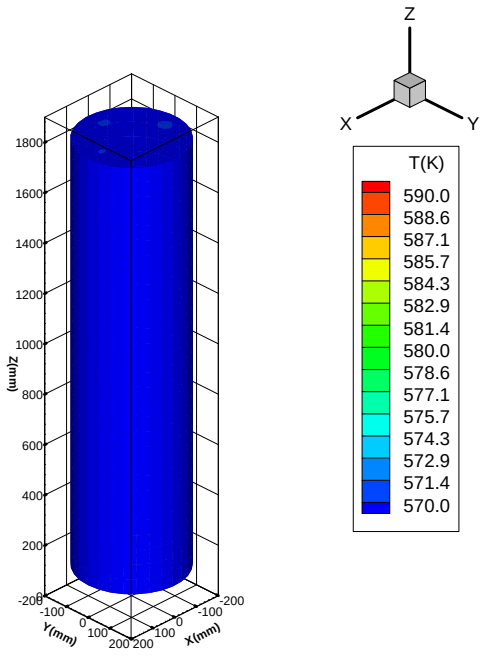

Shifted time=186.5 s
DAS time = 379.5 s

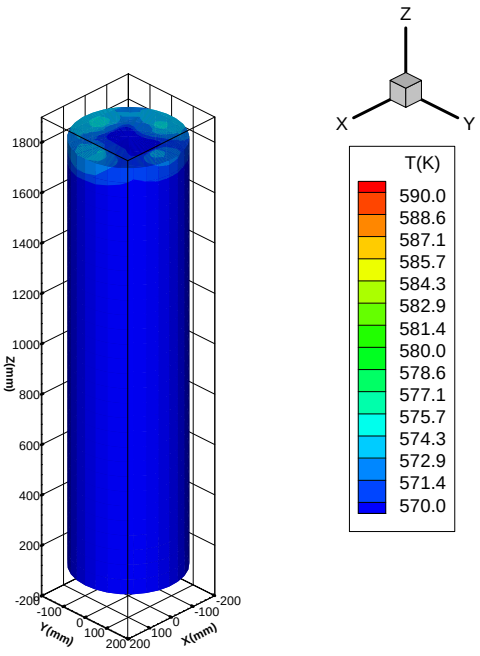

Shifted time=188.5 s
DAS time = 381.5 s

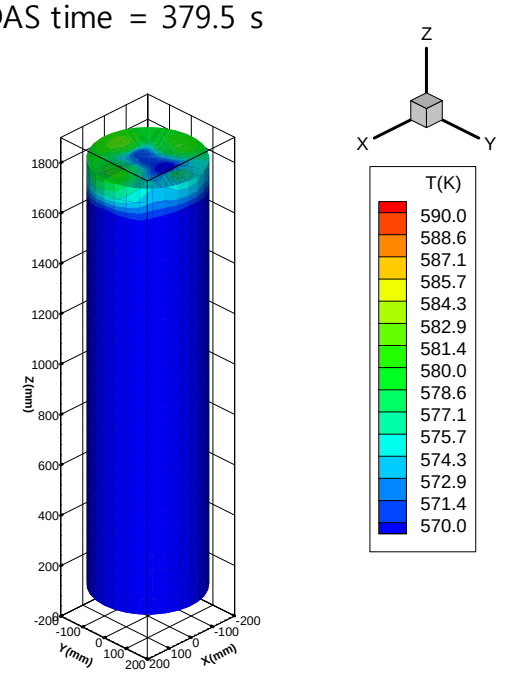

Shifted time=190.5 s
DAS time=383.5 s

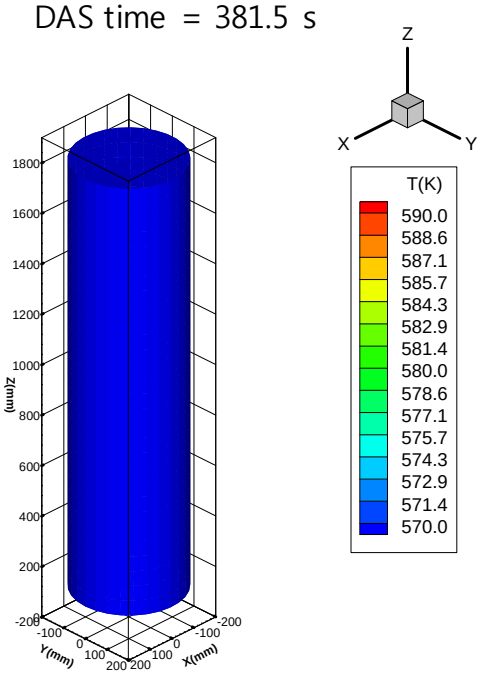

Shifted time=191.5 s
DAS time=384.5 s

Figure 8.2-4 TRACE prediction of the heater wall temperatures during temperature excursion

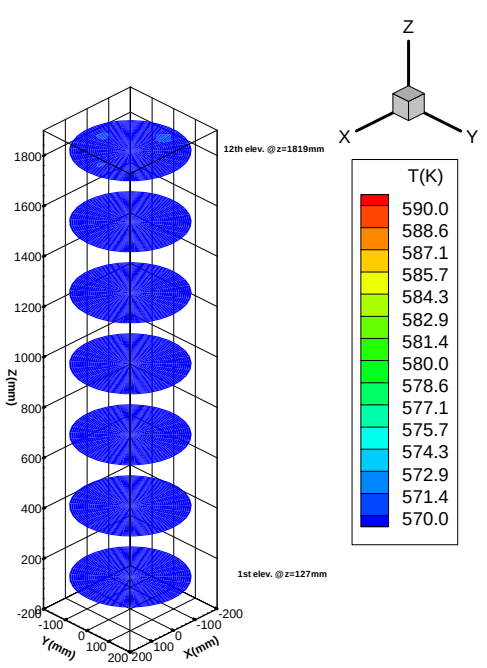

Shifted time=186.5 s
DAS time = 379.5 s

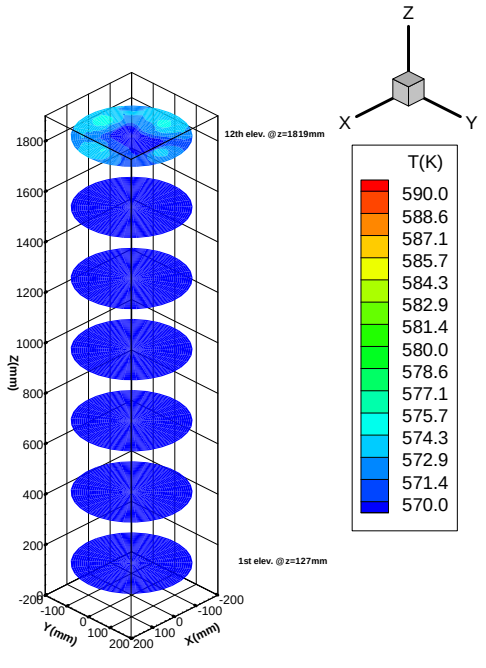

Shifted time=188.5 s
DAS time = 381.5 s

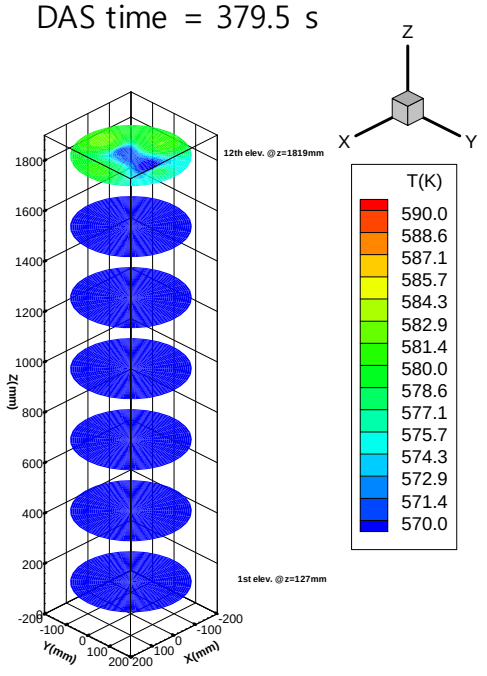

Shifted time=190.5 s
DAS time=383.5 s

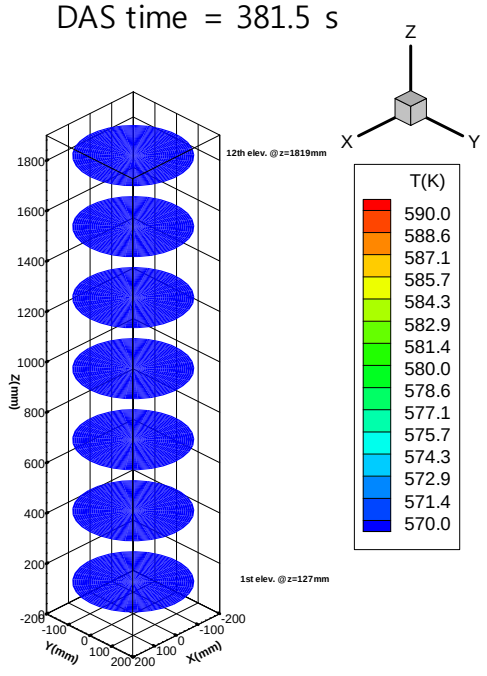

Shifted time=191.5 s
DAS time=384.5 s

Figure 8.2-5 TRACE prediction of the heater wall temperatures during temperature excursion in a z-plane

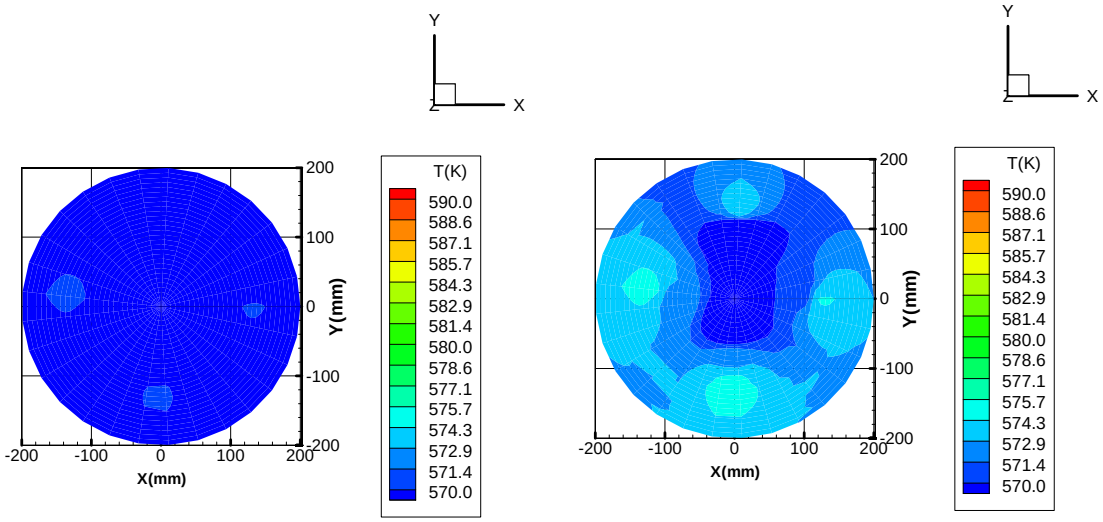

Shifted time=186.5 s
DAS time = 379.5 s

Shifted time=188.5 s
DAS time = 381.5 s

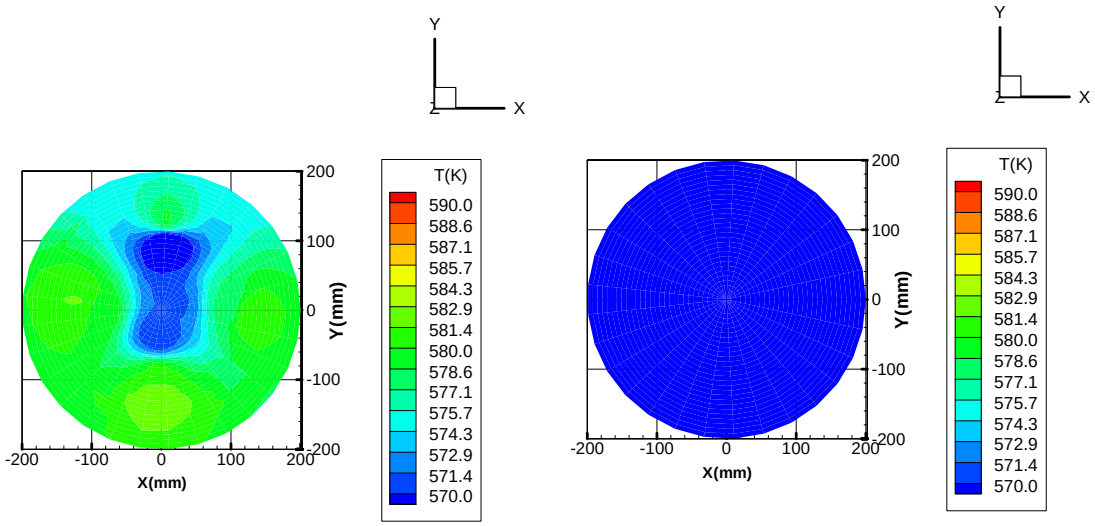

Shifted time=190.5 s
DAS time=383.5 s

Shifted time=191.5 s
DAS time=384.5 s

Figure 8.2-6 TRACE prediction of the wall surface temperature at the 20th elevation, z=1819mm

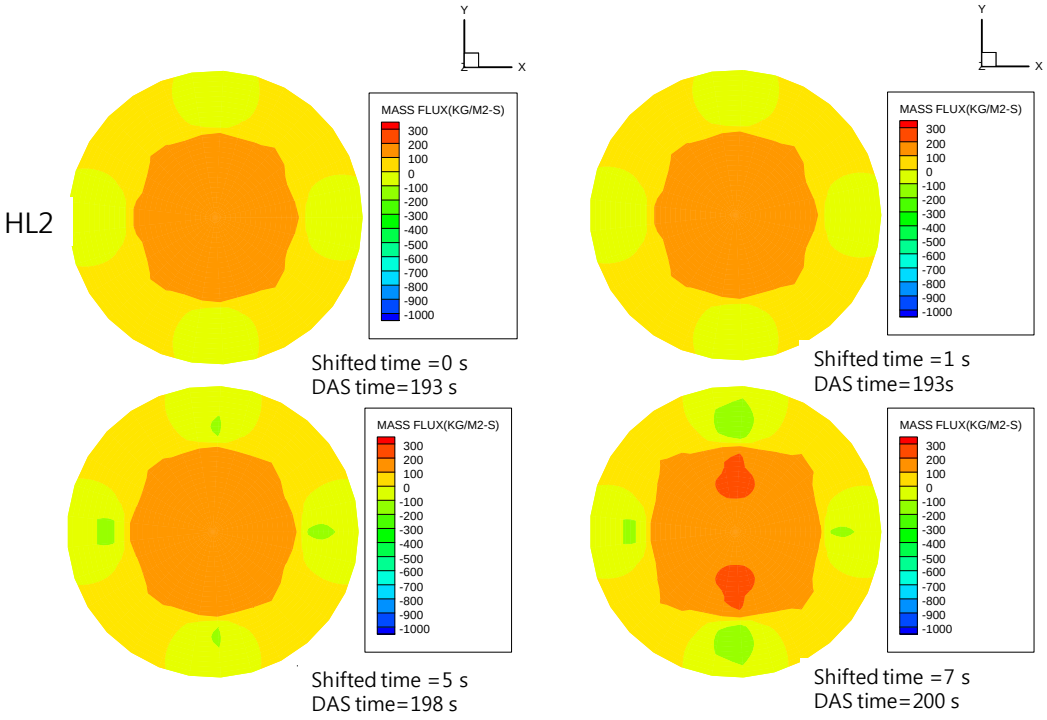

Figure 8.2-7 TRACE prediction of total mass flux at the top of the heated section, z=1905mm just after break

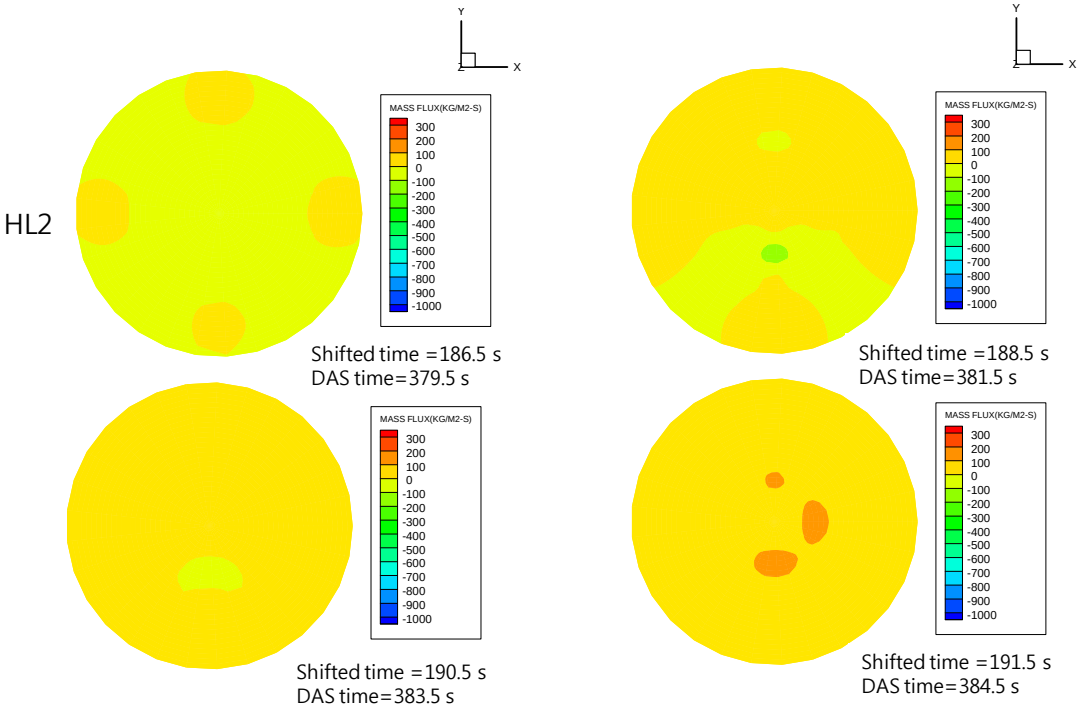

Figure 8.2-8 TRACE prediction of total mass flux at the top of the heated section, z=1905mm around loop seal clearing time

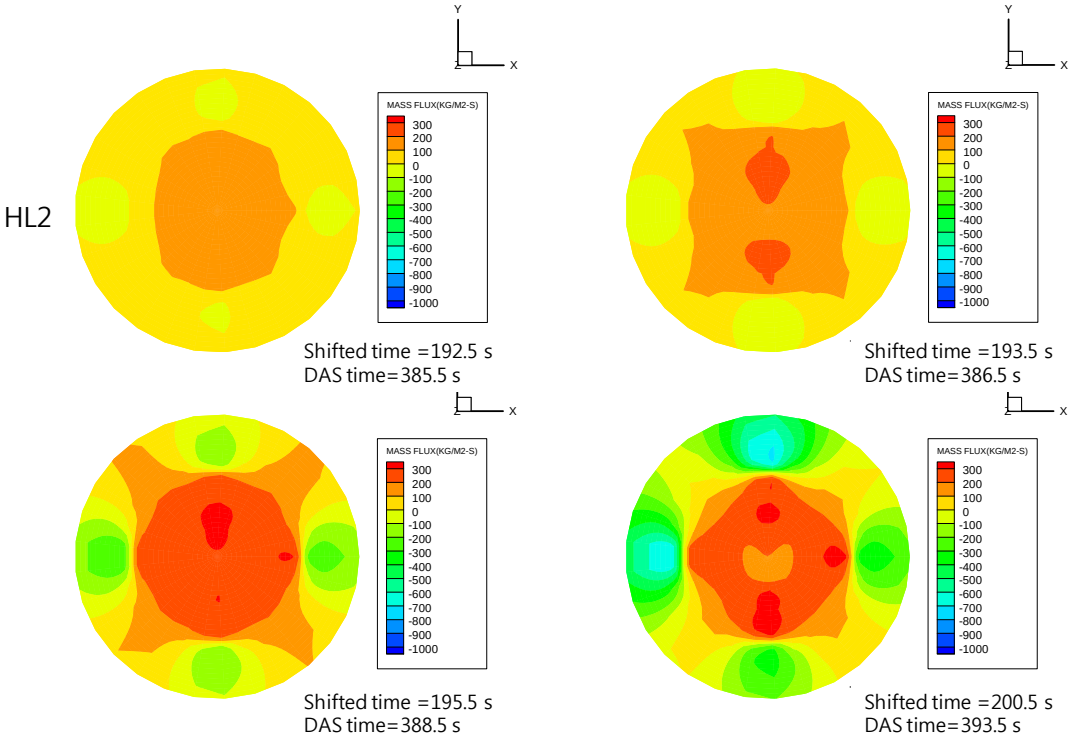

Figure 8.2-9 TRACE prediction of total mass flux at the top of the heated section, z=1905mm after loop seal clearing time

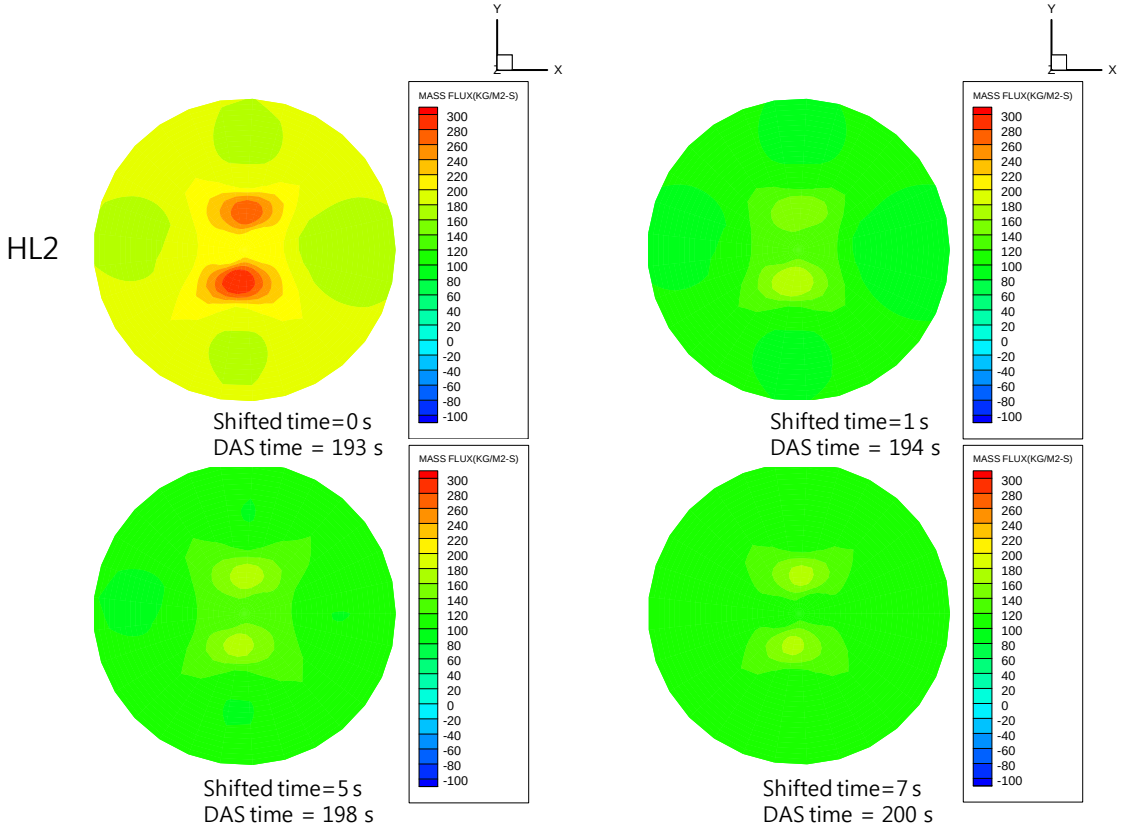

Figure 8.2-10 MARS-3D prediction of total mass flux at 11th elevation, z=1645mm

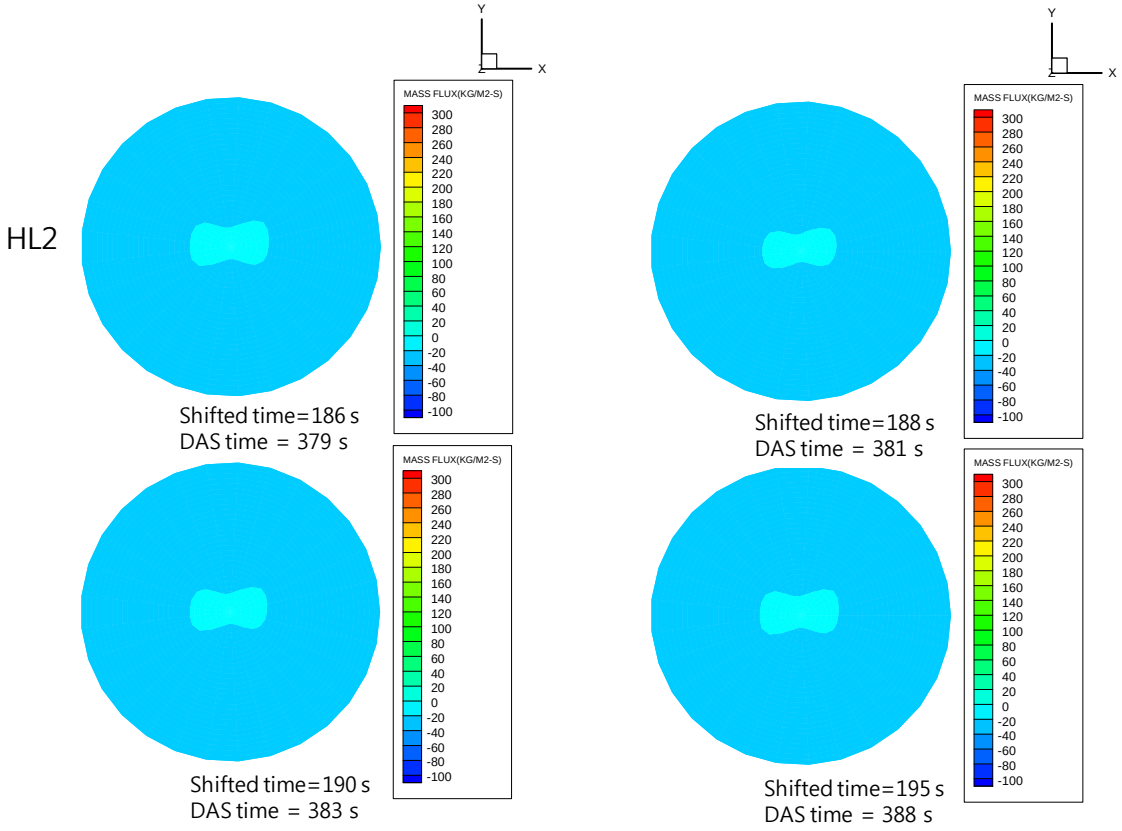

Figure 8.2-11 MARS-3D prediction of total mass flux at 11th elevation, z=1645mm around the loop seal clearing

8.3 Multi-dimensional behavior in the down-comer

Multi-dimensional fluid mixing in the down-comer region was highlighted in the present ISP-50 exercise. In order to investigate the down-comer mixing phenomena, the down-comer water levels need to be analyzed together with fluid temperature. The axial levels and the azimuthal sections in the down-comer region were defined in Section 3.5.12. Figure 8.3-1 shows the measured sectional collapsed water levels for upper down-comer from the axial level 4 through 7. Three typical phases can be identified based on the characteristics of the break flow. During the first phase from the break to 75 s, the sectional collapsed water level at the axial level 6 was full, where the broken DVI-4 was located. So it can be inferred that the break flow was a single-phase water discharge during this phase. During the second phase from 75 s to 200 s, the sectional collapsed water level at the axial level 6 maintained almost the same axial elevation of the broken DVI-4 and the break flow through the broken DVI-4 can be estimated to be in a 2-phase flow condition. Lastly after 190 s, the down-comer at the axial levels 5 and 6 were exposed to steam environment by the 1st loop seal clearing.

According to the above three phases, the down-comer fluid temperatures were examined.

In the first phase corresponding to the single-phase water discharge phase, most of the fluid temperatures in the down-comer decreased sharply by the upward cold fluid from the lower down-comer and then recovered to a certain value at the end of this phase as shown in Figure 8.3-2 and Figure 8.3-3. As the cold ECC water was injected at 54 s, it can be seen that the fluid mixing with the existing hot fluid started.

In the second phase corresponding to the two-phase discharge region, the fluid temperatures varied with respect to axial down-comer level. For example, in the lower axial levels 1 and 2, the fluid temperatures decreased slowly until the middle of the second phase and then increased to a certain value at the end of the second phase. But in the higher axial levels 5 and 6, the fluid temperatures showed quite large oscillations. In the middle axial levels 3 and 4, the fluid temperatures showed intermediate trends but close to those at the lower axial levels. Such fluid temperature oscillations started by actuation of the safety injection pump at 54 s. It could be concluded that the fluid temperatures in the higher down-comer region were affected by the cold ECC water from the safety injection pump.

It would be noteworthy here that the fluid temperature of the axial level 7 maintained the highest value during the first and second phases. From the collapsed water level as shown in Figure 8.3-1, it can be seen that the axial level 7 was quickly depleted during the first and the measured signal there indicated steam temperature rather than water temperature. So the steam temperature in the axial level 7 would be affected by the hot vessel wall. This seemed to be the reason why its temperature showed always higher than the others'.

In the following third phase corresponding to the single-phase steam discharge region, most of the fluid temperatures showed different trends from before. The test data showed that the amplitude of the oscillation was reduced and most of the fluid temperatures converged to a certain value then decreased according to the system pressure changes until 640 s as shown in Figure 8.3-4 and Figure 8.3-5. This would be explained by the fact that the down-comer region was exposed to steam environment after the loop seal clearings and major primary depressurization started by discharging the steam.

After 640 s, the temperature of the axial level 7 showed quite a large oscillation regardless of the subsections until the end of test. This would be due to evaporation of the ECC water from SITs by contacting the hot wall surface. For the other axial levels, the trends of the fluid temperatures between 2 subsections became different. In the subsection 2 where the broken DVI nozzle was located, all the fluid temperatures in the axial levels 1 through 6 showed the same trend as shown in Figure 8.3-4. However, in the subsection 4 which was the opposite side of the break, most of the fluid temperatures in the axial levels 1 through 5 showed the similar

trend as that in the subsection 2. But the temperature of the axial level 6 showed some oscillation as shown in Figure 8.3-5. This would be because of the effect of the ECC water from the safety injection tanks, which actuated at 468 seconds.

In the previous section 5.6.6, multi-dimensional effect in the down-comer fluid temperature was highlighted by comparing code calculation results with the data, focusing on azimuthal fluid mixing. The major multi-dimensional phenomena in the down-comer and code prediction capability can be summarized as follows:

Key phenomena

1. 1-Φ water discharge (0~75 s): typical blow-down trend, rapid drop in down-comer fluid temperature, no azimuthal temperature variation before the SIP injection
2. 2-Φ discharge (75~200 s): down-comer water level around the same elevation of the broken DVI nozzle, axial temperature stratification, well mixing of the ECC water from the SIP in azimuthal direction
3. 1-Φ steam discharge (200 s~): upper down-comer exposed to steam environment, nearly same temperature through the whole down-comer

Code predictions

1. 1-Φ water discharge (0~75 s): excellent agreement with the test data
2. 2-Φ discharge (75~200 s): weak thermal mixing of the ECC water from SIP in the axial and the azimuthal directions
3. 1-Φ steam discharge (200 s~): large temperature variations but nearly same temperature in the lower down-comer

It was found that the measured multi-dimensional phenomena during the 2-Φ discharge and 1-Φ steam discharge phases were not well predicted. Although the most calculations used two-dimensional approaches in the down-comer regions based on connection of 1-D cell with each other, this modeling was not sufficient to capture the multi-dimensional mixing behavior appeared in higher axial levels from 3 through 6.

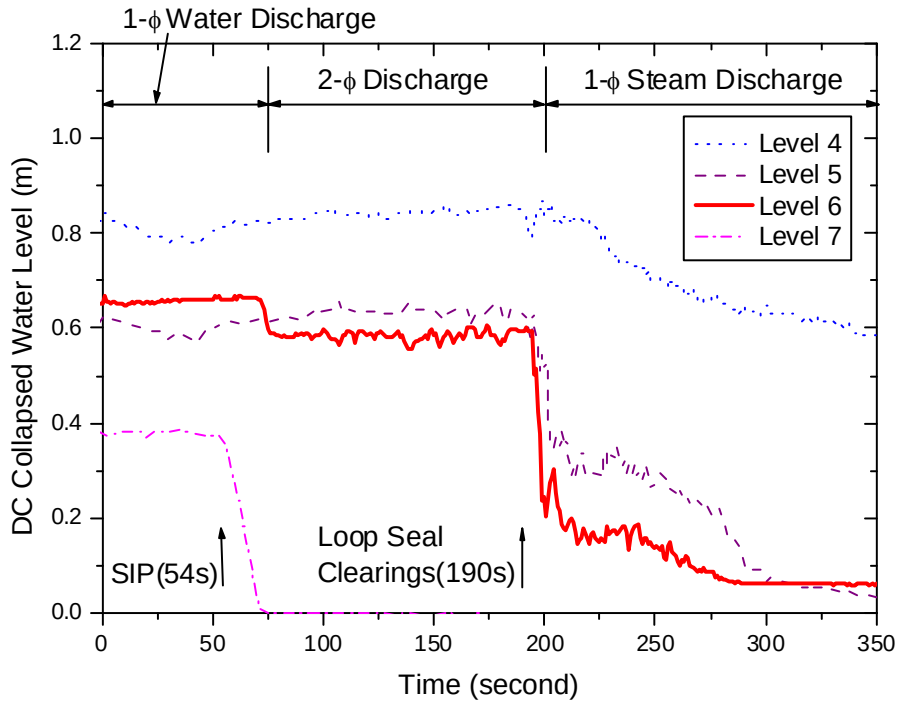

Figure 8.3-1 Measured collapsed water levels in the down-comer levels 4 through 7

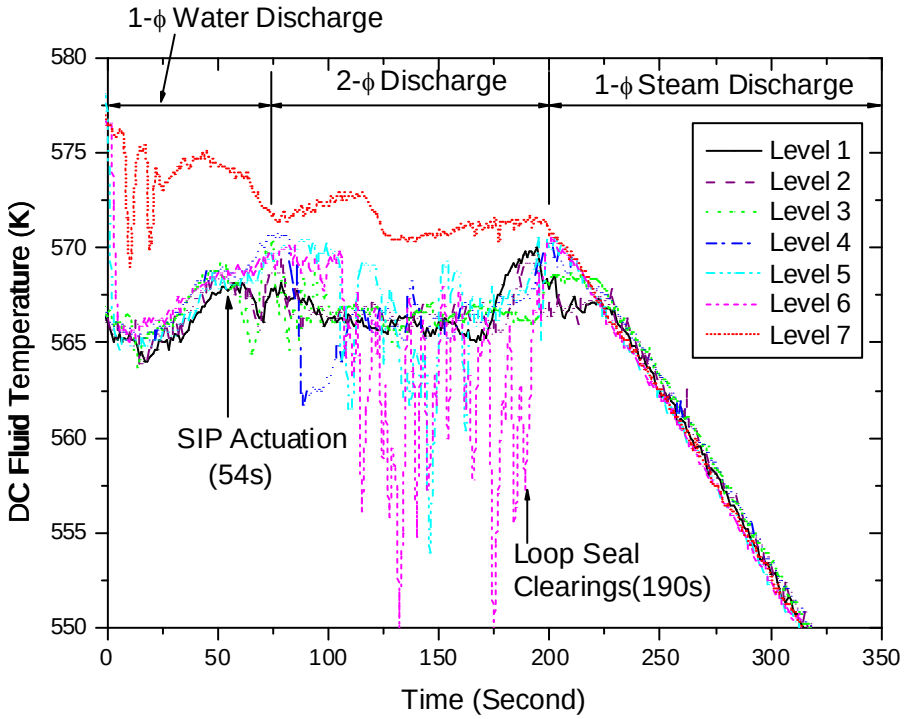

Figure 8.3-2 Down-comer fluid temperature distributions at subsection 2 during the initial period

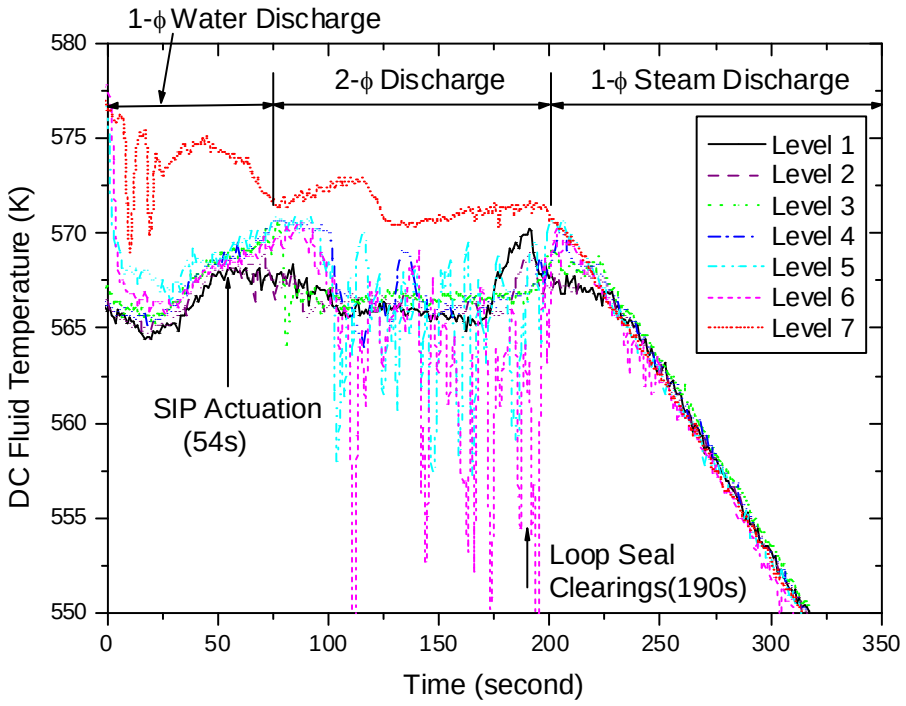

Figure 8.3-3 Down-comer fluid temperature distributions at subsection 4 during the initial period

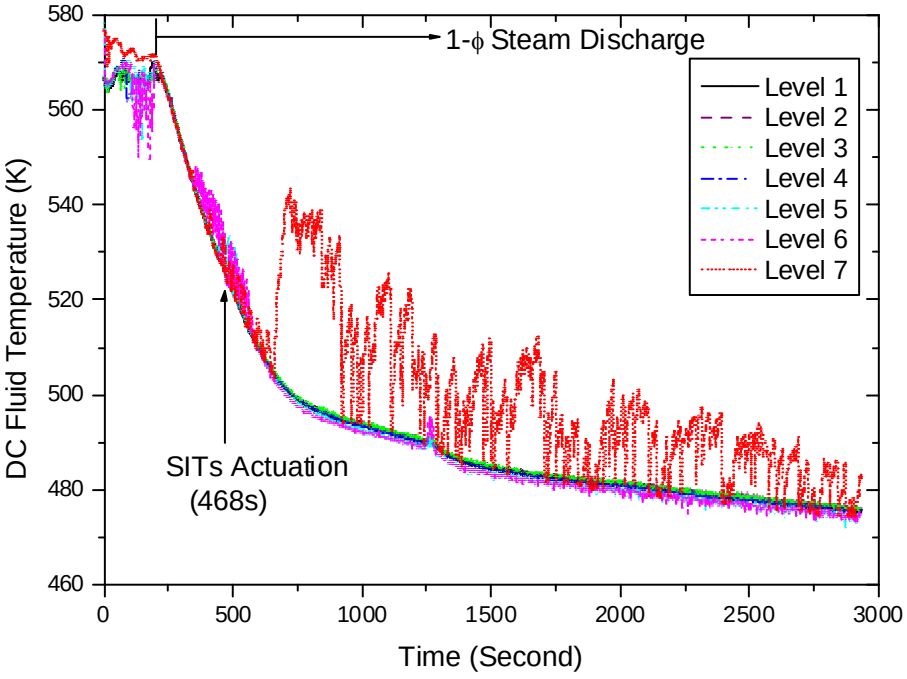

Figure 8.3-4 Down-comer fluid temperature distributions at subsection 2 during a single phase discharge period

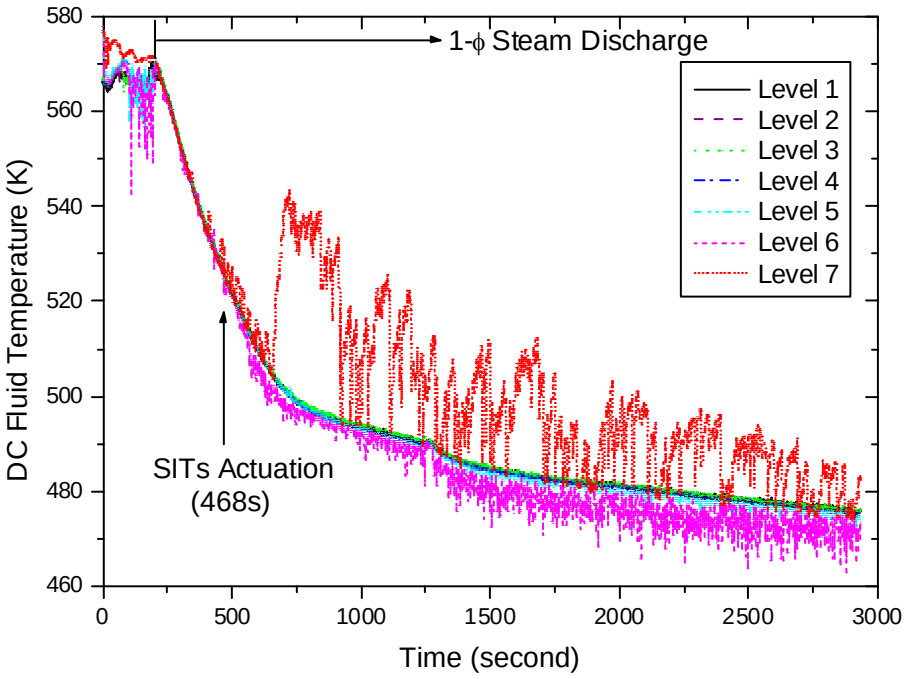

Figure 8.3-5 Down-comer fluid temperature distributions at subsection 4 during a single phase discharge period

8.4 Down-comer to upper head interaction

The bypass flow between the down-comer and the upper head is important because it is influential to the 3-D downcomer fluid behavior. This bypass flow was simulated by two external pipelines in the test as described in Section 3.5.15 and was also simulated by a simple junction in most calculations. The bypass flow pipeline is the only flow passage from the upper head to the broken DVI nozzle in the early period of the DVI line break scenario and the bypass flow rate is affected by the pressure built in the upper head. Thus, only the flow direction and the bypass flow rate are worthy of investigation as one of the important thermal-hydraulic phenomena. In general, the prediction accuracy of the bypass flow was not satisfactory in all the participant's calculations. The variations of the bypass flow rate according to the pressure build-up in the core were not calculated correctly. On break, negative bypass flow direction from the upper head to the down-comer is expected physically, because the break nozzle is located at the down-comer region. However, positive bypass flow rates were found in the calculations by KAERI, GP1, NRI, and VTT. It was obviously due to misunderstanding of the definition of the bypass flow direction. Therefore, such positive bypass flow directions were reversed by the operating agency for meaningful comparison as shown in Figure D.95.

In the Group A, NRC and KTH showed no bypass flow rates during the whole transient

period as shown in Figure D.95-A, implying that the bypass flow was not modeled. Whereas the KAERI's calculation showed the similar trend but the bypass flow rate was reduced earlier than the data. The KEPRI's calculation underestimated the bypass flow rate.

Comparison of the calculations in the Group B was shown in Figure D.95-B. CIAE did not model the bypass flow. On the other hand, the other participants predicted the similar bypass flow trends as the data, but they all underestimated the bypass flow rate. The KOPEC's calculation underestimated the bypass flow the most. They also showed earlier reduction in the bypass flow than the data, which was the same results found in the Group A. UNIPI predicted the initial high bypass flow rate as close as the data, though they slightly overestimated it.

In the Group C, GP1 was the only calculation to simulate the bypass flow as shown in Figure D.95-C. The initial bypass flow rate was greatly overestimated and the bypass flow rate was higher than the data during the whole transient.

In the Group D, the NRI's calculation showed extraordinarily high initial bypass flow rate and also a great value around 240 s. Initial period was enlarged for clear comparison and plotted together as shown in Figure D.95-D. VTT showed the best agreement with the data and GRS showed a little delayed bypass flow peak compared with the data.

The down-comer to upper head bypass flow has been known to affects the pressure and inventory distribution in the RPV significantly in the typical small break LOCAs. If the bypass flow is not simulated, the pressure in the core is easily built-up, resulting in deep depression in the core water level compared with the case where the bypass flow exists. Consequently, this induces an earlier and higher heater rod wall temperature. [Osakabe et al. 1988]. This behavior was also confirmed in the ATLAS tests.

On the other hand, the modeling of the bypass flow did not affect the major thermal-hydraulic phenomena such as the break flow rate, the primary system pressure, and the core water level in most calculations. It is recommended that the modeling of the bypass flow needs to be improved in the calculations.

8.5 Non-uniform loop seal clearing

A driving force of the loop seal clearing is a hydrostatic head imbalance between the reactor vessel down-comer and the top of the bend in the steam generator tubes. This hydrostatic head imbalance pushes the liquid in the steam generator outlet piping to below the spill-under elevation, and it causes the differential pressure between the down-comer and the upper part of the core region. Because the spill-under elevation is below the top of the core, the core

collapsed water level can be depressed below the top of the core, possibly allowing cladding temperature excursions. Therefore, the loop seal clearing phenomena has a consequential effect on the PCT during the SBLOCA sequence. Moreover, in the postulated DVI line break accident of the APR1400, the loop seal clearing phenomena is closely related to the multi-dimensional behavior in the down-comer due to the 1.05 m higher elevation of the DVI nozzles than those of the cold legs.

As mentioned in section 3.5.16, the loop seals in each loop show a different clearing behavior during the experiment. The loop seals of 1A, 1B were cleared at 190 s, and the loop 2A was not cleared during the whole period of the experiment. On the other hand, the loop 2B was cleared at around 1,236 s, which was about 790 s after the SIT actuation. When the first loop seal clearing was observed at the loop 1A and 1B, the differential pressure between the down-comer and the upper head region, measured by DP-DCUH1-01, reached its maximum value, and then this differential pressure rapidly decreased with the loop seal clearing at the corresponding loops until the SIT actuation at 467 s through the DVI nozzle -1, -2, and -3. With the SIT injection flow, the down-comer and upper head differential pressure steadily increased again, and the collapsed water levels in the upper down-comer region, measured by LT-DC-04, -05, and -06 also increased continuously.

The operating agency performed a series of DVI line break tests for the various break sizes from 5% to 100%. In all case, the loop seal clearing was observed, but the location and sequence of the loop seal clearing was different with each other. Summary of the sequence of events for various break sizes is shown in Table 8.5-1. Measured collapsed water levels from these transmitters were plotted from Figure 8.5-1 to Figure 8.5-7.

Summarizing the loop seal clearing observed in the DVI line break tests, the number of the loop seals cleared during the test is directly proportional to the break size. Also, it took more time for the loop seal clearing to occur as the break size became smaller. The case of the 100% break resulted in loop seal clearing in all four loops. The case of the 50% break brought about loop seal clearing in three loops, and so does the 25% break case. The 5% break case led to periodic loop seal clearing only in the loop 1B.

Figure 8.5-8 shows the measured fluid temperature trends in the two hot legs and the pressurizer. With the inception of the break, the fluid temperature in the hot leg-2 was decreased sharply due to the injection of relatively cold water in the surge line into the HL-2, and then it was restored with the hot water injection from the pressurizer. The fluid temperature of the surge line can be seen in Figure 8.5-9. After this fluctuation, the fluid temperature of the HL-2 showed a linear decreasing trend with the inventory discharging through the break point.

Then it maintained a constant temperature until the loop seal clearing occurred in IL-1A and -1B. During this phase, temperature of the HL-2 shows a nearly same value with that of the HL-1 within the uncertainty range. From this observation, it can be understood that the inventory injection from the pressurizer to the HL-2 has not significant effect on the loop unbalance which is a main factor for the asymmetric loop seal clearing.

Other possible reason for the asymmetric first loop seal clearing phenomena observed in the present experiment is an unbalanced water level in the primary pipes shown in Figure 8.5-10. As can be observed in Figure 8.5-10, the measured water level in the CL-2A was in the slightly higher level than those of the other cold legs. The higher water level in the CL-2A indicates that a relatively larger water inventory was accumulated in the loop-2 side than the loop-1 side. Considering that the water level in the hot leg was in the nearly same level before the first loop seal clearing period, this larger water inventory can be acted as a blocking force for the loop seal clearing. Therefore, the first loop seal clearing had occurred in the loop-1 only.

Table 8.5-1 Summary of the sequence of events for DVI line break simulations

Test ID	Break size (%)	Break (sec)	LPP (sec)	SIP (sec)	SIT (sec)	1st loop seal clearing (sec)/cleared loops	Remarks
SB-DVI-06*	5	202	400	428	-	8238~ 8244/1B	Oscillatory LSC
		0	198	226	-	8036~ 8042/1B	Shifted time
SB-DVI-04	25	195	242	269	1695	674 ~ 680/1A, 2B	partial 2nd LSC
		0	47	75	1500	479 ~ 485/1A, 2B	Shifted time
SB-DVI-05*	25	202	246	291	1665	674 ~ 688/1A, 1B, 2B	No 2nd LSC
		0	44	89	1463	472 ~ 486/1A, 1B, 2B	Shifted time
SB-DVI-07	50	202	226	254	671	379 ~ 385/1A, 1B	2nd LSC @1250s/2B
		0	24	52	469	177 ~ 183/1A, 1B	Shifted time
SB-DVI-09*	50	193	218	247	661	383 ~390/1A, 1B	2nd LSC @1429s/2B
		0	25	54	468	190 ~197/1A, 1B	Shifted time
SB-DVI-03	100	198	217	245	431	281 ~ 288/All	
		0	19	47	233	83 ~ 90/All	Shifted time
SB-DVI-08*	100	199	219	246	431	281 ~ 288/All	
		0	20	47	232	82 ~ 89/All	Shifted time

* reference case

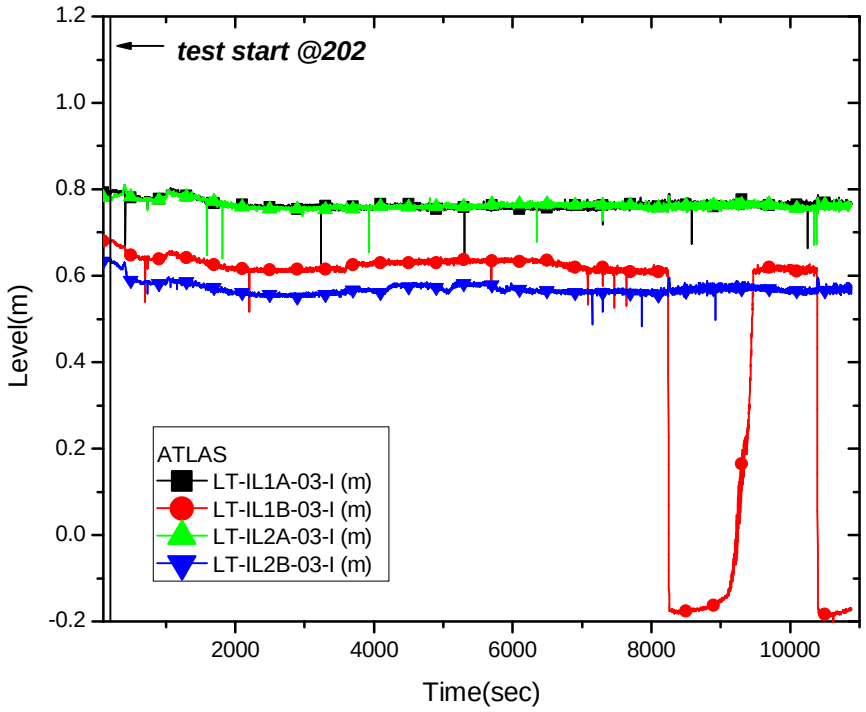

Figure 8.5-1 Collapsed water levels of the vertical intermediate legs for SB-DVI-06 (5%)

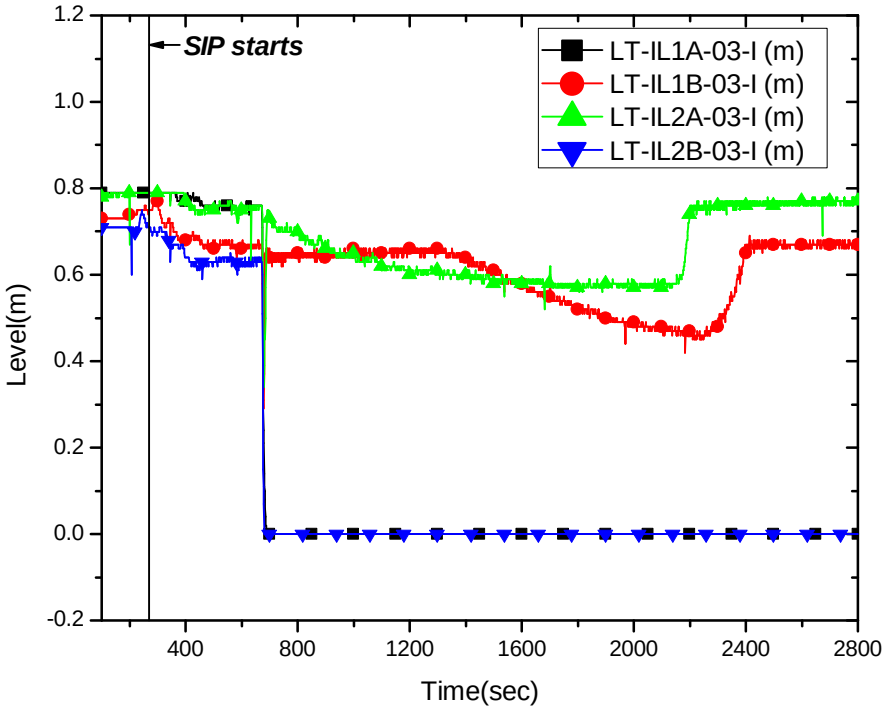

Figure 8.5-2 Collapsed water levels of the vertical intermediate legs for SB-DVI-04 (25%)

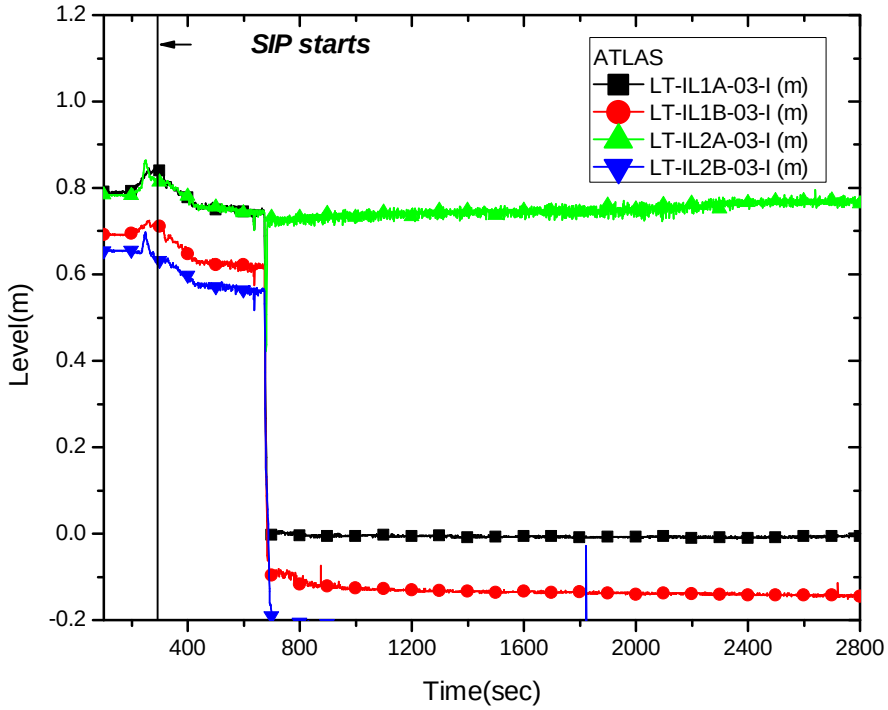

Figure 8.5-3 Collapsed water levels of the vertical intermediate legs for SB-DVI-05 (25%)

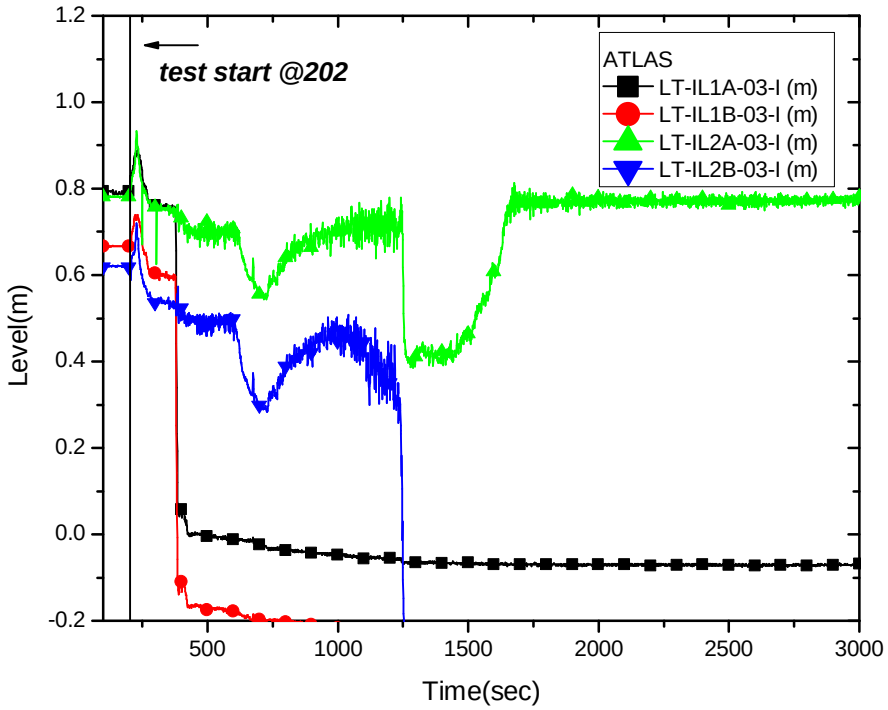

Figure 8.5-4 Collapsed water levels of the vertical intermediate legs for SB-DVI-07 (50%)

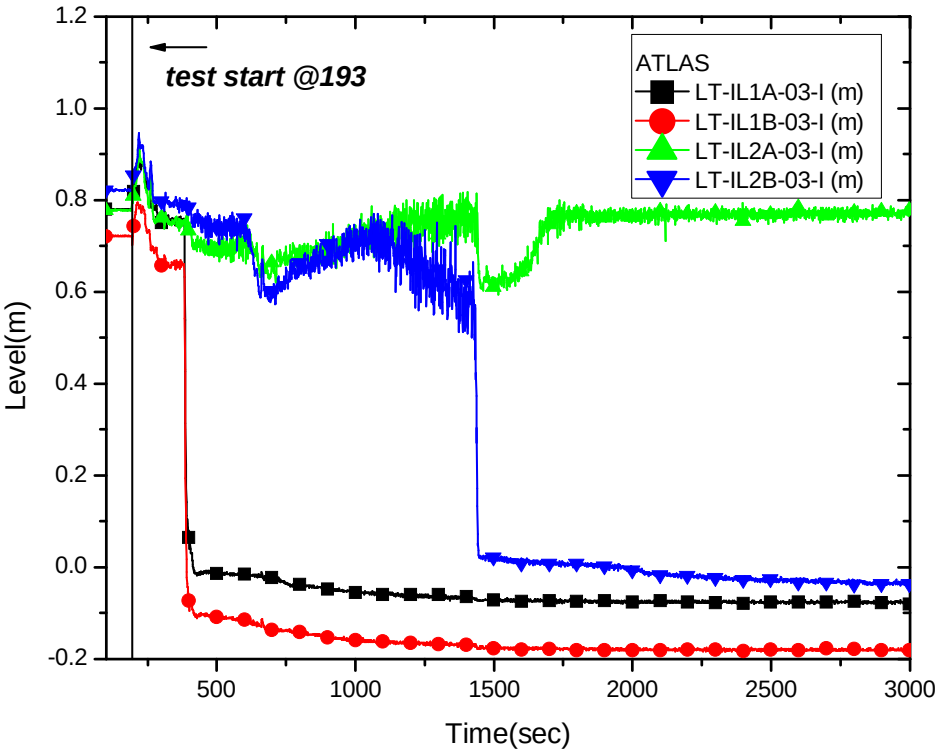

Figure 8.5-5 Collapsed water levels of the vertical intermediate legs for SB-DVI-09 (50%)

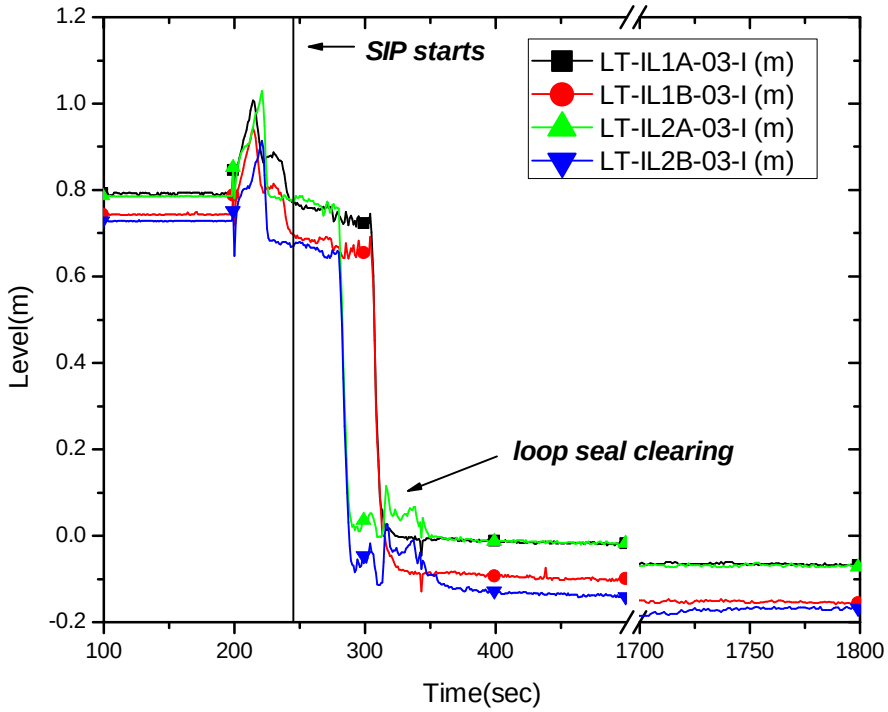

Figure 8.5-6 Collapsed water levels of the vertical intermediate legs for SB-DVI-03 (100%)

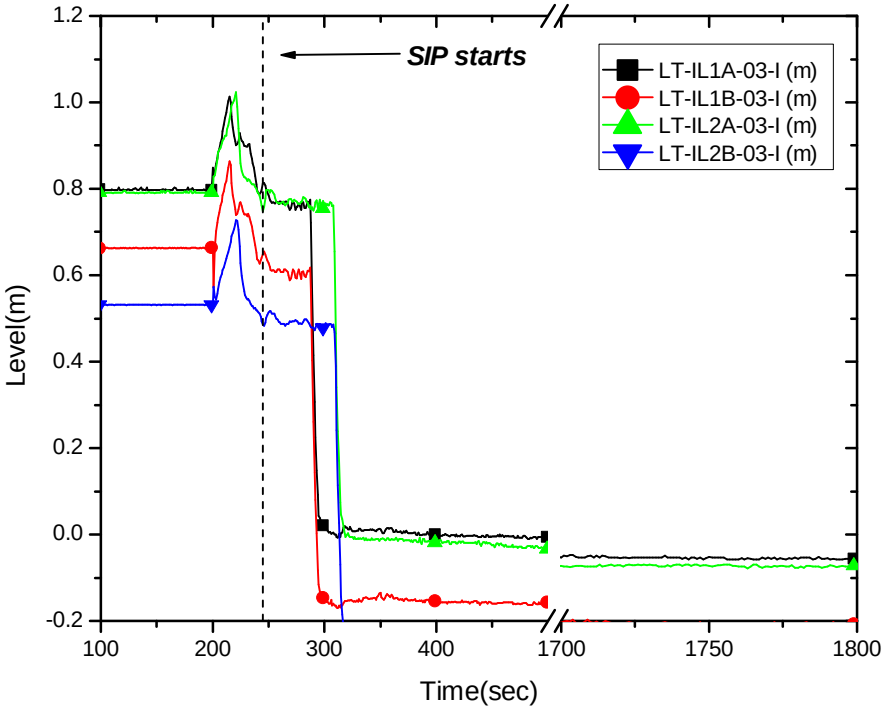

Figure 8.5-7 Collapsed water levels of the vertical intermediate legs for SB-DVI-08 (100%)

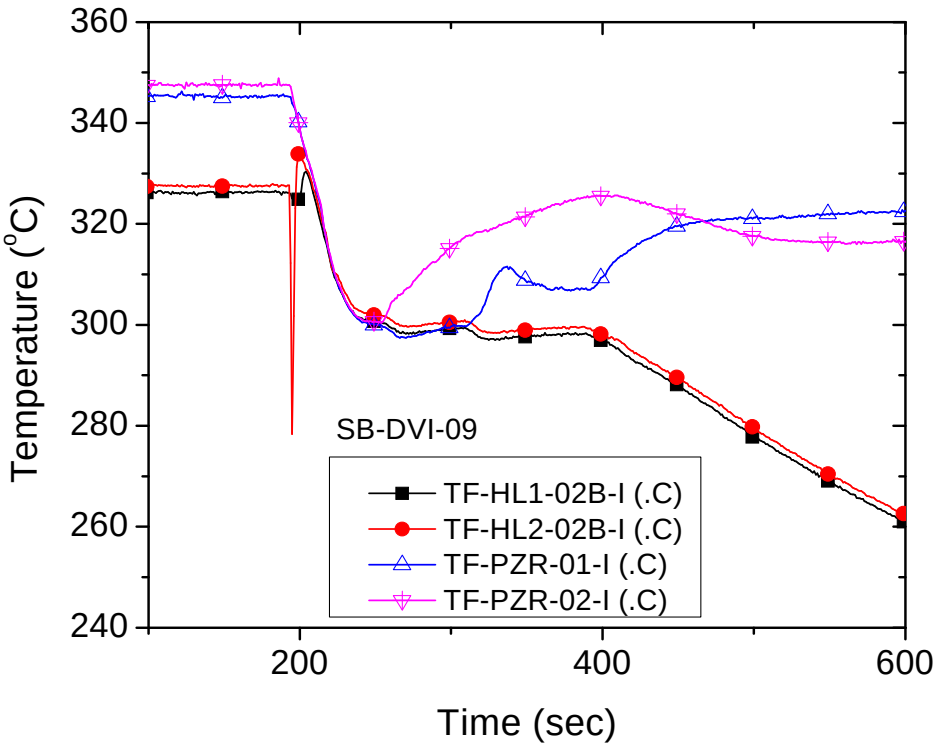

Figure 8.5-8 Comparison of fluid temperature in the hot leg and pressuizer for SB-DVI-09

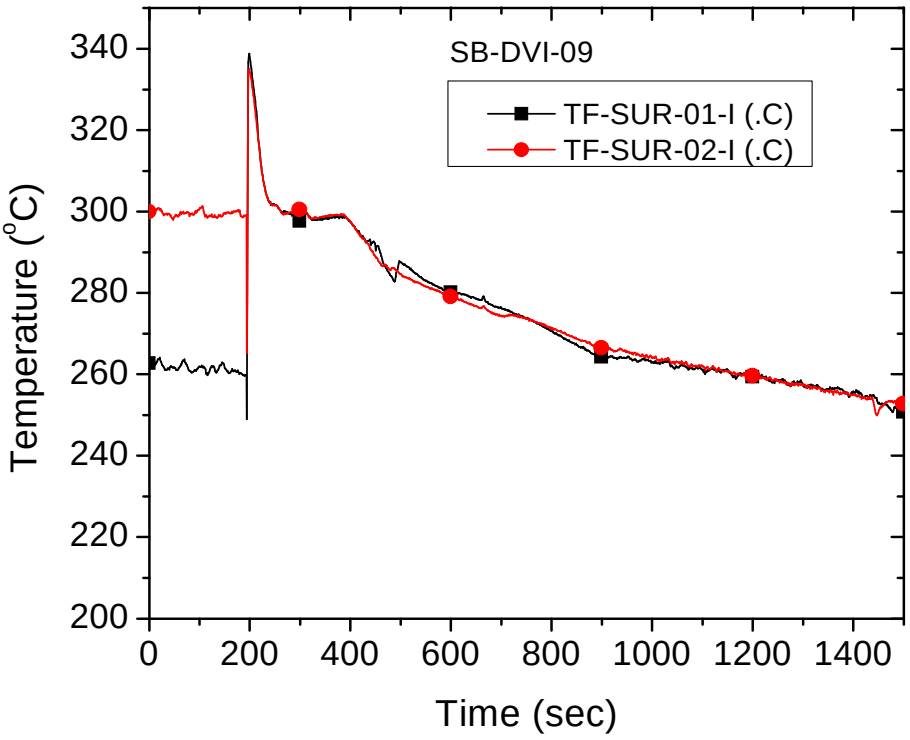

Figure 8.5-9 Fluid temperature in the surge-line of SB-DVI-09

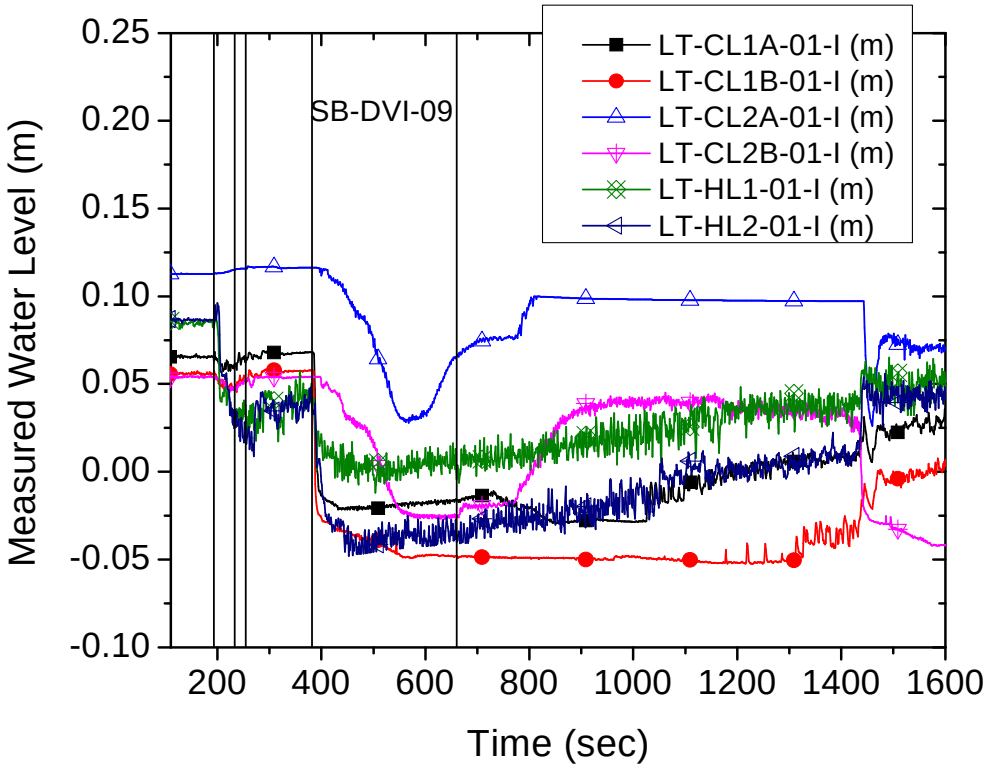

Figure 8.5-10 Water level behavior in the primary piping of SB-DVI-09

8.6 Secondary system pressure

While the prediction performance of the primary system pressure was relatively excellent, the secondary system pressures were not properly estimated in many calculations. Especially, the secondary system pressures subsequent to the MSSV opening were over-predicted. The plausible causes for the over-prediction of the secondary system pressure are the loop seal clearing behavior, the heat loss, and the fluid condition inside the U-tubes. If the loop seal clearing behavior was predicted to occur later than the data, the secondary system pressures show a tendency of over-estimation. When the loop seal is cleared, the U-tubes of the steam generators are emptied, causing secondary system depressurization by the reverse heat transfer. Otherwise, the reverse heat transfer rate is deteriorated after the heat-up of the steam confined inside the U-tubes. In the ISP-50 test, the primary heat loss at the initial condition was about 83 kW and the secondary heat loss of each steam generator was about 29 kW. During the test, the primary heat loss was compensated by adding it to the core decay power table with respect to time. The secondary heat loss, however, was not compensated in the test. Table 8.1-1 summarizes the detailed heat loss modeling and the prediction performance of the secondary system pressure in each calculation. The primary and the secondary heat loss were considered by using the constant heat transfer coefficient under the constant ambient temperature in many calculations. At this stage, a definite conclusion on the relation between the heat loss modeling and the secondary system pressure prediction cannot be made due to the lack of the detailed information on the code input modeling and also the use of the different codes in each calculation. However, it can be rationally expected that modeling of the heat loss at the steam generators affects the secondary system pressure behavior. In the KAERI calculation where the MARS code was used, modeling of the heat loss at the steam generators results in the difference of the secondary system pressure prediction. Figure 8.6-1 shows the comparison of the secondary system pressures between the ISP-50 test and the KAERI calculation. As a sensitivity study for the secondary heat loss, two cases of the calculations were performed. When the secondary heat loss was not modeled, the secondary system pressures were highly over-estimated as shown in Figure 8.6-1. On the other hand, when the secondary heat loss was modeled, the prediction performance of the secondary system pressures was significantly improved even though they were under-predicted after 750 seconds of the test period. Figure 8.6-2 shows the variations of the heat loss in both the ISP-50 test and the KAERI calculation. Compared to the ISP-50 test, the secondary heat loss was larger in the KAERI calculation. Excessive heat loss at the steam generators may induce the under-prediction of the secondary system pressures in the KAERI calculation. Despite the difference from a quantitative point of view, it can be found in the KAERI calculation result that the heat loss at the steam generators needs to be properly modeled for the accurate estimation of the secondary system pressures.

Another possible source of over-prediction of the secondary pressure is the quality of the steam entering the U-tubes after the loop seal clearing. If the steam quality at the U-tube inlet is lower in calculation than in the test, it would result in less reverse heat transfer from the secondary to the primary system and consequently higher secondary pressure than the data is obtained in calculation and vice versa. Unfortunately, however, the present ISP-50 test does not provide such detailed local information on the steam quality to support this reasoning.

Table 8.6-1 Detailed heat loss modeling and the prediction performance of the secondary system pressure in each calculation

Grp	Participant	Detailed heat loss modeling		SG pressure prediction performance
		Primary system	Secondary system	
A	KAERI	h: 8 W/m^{2}K @ 300 K	h: 8 W/m^{2}K @ 300 K	Good agreement with under-estimation later
	KEPRI	Not modeled	Not modeled	Over-estimation
	KTH	Not modeled	Not modeled	SG-1: good agreement SG-2: under-estimation
	USNRC	Not modeled	Not modeled	Under-estimation
B	CIAE	h: 12.44 W/m^{2}K	h: 5.33 W/m^{2}K	SG-1: over-estimation SG-2: good agreement
	KNF	Not modeled	Not modeled	SG-1: good agreement SG-2: over-estimation
	KOPEC1	Not modeled	Not modeled	Over-estimation
	PSI	h: 17.0 W/m^{2}K @ 298.15 K	h: 4.5 W/m^{2}K @ 298.15 K	Over-estimation
	UNIPI	Adjusted to the test condition	Adjusted to the test condition	SG-1: over-estimation SG-2: good agreement
C	AEKI/KFKI	h: 10.0 W/m^{2}K @ 298.15 K	h: 10.0 W/m^{2}K @ 298.15 K	Over-estimation
	GP1	Use of same correlation to the test	h: 4.5 W/m^{2}K @ 298 K	Over-estimation
	GP2	h: 18.0 W/m^{2}K @ 293 K	Not modeled	Over-estimation
	GP3	Not modeled	Not modeled	Over-estimation
D	GRS	h: 10.0 W/m^{2}K @ 298 K	h: 5.0 W/m^{2}K @ 298 K	Good agreement
	NRI	PZR (h: 14 W/m^{2}K) RPV (h: 15.4 W/m^{2}K) Loop (h: 15.3 W/m^{2}K)	h: 6.5 W/m^{2}K	SG-1: under-estimation SG-2: good agreement
	VTT	Constant HTC to adjust test condition	Constant HTC to adjust test condition	Under-estimation

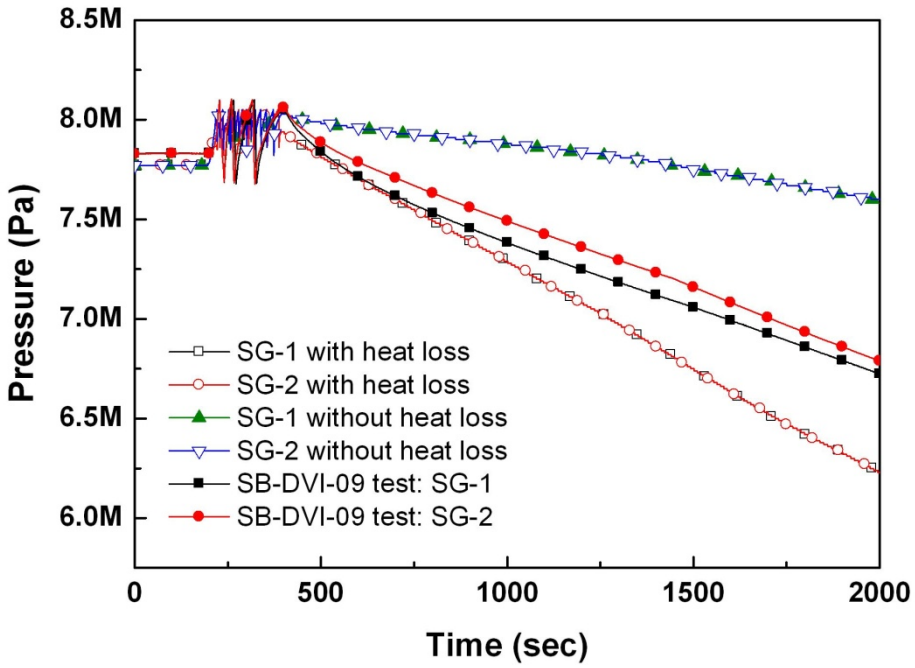

Figure 8.6-1 Comparison of the secondary system pressures between the ISP-50 test and the KAERI calculation

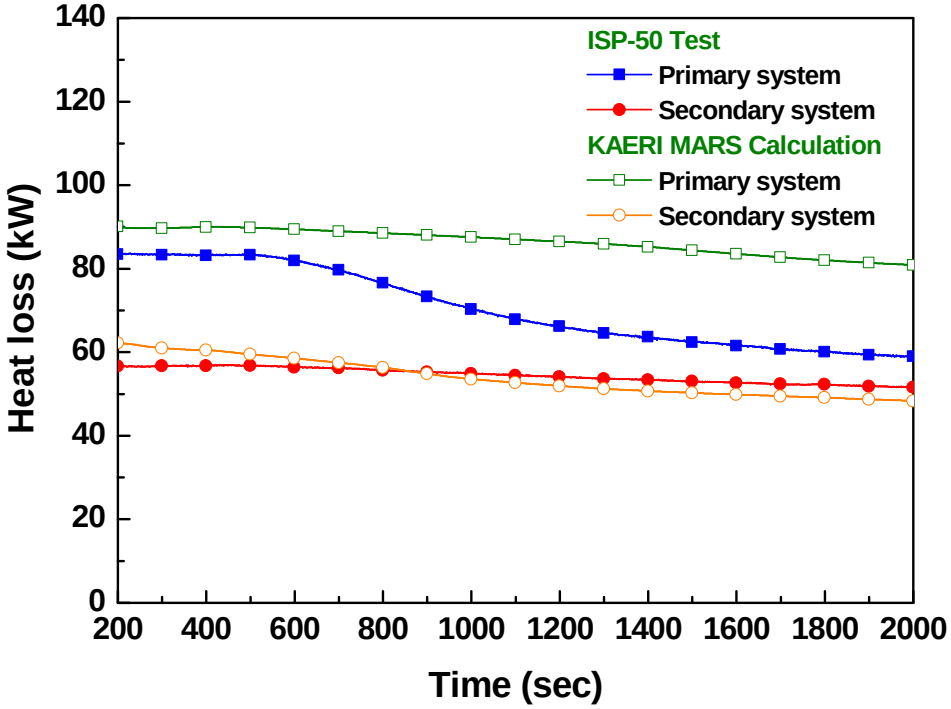

Figure 8.6-2 Variations of the heat loss in both the ISP-50 test and the KAERI calculation

9. Conclusions and Recommendations

This ISP-50 exercise was composed of blind and open phase calculations on a 50% DVI line break LOCA test with the ATLAS facility that simulates APR1400 reactor.

9.1 Pre-test (blind) calculation

In general, the present ISP-50 exercise gave a wide and very valuable outlook on actual status of the code performance because of two main reasons: a) different codes are tested against the same experiment; b) different users adopting the same code get different results. Seventeen calculation results were finally submitted for the "blind" calculation of the ISP-50. Seven different thermal-hydraulic safety analysis codes were used: MARS-KS, TRACE, RELAP5/MOD3.3 series, KORSAR, TECH-M-97, APROS and ATHLET. Most participants seemed to initialize their codes very well based on the provided facility description report. The prediction accuracy of the initial conditions was good by taking into account the difficulty in "blind" exercise. All the calculations qualitatively succeeded in simulating the typical transient behaviors during the DVI line break accident, including the primary pressure depressurization, the primary pressure plateau, the MSSV opening, the loop seal clearing, the RPV core water level depression, and the break flow. However, a few participants seemed not to have full understanding of the actual test conditions. Certain boundary conditions, for instance, the core power with respect to time or ECC flow rate, were not properly implemented in the code calculations.

On the whole, the prediction accuracy of each thermal-hydraulic phenomenon was not satisfactory. In particular, prediction discrepancies of the RPV core and the down-comer level were significant in most calculations. The SIT flow rate was also not properly predicted by most calculations. Regarding the break flow rate, accuracy of break flow simulation has long been the center of the discrepancy in the predicted result from the experiment result. This problem was confirmed still remaining in this ISP-50 too. This problem has also been recognized to be a main source to make the calculation results to have some time difference (shifting) from the experiment. Average prediction accuracy AA of the break flow for time interval of 300 s was found to be around 0.70.

In the blind phase, 3-D data for the fluid temperature in the down-comer region were not collected from participants because the one of the objectives of the blind phase was to investigate overall prediction capability of the existing thermal-hydraulic system codes.

Prediction accuracy quantification of the submitted calculations was performed by applying the FFTBM, which was developed by Prof. D'Auria's group in Univ. of Pisa. This method has been widely used in the previous ISPs: ISP-21, ISP-22, ISP-27, ISP-33, ISP-35, ISP-39, and ISP-42. Taking into account major phenomena of the DVI line break scenario identified from Phenomena Identification Ranking Tabulation (PIRT) process, three time frames were selected: (1) from break to 24 s, (2) from break to 300 s (3) from break to 2000 s. The first time frame corresponds to the pre-trip phase, the second extends to the post-trip phase, and the third includes the refill phase according to PIRT result. In order to apply the FFTBM to ISP-50, 22 key parameters considered to be sufficient to represent the present DVI line break scenario were selected for quantitative comparison through communication with Prof. D'Auria, including the core power, the primary pressure, the secondary pressure, the primary flow rate, the break flow rate, the ECC water flow rate, the PCT in selected axial locations, and the water levels in the core, the down-comer, the pressurizer, and the vertical intermediate loops. The cut-off frequency of 1.0 Hz was used to all variables and the standard weighting factors in the literature were used with the consideration from the measurement uncertainty, the safety relevance and the relevance with respect to primary pressure. On the whole, the prediction accuracy became worse as the time interval became longer.

Considering the third time interval of 2000 s, the best and the worst calculations were provided by CIAE and GP4, respectively. CIAE used the RELAP5/MOD3.3 code and the GP4 used the TECH-M-97 code. However, the present ranking does not imply that the RELAP5/MOD3.3 code has improved models compared with the TECH-M-97 code. The present disagreement of calculation with the test data is significantly affected by, so called, user effects. The user effects, in general, arise due to many reasons such as the ill-preparation of input caused by simple mistake, misunderstanding of the given boundary and initial condition(s), misunderstanding how to properly use the computer code, misunderstanding of the phenomena that appeared during the test scenario, misunderstanding of the models incorporated in the computer codes, etc. Several computer codes with various nodalization methods were also used. Therefore, it was surely hard to define them quantitatively in the present phase, but great user effects resulting from the combination of the possible reasons were again found, confirming that user effect is still one of the major issues in connection with the system thermal-hydraulic code application. It should be pointed out that very careful preparation of code input based on correct understanding of the target scenario is necessary to minimize the user effects.

9.2 Post-test (open) calculation

Sixteen calculations from eleven countries were collected and analyzed by comparing with the experimental data. Seven different safety analysis codes were used: MARS-KS, TRACE,

RELAP5/MOD3.3 series, KORSAR, APROS, CATHARE, and ATHLET. Five calculations with RELAP5, three with KORSAR, two with MARS-KS, TRACE, ATHLET, one with APROS, CATHARE were performed. Three-dimensional modeling for the core region was tried by NRC with the TRACE code. KAERI also tried three-dimensional modeling for the core region with MARS-3D and TRACE codes. The "MULTID" and "VESSEL" component was used for MARS-3D and TRACE, respectively. As these calculations were preliminary ones in order to examine the 3-D effects, detailed analysis was not performed, but some information was included in Appendix-F. UNIPI helped the operating agency in analyzing this exercise and recommending future investigation.

In most calculations, much improved prediction results compared with the "blind" case were found in the "open" calculation. This conclusion was obvious when the FFTBM was applied to both calculation results. Most open calculations resulted in very good prediction results. In the third time frame from break to 2000 s, the calculated AA_{tot} was around 0.3. Compared with the "blind" case, the improvement of AA_{tot} was more than 20%. A maximum of 45% improvement was observed in a certain calculation. Although a few calculations resulted in worse output than the "blind" case, it was not a big deal. Such degradation in the prediction accuracy was so small that it was very hard to reach any technical conclusion. Such improvement in the prediction capability implies that there are significant user effects in code validation. It is obvious that the user effects cannot be avoided completely in safety analysis. Nonetheless, the user effects have to be minimized in any case by appropriate measures. But, how to avoid the user effects was not an objective of this ISP-50 exercise. Having the calculation results, it can be postulated that most participants used their experience and expertise to correct their pre-test calculations. This correction was made in tuning the nodalization to reach better agreement between the test data and the calculation.

Observed major sequence of events were an opening of MSSV, a LPP trip, a RCP trip, a MFW isolation, a SIP actuation, and a SIT actuation and each set point is directly related to the primary or the secondary pressures. Thus, good prediction of the pressure behavior leads to good prediction of the calculated sequence of events. Most open calculations showed much better agreement with the data than the blind calculation. Especially, the participants who showed an excellent prediction of the primary pressure also showed an outstanding agreement in the major sequence of events. However, the reproduction of the asymmetric loop seal clearing behavior seemed to cause great difficulties for most participants. Acceptable reproduction of the loop seal clearing was not made in most calculations, particularly with respect to occurrence order and timing in four intermediate loops. Another difficulty in code prediction was found in prediction of the secondary pressure. Incorrect prediction of the secondary pressure caused different timing of the opening of the MSSVs. In addition, the opening of the MSSVs played a role in reducing the secondary pressure and the heat removal

rate from the primary system.

One of the most important code prediction capabilities during the small break loss of coolant accident is an estimation of the break flow discharging from the break location. The break flow is also the most dominant factor to determine the primary depressurization. The break flow is clearly influenced from the down-comer level. Most calculations reasonably predicted the overall measured trend of the break flow rate. Loss coefficient has been tuned to catch the mass discharged through the break. Prediction of the initial peak flow rate as well as the later single-phase steam flow rate was acceptable. Great uncertainty was found to come from the prediction of the discharge of two-phase mixture observed in the earlier phase prior to the loop seal clearing. Many participants adjusted the discharge coefficients and succeeded in calculating the reasonable two-phase break flow rate, but a few participants resulted in lower two-phase flow rate than the data. Probably liquid entrainment plays a role in the break flow behaviour, not properly simulated by the code. Thus additional investigation is expected to be done, considering that break mass flow rate is quite difficult to be measured. In the present ISP-50 test, complicated phenomena such as combination of 3-D flow coupled with mixture level fluctuation and/or swell with certain amount of liquid or vapor entrainment towards the DVI nozzle are involved in determining the break flow rate. Therefore, combination of several parameters such as noding, selection of break flow models and evaluation of coefficient(s) for each model such as 3-D flow model, inter-phase drag to properly estimate mixture level and liquid/vapor entrainment should be investigated comprehensively. Such comprehensive investigation was not done to distinguish the user effects in the present ISP-50.

The bypass flow path from the down-comer to the upper head can affect the pressure distribution between the core and the down-comer regions and the collapsed water level in the core. On break, inventory of the upper head flowed though the bypass path to the broken DVI nozzle. This is the only flow path for the inventory to be discharged before the loop seal is cleared. Measured temperature distribution in the upper head and upper down-comer was rather uniform and any multi-dimensional effect was not observed. Thus, this phenomenon was reasonably well reproduced in most code calculations.

The loop seal clearing was not correctly reproduced by most calculations, notwithstanding the tuning of the form loss coefficients (k) against the pressure drop data supplied by KAERI. In the ISP-50 test, two loop seals in the broken loop, 1A and 1B were cleared first, followed by the 2nd loop seal clearing in the loop 2B. The remaining loop 2A was not cleared during the test period. Many participants predicted the first loop seal clearing with reasonable accuracy. No participants, however, predicted the second loop seal clearing occurred at loop 2B in the experiment. To evaluate the relevance of the phenomenon in reactor safety, it should be

considered its duration and impact on the overall behaviour. Other systems intervention, such as hydro-accumulators and/or active emergency core cooling, has larger effect on the mass distribution and consequently affects the reactor pressure vessel level.

The influence of secondary side behaviour on the primary side was noticeable during the first phase of the experiment. Difficulties in reproducing the timing and the number of openings of the MSSVs have been encountered. The heat released from the secondary side to the primary side plays also a role for the evolution of the transient, even though heat loss may reduce such an effect. Secondary side behaviour is relevant from the reactor safety point of view taking into account the heat flow inversion. In general, the secondary pressure was over-predicted in most calculations. Possible sources of over-prediction of the secondary pressure are the heat loss modeling, the quality of the steam entering the U-tubes after the loop seal clearing. Modeling the secondary heat loss produced better prediction accuracy. Finally, the blocked loop seal prevents the steam from flowing the U-tubes and then significantly reduces the reverse heat transfer.

In this ISP-50, multi-dimensional aspects observed in the test were highlighted in terms of code prediction capability. In particular, detailed calculation results on down-comer fluid temperatures were requested and compared. During the ISP-50 test, cold ECC water was introduced by a SIP and three SITs at a different time. The SIP injected ECC water through the DVI nozzle opposite to the broken DVI nozzle into the annulus down-comer and three SITs injected ECC water through the intact three DVI nozzles. As the down-comer region was filled with water when the SIP started injection, mixing of the cold ECC water with the hot inventory was of the prime interest. Most codes did not succeed in predicting the mixing satisfactorily. Instead of mixing, azimuthal temperature stratification was predicted even in lower down-comer region. This incorrect prediction seems to be due to limitation of the one-dimensional code to treat ECC mixing. The NRC's calculation where three-dimensional modeling was used in the reactor vessel region showed better mixing than the others. Shortly after, the loop seal was cleared and then the loop seal clearing caused the cold ECC water to interact with the high temperature steam. In this period, condensation was expected to occur. When the SITs started injection later on, the water level of the down-comer region was below the cold leg elevation and much cold ECC water flowed down the down-comer region.

During the experiment, three-dimensional behaviour was observed in the heater surface temperature distribution. Notwithstanding the nodalization set up to predict possible 3-D effects, the use of 1-D component limited the possibility of computing such asymmetries in the heater surface temperature. It should be also mentioned that 3-D effects observed during the test are considerable. It was found that three dimensional code model resulted in better

prediction accuracy than the most 1-D models. Three dimensional effects are quite relevant from the reactor safety point of view especially in those transients in which this behaviour is remarkable. Strong asymmetries may yield to thermal crisis in part of the core while the rest is still covered.

Following the BEMUSE Phase II procedure for evaluating the nodalization quality, the primary and the secondary inventories of the code models were compared with the measured geometric data as the inventories significantly affect the transient behavior. Compared with the primary inventory, the secondary inventory showed much larger errors. About 50% calculations fulfilled the global acceptability Q_A<1.0 with an Acceptable Error (AE) of 5%.

The FFTBM was adopted in the open phase for quantification of the calculation results. The same number of parameters considered to be sufficient to represent the present DVI line break scenario was used for FFTBM calculation. Open calculations showed better prediction accuracy than the blind calculations in terms of average amplitude (AA) value. Average improvement for each time interval was 19%, 16%, and 12%, respectively. It has also been confirmed that the FFTBM is a useful method to quantify code prediction accuracy, though it has a few limitations. Finally being the facility configuration (including the break location) different from a typical PWR, it might be worth to analyze in deep whether new thermal-hydraulic phenomena appear or if already known phenomena change their relevance from the reactor safety point of view in those installations that adopt the DVI solution. A feedback on the CSNI Integral Test Facility validation matrix issued on July 1996 could be envisaged.

References

- W. Ambrosini, R. Bovalini, F. D'Auria, "Evaluation of accuracy of thermal hydraulic code calculations", *J. Energia Nucleare*, V. 2, (1990)
- W. P. Baek et al.[1)], "KAERI Integral Effect Test Program and the ATLAS Design," *Nuclear Technology*, **152**, 183-195 (2005).
- W. P. Baek et al.[2)], "Accident Simulation ATLAS for APWRs," *Nuclear Engineering International*, **53**, 21-25 (2008).
- W. P. Baek et al.[3)], "LBLOCA and DVI Line Break Tests with the ATLAS Integral Facility," *Nuclear Engineering and Technology*, **41**, 775-784 (2009).
- S. Cho et al, "Core Thermal Hydraulic Behavior during the Reflood Phase of Cold-leg LBLOCA Experiments using the ATLAS Test Facility," *Nuclear Engineering and Technology*, **41**, 1263-1274 (2009).
- K. Y. Choi et al.[1)], "Simulation Capability of the ATLAS Facility for Major Design-Basis Accidents," *Nuclear Technology*, **156**, 256-269 (2006).

- K. Y. Choi et al.[2)], "Integral Behavior of the ATLAS Facility for a 3-inch Small Break Loss of Coolant Accident," *Nuclear Engineering and Technology*, **40**, 199-212 (2008).
- K. Y. Choi et al.[3)], "Experimental Simulation of a Direct Vessel Injection Line Break of the APR1400 with the ATLAS," *Nuclear Engineering and Technology*, **41**, 655-676 (2009).
- K. Y. Choi et al.[4)], "Effects of Break Size on DVI Line Break Accidents of the ATLAS," *Nuclear Technology*, **175**, 604-618 (2011).
- K. Y. Choi et al.[5)], "ISP-50 Specifications for a Direct Vessel Injection Line Break Test with the ATLAS," KAERI/TR-3778 (2009).
- K. Y. Choi et al.[6)], "Detailed Information on Actual Test Conditions and Procedures for ISP-50," KAERI Interim report (2009).
- B.D. Chung et al., "Phenomena Identification and Ranking Tabulation for APR1400 Direct Vessel Injection Line Break," *NURETH-10*, Seoul, Korea, October 5-9, (2003).
- "EPRI Utility Requirement Documents for the Advanced Light Water Reactor (Chapter 15)," Electric Power Research Institute (1995).
- F. D'Auria, M. Mazzini, F. Oriolo, S. Paci, "Comparison report of the OECD/CSNI International Standard Problem 21 (Piper-one experiment PO-SB-7)," *CSNI Report No. 162,* (1989).
- F. D'Auria, M. Leonardi, R. Pochard, "Methodology for the evaluation of thermal hydraulic codes accuracy," *Proc. Int. Conf. on New trends in Nuclear System Thermohydraulics*, Pisa, 467–477 (1994).
- K.H. Kang et al.[1)], "ATLAS Facility and Instrumentation Description Report," KAERI/TR-3779, (2009).
- K.H. Kang et al.[2)], "Application of Averaging Bidirectional Flow Tube for Measurement of Single-Phase Flow Rate in a Piping System," *J. Mech. Sci. and Tech.*, **23**, 758-767 (2009).
- K.H. Kang et al. [3)], "Detailed Description Report of ATLAS Facility and Instrumentation," KAERI/TR-4316, (2011).
- Y. S. Kim et al, "Commissioning of the ATLAS Thermal-Hydraulic Integral Test Facility," *Annals of Nuclear Energy*, **35**, 1791-1799, (2008).
- M. Ishii et al., "The three level scaling approach with application to the Purdue University multi-dimensional integral test assembly (PUMA)," *Nuclear Engineering and Design*. **186**, 177–211, (1998).
- J. J. Jeong et al., "Development of a multi-dimensional thermal-hydraulic system code, MARS 1.3.1," *Annals of Nuclear Energy*, **26**, No.18, 1611-1642, (1999).
- R. F. Kunz, G. F. Kasmala, J. H. Mahaffy, C. J. Murray, "On the automated assessment of nuclear reactor systems code accuracy," *Nuclear Engineering and Design*, **211**, Issues 2-3, 245-272, (2002).
- OECD/NEA, "CSNI International Standard Problems (ISP) – Brief Descriptions (1975-1999)," NEA/CSNI/R(2000)5 (2000).
- OECD/NEA, "Re-Analysis of the ISP-13 Exercise, Post Test Analysis of the LOFT L2-5 Test

Calculation, " BEMUSE PHASE II Report, NEA/CSNI/R(2006)2 (2005).

- OECD/NEA, "CSNI International Standard Problem Procedures," NEA/CSNI/R(2004)5 (2004).
- H. S. Park et al.[1)], "An Assessment of a LBLOCA Similarity for a Reduced-Height Integral Effect Test Loop Design for PWRs," *Annals of Nuclear Energy*, **34**, 931-937 (2007).
- H. S. Park et al.[2)], "An Integral Effect Test on the LBLOCA Reflood Phenomena for the APR1400 using the ATLAS under a Best-Estimate Condition," *J. of Nuclear Science and Technology*, **46**, 1059-1069 (2009).
- H. S. Park et al.[3)], "A Separate Effect Test for a Low Reflooding Rate Condition During the Reflood Phase of a LBLOCA Using the ATLAS," KAERI/TR-4037 (2010).
- A. Prosek, F. D'Auria, and B. Mavko, "Review of Quantitative Accuracy Assessments with Fast Fourier Transform Based Method (FFTBM)," *Nuclear Engineering and Design*, **217**, 179-206, (2002).
- A. Prosek, F. D'Auria, D. J. Richards, and B. Mavko, "Quantitative assessment of thermal-hydraulic codes used for heavy water reactor calculations," *Nuclear Engineering and Design*, **236**, Issue 3, 295-308, (2006).
- B. J. Yun et al.[1)], "Development of an Average Bidirectional Flow Tube for a Measurement of the Single and Two Phase Flow," The 11th International Topical Meeting on Nuclear Reactor Thermal-Hydraulics (NURETH-11), Avignon, France, October 2~6 (2005).
- B. J. Yun et al.[2)], "Measurement of the Single and Two Phase Flow using a Newly Developed Average Bidirectional Flow Tube," *Nuclear Engineering and Technology*, **37**, 595-604 (2005)
- M. Osakabe et al., "Core Liquid Level Depression due to Manometric Effect during PWR Small Break LOCA," *J. Nuclear Science and Technology,* **25**, No. 3, 274-282, (1988).

CD supplement

1. Experimental data for 269 major TH parameters [Excel]
2. Experimental data for 264 heater surface wall temperature [Excel]
3. Output submission format [Excel]
4. Specifications for ISP-50 [pdf]
5. Updated facility description report (FDR) [pdf]
6. Final integration report for ISP-50, Volume I [pdf]
7. Final integration report for ISP-50, Volume II [pdf]
8. Final integration report for ISP-50, Volume III [pdf]

Acknowledgements

The authors are grateful to the Ministry of Education, Science and Technology (MEST) of Korea for their financial support for this exercise and to all the participants for their engagement in the ISP-50 by contributing the blind/open calculations, meeting, and comments made all along this exercise.

Appendix-A:
Measured Boundary Conditions

Table A.1 Measured boundary conditions

DAS Time	Qtotal	Qcore	Qloss	PT-CS-03	PT-DVIBS-01
(sec)	(kW)	(kW)	(kW)	(MPa)	(MPa)
-10	1635.384	1551.895	83.489	0.1051	15.653
-9	1635.507	1551.935	83.573	0.1051	15.654
-8	1636.372	1552.859	83.514	0.1051	15.655
-7	1635.548	1552.032	83.516	0.1051	15.655
-6	1635.507	1552.103	83.404	0.1051	15.654
-5	1635.466	1551.964	83.503	0.1051	15.651
-4	1638.432	1554.972	83.460	0.1051	15.653
-3	1637.485	1554.080	83.405	0.1052	15.652
-2	1638.515	1555.067	83.448	0.1051	15.653
-1	1635.425	1551.797	83.628	0.1051	15.654
0	1635.507	1551.978	83.529	0.1052	15.656
1	1635.507	1551.930	83.578	0.1051	15.653
2	1635.466	1551.936	83.530	0.1051	15.654
3	1636.414	1552.932	83.481	0.1051	15.652
4	1635.466	1551.939	83.528	0.1051	15.653
5	1636.414	1553.056	83.358	0.1051	15.653
6	1637.485	1553.841	83.644	0.1051	15.653
7	1635.548	1552.103	83.445	0.1051	15.654
8	1637.402	1553.845	83.558	0.1051	15.656
9	1637.444	1553.871	83.573	0.1051	15.654
10	1638.391	1554.899	83.493	0.1051	15.654
11	1637.444	1554.084	83.360	0.1051	15.653
12	1637.485	1553.962	83.523	0.1051	15.654
13	1638.432	1554.811	83.621	0.1051	15.654
14	1636.578	1552.985	83.594	0.1051	15.654
15	1635.548	1552.005	83.544	0.1051	15.655
16	1635.590	1551.963	83.626	0.1051	15.654
17	1634.354	1550.820	83.534	0.1051	15.655
18	1635.507	1552.002	83.505	0.1051	15.653
19	1635.384	1551.934	83.450	0.1051	15.652
20	1636.496	1553.063	83.433	0.1051	15.655
21	1635.548	1552.150	83.399	0.1052	15.654
22	1637.485	1554.151	83.334	0.1051	15.653
23	1639.339	1556.097	83.241	0.1051	15.654
24	1638.226	1554.843	83.384	0.1051	15.656
25	1637.320	1553.635	83.685	0.1051	15.654
26	1635.507	1552.185	83.323	0.1051	15.654
27	1636.414	1552.870	83.544	0.1051	15.653
28	1636.455	1552.930	83.525	0.1051	15.653
29	1634.477	1550.765	83.713	0.1051	15.654

30	1634.436	1550.936	83.500	0.1051	15.654
31	1635.507	1552.145	83.363	0.1051	15.654
32	1635.342	1552.020	83.323	0.1051	15.655
33	1635.384	1551.896	83.488	0.1051	15.653
34	1634.560	1551.096	83.464	0.1051	15.654
35	1635.507	1551.943	83.564	0.1051	15.654
36	1636.455	1553.077	83.378	0.1051	15.654
37	1635.425	1551.900	83.525	0.1051	15.653
38	1635.466	1551.990	83.476	0.1051	15.653
39	1635.301	1551.714	83.588	0.1052	15.654
40	1635.425	1551.822	83.603	0.1051	15.655
41	1635.466	1552.125	83.341	0.1051	15.653
42	1635.548	1552.260	83.289	0.1051	15.652
43	1635.466	1552.181	83.285	0.1051	15.653
44	1633.530	1549.987	83.543	0.1052	15.652
45	1635.507	1551.996	83.511	0.1051	15.650
46	1635.548	1551.923	83.625	0.1051	15.653
47	1635.507	1551.920	83.588	0.1051	15.653
48	1635.466	1552.165	83.301	0.1051	15.654
49	1635.342	1551.954	83.389	0.1051	15.652
50	1635.425	1551.861	83.564	0.1051	15.652
51	1635.507	1551.938	83.569	0.1051	15.652
52	1634.518	1551.112	83.406	0.1052	15.654
53	1635.466	1552.069	83.398	0.1051	15.653
54	1635.507	1552.050	83.458	0.1052	15.654
55	1635.466	1551.960	83.506	0.1051	15.654
56	1634.518	1550.735	83.784	0.1051	15.655
57	1634.436	1550.931	83.505	0.1051	15.653
58	1635.342	1551.949	83.394	0.1051	15.654
59	1635.425	1552.121	83.304	0.1052	15.653
60	1634.518	1551.192	83.326	0.1051	15.654
61	1635.466	1552.030	83.436	0.1052	15.653
62	1635.548	1551.997	83.551	0.1051	15.654
63	1635.425	1551.876	83.549	0.1051	15.655
64	1635.507	1552.046	83.461	0.1051	15.655
65	1635.466	1551.931	83.535	0.1051	15.655
66	1635.507	1552.011	83.496	0.1050	15.655
67	1636.331	1552.846	83.485	0.1051	15.655
68	1635.384	1551.870	83.514	0.1052	15.656
69	1634.560	1550.993	83.566	0.1051	15.655
70	1635.507	1552.115	83.393	0.1051	15.655
71	1635.631	1552.118	83.513	0.1051	15.655
72	1635.466	1551.977	83.489	0.1051	15.654
73	1635.425	1551.895	83.530	0.1051	15.655
74	1635.384	1552.030	83.354	0.1051	15.655

75	1636.414	1552.867	83.546	0.1051	15.655
76	1635.466	1552.006	83.460	0.1051	15.655
77	1635.466	1551.924	83.543	0.1051	15.655
78	1635.548	1552.041	83.508	0.1051	15.655
79	1635.466	1552.056	83.410	0.1051	15.655
80	1635.590	1552.030	83.560	0.1052	15.654
81	1635.507	1552.085	83.423	0.1051	15.655
82	1635.466	1551.976	83.490	0.1051	15.655
83	1635.466	1551.961	83.505	0.1051	15.656
84	1635.507	1552.038	83.469	0.1052	15.654
85	1635.425	1551.881	83.544	0.1051	15.655
86	1634.395	1550.907	83.488	0.1051	15.655
87	1633.447	1549.977	83.470	0.1051	15.654
88	1635.425	1552.072	83.353	0.1052	15.654
89	1634.518	1550.970	83.549	0.1051	15.655
90	1635.384	1551.799	83.585	0.1051	15.657
91	1637.361	1553.922	83.439	0.1051	15.656
92	1635.507	1551.983	83.524	0.1051	15.655
93	1635.548	1552.047	83.501	0.1051	15.656
94	1635.548	1552.076	83.473	0.1051	15.656
95	1635.507	1551.908	83.599	0.1051	15.656
96	1635.466	1551.796	83.670	0.1052	15.657
97	1634.436	1550.870	83.566	0.1051	15.657
98	1635.507	1552.112	83.395	0.1051	15.657
99	1632.500	1549.081	83.419	0.1051	15.656
100	1635.548	1552.063	83.485	0.1051	15.658
101	1635.425	1551.764	83.661	0.1051	15.656
102	1635.466	1551.940	83.526	0.1051	15.658
103	1635.548	1551.925	83.624	0.1051	15.658
104	1635.425	1551.906	83.519	0.1052	15.656
105	1635.425	1551.795	83.630	0.1050	15.657
106	1635.590	1552.142	83.448	0.1051	15.658
107	1635.507	1551.981	83.526	0.1051	15.657
108	1635.384	1551.917	83.466	0.1051	15.657
109	1635.466	1551.962	83.504	0.1052	15.655
110	1634.395	1550.885	83.510	0.1051	15.656
111	1634.436	1550.896	83.540	0.1051	15.656
112	1634.518	1550.926	83.593	0.1051	15.655
113	1634.518	1550.851	83.668	0.1051	15.655
114	1634.560	1551.122	83.438	0.1051	15.655
115	1633.653	1549.957	83.696	0.1051	15.655
116	1634.354	1550.950	83.404	0.1051	15.655
117	1635.590	1552.110	83.480	0.1051	15.654
118	1633.571	1549.965	83.606	0.1051	15.655
119	1634.477	1551.041	83.436	0.1051	15.655

120	1634.518	1550.856	83.663	0.1051	15.655
121	1633.406	1549.842	83.564	0.1051	15.654
122	1635.466	1551.939	83.528	0.1051	15.654
123	1634.477	1550.953	83.524	0.1051	15.655
124	1635.342	1551.995	83.348	0.1052	15.654
125	1633.447	1549.770	83.678	0.1051	15.654
126	1633.488	1550.002	83.486	0.1051	15.654
127	1635.507	1552.113	83.394	0.1051	15.654
128	1633.365	1549.901	83.464	0.1051	15.655
129	1634.518	1551.175	83.344	0.1051	15.655
130	1633.488	1550.003	83.485	0.1051	15.654
131	1634.477	1551.021	83.456	0.1051	15.654
132	1634.560	1551.035	83.525	0.1051	15.655
133	1633.447	1549.787	83.660	0.1051	15.656
134	1633.447	1549.870	83.578	0.1051	15.654
135	1634.518	1550.808	83.710	0.1052	15.656
136	1635.466	1551.916	83.550	0.1051	15.656
137	1632.500	1548.800	83.700	0.1051	15.656
138	1634.477	1550.891	83.586	0.1051	15.655
139	1635.507	1551.847	83.660	0.1051	15.657
140	1632.458	1548.965	83.494	0.1051	15.656
141	1635.425	1551.922	83.503	0.1051	15.656
142	1632.623	1549.130	83.494	0.1051	15.655
143	1635.466	1551.955	83.511	0.1051	15.656
144	1633.488	1549.851	83.638	0.1051	15.656
145	1633.571	1549.950	83.621	0.1051	15.656
146	1632.500	1548.772	83.728	0.1051	15.655
147	1635.384	1551.861	83.523	0.1051	15.655
148	1633.488	1549.901	83.588	0.1051	15.654
149	1633.530	1549.905	83.625	0.1051	15.656
150	1632.500	1549.037	83.463	0.1051	15.655
151	1634.395	1550.900	83.495	0.1051	15.655
152	1633.447	1549.835	83.613	0.1051	15.655
153	1635.466	1551.916	83.550	0.1051	15.656
154	1634.477	1550.855	83.623	0.1051	15.656
155	1634.436	1550.940	83.496	0.1051	15.655
156	1633.488	1549.773	83.715	0.1051	15.655
157	1634.395	1550.845	83.550	0.1052	15.656
158	1634.395	1550.775	83.620	0.1051	15.656
159	1634.518	1550.875	83.644	0.1051	15.656
160	1634.436	1550.769	83.668	0.1051	15.655
161	1635.507	1551.961	83.546	0.1051	15.656
162	1633.324	1549.677	83.646	0.1051	15.656
163	1634.436	1550.745	83.691	0.1051	15.656
164	1632.582	1549.052	83.530	0.1051	15.657

165	1634.436	1550.764	83.673	0.1051	15.656
166	1634.354	1550.751	83.603	0.1051	15.656
167	1634.436	1550.845	83.591	0.1051	15.657
168	1634.477	1550.810	83.668	0.1051	15.658
169	1633.447	1549.702	83.745	0.1051	15.658
170	1633.406	1549.900	83.506	0.1051	15.658
171	1632.623	1548.996	83.628	0.1051	15.657
172	1635.590	1552.053	83.536	0.1051	15.657
173	1632.417	1548.999	83.419	0.1051	15.658
174	1632.459	1548.655	83.804	0.1051	15.657
175	1633.365	1550.020	83.345	0.1051	15.657
176	1632.541	1549.240	83.301	0.1051	15.656
177	1635.548	1551.957	83.591	0.1052	15.658
178	1635.507	1551.940	83.568	0.1051	15.657
179	1633.488	1549.852	83.636	0.1051	15.657
180	1634.477	1550.785	83.693	0.1051	15.658
181	1633.488	1550.131	83.358	0.1051	15.656
182	1635.466	1551.809	83.658	0.1051	15.656
183	1633.530	1550.067	83.463	0.1051	15.656
184	1634.518	1550.833	83.685	0.1051	15.657
185	1634.518	1550.998	83.520	0.1051	15.656
186	1633.447	1549.936	83.511	0.1051	15.656
187	1635.507	1551.915	83.593	0.1051	15.657
188	1633.324	1549.659	83.665	0.1051	15.656
189	1632.417	1548.940	83.478	0.1052	15.656
190	1635.425	1551.860	83.565	0.1051	15.656
191	1634.436	1550.814	83.623	0.1051	15.657
192	1635.548	1551.830	83.719	0.1051	15.656
193	1633.612	1550.136	83.476	0.1051	14.826
194	1635.507	1551.772	83.735	0.1066	5.882
195	1634.477	1550.952	83.525	0.1273	4.634
196	1634.477	1551.050	83.428	0.1420	4.486
197	1633.406	1549.962	83.444	0.1472	4.506
198	1634.436	1550.885	83.551	0.1488	4.530
199	1633.612	1550.158	83.454	0.1489	4.526
200	1633.612	1549.933	83.679	0.1477	4.502
201	1633.571	1549.923	83.648	0.1452	4.475
202	1634.436	1550.777	83.659	0.1440	4.457
203	1634.395	1550.712	83.683	0.1444	4.438
204	1632.623	1548.892	83.731	0.1457	4.403
205	1634.395	1550.970	83.425	0.1474	4.351
206	1634.436	1550.734	83.703	0.1492	4.300
207	1633.612	1549.932	83.680	0.1511	4.260
208	1633.612	1550.102	83.510	0.1527	4.210
209	1631.511	1547.860	83.651	0.1535	4.158

210	1631.511	1547.936	83.575	0.1550	4.100
211	1633.406	1549.927	83.479	0.1566	4.042
212	1634.601	1551.075	83.526	0.1573	3.975
213	1632.623	1549.010	83.614	0.1574	3.897
214	1632.417	1548.881	83.536	0.1581	3.816
215	1633.571	1549.960	83.611	0.1585	3.753
216	1631.387	1547.750	83.638	0.1584	3.692
217	1631.552	1547.982	83.570	0.1579	3.633
218	1632.541	1549.113	83.428	0.1574	3.561
219	1633.365	1549.855	83.510	0.1566	3.486
220	1632.459	1548.865	83.594	0.1558	3.400
221	1635.466	1551.962	83.504	0.1547	3.310
222	1634.436	1550.917	83.519	0.1539	3.235
223	1634.436	1550.895	83.541	0.1525	3.156
224	1632.664	1549.144	83.520	0.1508	3.092
225	1633.488	1549.808	83.680	0.1495	3.041
226	1623.724	1540.057	83.668	0.1483	2.992
227	1600.035	1516.414	83.621	0.1467	2.953
228	1573.421	1489.762	83.659	0.1456	2.905
229	1542.686	1459.069	83.618	0.1444	2.861
230	1512.158	1428.651	83.508	0.1437	2.822
231	1479.570	1396.168	83.403	0.1425	2.784
232	1450.854	1367.316	83.539	0.1421	2.736
233	1422.304	1338.816	83.488	0.1411	2.701
234	1398.532	1315.043	83.489	0.1403	2.675
235	1379.787	1296.225	83.561	0.1395	2.653
236	1360.011	1276.528	83.484	0.1388	2.622
237	1339.247	1255.687	83.560	0.1380	2.589
238	1323.509	1239.879	83.630	0.1373	2.572
239	1306.741	1223.288	83.454	0.1368	2.564
240	1290.921	1207.454	83.468	0.1363	2.553
241	1276.131	1192.701	83.430	0.1360	2.536
242	1265.254	1181.782	83.473	0.1352	2.535
243	1251.576	1168.097	83.479	0.1348	2.527
244	1238.599	1155.032	83.566	0.1343	2.507
245	1227.846	1144.497	83.349	0.1341	2.498
246	1215.033	1131.428	83.605	0.1335	2.501
247	1201.190	1117.701	83.489	0.1331	2.497
248	1190.231	1106.620	83.611	0.1328	2.487
249	1182.321	1098.965	83.356	0.1328	2.484
250	1172.598	1089.116	83.483	0.1324	2.483
251	1163.658	1080.216	83.443	0.1323	2.481
252	1155.666	1072.203	83.463	0.1320	2.475
253	1146.931	1063.326	83.605	0.1316	2.473
254	1137.044	1053.430	83.614	0.1316	2.482

255	1129.051	1045.809	83.243	0.1312	2.469
256	1121.141	1037.679	83.463	0.1312	2.459
257	1116.280	1032.867	83.413	0.1312	2.443
258	1108.411	1025.001	83.410	0.1308	2.429
259	1101.572	1018.092	83.480	0.1308	2.424
260	1094.609	1011.174	83.435	0.1304	2.411
261	1088.512	1005.142	83.370	0.1304	2.391
262	1081.673	998.298	83.375	0.1301	2.381
263	1075.905	992.452	83.453	0.1301	2.378
264	1070.055	986.598	83.456	0.1297	2.368
265	1062.968	979.477	83.491	0.1297	2.364
266	1057.201	973.737	83.464	0.1294	2.356
267	1051.227	967.777	83.450	0.1294	2.349
268	1046.201	962.906	83.295	0.1294	2.127
269	1041.298	957.957	83.341	0.1285	1.969
270	1035.283	951.838	83.445	0.1273	2.153
271	1031.534	948.200	83.334	0.1269	2.053
272	1025.519	942.014	83.505	0.1267	1.931
273	1019.627	936.206	83.421	0.1259	1.913
274	1015.466	932.026	83.440	0.1251	1.896
275	1007.680	924.289	83.391	0.1248	1.940
276	1004.878	921.359	83.519	0.1243	1.895
277	999.770	916.262	83.508	0.1240	1.899
278	995.856	912.478	83.378	0.1238	2.077
279	992.848	909.481	83.368	0.1240	1.938
280	989.017	905.702	83.315	0.1238	1.862
281	983.084	899.623	83.461	0.1233	2.001
282	980.035	896.570	83.465	0.1234	1.952
283	977.151	893.711	83.440	0.1234	2.073
284	973.196	889.734	83.463	0.1234	1.974
285	969.241	885.946	83.295	0.1234	1.948
286	966.275	882.844	83.431	0.1230	1.943
287	961.372	878.034	83.339	0.1229	1.936
288	957.294	873.932	83.361	0.1229	1.941
289	953.297	869.865	83.433	0.1229	1.923
290	949.507	866.082	83.425	0.1225	2.062
291	945.552	862.130	83.423	0.1229	2.277
292	942.545	859.065	83.480	0.1234	2.422
293	937.601	854.029	83.571	0.1243	2.341
294	932.780	849.194	83.586	0.1248	2.217
295	931.668	848.196	83.473	0.1243	2.099
296	928.825	845.373	83.453	0.1240	1.980
297	923.882	840.435	83.446	0.1237	1.928
298	921.863	838.399	83.464	0.1234	1.936
299	918.896	835.553	83.344	0.1229	1.949

300	916.837	833.442	83.395	0.1229	2.021
301	913.788	830.388	83.400	0.1229	2.235
302	911.028	827.491	83.536	0.1231	2.372
303	908.926	825.485	83.441	0.1242	2.384
304	906.990	823.585	83.405	0.1249	2.418
305	903.035	819.656	83.379	0.1253	2.423
306	901.099	817.724	83.375	0.1255	2.453
307	898.132	814.621	83.511	0.1263	2.181
308	895.125	811.686	83.439	0.1259	2.394
309	893.271	809.883	83.388	0.1259	2.571
310	889.357	806.013	83.344	0.1266	2.497
311	887.173	803.683	83.490	0.1273	2.462
312	884.413	801.059	83.354	0.1274	2.530
313	881.447	797.902	83.545	0.1278	2.393
314	879.469	796.039	83.430	0.1278	2.319
315	877.409	794.054	83.355	0.1274	2.225
316	875.473	792.099	83.374	0.1266	2.331
317	872.466	789.222	83.244	0.1266	2.363
318	872.466	789.127	83.339	0.1270	2.424
319	871.436	788.048	83.388	0.1269	2.475
320	868.469	785.045	83.424	0.1273	2.333
321	867.480	784.084	83.396	0.1271	2.434
322	865.462	782.059	83.403	0.1274	2.144
323	864.555	781.100	83.455	0.1266	2.228
324	862.495	778.899	83.596	0.1263	2.010
325	861.507	778.070	83.436	0.1259	2.245
326	858.582	775.073	83.509	0.1255	2.360
327	857.593	774.200	83.393	0.1259	2.418
328	853.679	770.139	83.540	0.1266	2.413
329	852.773	769.554	83.219	0.1267	2.317
330	849.641	766.238	83.404	0.1266	2.141
331	847.746	764.399	83.348	0.1263	2.137
332	845.769	762.437	83.331	0.1259	2.162
333	844.739	761.419	83.320	0.1259	2.466
334	842.844	759.322	83.521	0.1263	2.368
335	839.960	756.662	83.298	0.1266	2.121
336	838.971	755.468	83.503	0.1263	1.881
337	836.870	753.545	83.325	0.1251	1.845
338	835.098	751.661	83.438	0.1244	1.890
339	833.986	750.740	83.246	0.1240	2.080
340	830.031	746.747	83.284	0.1240	2.357
341	829.083	745.535	83.549	0.1247	2.488
342	825.993	742.775	83.219	0.1258	2.457
343	825.005	741.708	83.296	0.1263	2.475
344	822.121	738.786	83.335	0.1269	2.507

345	819.196	735.774	83.421	0.1272	2.192
346	819.113	735.852	83.261	0.1266	2.095
347	817.218	733.926	83.293	0.1263	2.350
348	814.211	730.904	83.306	0.1266	2.573
349	814.211	730.948	83.263	0.1273	2.500
350	811.327	728.043	83.284	0.1277	2.412
351	811.244	727.994	83.250	0.1278	2.327
352	809.349	725.945	83.404	0.1277	2.276
353	807.372	724.129	83.243	0.1274	2.559
354	805.353	721.903	83.450	0.1281	2.462
355	805.394	722.160	83.234	0.1282	2.320
356	804.446	721.233	83.214	0.1281	2.405
357	803.458	720.180	83.278	0.1282	2.491
358	801.439	718.181	83.258	0.1285	2.432
359	801.357	717.909	83.448	0.1285	2.546
360	798.555	715.431	83.124	0.1286	2.597
361	797.525	714.326	83.199	0.1294	2.573
362	796.577	713.177	83.400	0.1297	2.527
363	794.559	711.269	83.290	0.1302	2.587
364	793.611	710.304	83.308	0.1301	2.543
365	792.540	709.107	83.433	0.1304	2.508
366	790.604	707.464	83.140	0.1305	2.447
367	788.544	705.479	83.065	0.1301	2.479
368	788.503	705.209	83.294	0.1302	2.445
369	785.536	702.256	83.280	0.1297	2.467
370	785.536	702.164	83.373	0.1301	2.456
371	783.641	700.326	83.315	0.1301	2.388
372	782.529	699.217	83.311	0.1297	2.382
373	779.686	696.416	83.270	0.1296	2.406
374	779.645	696.407	83.238	0.1294	2.438
375	777.708	694.346	83.363	0.1294	2.422
376	776.761	693.560	83.201	0.1295	2.416
377	774.825	691.680	83.145	0.1298	2.610
378	772.847	689.773	83.074	0.1299	2.648
379	770.911	687.617	83.294	0.1307	2.556
380	770.952	687.747	83.205	0.1308	2.424
381	768.933	685.666	83.268	0.1305	2.366
382	767.944	684.769	83.175	0.1300	2.540
383	766.873	683.664	83.209	0.1301	2.616
384	764.896	681.588	83.308	0.1308	2.612
385	763.783	680.496	83.288	0.1312	2.561
386	762.918	679.788	83.130	0.1311	2.378
387	760.982	677.777	83.205	0.1308	2.311
388	760.982	677.613	83.369	0.1302	1.957
389	759.004	675.913	83.091	0.1294	1.809

390	755.914	672.529	83.385	0.1278	1.896
391	756.120	672.975	83.145	0.1268	1.674
392	755.090	671.749	83.341	0.1259	1.554
393	751.959	668.797	83.163	0.1255	1.534
394	751.135	667.793	83.343	0.1245	1.468
395	750.146	666.954	83.193	0.1241	1.470
396	748.128	664.814	83.314	0.1234	1.452
397	747.098	664.058	83.040	0.1234	1.445
398	745.120	661.904	83.216	0.1229	1.464
399	745.038	661.833	83.205	0.1221	1.440
400	745.161	661.883	83.279	0.1218	1.432
401	744.214	660.915	83.299	0.1217	1.424
402	742.195	658.941	83.254	0.1213	1.389
403	742.195	658.969	83.226	0.1213	1.386
404	742.195	659.001	83.194	0.1209	1.409
405	739.188	655.813	83.375	0.1205	1.383
406	739.188	655.851	83.336	0.1205	1.390
407	738.116	654.890	83.226	0.1205	1.372
408	737.292	654.000	83.293	0.1202	1.344
409	737.210	653.858	83.353	0.1202	1.346
410	736.304	653.082	83.221	0.1202	1.354
411	734.244	651.014	83.230	0.1198	1.381
412	734.161	650.885	83.276	0.1194	1.328
413	733.296	650.036	83.260	0.1194	1.320
414	733.296	649.904	83.393	0.1195	1.314
415	732.266	648.884	83.383	0.1191	1.336
416	732.184	649.014	83.170	0.1190	1.308
417	730.248	647.030	83.218	0.1190	1.352
418	729.259	645.971	83.288	0.1187	1.309
419	728.394	645.182	83.211	0.1187	1.295
420	728.270	645.035	83.235	0.1187	1.299
421	728.394	645.216	83.178	0.1187	1.308
422	727.281	644.051	83.230	0.1183	1.336
423	724.397	641.134	83.264	0.1179	1.304
424	723.285	639.910	83.375	0.1179	1.314
425	723.450	640.261	83.189	0.1176	1.285
426	723.491	640.225	83.266	0.1175	1.323
427	722.420	639.207	83.213	0.1176	1.292
428	720.525	637.261	83.264	0.1176	1.312
429	720.483	637.355	83.129	0.1175	1.304
430	719.371	636.130	83.241	0.1173	1.305
431	719.495	636.121	83.374	0.1172	1.293
432	717.476	634.212	83.264	0.1173	1.265
433	716.322	633.141	83.181	0.1173	1.231
434	715.375	632.196	83.179	0.1176	1.240

435	714.427	631.105	83.323	0.1175	1.282
436	713.480	630.115	83.365	0.1172	1.279
437	712.450	629.276	83.174	0.1170	1.235
438	711.502	628.333	83.169	0.1173	1.192
439	711.502	628.361	83.141	0.1176	1.230
440	710.513	627.203	83.310	0.1173	1.249
441	710.472	627.107	83.365	0.1169	1.256
442	709.525	626.240	83.285	0.1168	1.211
443	707.465	624.178	83.286	0.1173	1.197
444	705.611	622.081	83.530	0.1172	1.201
445	705.611	622.217	83.394	0.1173	1.198
446	704.539	621.317	83.223	0.1168	1.198
447	704.581	621.138	83.443	0.1168	1.186
448	703.551	620.316	83.235	0.1168	1.176
449	702.644	619.312	83.333	0.1171	1.188
450	701.614	618.357	83.258	0.1170	1.179
451	700.626	617.312	83.314	0.1168	1.188
452	698.607	615.283	83.324	0.1165	1.173
453	698.648	615.453	83.195	0.1164	1.167
454	697.618	614.291	83.328	0.1167	1.150
455	696.588	613.407	83.181	0.1168	1.140
456	695.599	612.307	83.293	0.1169	1.142
457	694.611	611.313	83.298	0.1168	1.157
458	694.652	611.313	83.339	0.1164	1.133
459	693.663	610.322	83.341	0.1164	1.134
460	692.592	609.242	83.350	0.1164	1.119
461	691.727	608.417	83.310	0.1165	1.124
462	691.727	608.375	83.351	0.1164	1.100
463	690.656	607.364	83.291	0.1165	1.103
464	689.749	606.445	83.304	0.1164	1.098
465	687.648	604.311	83.338	0.1164	1.085
466	687.772	604.492	83.280	0.1165	1.092
467	687.813	604.508	83.305	0.1164	1.083
468	685.835	602.494	83.341	0.1162	1.090
469	684.847	601.602	83.245	0.1161	1.076
470	684.805	601.454	83.351	0.1161	1.069
471	683.817	600.545	83.271	0.1161	1.076
472	682.787	599.574	83.213	0.1160	1.069
473	681.963	598.683	83.280	0.1156	1.063
474	680.850	597.440	83.410	0.1156	1.063
475	680.768	597.478	83.290	0.1157	1.055
476	679.820	596.474	83.346	0.1157	1.048
477	678.790	595.488	83.303	0.1154	1.044
478	677.884	594.644	83.240	0.1153	1.040
479	676.854	593.653	83.201	0.1153	1.035

480	675.948	592.723	83.225	0.1153	1.033
481	675.000	591.705	83.295	0.1153	1.030
482	675.082	591.560	83.523	0.1153	1.025
483	673.970	590.570	83.400	0.1150	1.024
484	672.858	589.459	83.399	0.1153	1.021
485	672.075	588.831	83.244	0.1149	1.017
486	670.097	586.932	83.165	0.1149	1.012
487	669.026	585.652	83.374	0.1149	1.011
488	670.015	586.582	83.433	0.1149	1.008
489	668.985	585.629	83.356	0.1149	1.003
490	668.079	584.837	83.241	0.1149	1.002
491	668.120	584.807	83.313	0.1146	1.000
492	667.090	583.706	83.384	0.1146	0.998
493	665.030	581.747	83.283	0.1145	0.996
494	665.154	582.011	83.143	0.1146	0.991
495	664.000	580.636	83.364	0.1145	0.987
496	663.176	579.882	83.294	0.1145	0.987
497	663.176	579.740	83.436	0.1144	0.984
498	663.094	579.836	83.258	0.1142	0.982
499	663.217	579.916	83.301	0.1143	0.980
500	663.094	579.719	83.375	0.1143	0.976
501	662.146	578.949	83.198	0.1142	0.972
502	661.198	577.967	83.231	0.1142	0.969
503	661.157	577.991	83.166	0.1142	0.969
504	660.168	576.840	83.329	0.1142	0.966
505	660.210	576.948	83.261	0.1139	0.963
506	659.180	575.955	83.225	0.1138	0.960
507	659.138	575.892	83.246	0.1138	0.958
508	660.168	576.993	83.175	0.1138	0.954
509	660.210	576.996	83.214	0.1138	0.953
510	660.127	576.629	83.499	0.1138	0.950
511	659.138	575.940	83.199	0.1138	0.948
512	658.232	574.990	83.243	0.1138	0.945
513	657.243	574.003	83.240	0.1139	0.941
514	656.131	572.942	83.189	0.1134	0.940
515	656.172	572.895	83.278	0.1134	0.937
516	657.161	573.891	83.270	0.1134	0.935
517	656.213	573.017	83.196	0.1135	0.933
518	655.266	571.966	83.300	0.1135	0.929
519	655.142	572.023	83.119	0.1135	0.927
520	655.266	572.106	83.160	0.1132	0.924
521	654.236	571.022	83.214	0.1131	0.923
522	654.195	571.006	83.189	0.1130	0.918
523	654.236	571.170	83.066	0.1131	0.918
524	653.247	570.115	83.133	0.1131	0.915

525	653.206	569.927	83.279	0.1131	0.912
526	653.206	570.005	83.201	0.1130	0.910
527	653.123	570.052	83.071	0.1127	0.909
528	651.352	568.229	83.123	0.1130	0.907
529	653.206	570.085	83.121	0.1127	0.904
530	651.393	568.196	83.198	0.1128	0.903
531	651.146	568.085	83.061	0.1128	0.899
532	651.311	568.308	83.003	0.1128	0.896
533	651.270	568.040	83.230	0.1127	0.893
534	651.393	568.474	82.919	0.1127	0.892
535	650.157	567.100	83.058	0.1128	0.890
536	650.240	567.202	83.038	0.1127	0.886
537	648.221	565.373	82.848	0.1124	0.886
538	648.303	565.273	83.030	0.1124	0.883
539	648.386	565.523	82.863	0.1124	0.880
540	647.314	564.346	82.969	0.1124	0.878
541	648.221	565.321	82.900	0.1123	0.876
542	646.408	563.459	82.949	0.1124	0.873
543	646.243	563.322	82.921	0.1124	0.873
544	645.296	562.382	82.914	0.1124	0.869
545	644.348	561.324	83.024	0.1124	0.867
546	643.277	560.347	82.930	0.1120	0.866
547	644.472	561.524	82.948	0.1119	0.863
548	643.442	560.704	82.738	0.1120	0.862
549	643.277	560.381	82.896	0.1120	0.858
550	643.318	560.579	82.739	0.1120	0.854
551	643.359	560.593	82.766	0.1120	0.854
552	642.329	559.568	82.761	0.1120	0.851
553	640.352	557.506	82.846	0.1120	0.848
554	640.475	557.677	82.799	0.1120	0.847
555	640.393	557.533	82.860	0.1120	0.844
556	640.352	557.521	82.831	0.1120	0.843
557	640.393	557.584	82.809	0.1117	0.841
558	639.446	556.511	82.935	0.1116	0.838
559	639.528	556.947	82.581	0.1117	0.836
560	637.344	554.658	82.686	0.1116	0.834
561	636.397	553.822	82.575	0.1116	0.830
562	636.438	553.760	82.678	0.1116	0.828
563	636.520	553.922	82.599	0.1117	0.828
564	636.479	553.790	82.689	0.1117	0.825
565	634.543	551.845	82.698	0.1116	0.825
566	635.573	552.880	82.693	0.1116	0.821
567	634.502	551.898	82.604	0.1113	0.819
568	634.378	551.884	82.494	0.1113	0.817
569	634.502	551.892	82.610	0.1114	0.815

570	633.513	550.982	82.531	0.1113	0.814
571	632.442	549.790	82.651	0.1114	0.811
572	632.607	550.135	82.471	0.1113	0.809
573	632.565	549.873	82.693	0.1113	0.807
574	631.371	548.943	82.428	0.1113	0.805
575	631.535	549.124	82.411	0.1113	0.804
576	631.618	549.165	82.453	0.1114	0.800
577	630.423	548.193	82.230	0.1113	0.799
578	628.487	546.027	82.460	0.1113	0.797
579	630.547	548.023	82.524	0.1114	0.796
580	629.599	547.128	82.471	0.1108	0.793
581	629.475	547.017	82.459	0.1109	0.791
582	628.528	546.319	82.209	0.1109	0.789
583	628.610	546.301	82.309	0.1109	0.787
584	627.580	545.299	82.281	0.1109	0.786
585	626.591	544.395	82.196	0.1109	0.783
586	626.633	544.298	82.335	0.1108	0.780
587	626.674	544.275	82.399	0.1109	0.780
588	625.685	543.485	82.200	0.1109	0.776
589	625.685	543.579	82.106	0.1109	0.774
590	625.562	543.387	82.175	0.1109	0.773
591	624.696	542.251	82.445	0.1104	0.772
592	623.543	541.420	82.123	0.1104	0.770
593	623.584	541.386	82.198	0.1104	0.768
594	623.543	541.477	82.066	0.1104	0.767
595	622.760	540.664	82.096	0.1104	0.764
596	622.636	540.443	82.194	0.1104	0.762
597	621.730	539.879	81.851	0.1105	0.761
598	621.689	539.616	82.073	0.1105	0.759
599	622.678	540.741	81.936	0.1105	0.755
600	620.741	538.835	81.906	0.1104	0.755
601	619.753	537.709	82.044	0.1104	0.753
602	620.741	538.666	82.075	0.1105	0.751
603	620.700	538.768	81.933	0.1104	0.751
604	620.700	538.923	81.778	0.1104	0.747
605	619.711	537.816	81.895	0.1101	0.746
606	619.753	537.980	81.773	0.1100	0.743
607	620.659	538.864	81.795	0.1099	0.743
608	618.764	537.105	81.659	0.1100	0.740
609	619.753	537.944	81.809	0.1101	0.739
610	619.670	537.973	81.698	0.1100	0.738
611	618.764	536.869	81.895	0.1100	0.736
612	618.723	536.969	81.754	0.1100	0.734
613	618.681	536.946	81.735	0.1099	0.734
614	618.599	536.969	81.630	0.1100	0.731

615	618.599	536.849	81.750	0.1100	0.728
616	616.745	535.130	81.615	0.1101	0.728
617	618.681	536.929	81.753	0.1100	0.725
618	618.558	536.941	81.616	0.1100	0.725
619	616.704	535.188	81.516	0.1100	0.723
620	615.756	534.179	81.578	0.1097	0.722
621	615.715	534.229	81.486	0.1100	0.718
622	615.797	534.224	81.574	0.1097	0.718
623	615.797	534.310	81.488	0.1096	0.715
624	615.633	534.225	81.408	0.1101	0.713
625	615.633	534.099	81.534	0.1100	0.713
626	615.839	534.316	81.523	0.1100	0.712
627	614.685	533.344	81.341	0.1100	0.710
628	615.715	534.425	81.290	0.1100	0.708
629	615.715	534.280	81.435	0.1100	0.708
630	614.726	533.458	81.269	0.1101	0.705
631	614.809	533.406	81.403	0.1101	0.703
632	613.861	532.561	81.300	0.1101	0.702
633	613.779	532.609	81.170	0.1100	0.701
634	613.779	532.469	81.310	0.1099	0.700
635	612.708	531.621	81.086	0.1100	0.697
636	613.779	532.577	81.201	0.1101	0.696
637	612.831	531.792	81.039	0.1100	0.694
638	612.749	531.574	81.175	0.1099	0.692
639	611.842	530.764	81.079	0.1097	0.693
640	610.895	529.892	81.003	0.1097	0.689
641	610.854	529.744	81.110	0.1096	0.688
642	610.895	529.977	80.918	0.1096	0.688
643	609.906	528.934	80.973	0.1096	0.686
644	609.906	528.817	81.089	0.1096	0.684
645	610.771	529.800	80.971	0.1096	0.683
646	610.854	529.871	80.983	0.1096	0.682
647	609.824	528.997	80.826	0.1096	0.680
648	609.700	528.745	80.955	0.1097	0.678
649	609.782	528.822	80.960	0.1097	0.678
650	609.824	528.875	80.949	0.1096	0.677
651	609.906	528.980	80.926	0.1097	0.673
652	608.876	527.864	81.013	0.1096	0.673
653	608.794	527.881	80.913	0.1097	0.671
654	608.835	528.074	80.761	0.1096	0.670
655	608.835	528.172	80.663	0.1096	0.667
656	606.857	526.210	80.648	0.1097	0.667
657	607.805	527.087	80.718	0.1092	0.665
658	606.899	526.094	80.805	0.1092	0.664
659	608.011	527.510	80.501	0.1092	0.663

660	606.940	526.266	80.674	0.1092	0.663
661	606.940	526.350	80.590	0.1092	0.658
662	606.899	526.467	80.431	0.1092	0.656
663	605.951	525.253	80.698	0.1092	0.654
664	605.992	525.462	80.530	0.1092	0.651
665	605.910	525.285	80.625	0.1092	0.651
666	605.045	524.666	80.379	0.1092	0.645
667	604.962	524.486	80.476	0.1092	0.648
668	604.962	524.510	80.453	0.1092	0.644
669	605.951	525.691	80.260	0.1092	0.642
670	604.962	524.417	80.545	0.1092	0.641
671	604.921	524.687	80.234	0.1089	0.639
672	605.086	524.786	80.300	0.1088	0.638
673	603.809	523.600	80.209	0.1089	0.638
674	601.913	521.537	80.376	0.1088	0.635
675	603.108	522.751	80.358	0.1089	0.635
676	604.015	523.666	80.349	0.1088	0.634
677	602.985	522.780	80.205	0.1089	0.631
678	601.996	521.931	80.065	0.1088	0.631
679	601.913	521.800	80.114	0.1088	0.629
680	602.037	521.878	80.159	0.1089	0.629
681	602.037	521.893	80.144	0.1084	0.627
682	599.977	519.913	80.064	0.1085	0.626
683	600.060	520.067	79.993	0.1084	0.624
684	599.854	519.845	80.009	0.1084	0.624
685	598.824	518.856	79.968	0.1085	0.622
686	598.906	518.992	79.914	0.1085	0.621
687	598.988	518.925	80.064	0.1084	0.620
688	598.041	517.963	80.078	0.1086	0.618
689	598.988	519.142	79.846	0.1084	0.617
690	597.917	518.012	79.905	0.1084	0.616
691	597.958	518.113	79.845	0.1084	0.614
692	597.958	518.027	79.931	0.1085	0.614
693	597.011	517.041	79.970	0.1084	0.611
694	597.052	517.147	79.905	0.1085	0.611
695	596.970	517.093	79.876	0.1085	0.609
696	597.093	517.361	79.733	0.1084	0.606
697	597.011	517.193	79.818	0.1085	0.606
698	597.052	517.200	79.853	0.1085	0.606
699	596.970	517.272	79.698	0.1084	0.605
700	597.093	517.427	79.666	0.1084	0.602
701	596.887	517.203	79.684	0.1081	0.600
702	597.011	517.255	79.756	0.1081	0.600
703	593.962	514.273	79.689	0.1081	0.599
704	595.116	515.467	79.649	0.1081	0.597

705	594.127	514.431	79.696	0.1081	0.596
706	594.044	514.589	79.455	0.1081	0.595
707	594.951	515.443	79.508	0.1081	0.596
708	594.086	514.649	79.436	0.1081	0.593
709	594.086	514.643	79.443	0.1081	0.591
710	594.086	514.697	79.389	0.1081	0.589
711	593.962	514.626	79.336	0.1081	0.588
712	594.127	514.792	79.335	0.1081	0.587
713	594.127	514.774	79.353	0.1081	0.587
714	594.086	514.839	79.246	0.1081	0.584
715	594.003	514.656	79.348	0.1081	0.584
716	593.015	513.915	79.100	0.1081	0.583
717	593.097	513.983	79.114	0.1081	0.582
718	594.127	515.024	79.103	0.1081	0.580
719	593.056	513.953	79.103	0.1081	0.579
720	592.026	513.148	78.878	0.1081	0.578
721	591.202	512.123	79.079	0.1081	0.577
722	591.119	512.022	79.098	0.1081	0.576
723	591.161	512.108	79.053	0.1081	0.575
724	591.161	512.398	78.763	0.1081	0.573
725	590.089	511.244	78.845	0.1081	0.572
726	590.089	511.118	78.971	0.1080	0.570
727	590.131	511.271	78.860	0.1081	0.569
728	589.142	510.311	78.831	0.1081	0.568
729	589.265	510.462	78.804	0.1081	0.567
730	589.224	510.535	78.689	0.1081	0.567
731	589.183	510.469	78.714	0.1080	0.564
732	589.183	510.458	78.725	0.1078	0.564
733	589.101	510.367	78.734	0.1077	0.563
734	588.153	509.478	78.675	0.1077	0.561
735	588.194	509.522	78.673	0.1077	0.559
736	587.164	508.552	78.613	0.1077	0.558
737	587.206	508.668	78.538	0.1077	0.558
738	587.247	508.503	78.744	0.1078	0.557
739	587.164	508.586	78.579	0.1077	0.555
740	586.176	507.588	78.588	0.1077	0.553
741	586.093	507.706	78.388	0.1077	0.553
742	585.187	506.824	78.363	0.1076	0.551
743	586.217	507.647	78.570	0.1077	0.550
744	585.187	506.791	78.396	0.1077	0.550
745	585.146	506.913	78.233	0.1077	0.548
746	585.187	506.812	78.375	0.1077	0.548
747	585.269	507.039	78.230	0.1077	0.547
748	584.074	505.847	78.228	0.1077	0.545
749	585.187	506.926	78.261	0.1076	0.543

750	583.003	504.888	78.115	0.1076	0.542
751	585.228	507.235	77.993	0.1077	0.542
752	583.209	505.069	78.140	0.1076	0.541
753	582.303	504.347	77.956	0.1076	0.538
754	582.220	504.245	77.975	0.1077	0.538
755	581.149	503.203	77.946	0.1077	0.536
756	581.190	503.143	78.048	0.1077	0.536
757	581.232	503.287	77.945	0.1077	0.535
758	581.314	503.460	77.854	0.1077	0.532
759	581.108	503.216	77.893	0.1077	0.532
760	580.202	502.563	77.639	0.1077	0.531
761	580.243	502.549	77.694	0.1078	0.530
762	579.337	501.512	77.825	0.1077	0.529
763	579.254	501.453	77.801	0.1078	0.525
764	579.213	501.490	77.723	0.1078	0.526
765	579.337	501.690	77.646	0.1076	0.525
766	579.295	501.742	77.554	0.1074	0.524
767	579.295	501.709	77.586	0.1077	0.525
768	578.265	500.679	77.586	0.1077	0.522
769	578.224	500.813	77.411	0.1075	0.522
770	578.224	500.662	77.563	0.1076	0.520
771	578.224	500.808	77.416	0.1073	0.519
772	577.235	499.719	77.516	0.1077	0.519
773	577.153	499.751	77.403	0.1073	0.518
774	578.224	500.909	77.315	0.1073	0.515
775	577.277	499.914	77.363	0.1073	0.516
776	577.071	499.776	77.295	0.1073	0.513
777	577.153	499.843	77.310	0.1073	0.513
778	577.318	500.182	77.136	0.1073	0.513
779	577.235	500.069	77.166	0.1073	0.511
780	576.164	499.001	77.164	0.1073	0.511
781	577.277	500.068	77.209	0.1073	0.510
782	576.329	499.290	77.039	0.1073	0.508
783	574.269	497.197	77.073	0.1073	0.507
784	574.310	497.318	76.993	0.1073	0.507
785	574.269	497.290	76.979	0.1073	0.507
786	574.393	497.400	76.993	0.1073	0.505
787	574.310	497.422	76.889	0.1073	0.503
788	573.486	496.598	76.889	0.1073	0.504
789	573.322	496.554	76.768	0.1073	0.502
790	573.322	496.517	76.805	0.1073	0.500
791	573.280	496.435	76.845	0.1073	0.500
792	572.374	495.673	76.701	0.1073	0.500
793	572.292	495.529	76.763	0.1073	0.499
794	572.374	495.704	76.670	0.1073	0.498

795	571.344	494.188	77.156	0.1073	0.496
796	571.385	494.815	76.570	0.1073	0.495
797	571.426	494.908	76.519	0.1073	0.494
798	571.262	494.754	76.508	0.1073	0.496
799	571.344	494.760	76.584	0.1073	0.492
800	571.303	494.879	76.424	0.1073	0.490
801	571.468	495.114	76.354	0.1073	0.490
802	571.426	494.998	76.429	0.1073	0.490
803	571.468	495.004	76.464	0.1073	0.489
804	571.344	495.023	76.321	0.1073	0.489
805	571.385	495.088	76.298	0.1073	0.487
806	570.314	494.128	76.186	0.1073	0.488
807	569.366	493.146	76.220	0.1073	0.485
808	569.449	493.116	76.333	0.1073	0.484
809	569.366	493.139	76.228	0.1070	0.484
810	569.284	493.037	76.248	0.1072	0.483
811	569.408	493.271	76.136	0.1073	0.483
812	569.366	493.174	76.193	0.1072	0.481
813	569.366	493.231	76.135	0.1073	0.482
814	569.366	493.288	76.079	0.1073	0.482
815	568.460	492.436	76.024	0.1070	0.480
816	566.524	490.389	76.135	0.1072	0.477
817	566.483	490.598	75.885	0.1070	0.478
818	566.359	490.481	75.878	0.1069	0.478
819	566.483	490.600	75.883	0.1070	0.475
820	566.400	490.540	75.860	0.1069	0.476
821	566.359	490.538	75.821	0.1069	0.476
822	565.453	489.800	75.653	0.1069	0.474
823	565.411	489.725	75.686	0.1073	0.474
824	565.411	489.740	75.671	0.1069	0.472
825	565.453	489.879	75.574	0.1070	0.471
826	565.411	489.699	75.713	0.1069	0.471
827	565.411	489.850	75.561	0.1069	0.471
828	565.370	489.704	75.666	0.1069	0.469
829	564.423	488.954	75.469	0.1073	0.468
830	564.423	488.886	75.536	0.1069	0.469
831	565.535	490.104	75.431	0.1069	0.468
832	564.423	488.966	75.456	0.1068	0.468
833	564.505	489.088	75.418	0.1070	0.465
834	564.299	488.922	75.378	0.1069	0.464
835	563.557	488.170	75.388	0.1069	0.464
836	563.434	488.146	75.288	0.1069	0.464
837	563.475	488.310	75.165	0.1070	0.463
838	563.475	488.293	75.183	0.1069	0.462
839	562.569	487.252	75.316	0.1070	0.461

840	562.445	487.068	75.378	0.1069	0.461
841	562.445	487.291	75.154	0.1070	0.459
842	562.321	487.304	75.018	0.1070	0.458
843	562.363	487.229	75.134	0.1069	0.459
844	562.445	487.126	75.319	0.1069	0.458
845	561.539	486.390	75.149	0.1069	0.459
846	562.527	487.604	74.924	0.1069	0.457
847	562.486	487.524	74.963	0.1069	0.457
848	562.445	487.388	75.058	0.1069	0.456
849	561.456	486.674	74.783	0.1070	0.455
850	561.580	486.711	74.869	0.1069	0.451
851	561.498	486.653	74.845	0.1069	0.454
852	561.456	486.611	74.845	0.1070	0.453
853	560.468	485.500	74.968	0.1069	0.451
854	560.468	485.759	74.709	0.1069	0.451
855	560.344	485.664	74.680	0.1070	0.451
856	559.479	484.896	74.583	0.1069	0.450
857	560.509	485.982	74.526	0.1069	0.448
858	560.426	485.671	74.755	0.1069	0.447
859	560.468	485.876	74.591	0.1069	0.447
860	560.591	486.004	74.588	0.1069	0.447
861	559.602	485.166	74.436	0.1069	0.447
862	559.561	485.086	74.475	0.1069	0.445
863	559.479	485.036	74.443	0.1069	0.445
864	557.542	483.071	74.471	0.1069	0.444
865	557.625	483.154	74.471	0.1069	0.444
866	559.561	485.166	74.395	0.1069	0.444
867	557.666	483.345	74.321	0.1068	0.443
868	559.520	485.077	74.443	0.1069	0.441
869	557.584	483.405	74.179	0.1069	0.441
870	557.625	483.447	74.178	0.1069	0.439
871	557.542	483.331	74.211	0.1069	0.441
872	557.666	483.525	74.141	0.1069	0.439
873	557.707	483.560	74.148	0.1069	0.438
874	557.460	483.499	73.961	0.1069	0.436
875	557.584	483.409	74.175	0.1069	0.435
876	557.625	483.491	74.134	0.1069	0.436
877	557.501	483.441	74.060	0.1069	0.435
878	557.542	483.562	73.980	0.1069	0.434
879	557.584	483.689	73.895	0.1069	0.435
880	557.625	483.744	73.881	0.1069	0.433
881	557.378	483.413	73.965	0.1066	0.435
882	557.501	483.615	73.886	0.1067	0.432
883	555.482	481.692	73.790	0.1065	0.432
884	556.554	482.807	73.746	0.1069	0.433

885	555.524	481.694	73.830	0.1069	0.430
886	554.576	481.010	73.566	0.1067	0.430
887	554.453	480.798	73.655	0.1066	0.429
888	554.617	481.012	73.605	0.1069	0.429
889	554.576	481.012	73.564	0.1070	0.429
890	554.576	481.074	73.503	0.1065	0.427
891	554.617	481.097	73.520	0.1065	0.427
892	554.576	481.026	73.550	0.1069	0.426
893	554.576	481.145	73.431	0.1069	0.426
894	554.535	481.097	73.438	0.1066	0.425
895	554.535	481.354	73.181	0.1066	0.423
896	554.494	481.306	73.188	0.1065	0.423
897	554.576	480.972	73.604	0.1066	0.425
898	554.494	481.292	73.201	0.1069	0.422
899	553.587	480.225	73.363	0.1066	0.423
900	552.516	479.276	73.240	0.1069	0.422
901	554.494	481.249	73.245	0.1066	0.419
902	552.557	479.440	73.118	0.1066	0.420
903	552.557	479.322	73.235	0.1066	0.420
904	552.557	479.384	73.174	0.1065	0.417
905	553.546	480.429	73.118	0.1068	0.419
906	552.516	479.614	72.903	0.1066	0.418
907	552.640	479.566	73.074	0.1066	0.419
908	552.763	479.876	72.888	0.1065	0.416
909	552.599	479.519	73.080	0.1065	0.416
910	552.599	479.695	72.904	0.1065	0.416
911	551.569	478.695	72.874	0.1066	0.415
912	551.651	478.706	72.945	0.1065	0.413
913	552.599	479.744	72.855	0.1067	0.414
914	552.516	479.626	72.890	0.1065	0.413
915	551.610	478.739	72.871	0.1066	0.413
916	551.527	478.879	72.649	0.1066	0.413
917	550.621	477.774	72.848	0.1066	0.413
918	550.580	477.855	72.725	0.1066	0.410
919	550.662	478.007	72.655	0.1066	0.411
920	549.550	476.966	72.584	0.1066	0.412
921	549.591	477.011	72.580	0.1066	0.409
922	549.673	477.016	72.658	0.1066	0.411
923	549.673	477.311	72.363	0.1065	0.416
924	549.591	477.071	72.520	0.1066	0.413
925	548.561	476.069	72.493	0.1066	0.407
926	548.561	476.172	72.389	0.1066	0.407
927	548.643	476.193	72.450	0.1066	0.410
928	548.685	476.311	72.374	0.1066	0.408
929	548.602	476.134	72.469	0.1066	0.410

930	548.643	476.320	72.324	0.1066	0.406
931	549.715	477.418	72.296	0.1065	0.410
932	547.696	475.285	72.411	0.1066	0.406
933	546.584	474.447	72.136	0.1066	0.403
934	547.655	475.425	72.230	0.1065	0.419
935	548.602	476.311	72.291	0.1070	0.403
936	546.666	474.453	72.213	0.1066	0.408
937	546.666	474.477	72.189	0.1066	0.403
938	546.790	474.691	72.099	0.1066	0.403
939	546.584	474.574	72.010	0.1066	0.414
940	546.666	474.792	71.874	0.1066	0.406
941	546.666	474.661	72.005	0.1066	0.402
942	546.748	474.806	71.943	0.1066	0.399
943	546.501	474.616	71.885	0.1066	0.394
944	546.748	474.815	71.934	0.1066	0.413
945	546.707	474.753	71.954	0.1065	0.394
946	546.542	474.679	71.864	0.1066	0.410
947	546.584	474.792	71.791	0.1066	0.410
948	545.636	473.902	71.734	0.1066	0.395
949	545.677	473.888	71.789	0.1066	0.408
950	545.760	474.142	71.618	0.1065	0.397
951	544.647	472.923	71.724	0.1066	0.404
952	544.688	472.997	71.691	0.1066	0.396
953	544.688	472.940	71.749	0.1066	0.400
954	544.647	473.021	71.626	0.1066	0.398
955	544.647	473.063	71.584	0.1066	0.390
956	543.658	472.088	71.570	0.1066	0.398
957	543.617	472.034	71.584	0.1066	0.403
958	542.711	471.310	71.401	0.1065	0.396
959	542.793	471.382	71.411	0.1066	0.401
960	542.711	471.231	71.480	0.1066	0.410
961	542.670	471.267	71.403	0.1067	0.402
962	542.752	471.213	71.539	0.1066	0.401
963	542.670	471.126	71.544	0.1066	0.390
964	542.752	471.415	71.338	0.1066	0.397
965	542.711	471.296	71.415	0.1066	0.400
966	541.640	470.321	71.319	0.1065	0.393
967	541.763	470.501	71.263	0.1066	0.395
968	541.846	470.461	71.385	0.1066	0.398
969	541.681	470.362	71.319	0.1065	0.400
970	541.805	470.552	71.253	0.1066	0.392
971	541.763	470.667	71.096	0.1066	0.395
972	541.763	470.758	71.005	0.1066	0.392
973	541.846	470.572	71.274	0.1065	0.403
974	541.722	470.651	71.071	0.1066	0.397

975	541.681	470.633	71.048	0.1066	0.390
976	541.722	470.661	71.061	0.1065	0.384
977	541.763	470.680	71.084	0.1066	0.392
978	541.681	470.558	71.123	0.1066	0.395
979	541.805	470.752	71.053	0.1066	0.392
980	540.733	469.755	70.979	0.1066	0.397
981	540.692	469.711	70.981	0.1065	0.397
982	540.692	469.691	71.001	0.1066	0.392
983	539.786	468.938	70.848	0.1065	0.390
984	538.673	467.813	70.860	0.1066	0.402
985	538.756	467.923	70.833	0.1066	0.395
986	538.838	467.907	70.931	0.1065	0.390
987	538.879	467.804	71.075	0.1066	0.390
988	538.715	468.083	70.631	0.1066	0.392
989	538.879	468.132	70.748	0.1065	0.394
990	538.756	468.070	70.686	0.1065	0.394
991	538.632	467.982	70.650	0.1065	0.393
992	537.808	467.206	70.603	0.1066	0.390
993	537.808	467.238	70.570	0.1066	0.393
994	537.726	467.113	70.613	0.1066	0.390
995	537.726	467.156	70.570	0.1066	0.392
996	536.861	466.413	70.448	0.1066	0.385
997	536.696	466.271	70.425	0.1066	0.384
998	536.778	466.471	70.308	0.1066	0.397
999	536.943	466.616	70.328	0.1066	0.389
1000	536.737	466.193	70.544	0.1066	0.389
1001	536.737	466.306	70.431	0.1066	0.390
1002	536.778	466.343	70.435	0.1066	0.387
1003	536.778	466.493	70.285	0.1066	0.381
1004	535.666	465.482	70.184	0.1067	0.391
1005	535.831	465.537	70.294	0.1066	0.378
1006	535.789	465.582	70.208	0.1066	0.397
1007	536.696	466.492	70.204	0.1065	0.389
1008	535.707	465.423	70.284	0.1066	0.396
1009	535.789	465.562	70.228	0.1066	0.390
1010	535.789	465.654	70.135	0.1066	0.395
1011	535.789	465.748	70.041	0.1065	0.384
1012	535.748	465.752	69.996	0.1065	0.401
1013	535.789	465.781	70.009	0.1066	0.377
1014	534.760	464.720	70.040	0.1065	0.384
1015	534.883	464.849	70.034	0.1065	0.390
1016	534.842	464.791	70.051	0.1066	0.387
1017	534.966	464.961	70.005	0.1065	0.373
1018	533.730	463.833	69.896	0.1065	0.372
1019	532.906	463.197	69.709	0.1066	0.399

1020	532.906	463.122	69.784	0.1066	0.377
1021	533.771	463.851	69.920	0.1066	0.400
1022	533.936	464.002	69.934	0.1069	0.388
1023	532.823	463.096	69.728	0.1068	0.379
1024	532.864	463.229	69.635	0.1065	0.385
1025	532.823	462.808	70.015	0.1066	0.396
1026	532.988	463.378	69.610	0.1066	0.398
1027	532.782	463.017	69.765	0.1069	0.391
1028	532.782	463.096	69.686	0.1069	0.383
1029	532.823	463.164	69.659	0.1066	0.379
1030	532.864	463.136	69.729	0.1066	0.387
1031	531.834	462.284	69.550	0.1066	0.393
1032	531.917	462.436	69.481	0.1066	0.390
1033	531.999	462.529	69.470	0.1066	0.397
1034	531.834	462.424	69.410	0.1066	0.395
1035	531.876	462.389	69.486	0.1069	0.382
1036	531.793	462.279	69.514	0.1066	0.382
1037	531.010	461.817	69.194	0.1066	0.384
1038	530.846	461.436	69.410	0.1066	0.375
1039	530.804	461.459	69.345	0.1066	0.384
1040	530.928	461.682	69.246	0.1065	0.384
1041	531.052	461.722	69.330	0.1066	0.398
1042	529.939	460.633	69.306	0.1066	0.380
1043	529.898	460.594	69.304	0.1066	0.397
1044	530.928	461.672	69.256	0.1065	0.392
1045	529.939	460.712	69.228	0.1069	0.384
1046	529.774	460.511	69.264	0.1069	0.381
1047	529.939	460.603	69.336	0.1066	0.376
1048	530.063	460.929	69.134	0.1066	0.373
1049	529.898	460.774	69.124	0.1066	0.386
1050	529.816	460.728	69.088	0.1066	0.385
1051	528.951	459.873	69.078	0.1066	0.382
1052	528.951	459.846	69.105	0.1066	0.407
1053	528.992	459.938	69.054	0.1066	0.385
1054	527.879	458.932	68.948	0.1069	0.381
1055	528.868	459.856	69.013	0.1069	0.380
1056	528.868	459.869	68.999	0.1066	0.374
1057	527.921	458.866	69.055	0.1066	0.376
1058	527.921	459.058	68.863	0.1066	0.387
1059	527.879	459.162	68.718	0.1066	0.400
1060	527.879	459.316	68.564	0.1066	0.397
1061	527.921	459.048	68.873	0.1065	0.385
1062	527.962	459.147	68.815	0.1068	0.376
1063	528.909	460.056	68.854	0.1065	0.381
1064	527.962	459.217	68.745	0.1066	0.377

1065	527.921	459.183	68.738	0.1066	0.370
1066	526.891	458.151	68.740	0.1065	0.397
1067	526.932	458.227	68.705	0.1066	0.392
1068	525.984	457.305	68.679	0.1066	0.385
1069	524.954	456.189	68.765	0.1066	0.374
1070	524.954	456.293	68.661	0.1066	0.389
1071	524.954	456.302	68.653	0.1065	0.383
1072	525.037	456.483	68.554	0.1066	0.371
1073	524.913	456.316	68.598	0.1066	0.371
1074	525.037	456.404	68.633	0.1066	0.368
1075	524.913	456.332	68.581	0.1066	0.400
1076	524.872	456.388	68.484	0.1066	0.383
1077	524.954	456.387	68.568	0.1069	0.368
1078	524.913	456.494	68.419	0.1070	0.378
1079	524.872	456.486	68.386	0.1069	0.385
1080	524.954	456.555	68.399	0.1066	0.368
1081	524.048	455.605	68.443	0.1065	0.370
1082	524.872	456.468	68.404	0.1066	0.386
1083	523.924	455.477	68.448	0.1066	0.383
1084	524.007	455.758	68.249	0.1066	0.380
1085	523.100	454.790	68.310	0.1062	0.400
1086	522.853	454.563	68.290	0.1065	0.383
1087	523.018	454.777	68.241	0.1066	0.392
1088	522.935	454.559	68.376	0.1066	0.378
1089	522.935	454.720	68.215	0.1066	0.376
1090	523.059	454.870	68.189	0.1066	0.376
1091	523.059	454.944	68.115	0.1066	0.377
1092	523.018	454.908	68.110	0.1065	0.381
1093	523.018	454.852	68.166	0.1063	0.381
1094	522.894	454.732	68.163	0.1062	0.389
1095	521.947	453.709	68.238	0.1064	0.384
1096	523.059	454.993	68.066	0.1066	0.376
1097	522.029	453.952	68.078	0.1067	0.381
1098	522.029	454.042	67.988	0.1066	0.385
1099	522.070	454.192	67.879	0.1065	0.380
1100	522.029	454.053	67.976	0.1066	0.386
1101	521.082	453.093	67.989	0.1065	0.380
1102	520.917	453.031	67.886	0.1066	0.386
1103	522.029	454.168	67.861	0.1065	0.384
1104	520.999	453.034	67.965	0.1066	0.387
1105	521.040	453.225	67.815	0.1066	0.377
1106	520.010	452.008	68.003	0.1066	0.366
1107	520.093	452.307	67.786	0.1066	0.374
1108	519.928	452.233	67.695	0.1066	0.371
1109	520.010	452.243	67.768	0.1065	0.371

1110	520.093	452.268	67.825	0.1063	0.398
1111	520.010	452.289	67.721	0.1061	0.385
1112	520.010	452.345	67.665	0.1065	0.374
1113	519.969	452.149	67.820	0.1066	0.381
1114	520.052	452.334	67.718	0.1066	0.370
1115	520.093	452.433	67.660	0.1066	0.394
1116	520.093	452.488	67.605	0.1066	0.396
1117	520.010	452.308	67.703	0.1065	0.383
1118	518.980	451.509	67.471	0.1066	0.371
1119	518.033	450.437	67.596	0.1066	0.373
1120	518.074	450.558	67.516	0.1065	0.365
1121	517.950	450.524	67.426	0.1066	0.376
1122	518.074	450.447	67.628	0.1065	0.377
1123	518.033	450.560	67.473	0.1066	0.362
1124	518.115	450.703	67.413	0.1066	0.372
1125	518.074	450.412	67.663	0.1062	0.384
1126	518.115	450.604	67.511	0.1062	0.401
1127	518.115	450.851	67.264	0.1062	0.390
1128	517.126	449.571	67.555	0.1066	0.377
1129	515.025	447.560	67.465	0.1066	0.366
1130	515.108	447.790	67.318	0.1066	0.361
1131	516.179	448.689	67.490	0.1065	0.361
1132	516.097	448.914	67.183	0.1065	0.377
1133	517.003	449.692	67.311	0.1066	0.384
1134	516.055	448.747	67.309	0.1066	0.377
1135	516.055	448.798	67.258	0.1065	0.359
1136	515.067	447.880	67.186	0.1066	0.371
1137	516.097	448.844	67.253	0.1066	0.374
1138	515.108	447.868	67.240	0.1062	0.370
1139	516.097	449.017	67.080	0.1062	0.399
1140	515.067	447.845	67.221	0.1062	0.402
1141	515.108	447.890	67.218	0.1065	0.373
1142	515.108	447.966	67.141	0.1065	0.374
1143	515.067	447.910	67.156	0.1066	0.358
1144	515.067	448.005	67.061	0.1066	0.381
1145	515.149	448.080	67.069	0.1066	0.370
1146	514.078	447.048	67.030	0.1066	0.372
1147	515.067	448.149	66.918	0.1062	0.394
1148	514.160	447.009	67.151	0.1062	0.362
1149	513.995	446.839	67.156	0.1062	0.390
1150	513.995	447.089	66.906	0.1061	0.377
1151	514.037	447.083	66.954	0.1065	0.365
1152	514.037	447.095	66.941	0.1066	0.373
1153	514.037	447.069	66.968	0.1066	0.353
1154	514.078	447.118	66.960	0.1066	0.378

1155	514.078	447.220	66.858	0.1062	0.374
1156	513.048	446.169	66.879	0.1062	0.385
1157	513.048	446.207	66.841	0.1062	0.387
1158	513.130	446.241	66.889	0.1062	0.387
1159	513.007	446.198	66.809	0.1062	0.370
1160	512.306	445.497	66.809	0.1062	0.377
1161	513.048	446.303	66.745	0.1061	0.381
1162	512.141	445.308	66.834	0.1062	0.376
1163	513.007	446.187	66.820	0.1064	0.358
1164	511.194	444.465	66.729	0.1064	0.362
1165	511.153	444.474	66.679	0.1062	0.374
1166	511.153	444.413	66.740	0.1062	0.384
1167	511.029	444.374	66.655	0.1062	0.386
1168	511.029	444.380	66.649	0.1061	0.383
1169	511.153	444.539	66.614	0.1062	0.373
1170	511.029	444.318	66.711	0.1062	0.386
1171	511.070	444.467	66.604	0.1061	0.358
1172	511.070	444.499	66.571	0.1062	0.377
1173	511.029	444.538	66.491	0.1062	0.380
1174	511.153	444.616	66.536	0.1062	0.376
1175	511.111	444.531	66.580	0.1062	0.392
1176	511.070	444.524	66.546	0.1062	0.387
1177	509.093	442.554	66.539	0.1062	0.382
1178	510.164	443.743	66.421	0.1061	0.377
1179	509.175	442.546	66.629	0.1062	0.372
1180	509.134	442.784	66.350	0.1062	0.377
1181	509.216	442.693	66.524	0.1061	0.371
1182	509.216	442.824	66.393	0.1062	0.374
1183	509.216	442.876	66.340	0.1061	0.377
1184	509.134	442.628	66.506	0.1062	0.370
1185	508.186	441.633	66.554	0.1062	0.383
1186	509.134	442.774	66.360	0.1062	0.374
1187	508.145	441.775	66.370	0.1062	0.377
1188	509.175	442.753	66.423	0.1062	0.387
1189	509.216	442.970	66.246	0.1061	0.380
1190	509.216	442.960	66.256	0.1062	0.371
1191	509.134	442.835	66.299	0.1063	0.367
1192	508.063	441.773	66.290	0.1066	0.361
1193	507.115	440.938	66.178	0.1062	0.371
1194	507.280	441.169	66.111	0.1062	0.374
1195	507.198	440.973	66.225	0.1062	0.390
1196	506.126	440.009	66.118	0.1061	0.390
1197	507.033	440.774	66.259	0.1062	0.365
1198	507.115	441.056	66.059	0.1062	0.355
1199	506.209	439.978	66.231	0.1062	0.373

1200	507.198	441.178	66.020	0.1062	0.356
1201	506.209	439.961	66.248	0.1062	0.378
1202	506.250	440.221	66.029	0.1061	0.352
1203	506.209	440.049	66.160	0.1062	0.377
1204	506.168	440.199	65.969	0.1062	0.374
1205	506.168	440.151	66.016	0.1062	0.376
1206	506.168	440.140	66.028	0.1062	0.363
1207	506.250	440.211	66.039	0.1062	0.374
1208	506.126	440.159	65.968	0.1062	0.367
1209	505.138	439.246	65.891	0.1062	0.386
1210	506.126	440.089	66.038	0.1062	0.387
1211	506.209	440.228	65.981	0.1062	0.365
1212	506.126	440.193	65.934	0.1062	0.384
1213	506.126	440.315	65.811	0.1062	0.361
1214	506.209	440.340	65.869	0.1062	0.374
1215	506.209	440.278	65.931	0.1063	0.365
1216	505.261	439.487	65.774	0.1062	0.347
1217	506.250	440.395	65.855	0.1062	0.400
1218	504.231	438.448	65.784	0.1062	0.387
1219	503.242	437.392	65.850	0.1062	0.374
1220	505.138	439.435	65.703	0.1062	0.364
1221	503.284	437.656	65.628	0.1061	0.353
1222	504.190	438.483	65.708	0.1061	0.362
1223	503.325	437.599	65.726	0.1062	0.377
1224	503.407	437.715	65.693	0.1062	0.352
1225	503.201	437.523	65.679	0.1062	0.358
1226	504.231	438.459	65.773	0.1062	0.380
1227	503.325	437.494	65.831	0.1062	0.370
1228	503.160	437.459	65.701	0.1062	0.364
1229	503.160	437.305	65.855	0.1062	0.377
1230	503.160	437.400	65.760	0.1062	0.368
1231	502.254	436.629	65.625	0.1062	0.373
1232	503.160	437.548	65.613	0.1061	0.365
1233	503.242	437.497	65.745	0.1062	0.365
1234	503.366	437.896	65.470	0.1062	0.376
1235	502.295	436.706	65.589	0.1062	0.361
1236	501.265	435.624	65.641	0.1062	0.366
1237	501.347	435.740	65.608	0.1059	0.384
1238	500.276	434.742	65.534	0.1062	0.363
1239	500.276	434.854	65.423	0.1062	0.372
1240	500.276	434.892	65.384	0.1062	0.347
1241	500.276	434.841	65.435	0.1062	0.362
1242	500.194	434.620	65.574	0.1062	0.380
1243	500.235	434.765	65.470	0.1062	0.365
1244	500.235	434.980	65.255	0.1062	0.374

1245	500.194	434.858	65.336	0.1062	0.384
1246	500.235	434.660	65.575	0.1062	0.379
1247	499.411	434.122	65.289	0.1062	0.365
1248	500.235	434.975	65.260	0.1063	0.371
1249	500.235	434.784	65.451	0.1062	0.371
1250	500.317	434.986	65.331	0.1062	0.374
1251	499.287	433.889	65.399	0.1062	0.383
1252	500.317	435.130	65.188	0.1062	0.374
1253	499.287	434.004	65.284	0.1058	0.377
1254	499.287	434.097	65.190	0.1061	0.368
1255	498.299	433.044	65.255	0.1062	0.349
1256	497.351	432.192	65.159	0.1062	0.359
1257	500.317	435.171	65.146	0.1062	0.362
1258	497.310	431.994	65.316	0.1062	0.380
1259	497.351	432.196	65.155	0.1061	0.338
1260	497.351	432.144	65.208	0.1058	0.382
1261	497.351	432.164	65.188	0.1061	0.365
1262	497.269	432.195	65.074	0.1062	0.351
1263	497.351	432.259	65.093	0.1062	0.361
1264	497.310	432.377	64.933	0.1058	0.378
1265	497.310	432.339	64.971	0.1062	0.365
1266	497.351	432.257	65.094	0.1062	0.386
1267	497.269	432.170	65.099	0.1062	0.366
1268	497.392	432.284	65.109	0.1063	0.359
1269	497.392	432.352	65.040	0.1062	0.355
1270	497.351	432.357	64.994	0.1061	0.347
1271	497.351	432.310	65.041	0.1060	0.377
1272	497.351	432.281	65.070	0.1058	0.378
1273	497.351	432.334	65.018	0.1058	0.386
1274	497.310	432.436	64.874	0.1058	0.375
1275	496.280	431.276	65.004	0.1062	0.367
1276	497.310	432.207	65.103	0.1062	0.355
1277	495.374	430.432	64.941	0.1062	0.361
1278	495.332	430.447	64.885	0.1062	0.373
1279	495.332	430.344	64.989	0.1061	0.384
1280	495.374	430.427	64.946	0.1062	0.353
1281	494.344	429.326	65.018	0.1058	0.371
1282	494.344	429.446	64.898	0.1060	0.371
1283	494.385	429.535	64.850	0.1062	0.365
1284	495.374	430.637	64.736	0.1062	0.363
1285	495.332	430.571	64.761	0.1062	0.352
1286	494.302	429.609	64.694	0.1058	0.376
1287	494.344	429.472	64.871	0.1062	0.358
1288	494.302	429.595	64.708	0.1061	0.363
1289	494.385	429.652	64.733	0.1058	0.374

1290	494.261	429.424	64.838	0.1062	0.358
1291	494.302	429.426	64.876	0.1059	0.374
1292	494.385	429.571	64.814	0.1062	0.365
1293	494.344	429.601	64.743	0.1061	0.381
1294	494.302	429.429	64.874	0.1058	0.378
1295	494.261	429.581	64.680	0.1058	0.387
1296	494.426	429.726	64.700	0.1058	0.367
1297	494.385	429.720	64.665	0.1062	0.351
1298	493.272	428.655	64.618	0.1062	0.362
1299	493.396	428.830	64.566	0.1062	0.355
1300	493.355	428.617	64.738	0.1062	0.374
1301	493.355	428.760	64.595	0.1062	0.355
1302	493.314	428.591	64.723	0.1058	0.371
1303	491.254	426.701	64.553	0.1061	0.359
1304	491.336	426.676	64.660	0.1062	0.361
1305	491.418	426.848	64.570	0.1058	0.370
1306	491.254	426.735	64.519	0.1058	0.380
1307	492.490	428.076	64.414	0.1059	0.366
1308	491.460	426.951	64.509	0.1062	0.363
1309	491.542	426.981	64.561	0.1062	0.355
1310	491.377	426.910	64.468	0.1062	0.340
1311	491.336	426.822	64.514	0.1062	0.367
1312	491.377	426.920	64.458	0.1060	0.361
1313	491.418	426.905	64.514	0.1058	0.374
1314	491.377	426.916	64.461	0.1060	0.364
1315	490.430	426.053	64.376	0.1058	0.371
1316	488.493	423.976	64.518	0.1062	0.349
1317	490.471	426.015	64.456	0.1058	0.371
1318	489.359	425.006	64.353	0.1058	0.368
1319	489.400	424.987	64.413	0.1059	0.370
1320	488.452	423.915	64.538	0.1062	0.365
1321	488.329	424.000	64.329	0.1062	0.365
1322	489.400	425.053	64.346	0.1061	0.353
1323	488.329	423.955	64.374	0.1061	0.370
1324	488.411	424.073	64.338	0.1061	0.366
1325	488.370	424.137	64.233	0.1059	0.346
1326	488.370	424.005	64.365	0.1058	0.377
1327	488.452	424.176	64.276	0.1058	0.385
1328	488.411	424.056	64.355	0.1058	0.378
1329	488.370	424.029	64.341	0.1061	0.371
1330	488.411	424.187	64.224	0.1062	0.345
1331	488.452	424.187	64.265	0.1062	0.352
1332	488.329	424.120	64.209	0.1062	0.363
1333	488.493	424.417	64.076	0.1058	0.352
1334	487.381	423.330	64.051	0.1058	0.362

1335	488.452	424.220	64.233	0.1058	0.361
1336	488.370	424.222	64.148	0.1058	0.368
1337	488.493	424.285	64.209	0.1058	0.365
1338	488.452	424.233	64.219	0.1062	0.362
1339	487.422	423.328	64.094	0.1058	0.373
1340	487.463	423.263	64.200	0.1058	0.368
1341	487.381	423.176	64.205	0.1061	0.381
1342	487.299	423.285	64.014	0.1062	0.355
1343	487.422	423.227	64.195	0.1058	0.368
1344	487.505	423.353	64.151	0.1062	0.371
1345	487.463	423.340	64.124	0.1061	0.368
1346	487.546	423.417	64.129	0.1058	0.362
1347	487.422	423.431	63.991	0.1060	0.370
1348	487.381	423.243	64.138	0.1058	0.371
1349	486.433	422.462	63.971	0.1061	0.342
1350	486.392	422.393	63.999	0.1059	0.363
1351	486.516	422.431	64.085	0.1058	0.353
1352	486.433	422.443	63.990	0.1058	0.370
1353	486.351	422.195	64.156	0.1062	0.359
1354	486.351	422.294	64.058	0.1060	0.365
1355	485.527	421.505	64.023	0.1058	0.345
1356	485.362	421.240	64.123	0.1060	0.370
1357	486.351	422.401	63.950	0.1058	0.371
1358	484.538	420.682	63.856	0.1058	0.377
1359	485.403	421.490	63.914	0.1058	0.365
1360	485.445	421.517	63.928	0.1058	0.371
1361	484.373	420.387	63.986	0.1059	0.365
1362	484.579	420.651	63.929	0.1062	0.347
1363	484.456	420.713	63.743	0.1058	0.368
1364	484.497	420.607	63.890	0.1058	0.358
1365	484.538	420.601	63.938	0.1058	0.358
1366	484.497	420.570	63.928	0.1058	0.376
1367	484.415	420.557	63.858	0.1061	0.355
1368	484.579	420.788	63.791	0.1062	0.374
1369	484.497	420.763	63.734	0.1062	0.361
1370	484.456	420.576	63.880	0.1058	0.377
1371	484.456	420.446	64.010	0.1058	0.371
1372	483.508	419.600	63.909	0.1058	0.371
1373	483.426	419.460	63.966	0.1058	0.358
1374	483.426	419.587	63.839	0.1062	0.343
1375	483.426	419.683	63.743	0.1058	0.358
1376	483.302	419.402	63.900	0.1057	0.384
1377	483.508	419.817	63.691	0.1058	0.352
1378	483.426	419.812	63.614	0.1058	0.371
1379	481.448	417.748	63.700	0.1062	0.352

1380	482.520	418.643	63.876	0.1058	0.358
1381	483.591	420.104	63.486	0.1062	0.358
1382	481.490	417.713	63.776	0.1062	0.346
1383	482.561	418.952	63.609	0.1058	0.349
1384	482.437	418.888	63.549	0.1058	0.358
1385	481.448	417.881	63.568	0.1058	0.371
1386	481.448	417.962	63.486	0.1059	0.358
1387	482.478	418.673	63.805	0.1059	0.349
1388	482.520	418.853	63.666	0.1058	0.355
1389	481.490	418.003	63.486	0.1060	0.364
1390	481.366	417.618	63.748	0.1058	0.370
1391	481.531	418.030	63.501	0.1058	0.365
1392	480.542	417.062	63.480	0.1058	0.350
1393	481.448	417.867	63.581	0.1058	0.374
1394	480.501	416.901	63.600	0.1058	0.359
1395	481.448	417.810	63.639	0.1058	0.353
1396	480.501	416.996	63.505	0.1057	0.386
1397	480.542	416.874	63.668	0.1058	0.364
1398	480.542	416.922	63.620	0.1058	0.341
1399	479.594	415.899	63.695	0.1058	0.355
1400	479.553	415.967	63.586	0.1058	0.361
1401	479.594	416.327	63.268	0.1059	0.341
1402	477.493	414.050	63.444	0.1058	0.355
1403	478.482	415.015	63.468	0.1058	0.354
1404	478.606	415.191	63.415	0.1058	0.354
1405	477.576	414.061	63.515	0.1058	0.372
1406	478.606	415.243	63.363	0.1058	0.352
1407	478.441	415.183	63.258	0.1058	0.360
1408	477.617	414.151	63.466	0.1058	0.358
1409	477.534	414.058	63.476	0.1058	0.358
1410	477.534	414.138	63.396	0.1058	0.354
1411	477.699	414.208	63.491	0.1058	0.374
1412	477.576	414.374	63.201	0.1058	0.352
1413	477.617	414.062	63.555	0.1058	0.355
1414	476.587	413.253	63.334	0.1058	0.364
1415	476.711	413.372	63.339	0.1058	0.368
1416	476.587	413.426	63.161	0.1058	0.371
1417	475.722	412.383	63.339	0.1059	0.355
1418	476.628	413.384	63.244	0.1062	0.343
1419	476.546	413.183	63.363	0.1061	0.362
1420	475.681	412.788	62.893	0.1058	0.360
1421	475.722	412.298	63.424	0.1058	0.359
1422	475.475	412.093	63.381	0.1060	0.359
1423	475.681	412.284	63.396	0.1058	0.397
1424	475.681	412.294	63.386	0.1058	0.355

1425	475.722	412.512	63.210	0.1058	0.368
1426	475.639	412.434	63.205	0.1058	0.358
1427	475.557	412.303	63.254	0.1058	0.374
1428	474.651	411.402	63.249	0.1058	0.355
1429	474.692	411.502	63.190	0.1062	0.336
1430	474.692	411.467	63.225	0.1062	0.354
1431	474.568	411.514	63.054	0.1058	0.348
1432	474.609	411.309	63.300	0.1058	0.370
1433	474.527	411.388	63.139	0.1058	0.376
1434	474.527	411.341	63.186	0.1058	0.368
1435	473.744	410.568	63.176	0.1058	0.356
1436	473.538	410.361	63.178	0.1058	0.355
1437	473.621	410.426	63.195	0.1059	0.344
1438	473.621	410.584	63.036	0.1058	0.363
1439	473.579	410.397	63.183	0.1058	0.392
1440	473.538	410.333	63.205	0.1058	0.368
1441	473.703	410.617	63.086	0.1059	0.348
1442	474.651	411.612	63.039	0.1061	0.339
1443	472.632	409.564	63.068	0.1062	0.344
1444	472.591	409.527	63.064	0.1062	0.339
1445	472.508	409.408	63.100	0.1062	0.337
1446	472.673	409.608	63.065	0.1062	0.338
1447	472.591	409.679	62.911	0.1062	0.337
1448	472.755	409.693	63.063	0.1062	0.336
1449	472.591	409.474	63.116	0.1062	0.337
1450	472.632	409.643	62.989	0.1062	0.338
1451	472.673	409.721	62.953	0.1062	0.337
1452	472.714	409.718	62.996	0.1061	0.336
1453	472.673	409.632	63.041	0.1062	0.336
1454	472.714	409.748	62.966	0.1062	0.336
1455	472.591	409.618	62.973	0.1062	0.337
1456	472.632	409.731	62.901	0.1062	0.337
1457	472.591	409.579	63.011	0.1062	0.336
1458	472.755	409.825	62.930	0.1062	0.337
1459	472.632	409.826	62.806	0.1062	0.338
1460	471.602	408.648	62.954	0.1062	0.337
1461	471.767	408.950	62.816	0.1062	0.336
1462	471.849	408.872	62.978	0.1062	0.336
1463	471.643	408.714	62.929	0.1062	0.336
1464	470.778	407.990	62.788	0.1063	0.337
1465	470.696	407.833	62.863	0.1062	0.336
1466	470.737	407.797	62.940	0.1062	0.337
1467	470.778	408.015	62.763	0.1062	0.336
1468	470.778	407.923	62.855	0.1062	0.336
1469	470.695	407.909	62.786	0.1062	0.337

1470	469.707	407.059	62.648	0.1062	0.336
1471	469.748	407.052	62.696	0.1062	0.336
1472	469.707	406.905	62.801	0.1062	0.334
1473	469.542	406.898	62.644	0.1062	0.334
1474	469.748	407.024	62.724	0.1062	0.333
1475	469.624	406.891	62.734	0.1062	0.332
1476	469.748	407.037	62.711	0.1062	0.329
1477	469.624	406.842	62.783	0.1062	0.332
1478	470.819	408.170	62.649	0.1062	0.346
1479	469.707	407.015	62.691	0.1062	0.348
1480	469.789	407.010	62.779	0.1061	0.326
1481	470.696	407.979	62.716	0.1062	0.346
1482	469.748	406.838	62.910	0.1062	0.346
1483	469.789	407.207	62.583	0.1062	0.354
1484	469.707	406.873	62.834	0.1062	0.341
1485	469.666	407.153	62.513	0.1062	0.331
1486	469.707	406.962	62.745	0.1062	0.326
1487	469.707	407.034	62.673	0.1062	0.330
1488	469.707	406.897	62.810	0.1061	0.329
1489	468.759	406.277	62.483	0.1062	0.332
1490	469.748	407.084	62.664	0.1058	0.353
1491	469.666	407.079	62.586	0.1058	0.345
1492	469.830	407.067	62.764	0.1058	0.342
1493	468.594	405.913	62.681	0.1058	0.349
1494	468.718	406.112	62.606	0.1062	0.333
1495	468.594	406.261	62.334	0.1062	0.326
1496	468.842	406.130	62.711	0.1061	0.318
1497	468.718	406.012	62.706	0.1062	0.328
1498	468.842	406.302	62.540	0.1062	0.322
1499	468.718	406.325	62.393	0.1061	0.322
1500	467.688	405.077	62.611	0.1062	0.309
1501	466.864	404.319	62.545	0.1058	0.329
1502	468.636	406.097	62.539	0.1058	0.341
1503	466.740	404.114	62.626	0.1058	0.329
1504	466.782	404.189	62.593	0.1058	0.346
1505	466.782	404.172	62.610	0.1058	0.352
1506	466.823	404.240	62.583	0.1058	0.327
1507	466.823	404.175	62.648	0.1058	0.323
1508	466.782	404.252	62.530	0.1058	0.337
1509	466.782	404.394	62.388	0.1058	0.319
1510	466.740	404.105	62.635	0.1057	0.335
1511	465.834	403.457	62.378	0.1058	0.342
1512	465.875	403.406	62.469	0.1058	0.331
1513	464.886	402.513	62.374	0.1058	0.341
1514	463.857	401.345	62.511	0.1058	0.336

1515	465.834	403.315	62.519	0.1058	0.331
1516	466.740	404.320	62.420	0.1058	0.321
1517	464.845	402.358	62.488	0.1058	0.332
1518	464.845	402.357	62.489	0.1058	0.329
1519	464.722	402.400	62.321	0.1057	0.343
1520	463.857	401.488	62.369	0.1058	0.349
1521	464.845	402.548	62.298	0.1058	0.332
1522	463.898	401.601	62.296	0.1058	0.321
1523	463.774	401.525	62.249	0.1058	0.307
1524	463.857	401.478	62.379	0.1058	0.321
1525	463.857	401.389	62.468	0.1058	0.322
1526	463.815	401.565	62.250	0.1058	0.322
1527	463.815	401.538	62.278	0.1058	0.326
1528	463.857	401.605	62.251	0.1058	0.334
1529	463.857	401.520	62.336	0.1058	0.331
1530	463.939	401.594	62.345	0.1058	0.318
1531	463.857	401.560	62.296	0.1058	0.329
1532	462.868	400.495	62.373	0.1058	0.329
1533	463.815	401.629	62.186	0.1058	0.321
1534	463.857	401.393	62.464	0.1058	0.323
1535	463.857	401.550	62.306	0.1058	0.332
1536	463.815	401.584	62.231	0.1058	0.337
1537	463.733	401.507	62.226	0.1058	0.341
1538	463.815	401.494	62.321	0.1058	0.337
1539	462.744	400.604	62.140	0.1058	0.329
1540	463.857	401.622	62.235	0.1058	0.328
1541	463.774	401.658	62.116	0.1058	0.329
1542	461.838	399.588	62.250	0.1058	0.324
1543	462.950	400.773	62.178	0.1058	0.323
1544	462.909	400.796	62.113	0.1058	0.337
1545	463.939	401.741	62.198	0.1058	0.313
1546	462.868	400.685	62.183	0.1058	0.336
1547	463.774	401.664	62.110	0.1058	0.318
1548	461.961	399.726	62.235	0.1058	0.325
1549	461.961	399.803	62.159	0.1058	0.325
1550	461.961	399.708	62.254	0.1058	0.312
1551	461.797	399.575	62.221	0.1058	0.325
1552	461.879	399.635	62.244	0.1058	0.321
1553	461.755	399.673	62.083	0.1058	0.309
1554	461.838	399.634	62.204	0.1058	0.340
1555	461.838	399.789	62.049	0.1058	0.312
1556	461.838	399.622	62.216	0.1058	0.322
1557	461.879	399.750	62.129	0.1058	0.327
1558	460.890	398.741	62.149	0.1058	0.308
1559	461.920	399.841	62.079	0.1058	0.324

1560	460.808	398.644	62.164	0.1058	0.322
1561	460.931	398.949	61.983	0.1058	0.332
1562	460.931	398.871	62.060	0.1058	0.316
1563	460.973	398.933	62.040	0.1058	0.309
1564	460.931	398.929	62.003	0.1058	0.321
1565	460.849	398.760	62.089	0.1058	0.323
1566	460.931	398.968	61.964	0.1058	0.327
1567	459.901	397.848	62.054	0.1058	0.349
1568	460.808	399.045	61.763	0.1058	0.331
1569	460.849	398.984	61.865	0.1058	0.311
1570	460.931	398.959	61.973	0.1058	0.329
1571	459.819	397.832	61.988	0.1058	0.319
1572	460.808	398.854	61.954	0.1058	0.313
1573	460.973	399.104	61.869	0.1058	0.310
1574	460.931	398.866	62.065	0.1058	0.322
1575	459.819	397.932	61.888	0.1058	0.310
1576	459.943	397.989	61.954	0.1058	0.343
1577	459.860	398.010	61.850	0.1058	0.334
1578	459.984	398.111	61.873	0.1058	0.348
1579	459.901	398.094	61.808	0.1058	0.316
1580	459.901	398.136	61.765	0.1057	0.314
1581	458.954	397.008	61.946	0.1058	0.332
1582	459.943	398.130	61.813	0.1058	0.327
1583	459.943	398.046	61.896	0.1058	0.315
1584	459.901	397.981	61.920	0.1058	0.310
1585	459.901	398.233	61.669	0.1058	0.303
1586	459.819	397.918	61.901	0.1058	0.313
1587	458.913	397.069	61.844	0.1058	0.331
1588	459.778	397.838	61.940	0.1058	0.328
1589	458.954	397.071	61.883	0.1058	0.307
1590	459.943	398.293	61.650	0.1058	0.326
1591	458.954	397.285	61.669	0.1058	0.339
1592	459.860	397.953	61.908	0.1058	0.313
1593	458.871	397.213	61.659	0.1058	0.332
1594	458.913	397.086	61.826	0.1058	0.317
1595	458.995	397.269	61.726	0.1058	0.334
1596	458.748	396.950	61.798	0.1058	0.313
1597	458.830	397.080	61.750	0.1058	0.319
1598	458.871	397.118	61.754	0.1057	0.317
1599	458.913	397.334	61.579	0.1058	0.307
1600	458.830	397.137	61.694	0.1058	0.321
1601	458.954	397.124	61.830	0.1058	0.307
1602	457.924	396.073	61.851	0.1059	0.343
1603	457.924	396.441	61.483	0.1058	0.316
1604	457.924	396.064	61.860	0.1058	0.335

1605	457.965	396.291	61.674	0.1058	0.323
1606	457.883	396.066	61.816	0.1058	0.313
1607	456.976	395.321	61.655	0.1058	0.303
1608	457.718	396.153	61.565	0.1058	0.314
1609	457.883	396.208	61.675	0.1058	0.312
1610	457.883	396.353	61.530	0.1058	0.335
1611	457.924	396.260	61.664	0.1058	0.306
1612	456.935	395.258	61.678	0.1058	0.319
1613	456.853	395.311	61.541	0.1058	0.309
1614	456.935	395.374	61.561	0.1058	0.338
1615	455.988	394.556	61.431	0.1058	0.323
1616	456.935	395.495	61.440	0.1058	0.320
1617	455.823	394.292	61.531	0.1058	0.332
1618	456.935	395.399	61.536	0.1058	0.321
1619	457.018	395.486	61.531	0.1058	0.347
1620	456.976	395.469	61.508	0.1058	0.339
1621	456.853	395.270	61.583	0.1058	0.317
1622	456.935	395.418	61.518	0.1058	0.332
1623	456.853	395.450	61.403	0.1058	0.328
1624	455.946	394.378	61.569	0.1057	0.318
1625	454.999	393.766	61.233	0.1058	0.313
1626	454.875	393.524	61.351	0.1058	0.305
1627	454.916	393.585	61.331	0.1058	0.318
1628	454.958	393.455	61.503	0.1058	0.316
1629	455.040	393.656	61.384	0.1058	0.325
1630	454.999	393.483	61.516	0.1058	0.316
1631	454.958	393.459	61.499	0.1058	0.310
1632	455.040	393.655	61.385	0.1058	0.319
1633	453.969	392.509	61.460	0.1058	0.317
1634	454.916	393.395	61.521	0.1058	0.360
1635	453.886	392.426	61.460	0.1058	0.338
1636	454.916	393.570	61.346	0.1058	0.323
1637	454.875	393.506	61.369	0.1058	0.338
1638	453.928	392.514	61.414	0.1058	0.316
1639	454.958	393.606	61.351	0.1058	0.325
1640	454.010	392.645	61.365	0.1058	0.301
1641	455.040	393.660	61.380	0.1058	0.307
1642	454.834	393.649	61.185	0.1058	0.316
1643	454.051	392.706	61.345	0.1058	0.319
1644	454.999	393.695	61.304	0.1058	0.319
1645	454.010	392.759	61.251	0.1058	0.295
1646	452.939	391.694	61.245	0.1058	0.333
1647	453.062	391.831	61.231	0.1058	0.331
1648	453.021	391.789	61.233	0.1058	0.319
1649	452.980	391.654	61.326	0.1058	0.314

1650	453.021	391.656	61.365	0.1057	0.336
1651	452.074	390.770	61.304	0.1058	0.336
1652	451.991	390.665	61.326	0.1058	0.340
1653	451.909	390.719	61.190	0.1058	0.324
1654	451.950	390.604	61.346	0.1058	0.316
1655	451.950	390.766	61.184	0.1058	0.316
1656	452.115	390.740	61.375	0.1058	0.315
1657	451.991	390.740	61.251	0.1058	0.325
1658	452.032	391.047	60.985	0.1058	0.319
1659	452.032	390.947	61.085	0.1058	0.307
1660	451.950	390.695	61.255	0.1058	0.311
1661	452.032	390.910	61.123	0.1058	0.339
1662	452.032	390.914	61.119	0.1058	0.319
1663	451.950	390.771	61.179	0.1058	0.336
1664	451.991	390.780	61.211	0.1058	0.331
1665	452.032	390.867	61.165	0.1058	0.309
1666	451.991	390.826	61.165	0.1058	0.313
1667	452.032	390.990	61.043	0.1058	0.310
1668	449.973	388.821	61.151	0.1058	0.304
1669	450.961	389.929	61.033	0.1058	0.310
1670	450.920	389.759	61.161	0.1058	0.317
1671	450.014	388.976	61.038	0.1058	0.346
1672	450.014	388.952	61.061	0.1058	0.319
1673	450.055	388.975	61.080	0.1058	0.321
1674	450.055	389.056	60.999	0.1058	0.323
1675	450.055	389.136	60.919	0.1058	0.313
1676	450.137	389.139	60.999	0.1058	0.325
1677	450.055	389.317	60.738	0.1058	0.323
1678	450.137	389.159	60.979	0.1058	0.303
1679	449.890	389.024	60.866	0.1059	0.318
1680	449.973	389.203	60.770	0.1058	0.316
1681	449.025	388.145	60.880	0.1058	0.322
1682	450.014	389.081	60.933	0.1058	0.303
1683	449.025	388.241	60.784	0.1058	0.313
1684	450.014	389.149	60.865	0.1058	0.316
1685	449.107	388.265	60.843	0.1058	0.328
1686	449.066	388.244	60.823	0.1059	0.329
1687	449.025	388.346	60.679	0.1058	0.323
1688	449.025	388.235	60.790	0.1058	0.307
1689	448.943	387.973	60.970	0.1058	0.306
1690	449.025	388.336	60.689	0.1058	0.307
1691	449.025	388.307	60.718	0.1058	0.336
1692	449.025	388.079	60.946	0.1058	0.307
1693	449.107	388.356	60.751	0.1058	0.310
1694	449.066	388.262	60.804	0.1058	0.300

1695	449.149	388.389	60.760	0.1058	0.303
1696	449.066	388.667	60.399	0.1058	0.330
1697	447.995	387.273	60.723	0.1059	0.338
1698	448.160	387.309	60.851	0.1058	0.311
1699	448.077	387.292	60.785	0.1058	0.333
1700	448.077	387.402	60.675	0.1058	0.308
1701	447.130	386.316	60.814	0.1058	0.293
1702	447.006	386.251	60.755	0.1058	0.313
1703	447.047	386.362	60.685	0.1058	0.307
1704	448.036	387.294	60.743	0.1058	0.325
1705	449.231	388.571	60.660	0.1058	0.310
1706	448.036	387.204	60.833	0.1055	0.332
1707	447.995	387.185	60.810	0.1058	0.324
1708	447.171	386.462	60.709	0.1058	0.304
1709	447.089	386.431	60.658	0.1058	0.318
1710	447.006	386.417	60.589	0.1058	0.319
1711	446.100	385.566	60.534	0.1058	0.323
1712	446.100	385.511	60.589	0.1059	0.319
1713	446.141	385.417	60.724	0.1058	0.329
1714	447.130	386.550	60.580	0.1058	0.316
1715	447.047	386.462	60.585	0.1058	0.313
1716	446.059	385.287	60.771	0.1057	0.321
1717	447.089	386.550	60.539	0.1058	0.312
1718	446.059	385.414	60.645	0.1058	0.323
1719	446.100	385.487	60.613	0.1058	0.300
1720	446.100	385.644	60.456	0.1058	0.320
1721	446.100	385.524	60.576	0.1058	0.317
1722	446.182	385.604	60.579	0.1058	0.310
1723	446.182	385.575	60.608	0.1058	0.336
1724	446.141	385.414	60.728	0.1058	0.325
1725	446.059	385.479	60.580	0.1058	0.322
1726	446.059	385.609	60.450	0.1058	0.311
1727	446.141	385.534	60.608	0.1058	0.301
1728	446.100	385.659	60.441	0.1058	0.326
1729	446.182	385.536	60.646	0.1058	0.322
1730	446.059	385.407	60.651	0.1058	0.308
1731	446.141	385.666	60.475	0.1058	0.323
1732	446.059	385.549	60.510	0.1058	0.326
1733	446.100	385.661	60.439	0.1058	0.323
1734	446.100	385.491	60.609	0.1058	0.310
1735	445.070	384.624	60.446	0.1059	0.318
1736	445.111	384.426	60.685	0.1058	0.307
1737	443.999	383.462	60.536	0.1054	0.327
1738	445.029	384.515	60.514	0.1058	0.342
1739	444.040	383.692	60.348	0.1058	0.348

1740	443.134	382.790	60.344	0.1058	0.319
1741	443.134	382.549	60.585	0.1058	0.306
1742	444.164	383.704	60.460	0.1058	0.324
1743	444.164	383.760	60.404	0.1058	0.294
1744	443.175	382.713	60.461	0.1058	0.310
1745	444.122	383.637	60.485	0.1058	0.292
1746	443.134	382.706	60.428	0.1058	0.315
1747	443.175	382.695	60.480	0.1058	0.322
1748	443.092	382.807	60.285	0.1058	0.330
1749	442.186	381.905	60.281	0.1059	0.296
1750	443.134	382.801	60.333	0.1058	0.317
1751	442.969	382.499	60.470	0.1058	0.323
1752	443.092	382.797	60.295	0.1058	0.313
1753	442.021	381.621	60.400	0.1059	0.304
1754	443.134	382.829	60.305	0.1058	0.316
1755	441.980	381.707	60.273	0.1058	0.318
1756	443.134	382.871	60.263	0.1058	0.301
1757	442.104	381.772	60.331	0.1058	0.316
1758	442.104	381.729	60.375	0.1059	0.319
1759	442.104	381.810	60.294	0.1055	0.334
1760	443.134	382.749	60.385	0.1058	0.300
1761	442.062	381.737	60.325	0.1058	0.323
1762	442.145	381.731	60.414	0.1058	0.302
1763	442.104	381.719	60.385	0.1058	0.309
1764	442.104	381.705	60.399	0.1058	0.300
1765	442.062	381.652	60.410	0.1058	0.313
1766	442.104	381.742	60.361	0.1058	0.323
1767	442.062	381.777	60.285	0.1058	0.300
1768	442.062	381.876	60.186	0.1058	0.325
1769	442.145	381.641	60.504	0.1058	0.316
1770	442.104	381.790	60.314	0.1058	0.298
1771	442.227	381.852	60.375	0.1058	0.318
1772	442.021	381.631	60.390	0.1058	0.314
1773	442.062	381.721	60.341	0.1058	0.322
1774	440.991	380.620	60.371	0.1058	0.314
1775	442.062	381.687	60.375	0.1058	0.319
1776	441.032	380.761	60.271	0.1058	0.304
1777	442.104	381.761	60.343	0.1058	0.319
1778	440.085	379.942	60.143	0.1058	0.326
1779	441.115	380.862	60.253	0.1058	0.307
1780	441.156	380.747	60.409	0.1058	0.292
1781	441.156	380.825	60.331	0.1058	0.312
1782	440.085	379.854	60.231	0.1058	0.304
1783	442.104	381.812	60.291	0.1055	0.315
1784	441.115	380.805	60.310	0.1058	0.316

1785	441.197	381.061	60.136	0.1058	0.310
1786	439.096	378.920	60.176	0.1058	0.309
1787	441.074	380.817	60.256	0.1058	0.315
1788	440.044	379.796	60.248	0.1058	0.326
1789	440.126	379.865	60.261	0.1056	0.324
1790	440.167	379.906	60.261	0.1055	0.313
1791	439.096	378.850	60.246	0.1057	0.314
1792	439.055	378.797	60.258	0.1058	0.301
1793	440.085	379.820	60.265	0.1058	0.294
1794	440.167	379.982	60.185	0.1058	0.304
1795	440.250	380.095	60.155	0.1058	0.313
1796	440.167	379.791	60.376	0.1058	0.319
1797	440.085	379.847	60.238	0.1058	0.318
1798	439.220	379.001	60.219	0.1058	0.319
1799	439.137	379.047	60.090	0.1055	0.352
1800	439.055	378.817	60.238	0.1054	0.316
1801	439.137	379.009	60.129	0.1058	0.300
1802	439.137	378.914	60.224	0.1058	0.313
1803	440.085	380.015	60.070	0.1058	0.325
1804	439.096	378.897	60.199	0.1058	0.303
1805	440.085	379.967	60.118	0.1058	0.319
1806	439.096	378.959	60.138	0.1058	0.309
1807	439.178	379.140	60.039	0.1058	0.302
1808	439.261	379.110	60.151	0.1058	0.317
1809	439.178	379.002	60.176	0.1058	0.324
1810	439.055	379.002	60.053	0.1058	0.304
1811	439.137	379.200	59.938	0.1058	0.306
1812	439.178	379.153	60.025	0.1055	0.325
1813	440.126	379.975	60.151	0.1058	0.307
1814	439.220	379.211	60.009	0.1059	0.297
1815	439.178	379.061	60.118	0.1058	0.307
1816	439.096	378.964	60.133	0.1058	0.307
1817	439.302	379.316	59.986	0.1058	0.320
1818	439.137	379.165	59.973	0.1055	0.329
1819	439.178	379.307	59.871	0.1055	0.316
1820	438.066	378.114	59.953	0.1058	0.312
1821	439.178	379.192	59.986	0.1058	0.323
1822	438.149	378.074	60.075	0.1058	0.304
1823	438.149	378.092	60.056	0.1058	0.319
1824	437.119	377.219	59.900	0.1058	0.298
1825	437.242	377.261	59.981	0.1058	0.307
1826	437.160	377.126	60.034	0.1055	0.329
1827	437.119	377.244	59.875	0.1058	0.299
1828	438.149	378.172	59.976	0.1058	0.303
1829	437.119	377.149	59.970	0.1058	0.306

1830	437.160	377.340	59.820	0.1057	0.319
1831	437.119	377.229	59.890	0.1058	0.316
1832	437.077	377.169	59.909	0.1058	0.323
1833	437.201	377.311	59.890	0.1058	0.328
1834	437.160	377.175	59.985	0.1058	0.318
1835	437.201	377.338	59.863	0.1057	0.311
1836	436.130	376.259	59.871	0.1058	0.322
1837	436.171	376.391	59.780	0.1058	0.322
1838	436.047	376.227	59.820	0.1055	0.325
1839	437.077	377.310	59.768	0.1058	0.297
1840	436.253	376.445	59.809	0.1058	0.290
1841	437.119	377.352	59.766	0.1058	0.324
1842	436.089	376.436	59.653	0.1058	0.310
1843	436.130	376.435	59.695	0.1058	0.313
1844	436.006	376.236	59.770	0.1057	0.313
1845	436.130	376.305	59.825	0.1058	0.313
1846	436.253	376.573	59.680	0.1057	0.300
1847	436.212	376.478	59.734	0.1055	0.317
1848	436.171	376.378	59.793	0.1058	0.319
1849	435.223	375.401	59.823	0.1055	0.324
1850	435.141	375.546	59.595	0.1057	0.322
1851	436.212	376.355	59.858	0.1058	0.313
1852	436.171	376.523	59.648	0.1058	0.294
1853	435.223	375.342	59.881	0.1055	0.325
1854	436.171	376.533	59.638	0.1056	0.316
1855	435.182	375.473	59.709	0.1058	0.307
1856	435.141	375.385	59.756	0.1058	0.302
1857	435.141	375.482	59.659	0.1055	0.308
1858	435.223	375.541	59.683	0.1057	0.304
1859	435.265	375.675	59.590	0.1055	0.305
1860	435.306	375.563	59.743	0.1058	0.319
1861	435.182	375.497	59.685	0.1058	0.300
1862	435.223	375.452	59.771	0.1055	0.327
1863	435.223	375.667	59.556	0.1057	0.306
1864	435.265	375.821	59.444	0.1055	0.308
1865	435.223	375.505	59.719	0.1055	0.329
1866	434.193	374.573	59.620	0.1056	0.327
1867	435.182	375.538	59.644	0.1058	0.310
1868	435.265	375.702	59.563	0.1058	0.309
1869	434.235	374.382	59.853	0.1054	0.310
1870	435.223	375.608	59.615	0.1057	0.323
1871	434.152	374.600	59.553	0.1055	0.316
1872	435.141	375.616	59.525	0.1057	0.313
1873	434.193	374.722	59.471	0.1058	0.283
1874	433.246	373.636	59.610	0.1058	0.316

1875	434.193	374.631	59.563	0.1058	0.295
1876	433.246	373.570	59.676	0.1058	0.298
1877	434.193	374.526	59.668	0.1058	0.307
1878	434.235	374.643	59.591	0.1054	0.309
1879	433.205	373.628	59.576	0.1054	0.310
1880	433.246	373.655	59.591	0.1057	0.340
1881	434.317	374.831	59.486	0.1055	0.350
1882	433.287	373.801	59.486	0.1058	0.325
1883	433.246	373.778	59.468	0.1057	0.305
1884	433.205	373.757	59.448	0.1058	0.321
1885	433.205	373.557	59.648	0.1058	0.301
1886	433.205	373.632	59.573	0.1058	0.314
1887	434.111	374.677	59.434	0.1058	0.328
1888	433.205	373.803	59.401	0.1055	0.324
1889	433.246	373.926	59.320	0.1058	0.313
1890	433.246	373.651	59.595	0.1058	0.310
1891	433.205	373.788	59.416	0.1058	0.322
1892	432.298	372.788	59.510	0.1058	0.304
1893	432.339	372.787	59.553	0.1058	0.312
1894	432.298	372.836	59.463	0.1058	0.297
1895	432.257	372.796	59.461	0.1058	0.291
1896	431.227	371.737	59.490	0.1055	0.318
1897	431.104	371.707	59.396	0.1057	0.335
1898	430.238	370.686	59.553	0.1057	0.315
1899	432.216	372.806	59.410	0.1057	0.308
1900	431.227	371.771	59.456	0.1055	0.324
1901	430.115	370.571	59.544	0.1058	0.303
1902	430.238	370.900	59.339	0.1057	0.310
1903	430.280	370.788	59.491	0.1058	0.291
1904	430.197	370.811	59.386	0.1058	0.315
1905	430.362	370.913	59.449	0.1056	0.316
1906	430.362	371.052	59.310	0.1058	0.288
1907	430.280	370.888	59.391	0.1055	0.313
1908	430.280	370.865	59.415	0.1055	0.323
1909	430.197	370.873	59.324	0.1054	0.321
1910	430.197	370.796	59.401	0.1054	0.319
1911	430.403	371.004	59.399	0.1055	0.307
1912	430.403	370.999	59.404	0.1058	0.288
1913	430.197	370.806	59.391	0.1055	0.317
1914	430.362	370.867	59.495	0.1058	0.307
1915	430.238	370.748	59.490	0.1055	0.322
1916	430.197	370.878	59.319	0.1055	0.319
1917	430.280	370.917	59.363	0.1058	0.279
1918	429.250	369.943	59.306	0.1058	0.303
1919	430.403	371.113	59.290	0.1055	0.331

1920	430.197	370.953	59.244	0.1058	0.297
1921	430.115	370.915	59.200	0.1058	0.303
1922	429.332	369.979	59.353	0.1054	0.303
1923	430.280	370.863	59.416	0.1055	0.316
1924	429.373	370.082	59.291	0.1058	0.293
1925	429.250	370.011	59.239	0.1058	0.308
1926	429.373	370.029	59.344	0.1055	0.311
1927	430.280	370.965	59.315	0.1058	0.292
1928	429.291	370.122	59.169	0.1058	0.295
1929	429.208	369.946	59.263	0.1056	0.316
1930	429.291	370.056	59.235	0.1058	0.300
1931	429.250	369.910	59.340	0.1058	0.307
1932	428.302	368.950	59.353	0.1057	0.314
1933	428.220	369.090	59.130	0.1058	0.300
1934	429.250	370.050	59.200	0.1055	0.301
1935	428.220	368.871	59.349	0.1054	0.329
1936	428.261	368.907	59.354	0.1054	0.314
1937	429.291	369.990	59.301	0.1055	0.307
1938	429.291	370.000	59.291	0.1055	0.303
1939	428.343	369.057	59.286	0.1054	0.310
1940	429.291	369.995	59.296	0.1055	0.313
1941	429.250	370.130	59.120	0.1057	0.307
1942	428.302	369.225	59.078	0.1058	0.316
1943	428.302	368.958	59.344	0.1058	0.292
1944	428.302	369.158	59.144	0.1058	0.290
1945	428.261	369.170	59.091	0.1056	0.319
1946	428.261	369.011	59.250	0.1057	0.305
1947	427.190	368.065	59.125	0.1058	0.316
1948	428.343	369.091	59.253	0.1055	0.317
1949	428.302	369.215	59.088	0.1058	0.301
1950	428.302	369.228	59.074	0.1055	0.310
1951	428.261	369.307	58.954	0.1058	0.300
1952	428.220	369.198	59.021	0.1055	0.298
1953	427.231	368.121	59.110	0.1055	0.316
1954	427.313	367.984	59.329	0.1055	0.306
1955	427.190	368.070	59.120	0.1058	0.297
1956	428.261	369.117	59.144	0.1058	0.297
1957	427.396	368.408	58.988	0.1058	0.358
1958	428.302	369.410	58.893	0.1058	0.312
1959	428.343	369.318	59.025	0.1058	0.328
1960	427.231	368.048	59.183	0.1055	0.334
1961	427.354	368.368	58.986	0.1055	0.307
1962	427.313	368.064	59.249	0.1055	0.313
1963	427.313	368.117	59.196	0.1055	0.306
1964	427.396	368.284	59.111	0.1054	0.322

1965	426.366	367.256	59.110	0.1058	0.290
1966	426.283	367.187	59.096	0.1058	0.315
1967	427.272	368.213	59.059	0.1055	0.309
1968	426.242	367.198	59.044	0.1058	0.293
1969	427.272	368.098	59.174	0.1057	0.316
1970	426.324	367.196	59.129	0.1058	0.307
1971	427.190	368.378	58.811	0.1058	0.325
1972	426.324	367.452	58.873	0.1059	0.293
1973	426.283	367.140	59.144	0.1055	0.309
1974	426.242	367.266	58.976	0.1058	0.299
1975	426.324	367.237	59.088	0.1058	0.318
1976	426.283	367.321	58.963	0.1054	0.321
1977	426.324	367.222	59.103	0.1054	0.310
1978	426.407	367.497	58.910	0.1054	0.334
1979	426.324	367.377	58.948	0.1057	0.305
1980	426.242	367.298	58.944	0.1057	0.313
1981	427.272	368.291	58.981	0.1058	0.300
1982	426.201	367.176	59.025	0.1058	0.303
1983	426.283	367.263	59.020	0.1058	0.296
1984	426.242	367.240	59.003	0.1058	0.297
1985	425.253	366.205	59.049	0.1058	0.289
1986	426.201	367.218	58.983	0.1055	0.318
1987	425.336	366.548	58.788	0.1054	0.329
1988	426.324	367.256	59.069	0.1055	0.332
1989	426.324	367.401	58.924	0.1055	0.328
1990	425.336	366.408	58.928	0.1055	0.336
1991	426.283	367.248	59.035	0.1058	0.319
1992	426.283	367.268	59.015	0.1058	0.301
1993	425.253	366.352	58.901	0.1058	0.307
1994	425.294	366.331	58.964	0.1058	0.296
1995	426.242	367.293	58.949	0.1058	0.304
1996	425.336	366.292	59.044	0.1058	0.290
1997	425.377	366.504	58.873	0.1055	0.331
1998	425.377	366.518	58.859	0.1055	0.326
1999	425.294	366.292	59.003	0.1058	0.288
2000	424.306	365.281	59.025	0.1055	0.310
2001	424.429	365.561	58.869	0.1055	0.292
2002	426.324	367.357	58.968	0.1058	0.308
2003	426.324	367.404	58.920	0.1057	0.300
2004	425.418	366.569	58.849	0.1055	0.325
2005	425.377	366.492	58.885	0.1055	0.317
2006	423.317	364.411	58.906	0.1054	0.310
2007	423.399	364.484	58.915	0.1057	0.304
2008	423.358	364.361	58.998	0.1055	0.309
2009	424.429	365.604	58.825	0.1058	0.307

2010	424.388	365.421	58.968	0.1055	0.312
2011	423.399	364.554	58.845	0.1056	0.323
2012	423.441	364.521	58.920	0.1055	0.313
2013	423.441	364.668	58.773	0.1055	0.312
2014	423.358	364.338	59.020	0.1055	0.315
2015	423.317	364.473	58.844	0.1055	0.329
2016	423.358	364.332	59.026	0.1055	0.338
2017	423.317	364.434	58.883	0.1055	0.319
2018	423.358	364.486	58.873	0.1058	0.300
2019	423.358	364.504	58.854	0.1058	0.292
2020	423.399	364.407	58.993	0.1055	0.294
2021	423.317	364.459	58.858	0.1055	0.313
2022	423.317	364.469	58.848	0.1055	0.342
2023	423.399	364.517	58.883	0.1055	0.322
2024	423.441	364.734	58.706	0.1054	0.309
2025	422.411	363.572	58.839	0.1058	0.300
2026	422.369	363.646	58.724	0.1055	0.309
2027	422.369	363.506	58.864	0.1054	0.302
2028	422.534	363.638	58.896	0.1058	0.284
2029	422.369	363.463	58.906	0.1058	0.316
2030	421.381	362.484	58.896	0.1054	0.309
2031	422.328	363.436	58.893	0.1055	0.331
2032	422.411	363.548	58.863	0.1058	0.303
2033	422.369	363.421	58.949	0.1058	0.307
2034	422.328	363.446	58.883	0.1055	0.301
2035	422.328	363.483	58.845	0.1055	0.326
2036	422.452	363.607	58.845	0.1054	0.309
2037	422.328	363.456	58.873	0.1054	0.308
2038	421.381	362.726	58.655	0.1058	0.317
2039	420.392	361.604	58.788	0.1055	0.306
2040	421.339	362.624	58.715	0.1055	0.303
2041	421.298	362.778	58.520	0.1054	0.316
2042	420.392	361.577	58.815	0.1058	0.310
2043	421.257	362.370	58.888	0.1055	0.313
2044	420.309	361.537	58.773	0.1055	0.303
2045	420.474	361.688	58.786	0.1054	0.306
2046	420.309	361.523	58.786	0.1054	0.312
2047	420.351	361.512	58.839	0.1057	0.332
2048	421.422	362.826	58.596	0.1057	0.317
2049	420.309	361.576	58.734	0.1058	0.297
2050	420.392	361.562	58.830	0.1056	0.305
2051	420.392	361.528	58.864	0.1057	0.305
2052	420.351	361.641	58.710	0.1058	0.307
2053	420.392	361.634	58.758	0.1058	0.313
2054	420.392	361.576	58.816	0.1057	0.288

2055	420.392	361.584	58.808	0.1054	0.314
2056	420.433	361.689	58.744	0.1058	0.298
2057	420.392	361.628	58.764	0.1056	0.316
2058	420.309	361.571	58.739	0.1054	0.321
2059	420.392	361.629	58.763	0.1055	0.313
2060	420.474	361.677	58.798	0.1054	0.307
2061	419.403	360.644	58.759	0.1055	0.319
2062	419.321	360.667	58.654	0.1055	0.338
2063	419.321	360.666	58.655	0.1055	0.331
2064	420.309	361.552	58.758	0.1058	0.303
2065	420.309	361.502	58.808	0.1055	0.295
2066	419.362	360.699	58.663	0.1054	0.295
2067	418.332	359.807	58.525	0.1055	0.312
2068	419.362	360.751	58.611	0.1055	0.306
2069	419.403	360.821	58.583	0.1058	0.291
2070	419.485	360.707	58.779	0.1055	0.300
2071	419.444	360.714	58.730	0.1055	0.321
2072	418.332	359.744	58.588	0.1055	0.300
2073	419.362	360.594	58.768	0.1055	0.326
2074	418.373	359.819	58.554	0.1054	0.313
2075	419.403	360.793	58.610	0.1055	0.318
2076	419.321	360.772	58.549	0.1054	0.323
2077	419.238	360.552	58.686	0.1055	0.306
2078	418.332	359.634	58.698	0.1055	0.307
2079	418.373	359.662	58.711	0.1054	0.316
2080	418.373	359.697	58.676	0.1055	0.312
2081	418.373	359.819	58.554	0.1057	0.327
2082	418.497	359.962	58.535	0.1057	0.316
2083	417.384	358.778	58.606	0.1054	0.309
2084	417.426	358.867	58.559	0.1054	0.313
2085	418.414	359.769	58.645	0.1055	0.315
2086	418.373	359.601	58.773	0.1055	0.312
2087	418.414	359.759	58.655	0.1055	0.326
2088	418.373	359.672	58.701	0.1055	0.298
2089	417.384	358.821	58.564	0.1057	0.302
2090	417.426	358.868	58.558	0.1055	0.304
2091	418.414	359.741	58.674	0.1055	0.307
2092	417.426	358.791	58.635	0.1058	0.301
2093	417.467	358.998	58.469	0.1055	0.304
2094	417.384	358.823	58.561	0.1057	0.310
2095	416.354	357.772	58.583	0.1055	0.300
2096	416.478	357.915	58.563	0.1055	0.309
2097	416.437	357.877	58.560	0.1055	0.314
2098	417.426	358.853	58.573	0.1055	0.308
2099	417.384	358.922	58.463	0.1054	0.316

2100	416.396	357.866	58.530	0.1055	0.300
2101	417.467	358.880	58.586	0.1055	0.316
2102	416.396	357.913	58.483	0.1055	0.306
2103	416.396	357.804	58.591	0.1055	0.317
2104	416.437	357.894	58.543	0.1055	0.294
2105	416.437	357.974	58.463	0.1058	0.288
2106	416.437	357.903	58.534	0.1055	0.323
2107	416.437	357.802	58.635	0.1055	0.310
2108	417.384	358.954	58.430	0.1058	0.298
2109	417.426	358.953	58.473	0.1055	0.321
2110	416.437	358.019	58.418	0.1058	0.297
2111	415.407	356.862	58.545	0.1058	0.291
2112	416.396	357.862	58.534	0.1054	0.287
2113	416.437	357.958	58.479	0.1054	0.316
2114	416.437	357.887	58.550	0.1055	0.319
2115	416.396	358.056	58.340	0.1055	0.303
2116	416.478	357.962	58.516	0.1055	0.308
2117	416.437	357.926	58.511	0.1055	0.302
2118	416.396	357.884	58.511	0.1054	0.302
2119	415.489	356.897	58.593	0.1055	0.301
2120	416.396	357.884	58.511	0.1054	0.312
2121	416.396	357.947	58.449	0.1055	0.303
2122	416.478	358.028	58.450	0.1058	0.292
2123	415.530	356.994	58.536	0.1057	0.305
2124	416.396	357.908	58.488	0.1055	0.337
2125	415.448	356.979	58.469	0.1055	0.315
2126	415.530	357.105	58.425	0.1057	0.313
2127	414.418	355.926	58.493	0.1055	0.321
2128	414.500	356.109	58.391	0.1054	0.303
2129	414.377	356.076	58.301	0.1056	0.303
2130	415.407	356.991	58.416	0.1058	0.300
2131	414.583	356.267	58.316	0.1058	0.303
2132	415.530	357.117	58.414	0.1055	0.314
2133	415.489	357.078	58.411	0.1055	0.341
2134	414.418	355.964	58.454	0.1055	0.328
2135	413.470	355.035	58.435	0.1055	0.332
2136	413.470	355.049	58.421	0.1057	0.307
2137	413.470	354.878	58.593	0.1055	0.338
2138	413.429	355.042	58.388	0.1055	0.321
2139	412.564	354.329	58.235	0.1055	0.310
2140	413.429	355.179	58.250	0.1055	0.310
2141	413.512	355.034	58.478	0.1055	0.316
2142	413.429	354.942	58.488	0.1055	0.301
2143	413.470	355.259	58.211	0.1055	0.307
2144	413.429	355.032	58.398	0.1055	0.295

2145	412.523	354.202	58.321	0.1055	0.310
2146	413.512	355.115	58.396	0.1058	0.287
2147	413.635	355.243	58.393	0.1055	0.298
2148	413.512	355.400	58.111	0.1058	0.287
2149	413.470	355.160	58.310	0.1055	0.298
2150	413.512	355.263	58.249	0.1058	0.287
2151	412.482	354.214	58.268	0.1057	0.315
2152	412.399	353.924	58.475	0.1055	0.313
2153	411.493	353.267	58.226	0.1055	0.306
2154	412.440	354.072	58.369	0.1055	0.324
2155	412.605	354.255	58.350	0.1055	0.314
2156	412.440	354.109	58.331	0.1055	0.297
2157	412.564	354.124	58.440	0.1058	0.297
2158	412.482	354.127	58.355	0.1054	0.305
2159	411.493	353.248	58.245	0.1055	0.319
2160	410.504	352.149	58.355	0.1055	0.302
2161	411.411	353.181	58.230	0.1054	0.298
2162	411.534	353.270	58.264	0.1055	0.313
2163	410.587	352.257	58.330	0.1055	0.320
2164	411.534	353.323	58.211	0.1055	0.303
2165	410.628	352.382	58.246	0.1055	0.310
2166	411.534	353.157	58.378	0.1055	0.321
2167	411.493	353.058	58.435	0.1055	0.297
2168	411.493	353.210	58.283	0.1054	0.300
2169	411.411	353.047	58.364	0.1055	0.303
2170	410.504	352.125	58.379	0.1057	0.310
2171	411.575	353.297	58.279	0.1055	0.303
2172	410.463	352.199	58.264	0.1058	0.303
2173	410.751	352.489	58.263	0.1055	0.309
2174	411.493	353.209	58.284	0.1055	0.328
2175	410.463	352.142	58.321	0.1055	0.297
2176	410.504	352.293	58.211	0.1055	0.329
2177	410.504	352.327	58.178	0.1054	0.324
2178	409.433	351.240	58.193	0.1055	0.313
2179	409.557	351.317	58.240	0.1055	0.315
2180	410.504	352.412	58.093	0.1055	0.312
2181	410.504	352.308	58.196	0.1058	0.296
2182	410.545	352.294	58.251	0.1058	0.281
2183	409.515	351.455	58.060	0.1055	0.311
2184	409.515	351.272	58.244	0.1055	0.315
2185	409.598	351.615	57.983	0.1055	0.295
2186	409.474	351.334	58.140	0.1055	0.319
2187	410.504	352.330	58.174	0.1055	0.319
2188	409.598	351.244	58.354	0.1058	0.292
2189	410.545	352.405	58.140	0.1055	0.310

2190	409.474	351.133	58.341	0.1054	0.299
2191	409.680	351.498	58.183	0.1055	0.313
2192	409.515	351.465	58.050	0.1055	0.315
2193	409.515	351.415	58.100	0.1055	0.304
2194	409.557	351.255	58.301	0.1057	0.297
2195	409.433	351.317	58.116	0.1054	0.316
2196	408.444	350.257	58.188	0.1055	0.307
2197	408.609	350.454	58.155	0.1058	0.300
2198	409.515	351.375	58.140	0.1056	0.306
2199	408.650	350.381	58.269	0.1058	0.289
2200	407.497	349.367	58.130	0.1055	0.300
2201	408.527	350.259	58.268	0.1055	0.304
2202	407.538	349.505	58.033	0.1055	0.304
2203	407.497	349.428	58.069	0.1058	0.302
2204	408.527	350.464	58.063	0.1055	0.313
2205	407.579	349.454	58.125	0.1057	0.294
2206	407.538	349.355	58.183	0.1054	0.316
2207	407.620	349.489	58.131	0.1055	0.301
2208	407.579	349.482	58.098	0.1055	0.316
2209	407.538	349.513	58.025	0.1054	0.303
2210	406.508	348.598	57.910	0.1055	0.298
2211	407.703	349.444	58.259	0.1055	0.325
2212	407.538	349.498	58.040	0.1055	0.319
2213	407.661	349.621	58.040	0.1054	0.298
2214	407.620	349.589	58.031	0.1054	0.300
2215	408.609	350.530	58.079	0.1055	0.319
2216	407.579	349.478	58.101	0.1055	0.305
2217	407.455	349.458	57.998	0.1055	0.297
2218	406.590	348.534	58.056	0.1055	0.318
2219	407.579	349.568	58.011	0.1054	0.300
2220	407.620	349.589	58.031	0.1058	0.315
2221	407.497	349.557	57.940	0.1055	0.320
2222	407.497	349.670	57.826	0.1055	0.292
2223	407.538	349.678	57.860	0.1055	0.292
2224	407.620	349.590	58.030	0.1058	0.303
2225	407.455	349.434	58.021	0.1055	0.322
2226	407.579	349.518	58.061	0.1054	0.305
2227	407.579	349.510	58.069	0.1055	0.319
2228	407.497	349.345	58.151	0.1058	0.289
2229	406.549	348.332	58.218	0.1058	0.291
2230	406.590	348.479	58.111	0.1058	0.294
2231	407.703	349.729	57.974	0.1058	0.307
2232	407.538	349.569	57.969	0.1058	0.301
2233	407.620	349.780	57.840	0.1055	0.352
2234	406.549	348.567	57.983	0.1057	0.307

2235	406.631	348.715	57.916	0.1054	0.313
2236	406.714	348.716	57.998	0.1057	0.297
2237	406.631	348.724	57.908	0.1059	0.301
2238	406.549	348.462	58.088	0.1055	0.349
2239	407.579	349.602	57.978	0.1057	0.310
2240	406.549	348.509	58.040	0.1058	0.309
2241	406.549	348.390	58.159	0.1058	0.293
2242	406.590	348.610	57.980	0.1057	0.306
2243	406.590	348.673	57.918	0.1058	0.310
2244	405.560	347.633	57.928	0.1058	0.334
2245	406.755	348.829	57.926	0.1054	0.297
2246	404.613	346.573	58.040	0.1058	0.310
2247	406.631	348.633	57.999	0.1058	0.326
2248	405.560	347.690	57.870	0.1058	0.320
2249	404.695	346.798	57.898	0.1058	0.303
2250	404.654	346.776	57.878	0.1058	0.293
2251	404.613	346.678	57.935	0.1058	0.329
2252	405.602	347.667	57.935	0.1058	0.312
2253	404.530	346.567	57.964	0.1058	0.315
2254	405.478	347.519	57.959	0.1058	0.326
2255	404.572	346.645	57.926	0.1058	0.306
2256	404.613	346.630	57.983	0.1058	0.292
2257	404.572	346.613	57.959	0.1055	0.310
2258	404.654	346.846	57.808	0.1055	0.308
2259	404.613	346.644	57.969	0.1058	0.298
2260	404.613	346.810	57.803	0.1058	0.290
2261	404.613	346.800	57.813	0.1055	0.316
2262	404.572	346.922	57.650	0.1058	0.288
2263	404.572	346.749	57.823	0.1058	0.307
2264	404.489	346.543	57.946	0.1058	0.305
2265	404.572	346.535	58.036	0.1058	0.298
2266	404.572	346.588	57.984	0.1058	0.310
2267	404.654	346.914	57.740	0.1054	0.330
2268	404.695	346.745	57.950	0.1054	0.311
2269	404.572	346.730	57.841	0.1058	0.307
2270	404.572	346.799	57.773	0.1055	0.318
2271	404.695	346.931	57.764	0.1058	0.304
2272	404.572	346.740	57.831	0.1058	0.290
2273	404.572	346.732	57.840	0.1058	0.307
2274	404.572	346.617	57.955	0.1058	0.278
2275	404.613	346.629	57.984	0.1058	0.291
2276	404.695	346.746	57.949	0.1057	0.281
2277	404.572	346.760	57.811	0.1058	0.310
2278	404.572	346.807	57.765	0.1058	0.300
2279	404.572	346.679	57.893	0.1055	0.308

2280	404.654	346.794	57.860	0.1055	0.317
2281	403.583	345.538	58.045	0.1055	0.304
2282	404.613	346.754	57.859	0.1055	0.316
2283	404.613	346.659	57.954	0.1055	0.328
2284	404.654	346.776	57.878	0.1055	0.341
2285	404.654	346.818	57.836	0.1058	0.296
2286	403.624	345.831	57.793	0.1058	0.291
2287	403.542	345.852	57.690	0.1058	0.314
2288	403.665	345.929	57.736	0.1055	0.307
2289	403.665	345.781	57.884	0.1058	0.319
2290	404.613	346.838	57.775	0.1058	0.310
2291	404.530	346.690	57.840	0.1058	0.288
2292	404.654	346.995	57.659	0.1058	0.283
2293	404.613	346.839	57.774	0.1058	0.310
2294	404.572	346.792	57.780	0.1058	0.282
2295	403.665	345.864	57.801	0.1058	0.313
2296	403.665	345.814	57.851	0.1058	0.292
2297	403.665	345.840	57.825	0.1058	0.310
2298	402.841	345.166	57.675	0.1055	0.329
2299	402.635	344.743	57.893	0.1055	0.292
2300	402.635	344.819	57.816	0.1058	0.307
2301	404.654	346.794	57.860	0.1055	0.319
2302	403.665	345.820	57.845	0.1058	0.303
2303	403.748	345.926	57.821	0.1057	0.295
2304	403.665	345.824	57.841	0.1057	0.328
2305	402.676	344.780	57.896	0.1058	0.295
2306	403.542	345.687	57.855	0.1057	0.325
2307	403.583	345.714	57.869	0.1057	0.298
2308	403.789	345.766	58.023	0.1055	0.307
2309	403.583	345.763	57.820	0.1058	0.297
2310	402.594	344.729	57.865	0.1058	0.289
2311	403.706	345.846	57.860	0.1055	0.292
2312	403.748	345.826	57.921	0.1054	0.323
2313	401.688	343.776	57.911	0.1058	0.303
2314	401.646	343.783	57.864	0.1058	0.313
2315	401.729	343.855	57.874	0.1058	0.297
2316	401.729	343.883	57.846	0.1058	0.336
2317	402.676	344.798	57.879	0.1058	0.289
2318	401.605	343.764	57.841	0.1058	0.319
2319	401.605	343.991	57.614	0.1055	0.346
2320	401.770	343.749	58.021	0.1056	0.342
2321	401.605	343.854	57.751	0.1055	0.309
2322	401.646	344.048	57.599	0.1055	0.333
2323	401.646	343.963	57.684	0.1057	0.300
2324	401.688	343.953	57.735	0.1058	0.312

2325	402.512	344.575	57.936	0.1058	0.307
2326	401.688	343.856	57.831	0.1058	0.297
2327	401.605	343.655	57.950	0.1055	0.314
2328	402.553	344.699	57.854	0.1054	0.302
2329	401.605	343.690	57.915	0.1058	0.309
2330	401.564	343.728	57.836	0.1059	0.297
2331	401.770	343.883	57.888	0.1058	0.289
2332	401.564	343.853	57.711	0.1058	0.297
2333	401.770	343.934	57.836	0.1058	0.288
2334	401.564	343.923	57.641	0.1057	0.314
2335	401.688	343.886	57.801	0.1054	0.316
2336	401.688	343.805	57.883	0.1058	0.316
2337	401.605	343.723	57.883	0.1058	0.313
2338	401.688	343.931	57.756	0.1058	0.323
2339	401.770	344.058	57.713	0.1058	0.297
2340	401.564	343.777	57.788	0.1057	0.293
2341	401.440	343.735	57.705	0.1055	0.321
2342	401.770	344.025	57.745	0.1057	0.295
2343	401.646	343.834	57.813	0.1058	0.297
2344	401.688	343.933	57.755	0.1058	0.297
2345	401.688	343.819	57.869	0.1055	0.301
2346	401.605	344.123	57.483	0.1055	0.335
2347	401.688	343.885	57.803	0.1058	0.300
2348	399.628	341.835	57.793	0.1058	0.331
2349	399.628	341.910	57.718	0.1055	0.309
2350	400.616	342.905	57.711	0.1056	0.298
2351	400.658	342.931	57.726	0.1055	0.300
2352	400.699	343.105	57.594	0.1058	0.278
2353	400.658	342.969	57.689	0.1058	0.295
2354	398.557	340.864	57.693	0.1058	0.296
2355	400.616	342.646	57.970	0.1055	0.310
2356	399.669	341.919	57.750	0.1055	0.318
2357	399.669	341.981	57.688	0.1058	0.325
2358	401.646	343.761	57.885	0.1055	0.332
2359	399.710	342.108	57.603	0.1055	0.307
2360	399.710	342.056	57.654	0.1058	0.307
2361	398.557	340.905	57.651	0.1055	0.295
2362	398.639	340.789	57.850	0.1058	0.299
2363	399.669	341.924	57.745	0.1058	0.323
2364	398.804	341.091	57.713	0.1055	0.310
2365	399.669	342.003	57.666	0.1055	0.309
2366	398.721	340.986	57.735	0.1055	0.303
2367	398.680	340.944	57.736	0.1058	0.307
2368	398.721	340.989	57.733	0.1058	0.286
2369	398.639	340.889	57.750	0.1058	0.282

2370	398.639	341.008	57.631	0.1058	0.299
2371	398.680	340.759	57.921	0.1058	0.319
2372	398.763	341.050	57.713	0.1055	0.302
2373	398.763	341.008	57.755	0.1058	0.307
2374	398.639	341.011	57.628	0.1058	0.307
2375	398.804	341.047	57.756	0.1057	0.316
2376	398.721	340.943	57.779	0.1057	0.301
2377	398.721	340.961	57.760	0.1057	0.289
2378	398.721	340.971	57.750	0.1058	0.308
2379	398.680	341.039	57.641	0.1057	0.296
2380	398.680	340.940	57.740	0.1057	0.310
2381	398.598	340.819	57.779	0.1058	0.281
2382	398.639	340.999	57.640	0.1057	0.321
2383	398.680	340.901	57.779	0.1055	0.312
2384	398.639	340.955	57.684	0.1055	0.310
2385	398.515	340.823	57.693	0.1055	0.304
2386	398.721	340.885	57.836	0.1054	0.300
2387	398.680	340.924	57.756	0.1055	0.316
2388	398.721	341.061	57.660	0.1055	0.310
2389	398.639	340.840	57.799	0.1055	0.310
2390	398.639	340.955	57.684	0.1058	0.281
2391	398.804	341.225	57.579	0.1057	0.289
2392	398.680	340.876	57.804	0.1055	0.291
2393	398.639	341.036	57.603	0.1058	0.294
2394	398.721	341.153	57.569	0.1058	0.292
2395	398.763	341.184	57.579	0.1058	0.294
2396	398.680	340.968	57.713	0.1058	0.300
2397	397.650	340.066	57.584	0.1054	0.313
2398	398.598	340.946	57.651	0.1054	0.292
2399	396.744	339.336	57.408	0.1055	0.307
2400	397.691	340.160	57.531	0.1055	0.313
2401	398.721	341.004	57.718	0.1055	0.316
2402	397.733	340.048	57.685	0.1055	0.311
2403	396.661	339.239	57.423	0.1058	0.280
2404	396.579	338.991	57.588	0.1058	0.310
2405	397.691	339.990	57.701	0.1055	0.313
2406	396.744	339.269	57.475	0.1058	0.284
2407	395.755	338.243	57.513	0.1055	0.283
2408	396.661	339.039	57.623	0.1058	0.275
2409	398.639	341.090	57.549	0.1057	0.307
2410	396.661	339.178	57.484	0.1055	0.327
2411	396.661	339.263	57.399	0.1055	0.304
2412	397.733	340.263	57.470	0.1058	0.291
2413	395.673	338.269	57.404	0.1055	0.309
2414	397.650	340.209	57.441	0.1054	0.289

2415	395.714	338.286	57.428	0.1054	0.309
2416	395.673	338.194	57.479	0.1055	0.303
2417	395.631	338.011	57.620	0.1055	0.291
2418	395.631	338.183	57.449	0.1058	0.294
2419	395.631	338.058	57.574	0.1058	0.292
2420	395.631	338.129	57.503	0.1055	0.316
2421	396.579	339.110	57.469	0.1057	0.280
2422	395.590	338.281	57.309	0.1055	0.286
2423	395.673	338.228	57.445	0.1055	0.310
2424	396.703	339.310	57.393	0.1055	0.297
2425	395.673	338.121	57.551	0.1058	0.303
2426	395.631	338.305	57.326	0.1055	0.316
2427	395.631	338.124	57.508	0.1055	0.312
2428	395.631	338.014	57.618	0.1058	0.294
2429	395.673	338.404	57.269	0.1058	0.285
2430	395.631	338.063	57.569	0.1057	0.286
2431	395.714	338.296	57.418	0.1058	0.296
2432	395.714	338.664	57.050	0.1054	0.289
2433	395.673	338.189	57.484	0.1055	0.300
2434	395.673	338.161	57.511	0.1055	0.300
2435	395.755	338.291	57.464	0.1055	0.319
2436	395.673	338.226	57.446	0.1058	0.317
2437	395.631	338.194	57.438	0.1055	0.329
2438	395.590	338.125	57.465	0.1055	0.310
2439	395.879	338.467	57.411	0.1055	0.306
2440	395.673	338.189	57.484	0.1055	0.302
2441	395.631	338.158	57.474	0.1058	0.294
2442	395.673	338.318	57.355	0.1058	0.280
2443	395.673	338.209	57.464	0.1055	0.286
2444	395.673	338.280	57.393	0.1055	0.318
2445	395.796	338.460	57.336	0.1055	0.300
2446	395.714	338.155	57.559	0.1058	0.294
2447	395.673	338.418	57.255	0.1057	0.303
2448	395.590	338.193	57.398	0.1055	0.299
2449	394.766	337.457	57.309	0.1057	0.307
2450	395.673	338.235	57.438	0.1058	0.304
2451	395.714	338.316	57.398	0.1056	0.287
2452	395.631	338.194	57.438	0.1057	0.303
2453	395.590	338.184	57.406	0.1054	0.291
2454	394.725	337.303	57.423	0.1057	0.303
2455	395.631	338.299	57.333	0.1055	0.292
2456	394.766	337.450	57.316	0.1054	0.335
2457	395.590	338.193	57.398	0.1054	0.312
2458	395.755	338.471	57.284	0.1055	0.311
2459	394.725	337.350	57.375	0.1055	0.289

2460	394.766	337.426	57.340	0.1058	0.301
2461	395.590	338.456	57.134	0.1055	0.297
2462	394.766	337.559	57.208	0.1055	0.294
2463	395.590	338.311	57.279	0.1054	0.313
2464	395.673	338.374	57.299	0.1058	0.284
2465	393.777	336.422	57.355	0.1058	0.270
2466	393.695	336.240	57.455	0.1058	0.288
2467	393.695	336.425	57.270	0.1058	0.285
2468	393.695	336.306	57.389	0.1058	0.317
2469	393.654	336.190	57.464	0.1055	0.314
2470	395.673	338.379	57.294	0.1055	0.290
2471	393.777	336.485	57.293	0.1054	0.310
2472	393.695	336.505	57.190	0.1055	0.297
2473	392.583	335.309	57.274	0.1055	0.303
2474	392.871	335.816	57.055	0.1058	0.288
2475	392.789	335.624	57.165	0.1055	0.288
2476	392.706	335.441	57.265	0.1058	0.283
2477	392.706	335.471	57.235	0.1055	0.321
2478	393.695	336.503	57.193	0.1054	0.290
2479	392.789	335.476	57.313	0.1058	0.280
2480	392.748	335.554	57.194	0.1055	0.294
2481	392.789	335.471	57.318	0.1055	0.297
2482	392.624	335.410	57.214	0.1055	0.300
2483	392.706	335.531	57.175	0.1055	0.304
2484	392.789	335.439	57.350	0.1058	0.270
2485	392.542	335.324	57.218	0.1055	0.307
2486	392.624	335.605	57.019	0.1057	0.287
2487	392.789	335.570	57.219	0.1057	0.300
2488	392.665	335.420	57.245	0.1055	0.275
2489	392.789	335.447	57.341	0.1055	0.305
2490	392.789	335.509	57.280	0.1055	0.326
2491	392.706	335.508	57.199	0.1054	0.322
2492	392.789	335.485	57.304	0.1058	0.323
2493	392.748	335.559	57.189	0.1058	0.291
2494	392.624	335.496	57.128	0.1055	0.292
2495	392.665	335.315	57.350	0.1058	0.280
2496	392.830	335.721	57.109	0.1055	0.307
2497	392.789	335.639	57.150	0.1055	0.304
2498	392.706	335.480	57.226	0.1058	0.287
2499	392.871	335.611	57.260	0.1058	0.288
2500	392.748	335.615	57.133	0.1055	0.309
2501	391.635	334.599	57.036	0.1055	0.293
2502	392.748	335.569	57.179	0.1055	0.300
2503	391.841	334.657	57.184	0.1058	0.323
2504	392.871	335.531	57.340	0.1055	0.326

2505	392.912	335.739	57.174	0.1055	0.307
2506	392.706	335.536	57.170	0.1054	0.307
2507	392.706	335.536	57.170	0.1058	0.307
2508	392.706	335.520	57.186	0.1055	0.317
2509	392.789	335.634	57.155	0.1058	0.295
2510	391.800	334.672	57.128	0.1055	0.287
2511	392.789	335.429	57.360	0.1054	0.300
2512	392.706	335.756	56.950	0.1058	0.310
2513	391.718	334.505	57.213	0.1057	0.291
2514	392.748	335.674	57.074	0.1058	0.286
2515	391.718	334.444	57.274	0.1055	0.300
2516	391.841	334.854	56.988	0.1055	0.303
2517	391.676	334.603	57.074	0.1055	0.287
2518	392.830	335.894	56.936	0.1058	0.291
2519	391.800	334.702	57.098	0.1057	0.298
2520	391.800	334.802	56.998	0.1055	0.314
2521	392.789	335.714	57.075	0.1058	0.278
2522	391.718	334.610	57.108	0.1054	0.307
2523	391.718	334.490	57.228	0.1054	0.294
2524	390.770	333.696	57.074	0.1055	0.287
2525	391.759	334.679	57.080	0.1056	0.293
2526	391.800	334.930	56.870	0.1055	0.280
2527	390.729	333.620	57.109	0.1056	0.298
2528	389.740	332.580	57.160	0.1055	0.321
2529	389.740	332.660	57.080	0.1054	0.292
2530	389.740	332.712	57.028	0.1054	0.306
2531	389.699	332.594	57.105	0.1055	0.304
2532	390.729	333.703	57.026	0.1056	0.306
2533	389.699	332.615	57.084	0.1055	0.316
2534	389.822	332.700	57.123	0.1055	0.294
2535	389.864	332.751	57.113	0.1055	0.316
2536	389.864	332.664	57.200	0.1058	0.287
2537	389.740	332.556	57.184	0.1058	0.284
2538	389.781	332.760	57.021	0.1055	0.288
2539	389.781	332.630	57.151	0.1055	0.280
2540	389.699	332.634	57.065	0.1055	0.305
2541	389.740	332.702	57.038	0.1054	0.294
2542	389.781	332.602	57.179	0.1058	0.313
2543	389.864	332.732	57.131	0.1058	0.297
2544	389.658	332.693	56.965	0.1055	0.304
2545	389.864	332.869	56.995	0.1055	0.307
2546	389.822	332.877	56.945	0.1055	0.303
2547	389.740	332.770	56.970	0.1055	0.332
2548	389.781	332.879	56.903	0.1055	0.306
2549	389.740	332.664	57.076	0.1055	0.298

2550	389.699	332.456	57.243	0.1058	0.291
2551	389.740	332.866	56.874	0.1055	0.297
2552	389.781	332.667	57.114	0.1055	0.297
2553	389.864	332.911	56.953	0.1054	0.297
2554	389.822	332.771	57.051	0.1058	0.306
2555	389.781	332.631	57.150	0.1058	0.294
2556	389.740	332.575	57.165	0.1055	0.303
2557	389.740	332.675	57.065	0.1055	0.283
2558	389.616	332.660	56.956	0.1055	0.293
2559	389.699	332.605	57.094	0.1055	0.293
2560	389.699	332.780	56.919	0.1054	0.324
2561	388.834	331.715	57.119	0.1055	0.312
2562	388.834	331.715	57.119	0.1055	0.283
2563	388.792	331.689	57.104	0.1056	0.289
2564	388.792	331.499	57.294	0.1058	0.321
2565	388.710	331.574	57.136	0.1055	0.295
2566	388.792	331.655	57.138	0.1055	0.315
2567	388.792	331.747	57.045	0.1054	0.309
2568	388.792	331.760	57.033	0.1055	0.303
2569	388.751	331.630	57.121	0.1055	0.295
2570	388.834	331.669	57.165	0.1054	0.275
2571	388.875	331.834	57.041	0.1058	0.296
2572	388.628	331.549	57.079	0.1058	0.288
2573	388.792	331.775	57.018	0.1055	0.309
2574	388.751	331.552	57.199	0.1055	0.300
2575	387.804	330.757	57.046	0.1058	0.293
2576	388.751	331.842	56.909	0.1058	0.284
2577	387.845	330.780	57.065	0.1058	0.300
2578	387.804	330.795	57.009	0.1055	0.300
2579	387.721	330.779	56.943	0.1054	0.301
2580	387.721	330.618	57.104	0.1054	0.295
2581	387.845	331.027	56.818	0.1054	0.300
2582	387.804	330.782	57.021	0.1054	0.341
2583	387.721	330.785	56.936	0.1055	0.306
2584	388.669	331.684	56.985	0.1058	0.274
2585	387.927	330.890	57.038	0.1058	0.293
2586	387.845	330.841	57.004	0.1058	0.294
2587	387.721	330.726	56.995	0.1055	0.304
2588	387.804	330.832	56.971	0.1055	0.275
2589	387.680	330.681	56.999	0.1058	0.294
2590	387.762	330.745	57.018	0.1055	0.300
2591	387.680	330.734	56.946	0.1055	0.277
2592	386.856	329.761	57.095	0.1057	0.287
2593	387.762	330.850	56.913	0.1055	0.276
2594	387.845	330.770	57.075	0.1058	0.307

2595	387.845	330.827	57.018	0.1055	0.294
2596	386.815	329.750	57.065	0.1056	0.286
2597	387.804	330.820	56.984	0.1056	0.297
2598	386.856	329.835	57.021	0.1055	0.313
2599	386.815	329.796	57.019	0.1055	0.299
2600	387.804	330.795	57.009	0.1055	0.326
2601	387.886	330.892	56.994	0.1054	0.332
2602	386.897	329.884	57.014	0.1055	0.329
2603	385.909	328.939	56.970	0.1055	0.291
2604	387.845	330.946	56.899	0.1054	0.312
2605	386.815	330.106	56.709	0.1055	0.324
2606	386.897	329.899	56.999	0.1055	0.280
2607	387.804	330.852	56.951	0.1058	0.286
2608	386.774	330.096	56.678	0.1055	0.292
2609	386.815	329.889	56.926	0.1055	0.270
2610	386.815	329.892	56.923	0.1056	0.288
2611	387.721	330.731	56.990	0.1055	0.295
2612	386.691	329.898	56.794	0.1058	0.295
2613	385.826	329.035	56.791	0.1057	0.271
2614	386.856	329.876	56.980	0.1055	0.274
2615	386.815	329.935	56.880	0.1055	0.290
2616	386.897	330.014	56.884	0.1054	0.282
2617	386.815	329.916	56.899	0.1054	0.303
2618	385.785	328.852	56.933	0.1058	0.299
2619	385.867	329.079	56.789	0.1054	0.307
2620	385.826	328.865	56.961	0.1055	0.305
2621	385.826	328.995	56.831	0.1055	0.335
2622	385.785	328.885	56.900	0.1055	0.303
2623	385.826	328.937	56.889	0.1058	0.291
2624	385.785	328.900	56.885	0.1058	0.290
2625	385.867	329.140	56.728	0.1058	0.291
2626	385.785	328.844	56.941	0.1055	0.298
2627	385.785	328.937	56.848	0.1054	0.286
2628	385.950	329.027	56.923	0.1055	0.294
2629	385.826	328.819	57.008	0.1054	0.282
2630	385.867	329.007	56.860	0.1055	0.306
2631	385.826	328.924	56.903	0.1055	0.319
2632	385.703	328.870	56.833	0.1055	0.295
2633	385.909	328.897	57.011	0.1055	0.295
2634	385.909	329.042	56.866	0.1055	0.291
2635	385.867	329.182	56.685	0.1055	0.292
2636	385.867	329.020	56.848	0.1055	0.297
2637	385.867	329.064	56.804	0.1055	0.305
2638	385.785	329.176	56.609	0.1054	0.292
2639	385.909	329.144	56.765	0.1054	0.332

2640	385.950	329.203	56.746	0.1055	0.297
2641	385.826	329.019	56.808	0.1056	0.288
2642	385.909	329.057	56.851	0.1055	0.300
2643	385.909	329.129	56.780	0.1055	0.291
2644	385.909	329.071	56.838	0.1057	0.271
2645	385.867	328.906	56.961	0.1058	0.269
2646	385.909	329.062	56.846	0.1055	0.287
2647	385.867	329.011	56.856	0.1055	0.304
2648	384.961	328.077	56.884	0.1055	0.295
2649	385.909	328.929	56.980	0.1057	0.284
2650	385.826	329.011	56.815	0.1055	0.310
2651	385.867	329.067	56.800	0.1058	0.310
2652	384.879	328.122	56.756	0.1055	0.282
2653	385.867	329.097	56.770	0.1055	0.303
2654	385.950	329.141	56.809	0.1055	0.332
2655	384.837	327.976	56.861	0.1055	0.321
2656	383.890	327.174	56.716	0.1058	0.323
2657	385.826	329.041	56.785	0.1055	0.287
2658	384.013	327.342	56.671	0.1055	0.283
2659	383.890	327.044	56.846	0.1055	0.306
2660	384.755	328.004	56.751	0.1055	0.304
2661	384.796	328.082	56.714	0.1055	0.291
2662	383.931	327.236	56.695	0.1057	0.274
2663	383.890	327.134	56.756	0.1057	0.289
2664	383.890	327.225	56.665	0.1058	0.277
2665	383.890	327.176	56.714	0.1058	0.285
2666	383.890	327.192	56.698	0.1055	0.297
2667	383.972	327.277	56.695	0.1055	0.288
2668	383.725	327.050	56.675	0.1054	0.295
2669	383.766	326.986	56.780	0.1054	0.307
2670	383.890	327.180	56.710	0.1054	0.286
2671	382.860	326.119	56.741	0.1055	0.304
2672	382.860	326.200	56.660	0.1056	0.305
2673	382.942	326.285	56.658	0.1057	0.287
2674	382.860	326.009	56.851	0.1058	0.276
2675	382.860	326.050	56.810	0.1058	0.271
2676	383.890	327.347	56.543	0.1055	0.316
2677	382.819	326.080	56.739	0.1055	0.289
2678	382.860	326.165	56.695	0.1057	0.321
2679	382.777	326.204	56.574	0.1055	0.315
2680	382.819	326.039	56.780	0.1057	0.304
2681	383.849	327.125	56.724	0.1055	0.314
2682	383.890	327.056	56.834	0.1055	0.310
2683	382.819	326.039	56.780	0.1055	0.325
2684	382.819	326.161	56.658	0.1054	0.319

2685	382.777	326.094	56.684	0.1055	0.310
2686	382.860	326.100	56.760	0.1055	0.291
2687	382.860	326.165	56.695	0.1057	0.274
2688	382.819	326.171	56.648	0.1058	0.303
2689	382.819	326.110	56.709	0.1057	0.310
2690	382.819	326.144	56.675	0.1055	0.290
2691	382.777	326.082	56.695	0.1055	0.293
2692	382.819	326.186	56.633	0.1055	0.303
2693	382.819	326.144	56.675	0.1055	0.285
2694	382.901	326.302	56.599	0.1055	0.279
2695	382.819	326.301	56.518	0.1055	0.295
2696	382.901	326.354	56.548	0.1057	0.285
2697	382.819	326.159	56.660	0.1055	0.295
2698	382.819	326.200	56.619	0.1055	0.294
2699	382.860	326.099	56.761	0.1058	0.310
2700	382.860	326.166	56.694	0.1055	0.298
2701	382.860	326.307	56.553	0.1055	0.291
2702	382.819	326.182	56.636	0.1055	0.284
2703	382.983	326.288	56.695	0.1055	0.291
2704	382.860	326.175	56.685	0.1057	0.291
2705	382.819	326.249	56.570	0.1055	0.295
2706	382.860	326.217	56.643	0.1055	0.290
2707	382.777	325.987	56.790	0.1055	0.276
2708	382.777	325.940	56.838	0.1055	0.300
2709	382.901	326.382	56.519	0.1055	0.307
2710	382.901	326.354	56.548	0.1055	0.313
2711	382.860	326.185	56.675	0.1054	0.311
2712	380.841	324.271	56.570	0.1055	0.294
2713	382.819	326.109	56.710	0.1055	0.298
2714	382.942	326.376	56.566	0.1057	0.272
2715	382.983	326.556	56.428	0.1055	0.286
2716	382.901	326.201	56.700	0.1056	0.294
2717	382.860	326.144	56.716	0.1055	0.290
2718	382.819	326.214	56.605	0.1056	0.286
2719	382.860	326.180	56.680	0.1057	0.267
2720	382.983	326.166	56.818	0.1055	0.274
2721	381.871	325.149	56.723	0.1055	0.297
2722	380.923	324.305	56.619	0.1058	0.278
2723	381.995	325.603	56.391	0.1055	0.303
2724	382.901	326.179	56.723	0.1054	0.292
2725	381.871	325.239	56.633	0.1055	0.300
2726	380.923	324.258	56.665	0.1055	0.310
2727	380.882	324.369	56.514	0.1055	0.292
2728	380.759	324.089	56.670	0.1054	0.303
2729	380.923	324.277	56.646	0.1055	0.313

2730	381.912	325.356	56.556	0.1054	0.305
2731	379.852	323.205	56.648	0.1055	0.298
2732	380.923	324.316	56.608	0.1055	0.287
2733	380.800	324.216	56.584	0.1054	0.272
2734	380.882	324.160	56.723	0.1055	0.294
2735	380.882	324.307	56.575	0.1055	0.297
2736	379.811	323.087	56.724	0.1054	0.279
2737	380.841	324.132	56.709	0.1055	0.290
2738	380.882	324.422	56.460	0.1054	0.308
2739	380.841	324.215	56.626	0.1055	0.288
2740	380.759	324.117	56.641	0.1054	0.292
2741	379.976	323.391	56.585	0.1055	0.292
2742	380.841	324.332	56.509	0.1057	0.293
2743	380.841	324.076	56.765	0.1056	0.287
2744	381.006	324.355	56.651	0.1057	0.293
2745	381.006	324.283	56.723	0.1057	0.291
2746	379.811	323.121	56.690	0.1055	0.284
2747	379.852	323.259	56.594	0.1055	0.300
2748	380.882	324.379	56.504	0.1057	0.282
2749	380.882	324.364	56.519	0.1055	0.288
2750	380.965	324.490	56.475	0.1055	0.276
2751	379.976	323.291	56.685	0.1055	0.294
2752	379.935	323.392	56.543	0.1055	0.274
2753	379.976	323.296	56.680	0.1055	0.310
2754	380.923	324.486	56.438	0.1054	0.310
2755	380.017	323.442	56.575	0.1055	0.340
2756	379.893	323.351	56.543	0.1058	0.316
2757	379.852	323.300	56.553	0.1055	0.294
2758	379.976	323.367	56.609	0.1055	0.288
2759	381.006	324.435	56.571	0.1055	0.276
2760	380.017	323.461	56.556	0.1057	0.297
2761	379.893	323.256	56.638	0.1058	0.316
2762	379.976	323.530	56.446	0.1058	0.290
2763	379.852	323.292	56.560	0.1058	0.292
2764	379.976	323.300	56.676	0.1055	0.282
2765	379.893	323.357	56.536	0.1055	0.284
2766	379.852	323.412	56.440	0.1055	0.300
2767	379.852	323.477	56.375	0.1055	0.294
2768	379.852	323.320	56.533	0.1054	0.315
2769	379.976	323.411	56.565	0.1054	0.300
2770	379.852	323.271	56.581	0.1055	0.303
2771	379.935	323.335	56.600	0.1055	0.332
2772	379.935	323.417	56.518	0.1055	0.312
2773	379.935	323.435	56.500	0.1055	0.271
2774	379.893	323.393	56.500	0.1054	0.291

2775	379.935	323.555	56.380	0.1058	0.303
2776	379.852	323.206	56.646	0.1055	0.290
2777	379.893	323.313	56.580	0.1055	0.279
2778	380.017	323.578	56.439	0.1055	0.287
2779	379.852	323.372	56.480	0.1055	0.288
2780	379.852	323.575	56.278	0.1057	0.285
2781	380.017	323.493	56.524	0.1055	0.302
2782	380.058	323.525	56.534	0.1057	0.307
2783	379.935	323.370	56.565	0.1055	0.298
2784	379.935	323.435	56.500	0.1055	0.307
2785	379.935	323.473	56.461	0.1055	0.286
2786	379.893	323.437	56.456	0.1058	0.281
2787	379.852	323.477	56.375	0.1057	0.286
2788	380.058	323.463	56.595	0.1058	0.287
2789	379.852	323.467	56.385	0.1055	0.300
2790	379.976	323.647	56.329	0.1057	0.301
2791	380.058	323.521	56.538	0.1058	0.297
2792	379.935	323.498	56.436	0.1057	0.290
2793	379.976	323.496	56.480	0.1058	0.291
2794	379.852	323.386	56.466	0.1055	0.310
2795	379.893	323.493	56.400	0.1055	0.304
2796	378.864	322.560	56.304	0.1058	0.304
2797	379.852	323.449	56.404	0.1057	0.282
2798	380.017	323.632	56.385	0.1054	0.311
2799	379.976	323.587	56.389	0.1055	0.294
2800	378.905	322.677	56.228	0.1055	0.289
2801	379.935	323.560	56.375	0.1054	0.276
2802	379.935	323.488	56.446	0.1054	0.299
2803	380.017	323.570	56.448	0.1054	0.303
2804	379.852	323.320	56.533	0.1057	0.311
2805	377.916	321.521	56.395	0.1058	0.286
2806	379.976	323.567	56.409	0.1055	0.297
2807	379.028	322.530	56.499	0.1055	0.313
2808	378.946	322.561	56.385	0.1058	0.284
2809	379.935	323.526	56.409	0.1058	0.300
2810	379.935	323.492	56.443	0.1055	0.289
2811	378.905	322.511	56.394	0.1055	0.309
2812	378.864	322.477	56.386	0.1054	0.280
2813	377.875	321.514	56.361	0.1055	0.286
2814	376.968	320.570	56.399	0.1055	0.307
2815	377.875	321.519	56.356	0.1054	0.294
2816	377.957	321.591	56.366	0.1055	0.313
2817	377.834	321.320	56.514	0.1055	0.283
2818	378.946	322.547	56.399	0.1055	0.298
2819	378.987	322.651	56.336	0.1055	0.303

2820	377.875	321.439	56.436	0.1058	0.287
2821	377.998	321.571	56.428	0.1058	0.284
2822	377.998	321.480	56.519	0.1055	0.287
2823	377.957	321.625	56.333	0.1055	0.292
2824	378.040	321.548	56.491	0.1054	0.277
2825	376.968	320.663	56.305	0.1055	0.283
2826	377.875	321.327	56.548	0.1055	0.281
2827	377.916	321.388	56.528	0.1057	0.282
2828	377.957	321.648	56.309	0.1058	0.294
2829	376.968	320.682	56.286	0.1055	0.309
2830	377.957	321.548	56.409	0.1055	0.308
2831	376.886	320.382	56.504	0.1055	0.287
2832	376.886	320.420	56.466	0.1054	0.275
2833	376.886	320.486	56.400	0.1055	0.290
2834	376.968	320.607	56.361	0.1055	0.344
2835	376.886	320.520	56.366	0.1055	0.316
2836	377.792	321.441	56.351	0.1055	0.288
2837	376.886	320.511	56.375	0.1055	0.343
2838	376.968	320.702	56.266	0.1054	0.291
2839	376.927	320.625	56.303	0.1055	0.282
2840	376.886	320.630	56.256	0.1054	0.294
2841	376.968	320.508	56.460	0.1055	0.319
2842	376.968	320.702	56.266	0.1055	0.298
2843	376.886	320.381	56.505	0.1059	0.294
2844	376.886	320.330	56.556	0.1055	0.298
2845	376.968	320.660	56.309	0.1058	0.299
2846	377.092	320.722	56.370	0.1055	0.268
2847	376.968	320.716	56.253	0.1054	0.281
2848	376.968	320.816	56.153	0.1055	0.300
2849	376.886	320.463	56.423	0.1055	0.281
2850	376.886	320.563	56.323	0.1055	0.287
2851	376.968	320.546	56.423	0.1055	0.279
2852	376.927	320.447	56.480	0.1058	0.280
2853	376.886	320.568	56.318	0.1055	0.280
2854	376.968	320.546	56.423	0.1055	0.282
2855	376.845	320.492	56.353	0.1054	0.276
2856	376.968	320.665	56.304	0.1055	0.284
2857	374.991	318.686	56.305	0.1055	0.316
2858	375.032	318.880	56.153	0.1055	0.291
2859	376.927	320.557	56.370	0.1055	0.276
2860	374.950	318.607	56.343	0.1057	0.278
2861	375.980	319.590	56.390	0.1058	0.278
2862	375.980	319.605	56.375	0.1056	0.290
2863	375.073	318.746	56.328	0.1055	0.301
2864	374.991	318.691	56.300	0.1055	0.300

2865	375.032	318.686	56.346	0.1054	0.288
2866	375.073	318.854	56.219	0.1055	0.302
2867	374.991	318.645	56.346	0.1055	0.303
2868	374.908	318.686	56.223	0.1055	0.300
2869	375.032	318.676	56.356	0.1055	0.297
2870	374.991	318.648	56.343	0.1055	0.290
2871	374.950	318.550	56.400	0.1055	0.298
2872	374.908	318.390	56.519	0.1055	0.288
2873	374.950	318.716	56.234	0.1058	0.278
2874	374.991	318.763	56.228	0.1055	0.304
2875	374.950	318.651	56.299	0.1057	0.288
2876	375.032	318.780	56.253	0.1058	0.292
2877	374.908	318.623	56.285	0.1054	0.319
2878	374.908	318.685	56.224	0.1054	0.289
2879	374.908	318.566	56.343	0.1055	0.297
2880	374.867	318.616	56.251	0.1055	0.292
2881	374.826	318.761	56.065	0.1055	0.283
2882	375.032	318.727	56.305	0.1058	0.290
2883	374.867	318.639	56.229	0.1055	0.275
2884	374.867	318.625	56.243	0.1055	0.311
2885	374.991	318.650	56.341	0.1055	0.305
2886	375.073	318.826	56.248	0.1055	0.292
2887	374.867	318.530	56.338	0.1054	0.284
2888	375.032	318.686	56.346	0.1058	0.291
2889	375.032	318.702	56.330	0.1055	0.285
2890	374.950	318.597	56.353	0.1055	0.287
2891	375.032	318.766	56.266	0.1056	0.284
2892	374.908	318.552	56.356	0.1055	0.277
2893	374.991	318.748	56.243	0.1054	0.304
2894	374.991	318.701	56.290	0.1055	0.303
2895	374.991	318.652	56.339	0.1055	0.294
2896	374.991	318.928	56.063	0.1055	0.281
2897	374.950	318.598	56.351	0.1054	0.291
2898	374.950	318.793	56.156	0.1054	0.276
2899	375.073	318.783	56.290	0.1055	0.284
2900	375.114	318.829	56.285	0.1054	0.280
2901	374.908	318.642	56.266	0.1054	0.284
2902	374.950	318.417	56.533	0.1058	0.311
2903	375.156	318.979	56.176	0.1055	0.288
2904	374.084	317.737	56.348	0.1055	0.293
2905	374.991	318.710	56.281	0.1055	0.271
2906	374.084	317.804	56.280	0.1055	0.296
2907	375.032	318.732	56.300	0.1055	0.274
2908	374.950	318.707	56.243	0.1058	0.281
2909	373.920	317.492	56.428	0.1055	0.297

2910	374.950	318.697	56.253	0.1055	0.285
2911	375.032	318.556	56.476	0.1057	0.301
2912	374.043	317.787	56.256	0.1055	0.294
2913	374.002	317.785	56.218	0.1055	0.310
2914	375.032	318.781	56.251	0.1055	0.291
2915	372.972	316.801	56.171	0.1055	0.302
2916	374.950	318.712	56.238	0.1055	0.316
2917	374.908	318.590	56.319	0.1055	0.293
2918	374.043	317.902	56.141	0.1055	0.297
2919	374.908	318.615	56.294	0.1054	0.291
2920	374.126	317.998	56.128	0.1055	0.284
2921	374.991	318.715	56.276	0.1055	0.285
2922	373.920	317.743	56.176	0.1054	0.275
2923	373.096	316.804	56.291	0.1055	0.305
2924	374.950	318.755	56.195	0.1057	0.291
2925	374.002	317.802	56.200	0.1055	0.297
2926	374.002	317.932	56.070	0.1055	0.297
2927	374.084	317.913	56.171	0.1055	0.282
2928	374.002	317.737	56.265	0.1054	0.277
2929	375.032	318.900	56.133	0.1055	0.284
2930	373.920	317.638	56.281	0.1055	0.277
2931	373.920	317.853	56.066	0.1055	0.315
2932	373.013	316.742	56.271	0.1055	0.295
2933	373.878	317.722	56.156	0.1055	0.288
2934	373.013	316.862	56.151	0.1055	0.300
2935	374.084	318.023	56.061	0.1055	0.319
2936	374.002	317.866	56.136	0.1055	0.287
2937	374.002	317.931	56.071	0.1055	0.282
2938	371.983	315.847	56.136	0.1055	0.287
2939	374.084	317.933	56.151	0.1055	0.279
2940	372.025	315.930	56.095	0.1056	0.275
2941	373.055	316.893	56.161	0.1057	0.283
2942	374.043	317.805	56.239	0.1055	0.291
2943	371.983	315.921	56.063	0.1057	0.279
2944	373.920	317.530	56.390	0.1055	0.288
2945	373.013	316.986	56.028	0.1054	0.280
2946	374.002	317.761	56.241	0.1055	0.265
2947	372.931	316.812	56.119	0.1055	0.313
2948	372.025	315.815	56.210	0.1055	0.279
2949	373.055	317.012	56.043	0.1055	0.291
2950	372.025	315.815	56.210	0.1054	0.294
2951	371.983	315.745	56.239	0.1055	0.319
2952	372.025	315.892	56.133	0.1055	0.282
2953	371.860	315.688	56.171	0.1057	0.292
2954	371.942	315.838	56.104	0.1054	0.276

2955	372.025	315.948	56.076	0.1055	0.294
2956	372.025	315.941	56.084	0.1055	0.283
2957	372.066	316.037	56.029	0.1054	0.278
2958	372.107	315.983	56.124	0.1055	0.320
2959	373.055	317.193	55.861	0.1055	0.316
2960	372.025	315.918	56.106	0.1055	0.278
2961	371.942	315.891	56.051	0.1058	0.277
2962	372.107	315.944	56.163	0.1059	0.272
2963	372.066	315.724	56.341	0.1058	0.281
2964	372.066	315.899	56.166	0.1055	0.293
2965	372.025	315.801	56.224	0.1055	0.279
2966	372.025	315.901	56.124	0.1055	0.327
2967	372.066	316.033	56.033	0.1057	0.285
2968	372.107	315.983	56.124	0.1055	0.304
2969	372.148	315.958	56.190	0.1054	0.298
2970	372.025	316.057	55.968	0.1054	0.312
2971	372.066	316.038	56.028	0.1055	0.290
2972	372.148	316.011	56.138	0.1055	0.283
2973	372.066	315.932	56.134	0.1056	0.276
2974	372.066	316.018	56.048	0.1055	0.285
2975	371.036	314.945	56.091	0.1056	0.268
2976	372.066	316.048	56.018	0.1054	0.268
2977	372.066	315.937	56.129	0.1055	0.276
2978	372.066	316.028	56.038	0.1055	0.271
2979	372.025	315.911	56.114	0.1054	0.280
2980	372.025	316.072	55.953	0.1055	0.303
2981	372.025	316.043	55.981	0.1055	0.283
2982	372.189	316.148	56.041	0.1057	0.303
2983	371.077	315.016	56.061	0.1055	0.291
2984	372.025	315.952	56.073	0.1058	0.267
2985	370.995	314.937	56.058	0.1055	0.278
2986	371.077	315.077	56.000	0.1055	0.290
2987	372.025	315.968	56.056	0.1055	0.273
2988	371.036	315.187	55.849	0.1054	0.280
2989	372.148	316.207	55.941	0.1055	0.282
2990	371.118	315.061	56.058	0.1057	0.294
2991	372.025	316.035	55.990	0.1058	0.266
2992	371.036	315.042	55.994	0.1058	0.313
2993	372.025	316.020	56.005	0.1055	0.304
2994	371.036	314.907	56.129	0.1054	0.298
2995	372.107	316.024	56.083	0.1054	0.274
2996	370.953	315.148	55.805	0.1055	0.278
2997	370.953	314.887	56.066	0.1055	0.274
2998	371.077	314.929	56.148	0.1055	0.282
2999	371.036	314.893	56.143	0.1058	0.273

3000	372.148	316.287	55.861	0.1054	0.287
3001	372.107	315.873	56.234	0.1055	0.292
3002	371.201	315.162	56.039	0.1055	0.281
3003	371.077	314.902	56.175	0.1055	0.303
3004	371.159	314.964	56.195	0.1055	0.311
3005	371.118	315.213	55.905	0.1054	0.294
3006	371.077	314.952	56.125	0.1054	0.281
3007	371.118	314.932	56.186	0.1055	0.299
3008	371.036	315.096	55.940	0.1055	0.287
3009	371.036	314.941	56.095	0.1055	0.309
3010	371.118	315.156	55.963	0.1055	0.298
3011	371.036	314.945	56.091	0.1055	0.283
3012	371.118	315.133	55.985	0.1055	0.284
3013	371.118	315.276	55.843	0.1055	0.290
3014	370.047	313.771	56.276	0.1055	0.262
3015	371.036	315.050	55.986	0.1055	0.301
3016	370.212	314.227	55.985	0.1055	0.305
3017	370.953	315.006	55.948	0.1055	0.287
3018	371.036	315.070	55.966	0.1055	0.290
3019	370.047	313.971	56.076	0.1055	0.272
3020	371.118	315.189	55.929	0.1055	0.285
3021	370.129	313.911	56.219	0.1055	0.280
3022	371.201	315.096	56.105	0.1055	0.298
3023	370.212	314.241	55.971	0.1055	0.276
3024	369.099	313.052	56.048	0.1058	0.279
3025	371.159	315.126	56.034	0.1054	0.279
3026	370.171	314.161	56.010	0.1055	0.276
3027	370.171	314.066	56.105	0.1055	0.288
3028	370.171	314.194	55.976	0.1055	0.281
3029	369.099	313.179	55.920	0.1055	0.265
3030	370.047	314.047	56.000	0.1055	0.281
3031	370.129	314.053	56.076	0.1055	0.283
3032	370.088	314.002	56.086	0.1054	0.300
3033	369.182	313.224	55.958	0.1054	0.326
3034	369.099	313.063	56.036	0.1055	0.298
3035	369.141	313.112	56.029	0.1055	0.284
3036	370.088	314.064	56.024	0.1055	0.313
3037	369.182	313.153	56.029	0.1054	0.303
3038	370.088	313.983	56.105	0.1055	0.291
3039	369.141	313.073	56.068	0.1055	0.310
3040	370.212	314.236	55.976	0.1055	0.279
3041	369.017	312.970	56.048	0.1055	0.282
3042	369.058	313.138	55.920	0.1055	0.288
3043	370.088	314.134	55.954	0.1055	0.274
3044	369.058	312.992	56.066	0.1055	0.282

3045	369.058	313.173	55.885	0.1054	0.276
3046	369.017	312.907	56.110	0.1058	0.265
3047	369.141	313.232	55.909	0.1054	0.291
3048	369.223	313.242	55.981	0.1055	0.276
3049	369.141	313.097	56.044	0.1056	0.277
3050	369.099	313.199	55.900	0.1054	0.290
3051	369.058	313.101	55.958	0.1055	0.297
3052	369.058	313.216	55.843	0.1054	0.279
3053	369.141	313.207	55.934	0.1055	0.278
3054	369.182	313.458	55.724	0.1055	0.287
3055	369.099	313.133	55.966	0.1055	0.294
3056	369.141	313.216	55.925	0.1058	0.300
3057	369.223	313.352	55.871	0.1055	0.313
3058	369.017	313.136	55.881	0.1055	0.310
3059	369.141	313.312	55.829	0.1054	0.281
3060	369.141	313.163	55.978	0.1055	0.280
3061	369.182	313.182	56.000	0.1058	0.273
3062	369.141	313.293	55.848	0.1055	0.278
3063	369.099	312.991	56.109	0.1055	0.266
3064	369.141	313.139	56.001	0.1055	0.277
3065	369.058	313.133	55.925	0.1055	0.297
3066	368.028	311.986	56.043	0.1055	0.277
3067	369.099	313.256	55.844	0.1055	0.253
3068	369.182	313.178	56.004	0.1055	0.297
3069	369.058	313.186	55.873	0.1054	0.278
3070	369.141	313.231	55.910	0.1055	0.291
3071	369.141	313.308	55.833	0.1054	0.297
3072	368.111	312.163	55.948	0.1055	0.297
3073	369.182	313.244	55.938	0.1055	0.295
3074	369.182	313.234	55.948	0.1054	0.285
3075	368.152	312.147	56.005	0.1055	0.321
3076	368.069	312.287	55.783	0.1055	0.297
3077	369.141	313.249	55.891	0.1054	0.280
3078	368.193	312.221	55.973	0.1055	0.325
3079	369.141	313.422	55.719	0.1056	0.283
3080	368.234	312.424	55.810	0.1058	0.274
3081	369.099	313.247	55.853	0.1055	0.277
3082	368.152	312.186	55.966	0.1055	0.287
3083	368.152	312.323	55.829	0.1057	0.298
3084	368.111	312.211	55.900	0.1056	0.283
3085	368.111	312.301	55.810	0.1054	0.278
3086	368.152	312.194	55.958	0.1057	0.270
3087	368.152	312.179	55.973	0.1054	0.282
3088	368.234	312.396	55.839	0.1055	0.271
3089	368.111	312.286	55.825	0.1055	0.284

3090	368.069	312.163	55.906	0.1054	0.278
3091	368.152	312.223	55.929	0.1055	0.313
3092	368.152	312.243	55.909	0.1055	0.283
3093	368.111	312.372	55.739	0.1055	0.307
3094	368.152	312.533	55.619	0.1055	0.274
3095	367.163	311.239	55.924	0.1055	0.288
3096	368.111	312.349	55.761	0.1058	0.295
3097	367.987	311.992	55.995	0.1055	0.304
3098	368.069	312.117	55.953	0.1054	0.276
3099	368.028	311.886	56.143	0.1055	0.278
3100	368.069	312.231	55.839	0.1055	0.295
3101	368.152	312.167	55.985	0.1055	0.301
3102	367.081	311.186	55.895	0.1055	0.281
3103	367.163	311.268	55.895	0.1058	0.277
3104	368.069	312.071	55.999	0.1055	0.276
3105	368.111	312.192	55.919	0.1058	0.274
3106	368.069	312.353	55.716	0.1055	0.284
3107	368.152	312.361	55.791	0.1055	0.281
3108	367.204	311.428	55.776	0.1055	0.306
3109	367.987	312.250	55.738	0.1054	0.300
3110	367.081	310.933	56.148	0.1055	0.309
3111	368.234	312.263	55.971	0.1055	0.287
3112	367.163	311.183	55.980	0.1054	0.272
3113	368.069	312.139	55.930	0.1055	0.276
3114	367.946	312.012	55.934	0.1054	0.292
3115	368.111	312.314	55.796	0.1057	0.312
3116	368.152	312.232	55.920	0.1057	0.289
3117	368.152	312.394	55.758	0.1055	0.274
3118	367.163	311.229	55.934	0.1055	0.263
3119	367.039	311.221	55.819	0.1055	0.310
3120	367.122	311.232	55.890	0.1055	0.288
3121	368.028	312.186	55.843	0.1054	0.282
3122	368.069	312.174	55.895	0.1055	0.302
3123	367.081	311.081	56.000	0.1055	0.284
3124	368.193	312.321	55.873	0.1055	0.305
3125	366.998	311.198	55.800	0.1055	0.284
3126	368.152	312.323	55.829	0.1055	0.281